Advances in Intelligent Transportation System and Technology

Edited by
Decheng Feng

TTP TRANS TECH PUBLICATIONS

Advances in Intelligent Transportation System and Technology

Edited by
Decheng Feng

Advances in Intelligent Transportation System and Technology

Selected, peer reviewed papers from the
1st International Doctoral Annual Symposium on
Intelligent Transportation Technology and Sustainable Development
September 15-16, 2012, Harbin, China

Edited by

Decheng Feng

TTP

Trans Tech Publications Ltd
Kreuzstrasse 10
CH-8635 Durnten-Zurich
Switzerland
http://www.ttp.net

Volume 5 of
Advanced Engineering Forum
ISSN 2234-9901

Full text available online at *http://www.scientific.net*

***Distributed** worldwide by*

Trans Tech Publications Ltd
Kreuzstrasse 10
CH-8635 Durnten-Zurich
Switzerland

Fax: +41 (44) 922 10 33
e-mail: sales@ttp.net

and in the Americas by

Trans Tech Publications Inc.
PO Box 699, May Street
Enfield, NH 03748
USA

Phone: +1 (603) 632-7377
Fax: +1 (603) 632-5611
e-mail: sales-usa@ttp.net

Preface

The 1st International Doctoral Annual Symposium on Intelligent Transportation Technology and Sustainable Development was held by School of Transportation Science and Engineering, Harbin Institute of Technology. This symposium encompasses all aspects of intelligent transportation technology, bridge monitoring and maintenance, road engineering and material science. The aim of this symposium is to build the platform for communication between graduate students in different countries, to bring together some best and newest work that have been done in the field of transportation engineering, and to stimulate and promote research into related fields.

Organization

Conference chair: Prof. Shi An
Executive chair: Prof. Xiangshen Hou
Academic chair: Prof. Yiqiu Tan
Secretariat chair: Prof. Decheng Feng
Organizing secretariat: Prof. Ning Xie, Prof. Yang Liu, Prof. Hua Wang,
Dr. Junyan Yi, Dr. Feng Zhang, Ms. Qi Wang

Committees & Sponsors

Harbin Institute of Technology, China
Research Institute of Highway Ministry of Transport, China
University of Illinois at Urbana-Champaign, U.S.A
Texas A&M University, U.S.A
Northeastern University, U.S.A
Tongji University, China
Southeastern University, China
Chang An University, China

Table of Contents

Chapter 2: Bridge Monitoring, Safety and Maintenance

Chapter 3: Advanced Technique in Road Engineering and Material Science

CHAPTER 1:

Intelligent Transportation Technique

doi:10.4028/www.scientific.net/AEF.5.3

Classification of mobility of cellular phone using linear classification and k-clustering

Shilong Wang, Hua Wang

School of Transportation Science and Engineering, Harbin institute of technology
School of Transportation Science and Engineering, Harbin institute of technology
wangshilongjms@126.com,wanghua@hit.edu.cn.

Keywords: multiple base station; cellular phone classification and recognition; linear classification; k–clustering.

Abstract: Road traffic data is a fundamental element of intelligent traffic system. However, due to the high investment of the road sensor, the availability of the traffic data is so limited that it can't satisfy the requirement of current situation. Using cellular phone information as road traffic data becomes an attractive alternative because of its low cost, widespread and high cover rate. Until now, there are several algorithms to process the cellular phone information and most of them present promising conclusion. In this paper, we proposed a process to collect the information of cellular phone based on the simulation of working mode of the real base station, i.e., putting an appropriate instrument on the side of the road to detect the cellular phone passing by. Using the data we got, then we proposed a method to classify the mobility of the cellular phone, which is the critical problem of the analysis of the cellular phone information. Two key attributes are the average vehicle velocity and the variance of the vehicle velocity.

I. Introduction

According to the up-to-date statistics, there are already 1.3 billion mobile phone users in China. The cellular phone penetration rate has reached 100% in some large and middle cities in China. The enormous mobile phone users can provide considerable potential traffic data for the location of mobile phone. And as the development of the 3g technique, the speed of wireless transmission is becoming quite fast[1]. These conditions put a solid foundation to the technique of traffic data detecting. However, since the work pattern of the base station, the data collected from cellular phones contain various carrier types such as pedestrians, travelers on bus, in car and by bicycle. Among these carrier types, the phones carried by travelers on buses and in cars are the objects we most care about. On the other hand, except for these two types, the rest of types (we can call them voice) can cause obvious error of analysis for traffic flow. If each carrier type of cellular phone can be accurately identified, cellular phone information can become essential source of road traffic data in the future. According to the literature, there are several algorithms to classify the mobility of cellular phone into pedestrian and vehicle, such as neural network[2], naive Bayes model and many other methods[3]. While, these methods either assume the voice has already been filter out or need a large amount real samples to train the model.

In this paper, we proposed a classification method which has two steps based on pattern recognition. And we got the cellular data from using an appropriate instrument with the similar function as the base station which can detect the cellular phone passed by it, and, at the same time, record the phone's ID and the passing time. The structure of this paper is as follows. Section 2 describes related work about the working pattern of base station. Section 3 presents preliminary

process of the cellular phone data to get the velocity of the vehicle and classification of the cellular phone by two steps, linear classification and k-clustering. In section 4, analysis of the classification result is presented. We draw conclusion in section 5.

II. Related work

Cellular phones in work keep touch with the base stations cover it through GSM protocol by the way of high frequency wireless[4]. The radio frequency unit in the phone can transmit the phone's information we need to the base station. The information includes the ID of the phone and the register time. In the meanwhile, the phone can also receive signals from the base station. According to the strength of the signal, mobile phone registers to the nearest base station in order to make itself known to the network. When the phone moves from one cell into another cell, it needs to register again to the new nearest base station. The duration between the two operations of register is called cell dwell time (which is known as CDT) as shown in figure 1 and Eq.1.

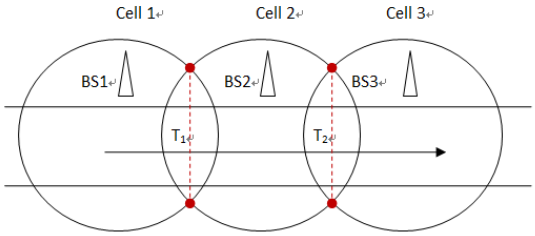

Fig 1 Principles of CDT

$$CDT=T_1-T_2 \tag{1}$$

III. Methodology

A. Data collection. Cellular phone data is collected by several instruments which have similar function as the base station. They are able to collect the ID and the corresponding register time of the phone passing by the instrument and store the data into data base. Every single instrument consists of radio frequency antenna and mainframe box and it can be powered by battery of car.

We choose the Bridge of Songhua River as the experiment location because of following reason. 1. The component of the traffic flow on the bridge is as same as the component of city area which consists of vehicle, bus, bicycle and pedestrian and there are some bus stops on the bridge.2.There is no traffic signal on the bridge. Therefore, the distributions of the velocity of each means of transportation conform to normal distribution which is easy to analyse.

The data collecting took place at day time from 7:30 to 10:00. The locations of the six instruments number 1 to number 6 are assigned as figure 3 shows.

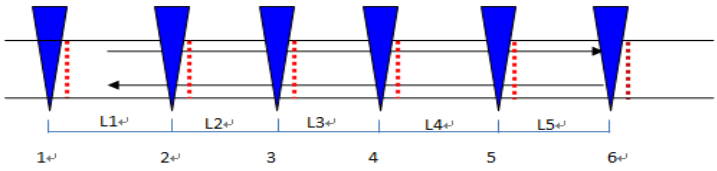

Fig 2 The locations of instruments

The triangle area represent the detect area of the instrument and L1-L5 represent the interval distance between the two close instruments. And the dotted lines represent the imaginary line to count the real traffic volume and the velocity of floating car.

Part of the original data we collected is shown in table 1.

Table 1 The original data

Instrument number	International identity number	Register time
1	460000334311710	25/03/2010 07:37:19
2	460021345529663	25/03/2010 07:48:07

Then we use each ID of the each phone to match its register time from each instrument by the software. During the experiment time, we set several floating cars to shuttle between the experiment area to get the real value of the velocity of cellular phones in it, and we've already known these phones' ID. Up to now, we have got the original data.

B.Preliminary data process. After the register time matching, we are able to work out the CDT of each phone between each two instruments. And the distance between each two close instruments we've already known. Therefore the estimated value of velocity of each phone can be calculated as Eq.2.

$$V=L/CDT \tag{2}$$

And the real values of velocity of some phones have been recorded by the method of floating car. Part of the consequence of contrast is listed in table 2.

Table 2 Error of estimation

Real value	Estimated value	Error
35.4 km/h	34.2 km/h	3.39%
25.7 km/h	25.2 km/h	1.95%
27.8 km/h	26.9 km/h	3.24%
40.4 km/h	42.6 km/h	5.45%

As shown in table 3, the maximum error of velocity estimation is lesser than 6%, which means the method reach a very high accuracy of velocity estimation. The high accuracy of velocity estimation put a solid foundation to the phase of data classification. 6 instruments have 5 intervals and we could get 5 CDTs from which the 5 values of velocity of each cellular phone calculated as shown in table 3.

Table 3 Result of preliminary process ,km/h

V_{1-2}	V_{2-3}	V_{3-4}	V_{4-5}	V_{5-6}	standard deviation	average
5.98	5.992786	6.055501	5.870521	5.752636	0.12	5.93
27.51	26.47069	25.47287	4.484469	4.680591	4.89	11.96
15.51	15.17947	15.7017	15.59274	15.5054	0.19	15.50
35.74303	35.62304	32.64834	5.178054	5.133856	15.21	24.73
24.71582	25.35427	26.28661	27.65894	27.55467	1.59	25.87
10.36	10.78132	10.557	10.29623	10.89844	0.26	10.58

Thus, every phone got through the experiment area can be denoted by follow vector as Eq.3.

$$\mathbf{P_i}= (V_{1-2}, V_{2-3}, V_{3-4}, V_{4-5}, V_{5-6}) \tag{3}$$

Where $\mathbf{P_i}$ is to represent the cellular phone passed through all the instrument.V_1-V_5 are the values of velocity of corresponding interval.

C. Classification of mobility. Consider the travel between instrument 1 and instrument 6 could be finished by 2 sorts of traffic modes, i.e., mode 1, the phone carried only by just one kind of means of travel within the whole journey, such as only by pedestrian, only by vehicle or only by bicycle. Mode 2, there is at least one time of switch of means of travel happened within the journey between instrument 1 and instrument 6. There are so kinds of switch within the journey that we can not use k-clustering directly. Here is a simplest instance, one phone carrier travels from instrument 1 to the instrument 3 by bus, and finish the rest of travel from instrument 3 to instrument 6 on foot. It is easy to draw a conclusion that the variance of series estimated velocity of mode 1 could be much lesser than mode 2 in the normal condition in which we took our experiment. Also consider that there are pedestrian, vehicle and bicycle, 3 types of phone carrier. And we can group these 3 types into two types for the reason that in traffic regulation and control, the flow of vehicle in mode 1 is what we most care about. So, the two new carrier types are motor vehicle type (such as car, bus, truck) and non-motor vehicle type (such as bicycle and pedestrian). And these two types' velocity has remarkable distinction from each other. Thus, the average of 5 values of velocity of one single phone is fit for being the characteristic value to involve in the classification. But, before we finish separating mode 1 from mode 2, we could not use this value to classify the types of carrier because of the average value of velocity of each phone can be full of the one dimension number axis and no obvious interval can be used to classify. Until now, we've got two characteristic value which can be applied to classify, i.e. σ_i=variance(P_i) and μ_i=average(P_i). Finally we rewrite the feature vector of $\mathbf{P_i}$ as Eq.4.

$$\mathbf{P_i}=(\sigma_i, \mu_i) \tag{4}$$

The scatter diagram of $\mathbf{P_i}$ (about 500 points collected in 10 minutes)is shown in figure 4.

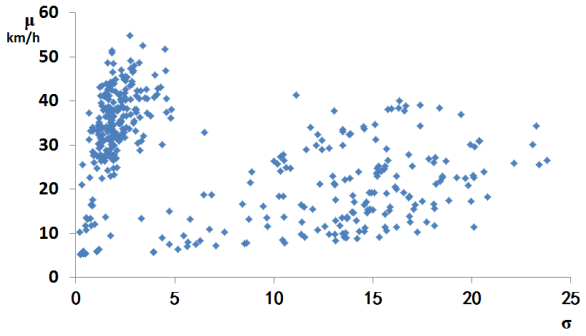

Fig 4 The scatter diagram of $\mathbf{P_i}$

As shown in figure 4, the two kinds of traffic mode are obviously grouped into two areas in the diagram. Considering the accuracy of using K-clustering right now is not enough, we take the method of linear classification as the first step processing.

$$\boldsymbol{w}(k+1)\begin{cases}\boldsymbol{w}(k) & ,\mathbf{w}^{\mathrm{T}}(\mathrm{k})\mathbf{x}_{\mathrm{k}} > 0\\ \boldsymbol{w}(k)+p\mathbf{x}_{\mathrm{k}} & ,\mathbf{w}^{\mathrm{T}}(\mathrm{k})\mathbf{x}_{\mathrm{k}} \le 0\end{cases} \tag{5}$$

Step 1: linear classification. In order to separate voice mode 1 from mode 2 and improve the accuracy of next classification, we use linear classification which perform perfectly in classifying two kinds of problem. The training procedure is processed by the principle above in Eq.5. The vector **w** is the augment weight vector. And the so called samples used to train the weight vector are extracted from data collected by the instruments, therefore, in fact, we didn't use any real sample to train the model. And by conscribing the longevity of samples extracting, we can also get a good real-time property. The result of linear classification is shown in figure 4 and figure 5.

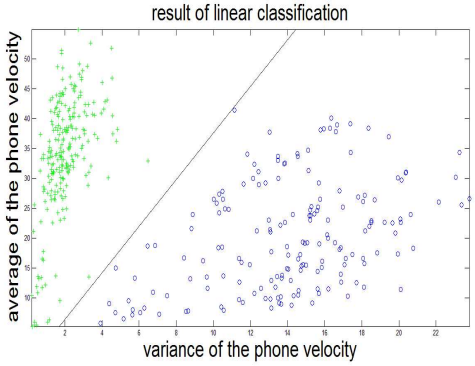

Fig 4 Result of linear classification

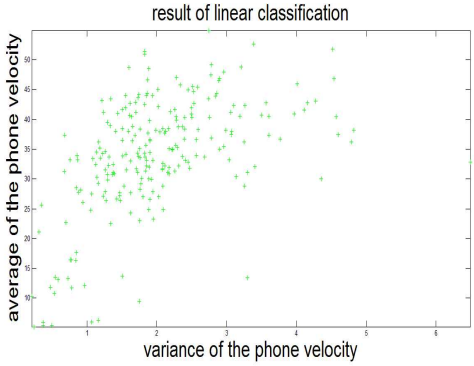

Fig 5 Result of linear classification

As shown in figure 4, the cycles under the line present the mode 2 and the crosses present the mode 1. The result of separating the cycle from the cross is shown in figure 5. Until now, the mode 1 has been separated out waiting for the next processing.

Sept 2: K-clustering. K-clustering is an unsupervised learning algorithm and when the different clusters in the scatter diagram are apparent, the effect of clustering could be accurate enough just like the condition in our case. The result of K-clustering is shown in figure 6.

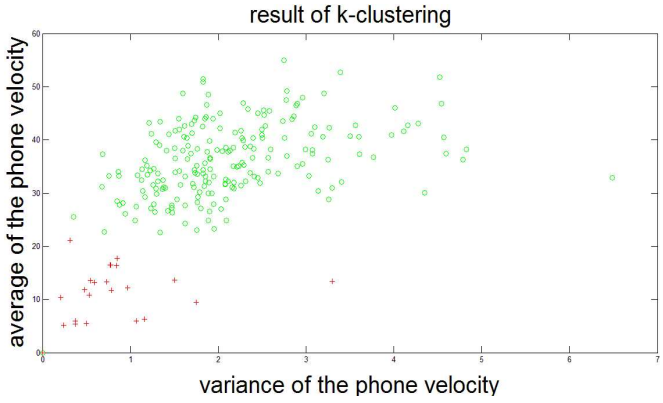

Fig 6 Result of k-clustering

Finally, the circles are the cellular phones of vehicle type in mode 1. The parameters of this phone type are what we need for the traffic regulation and control because that they can represent the parameter of real traffic flow.

IV. Analysis of result

In order to evaluate the result of classification, some statistics of the crosses data (mode 1, vehicle) and the circles data (mode 1, non-vehicle) in figure 6 have been done. The frequency distribution histogram of the crosses data and the probability density distribution of crosses data are shown in figure 7 and figure 8 respectively.

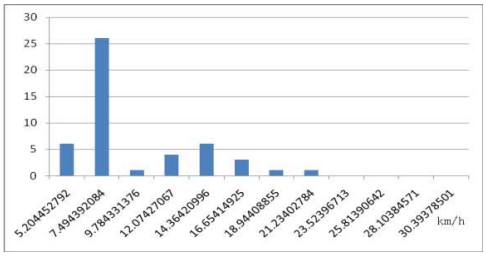

Fig 7 The frequency distribution histogram

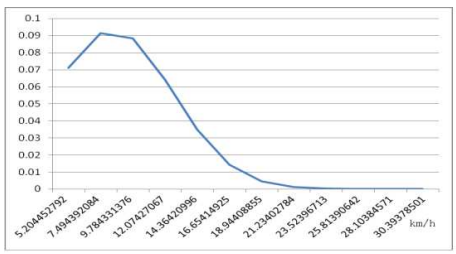

Fig 8 The probability density distribution

As shown in figure 7 and figure 8, no obvious regular pattern of distribution has been found. According to the knowledge of statistic, we can get the maximum value and the minimum value of velocity respectively is 21.07km/h and 5.2km/h and they are basically corresponded to the traffic characteristic of non-vehicle.

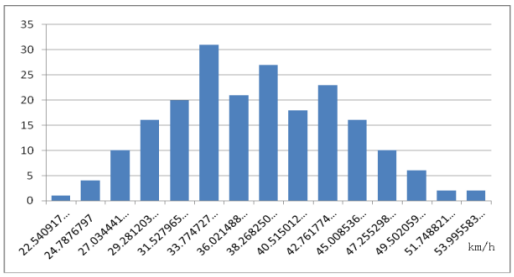

Fig 9 The frequency distribution histogram

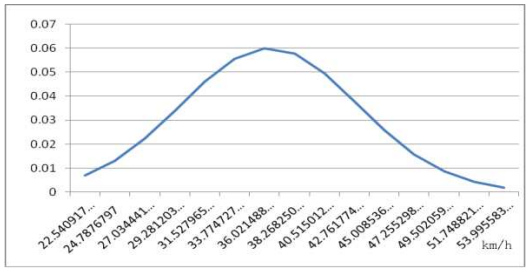

Fig 10 The probability density distribution

As shown in figure 9 and figure 10, the distribution of circles data accords with normal distribution, with μ=36.37km/h and σ=6.63, which is corresponded to the traffic characteristic of vehicle.

V. Conclusion

Cellular phone as the probe to detect the information of traffic flow has been becoming more and more attractive because of its advantage of high cover rate and low cost. And the essential problem of processing the cellular phone data is to separate the voice (non-vehicle phone) from the vehicle phone. In this paper, we proposed a new method to classify the mobility of cellular phone by two steps, i.e. 1) linear classification to separate the traffic mode with switches from the traffic mode with no switch. 2) K-clustering to classify the mode with no switch into two types of mobility, vehicle phone and non-vehicle phone. Based on the statistics of the classification result, we could believe that this method has an encouraging performance.

Acknowledgments

This research was supported by the China National Science Foundation Grant No. 51138003.

Reference

[1] Schneider W., Mrakotsky E. Mobile Phones as a Basis for Traffic State Information.Proceedings of the 8th International TB5.1 .IEEE Conference on Intelligent Transportation Systems Vienna, Austria, September 13-16, 2005.

[2] Wasan Pattara-atikom ,Ratchata Peachavanish. Estimating Road Traffic Congestion from Cell Dwell Time using Neural Network. 1-4244-11 78-5/07(C)2007 IEEE.

[3] Anum L.EnlilCorral-Ruiz,Felipe A.Cruz-Pérez,and Genaro Hernández-Valdez. Teletraffic Model for the Performance Evaluation of Cellular Networks with Hyper-Erlang Distributed Cell Dwell Time.

[4] Arwa Zabian.Mobile Cellular Networks and Traffic Road:a new Paradigm.Department of CIS Irbid National University Irbid-Jordan.

doi:10.4028/www.scientific.net/AEF.5.9

A Review on Intelligent Distribution for Passenger Service Resources in Airport Terminal Building

Shang Difeia, Zhang Yapingb, Cheng Shaowuc

[a] School of Transportation Science and Engineering, Harbin Institute of Technology, Harbin 150090, China

[a] sdf19888107@163.com, [b]zxlt0905@163.com, [c]105164467@qq.com

Keywords: airport; terminal; passenger behavior; simulation

Abstract: Airport terminal is a kind of important resource. It plays an vital role in transportation for people and goods. Ensuring scheduled flight security and punctual is a basic requirement of civil aviation. In the premise that existing service resources unchanged, intelligent distribution and dispatch for passenger service resources in airport terminal building is an effective way to solve problems of delays for passengers. To study passenger departure processes in airport terminals, improve the operation efficiency, service quality and reduce delay, a research on intelligent distribution for passenger service resources is developed using data integration methods, flow prediction method and intelligent simulation optimization algorithm.

1. Introduction:

Air travel has increased considerably in recent years, the number of passengers of China civil aviation has brokenthrough 260 million, China has become second air transport power country because of the increace of passenger flow, To guarantee scheduled flight safe and punctual is the basic requirement of civil aviation transportation.passengers often strand for a long time in security area and check-in area. It is easy to trigger group events and bring a lot of negative effects to civil aviation transportation. Intelligent distribution for passenger service resources is the focus of the problem. The United States has started research of related theory for terminal building intelligence of distribution and scheduling. the domestic research has just started00. At present domestic terminal mainly use vulgar methods based on the resource distribution density of flight0. The disadvantage of this method is Lack of accurate grasp toward passenger flow change real-time and the necessary distribution and scheduling resources scientific basis and technology. The specific performance is:

(1) Without Allocated resources and scheduling policy decision analysis for air ticket reservation, flight scheduling, check-in, security check, boarding scheduling, baggage processing system information

(2) Lack of methods of passengers flow quantitatively forecasting, it is difficult to distribute and schedule passenger terminal building service resources according to the change of the passenger flow.

(3) Lack of complete theoretical system for passenger terminal building service resources allocation and scheduling, it is difficult to Realize the terminal passenger services resources allocation and the intelligent scheduling

To solve above problems, describe the logical relation, information flow, resource allocation and scheduling plan between activities of passenger terminal building service process, research the coordination mechanism between passengers flow process and baggage flow process on the basis of dyeing time Petri nets; Use the three-stage activities scanning simulation strategy to establish the simulation algorithm for discrete event of passenger service process. Then use genetic algorithm to optimize the allocation of resources and scheduling plan.

2. Experimental Section

The solution process and assumptions:

Study passenger departure processes in airport terminals, model passenger service process. Fig 1 shows flow of departure passenger at airport terminal

(1) Simulation on the logical relation, information flow, resource allocation and scheduling plan between business activities of passenger terminal building service process.

(2) Using the genetic algorithm to optimize the allocation of resources operation time and scheduling plan.

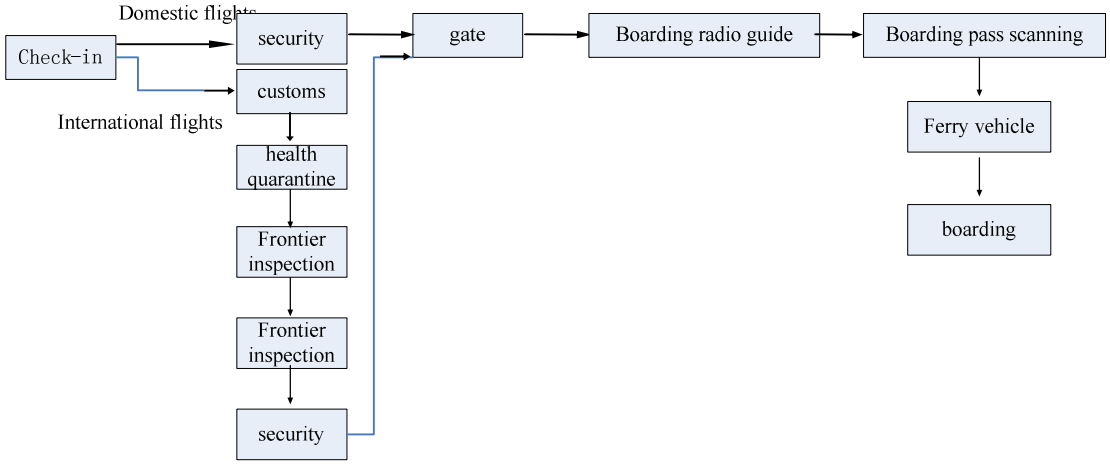

Fig 1 Flow of departure passenger at airport terminal

There are some researches worthy to study0:

H. Van Landeghem , A. Beuselinck from Department of Industrial Management, Ghent University do some research in reducing passenger boarding time in airplanes than allowed, but up to now has been largely neglected in reengineering projects. Their paper investigates dierent boarding patterns, in order to detect to what extent boarding time can be reduced. Findings indicate quite some discrepancy between current practices and optimal patterns. The results are analyzed with regard to airline objectives as well as to customer objectives, and implementation issues are considered.

Shangyao Yan, Ching-Hui Tang in Department of Civil Engineering, National Central University do some research in heuristic approach for airport gate assignments for stochastic flight delays. Their framework includes three components, a stochastic gate assignment model, a real-time assignment rule, and two penalty adjustment methods. The test results are based on data supplied by a Taiwan international airport, and show that the proposed framework performs better than the current manual assignment process and the traditional deterministic model.

Wonkyu Kim, Yonghwa Park,, Byung Jong Kim in School of Air Transport, Transportation and Logistics, Hankuk Aviation University do some research in estimating hourly variations in passenger volume at airports using dwelling time distributions. They use a mathematical model using a probability density function of the terminal dwelling time distribution is developed to estimate the number of passengers arriving at an airport terminal at various times. A two-way ANOVA that tests the effects on different airports and access time durations were carried out, and the results showed a signicant difference between terminal dwelling times among airports. The paper also provides some insight into airport terminal operation when there are signicant changes to fight schedules and the introduction of new airlines.

3. Summary:

In this research, We focus on solving terminal passenger services resources allocation and scheduling of the basic theory of intelligent, through the research of intelligent terminal passenger service resources allocation and scheduling of data integration, the passenger flow forecast method The passenger terminal building service resources allocation and scheduling of intelligent simulation optimization algorithm , construct theory system on the basis on airport data integration, With the core technology of passenger flow forecast and terminal services process intelligent simulation optimization, and provide theoretical support for realizing the terminal passenger services intelligent distribution and scheduling system resources.

4. Conclusions:

(1) Establish the Passenger service resources distribution terminal intelligent and scheduling theory system melting passenger services resources data integration methods, allocation and the intelligent scheduling, passenger flow forecast method, Passenger service process intelligent simulation optimization method.

(2) Make passenger service resources to terminal intelligent distribution and dispatching data integration as the foundation, put forward the passenger flow terminal real-time prediction methods.

(3) Based on the evolutionary computation theory and process simulation optimization technique, Put forward the passenger terminal building service resources allocation and the simulation of intelligent scheduling optimization algorithm.

Acknowledgments:

The cooperation we enjoyed from operations people of School of Transportation Science and Engineering, Harbin Institute of Technology is gratefully acknowledged. This paper also beneted from numerous remarks from the anonymous referees, which we thank. This paper is funded by the national natural science funds(No.61179096).

References:

[1] Florian Jaehn，Solving the flight gate assignment problem using dynamic programming, Zeitschrift für Betriebswirtschaft，2010，80（10）：1027-1039,

[2] Mahmoud Saffarzadeh, John P. Braaksma，Optimum Design and Operation of Airport Passenger Terminal Buildings，Journal of the Transportation Research Board，2007，Volume 1703 （2000）: 72-82

[3] Sydney C. K. Chu, Minyue Zhu and Liang Zhu，Multiple Criteria Decision Making for Sustainable Energy and Transportation Systems，Lecture Notes in Economics and Mathematical Systems, 2010, 634（2）：189-199

[4] H. Van Landeghem, A. Beuselinck, Reducing passenger boarding time in airplanes:A simulation based approach, European Journal of Operational Research，142 (2002)：294–308

[5] Shangyao Yan, Ching-Hui Tang，A heuristic approach for airport gate assignments for stochastic flight delays，European Journal of Operational Research,2007,180（2）：547-567

[6] Wonkyu Kim, Yonghwa Park, Byung Jong Kim，Estimating hourly variations in passenger volume at airports using dwelling time distributions，Journal of Air Transport Management 10 (2004)：395–400

[7]LiMing, Zhang Sanyuan, Zhao Xiaojing, Design and Implementation of Information Integration for A irport Based on Data Exchanging Platform (in Chinese), Journal of Science Techology and Engineering, 2009,9 (20): 6235-6238

[8] Craig V. Robertson, Shelly Shrader, David R. Pendergraft, Lisa M. Johnson, Kenneth S. Silbert, The Role Of Modeling Demand In Process Re-Engineering, Proceedings of the 2002 Winter Simulation Conference,1454-1458

[9] Shen Yang, Architecture of Airport Operation Database System，The 1st International Conference on Information Science and Engineering (ICISE2009), 2009, 2278-2281

[10] Lu Xu, Tang Xiaowei, Zhu Jinfu, Airport Luggage Process Modeling and Simulation, Journal of system Simulation(in Chinese), Vol. 2008，20（14）;3876-3880

[11] Chung, C.A., Sodeinde, T., Simultaneous service approach, for reducing air passenger queue time. Journal of Transportation Engineering 2000，126 (1)：85–88.

[12] Analysis and Recommendations for Developing Integrated Airport Information Systems, Contracto's Final Report for ACRP Project 1-03，Submitted October 2008

[13] Ioanna E. Manataki, Konstantinos G. Zografos，Assessing airport terminal performance using a system dynamics model，Journal of Air Transport Management，16 (2010)：86–93
[14] Lu Xu, Tang Xiaowei, Zhu Jinfu, Simulation analysis of passenger departure procedure in airport terminals(in Chinese), Journal of Southwest Jiaotong University, 2009, 44(1): 135-140
[15] Liu Jingli, Wang Zhiqing, Ning Xuanxi, A research on passenger terminal building process simulation (in Chinese), Journal of Aeronautical Computing Technique, 2005, 35(2): 45-49
[16] Liene Freivalde, Lelde Lace，Improvement Of Passenger Flow Management In An Airport Terminal，5th international Science Conference Bussiness and Managemnet'2008,16-17 May 2008, Vilnius, Lithuania,659-664
[17] K. C. James,Performance Improvement Studies of An Airport Terminal Using Discrete-Event Simulation，Computer Modelling and New Technologies, 2009, 13（3）：58–64

doi:10.4028/www.scientific.net/AEF.5.14

Multi-stakeholders Comparative Assessment of Freeway Traffic Conditions by Data Envelopment Analysis

Shen Zhang[1, a] and Wei Quan[1,b]

[1]School of Transportation Science and Engineering, Harbin Institute of Technology, Harbin, China

[a]shenzhang@hit.edu.cn, [b]qw.quanwei@163.com

Keywords: Freeway Traffic Conditions; Multiple Stakeholders; Data Envelopment Analysis.

Abstract. Effective assessment of traffic conditions is a key issue involved in alleviating freeway congestion, evaluating capital improvements and estimating travel time. Since the goals and objectives of assessment are inherently an expression of the various stakeholders affected by the traffic conditions, the assessment process and result must address the interests of all stakeholders. In this paper, a methodology and its application to assess traffic conditions on urban freeways are described. The methodology, which synthesizes Data Envelopment Analysis (DEA) and Analytical Hierarchy Process (AHP), can devise an overall traffic conditions assessment regarding various stakeholders' preferences. Application of the methodology to six real-life freeway corridors in Jilin Province indicated that the stakeholders can gain new insight into the overall traffic conditions behind multiple performance measures with our method, and the assessment results is helpful in identifying transportation investment priorities for specific regions and improving resource utilization among competing sectors.

1. Introduction

Understanding the temporal and spatial evolution of traffic conditions is a critical step toward improving freeway modeling and operations. With this clear understanding, administrators at any time can manage traffic congestion and incidents, Planners can determine whether congestion bottlenecks can be alleviated by improving operations or by minor capital improvements. Commuters can obtain the shortest route and travel time estimation to plan their trips. The widespread availability of freeway sensor data makes multivariate traffic condition analysis possible in ways that were not available in the past. However, there are two issues needed to be addressed during the process.

Firstly, the goals and objectives of traffic conditions assessment are inherently an expression of the various stakeholders affected by transportation system. This includes not only the administrators and the planners of transportation but also the commuters that experience their trips. In the principles of some multivariate statistical methods, all the stakeholders are treated as Decision Makers (DM), who have preferences to which of the measures they consider to be "strong important", "equal important" or "less important" measures. Performance assessment should allow decision makers to compare actual performance with desired performance as well as to provide the basis for making decisions to improve traffic conditions. Therefore, it is an urgent need to proactively involve various kinds of decision makers in the measurement process, and ensure the result to reflect their goals and objectives.

Secondly, identification of the need for and the effect of transportation infrastructure investment is particularly important in the assessment when development resources are scarce as in the case of developing countries or regions. From the perspective of public development agencies and planning authorities, investment of resources involves the identification and assessment of the need for infrastructure development as well as an accurate measurement of the need to allow for effective allocating of resources. For example, when the decision makers find that an increase in the road width can result in a more than proportional increase in the traffic volume and flow speed, they may intend to initiate development processes through proactive measures such as infrastructure investment, and

vice versa. Therefore, the analysis of transportation investment needs and optimal allocation of resources seem to exhibit returns to scale, which is of considerable importance for the multivariate analysis of traffic conditions.

This paper introduces a novel hybrid method based on Data Envelopment Analysis (DEA) and Analytical Hierarchy Process (AHP). This method can assess traffic conditions of each freeway section relative to others by considering various stakeholders' preferences in multiple performance measures. In particular, this paper summarizes how the method uses surveillance data to assist in assessing freeway conditions, evaluating capital and operational improvements, it assesses the traffic conditions of 6 freeway sections in Jilin Province by incorporating two types of stakeholders' preferences, and multiple measures are established on the basis of the 12-month loop data for the year 2011. As a result, the best sections and others' performance gaps can be identified. The conclusions indicate the stakeholders can gain new insight into the overall traffic conditions behind multiple performance measures with our method, and the analysis of returns to scale can generate references for infrastructure investment and facilitate optimal allocation of resources It should be noted that this study is not intended as the definitive work on freeway capability measurement; instead, it describes our experience in learning more about freeway conditions assessment.

This paper is outlined as follows. Section 2 discusses the state of the art. Section 3 presents the hybrid evaluation model based on DEA and AHP, then details fundamental strategy of incorporating Decision-Making preference and estimating returns to scale. To verify the proposed method, an experiment is demonstrated and its results are analyzed in Section 4. Section 5 closes with a conclusion.

2. Related Work

In recent years, demands for a better understanding of the traffic conditions have stimulated a considerable research interest. Choe and Chen et al. developed a freeway performance measurement system (PeMS) for all of California [1], while Bertini et al. described the evolution of traffic conditions and measured bottleneck outflows by using this system [2]. Although PeMS can assist users compute some basic performance measures by processing real-time detector data, it hasn't devised an overall traffic conditions evaluation based on the multiple performance measure**s**. Zuduo et al. analyzing important features related to bottleneck activations by Using wavelet transform, WT method can effectively identify the location of an active bottleneck, but lacks the capability to identify the relative congested or clear corridors [3]. Kamarianakis et al. forecasted the traffic flow conditions in an urban network based on data sets from loop detectors [4]. They concentrated on statistical methods, such as ARIMA, VARMA, and STARIMA models, but took the relative velocity as the only measure for traffic conditions. Hussein et al. demonstrated the feasibility of developing data fusion neural network architectures for incident risk detection on urban arterials using data from loop detector and probe vehicles [5]. However, the NN applications in transportation do not target interpretation of effects and signs, but rather aim at providing predictions for the phenomenon [6]. Turochy et al. measured variability in traffic conditions by applying principles of MSQC (multivariate statistical quality control) to derive a variability index [7]. In their study, the variability index is computed by measuring the size (spatial volume), mean speed, and occupancy with the detector data. While Catbagan et al. analyzed and compared possible two-lane expressway performance measures and recommended the suitable measures that would best describe the traffic flow characteristics [8]. The measures stated above are also proposed in our study to evaluate the traffic conditions.

3. Methodology

In this section, we will briefly formulate and discuss our integrated evaluation method based on DEA and AHP, the steps in incorporation of stakeholders' preferences and estimation of returns to scale will be introduced in the following subsections as well.

3.1 Method Description

Let us assume that there are n freeway sections to be assessed, which can be written as: S= (S_1, S_2,...,S_n). Each section consumes varying amounts of m different inputs to produce s different outputs. The input measures can be any factors used as a resource by the freeway, for example, the time, capital investment and transportation infrastructure. The output measures are the vehicle volume, occupancy density, incidents or other outcomes accommodated or produced by the freeway.

We first establish the freeway conditions evaluation models by synthesizing the cone ratio DEA model (C^2WH) (Charnes and Cooper, 1989) and AHP. Our hybrid assessment model can be expressed in linear program (LP) form Eq. 1 and dual form Eq. 2 as shown below.

$$\left(P_{C^2WH-AHP}\right)=\begin{cases}\theta_u=\max(\mu^T y_u)\\ \omega^T x_j-\mu^T y_j\ge 0, j=1,\ldots,n\\ \omega^T x_u=1\\ \omega\in V_{AHP},\mu\in U_{AHP}\end{cases} \tag{1}$$

$$\left(D_{C^2WH-AHP}\right)=\begin{cases}\min(\theta_u)\\ \sum_{j=1}^{n} x_j\lambda_j-\theta x_u\in V^*_{AHP}\\ -\sum_{j=1}^{n} y_j\lambda_j+y_u\in U^*_{AHP}\\ \lambda_j\ge 0,\ j=1,2,\ldots,n\end{cases} \tag{2}$$

In our assessment model, the Decision-Making preferences of stakeholders are introduced in the form of V_{AHP}, V^*_{AHP}, U_{AHP} and U^*_{AHP} generated using AHP.

The scalar variable θ in Eq. 1 and Eq. 2 represents the nonnegative performance score of each freeway section, and it ranges from 0 to 1. If S_u ($S_u \in S$) receives the optimal value $\theta_u = 1$, then it is of relative high performance, but if $\theta_u < 1$, it is of relative low performance.

Furthermore, since the value of θ_u means that S_u can still achieve a minimum decrease of θ_u times in its inputs without decreasing the production for any outputs, the performance of S_u is relatively lower when the θ_u is relatively smaller.

Besides the performance score θ in Eq. 1 and Eq. 2, we also calculate another two variables: ω and μ.

The $\omega=(\omega_1, \omega_2, \ldots, \omega_m)^T$ and $\mu=(\mu_1,\mu_2, \ldots, \mu_m)^T$ in (1) are the preference weights of input and output measures, so the values of ω and μ reflect the relative importance of the input and output measures in stakeholders' preferences.

3.2 Preference Incorporation

The hybrid assessment model can incorporate preference in order to bring the results closer to the prior perceptions of stakeholders. The preferences are aggregated into "input /output preference cones", which are in the form of V_{AHP} and U_{AHP} (see Eq. 1), while V^*_{AHP} and U^*_{AHP} (see Eq. 2) are the negative polar cones of V_{AHP} and U_{AHP}. The "input/output cone" reflects the relative importance of each input/output measure regarding various stakeholders' preferences.

The AHP method is utilized to provide a vector of preference weights expressing the relative importance for each traffic measure and construct the "preference cones". The scale of relative importance is defined according to Satty 1–9 scale for pairwise comparison (Satty,1990). According to group AHP theory (Lai and Wong, 2002), single stakeholder's judgment can also be aggregated into a group judgment. Therefore, we obtain a m×m matrix A_m for input measures and a s×s matrix B_s for output measures. A_m and B_s are called judgment matrix.

Then the input/output preference cones U, U^*, V and V^* can be constructed using the following Eq. 3 (E is identity matrix, λ is the max eigenvalue):

$$\begin{aligned} &A=A_m-\lambda_A E_m \quad V_{AHP}=\{\omega\mid A\omega\ge 0\} \quad V^*_{AHP}=\{A^T\omega\mid \omega\le 0\}\\ &B=B_s-\lambda_B E_s \quad U_{AHP}=\{\mu\mid B\mu\ge 0\} \quad U^*_{AHP}=\{B^T\mu\mid \mu\le 0\}\end{aligned} \tag{3}$$

In the above formula, the AHP solution is used to provide a regional value of traffic stakeholders' preferences. Since the regional value actually represents the preference weight region for input and output measures, the DEA model weighted by AHP proposed in our study is adopted to identify the optimal weight vectors in this solution region, and then evaluate the relative traffic conditions regarding preferences of various stakeholders. Therefore, this synthesis method can lead to a reasonable evaluation result that considers both objective loop-data characteristic and subjective stakeholders' preferences.

4. Experimental Design

4.1 Data

To illustrate our approach, the traffic conditions are evaluated with respect of various preferences by using the monthly data from Jilin Highway Administration. The data is mainly derived from the loop detector network, taken at 20-second intervals. Our experiment covers the period from January 1, 2010 to December 31, 2010 and is for up to 6 sections on urban freeway network, the 12-month data for one section is treated as 12 sets of data from 12 different pseudo freeway sections. This generates 72 (12×6) data sets to be evaluated across time and space. The 6 freeway study stations are K41+145, which is located on Yanji, southbound mainline; K78+175, which is located on Yitong, southbound mainline; K93+005, which is located on Dunhua, eastbound mainline; K126+695, which is located on Tonghua, southbound mainline; K150+85, which is located on Songyuan, eastbound mainline; and K184+65, which is located on Liaoyuan, eastbound mainline.

4.2 Computed Measures

A large catalogue of measures can be computed from a stream of 20-second observations of loop detectors network and other surveillance systems. Six promising indicators including observation time, Investment amount, lane number, station total volume, station total occupancy, and station total weighted speed, which can reflect traffic conditions in a clear way, are derived for the assessment process. Other potential measures, such as incidents and vehicle length, are not analyzed.

Among the 6 chosen measures, the observation time, investment amount and lane number are taken as the input performance measures, while the rest will be treated as the output performance measures used in our assessment models.

4.3 Results and Analysis

To discuss the merits of our method, we prepare the stakeholders' preferences regarding the six input and output measures stated above. To simplify our discussion, we only consider the impact of subjective preference on the three output factors. Further, suppose there are two types of stakeholders, administrators and commuters. Administrators need to make strategic decisions on transportation infrastructure improvement occasionally, so they may prefer traffic volumes and vehicle density to flow speed. When they have "strong important" perception on the former, a judgment matrix B_{admin} can be calculated (see Section 3.2). On the other hand, commuters pay more attention to the shorter travel time and more comfortable experience, so they may prefer vehicle speed and density to volumes. When they have "strong important" perception on the former, another judgment matrix $B_{commuter}$ is established. The two matrices are given as follows:

$$B_{admin} = \begin{bmatrix} 1 & 1 & 5 \\ 1 & 1 & 5 \\ 1/5 & 1/5 & 1 \end{bmatrix} \qquad B_{commuter} = \begin{bmatrix} 1 & 1/5 & 1/5 \\ 5 & 1 & 1 \\ 5 & 1 & 1 \end{bmatrix}$$

Then the output preference cones U_{admin} and $U_{commuter}$ can be constructed based on the Eq. 3 . By incorporating these preference cones into the Eq. 1, the performance evaluation results of these 72 dataset regarding two types of preference are calculated and shown in Fig. 1 and Fig. 2. Fig. 1 displays the preference score incorporating U_{admin}, while Fig. 2 describes the score incorporating $U_{commuter}$. The 6 series represent separately evaluation results of the 6 selected roadway segments.

As stated in Section 3.1, the plotted points, which fall on the horizontal solid black line in Fig. 1 and Fig. 2, are identified as relatively high performance ones. While the other points, which fall below the horizontal black line, are all of relative low performance in these series, and the performance gaps

can be further identified with reference to their values. As a result, the traffic conditions of February, March and June observed in K184+65, the conditions of February observed in K126+695, and the conditions of July observed in K78+175 are the best from administrator's perspective. While the conditions of February, July and September observed in K126+695 are the best from commuter's perspective.

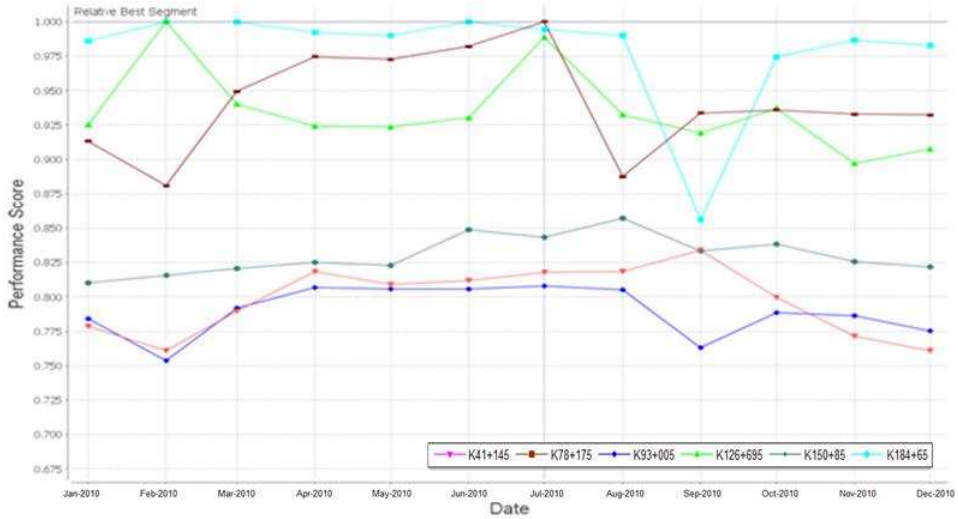

Figure 1 Performance score distribution with preferences of administrators

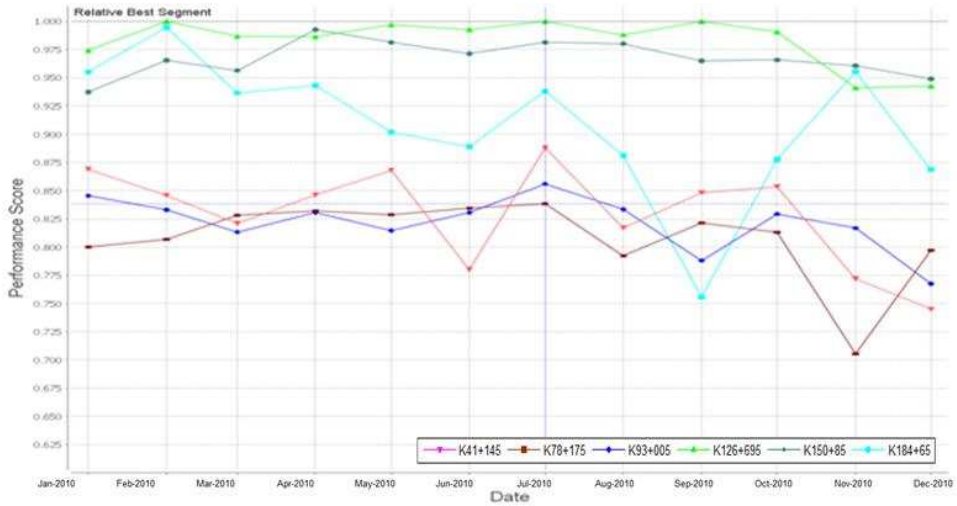

Figure 2 Performance score distribution with preferences of commuters

However, from the above figures, it can be observed that the same freeway segment's evaluation results may sometimes vary significantly across months. For example, the brown series in Fig. 1, which represents the K78+175, has a best performance score θ=1 at July, but surprisingly, it has a steeply falling at August and its score θ is just 0.887554. The average volume per minute Q/T and the average occupancy O/T of July is (58.358, 8.36%), while these measures of August is (51.151, 8.582%). The difference of the two-month measures causes the performance variation. There is still two issues should explained. Firstly, the reason, why the comparison of volume (58.358 > 51.151) leads to an undesirable result—occupancy (8.36% <8.582%), is that the weighted average speeds V/Q of July and August are (58.99 > 55.74), so the higher speed results in a lower vehicle density. Secondly, the likely reason for the large variation in volume is that July is a month of atypical traffic flow characteristics because most of the region population takes vacation at that time, whereas August is considered a typical one. As expected, the volumes of Yitong southbound mainline are separately 58.358 and 51.151 in July and August.

Besides, according to the comparison of Fig. 1 and Fig. 2, we find that the same dataset' score θ with different preferences may also differ widely from each other. Once again, take K78+175 for example, the brown series has the best score θ=1 at July as shown in Fig. 1, but in Fig. 2 its capability

score θ is just around 0.6 when evaluation process incorporates commuters' preference $U_{commuter}$. The reason for this difference can be attributed to the impact of Decision-Making preferences. To help clarify these issues, we adopt Eq. 1 in (see Section 3.1) to calculate the preference weights of output metrics (μ) and explain the discrepancy. The weights vector μ for output metrics under different restrictions are shown below.

When with administrators' preferences U_{admin}:.

$$S_{July}:\ \theta_a = 1.000 \quad \mu = (\mu_{volume}, \mu_{occupancy}, \mu_{speed})^T = (4.22, 4.42, 1.28)^T$$

When with commuters' preferences $U_{commuter}$.

$$S_{July}:\ \theta_c = 0.838 \quad \mu = (\mu_{volume}, \mu_{occupancy}, \mu_{speed})^T = (1.25, 4.09, 4.54)^T$$

It is obvious that the distinct output weights have imposed preference restrictions for the output measures. While the evaluation process adopts the preference cone U_{admin}. "volume" and "occupancy" have the greatest impact on the final results. Since S_{july} of K78+175 holds a very high value for Q against the other 11-month datasets in Fig. 1. the performance scores of the other 11 datasets generally appear with relative low values. However, when the evaluation process incorporates $U_{commuter}$, the measures of "speed" and "occupancy" have the greatest weights. Because all the datasets of K78+175 have nearly the same value for V except the dataset from November, the brown series has a relative smooth curve in Fig. 2, except for the eleventh point. This can explain the reason why S_{july} of K78+175 varies significantly with different output preference cones.

Acknowledgements

This research is supported by the State Key Program of National Natural Science of China (Grant No. 51138003), and the Fundamental Research Funds for the Central Universities (Grant No. HIT.NSRIF.201184).

References

[1] T. Choe, A. Skabardonis, and P. Varaiya. Freeway Performance Measurement System: Operational Analysis Tool. In *Transportation Research Record: Journal of the Transportation Research Board, No. 1811,* Transportation Research Board, Washington, D.C., (2002) 67–75.

[2] R. L. Bertini, and A. M. Myton. Use of Performance Measurement System Data to Diagnose Freeway Bottleneck Locations Empirically in Orange County, California. In *Transportation Research Record: Journal of the Transportation Research Board, No. 1925,* Transportation Research Board, Washington, D.C., (2005) 48–57.

[3] Z. Zuduo, A. Soyoung, C. Danjue and L. Jorge. Applications of wavelet transform for analysis of freeway traffic: Bottlenecks, transient traffic, and traffic oscillations. *Transportation Research Part B*, 45, (2011) 372–384.

[4] Y. Kamarianakis, and P. Prastacos. Forecasting Traffic Flow Conditions in an Urban Network: Comparison of Multivariate and Univariate Approaches. In *Transportation Research Record: Journal of the Transportation Research Board, No. 1857,* Transportation Research Board, Washington, D.C., (2005) 74–84.

[5] D. Hussein and T. Kim. Development and evaluation of arterial incident detection models using fusion of simulated probe vehicle and loop detector data. *Information Fusion*, 12, (2011) 20–27.

[6] M.G. Karlaftis and E.I.Vlahogianni. Statistical methods versus neural networks in transportation research: Differences, similarities and some insights. *Transportation Research Part C*, 19, (2011) 387–399.

[7] R. E. Turochy, and B. L. Smith. Measuring Variability in Traffic Conditions by Using Archived Traffic Data. In *Transportation Research Record: Journal of the Transportation Research Board, No. 1804,* Transportation Research Board, Washington, D.C., (2002) 168–172.

[8] J. L. Catbagan, and H. Nakamura. Evaluation of Performance Measures for Two-Lane Expressways in Japan. In *Transportation Research Record: Journal of the Transportation Research Board, No. 1988,* Transportation Research Board, Washington, D.C., (2006) 111–118.

doi:10.4028/www.scientific.net/AEF.5.20

A Cell-based Regional Evacuation Model with Contra-flow Lane Deployment

Zhang Xinming [1, a], An Shi [1,b] and Xie Binglei [2,c]

[1]School of Transportation Science and Engineering, Harbin Institute of Technology, Harbin, China

[2]School of Urban Planning and Management, Harbin Institute of Technology Shenzhen Graduate School, Shenzhen, China

[a]zxinming@yahoo.cn, [b]anshi@hit.edu.cn, [c]xiebinglei@126.com

Keywords: regional traffic evacuation, DTA, cell, one-destination evacuation, contra-flow lane

Abstract: In this paper, a traffic evacuation model is proposed with a framework of SO-DTA model and one-destination evacuation embedded. The network is described as cells and nodes, so that a regional traffic evacuation model which embeds CTM and point-queue is proposed. This paper also optimized the deployment strategy of the contra-flow lane in the premise of system optimization. In the end, a numerical experiment is conducted to analysis the effectiveness of the model. Compared with the CTM, the model constructed reduced the gross evacuation time and the clear time of the road net, and solved the unnecessary "traffic holding" problem.

1 Introduction

With the developing and expanding of cities, security issues are potential threatened by various disasters. When the degree of disasters reach some threshold level, an emergency evacuation is necessary in order to avoid or reduce the loss of life and property. Transportation plays an important role in evacuation. Constructing models is the core of an evacuation.

In previous studies, the Cell Transmission Model (CTM), proposed by Ziliaskopoulos[1], is considered to be a better basic model for evacuation. But the "traffic holding" problem often happens in this model and its cell-connector topology structure increases the constraints. In part, these observations motivated our study

The first and primary goal of this paper is to construct a cell-based regional evacuation model, which embeds the idea of one-destination evacuation. And using point-queue model, the road network is converted to cell-node topology structure to reduce constraints. The "traffic holding" problem also be solved in the model by an OSP constraint.

Secondly, based on the model proposed, the deployment strategy of contra-flow lane in the premise of system optimization is also optimized in this paper to improve the efficiency of evacuation.

Finally, a numerical experiment is conducted to verify the proposed model.

2 Literature review

Existing regional evacuation models can be classified into two basic models: network flow models and dynamic traffic assignment models.

The traditional graph theory is the basic theory of network flow models. The nodes and arcs are used to represent generating points and roads in network flow models[2]. Yamada considered the regional evacuation as a minimal cost flow problem, aimed to minimize the driving distance[3].

Cova and Johnson believed that delays in regional evacuation often occurred at intersections and presented a network flow model for identifying optimal lane-based evacuation routing plans in a complex road network. The model is an integer extension of the minimum cost flow problem[4].

SO-DTA has been recognized to be a better basic model to solve evacuation problems. Ziliaskopoulos brought CTM to SO-DTA, but limited to only one destination[1]. Han proposed the concept of one-destination evacuation which could significantly simplified evacuation problem[5].

Each model has its advantages and disadvantages. Network flow models describe the traffic flow using graph vividly, but it cannot effectively reflect some dynamic characteristics of traffic flow, such as queues. Most agree that SO-DTA based on CTM could be a better model for evacuation. But the model is limited to only one destination in evacuation. When more destinations exist, it would become complex. One-destination evacuation[6], proposed by Han, can solve the problem suitably.

There is another problem in CTM. Under the premise of system optimization, the "traffic holding" problem often happens at interactions. Some "traffic holding" is necessary but some is unnecessary. Unnecessary "traffic holding" is hardly understood by evacuees. The model this paper proposed can solve the problem.

3 A cell-based regional evacuation model

3.1 One-destination evacuation network

In daily traffic, every person has his own destination. While in evacuation, the primary purpose is to reach the shelters as soon as possible. It is not important that which paths or shelters should be chosen. So Han assumed that there was a most-desirable-destination, that is, one-destination evacuation[5].

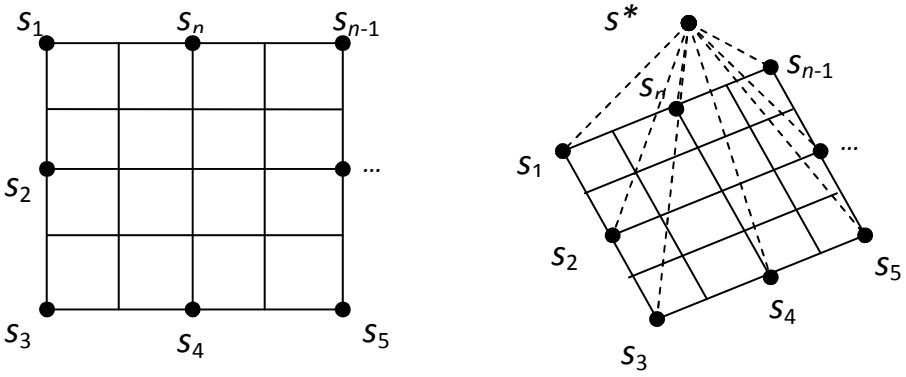

(a) The original multiple-destination network (b) The one-destination network

Figure 1: The network transformation

In Figure 1(a), there are m origins and n destinations in the evacuation. In previous studies, we will have an O-D matrix with m rows and n columns. Strictly speaking, when we get the O-D matrix by the Shortest Path Method or other methods, the system optimization is not considered. Han added a "dummy-destination point", denoted as S^*, to the network, as shown in Figure 1(b). Then "dummy links" were used to lead from each real-world destinations to S^*. It is assumed that all these dummy links have infinite capacity and zero cost. Thus the O-D matrix has been simplified to m rows and only one column. At the same time, destinations and paths are chosen synchronously. This is consistent with the system optimization.

3.2 A cell-based regional evacuation model

Consider a network $G(N,A)$, where N and A are the sets of nodes and links respectively. Let R represent the set of origins and s^* the single destination. The assignment horizon is divided into a finite number of discrete time intervals indexed by $\{t:t = 0,1,\ldots,T\}$.

Let $O(i)$ and $I(i)$ be the sets of outgoing and incoming cells of node $i \in N$, Let $Q_{rs*}(t)$ be the travel demand between O-D pair *r-s** departing at time *t*, and the numbers of vehicles on, entering, and exiting a link *a* at time *t* are denoted by $X_a(t)$, $U_a(t)$ and $V_a(t)$ respectively.

Merchant and Nemhauser constructed a basic dynamic traffic assignment model in 1978, Carey modified the model as follows[7]:

$$\min \sum_{t=1}^{T} \sum_{a \in A} X_a(t) \tag{1a}$$

$$s.t. \quad X_a(t+1) = X_a(t) - V_a(t) + U_a(t) \tag{1b}$$

$$\sum_{a \in O(i)} U_a(t) = Q_{is^*}(t) + \sum_{a \in I(i)} V_a(t) \tag{1c}$$

$$X_a(0) = R_a \geq 0 \tag{1d}$$

$$X_a(t), V_a(t), U_a(t) \geq 0 \tag{1e}$$

Constraint (1b) describes traffic flow propagation; Constraint (1c) represents node flow conservation; Constraint (1d) is the initial condition while (1e) is nonnegative constraint.

Note that the model above does not reflect the queue. Thus we embed the point-queue model into M-N model. So at time *t*, we can divide the numbers of vehicles on a link *a* into two parts: the queued flow $P_a(t)$ at the end of time *t* and the exit flow $V_a(t)$ during time *t*. That is,

$$X_a(t) = P_a(t) + V_a(t) \tag{2}$$

Then the model can be written as:

$$\min \sum_{t=1}^{T} \sum_{a \in A} (P_a(t) + V_a(t)) \tag{3a}$$

$$s.t. \quad P_a(t+1) = P_a(t) - V_a(t+1) + U_a(t) \tag{3b}$$

$$\sum_{a \in O(i)} U_a(t) = Q_{is^*}(t) + \sum_{a \in I(i)} V_a(t) \tag{3c}$$

$$P_a(0) + V_a(0) = R_a \tag{3d}$$

$$U_a(t) \geq 0 \tag{3e}$$

$$0 \leq V_a(t) \leq V_{am} \tag{3f}$$

$$P_a(t) > 0 \Rightarrow V_a(t) = V_{am} \tag{3g}$$

Where V_{am} is the maximum outflow of a link *a*. Constraint (3g) requires the link to be operated at capacity at *t* when a queue is present at the end of *t*. That is the OSP constraint. Violating this condition thus implies "holding" flows when there is still spare capacity.

In the model 3, the queue has been reflected but it cannot propagate. Learning from the CTM, we transform the original network into a cell-node network. Thus link *a* is divided into several cells so that we can use cell *a* instead. According CTM,

$$U_a(t) \leq U_{am} \tag{4a}$$

$$U_a(t) \leq \omega / v_f [N_j(k) - X_j(k)] = \omega / v_f [H_a - P_a(t) - V_a(t)] \tag{4b}$$

Where U_{am} is the maximum inflow of a cell *a* and H_a is the maximum vehicles cell *a* can hold. Let a^+ be the downstream node of cell *a*. Then the OSP constraint can be written as

$$\begin{aligned} &P_a(t) > 0 \Rightarrow V_a(t) = V_{am}, \\ &\quad \text{or} U_{a^+}(t) = U_{a^+m}, \\ &\quad \text{or} U_{a^+}(t) = \omega / v_f [H_{a^+} - P_{a^+}(t) - V_{a^+}(t)] \end{aligned} \tag{5}$$

Adding the constraint of the holding capacities of real destinations, we can obtain a cell-based regional evacuation model as follows:

$$\min \sum_{t=1}^{T} \sum_{a \in A} (P_a(t) + V_a(t)) \tag{6a}$$

s.t. [Original Constraints](3b-3f) (6b)

$$U_a(t) \le \omega / v_f \,[H_a - P_a(t) - V_a(t)] \quad (6c)$$

$$\sum_{t=1}^{T} U_{l_i}(t) \le H_{S_i} \quad (6d)$$

[OSP Constraints](5) (6f)

3.3 The contra-flow lane deployment

Let cell a and cell $-a$ are the two cell of a link with opposite directions. The two have the same characteristic except direction. Let v_{am} (u_{am}) is the capacity of a lane in cell a, h_a is the holding capacity of a lane in cell a, n_a is the number of lane that cell a have and ρ_a is the number of contra-flow lanes in cell a. If $\rho_a < 0$, it means $|\rho_a|$ contra-flow lanes are needed in cell $-a$.

When contra-flow lanes are deployed on cell a, the capacity V_{am} and the holding capacity H_a of cell a are changed as Table 1.

Table 1 The capacity V_{am} and the holding capacity H_a of cell a changed

cell	V_{am} before	V_{am} after	H_a before	H_a after
a	V_{am}	$V_{am} - \rho_a * v_{am}$	H_a	$H_a - \rho_a * h_a$
$-a$	V_{-am}	$V_{-am} + \rho_a * v_{am}$, or $V_{-am} - \rho_{-a} * v_{-am}$	H_{-a}	$H_{-a} + \rho_a * h_a$, or $H_{-a} - \rho_{-a} * h_{-a}$

Then the model can be shown as follows:

$$\min \sum_{t=1}^{T} \sum_{a \in A} (P_a(t) + V_a(t)) \quad (7a)$$

s.t. [Original Constraints](3b-3f) (7b)

[Holding Capacity Constraints](6d) (7c)

$$V_a(t) \le V_{am} - \rho_a * v_{am} \quad (7d)$$

$$U_a(t) \le U_{am} - \rho_a * v_{am} \quad (7e)$$

$$U_a(t) \le \omega / v_f \,[H_a - \rho_a * h_a - P_a(t) - V_a(t)] \quad (7f)$$

$$P_a(t) > 0 \Rightarrow V_a(t) = V_{am} - \rho_a * v_{am},$$
$$\text{or} U_{a^+}(t) = U_{a^+m} - \rho_{a^+} * v_{a^+m},$$
$$\text{or} U_{a^+}(t) = \omega / v_f \,[H_{a^+} - \rho_{a^+} * h_{a^+} - P_{a^+}(t) - V_{a^+}(t)] \quad (7g)$$

$$-n_a \le \rho_a \le n_a, \quad \rho_a \text{ is an integer} \quad (7h)$$

$$\rho_{-a} + \rho_a = 0 \quad (7i)$$

3.4 Algorithm

Noted that without thinking constraint 7g (OSP constraint), model 7 is an integer programming model, we can use traditional algorithm to solve the model. Thinking about OSP constraint, Ho designed an efficient algorithm in 1980[8]. We improve it and design a new algorithm as follows:

Step 0: Solve the integer programming problem to get the optimal system cost Z_T^*. Set $w = T$.

Step 1: Test the OSP constraint, stop if satisfied; otherwise, go to Step 2.

Step 2: Solve the following integer programming problem and get E_{w-1}^*.

$$\max E_{w-1} = \sum_{t=1}^{w-1} \sum_{a \in A} V_a(t) \quad (8a)$$

s.t. [Constraints](7a-7f, 7h, 7i) (8b)

$$\sum_{t=1}^{T} \sum_{a \in A} (P_a(t) + V_a(t)) = Z_T^* \quad (8c)$$

Step 3: Set $w = w$-1; test the OSP constraint, stop if satisfied; otherwise, add the following constraint into model 8: $\sum_{t=1}^{w-1}\sum_{a\in A} V_a(t) = E^*_{w-1}$, and then go back to Step 2.

4 Numerical example

A numerical example is briefly described in the following. In Figure 2, There are 12 nodes and 17 links in the network. Each link has 6 lanes. The evacuation demand 1150, 850 and 1000 are loaded into the network by three points-O1, O2, and O3 respectively. J and K are the real destinations with 2000 holding capacities both. Point s is the dummy-destination.

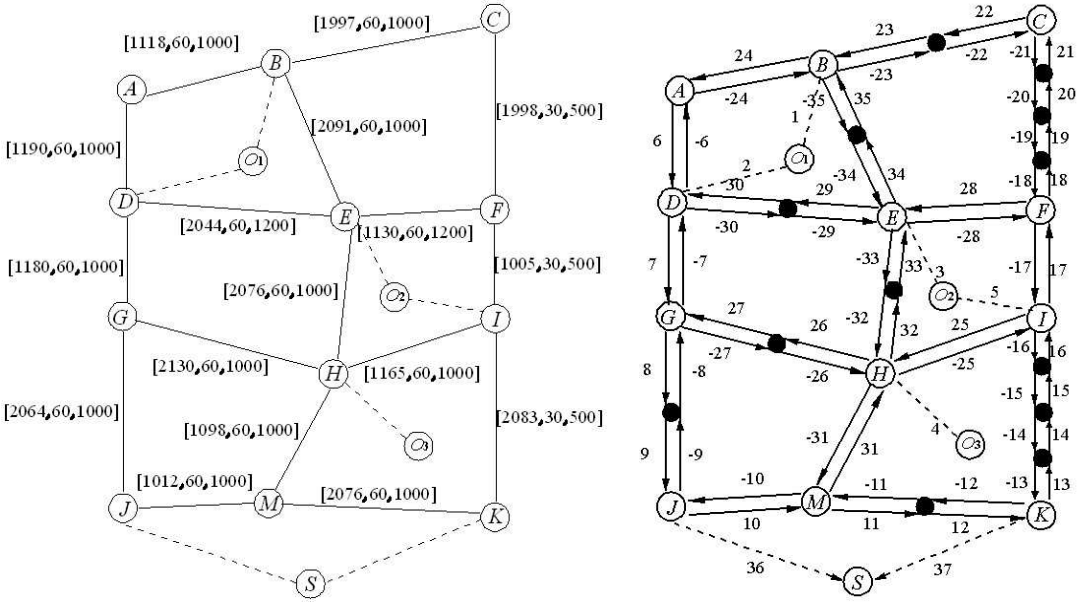

(a) Original network[length (m), speed(km/h), capacity (veh/h)] (b) cell-node network

Figure 2 The evacuation network:

The analysis period is 30 minutes, divided into 30 time intervals. The model is solved using "lingo" and the result we get is that :

(1)The system cost is 22 350 minutes and the time for evacuation is 16 minutes.

(2)To improve the efficiency of evacuation, we also can obtain from the result that these links, including GD, JG, KM, JM, KI, IF, FC and MH, need to deploy contra-flow lanes keeping the system optimal.

(3)By analysis the result seriously, "traffic holding" problem do not happen in our model.

(4)Also, we can get that how much demand is loaded into the network every time interval. Like Table 2.

Table 2 Demand loading

	0-1	1-2	2-3	3-4	4-5	5-6	6-7	7-8
O_1	360	360	210	150	70	0	0	0
O_2	240	210	50	100	50	50	100	50
O_3	250	150	200	150	130	100	20	0

Conclusions

A new model for evacuation based on cell is proposed in this paper. In the model, we make use of the CTM and point-queue model. Based on the model, the road network is converted to the cell-node topology structure so that the constraints of evacuation model are significantly reduced. The idea of one-destination evacuation makes the feasibility of our model.

By adding a new constraint, called OSP constraint, the “traffic holding” problem is solved. And we improve the model to get contra-flow lanes deployment in evacuation. This improves the efficiency of evacuation significantly.

In the model proposed, when the network becomes more complex, the solution of the model will be more different. So a more efficient algorithm will be designed in the future study. Besides, it would better if other management of evacuation can be embedded into the model, such as staged evacuation.

Acknowledgements

This work was partially supported by the NSFC under Grant No. 70973032 and No.71173061.

References

[1] Ziliaskopoulos A K. A Linear Programming Model for The Single Destination System Optimum Dynamic Traffic Assignment Problem[J]. Transportation Science, 2000,34(1):37-49.

[2] Hamacher H W, Tjandra S A. Mathematical Modeling of Evacuation Problems - a state of art[C]. Pedestrian and Evacuation Dynamics, 2001:59-74.

[3] Yamada T. A Network Flow Approach to A City Emergency Evacuation Planning[J]. International Journal of Systems Science, 1996, 27(10):931-936.

[4] Cova T J，Johnson J P. A Network Flow Model for Lane-based Evacuation Routing[J]. Transportation Research Part A: Policy and Practice, 2003, 37(7):579-604.

[5] Han D L. Evacuation Modeling and Operations Using Dynamic Traffic Assignment and Most-desirable-destination Approaches[C]. Washington D.C.: The 84th Transportation Research Board Annual Meeting, 2005:964-969.

[6] Han D L. Evacuation Modeling and Operations Using Dynamic Traffic Assignment and Most-desirable-destination Approaches[C]. Washington D.C.: The 84th Transportation Research Board Annual Meeting, 2005:964-969.

[7] Carey M. Optimal Time-varying Flows on Congestion Networks[J]. Operations Research, 1987, 35(1):58-69.

[8] Ho J K. A Successive Linear Optimization Approach to The Dynamic Ttraffic Assignment Problem[J]. Transportation Science, 1980, 14(4):295-305.

doi:10.4028/www.scientific.net/AEF.5.26

Research on Traffic Characteristics and Traffic Conflicts of the One-way-closure Work Zone on Freeway

Lai Zheng[1, a], Xianghai Meng[2,b]

[1] School of Transportation Science and Engineering, Harbin Institute of Technology, Harbin, China

[2] School of Transportation Science and Engineering, Harbin Institute of Technology, Harbin, China

[a] zhenglai1985@163.com, [b]mengxianghai100@126.com

Keywords: freeway; one-way-closure; work zone; traffic characteristic; traffic conflict.

Abstract. By analyzing the traffic characteristics and traffic conflicts of the typical one-way-closure work zone on four-lane freeways, the queuing characteristics of vehicles are determined, and the Erlang distribution model which can describe the distribution of time headway is calibrated. The speed distribution characteristics of each component of the work zone are concluded, and the speed limit scales for these components are put forward based on the statistic analysis. The types of traffic conflicts are firstly concluded, and then the identification method of the rear-end conflicts' severity degree based on TTC technique as well as the prediction model of rear-end conflicts based on Negative Binomial distribution are put forward. The research results are useful to the analysis of traffic conditions of work zones, and they can also be used to evaluate the safety situations of freeway work zones.

Introduction

Heavy repair or maintenance is one of the main problems for expressways which opened to operation for many years. To ensure the operation of the expressway, "constructing while operating" is the most common adopted way. Under this condition, it needs to close parts of lanes even one-way-closure, which caused the reduction of capacity as well as the traffic condition change for the lanes allowing vehicle to run, and this will bring traffic congestion, road traffic accident occurrence and other problems. Thus, it is very important to analyze the traffic organization and optimization method during the heavy repair or maintenance period, and then improve the traffic operating efficiency and the safety level of the expressway.

In the early 1980s, developed countries began to do research on expressway work zones, and the focus of that time is speed limits. To 1990s, there was much further research on the operating speed of vehicles[1,2], and capacity, queuing and delay became the research hot points[3,4]. Recently, the research on how queuing and delay influencing traffic operating efficiency and road safety becomes popular[5-7]. As the expressways constructed in early years in China beginning to heavy repair or maintenance, domestic researchers pay close attention to the traffic flow characteristics of work zones, and traffic characteristics and influence factors, speed distribution, time headway distribution and other related research works are conducted[8,9].

Road safety of work zones is one of the main problems, and foreign researchers have done a lot of research works, including relationships between accident rates and working time as well as length of work zone, influencing factors of accidents, safety assessment, and accident prediction[10-12]. Since there are systemic and completed accident data from work zones, their research results are more reliable and applicable. Based on the experience from abroad, the domestic researchers have get some achievements in recent years, e.g., the risk prediction model of work zones are put forward, the influence factors of hazardous locations in work zones are analyzed, and the counter measures to improve road safety level are developed[13,14]. Regarding to there is not enough accident data of work zones in China up until now, the road safety research based on traffic conflict technique is put forward in this paper.

Field Investigation and Data Collection

Based on the project of "Research on traffic control and safety guarantee technique during the construction of expressway", which is authorized by Transportation department of Heilongjiang province, the field investigation were conducted at the Harbin to Yagou segment of Suiman highway, Beian to Wudalianchi segment of Qianfeng Farm to Nenjiang Expressway, and Hailun to Beian segment of Suihua to Beian Expressway. The contents of investigation includes traffic volume, speed, time headway, traffic conflict and travel time, et al. 8 work zones are investigated and traffic data of 12h or 24h are obtained for each work zone. Traffic investigation sites and investigation method are shown in Fig.1.

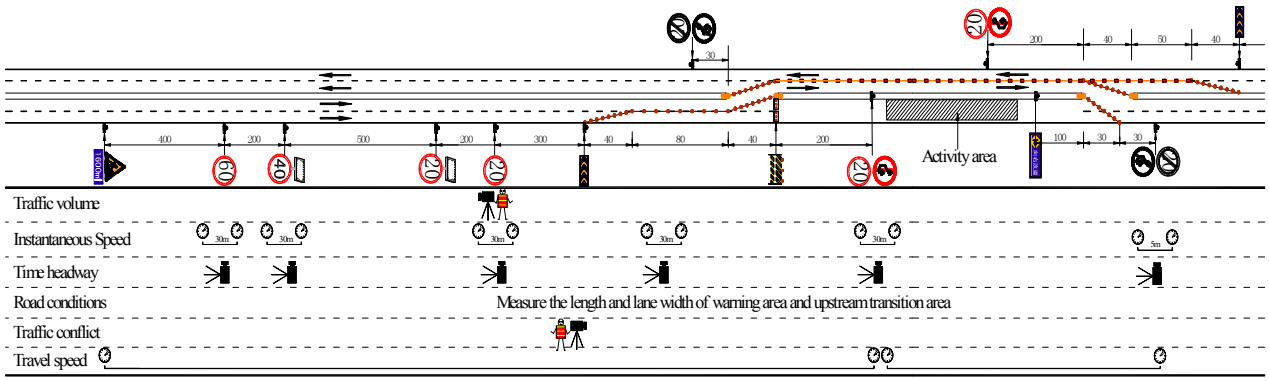

Fig.1 Investigation sites and investigation method

Vehicle Queuing Characteristics and Time Headway Analysis

Vehicle Queuing Characteristics

At the upstream transition area, vehicles on the two lanes need to merge into one lane, and then run into the opposite way, which will form an obvious bottleneck at this segment. Vehicles need to slow down and pass the bottleneck in a queue. By statistic analysis, the characteristics of vehicle queuing during the peak time are as follows: the proportion of queuing vehicles for all kinds of vehicles is 41.18%; the proportion of queuing vehicles for light-duty vehicles is 41.18%; the proportion of queuing vehicles for medium vehicles is 42.67%; the proportion of queuing vehicles for oversized vehicles is 52.84%. The queue length with a light-duty vehicle as leading is 3.72 vehicles; the queue length with a medium vehicle as leading is 3.04 vehicles; the queue length with an oversized vehicle as leading is 3.87 vehicles; the maximum queue length is 14 vehicles; the average queue length for all the vehicles is 4.96 pcu.

The queuing characteristics, especially the queue length, are very important to determine the proper length of transition area. If the average queue length is 4.96 pcu, and the speed limit is 20 to 40 km/h, the minimum length of transition area should be 45 to 70m, which is longer than 40m required by the "Safety Work Rules for Highway Maintenance".

Time Headway Analysis

All the time headways less than 30s are taken as samples, and the statistic results are shown in Table 1. The average time headway is 5.75s, and 2s time headway is most frequent. Negative exponential distribution, shifting negative exponential distribution, Erlang distribution and Weibull distribution are employed to fit the data, and the result shows that Erlang distribution is the best for both the peak time period and the off-peak time period.

Table 1 Statistical Results of Time Spaces of Vehicles

Average	Standard error	Median	Mode	Standard deviation	Minimum	Maximum
5.75	0.17	3.70	2.00	5.42	0.20	29.20

The function of Erlang distribution is as follows:

$$P(h \geq t) = \sum_{i=0}^{r-1} \frac{(\lambda t)^i}{i!} e^{-\lambda t} \tag{1}$$

where, t is the time headway, s; r is the order of the Erlang distribution(the larger the r, the traffic is more congested).

r and λ can be determined by the average(E) and variance (S^2) of the samples, and the calculation formula are $r = E^2 / S^2$ and $\lambda = E^2 / S^2$. The calculation results show that the time headways of peak time, off-peak time and all time agree with the Erlang distribution with r=2, r=1 and r=1, respectively. The Erlang distribution with r=1 is actually the negative exponential distribution. The fitting of the time headways for peak time and off-peak time are shown in Fig.2. The distribution of time headway can be used to identify the traffic conflict and determine the situation of traffic operation.

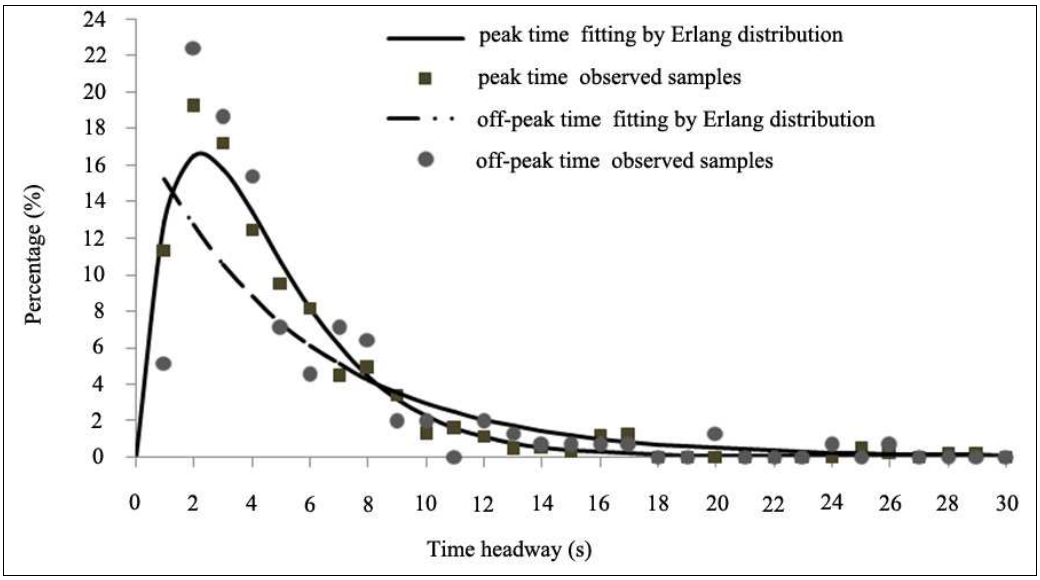

Fig.2 Time headways on peak and off-peak time

Speed Distribution and Speed Limit Scale based on Statistic Analysis

Speed Distribution of Work Zones

The speed frequencies of the investigate sites at the speed limit signs of 80km/h (60km/h), 60km/h (40km/h), 40km/h (20km/h) in upstream of work zones, buffering spaces, activity areas, and downstream segments are listed in Table 2.

Table 2 Statistical results of speeds on each component of work zone

No.	Statistic indexes	80 (60)km/h	60 (40)km/h	40 (20)km/h	Buffering space	Activity area	Downstream segment
1	Average (km/h)	91.697	72.345	61.273	38.354	61.763	87.310
2	Median (km/h)	90.0	70.054	61.463	38.710	61.685	87.273
3	Standard error	1.347	0.956	0.69	0.46	0.95	1.15
4	Standard deviation	22.1	16.6	12.3	8.8	17.3	18.0
5	Variance	489.91	275.85	150.99	77.87	299.14	325.35
6	Number of samples	270	300	314	371	334	245
7	e+δ	113.797	88.945	73.573	47.154	79.063	105.31
8	e-δ	69.597	55.745	48.973	29.554	44.463	69.31

Speed Limit Scale based on Statistic Analysis

The speed limit scales of each component of the work zone can be calculated by the formula below:

$$V_i^{upper} = E_i + 1 \times \delta_i \tag{2}$$

$$V_i^{lower} = E_i - 1 \times \delta_i \tag{3}$$

where, V_i^{upper} is the upper speed limit of segment *i*; V_i^{lower} is the lower speed limit of segment *i*; E_i is the average speed of segment *i*; δ_i is the standard deviation of speeds at segment *i*.

The determined speed limit values are shown as Row 7 and 8 in Table 2. When the traffic volume is low, the upper limits can be taken as the speed limit values, while the traffic volume is high, the lower limits should be taken as the speed limit values.

Traffic Conflict Characteristics Analysis and Prediction

Categories of traffic conflicts of work zone

Because of the lane merging or changing, vehicles running in the work zone are often very close to each other. There will be a traffic conflict even a traffic accident, if any of the two approximating vehicle does not take counter measures such as slowing down or changing the direction.

The categories of traffic conflicts of work zone mainly include rear-end conflicts and side conflicts, and the detailed forms are rear-end conflicts in passing carriageway of warning areas, rear-end conflicts in carriageway of warning areas, side conflicts in upstream transition areas, rear-end conflicts in activity area, and rear-end conflicts in downstream transition area. The locations where the five traffic conflicts occurred are shown in Fig.3.

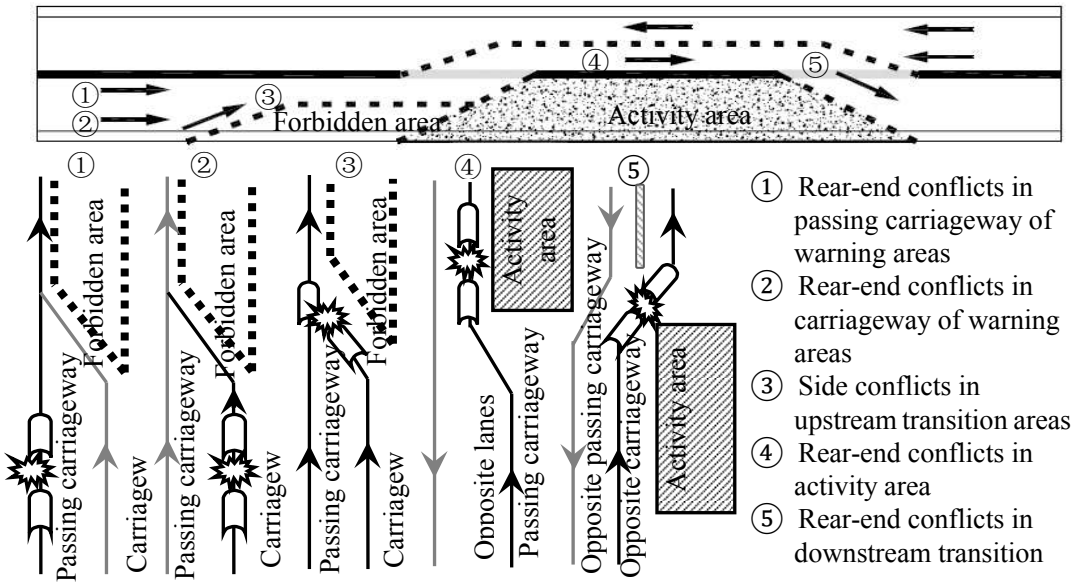

Fig.3 Types of traffic conflict of work zone

Identification of Rear-end Conflict Severity based on TTC

The first thing to apply traffic conflict technique is to determine the identification method of traffic conflict severity, and the identification method based on TTC is employed in this paper. Given two vehicles running while queuing on the same lane, if the speed of the follower is faster than that of the leader and the distance between them is short, there will be a rear-end conflict. The time TTC (time to collision) for the follower vehicle hit the leader is calculated as follows:

$$TTC_i = \frac{x_{i-1}(t) - x_i(t) - l_{i-1}}{\dot{x}_i(t) - \dot{x}_{i-1}(t)} \quad \forall \dot{x}_i(t) > \dot{x}_{i-1}(t) \tag{4}$$

where, $x_{i-1}(t)$ and $x_i(t)$ is the location of the leader vehicle and the follower vehicle at time *t*, respectively, shown in Fig.4; l_{i-1} is the length of the leader vehicle; $\dot{x}_{i-1}(t)$ and $\dot{x}_i(t)$ is the instantaneous speed of the leader vehicle and the follower vehicle, respectively.

Since the vehicles are always moving, it is much easier to get the time headway than the space headway. Thus, the formula is adjusted as follows:

$$TTC_i = \frac{\dot{x}_i(t)}{\dot{x}_i(t) - \dot{x}_{i-1}(t)} \left(h_i - \frac{l_{i-1}}{\dot{x}_i(t)} \right) \tag{5}$$

where, h_i is the time headway, s.

The samples with short time headways as well as the follower vehicle faster than leader one are selected from the data, and the TTCs are calculated by formula (5). After the statistic analysis of the TTC data, TTCs less than 2s are defined as the severe conflicts, and TTCs more than 2s and less than 6s are defined as normal conflicts. The proportion of severe conflict, normal conflict and no conflict are 2.73%, 5.12% and 92.15%, respectively, shown in Fig.5.

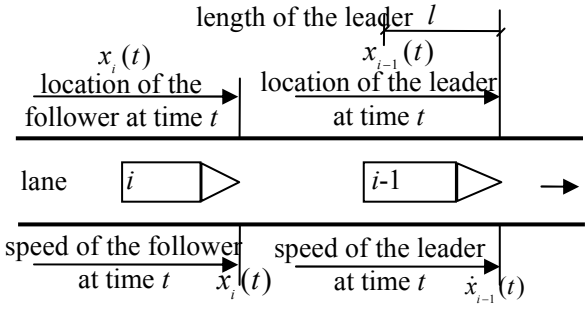

Fig.4 Schematic diagram of rear-end conflict of work zone

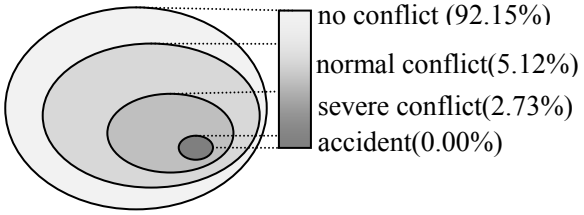

Fig.5 Safety situation of work zone

Traffic Conflict Prediction Model of Rear-end Conflict in Work Zone

The statistic analysis shows that the variance of the samples is much higher than the mean, so the negative binomial distribution is adopted to model the occurrence of traffic conflicts. Combining the traffic flow and traffic conflict data, applying the maximum likelihood estimation, the prediction model is calibrated as follows:

$$P_i(n) = \frac{\Gamma(\frac{1}{0.328} + n)}{\Gamma(\frac{1}{0.328}) \cdot n!} \cdot (\frac{1}{1 + 0.328\lambda_i})^{\frac{1}{0.328}} \cdot (\frac{\lambda_i}{\frac{1}{0.328} + \lambda_i})^n \tag{6}$$

$$\lambda_i = \exp(2.812 + 0.00734x_q + 4.889x_b + 0.0346x_{\Delta v} - 0.538x_h) \tag{7}$$

where, $P_i(n)$ is the probability of *n* rear-end t conflicts at site *i*; λ_i is the expectation number of rear-end conflicts at site *i*; x_q is the traffic volume of the lane, pcu/15min; x_b is the percentage of oversized vehicles, %; $x_{\Delta v}$ is the speed difference of two vehicles, m/s; x_h is the time headway, s.

Summary

The one-way-closure work zone is selected as the research focus, and the field investigation of traffic flow and traffic conflict are conducted. The queuing characteristics, time headway distribution, and speed distribution of each component of the work zone are analyzed base on the investigation data and statistic analysis. Then the traffic conflict prediction model based on TTC technique is put forward. The research results of this paper can provide reference to the analysis of work zones' traffic characteristics and traffic conflicts.

References

[1] Virginia P. Sisiopiku, Richard W. Lyles. Study of Speed Patterns in Work Zones. Transportation Research Board, Washington, D.C., (1999) 978-992.

[2] James Migletz, Jerry L. Graham, Ingird B. Anderson, Douglas W. Harwood, Karin M. Bauer. Work Zone Speed Limit. Transportation Research Board, Washington, D.C., (1999) 584-596.

[3] Karen K. Dixon, Joseph E. Hummer, Nagui M. Rouphail. Comparison of Rural Freeway Work Zone Queue Length Estimation Techniques: A Case Study. Transportation Research Board, Washington D.C., (1998).

[4] A. T. Vemuri, M. M. Polycarpou, P. D. Pant. Short-term Forecasting of Traffic Delays in Highway Construction Zones Using On-line Approximators. Mathematical and Computer Modelling, 27 (1998), 311-322.

[5] Dazhi Sun, Rahim F. Benekohal. Analysis of Car Following Characteristics for Estimating Work Zone Safety. Transportation Research Board, Washington D.C., (2004) 4883-4908.

[6] Madhav V. Chitturi, Rahim (Ray) F. Benekohal. Effect of Work Zone Length and Speed Difference between Vehicle Types on Delay-Based Passenger Car Equivalents in Work Zones. Transportation Research Board, Washington D.C., (2008) 3021-3034.

[7] Madhav V. Chitturi, Rahim (Ray) F. Benekohal. Work Zone Queue Length & Delay Methodology. Transportation Research Board, Washington D.C., (2010) 112-130.

[8] LUO Xia, DU Jin-you, CHEN Ying-wen. Analyses on Multi-Traffic Flow's Characteristics. Journal of Southwest Jiaotong University, 3 (2000) 297-300.

[9] CHEN Xiao-hong, XIAO Hai-feng. Micro-simulation Study of the Characteristics of Waving Area. China Journal of Highway and Transport, 12 (2001) 89-91.

[10] Asad J. Khattak, Aemal J. Khattak, Forrest M. Council. Effects of Work Zone Presence on Injury and Non-injury Crashes. Accident Analysis and Prevention, 34 (2002) 19-29.

[11] Jian Xing, Hideki Takahashi, Kazuhiko Iida. Analysis of Bottleneck Capacity and Traffic Safety in Japanese Expressway Work Zones. Transportation Research Board, Washington D.C., (2010).

[12] David Arditi, Dong-Eun Lee, Gul Polat. Fatal Accidents in Nighttime vs. Daytime Highway Construction Work Zones. Journal of Safety Research, 38 (2007) 399-405.

[13] WU Bing, YANG Pei-kun. Forecasting the Risk of Traffic Accident during Highway Maintenance. Chinese Journal of Ergonomics, 1 (1995) 32-34.

[14] SU Zhi-qiang. Analysis of Freeway Work Zone Safety. Computer and Communications, 26 (2008) 40-43.

doi:10.4028/www.scientific.net/AEF.5.32

A Dynamic Emergency Evacuation Network Optimization Problem with Crossing Elimination Strategy

Wang Ze[1, a], Ma Shiyong[2, b], An Shi[1, c]

[1]School of Transportation Science and Engineering, Harbin Institute of Technology, Harbin, 150090, China

[2]School of Management, Harbin Institute of Technology, Heilongjiang institute of science and technology, Harbin, 150027, China

[a]sunshineym@163.com, [b]mashiyong1009@126.com, [c]anshi@hit.edu.cn

Keywords: Evacuation Planning; Dynamic Traffic Assignment; Cell Transmission Model; Crossing Elimination

Abstract. This paper presents a dynamic evacuation network optimization problem that incorporates crossing elimination strategy. Bottleneck problem at intersections during evacuation process is analyzed for the effective evacuation planning. The developed model is formulated as a system-optimum traffic assignment based on cell transmission model (CTM), which can effectively investigate the characteristics of randomness and dynamics of evacuation flow's spatial and temporal distribution. The numerical results show that the model can provide crucial theoretical support for evacuation decision-making for traffic managers.

Introduction

Evacuation has been widely used as an effective emergency response and mitigation strategy to protect people against natural and man-made emergency events, such as hurricanes, wildfires, floods, chemical spills, or terrorist attacks. The overall efficiency of the evacuation plan is a key factor for evacuation success in a large-scale urban region. It is widely known that traffic jams may easily be formed in the intersections of the road network, and intersection capacity may restrict the accessibility of evacuation flow especially when the evacuation demand soars up in the short time. As a matter of fact, traffic signal can separate the conflict flow from different directions by different timings in order to ensure traffic safety and improve operation efficiency. However, under the extreme condition, the signal facilities of the intersection may be destroyed due to the failure of electric power, damage of traffic sensors and communication interruption, and the signal lights cannot be functional described by Ardekani and Hobeika [1]. The evacuation may be a new disaster unless the disruptive intersections are not managed well, so the intersection crossing elimination is paying more and more attention in evacuation management in recent years. The primary research was carried out by Cova and Johnson [2] and a lane-based routing plan was generated that traded total vehicle travel-distance against merging, while preventing traffic crossing-conflicts at intersections.

There are some important considerations of implementing the intersection crossing elimination strategy in evacuation planning. First, the abnormally high evacuation demand may easily cause a wide range of traffic congestion and severe delays when the key intersection suffers from little disturbance. Second, it is extremely difficult to make a reasonable signal control plan to maximize the global evacuation efficiency because of the difficulty of an accurate traffic volume prediction, after all the traffic volume may stuck into a unstable fluctuation. Third, drivers under the emergency often become so impatient and panic that they may violate the traffic regulations and drive illegally through a red light timing. This behavior will greatly reduce the evacuation efficiency and traffic safety of the intersection.

The theoretical basis of the evacuation strategy is to grasp the evacuees' behavior and characteristics of evacuation traffic flow. At present, domestic and foreign scholars on disaster management caused by large-scale regional evacuation modeling approach adopted is broadly divided

into: network flow theory, traffic assignment theory and computer simulation method based on a simple path selection rules [3-6]. The paper discusses the intersection crossing elimination strategy in a traffic assignment frame based on modified cell transmission model (CTM), which can effectively investigate the characteristics of randomness and dynamics of evacuation flow's spatial and temporal distribution. The cell transmission model is proposed by Daganzo[7], which is firstly used to simulate a highway traffic flow, and applied into the transport network. Compared with node-arc network, cell network description can better express the transmission and evolution mechanism of evacuation traffic flow, including potential queue forming and dissipation. We conduct our study in the following sequence. Crossing elimination methods are first analyzed and then cell network with is described. Secondly we formulate a cell-based evacuation network optimization model with the crossing elimination strategy. Finally, our case and its results are showed in the last section.

Evacuation optimization model with crossing elimination strategy

Evacuation optimization model based on dynamic system optima is built up in the frame of CTM, with the objective of minimizing the evacuation clearance time, with the main conditions of model contained flow conservation, flow transmission and sending-receiving balance in cell network.

Firstly, we analyses the crossing elimination strategy. The basic rule of carrying out this technique is to make the flow through an intersection be uninterrupted, such as blocking lane entries and limiting flow directions by the use of traffic control device, such as barrier and other police support. Take a four-leg intersection as an example, there are 16 conflict points in the signal intersection including crossing points, and all of them can be eliminated as shown in the Fig 1.

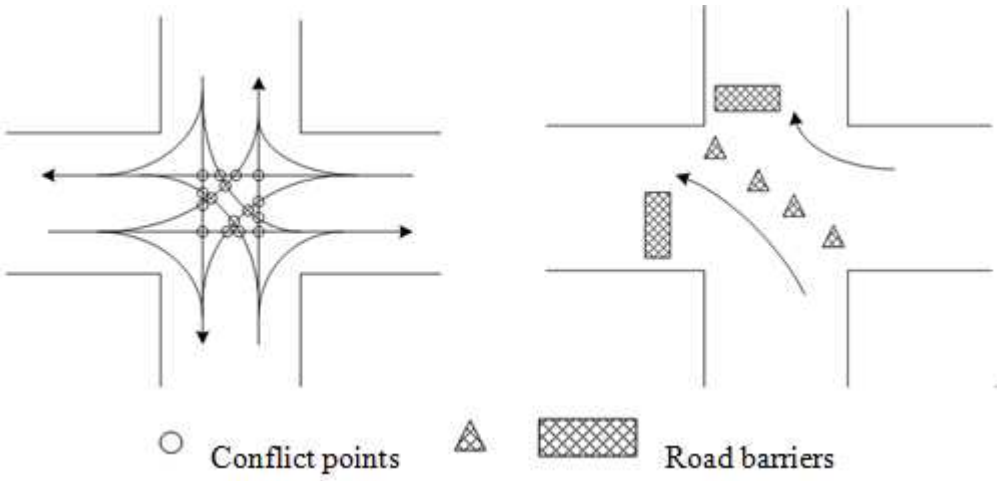

Fig.1 Traffic organization strategies in a four-leg intersection

Secondly, we describe the cell network description. The way to express the cell network can be found in our past work [8]. An example of the conventional intersection is shown in Fig.2, and we can get the cell-connection graph of the road network in this way. In order to facilitate the evacuation study, the single destination is considered here.

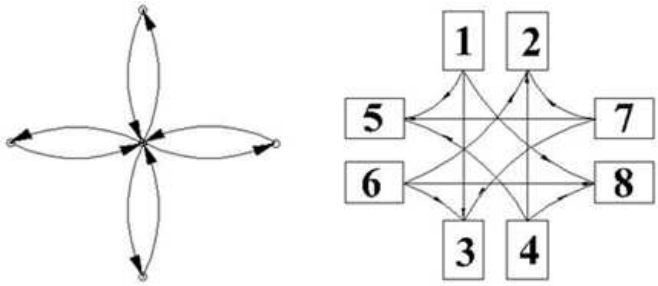

Fig.2 Cell-connection model of a four-leg intersection

Now, we can formulate the system-optimum optimization model, which is based on dynamic traffic assignment of the road work. This modified CTM model can accurately capture the randomness and evolution process of the traffic flow in the time and space. The objective of the model is to make the total evacuation time minimum. Total travel time of the system can be explained as follows:

$$\min Z = \sum_{t\in\Omega/\{0\}} \sum_{i\in\mathfrak{V}/\{\mathfrak{V}_p\}} x_i^t \tag{1}$$

$$\text{s.t.}\quad x_i^{t+1} = x_i^t + \sum_{k\in\psi^-(i)} y_{ki}^t - \sum_{j\in\psi(i)} y_{ij}^t + r_i^t \qquad \forall t\in\Omega/\{T\}, \forall i\in\mathfrak{V} \tag{2}$$

$$\begin{aligned} &\sum_{j\in\psi(i)} y_{ij}^t \le x_i^t; \forall t\in\Omega/\{T\}, \forall i\in\mathfrak{V} \\ &\sum_{j\in\psi(i)} y_{ij}^t \le Q_i^t; \forall t\in\Omega/\{T\}, \forall i\in\mathfrak{V} \end{aligned} \tag{3}$$

$$\begin{aligned} &\sum_{k\in\psi^-(i)} y_{ki}^t \le \delta_i^t[N_i^t - x_i^t]; \forall t\in\Omega/\{T\}, \forall i\in\mathfrak{V} \\ &\sum_{k\in\psi^-(i)} y_{ki}^t \le Q_i^t; \forall t\in\Omega/\{T\}, \forall i\in\mathfrak{V} \end{aligned} \tag{4}$$

$$x_p^T = \sum_{t=0}^{T-1} \sum_{i\in\mathfrak{V}_s} r_i^t, p\in\mathfrak{V}_p \tag{5}$$

$$\pi_{ij} + \pi_{mn} \le 1 \quad \forall (i,j)\in\chi, (m,n)\in\Psi(i,j). \tag{6}$$

$$y_{ij}^t \le M_{ij}.\pi_{ij} \quad \forall i\in\mathfrak{V} \tag{7}$$

$$x_i^0 = 0 \quad \forall i\in\mathfrak{V} \tag{8}$$

$$x_i^t \ge 0, \forall t\in\Omega, \forall i\in\mathfrak{V} \tag{9}$$

Equation (1) minimizes the evacuation time of the whole system, and it means the sum of every product of the number of vehicles in all cells except the sink cell $\mathfrak{V}_p$ and time interval unit τ .Equation (2) denotes cell flow conservation and flow propagation equations can be express as sending and receiving vehicle constraint seperately in equation (3) and equation (4). The next equation (5) is balance constraint of the cell transmission model. Equation (6) and (7) are crossing elimination constraint. As for the former equation, it is used to ensure the rationality that only one direction can go through vehicles, because the sum of the two binary indicators is not greater than 1 for any flow directions $(i,j)\in\chi$. The latter equation constructs the relationship between binary indicator π and the connector flow y , which can restrict the capacity of the direction in the connector. Equation (8) and (9) are balance constraint including non-negative and initial constraints.

The model can be formed as a mixed integer programming model with decision variables including x_i^t , y_{ij}^t and π_{ij} . π_{ij} is used to help to set the flow direction, which is a binary variable .We can get the number of vehicles in any cell, the optimum flow of the connecter between two cells and the organization of intersections in a determined time period.

Here, $LN(I)$ denotes lane set of road link $I\in A$; $\mathfrak{V}(I)$ denotes cell sets of link I ; Q_i denotes the maximum inflow of the cell in a unit time interval; N_i denotes maximum vehicles of the link cell; $\Psi(i,j)$ denotes flow direction set where the direction clash with the direction (i,j) in the intersection.

Numerical studies

Finally, taking road network as an example to analyze and verify the proposed model, numerical experimental results show that evacuation efficiency can be improved significantly under optimal management strategy. There are 9 signalized intersections, and node no.7and no 9 are destinations. Traffic zone 1 covers the scope including node no. from 1 to 6 with 25,000 vehicles, and traffic zone 2 covers the scope including node no. from 4 to 9 with 15,000 vehicles. Here, the number of vehicles is got according to the population. Basic data of links are presented in the table.

Tab.1 Basic data of links in evacuation area

no.	lanes one-way	capacity one-way (veh/h)	free speed (km/h)	length (km)
1, 2	3	2200	60	1.8, 1.1
6,7	3	2200	60	1.7, 1.6
11,12	3	2200	60	1.1, 2.1
3,8	3	2200	60	1.4, 1.5
5,10	3	700	30	1.9, 1.6

We assume that the evacuation demand is loading according to the classical type in MASSVAC. The time range is 30 minutes, and the unit time interval $\tau = 1\,\text{min}$, according to the basic information of the link, the road network on the left can be converted into the cell-connector model on the right in Fig.5. The no. 1 and 2 of cells are origin cells, no.50 and 51 are destination cells, and the no.52 is sink destination cell.

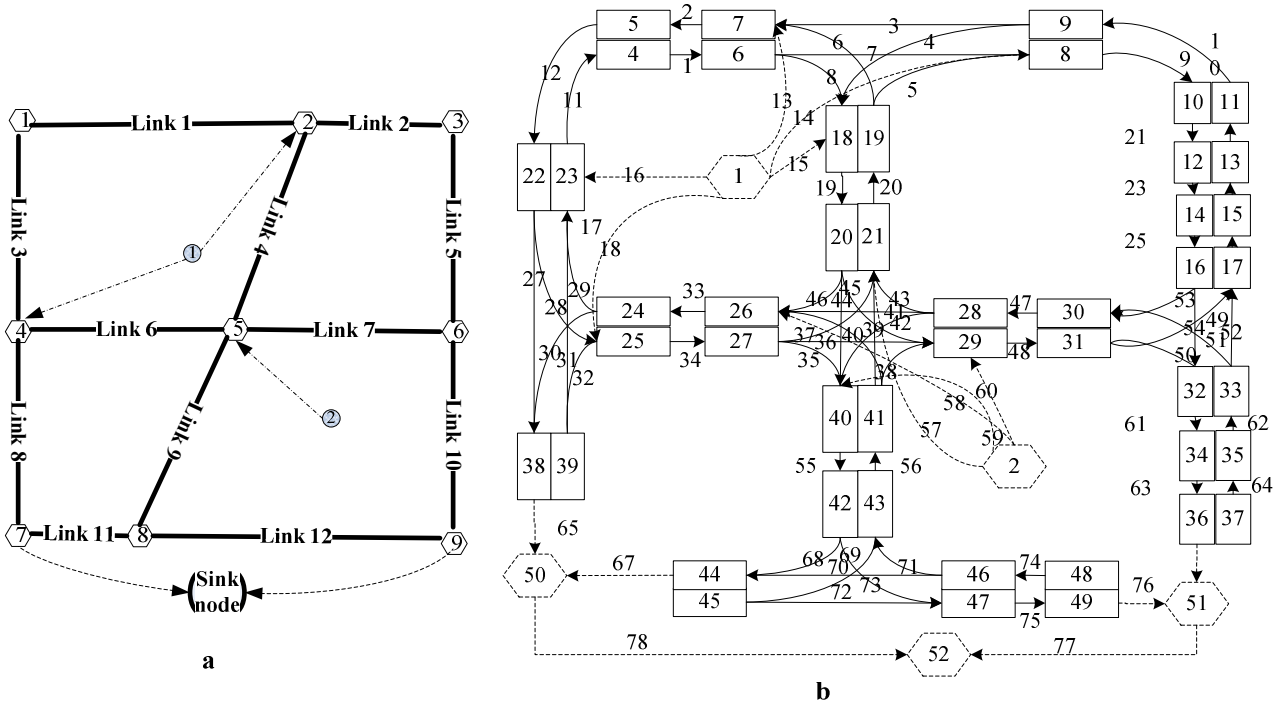

Fig.3 The cell-connector model of the evacuation road network

Based on the above data, this paper uses the Matlab and the function Miprog() to solve the model. Solution results show during 30 time intervals the, the number of total evacuation vehicles are 15738, including 10174 of destination 1 and 5564 of destination 2. Fig. 6 shows optimization layout of the evacuation area.

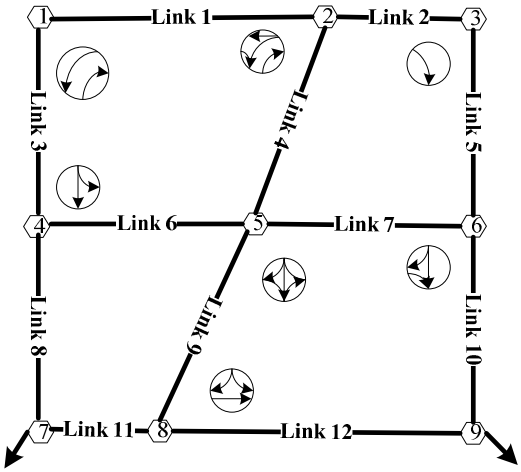

Fig.4 The setting results of crossing elimation

Conclusions

Under the conditions of emergency evacuation, applying crossing elimination is a critical and necessary measure to improve the efficiency significantly instead of the stop-and-go traffic control when drivers traverse though the intersection, because the intersection can be converted to be an uninterrupted flow facility. Our paper provides a reasonable model to get the organization and layout of the intersections, which is practical to a real evacuation plan. Urban ability dealing with all kinds of disaster may be strengthened by the implementation of scientific traffic emergency management plan. The research makes contribution to deeply understand the operation mechanism of evacuation traffic flow and provides crucial theoretical support for making evacuation traffic management strategies for decision maker. The model established in this paper is essentially a mixed integer programming model with lots of 0-1 decision variables. As the expansion of road network, the increasing in discrete time intervals, it will become more difficult to get optimization solutions. Thus, future research should be investigated on heuristic algorithm design for large-scale evacuation situation.

Acknowledgements

This research was supported by National Natural Science Foundation of China (Project No. 70973032).

References

[1] Ardekani, S.A., Hobeika, A.G.. Logistics problems in the aftermath of the 1985 Mexico City earthquake, J. Transportation Quarterly. 1998, 42 (1) 107-124.

[2] Cova, T.J., Johnson, J.P.. A network flow model for lane-based evacuation routing, J. Transportation Research Part A. 2003, 37 (7) 579-604.

[3] An Shi, Cui Jianxun, Wang Jian. An International Review of Road Emergency Transport and Evacuation [J]. Journal of Transportation Systems Engineering and Information Technology. 2008, 8(6) 38-45.

[4] Chen Yueming, Xiao Deyun. Emergency Evacuation Model and Algorithms, J.Journal of Transportation Systems Engineering and Information Technology. 2008, 8(6) 96-100.

[5] Liu, X.M., Hu, H. Research status and prospect of emergency transportation evacuation [J]. Journal of Traffic and Transportation Engineering, 2008, 8(3) 108-121.

[6] Liu, Y. Two-Level Integrated Optimization System for Planning of Emergency Evacuation [J]. Journal of Transportation Engineering. 2006, 132(10) 800-807.
[7] Daganzo, F C. The cell transmission model: A dynamic representation of highway traffic consistent with the hydrodynamic theory, J. Transportation research Part B. 1994, 28(4) 269-287.
[8] Cui Jianxun, An Shi, Cui Na. Dynamic regional evacuation traffic assignment based on cell transmission model. Journal of Harbin Institute of Technology. 2010, 42(1) 123-127.

doi:10.4028/www.scientific.net/AEF.5.38

A Game theory approach for the operators' behavior analysis in the urban passenger transportation market

Xiaowei HU [1, a], Jian WANG [2,b], and Guanglin SUN [3,c]

[1] School of Transportation Science and Engineering, Harbin Institute of Technology, 150090, China

[2] School of Transportation Science and Engineering, Harbin Institute of Technology, 150090, China

[3] School of Transportation Science and Engineering, Harbin Institute of Technology, 150090, China

[a] hxwhit@163.com, [b] wang_jian@hit.edu.cn, [c] mumulinhit@126.com

Keywords: game theory; bi-level programming; urban passenger transportation market; Nash Equilibrium.

Abstract. Urban passenger transportation market in China now is composed by three public transportation modes, including the conventional bus, taxi and subway (or light rail). There are both cooperation and competitive behavior among these three different transportation modes. This paper aims to describe how these three operators make their operational decisions in the competitive environment. A bi-level programming operational model is proposed to model urban passenger transportation operators' decision behavior, which is based on the game theory to describe the behavioral conjectures among the management authority, different operators and passengers. The upper-level model described the management authority' regulation on the fares of each mode, which aimed to achieve the comprehensive social objectives, indexed by the travel time cost, air pollution cost and energy consumption cost. The lower-level model described the three operators' aiming to maximize the profit by determining the service frequency, which can reflect the operators' cooperation and completive behavior under the urban passenger transportation economic policy. A logit model is proposed to analyze passengers' mode choice behavior with the maximization of their travel utilities, which considers the total travel time, waiting time and total travel fare of each mode. This research will provide more evidence for urban passenger transportation development and contribute to urban passenger transportation economic policy establishment and implementation.

1. Introductions

Urban passenger transportation service in China now is mainly provided by conventional bus, with the supplementation of taxi service; the rail transit is gradually introduced in large urban area. In 2011, there are twelve cities have operated urban rail transit, and fourteen cities have been constructing urban rail transit. Rail transit can not only provide a more convenient, huge-capacity, punctuality and comfortable service for travelers, but also can meet the urban modernization needs, alleviate the urban road traffic congestion, reduce road traffic air pollution emissions, promote urban passenger transportation sustainable development [1, 2].

There are conventional bus operator, taxi operator and rail transit operator in the urban passenger transportation market, while both cooperation and competitive relationship exist among these different operators [3]. Different operators will make their decision according to their own

development goals; each operator's decision-making process would often be impacted by other operators. How to design and schedule the operational programs to achieve the maximum profit is one of the keys to optimize the urban passenger transport system.

Due to the open and competition in the urban passenger transportation market, the competition and cooperation among different operators have been increasing and more severe; the research on the different operators' competition and cooperation strategies has been paid more attention during recent years, which can be referred to the studies of [4-8].

The aim of this paper is to provide the cooperation and completive behavior analysis among different urban passenger transportation operators, and to apply this study to analyze the reason of the different behavior change among different operators. This research will provide more evidence for urban passenger transportation development and contribute to urban passenger transportation economic policy establishment and implementation.

The paper is organized as follows. Section 2 describes the urban passenger transportation operators' relationship. Section 3 analyzes and models the urban passenger transportation operator's behavior in detail. In Section 4, we summarize this paper.

2. The urban passenger transportation operators' relationship analysis

As a typical complex system, there exists mutual cooperation and mutual competition relationship among the different passenger transportation operators. Each balanced state of the urban passenger transport system is formed when all the operators make their own decision after taking into account the decision-making of other operators.

The cooperative relationship among the urban passenger transportation different operators can be regarded as, the different transportation mode in accordance with its own technical and economic characteristics, playing its own respective role in its reasonable transportation scope; then reasonable convergence with other transportation modes, jointly to accomplish the passengers transport service from the origin to the destination. This cooperative relationship can effectively reduce transportation costs, and improve the passenger transportation efficiency, which make the passenger safety, convenience and fast reach the destination. The coordination and cooperation among the urban passenger transportation operators will meet the different categories passengers travel demand; thereby improve the public's satisfaction and support of the urban passenger transportation system [9]. The cooperative behavior among the he urban passenger transportation operators can be referred to [7, 10-12].

The competition relationship among the urban passenger transportation different operators can be achieved when all the transportation modes' services fully reflect its true social cost. The competition relationship will improve the passenger transportation systems productively, save one unit operating costs, and increase the average service number per unit expenditure [13]. Fox (2000) considered that the competitions between the urban passenger transportation are often reflected in the few visible businesses, such as the introduction of new technologies, financial performance and the advanced service function [14]. In China these can be mainly reflected by the electronic bus stop board, taxi GPS dispatching system and the IC card service. At present the competition behavior among the urban passenger transportation operators can be referred to [4-5, 15-17].

3. Model formulation

This section presents a bi-level programming model – an operational model for urban passenger transportation market, which describes the operators' cooperation and competition behavior relationship in the urban passenger transportation market.

The game among the urban passenger transport different operators has taken the different transportation mode's service price as objective; modeling the different pricing strategies set, and thus obtains the Nash equilibrium price or a stable equilibrium point. Around the world, the introduction of game theory into the passenger transportation research filed began from Fisk's (1984) study [18]. Different authors apply game theory have achieved more useful research results on the multi-player games [4-8, 10]. With the introduction and development of the subway transit in the urban passenger transportation, existing researches can not be suitable to reflect the cooperation and competition relationship among the three different mode operators, which is difficult to ensure the passenger transport management policy achieve the expected effect.

According to the gaps between previous researches and the reality, this paper will based on the existing studies to explore urban passenger transportation operator's cooperation behavior under the introduction of rail transit service. This paper will be helpful for the cooperation and completive strategy selection among different urban passenger transportation mode operators.

3.1 Model assumptions

Considering in the urban passenger transportation market, existing three public passenger transportation modes (bus, taxi and subway), and the private car mode. For simplicity, each public passenger transportation mode is assumed to be operated by only one operator under a regulated fare. The Nash Equilibrium will be achieved when the bus, taxi, subway and car compete with each other; meanwhile there no one acts as a leader in the four modes' competition. The bi-level operational model is established to determine the optimal fare and service frequency for each mode. The basic model assumptions are as follows:

ⅰ. The management authority aims to regulate the fares and subsidy to achieve overall market equilibrium; the operators determine the service frequency to maximize their profits under the fares restricted by the management authority;

ⅱ. The Nash Equilibrium among the different operators with the competition with each other in the service frequency, that means the operators behave in a non-cooperative manner in which each operator acts as given the other operators' operational decisions when determining its own strategy;

ⅲ. The capacity and travel time are fixed for the four passenger transportation modes;

ⅳ. Passengers based on their personal income and car ownership, they can choose different passenger transportation modes to maximize their utilities, including the conventional bus, taxi, subway and private car; A logit model is proposed to analyze passengers' mode choice behavior with the maximization of their utilities, which considers the total travel time, waiting time and total travel fare of each mode.

3.2 The bi-level programming operational model

The bi-level programming operational model of the urban passenger transportation market can be formulated as follows:

Upper level

$$\underset{f_i}{Min}\ SC = TC + AP + EC\,. \tag{1}$$

$$TC = \sum_{i=1}^{3}\left[b_{i1}\times R\times \mathrm{Pr}_i\times\left(t_{T,i}+t_{W,i}\right)\right]+b_{41}\times R\times \mathrm{Pr}_4\times t_{T,4} \quad \text{for } i=1,\ 2,\ 3. \tag{1.1}$$

$$AP = \sum_{i=1}^{3}\left[b_{i2} \times F_i \times d\right] + b_{42} \times \frac{R \times \mathrm{Pr}_4}{H_4} \times d \quad \text{for } i=1, 2, 3. \tag{1.2}$$

$$EC = \sum_{i=1}^{3}\left[b_{i3} \times F_i \times d\right] + b_{43} \times \frac{R \times \mathrm{Pr}_4}{H_4} \times d \quad \text{for } i=1, 2, 3. \tag{1.3}$$

In the Eq. (1), *SC* is the total social cost, where *TC, AP* and *EC* respectively represent the total costs of travel time cost, air pollution cost and energy consumption cost. Where b_{ij} is the unit cost of social cost index *j* (*j=1* represents for travel time cost, 2 for air pollution cost, 3 for energy consumption cost) of transport mode *i* (*¥/trip* or *¥/veh·km*), operator *i* for bus (*i=1*), subway (*i=2*), taxi (*i=3*). *R* is the ridership of the passengers (trips per hour). *d* is the distance between the origin to the destination (*km*). Pr_i is the passenger transportation market share of mode *i* (%). $t_{T,i}$ and $t_{W,i}$ is the travel time and the average waiting time of mode *i*. The average waiting time of bus and subway can be assumed as one-half of its headway, that is $t_{W,i} = (1/2F_i)$, *i=1, 2.* The average waiting time of taxi can be assumed in the time interval [5, 10] minutes.

Lower level i

$$\underset{F_i}{Max}\ \pi_i = f_i \times R \times \mathrm{Pr}_i - F_i \times c_i \quad \text{for } i=1, 2, 3. \tag{2}$$

s.t.

$$0 < R \times \mathrm{Pr}_i \le F_i \times H_i \quad \text{for } i=1, 2, 3. \tag{2.1}$$

$$0 < F_i \le F_{\max,i}, \quad F_i \in \text{integer}, \text{ for } i=1, 2, 3. \tag{2.2}$$

$$0 < f_i, \text{ for } i=1, 2, 3. \tag{2.3}$$

$$\mathrm{Pr}_i = \frac{e^{\alpha_1 \cdot t_{T,i} + \alpha_2 \cdot t_{W,i} + \alpha_3 \cdot f_i}}{\sum_{i=1}^{3} e^{\alpha_1 \cdot t_{T,i} + \alpha_2 \cdot t_{W,i} + \alpha_3 \cdot f_i} + e^{\alpha_1 \cdot t_{T,4} + \alpha_3 \cdot f_4}} \quad \text{for } i=1, 2, 3. \tag{2.4}$$

$$\mathrm{Pr}_4 = \frac{e^{\alpha_1 \cdot t_{T,4} + \alpha_3 \cdot f_4}}{\sum_{i=1}^{3} e^{\alpha_1 \cdot t_{T,i} + \alpha_2 \cdot t_{W,i} + \alpha_3 \cdot f_i} + e^{\alpha_1 \cdot t_{T,4} + \alpha_3 \cdot f_4}} \quad \text{for private car.} \tag{2.5}$$

Where f_i is the fare rate of passenger transportation operator *i* (*¥/trip*) for bus (i=1), subway (i=2), taxi (i=3), and for private car, respectively. F_i is the service frequency of operator *i* (number of scheduled buses, scheduled subway trains, and scheduled taxi per day). f_i and F_i are the decision variables at upper level and lower level, respectively. H_i is seat capacity of mode *i* (passengers per bus, passenger per train, or per taxi).

Eq. (2) is the profit (π_i) of operator *i* (*¥*) for bus, subway and taxi. c_i is the average operational cost per service of operator *i* for bus, subway and taxi. Restriction (2.1) means that the seat capacity of operator *i* must equal or exceed its passenger demand of bus, subway and taxi. Eq. (2.4) and (2.5) represent the Logit-choice model for the mode *i* (%) market share. *v* is the time of value of different categories passenger (*¥/hour*). α_1, α_2, and α_3 are three negative parameters for the travel time, average waiting time and fare, respectively, which can be obtained by the parameter calibration method [19].

The upper level model is to determine the optimal fare for each passenger transportation mode, which is based on the management authority's objective. Once the fares are fixed at the upper level, the lower level of the model is to determine the optimal operational service for each mode.

3.3 Model solution

As a bi-level programming model, the presented operational model can be solved by kinds of method, referring to the research of [20, 21], this model can be solved by Branch-and-bound method, Complementary pivoting method, Descent methods, Penalty function methods, and Trust-region methods. The Genetic Algorithm can also be introduced to solve this model; the detail can be referred to the research of [8] and [19] to solve this problem. Meanwhile, the software GAMS can also be adopted to solve this model [6].

4. Summary

In order to describe and analyze different kinds of passenger transportation operators operational decision behavior, this paper based on game theory to establish a bi-level programming operational model. The upper-level model described the management authority' regulation on the fares of each mode, and the lower-level model described the three operators' aiming to maximize the profit by determining the service frequency, which provides the cooperation and completive behavior analysis among different urban passenger transportation operators. The future work is to set parameters and analyze the operators' competition behavior under different strategies.

Acknowledgments

This research is supported by Program for New Century Excellent Talents in University (NCET-10-0065) and National Natural Science Foundation of China (Project No. 71073035). The authors would like to express their sincere thanks to the anonymous reviewers for their helpful comments and valuable suggestions on this paper.

References

[1] M. Wardman, Demand for rail travel and the effects of external factors, Transportation Research Part E. 42 (2006) 129-148.

[2] C.M. Werner, B.B. Brown, J. Gallimore, Light rail use is more likely on"walkable" blocks: Further support for using micro-level environmental audit measures, Journal of Environmental Psychology. 30 (2010) 206-214.

[3] J. Wang, X. Hu, A review of urban passenger transport economic management policy, Journal of Transportation System Engineering and Information Technology. 11 (2011) 24-31 (In Chinese).

[4] J.Y.T. Wang, H. Yang, A game-theoretic analysis of competition in a deregulated bus market, Transportation Research Part A. 41 (2005) 329-355.

[5] J. Zhou, W.H.K. Lam, B.G. Heydecker, The generalized Nash equilibrium model for oligopolistic transit market with elastic demand, Transportation Research Part B. 39 (2005) 519-544.

[6] P. Zito, K. Salvo, L.L. Franca, Modelling Airlines Competition on Fares and Frequencies of Service by Bi-level Optimization, Procedia Social and Behavioral Sciences. 20 (2011) 1080-1089.

[7] A. Roumboutsos, S. Kapros, A game theory approach to urban public transport integration policy, Transport Policy. 15 (2008) 209-215.

[8] Y.-C. Chiou, L.W. Lan, K.-L. Chang, Sustainable consumption, production and infrastructure construction for operating and planning intercity passenger transport systems, Journal of Cleaner Production. (2010) doi:10.1016/j.jclepro.2010.09.004.

[9] R. Vickerman, Provision of public transport under conflicting regulatory regimes, Transportation Research Part A. 42 (2008) 1176-1182.

[10] B.B. Su, H. Chang, Y.Z. Chen, D.R. He, A game theory model of urban public traffic networks, Physica A. 379 (2007) 291-297.

[11] G. Santos, H. Behrendt, A. Teytelboym, Part II: Policy instruments for sustainable road transport, Research in Transportation Economics. 28 (2010) 46-91.

[12] N. Sharaby, Y. Shiftan, The impact of fare integration on travel behavior and transit ridership, Transport Policy. 21 (2012) 63-70.

[13] W. Cox, B. Duthion, Competition in urban public transport: A world view. 2001, Presented to the 7th International Conference on Competition and Ownership in Land Passenger Transport (Thredbo 7) Molde, Norway, June 2001.

[14] H. Fox, Review of urban public transport competition (draft final report), Department for International Development. May 2000. Halcrow Group Limited 2000.

[15] B. De Borgera, I. Mayeres, Optimal taxation of car ownership, car use and public transport: Insights derived from a discrete choice numerical optimization model, European Economic Review. 51 (2007) 1177-1204.

[16] H. Cavusoglu, S. Raghunathan, Configuration of detection software: a comparison of decision and game theory approaches, Decision Analysis. 1 (2004) 131-148.

[17] Y. Hollander, J.N. Prashker, The applicability of non-cooperative game theory in transport analysis, Transportation. 33 (2006) 481-496.

[18] C.S. Fisk, Game theory and transportation systems modeling, Transportation Research Part B. 18 (1984) 301-313.

[19] J. Wang, Research on bus fee under urban road congestion pricing. Dissertation of Harbin Institute of Technology. 2003 (In Chinese).

[20] A. Migdalas, Bilevel programming in traffic planning: Models, methods and challenge, Journal of Global Optimization. 7 (1995) 381-405.

[21] B. Colson, P. Marcotte, G. Savard, An overview of bilevel optimization, Annuals of Operations Research. 153 (2007) 235-256.

doi:10.4028/www.scientific.net/AEF.5.44

Price transmission mechanism of transit service in city

GUANGLIN SUN[1,a], JIAN WANG[2,b]

[1]School of Transportation Science and Engineering, Harbin Institute of Technology, Harbin, China

[2] School of Transportation Science and Engineering, Harbin Institute of Technology, Harbin, China

[a]mumulinhit@126.com, [b]wang_jian@hit.edu.cn

Keywords: transit price; transmission mechanism; transmission network

Abstract. Price transmission of transit service is a distinct mechanism with common characters. This paper aims to provide the nature and law of price transmission of transit service. The transmission of transit service prices is defined and transmission routes are classified into vertical and horizontal. The cost-push and demand-push are to drive the price carriers along transmission routes, which produces the price transmission network. Augmented Dickey-Fuller (ADF) and Granger co-integration test are used to measure the cost-push price transmission. For demand-push price transmission, the demand elasticity was used to model the relationship between transit demand and prices.

Introduction

The price transmission is defined to the intrinsic mechanism described by the price change due to price fluctuation of some products or service [1]. In addition, the coverage and degree of price transmission are depended on economic and policy environment [2]. The public transportation is indispensable infrastruction with semi-public goods property, and a global and fundamental service industry, determining the function of city. Therefore, the specific characteristics lead to the difference in transit price form and transit price transmission mechanism.

The public transport service is typical semi-public goods with production indivisibility, consumption separation, and enjoyment existing in consumption course. For this reason, the transit services are supplied by private or public department, and the services' price are formed according to market value rules and subsidized and controlled by government [3]. Hence the transit service prices simultaneously have common and specific characteristics as to the consequence of interaction among market, operator and government.

The research on price transmission mechanism may provide the means to stabilize public service price and adjust industrial structure. This paper is structured as follow: section 2 gives the definition and attributes of public transport price; section 3 provides the carrier, route and network of price transmission; the quantity to price transmission derived by cost and demand presents in section 4; section 5 concludes.

The definition and attributes of price transmission

(1) Definition

The price transmission is the process of price change of up-stream product effects on the price of down-stream product in term of industry chain relationship. Therefore, the price transmission of public transport can be defined as the price fluctuation mechanism due to cost, demand or some transit service price.

The price transmission mechanism is to exist in price operation of product or service and be affected by many factors. It relates to interior price or external environment by some way [4]. The transmission mechanism of public transport price includes three meaning:

1) the way of price transmission, including cost-push or demand-push;

2) the route of price transmission, including transmission chain and network;

3) the influence of many factors on price transmission.

The price transmission of public transport occurs along to vertical and horizontal route under action of impact factors.

(2) Attributes

The attribute of semi-public product of public transport service promotes the government to a leading role, and presents the particularity of transmission way, route and factors.

1) the way of price transmission

In this paper, the way of price transmission can be classified into two kinds: cost-push and demand-push.

- cost-push

The nature attribute of cost-push is the effects of price change of up-stream products on the price of down-stream product. The up-stream product prices of public transport is related to transportation cost including energy, material and power etc., which to be as production factors whose value being transferred into the revenue of public transport service. When the transportation cost increasing, it must lead to the rise of operation cost, then the price will transmit along vertical direction if the public transport operator cannot internalize the factors of price rising.

- demand-push

The service provided by public transport has "congestion" attribute. When the number of passenger increasing beyond a threshold, congestion will occur and marginal cost is positive, which results in the decline of passengers utility with passengers growing. At this time, the rising of service price can improve the revenue of enterprise, as can supply the motivation and condition for more transportation service. Additionally, the change of service price can raise the share of public transport to gain new market equilibrium, when the contradiction between supply and demand appearing. The contradiction aroused by public transport demand is the power to promote the transport service price transmitting along horizontal direction due to the new equilibrium in transport service price system.

The mechanism of price transmission is objective law in price operation. However, the price change of up-stream product or demand cannot reflect absolutely at the service price in time, but the happening of price transmission is just time and degree problems.

2) the route of price transmission

According to price theory, the price system formed by organic connections among every kind of products and service price, performs the join of chain. It is general rule that the fluctuation of price of product and service at a link of chain will transmit to other link by cost-push or demand-push. The transmission chain of public transport price is promoted by transport cost-push and demand-push along vertical or horizontal direction. Assuming without external constrains, the public transport enterprise will be a receptor rather than a constitutor, and the efficiency of resource allocation will be distorted. The results lead to lost public welfare of public transport. Therefore, the government control to price formation and transmission route play a role in transmission direction and occurring.

3) the influence of many factors

The influencing factors may bring about the variability of transmission or transmission delay. Market general equilibrium aroused by change of a product or service price exists and the transmission of price change has no delay under perfect commodity economy condition. The formation of price and public vehicle operation may be influenced by government control, cost and demand etc. which generates the variation of price transmission.

Transit price transmission mechanisms

(1) cost-push price transmission

1) transmission carriers and routes

The prices of the fixed investments, energy, and raw materials and labor power are the origin of price transmission of general industrials chain, which can affect the price of industrial or semi-finished products and determine the price [5]. The providing of public transport service needs human resource including drivers, managers, service personals, and means of production such as fuel,

vehicles etc. The means of products including metal, fuel and machine are from some semi-finished and finished products transformed from mineral resources, energy and raw materials. These productions are further processed into the elements needed in public transport operation. Therefore, the prices of mineral, energy etc. named up-stream products are important carriers in chain; the prices of fuel, vehicle etc. are the prices of medium-stream products; the price of public transport service is the price of down-stream products.

Hence, the cost-push price transmission can be represented as follow:

The prices of labor and products↑→ the prices of vehicle and fuel↑→ the price of public transport service; where all of the price transmission are positively related, and "↑" presents price rising. The vertical transmission route of public transport service price is represented in Figure 1:

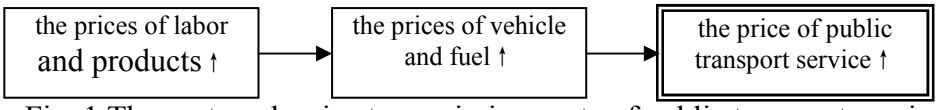

Fig. 1 The cost-push price transmission route of public transport service

The vertical price transmission of public transport service is the reflection at operation cost with the price of up-stream products and further transmitting to the price of public transport service.

2) transmission network

The operation cost is the power to change the price and transmit along vertical route. Consequently, the price of public transport service reflects the price change of up-stream products. The transmission network formed by transmission routes is provided in Figure 2.

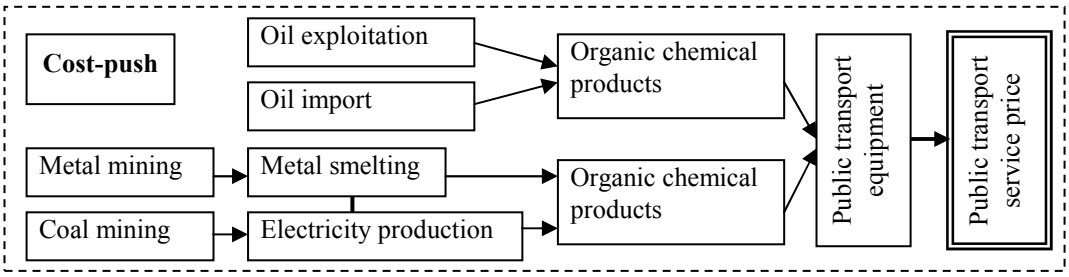

Fig. 2 The cost-push price transmission network of public transport service

(2) demand-push price transmission

1) transmission carriers and routes

Another power of price transmission is from the fluctuation of transit demand. One reason for demand fluctuation is the change of travel mode choice; the other is the policy effects on demand. The variation of mode share in public transport market may lead to congestion or idle of the usage of traffic resources, which can decrease the efficiency of public transportation. Therefore, the rational price is an efficient way to regulate transit demand; oppositely, the demand assignment can examine the rationality of price. In other words, the transit demand and service price are mutually carrier, and the transmission route is following.

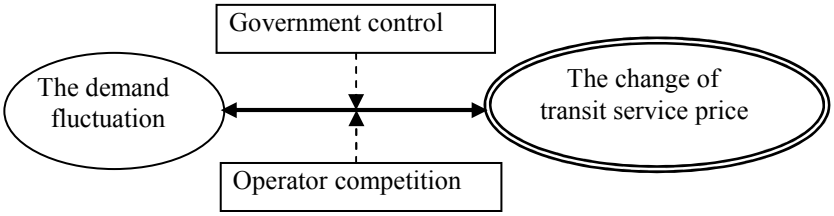

Fig. 3 The demand-push price transmission route of public transport service

2) transmission network

The variation of demand and cost is the power to price transmission along vertical and horizontal route, which reflects the price change of up-stream products. The transmission network formed by transmission network is presented in Figure 4.

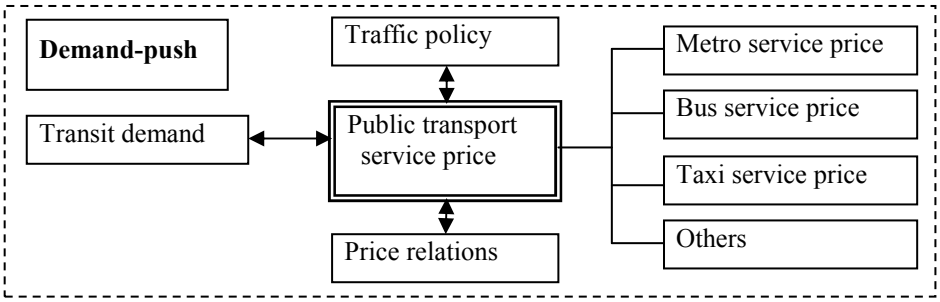

Fig. 4 The demand-push price transmission network of public transport service

(3) transmission results

Whatever the vertical or horizontal price transmission of up-stream products, it generates the price variation of public transport service (cost-push or demand-push). Under the condition for transit service prices as up-stream products and others as down-stream products, transit service prices will transmit to price system of public transportation along transmission routes. The price transmission of passenger transportation system is reported by Figure 5.

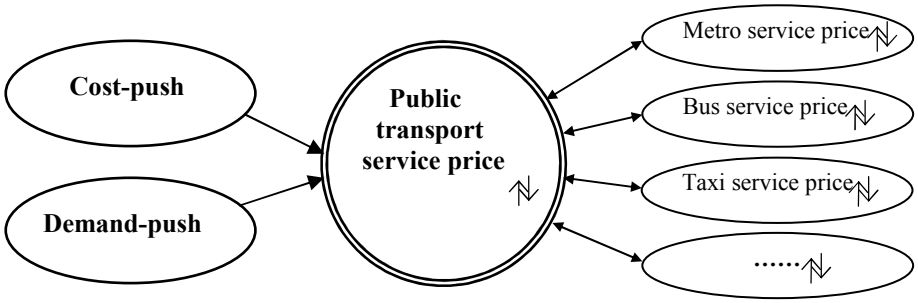

Fig. 5 The comprehensive price transmission network of public transport service

The price transmission is no longer successive as to the global and information market economy. The variation of cost or relationship between demand and supply may directly transmit from initiation to end without intermedium process. Therefore, keeping the public transport price steady needs enough government control.

Transit price transmission pattern

(1) cost-push price transmission

The cost-push is the nature of transit price transmission. For this reason, the regression model can be used to the stable price time series and Pearson coefficient model is adopted to calculate the correlation degree between price index at each link [6]. In this paper, the prices with no stable time series are analyzed by Augmented Dickey-Fuller (ADF) test and Johansen co-integration analysis base on co-integration theory proposed by Engle and Granger [7, 8, 9].

1) ADF test

The stable property of up-stream product prices and transit service prices must be examined before co-integration test. Firstly, both of the prices of up-stream products Pt and transit service prices Ft are treated into difference sequence ΔPt and ΔFt to do the unit root test for removing the time trend terms in order to satisfy stable series condition. These treatments can confirm the single whole order numbers of Pt and Ft when single whole order numbers of 2 series above are same, the co-integration correlation may be existing. The ADF model can be presented following.

$$\Delta X_t = \alpha + \beta X_{t-1} + \sum_{i=1}^{n} \delta_i \Delta X_{t-i} + \varepsilon_i \tag{1}$$

where $\Delta X_t = X_t - X_{t-1}$, $\Delta X_{t-i} = X_{t-i} - X_{t-i-1}$; X_t is the prices series of up-stream products when ADF test for up-stream products, otherwise X_t presents the prices of public transport service. ε_t is white noise; n is delay periods.

2) Johansen co-integration test

The VAR (Vector Auto Regression, VAR) is the basic model for Johansen co-integration test, which is reported as follow [8].

$$\begin{bmatrix} \Delta P_t \\ \Delta F_t \end{bmatrix} = \begin{bmatrix} a_1 \\ a_2 \end{bmatrix} + \begin{bmatrix} \pi_{11}-1 & \pi_{12} \\ \pi_{21} & \pi_{22}-1 \end{bmatrix} \begin{bmatrix} P_{t-1} \\ F_{t-1} \end{bmatrix} + \begin{bmatrix} u_{1t} \\ u_{2t} \end{bmatrix} \tag{2}$$

where a_1 and a_2 are constants; π_{11}, π_{12}, π_{21}, π_{22} are coefficients; u_{1t} and u_{2t} are random error terms;

Identifying the relationship between the prices of up-stream products and transit service prices must develop the binary model including Pt and Ft. Granger causal relationship model is following.

$$P_t = a_0 + \sum_{i=1}^{p} a_i P_{t-i} + \sum_{j=1}^{p} b_j F_{t-j} \tag{3}$$

$$F_t = c_0 + \sum_{i=1}^{p} c_i P_{t-i} + \sum_{j=1}^{p} d_j F_{t-j} \tag{4}$$

If $b_1=b_2=\ldots=b_p=0$, F is not the Granger reason for P, namely F cannot explain and predict P; If $c_1=c_2=\ldots=c_p=0$, P is not the Granger reason for F; if both of them are admitted, no causal relationship between them.

(2) demand-push price transmission

The transit demand elasticity can be used to describe demand-push price transmission. According to the principles of economics [10], the transmission relationship between public transport turnover Q and service price P can be indicated as follow [11, 12].

$$Q = \alpha P^{\beta} \tag{5}$$

where Q is public transport turnover (e04 passengers · km); P is service price (yuan); α is constant; β is coefficient of price elasticity of passenger turnover.

(3) transmission delay of transit service price

The price transmits without time delay under perfect market economics. The government can carry out enough controls to regulate the price of public transport service, such as public administration, industry policy etc. The variation of up-stream product prices may be neutralized and reversed the adverse impacts by tax, subsidy, special fund etc, as will produce the transmission delay. In other words, the variation of up-stream product prices has no reflection in down-stream transit service prices in time.

Conclusions

In this paper, we defined the transmission of transit service prices and provided the transmission attributes in way, route and impact factors. Presenting the carriers, routes and transmission network of transit service price, and developing the ADF test and multiple co-integration analysis method were to measure the cost-push price transmission. For demand-push price transmission, the demand elasticity was used to model the relationship between transit demand and prices. The law of price transmission can clear the correlations among departments of transit service, meanwhile provide theory basis for controlling the transit demand and supply equilibrium.

References

[1] Zhou Shuai, Yu Miao, The case study on price transmission mechanism, China Price, 2008, 9, pp. 9-12.

[2] Leng Shulian, Jiang Yejun, The analysis of price transmission mechanism, Price World, 2004, 12, pp. 10-13.

[3] Wang Jian, An Shi, Development and Experience from Toll Theory of Public Transport, Journal of Transportation Systems Engineering and Information Technology, 2004, 4(3), pp. 105-109.

[4] Wang Yongzhi, Some questions of price transmission mechanism, Price: Theory & Practice, 2005, (2), pp. 10-13.

[5] Sun Shengxiang, Li Zhenyu, Research on Conduction Mechanism of Naval Equipment Prices, JOURNAL OF WUT (INFORMATION &MANAGEMENT ENGINEERING), 2008, 30(6), pp. 955-958.
[6] J Eggers, R Bauml, R Tzschoppe et al, Scalar Costa Scheme for Information Embedding, IEEE Trans on Signal Processing, 2003, 51, pp. 1003-1019.
[7] Engle R F, Granger C W J, Cointegration and error correction: representation, estimation and testing, Econometrica, 1987, 55, pp. 251-276.
[8] Johansen S, Statistical analysis of co-integration vectors, Journal of Economic Dynamic and Control, 1988, 12(2), pp. 231-254.
[9] Dickey D A, Fuller W A, Likelihood ratio statistics for auto regressive time series with unit root, Econometrica, 1981, 49, pp. 1057-1072.
[10] Alfred Marshall, Zhu Zhitai translate, Principles of economics, Beijing: The Commercial Press, 2005.
[11] Wang Dianhai, Wu Juan, Li Hongqiang, Study on Method of Deciding Bus Ticket Price for Typical Route, JOURNAL OF HIGHWAY AND TRANSPORTATION RESEARCH AND DEVELOPMENT, 2000, 17(6), pp. 10-12.
[12] Tong Yunhuan, Optimal Fare-Pricing for Urban Rapid-Transport Line Project and Government Compensation, System Engineering Theory & Practice, 2001, (4), pp. 88-91.

doi:10.4028/www.scientific.net/AEF.5.50

Transit OD Generation Based on Information Technology

LIBING CHI[1,a] , JIAN WANG[2,b]

[1]School of Transportation Science and Engineering, Harbin Institute of Technology, Harbin, China

[2] School of Transportation Science and Engineering, Harbin Institute of Technology, Harbin, China

[a]16725684@qq.com , [b]Wang_jian@hit.edu.cn

Keywords: GPS data; IC card data; Transit OD matrix

Abstract: As developing in computer and information technology, data access and collection have becom more and more convenient. In many cities' transit system of the world, transit vehicle GPS data and passenger IC card data could be provided with database. This paper focuses on how to use the passenger IC card data (only record once per trip) and transit vehicle GPS data to generate the transit OD matrix. With the characteristic of transit trips, The continuity of transit trips is definited . By this definition, this paper presents a search method to generate the transit OD matrix. The validity of this method has been tested in the modeling Zhengzhou city's comprehensive transportation system.

Introduction

How to use public transportation IC card data has done in many literatures [1-3]. Previous studies focused on the use of public transportation IC card data to get the demand on-site car; in addition, considering certain characteristics of the bus passenger flow to estimate approximate number of passengers alighting on stops. The gravity model is adopted to generate OD between bus stops with constrains on the number of passengers boarding and alighting. More complex approach was to develop a bi-level mathematical programming model, the upper-level issue is responding to least squares model, the lower-level is the problem of public transportation network equilibrium assignment [4]. Due to lack of bus GPS data, these methods gain the information from the bus IC card and application of a number of vehicles on the site, meanwhile applied to the bus OD estimation process.

With the development of information technology in recent years, more and more cities begin to cellect the bus GPS data. Recently some studies pay attention to explore the basis of the bus GPS and bus IC card data fusion to generate a bus OD [5]. However, the assumptions lead to that the method can be applied only in a single bus line. How to effectively utilize large amounts of data in computers and IT development is still a very interesting research direction.

This paper focused on how to use public transportation IC card data (only the case of credit card on the bus) and bus GPS data to generate a bus OD. Different from previous studies, In this study, not only presenting a model to estimate the bus OD, but searching alighting stops is conducted by the bus travel characteristics of the credit card records with meeting certain conditions to reflect the public transport of bus travel the inherent law of the OD. Bus OD generated from the existing methods are mostly corresponding to a certain extent. The new methed is to use the concept of continuity of bus travel "to reproduce" the number of on-site car and bus OD generated by the new method in the overall evaluation on the bus travel through the survey data. As the hypothesis conditions, most applications on a virtual network are to verify its effectiveness. This method has been successfully used in the traffic model of zhengzhou, and generated the article dynamic bus OD with more than ninety thousand of the GPS data and millions of bus card record.

Bus GPS and IC card data

This study is based on two basic database of bus GPS and bus IC, data record provided by the Zhengzhou Public Transport Company (May 18, 2010 all-day bus operators).

Bus GPS data can describe the detail time of each bus arriving in the stations etc. The data tables can provide the information comprising of company names, bus lines, the number of vehicles, operation directions, the station number, station name, arrival time. There are a total of 90 million records in a all-day data (per vehicle to reach each site for a record).

Tab.1 Example of GPS data for transit vehicles

Company	Line	Vehicle number	Uplink and downlink	Site number	Name of the station	Arrival time
The second company	62	3847	Uplink	1	Garden Road Liuzhuang	7:28:18
The second company	62	3847	Uplink	2	Lu gang xiao zhen	7:30:37
The second company	62	3847	Uplink	3	Tian Rong international building materials Port	7:32:12
The second company	62	3847	Uplink	4	New LiuLu garden road station	7:33:59

Public transportation IC card data can record detailed information of each riding on transit vehicle, and the information tables are consisted of six fields: the card number, card type, using card date, using card time, using bus line, the vehicle number. There are a total of 129 million records in a all-day (each passenger per ride card information for a record).

Tab.2 Example of transit IC data

Card Type	IC card number	Card time	Take the vehicle number	Line
Classic Card	268970105	7:29:12	3847	62
Classic Card	268970105	8:25:53	1955	61
Classic Card	268970105	19:37:52	1958	61
Classic Card	268970105	19:50:46	4483	9
Adult concession card	292659705	7:24:34	2614	41
Adult concession card	292659705	18:33:09	2615	41

The analysis of bus OD needs to match the bus GPS and IC card data on line, additionally using vehicles and taking time. After the inspection for matching, a total of 88 million bus GPS data and 118 million bus IC card data can be in exact match. The rest of the data is not directly used due to various reasons caused by no match between bus GPS or IC card.

Characters of resident's bus travel

The analysis of survey data on the bus characteristics of residents are from Zhengzhou City, June 2010 household travel characteristics survey. The principles of extraction of data sources are: (1) taking a person as a unit, the survey object (personal) has one trip at least in a day; (2) the survey object is completed in survey space, namely the first trip is from his/her home and the last trip destination is also his/her home. According to the above principles, there are a total of 8547 subjects extracted from survey data. Since the families surveyed are subjected to uniform distribution in space, we can approximately consider that the survey objects are similarly subjected to uniform distribution in space.

(1) The distribution of frequency of bus usage

Only 11.32% travelers have a bus trip within public transport survey in one day, and 68.71% travelers take two bus trips in one day. Analysis of residents of bus travel, the bus mode chosen by traveler is dominant role with 70.98% trips in all.

Tab.3 Travel mode structure for persons with transit trips

Travel modes	Passenger trips	Proportion
Bus	18945	70.98%
Other	7744	29.02%
Total	26689	100.00%

(2) The continuity of bus travel

The continuous characteristics with two bus trips in one day are: the next travel origin is generally the destination of this trip, namely the other transit modes are rarely used by passengers between two trips when to choose travel modes. Therefore, we can define the continuity of a bus trip: when travelers have many trips in a day, if the destinations of their next trip were the origins of this trip, this bus trip can be called the continuity trip. For the last trip in one day, if the destination of trip is the origin of this trip, the last trip is also the continuity trip.

According to the definition above, if there is only a bus trip in one day, this bus trip is non-continuous. The continuity trip is a proportion 89.79% with the statistics source. If we take out the trip with one travel process, the continuity trips can be 94.7%. In other words, the most bus trips are the continuity trips.

Tab.4 Rate of continuous transit trips

Bus travel classification	All bus travelers		Use the bus twice and more than twice the travel	
	Number of times	Proportion	Number of times	Proportion
Continuous bus travel	17010	89.79%	17010	94.7%
Non-continuity of bus travel	1935	10.21%	959	5.3%
Total	18945	100.00%	17969	100.0%

Analyzing the non-continuity of bus travel for travel using public transportation more than once, about 60% are with non-continuity trips. This indicates that the destination is closer to the travel origin of the non-continuity trip. In addition, taxi and car (take) modes chosen are often accompanied by bus non-continuity trips. This shows that there are no convenient bus lines until the next time.

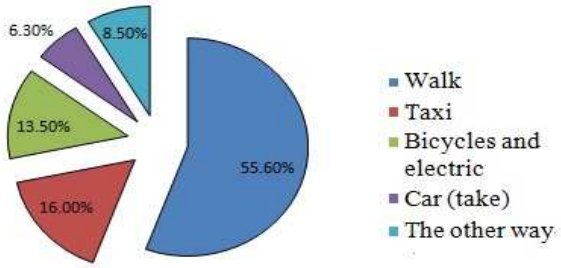

Fig.1 Non-transit travel mode composition for trips following the non-continuous transit trips

Search algorithm between O and D

(1) Typical bus trips

Using the concept of bus continuity trip, the records with many using in a card within IC card data on Zheng Zhou city network. The typical transit trip behavior can be summarized as the following three forms: (A) Travelers (morning); the first bus trip from the stop *i*, getting off at stop *j*; (at night) the second bus trip from the *j* stop and get off at the stop *i*; (B) Travelers (morning); the first bus travel in the stop *i*, transfer at stop *j*, and get off at *n*-stop, (at night) the second bus travel in the *n*-stop, transfer at stop *j*, and get off at the stop *i*; (C) Travelers (morning) first bus travel in the stop *i*, get off at stop *j*, at the second bus travel in the *j* stop ... and get off near the n-stop, (at night) the most the first bus travel in the *n*-stop on the car, get off at the stop i. The typical transit trip behavior is provided in Figure 2.

(2) Algorithm description

Firstly, the records of same number cards should be extracted(including each card on the train line, direction, and site information) and sorted by charge time. Search every get-off records, and the search method: the next records site location as the target, the line get-on this time as the search direction, on-line follow-up site for the search site collection. When the shortest distance of a station in the follow-up site of this on the is found, the site is recorded as get-off site. When the card records the the last one, the target location was the location of the first sites charged.

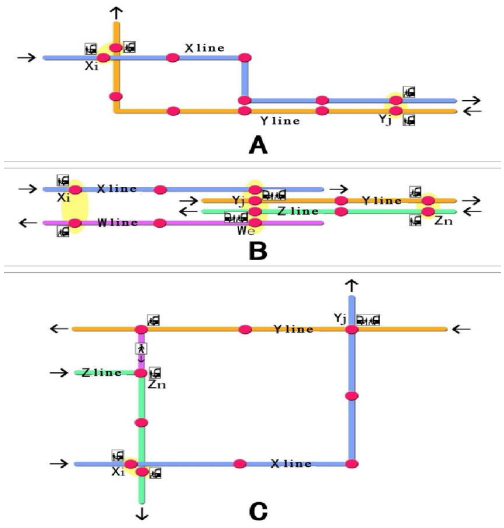

Fig2. Three typical situations for transit trips

In other words, when passengers who have twice and more records in the IC card c, the $n(n \geq 2)$ credit card records could be expressed as according to the time: $(l_1^x, l_2^y, l_3^z \ldots\ldots, l_n^w)$, where l_n^w is n times bus line of the w station, $w < \bar{l}_n$, $\bar{l}_n$ is the largest serial number station (terminus) of the n times bus line. According to the above description, next credit card by the card location of the site is generally oriented goals when passengers continuously charged the card. Therefore, get off site $l_n^{i^0}$ can be calculated by next formulas:

$$l_1^{i^0} = \min_i \left\| l_1^{x+i} - l_2^y \right\|, (i = 0,1,2,\ldots\ldots, \bar{l}_1 - x)$$

$$l_2^{i^0} = \min_i \left\| l_2^{y+i} - l_3^z \right\|, (i = 0,1,2,\ldots\ldots, \bar{l}_2 - y)$$

$$l_n^{i^0} = \min_i \left\| l_n^{w+i} - l_1^x \right\|, (i = 0,1,2,\ldots\ldots, \bar{l}_n - w)$$

Obviously, the search algorithm on every card records (including the last credit card records) can be found in the corresponding get off site. But not all the bus travel are continuous, so there will be searches that get-off site and get-on site is the same(i = 0). In this case, the OD between the card records stations could be regarded as invalid.

(3) Algorithm evaluation

The search algorithm showed good adaptability to be able to handle a variety of complex situations. Firstly, for the continuity of bus travel, the search algorithm can get accurate get-off site, typical bus travels cases (A) and (B) as shown in Figure 1. According to the proportion of the continuity of bus travel in the travel survey of households, the accuracy of the search algorithm can achieve about 95%. Secondly, for some of the non-continuity of bus travel, the search algorithm can be accurate to get off site. Figure 1, a typical bus travel (C) of the case, for example, when the passengers between the two bus trip mixed up with other ways, the search algorithm is still applicable. According to the characteristics of non-continuity of bus travel, the search algorithm could find a relatively accurate or relatively close method to get off site most of the non-continuity of bus travel. Finally, for some non-continuity of bus travel, get-off sites found through the search algorithm is invalid (as the situation that the get-on site and the get –off site are the same one). When this records are regarded as invalid, the bus station between the OD can get higher accuracy by the search algorithm.

The generation of the bus OD

The search algorithm can get most of the card records of the OD between bus stations, but it can't deal with only one credit card record and some non-continuous bus travel card records. As the large number data of the OD between bus stations get a high accuracy, OD between bus stations would be got through by loft on-site car (credit card) number for the whole sample.

Card records corresponding to get off site can also match its corresponding off time by bus GPS data. For many of the same card number records, the OD between bus stations could be transformed to the bus OD by the judgment of the transfer site. Because of bus GPS data, the transfer site definitions can be very precise, such as the combination of the two stations (site on the car and get off the site) the spatial distance, vehicular arrival and the time interval for the comprehensive judgment. As normal circumstances, the level peaks on the get off at the time of a passenger in a site before the next time in less than 25 minutes can be considered the site (ie, get off the site and the site on the car) for the transfer points. Peak within 30 minutes can be considered as a transfer site (due to the peak is very crowded, and passengers may not be squeezed into the vehicles to take the line first to reach). When a site has been identified as a transfer site, the bus trip and the next one will be combined (to retain the previous site on the train and get off of after times site). All card records does not exist to meet the conditions of the transfer site, the OD between bus stations was converted into a bus OD. Different from bus station OD, bus OD expression is public transportation amount of spatial relations, rather than public transit passenger volume of spatial relations.

Tab.5 Results of transit OD generation

ID	Travel sequence	On the bus line	Uplink and downlink	On the train site number	On the train site time	Travel sequence	Get off line	Uplink and downlink	Get off the site number	Get off site time
1	1	62	0	1	7:28:18	2	61	0	31	8:29:05
2	3	61	1	5	19:38:17	4	9	1	24	20:17:46
3	5	22	0	12	7:27:20	5	22	0	12	8:16:13
4	6	22	1	1	19:52:49	6	22	1	1	20:30:00
5	7	41	0	5	7:22:29	7	41	0	5	8:06:04
6	8	41	1	15	18:32:30	8	41	1	15	19:03:26
7	9	130	0	11	9:27:26	10	88	1	9	10:31:02
8	11	210	0	12	16:06:06	11	210	0	12	16:36:21
9	12	95	1	2	18:08:49	12	95	1	2	18:43:07
10	13	77	1	28	19:31:39	13	77	1	28	19:36:04

Zhengzhou bus OD generated results in Table 5. In Table 5 with a record on the train line and get-off the line is inconsistent with the description of bus travel after the transfer. When getting on line and getting off line consistent (right now travel sequence time is also consistent), there is no change to bus travel. It can be got from Table 5, the bus OD obtained by the new method is dynamic.

Figure 3 is a bus company statistics IC card credit card traffic generated bus OD allocation in the model line statistical results of the comparison. It can be seen, each line card statistics of traffic and the bus company forecast results have a very high goodness of fit (0.97), which also illustrates the bus OD generated by the above method has a very high accuracy.

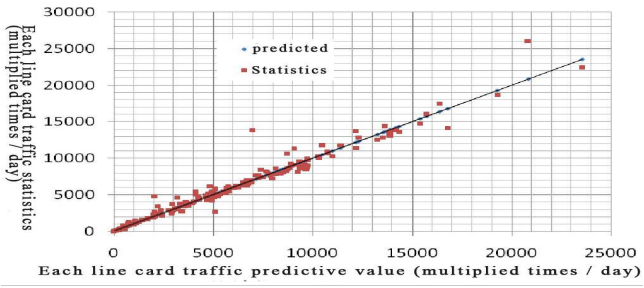

Fig3. Comparison of forecasted and reported line ridership

It should be noted that the above method is applicable to passengers in the IC card bus travel OD generated. A considerable portion of bus passenger is coin-operated ride the city bus. The features of bus travel card passengers (usually urban resident population as the main body) and the coin passengers (floating population) are significant difference. Therefore, the generated based on the IC card data bus OD should not loft to generate the overall bus OD.

In the case of the lack of coin-operated passenger, bus travel data can be assumed to constitute a card passengers urban resident population, and using the above-generated credit card passenger bus trip OD, bus service level measurements and land use data (population, employment, etc.) to calibrate

passenger transport model [6]. The flow of population distribution can be used to predict on the basis of the calibration of the passenger traffic model and the coin passenger bus travel OD (or floating population). Credit card passengers and coin-operated passenger bus trip OD are merged to generate the overall bus OD. Figure 4 shows the results for the overall bus OD in Zhengzhou city, assigned bus network.

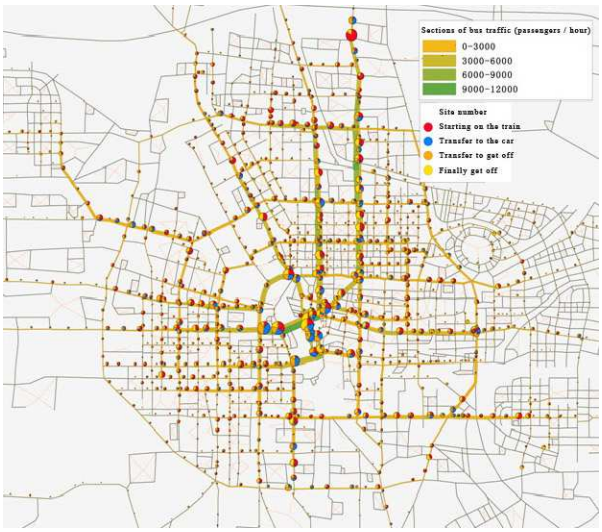

Fig4. Transit assignment results in AM peak period for Zhengzhou city

Obviously, the exact extent of the coin passenger bus travel OD have a certain impact on the quality of the overall transit trip OD, but the bus trip data is difficult to get through the survey. The future can be combined with sections of cross-section survey of passenger transport, back stepping.

5 Conclusions

This paper is based on the analysis of bus travel characteristics of the concept of continuity of bus travel. Based on the concept of continuity and bus system (bus GPS and IC card data), this paper constructs a search algorithm to generate the OD between the bus station, which to generate other types of bus OD. Different from previous studies is that the proposed method can be easily applied to the reality of the bus system; bus OD generated can reproduce the inherent law of bus travel. The bus OD generated should be noted as to the bus GPS and IC card data. It can accurately reflect the general urban population (or credit card passengers) bus travel distribution, and the floating population (or coin passengers) bus trip distribution in future is still needs further research.

References

[1] Xue-Wu Chen, Dai Xiao, Chen Qian. Bus IC card information collection, analysis and application [J]. Civil Engineering, 2004, 37 (2): 105-110.
[2] Shi Fumin.OD matrix construction method based on the IC card data bus. Journal of Jilin University [D], 2004, 11-39.
[3] Zhou Tao, Zhai Changxu, Gao Zhigang. Based on the OD of the bus IC card data projection technology [J], the urban traffic, 2007, 5 (3): 48-52.
[4] Zhou Jing, Zhang Lunke. using the IC card data to estimate the bus OD matrix model and algorithm . Theory and practice of systems engineering, 2006 (4): 130-135.
[5] Xu Jianmin, Xiong Wenhua, You Feng. Based on GPS and IC card single-wire bus OD generation method [J]. Microcomputer Information, 2008, 22: 221-222.
[6] Wu Zixiao, Ren Xifeng, Hu Jingyu. Based on the bus GPS and IC card data traffic modeling and new ideas [J], the urban traffic, 2011, 9 (1): 47-51.
[7] INRO Consultants Inc. (2010). EMME 3 User's Manual.

doi:10.4028/www.scientific.net/AEF.5.56

Slow Traffic System Planning Should Pay Attention to Several Issues in Central Area of Cold Region—Take Harbin for Example

Yao Xu [1,a], Zhang Yaping [1,a], Yang zhichao [1,a]

[1]School of Transportation Science and Engineering, Harbin Institute of Technology, Harbin 150090, China

[a] hrbyao@163.com

Key words: Cold region; slow traffic system; limited time non-motorized vehicles

Abstract. Starting from the definition of slow traffic system, taking Harbin for example, and by analyzing the characteristics and trip features of slow traffic system in cold region, the paper proposes that the central area should increase the pedestrian streets and underground warm gallery in cold city to improve walking environment in winter. At the same time, the paper puts forward that road cross- section planning and design should emphasis focus on the safety of non-motorized mode, and proposes specific measures, such as setting limited time of non-motorized vehicle lanes, slow integration design of non-motor vehicle lanes and sidewalk.

Introduction

In cold region, the winter that has large snowfall, short daytime and long night is long and cold. The outdoor season usually lasts six months or six months following. The negative impact of climate cold city is manifested in many ways. Climate has a significant impact not only on the residents travel, the city traffic, but also on slow traffic.

The concept of slow traffic appeared earlier at the Shanghai Urban Transport Development White Paper[1]. Slow traffic refers to is travelling on foot or by bicycle that occupy the highest priority in the green transport system. Specifically it refers to the speed below 15km/h, people-oriented, the focus on equity and sustainable development in close travel modes of transportation. Slow traffic, including pedestrian and non-motorized transport, contains walking, wheelchair, bicycle, tricycle, electric bicycle, car batteries, roller skating and jogging and other various modes of transportation in the broad sense. Because non-motorized transport in many cities is the bicycle traffic, so the main body of slow traffic generally is to walk and bicycle traffic[3].

Domestic and international planning and design to slow traffic often only consider the state of the warm season, neglect of alternating periods of climatic factors and lack planning and design in accordance with the needs of the seasonal characteristics of countermeasures. It leads that slow traffic planning and design in cold region are lack of geographical conditions, climatic characteristics the geographical and cultural considerations and local characteristics. Therefore, walking and bicycle traffic planning and design in cold region must take full account of the climate characteristics of the cold region, reflecting people oriented and the cold city's natural environment, geographical and cultural characteristics.

Research status

In order to reduce the impact of the cold climate of pedestrian traffic and bicycle traffic, many winter cities provide effective climate protection measures to make the residents get more humanistic care, compensation of adverse weather conditions brought negative effect. For example, Toronto and Montreal are famous for huge system of underground public space that is not subject to seasonal effects. St. Paul, the United States and Canada, Calgary, Minneapolis and other cities have vehicle-separation and winter weather protection footbridge trail system. Many European and

American Cold City have also established a large indoor public space, such as indoor public street and indoor activity center and it brings outdoor sunlight, plants, water and other natural factors into indoor by air conditioning technology to make the room warm as in spring. People in these public spaces can still fully enjoy the flowers and lush spring beauty, and completely forget the outdoor ice and snow of winter. There are a number of other climate protection measures. For example, Canadian winter city construct the glass roof of the sidewalk that can open or close according with season and internal heating device of the bus shelters, rest kiosks. Japan, Iceland and other countries in Cold urban construct the sidewalk which can melt the snow and is of the convenience of passers-by walking on. Stuttgart, in 1974-1978, constructed the Kaer Wei indoor pedestrian street. This is the world's first modern indoor pedestrian street.

Slow traffic in China's urban development is slow. Developed cities in the south ,such as Shanghai, Hangzhou, Shenzhen, completed the preparation of the slow transport system planning. However, slow traffic in the cold northern region city system planning studies is still in its infancy and planning for the protection of pedestrians and bicycles in the winter safe and comfortable travel is in the blank.

Slow traffic characteristics and the characteristics of the trips in cold region

Slow traffic characteristics in cold region.

(1) The difficulties of Winter walking traffic

The negative impact of climate on cold city's largest winter is traffic problems. Due to frequent snowfall and not timely clearance, the cold weather makes the road continued smooth and leads to walking slowly. Thus it affects a variety of consumer and leisure activities in the commercial street.

(2) The limited Behavior

In cold region, climate affects people's behavior, including the person's lifestyle and leisure. Winter outdoor temperature is low and a long duration. In order to avoid the cold and traffic inconvenience, people travel is less than that in other seasons, Especially the elderly, children and people with disabilities. Pedestrian street usage is affected. Sunshine time is short and the nightlife of urban public has been greatly affected.

(3) Climate impacting on the way to travel

Winter temperatures are low and the sunshine is short, so non-motorized travel that people choose is greatly reduced.

Characteristics of walking and cycling trips in cold region

(1) Trip distance

By investigating, Harbin summer walking distance is less than 30 minutes and the average trip distance is 1.8 km; winter walking distance is less than 12 minutes and the average trip distance is 0.8 km. In winter, residents' travel time and travel distance drop significantly, decreased by about 60%.

(2) Travel changes in the number

According to the Residents Travel Survey Harbin (2000), summer daily number of trips per capita is 2.2 times; the number is 2.02 times in winter. The resident trip times in winter decreased by about 8% than in summer.

(3) Travel pattern

Comparing city in cold region with any other city, walking and bicycle travel has obvious seasonal characteristics. Generally speaking, walking and bicycle travel are no significant difference in cold region in the spring, summer and autumn. Walking is one of the main modes of travel of the residents. The average walking travel of China's urban residents is 34% and the distance is 1.2km at now. According to the survey in Harbin, walking travel accounts for 37.2% and bicycle travel accounts for 15% in summer. Then walking travel accounts for 25.7% and bicycle travel accounts for 5.7% in winter. It can be seen that the non-motorized travel declines in the proportion of about 25% during up to six months in Harbin.

Pedestrian traffic is necessary form trip starting point to the end, so share rate does not change significantly in winter and summer. And there are three reasons for declined share rate of bicycle traffic:

(1) With the development of the city , the increased average distance of resident trip is more than the range of the bicycle travel's advantage. Currently, the average trip distance of residents is nearly 7 km in Harbin and greatly exceeds the 5km range of the advantages of travel of the bicycle traffic.
(2) As the urban infrastructure has improved steadily, cars, regular public transport and rail transport get to great efforts to develop, further reducing the competitiveness of bicycle traffic.
(3) As people's incomes increase, the travel traffic requires a significant comfort level. In winter, the weather is cold and the pavement is smooth. It leads that less and less people choose the bicycle mode to travel year by year.

Several key issues that need to be addressed in slow traffic planning in Harbin central area

Compared to other cities, Harbin winter is long and climate has a great influence on urban environmental quality and human activity patterns. In winter, people will minimize the number of trips in order to escape the harsh outdoor weather, resulting in reduced time outdoors. Residents in cold region relative to the residents in the mild climate are more eager to have a comfortable outdoor living. Therefore, requirements about the slow system are higher. The slow system is not only the residents' leisure, the main way of exercise, but also the main way of short-distance travel. Slow system is the real green transportation. So, walking streets are essential in the lives of residents in the cold. But at the same time it is also affected by climate and need to be improved.

Cold climate and pedestrian travel

Usually walking travel contains travel behavior and travel environment. From the walking behavior, literature will group walk into four forms: passing behavior, travel / arriving behavior, pause behavior and free movement. And the travel environment contains comfortable environment and uncomfortable environment. Walk behavior is greatly affected by the environment. To improve the walking environment is the focus of planning of the central area in Harbin.

In Harbin, the annual average temperature is 3.6 ℃. Harbin central area is divided into seven major functional areas: Fanghong tower square, central avenue business district, O luoba business district, Mai-kai business district, Ha yibai business district, Sofia Leisure Square and Manhattan shopping center. The seven functional areas are relatively independent and are lack of organic walk contact system among them. Walking links between the various functions of the status quo take rely mainly on the ground crosswalk and underground commercial street connection. Because of concentration of people and vehicles in the region, ground traffic walking system is inefficient. Underground shopping street for their own camps, most can only use as a cross-channel. Therefore the region both ground system on foot and in the underground shopping center is without forming a complete set of contact 7 Ribbon pedestrian traffic system.

Measures:

(1) Perfect ground walking system, improved pedestrian environment

Considering the central street, Mai-Kai shopping mall and 100 Central Avenue area are lack of walk traffic contact system, plan to build Ten West Road walking street(central street-Shangzhi Street). After the completion of the street, it will greatly improve the accessibility of central walk and bring big improvement in walking environment.

(2) Build underground warm gallery system as the principal centre of winter walking system

Plan to build new underground civil air defense engineering along Shangzhi Street and it will connect nine west road and thirteen west road civil air defense engineering, connect Rail transit Line 2 and Line 3 on line interchange station(Zhao Lin Park Station) and connect Ha100 Shopping Plaza. Plan to build new underground civil air defense engineering along Youyi Street (Tongjiang Street-Shangzhi Street) and it will connect Fanghong tower square, central avenue business district, Ha100 and so on. Plan to build new underground civil air defense engineering along Toulong Street

(Maimai Street-Shangzhi Street) and it will connect Shangzhi Street, Rock Street, Maimai Street and Zhaolin Street civil air defense engineering. It will form underground pedestrian system and contact 7 ribbon pedestrian traffic systems.

Cross section design of roads in winter and in summer

Cross section of road is one of the key elements of the planning. Cross design affects road traffic function of traffic environment with the traveler and to some extent determines the taste and image of the city. Cross section type of road in Harbin city is rich in one, two and three plate's type of cross section. As cities of the growing number of cars, and non-motorized vehicle usage continues to decline, it result that three silver shift gradually to a board. Bicycles give way to vehicles, bike paths being seriously compressed, and there is only one lane. Bike has no independent security driven space and cross section's change shows that the Harbin road function changes to mobile service delivery. Compared to other seasons, Harbin winter bicycle traffic space is greatly compressed. Snow cover over the original narrow passage space and bike has to contend with a motor vehicle, leading to frequent traffic accidents.

Measures:

(1) For characteristics of Harbin, in order to make road function into full play, road cross-section planning should ensure that use on road of travelers in different season, fully reflect the human text.

(2) For all new and rebuilding road, pavement width in accordance with specifications increases by 1 m, as a response to the snow of sidewalks during the winter reservations.

(3) For three panels on the center road, it is proposed to retain its cross section form and increase the sidewalk width. Des Voeux Road Central is set to limit non-motorized vehicle lane (every year from April 1 to November 1), and in the remaining time, it is set to bus lane. Slow bicycle road and sidewalk design use slow integration. Bicycle lanes and sidewalks are designed in the same plane and use bridges between wooden flexible isolation.

(4) Center one plate and two plates of roads use slow integration. Bicycle lanes and sidewalks are designed in the same plane and use bridges between wooden flexible isolation.

Conclusion

Resident's travel in cold region is affected by climatic conditions, especially wind, snow in winter and low temperature environment. So, slow system planning of city in cold region should take full account of the climate characteristics to reflect people oriented and adapt to the natural environment and local culture. It should focus on slow systems of safety, comfort and accessibility and gradually standardize and guide the city facilities to meet travel needs in different ways as far as possible to build harmonious traffic.

Acknowledgements

This research is funded by Heilongjiang Province Natural Science Foundation of China (Grant No. E200940).

References

[1] Liu Dongfei. Green Transport: means of achieving urban traffic sustainable development [J]. Study of modern city planning, 2003.

[2] Wang Yuna; Application of Human Basis Slow Traffic in Municipal Construction[J];Urban Roads Bridges & Flood Control;2010-10

[3] LI Feng-qing HUANG Huang; China's Future Aged Society and Related Planning Strategies[J];Modern Urban Research;2010-07

[4] XIA Tian(School of Traffic and Transportation, Beijing Jiaotong University, Beijing 100044,China);Strategies for Designing Urban Slow Traffic System[J];Journal of Transport Information and Safety;2010-05

[5] WANG Zhao-fei,LI Xiao-hua, SHAO Xiao-dong, GENG Juan (College of Civil Engineering, XI'AN University of Architecture and Technology, Xi'an 710055, China);Research on the Planning Strategy of Slow Traffic System in Big Cities[J];Logistics Engineering and Management;2009-06

[6] YUN Mei-ping1,YANG Xiao-guang1,LI Sheng2(1.School of Traffic and Transportation Engineering, Tongji University, Shanghai 201804,China;2.Laboratory of "City, Mobility, Transport", The National Ecole of Route and Bridge, Paris 77455,France);A Brief Review of Planning for Ped and Bike System[J];Urban Transport of China;2009-02

[7] WANG Wei ZHANG Yongqiang QI Xiang DONG Wencong; Urban Road Humanity Management Design[J];Shanghai Construction Science & Technology;2008-05

[8] Chen lei, Sun Honggang. Efficiency and vitality: modern urban street structure [m]. Beijing: China architecture and building press, 2007

[9] Peid E.Traffic calming:State of the practice [J].Washington,D.C.:Institute of Transportation Engineers.August 1999.

[10] Yun Meiping, Yang Xiaoguang. Road transport management, notes on slow traffic system planning, 2009

doi:10.4028/www.scientific.net/AEF.5.61

Risk factors for the injury severity of fatigue-related traffic accidents

Lianzhen Wang[1, a], Yulong Pei[1, b], Botong Liu[1, c]

[1] School of Transportation Science and Engineering, Harbin Institution of Technology, Harbin, 150090, China

[a] rock510@163.com,[b] yulongp@263.net, [c] 291169750@qq.com,

Key words: Fatigue-related traffic accidents, drivers' fatigue, Stepwise logistic regression, risk factors, road safety

Abstract. Traffic accidents caused by drivers' fatigue carry less than one percent of the whole accidents in HLJ Province during the years 2006 to 2008. However, more than forty percent of such accidents accompanied fatalities. Drivers' fatigue is usually hard to be identified and there are no valid measures that could make real-time detection for it. Accordingly, variables such as drivers' characteristics, time of accident and whether using seat belt are considered to have close association with the injury severity in fatigue-related traffic accidents. This research focuses on analyzing injury severities of traffic accidents caused by drivers' fatigue, utilizing stepwise logistic regression method. Potential risk factors such as human, environment, road, and so on, were examined. Driving year, road pavement type, road grade and alignment, terrain, time and type of the accident, streetlight condition, vehicle type, speed limit, the number of vehicles involved, and whether using seat belt are significant factors impacting the injury severity. Identifying the high risk factors influencing the injury severity of fatigue-related accidents helps prevent the occurrence of drivers' fatigue and improve road safety conditions.

Introduction

With the great development of economy and rapid increase of automobiles in China, the problem of road traffic safety is more and more serious. Fatigue-related traffic accident is one of the most popular accident types which takes away lots of lives and properties every year. The hazard of fatigue-related accidents is very great.

Utilizing both the MNL model and the LCL model, factors such as driver age, influence of alcohol or drug, seat belt usage, speed are found to be closely related to driver injury severity levels in rural single-vehicle accidents[1]. Using a stepwise logistic regression model, the district board, road type, speed limit, time of the accident, driver's gender, and vehicle type are significant factors influencing the injury severity in multiple-vehicle traffic accidents in Hong Kong[2]. In single vehicle traffic accidents, district board, gender of driver, age of vehicle, and street light conditions are significant factors determining injury severity for private vehicles[3]. Complete or partial ejection, a lack of seatbelt use, a greater number of roof inversions, far side seating position and older occupant age significantly increased the risk of all types of injuries in rollover crashes[4]. Factors such as dynamics of the accident, seating position of occupant, use of seat belts, and age of occupant involved affect the accident severity[5]. There is a study confirming that the injury risk is higher in accidents occurring between heavy cars than for accidents between lighter cars[6]. In highway accidents, there are studies proving that average daily traffic per lane, average daily truck traffic, truck percentage, interchanges per mile, the number of horizontal curves, number of grade breaks per mile, pavement friction and weather effects are significant factors affecting road accidents severity[7].

This study aims to identify contributory factors for the injury severity of fatigue-related accidents. Several factors including accident type, seatbelt use, speed limit, time, weather, streetlight condition, road condition, road type, and professional driving years of the drivers were considered. To find significant factors of the injury severity, stepwise logistic regression was used to analyze the data of traffic accidents during the years 2006~2008 in Hlj Province.

Materials and methods

The traffic data used in this study were obtained from Hlj Provincial Department of Public Security Traffic Administrative Bureau Data System. Data about time, vehicle, driver, and environment were extracted from the system. Fatigue-related accidents were picked out from the system and researched in this study. According to the casualties and property loss in the accidents, accident severity was categorized into three groups: fatal, serious and slight.

In the study, contingency tables were constructed to examine the factors distribution according to each potential factor variable, which were used to assess the association between accident severity and the factors. And also the stepwise logistic regression was used to identify significant factors affecting the injury severity of fatigue-related accidents. Factors studied in this paper include human, road, environment, accident type, safety, vehicle and site.

Results

Applying logistic regression analysis to the data of accidents caused by driver fatigue, fifteen factors are determined to have a significant association with the injury severity of the fatigue-related accidents. Detailed results are shown in Tab. 1. The period from 0:00 to 5:59 shows the highest risk for fatal accidents caused by driver fatigue, while the lowest risk period is from 6:00 to 11:59. Besides, the period from June to August has the lowest risk, while the period from December-February and the period from September-November have a higher risk. Fatal accidents caused by driver fatigue are more likely to occur on roads without good lighting at night time. Drivers with less than 2 years of driving experience are more likely to be involved in fatal accidents. Driving on the straight road segment has a lower risk for the occurrence of fatal accidents, while driving both on the horizontal curve and vertical curve segments have higher risk. There is also greater risk while driving on the road in the mountain area or hilly region than in the plain area. Driving in the bad weather days, such as rainy day, snowy days, and foggy days, has much higher risk for fatal accidents than in good days. Giving the accident type, side impact, rear-end collision and bump fixation matter have a higher risk of fatal injury while frontal impact and scrape have a lower risk. Accidents occurred on the second-class highway have much more fatal injury, on the contrast, expressway, first-class highway, third-class highway and below have less fatal injury accidents. On the aspect of speed limit, the higher speed limit, the more severe accidents are, that is above 80 km/h having the highest risk. Road without the central reserve have higher risk for the fatal accidents. If roads have bad condition, such as overflow, ice-snow covered, bumpy, the probability of fatal accidents will be higher. The involvement of heavy trucks and buses has a much higher risk of fatal injury. The number of vehicles involved in fatigue-related accidents has a great association with the injury severity. The more vehicles involved, the more severe the accident is, single vehicle, double vehicles, multiple vehicles. Drivers using seat belt have lower risk of being involved in fatal accidents than those without using seat belt.

Discussion

This study analyzed all of the vehicle accidents occurring during the 3-year period from 2006 to 2008 in Hlj province. Data of fatigue-related traffic accidents were extracted in order to find the high risk factors affecting the injury severity of such accidents. On the basis of the results obtained in previous section, time of the accident was identified to be an important factor which could increase the risk of fatal accidents. In particular, the period from 0:00 to 5:59 has the highest risk for

such fatal accidents. This is because during this period people should have enough sleep, according to the physiological rhythm of people, but they have to be in the car rather than in the bed. So, drivers during this period are easy to become sleepy. It is too late to take any measures before the accident occurs while the vehicle is still with high speed. Thus, it will be very severe once the accident happens. Besides, night-time driving without good street lighting is another high risk factor. The first reason is that in this condition drivers need to always keep their eyes wide open in order to avoid accidents or not get lost, which will make them tired quickly. And the second is that the darkness will reduce the right judgement of drivers due to decreased vision. Drivers with less than 2-years of driving experience have the highest risk for the fatal fatigue-related accidents. Due to lack of operational experience, inexperienced drivers are prone to be nervous and take the wrong measures when they are in face with dangerous conditions, which will increase the probability of fatal accidents.

Tab. 1 Adjusted odds ratios in stepwise logistic regression analysis

Factors	O.R.	Factors	O.R.
Time of the accidents		Accident type	
0:00-5:59	2.109	side impact	1.029
Month		rear-end collision	1.402
December-February	1.281	bump fixation matter	2.107
September-November	1.010	Others	2.199
Streetlight condition		Road cross section	
no lighting at night time	2.991	without the central reserve	1.552
Road alignments		Road grade	
Horizontal curve	1.638	second-class highway	1.042
vertical curve	6.541	Road condition	
Terrain		Overflow	1.520
hilly region	1.620	Ice-snow covered	2.153
mountain area	2.269	Bumpy	1.316
Weather		No seatbelt use	3.547
Rainy	1.020	Speed limit (km/h)	
Snowy	1.515	41-80	1.025
Foggy	1.516	⩾80	2.742
Driving years		Vehicle type	
⩽2	3.081	Buses	1.221
Number of vehicles involved		Heavy truck	3.450
double vehicles	1.635		
multiple vehicles	3.705		

The results also show that people driving both on the horizontal curve road segment and on the vertical curve road segment have much more risk for fatal accidents than on the straight road segment, especially the vertical curve road segment having the highest risk. This is probably because drivers on the vertical curve or the horizontal curve road segment do not have good sight distance. Their declining alertness will exacerbate the bad condition, which could result in serious accidents. Another condition is that driving on the roads in the hilly region or mountain area is prone to be involved in fatal accidents. As we can see, vehicles will usually roll violently and do great harm to passengers' lives.

Vehicle type is also an important risk factor for fatigue-related accidents involving buses or heavy trucks exhibiting much higher risk of fatal accidents. This is because much more people will be involved in an accident once there is a bus to be involved in, which will increase the probably for fatal or serious injury. And besides, heavy trucks are at greatest risk than any other kinds of vehicles because they all have great masses and are hard to be braked. Once they collide with smaller vehicles, they usually maintain undamaged, while other vehicles yield serious deformation, reducing the survival chances of drivers. The number of vehicles involved in the accident is also another risk factor affecting the injury severity. The more vehicles involved in an accident, the more people to be involved which in turn increases fatal injury occurrence.

The results also show speed and road type to be important factors. Higher speed limits on road imply higher speeds of vehicles on road. So, it is more probable that fatal accidents happen on road with high speed limits. However, expressways do not have the highest risk for fatal accidents, but the second-class highways do. This is probably because second-class highways in HLJ account for the most proportion of all roads, and traffic volumes on these roads are usually heavy. Besides, expressways usually have favorable safety facilities, such as guardrail and median strip, keeping drivers away from serious accidents. That is also why accidents occurred on the roads with the central reserve have lower risk of fatal injury. As we know, the function of seatbelts is to protect drivers away from serious injuries. So, drivers involved in an accident without seatbelt use have much more probability of fatal injury.

The weather of the accidents seems to be related with the occurrence of fatal of severe fatigue-related accidents. There may be more fatal accidents in bad weather days, such as rainy, foggy, or snowy days. This is most largely because that bad weathers increase the difficulties of driving and severity of accidents. The same condition applies to driving on the of roads with bad conditions, such as overflow, ice-snow covered, increasing the wet traction of roads. As we know, the period from December to February in HLJ is winter, coldest and most snow and ice on the roads, which will lead to greater number of accidents, and increase the probability of fatal accidents. Side impact, rear-end collision, and bump fixation matter have much higher of fatal injury. This is probably because of the collision point of vehicles. The side and back of vehicles are the most fragile, once vehicles collide with each other at these parts, the consequences will usually be serious.

Although fatigue-related accidents account for less proportion of all accidents, the severity of them is much higher. Because once the drivers get asleep when they drive at a high speed, they don’t even have any time to take measures before the vehicles collide with each other. More and more efforts have been done to prevent fatigue-related accidents and keep drivers away from dangers. Identifying the high risk factors of fatal fatigue-related accidents helps prevent the occurrence of drivers’ fatigue and improve road safety conditions.

Acknowledgements

This work was financially supported by the National Natural Science Foundation of China (51178149).

References

[1] Yuanchang Xie, Kaiguang Zhao, Nathan Huynh. Analysis of driver injury severity in rural single-vehicle crashes[J]. Accident Analysis and Prevention, 2012, 47: 36-44

[2] Kelvin K.W. Yau, H.P. Lo, Sherrice H.H. Fung. Multiple-vehicle traffic accidents in Hong Kong[J]. Accident Analysis and Prevention, 2006, 38(6): 1157-1161

[3] Kelvin K.W. Yau. Risk factors affecting the severity of single vehicle traffic accidents in Hong Kong[J]. Accident Analysis and Prevention, 2004, 36(3): 333-340

[4] Parviz A. Koushki, Mahmood A. Bustan, Nabil Kartam. Impact of safety belt use on road accident injury and injury type in Kuwait[J]. Accident Analysis and Prevention, 2003, 35(2): 237-241

[5] F.F. Saccomanno, S.A. Nassar1, J.H. Shortreed. Reliability of Statistical Road Accident Injury Severity Models[J]. Transportation Research Record: Journal of the Transportation Research Board. 2007, 1542: 14-23

[6] Tarriere. C, MORAN. Y, Steyer. C, BELLOT. D. Accident research and experimental data useful for an understanding of the influence of Car Structural Incompatibility on the Risk of Accident Injury[J]. Proceedings of the 14th International Technical Conference on Enhanced Safety of Vehicles, 1994: 593-610

[7] John C. Milton, Venky N. Shankar, Fred L. Mannering. Highway accident severities and the mixed logit model: An exploratory empirical analysis[J]. Accident Analysis and Prevention, 2008, 40(1): 260-266

doi:10.4028/www.scientific.net/AEF.5.66

Theory of Allocating and Scheduling Resources at Airport Passenger Terminals: A Review

Shaowu Cheng[1,a] , Yaping Zhang[2,b] and Yuanyuan Guo[2,c]

[1]Department of Traffic Information and Control Engineering, Harbin Institute of Technology, Harbin, China, 150006

[2]Department of Traffic Engineering, Harbin Institute of Technology, Harbin, China, 150006,

[a]csw_h@hit.edu.cn, [b]zxlt0905@163.com, [c]hitgyy@126.com

Keywords: Allocating and Scheduling, Resource, Airport Passenger Terminal

Abstract: This paper reviews theory of allocating and scheduling resources at airport passenger terminals, from three aspects, that are method of integrating airport operational data, method of predicting passenger flow at airport terminals and optimization method of allocating and scheduling resources at airport terminals. Directions and challenges of future research are identified.

Introduction

The guarantee of flight safety and punctuality is the basic requirements of the civil aviation convenient transportation, the United States established a clear development goals aiming at the efficiency of air transport in the Next Generation Air Transport System (NextGen): travelers can take off after reaching the terminal within 30 minutes except in very bad weather conditions. In 2010, China's civil aviation passenger traffic exceeded 260 million, ranking in the world second. Management of airport terminals is becoming more and more important.

On one hand, in large hub airport terminals, for passenger traffic increased rapidly, long stranded passengers in check-in, security and other areas can easily lead to group events, which bring a great deal of negative impact to the civil aviation industry. Reduce the residence time in the airport terminal building has two ways: first, increase the terminal passenger service resources; second, according to passenger flow fluctuation at different times, take a reasonable allocation and scheduling of the terminal passenger service resources. Under the premise of not increasing existing resources, the latter is an effective way to resolve the problem of passengers long time stuck.

On the other hand, in the small airport terminal, due to a lack of passenger traffic, coupled with resource allocation and scheduling without considering passenger flow fluctuation, passenger service resources is idle in some periods, which artificially reduced the use efficiency of passenger service resources and increase operational costs of airport terminals. According to passenger flow fluctuation at different periods, taking a reasonable allocation and scheduling of the terminal passenger service resources benefits reducing the operational costs of the airport terminal, and improving the operational efficiency of the airport.

The United States has started to study theoretical problem of the intelligent allocation and scheduling of terminal passenger service resources [1,2]. China just started the research in this field [3]. At present, theoretical research in intelligent allocation and scheduling of the terminal resources fall into three fields: first, method of integrating airport operation data, second, method of predicting passenger flow at airport passenger terminals, third, optimization method of allocating

and scheduling passenger service resource at airport terminals. This paper reviews the theoretical study on these three fields, and identifies directions and challenges of future research in the field of intelligent allocation and scheduling of terminal resource.

Method of integrating airport operation data

In aspect of integrating airport operation data, research focus on the airport information systems integration technology for ensuring safety and efficiency of airport operations. The U.S. Department of Transportation provides guidance for the development of integrated airport information system through the airport cooperative research program [4]. Shen Yang proposed the multi-layer distributed database architecture for integrating airport operation data, based on Web Service and the message queue [5]. Li Ming etc. studied the technology of airport data exchange platform in a distribution heterogeneous environment [6].

The above studies involved in framework of airport information systems, architecture of airport operations database and technology of airport information systems integration, but didn't involve method of needs analysis and logical modeling aiming at data integration for smart allocation and scheduling the airport passenger service resources. Therefore, it is difficult to get the accurate data demand from intelligent allocation and scheduling airport passenger service resources, also difficult to guarantee the logic rationality and query efficiency of data integration. The data integration methods, oriented terminal passenger services resources intelligent allocation and scheduling, in data integration needs analysis and logical modeling method centered, needs to be studied.

Method of predicting airport terminal passenger flow

Evaluation index of airport terminal operation efficiency and service level include available space for per passenger, passenger queuing time in a key part of business process and the total time required by a passenger departure process. Values of these indices are determined by the variation of airport terminal passenger flow. Accurately predicting airport terminal passenger flow and reasonably allocating and scheduling terminal passenger service resources in accordance with the terminal passenger flow fluctuations, can ensure that values of these indices are not affected by passenger flow fluctuations. Therefore, airport terminal passenger flow is basis of allocating and scheduling terminal passenger service resources.

At present, there are two methods forecasting the airport terminal passenger flow. One method is based on the data obtained from manual counts [7], using of mathematical statistical methods to obtain the probability density function of passenger's stranded time at airport terminal, and to estimate passenger number reaching at terminal in different periods of a day. Another method use flight scheduling data, check-in passenger's number distribution, and flight operations data, by simple data statistics, to establish passenger flow distribution model with one week cycle [8]. The two forecasting methods are based on the assumption that passenger flow distribution repeats at constant cycle.

In fact, with air transport demand change, passenger flow changes on the time scale of the year, seasons, months, weeks, days and hours, has not only periodicity but also randomness. The passenger flow forecasting method based on assumption that passenger flow distribution cyclically changes, ignores randomness of terminal passenger flow changes, and cannot reflect the complexity of terminal passenger flow fluctuation. Research is required for prediction method of airport terminal passenger flow, considering both periodicity and randomness characteristics of airport terminal passenger flow fluctuation.

Optimization method of allocating and scheduling resource of airport passenger terminals

Research on terminal passenger service resource allocation and scheduling focus on resource scheduling problem of a part of airport business process (such as parking bays scheduling [9], check-in counter scheduling [10], baggage carousels scheduling [11]) and the optimization methods of key index about airport terminal operations service levels (such as lower check-in aspects waiting time of passengers [12], reducing the boarding process time [13]).

In fact, simply optimizing a part of passenger service process, often results in blockage of the downstream parts [14], for example, too fast passenger flow at check-in areas will result in traveler strand at security control areas. Therefore, the optimization of allocation and scheduling resources should consider airport business process as a whole. At present, optimization methods of terminal passenger service resource allocation and scheduling include mathematical programming method and process simulation method. Application scope of mathematical programming method is restricted, because it assumes that passenger flow satisfies some probability distribution, and requires necessary simplification of the model, [10]. Therefore, process simulation and optimization, with target to improve overall performance of terminal passenger service process, become a main optimization method of allocating and scheduling airport terminal resources [15,16].

At present, the process simulation and optimization method to improve overall performance of airport terminal passenger service process requires a number of simulation test, with parameter values of each simulation test set by person's experience, and with lack of scientific basis. In addition, it is impossible for process simulation to traverse all possible combination of resources, because of the "combinatorial explosion" problem. Therefore, it is necessary to develop an intelligent method of setting simulation parameter values, and to establish an intelligent optimization method of allocating and scheduling airport terminal resources.

Directions of future research

The main research direction of airport terminal resource allocation and scheduling theory is to factor improvement of passenger service levels and airport terminal operation efficiency, airport data integration, passenger flow forecasting and baggage demand prediction, resource allocation and scheduling, as well as passenger service process simulation and optimization into a unified theoretical framework, and to reveal quantitative relationship among airport operational information, passenger flow, baggage demand, resource allocation and scheduling, passenger service levels and operational efficiency, and establish a theory system of intelligent allocation and scheduling of airport terminal resources, with airport operational data integration on a basis, and with passenger flow forecasting and passenger service process simulation and optimization as a core technology. To achieve the above objectives, research for following theoretical issues is required.

Data integration method of intelligent allocation and scheduling of airport passenger terminal resources. According to data demand of passenger flow prediction and business process simulation & optimization, taking into account efficiency of data querying and future expansion capabilities of data integration , build the logic model of data integration for intelligent allocation and scheduling of airport passenger terminal resources, using data warehouse modeling theory, verify the logical model and improve it by testing data query, and lay theoretical foundation for implementing a data warehouse used to allocate and schedule airport passenger terminal resources.

Information fusion method of predicting passenger flow at airport terminals. Predict variation of passenger flow at airport passenger terminals, fusing ticket booking information and passenger flow monitoring information, based on nonlinear modeling theory such as BP neural network, theory of chaotic time series etc.

Warning method of passenger flow anomaly at airport terminals. Set up a 'normal' value for passenger flow at distinctive period, and then difference between the real-time monitoring passenger flow and the "normal" value of passenger flow at corresponding period, is used as indicators to evaluate state of passenger flow, and determine threshold of passenger flow anomaly by experiment method.

Prediction method of passenger baggage demand. Airport terminal passenger baggage demand is closely related to passenger flow at airport terminals. Using passenger flow monitoring data and passenger baggage historical data obtained from departure system as data of training neural network, establish a BP neural network model to predict passenger baggage demand.

Intelligent simulation optimization method of airport passenger terminal resource allocation and scheduling. Based on dyeing time Petri net, describe logical relationship and information flow among business activities, allocation and scheduling plan of resources used by business activities at airport terminals, as well as coordination mechanism between passenger departure process and baggage handling process. Design discrete event simulation algorithm of passenger service process at airport terminals, using the Three-Phase approach. Optimize resource allocation and scheduling plan for each simulation run, based on genetic algorithm.

Remarks and conclusion

This paper reviews theory of allocating and scheduling resources at airport passenger terminals, from three aspects, that are method of integrating airport operational data, method of predicting passenger flow at airport terminals and optimization method of allocating and scheduling resources at airport terminals. The main direction of future research is to factor improvement of passenger service level and airport terminal operation efficiency, airport operational data integration, passenger flow prediction and baggage demand prediction, resource allocation and scheduling, as well as passenger service process simulation and optimization into a unified theoretical framework, and establish a theory system of intelligent allocation and scheduling of airport terminal resources, with airport operational data integration on a basis, and with passenger flow forecasting and passenger service process simulation and optimization as a core technology. Challenges of future research include:

(1) How to describe data demand of airport terminal passenger flow prediction and business process simulation & optimization, and build logical data model to meet the demand.
(2) How to build quantitative relationship among passenger flow fluctuation, flight ticket booking information, flight scheduling, and historical passenger flow information.
(3) How to identify disturbance factors and cycle of passenger flow fluctuation, and determine threshold of potential passenger flow anomaly.
(4) How to describe collaborative mechanisms among passenger service processes and build a formal model of resource allocation and scheduling plan, and how to design intelligent simulation optimization algorithm for airport passenger terminal resource allocation and scheduling.

Acknowledgements

This research is funded by National Natural Science Foundation of China (Grant No. 61179069) and Heilongjiang Province Natural Science Foundation of China (Grant No. E201114).

References

[1] F. Jaehn, Solving the flight gate assignment problem using dynamic programming, Zeitschrift für Betriebswirtschaft, 10(2010) 1027-1039.

[2] M. Saffarzadeh, J.P. Braaksma, Optimum design and operation of airport passenger terminal buildings, Journal of the Transportation Research Board, 1703(2000) 72-82.

[3] M. Ehrgott, B. Naujoks, T.J. Stewart, J. Wallenius(eds.), Multiple Criteria Decision Making for Sustainable Energy and Transportation Systems, 1st ed. , Springer, Berlin, 2010.

[4] C. Stocking, J. DeLong, V. Braunagel. T. Healy and S. Loper, Analysis and Recommendations for Developing Integrated Airport Information Systems, Contractor's Final Report for ACRP Project 1-03, Submitted (2008).

[5] Y. Shen, Web service-based architecture of airport operation database system, Journal of Value Engineering (in Chinese), 5(2011) 154-155.

[6] M. Li, S.Y. Zhang, X.J. Zhao, Design and implementation of information integration for airport based on data exchanging platform, Journal of Science Technology and Engineering(in Chinese), 20(2009) 6235-6238.

[7] K. Wonkyu, P. Yonghwa, J.K. Byung, Estimating hourly variations in passenger volume at airports using dwelling time distributions, Journal of Air Transport Management, 10(2004) 395-400.

[8] C.V. Robertson, S. Shrader, D.R. Pendergraft, L.M. Johnson, K.S. Silbert, The role of modeling demand in process re-engineering, in: Proceedings of the 2002 Winter Simulation Conference(WSC'02), IEEE Computer Society Press, New York, 2002, pp.1454-1458

[9] S.Y. Yan, C.H. Tang, A heuristic approach for airport gate assignments for stochastic flight delays，European Journal of Operational Research, 2(2007) 547-567.

[10] C.Y. Liu, Z.N. Deng, J.J. Zhang, Research on check-in problem in airport terminal building, in: Proceedings of 2007 Control and Decision Annual Conference of China(in Chinese), Control and Decision Press, Shenyang, China, 2007, pp.789-792.

[11] X. Lu, J.F. Zhu, X.W. Tang, Airport Luggage process modeling and simulation, Journal of System Simulation, 14(2008) 3876-3880.

[12] C.A. Chung, T. Sodeinde, Simultaneous service approach for reducing air passenger queue time. Journal of Transportation Engineering, 1(2000) 85-88.

[13] H.Van Landeghem, A. Beuselinck, Reducing passenger boarding time in airplanes: A simulation based approach, European Journal of Operational Research, 2(2002) 294-308.

[14] I.E. Manataki, K.G. Zografos, Assessing airport terminal performance using a system dynamics model, Journal of Air Transport Management, 16 (2010) 86-93.

[15] Liene Freivalde, Lelde Lace, Improvement of passenger flow management in an airport terminal, in: Proceedings of the 5th international Science Conference Business and Management, Vilnius, Lithuania, 2008, pp.659-664.

[16] K. C. James, Performance improvement studies of an airport terminal using discrete-event simulation, Journal of Computer Modeling and New Technologies, 3(2009) 58-64.

doi:10.4028/www.scientific.net/AEF.5.71

Study on the Scale Determination of Urban Rail Transfer Station

Yuping Wang [1,3, a], Yaping Zhang[3,b], Huizhi Xu [2,3,c]

[1] The Preparation Research Centre, Harbin Urban and Rural Planning Bureau, Harbin, 150000, China [2] Harbin Metro Group Corporation Ltd, Harbin, 150000, China,[3] Harbin Institute of Technology, Harbin, 150090, China

[a] wangyuping004997@163.com,[b] 895679648@qq.com, [c] 353812396@qq.com

Key words: urban rail transit, transfer station, facilities, scale

Abstract. As the major distributing center and intermediate transit point, the scale of transfer station in urban rail transit system directly affects the operational efficiency and overall cost of the entire system. So, accurately controlling the scale of transfer station becomes one of the most important aspects in improving service level and reducing the overall project cost. On the basis of summarizing the method on determining the scale of transfer station both home and abroad, the paper describes the role of the various facilities in rail transfer station, and illustrates the problems of our rail transfer station. Following the above discussion and investigation, the sizes of typical transfer station facilities are discussed and improved (e.g. vertical elevator). Taking the Longjiang Street station as an example, the proposed methods and models are verified and the analysis result shows that this transfer station should use parallel transfer mode.

Introduction

With the improvement of urbanization level, the serviceability of public transport facilities is becoming harder and harder to adapt to the increasing travel demands. Thus, more and more cities in China begin to turn their attention to urban rail transit system, which has the characters of high speed, large volume and high punctuality rate. However, because of the particularity, the construction cost of the urban rail transit is huge. As the important node for passengers to gather and leave, the scale of transfer station will directly impact the operational efficiency and overall cost of the entire system. So, accurately controlling the scale of transfer station becomes one of the most important aspects in improving service level and reducing the overall project cost.

Vladimir[1] established 0-1 Linear Programming model, which was suitable for the determination of airport scope. Bates[2] introduced the function and form of the transfer facilities, elaborated the right scale of each kind of transfer station, and discussed the improvement measures of transfer facilities. Dickins[3] gave some recommendations on the location, layout and scale of inner facilities, and summarized the factors that affected efficient use of the facilities by investigating the transit rail systems of 51 cities in Europe and South America. Miclea[4] studied the scale of the pedestrian facilities underground from the security point of view, and proposed the minimum design standards meeting the safety need of every facility. Shen Jingyan[5] analyzed dynamic variation of passengers on the platform, concluded the distribution graphics and related parameters, studied the reasonable scale of platform, gave simple calculation method. Tan Yu[6] studied the demands of facilities, the transfer form, and the connection between rail transit and other transportation from the single station point of view. Wang Xiaorong[7] proposed implementation doctrine of public zone, platform and equipment rooms.

Following the above discussion, the sizes of typical transfer station facilities are discussed and improved (e.g. vertical elevator, automatic fare collector). Taking the Longjiang Street station (connecting Harbin Metro Line 1 & Line 5 together) as an example, the proposed methods and models are verified and the analysis results show that this transfer station should use parallel transfer mode.

Inner facilities in transfer station

In principle, transit rail station consists of waiting room, platforms, station buildings, passageways and stairs. The platform is the most basic part which must be set. Other parts usually should be set, and sometimes they might be simplified for some special condition or meeting the function.

Waiting room. The function of waiting room is guiding the passengers along the way from platform to gateway quickly, safely and conveniently. It is transitional space for passengers boarding. So, it is necessary to set Automatic Fare Collection System and query facilities. Besides, there are other facilities in the waiting room need to be set, such as equipment and management room, and lifting equipment.

Platform. The platform is the site providing boarding and waiting space for passengers, and it is one of the most important parts in the rail transit system facilities. The platform could be set either above, under or parallel to the waiting room, and can be classified into two kinds, island platform and side platform, according to the layout form of the station.

Automatic Fare Collection System. AFC can realize the processes of booking, checking, and charging automatically, which would not only reduce the time of passengers' ticket into station, but also improve the efficiency of the station management to some extent. The scale of AFC should meet the need of serving passengers. It is should also be avoided too much configuration, which would result in a waste of construction costs.

Vertical mobile facilities. Vertical movement facilities include stairs, escalator, elevator and incline, which are mainly set up at the gateway and fee area. The incline is usually set up to serve the handicapped and people with big luggage[8].

Determination models for transfer station scale

Determination of platform scale. The size of the platform refers to the width, length and height. The length should at least meet the need of train stopping. It can be calculated by formula (1).

$$L = L_0 + L_u \tag{1}$$

L is the length of platform, L_0 is the length of marshalling in the future, and L_u is uncertain distance of the train stopping allowed, usually taking 4 to 10 meters.

The width of platform is determined by the passenger volume during peak hours in the future, platform type, layout of station house, stairs, escalator, and so on, meeting the least width.

Platform is divided into island and side. If the width of side platform is B_c, the width of island platform will be as follows.

$$W_d = 2B_c + n \cdot W_z + W_l \tag{2}$$

W_z means the width of an upright, W_l means the width of the stair or the escalator, and n is the number of uprights in the direction of platform cross section. Before the train arriving, the main function of the platform is waiting. Assuming passengers are uniformly distributed, not occupying the width of safety area[5]. Then the width of platform can be calculated as follows:

$$W_{c1} = (Q_{in} + Q_{transfer})\beta / (q \cdot L\rho_1) + W_a \tag{3}$$

W_{c1} means the calculated width of platform before the train arriving, Q_{in} means the passenger volume pulling in during peak hours, and $Q_{transfer}$ means the passenger volume need to transfer. β is the peak hour factor, usually taking 1.2 to 1.4. q is the rate of train flow, relevant to departure interval time. L means the effective length of the platform, ρ_1 is the standing density of passengers before the train arriving, and W_a is the width of safety area. When the train arrives, passengers getting on will crowd at both sides of the door. Then the length of passengers on the platform equals to the effective length of platform subtract sum of all doors' width. The width of waiting area on the platform when the train arriving is as follows:

$$W_{c2} = (Q_{in} + Q_{transfer})\beta / q \cdot (L - nb)\rho_2 + W_a \tag{4}$$

n means the number of marshalling, b is the width of each door, and ρ_2 means the standing density of passengers when the train arriving. The difference between the widths before the train arriving and when arriving, can be seen as the width of passageway for passengers getting off the train.

$$W_{c3} = W_{c1} - W_{c2} \tag{5}$$

Usually the width of side platform should meet the following conditions. That is:

$$W_{c3} = W_{c1} - W_{c2} \geq 1.0, \quad W_{c1} \geq W_{c2} + 1.0 \tag{6}$$

The transfer style can be classified into three kinds: side with side, island with island and island with side, just as figure 1 to figure 3 show. Assuming that there are two lines interweaved together, Line M and Line L. The width of platform transferring on the same layer can be divided into six parts: the width of waiting area for Line M uplink, the width of waiting area for Line L uplink, the width of waiting area for Line M downlink, the width of waiting area for Line L downlink, the width of stairs or escalator and the width of uprights. The passenger volumes are different for different waiting areas. The width of platform for island with island transfer style is as follow:

$$W_1 = (Q_{MU} + Q_{MD} + Q_{LU} + Q_{LD})\beta / (q \cdot L\rho_1) + 4W_a + nW_z + 2W_l \tag{7}$$

In a similar way, the width of platform for island with side transfer style is as follow:

$$W_2 = (Q_{MU} + Q_{MD} + Q_{LU} + Q_{LD})\beta / q \cdot (L\rho_1) + 4W_a + nW_z + 3W_l \tag{8}$$

Q_{MU} refers to passenger volume for Line M uplink, Q_{MD} refers to passenger volume for Line M downlink, Q_{LU} refers to passenger volume for Line L uplink, and Q_{LD} refers to passenger volume for Line l downlink.

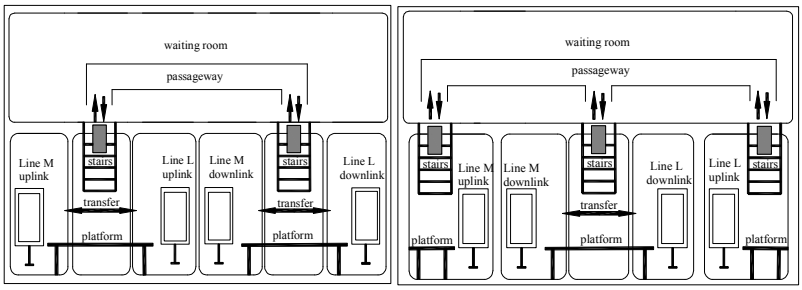

(a) island with island W_1 (b) island with side W_2

Figure 1 Parallel transfer on the same platform

There is another transfer style on the different layers, just as figure 2 shows. The widths of platform transferring on different layers can be calculated as follows:

$$W_3 = (Q_{MU} + Q_{LU})\beta / (q \cdot L\rho_1) + 2W_a + nW_z + W_l \tag{9}$$

$$W_4 = (Q_{MD} + Q_{LD})\beta / (q \cdot L\rho_1) + 2W_a + nW_z + W_l \tag{10}$$

W_3 refers to the platform width on the second floor, and W_4 refers to the platform width on the third floor. The final width of the platform should take the maximum of the two widths.

$$W_5 = \max\{W_3, W_4\} \tag{11}$$

Besides, there is another kind of transfer style, node transfer. There are three layers in such station, and different rail lines are located at different layers, linked with each other by stairs or escalator, just as figure 3 shows.

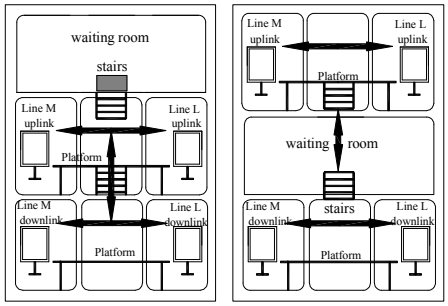

Figure 2 Parallel transfer on the different floor layers

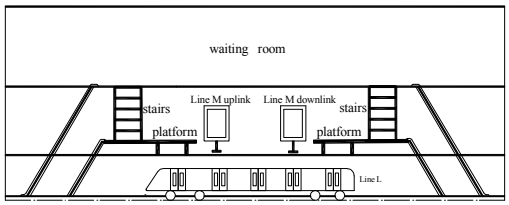

Figure 3 Platform for node transfer style

Width of platform on the second floor underground:

$$W_6 = (Q_{MU} + Q_{MD})\beta / (q \cdot L\rho_1) + 2W_a + 2W_l \tag{12}$$

Width of platform on the third floor underground:

$$W_7 = (Q_{LU} + Q_{LD})\beta / (q \cdot L\rho_1) + 2W_a + nW_z + W_l \tag{13}$$

Determination of vertical mobile facilities scale. The number and width of stairs or escalators should meet the requirements for timely evacuation. They are also connected with delivery capacity and passenger volumes during peak hours in the future[9].

The width of stairs should be determined by the passenger volumes both getting on and off the trains, on the basis of meeting disaster prevention requirements.

The width of stairs shown in figure 1 can be calculated as follows:

$$W_l = (Q_{lU} + Q_{lD})\beta / NC + W_f \tag{14}$$

W_l is the width of stairs, Q_{lU} and Q_{lD} are passenger volumes for uplink and downlink respectively. C is the capacity of per meter of stair for passenger both up and down. β refers to peak hour factor, usually taking between 1.2 and 1.4, N is the number of stairs, and W_f is the width of stair railing.

The number of escalators can be calculated by the following formulas.

$$N_U = Q_U\beta / Ck, \quad N_D = Q_D\beta / Ck \tag{15}$$

N_U, N_D are the number of escalators for uplink and downlink respectively. Q_{IU} and Q_{ID} are passenger volumes for uplink and downlink. k is the utilization of the escalator per hour, usually taking 0.8.

Determination of AFC scale. The main equipments of AFC are the fare gates for getting in and out of the station. They are determined according to the passenger volumes during peak hours, just as follows.

$$N_{IN} = INT[Q_{in}\beta / C_I], \quad N_{OUT} = INT[Q_{out}\beta / C_O] \tag{16}$$

N_{IN}, N_{OUT} are the number of fare gates for in and out respectively. Q_{IN}, Q_{OUT} are the passenger volumes getting in and out of the station. C_I, C_O are ticket checking capacities.

Case

Taking Longjiang Street Station in Harbin for example. The designers designed two kinds of transfer styles for the station, parallel transfer on the same side of platform and cross-shaped node transfer on different layers, just as figure 4 shows.

The passenger volumes of Line one and Line five are 33500 persons per hour and 20900 persons per hour respectively. Assuming that it takes B type vehicle, with four gates on each side, and 1.2 meters for each gate. And the width of each escalator is one meter, and the utilization is 0.8. The utilization of ticket vendors in the station is sixty percent

Platforms of different transfer styles have different length, width and escalator number, just as Tab. 1 and Tab.2 show. From the result, it can be concluded that the scale of platform transferring on the same side is less than the scale of platform transferring through node on different layers. And besides, there are only two layers of floors in the platform transferring on the same side. So the paper recommends the former as the station style in Longjiang Street Station.

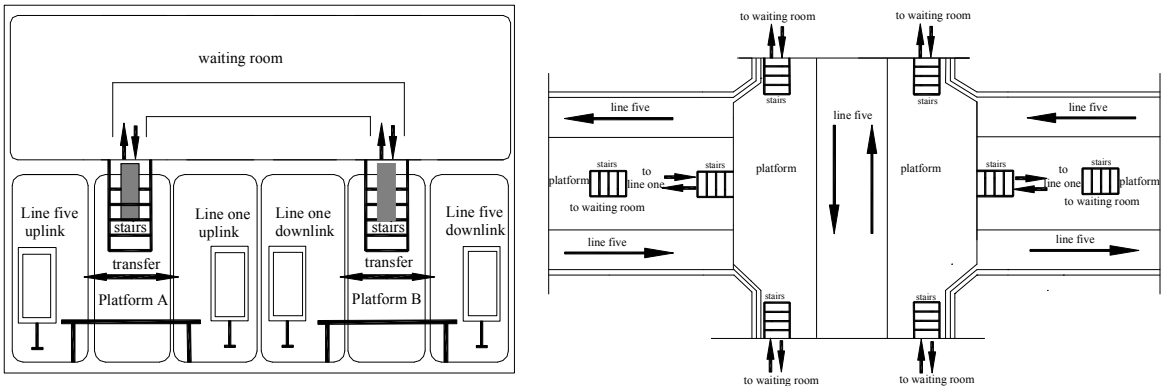

(a) parallel transfer (b) cross-shaped node transfer

Figure 4 The station style in Longjiang Street Station

Conclusion

The paper proposes scale determination methods of typical facilities in transfer station for both parallel transfer and node transfer. The study improves the calculation methods of the sizes for platform, stairs, escalators ticket vendors, and checkers. Taking the Longjiang Street station as an example, the case study proves the validity and operability of the proposed method.

Tab. 1 The scale of facilities for different transfer styles (platform and stairs)

Transfer style	platform		stairs	
	length	Width(with stairs and escalators)	number	width
parallel transfer	96~102	21.15	4	11.1
node transfer	96~102	21.74	8	18.3
	82~88			

Tab. 2 The scale of facilities for different transfer styles (other facilities)

Transfer style	escalator qualities	ticket vendors	ticket checkers
parallel transfer	5	20	17
node transfer	6		

Acknowledgements

The authors would like to thank Harbin Metro Group Corporation Ltd. and Harbin Urban and Rural Planning Bureau for providing the useful data about the rail transit.

References

[1] VlmadimiMrarinao, DnaielSerra, Location of Hubsina Competetitive Envionment[J]. Euorpean Joumal of Operational Research, 2005, 23(3): 121-129.

[2] Bates E. A Study of Passenger Transfer Facilities[J]. TRR, 1998: 662.

[3] Diekins, S.J.Ian. Park and Ride Facilities on Light Rail Transit Systems[J].Transportation, 2001: 23-36.

[4] Miclea. International tunnel fire-safety design practices[J]. ASHRAE Journal, 2007: 50-60.

[5] Shen Jingyan. Simplified Calculation for the Width of On and Off Region of Station Platform[J]. Urban Rapid Rail Transit, 2008, 21(5): 9-13.

[6] Tan Yu. Study on the theory of panning & design for urban rail transit hub[D]. Doctoral Dissertation in Tongji University, 2002: 31-33.

[7] Wang Xiaorong, et al. On the Scale of Subway Stations[J]. Modern Tunnelling Technology, 2008, 45(3): 22-28.

[8] Wang Lihua. Preliminary Approach to Design of Subway Station Building[J]. Northern Communications, 2008, (2): 164-166.

[9] Yao Lan. Design for scale control of subway station[J]. Quality of Civil Engineering and Construction, 2006, (7): 48-51.

doi:10.4028/www.scientific.net/AEF.5.77

Driving Mode at Pothole-Subsidence Pavement Based on Wheel Path & Speed

Yulong Pei[1, a], Chengyuan Mao[1, b] and Mo Song [1, c]

[1] School of Traffic Science and Engineering, Harbin Institution of Technology, Harbin 150090,China

[a]yulongp@263.net, [b]maozhang1982@126.com, [c]07smhit@163.com

Key words: Driving Mode; Wheel Path; Speed; Pavement; Pothole-Subsidence

Abstract. The pavement distress has considerable influence with drivers. Considering the fact that the forms of asphalt pavement potholes, subsidence and cement pavement potholes (collectively defined as pavement pothole-subsidence) are similar and they can influence traffic flow significantly, we put forward to use indexes such as Tangential Diameter Length, Normal Diameter Length, Depth, Lateral distance, etc to describe the characteristics of pothole-subsidence. According to different wheel paths & speed, driving modes was classified into several types, influences of various pothole-subsidence on driving mode and speed was analyzed. By the research, we get that Pothole-Subsidence Pavement significantly influenced the variation of vehicle trajectory , and the relationship between driving speed and driving mode choosing is correlative tightly, the main driving mode choosing influence factor are lane number, driving speed, traffic and the PS' size and figure.

Introduction

The phenomena, such as overloading vehicle and pavement wear fatigue, are inevitable. Unlike shaped crack or dislocation, slight damage of lower degree or less distinctive such as asphalt pavement potholes, subsidence and cement pavement potholes are more likely to be ignored, which however, can influence the safety and efficiency of vehicle operation in various degrees. There exist a great many studies on the emergence and maintenance of asphalt pavement potholes, subsidence and cement pavement pothole at home or abroad[1-3], yet theories about its influence on driving behavior，vehicle trajectory and operation mode of traffic flow are rarely published. On the base of analyzing different aspects such as the figure and location of road potholes or subsidence as well as traffic flow we analyzed their influence on driving mode and traffic flow， thus we provided theoretical basis for further study of actual urban road capacity and mark-setting under the circumstance of defective pavement.

Definition of pavement pothole and shape characterization indexes

According to *Urban road* m*aintenance technical specifications* the definitions and concept definitions of asphalt pavement pothole, subsidence and cement pavement pothole are as follows[4]:

Definitions.(1) Asphalt pavement pothole: pothole formed after the loss of pavement materials, belonging to damage of loose class.

(2) Asphalt pavement subsidence: partial pavement subsidence, belonging to damage of deformation.

(3) Cement pavement pothole: holes appeared on the surface of cement panel whose diameters ranged from 25 to 100mm while depths ranged from 1 to 50mm.

Concept Definitions. Asphalt pavement pothole: when the depth of certain pothole reaches 20mm and its area reaches 0.04m^2 it can be demarcated as pothole. For gathered small area pothole, if their distances are less than 0.2m they should be measured together.

Asphalt pavement subsidence: when there are vertical deformations of roadbed and asphalt pavement and the depth of pavement concave is above 30mm it can be demarcated as subsidence.

Cement pavement pothole: partial potholes whose areas are above 0.01m^2 formed due to the fall of coarse aggregate on cement pavement can be demarcated as pothole.

For the convenience of research，we collectively define asphalt pavement pothole, asphalt pavement subsidence and Cement pavement pothole as pavement pothole-subsidence(***PS*** in abbreviation).

Characterization indexes about the figure of *PS* are as follows, shown as fig.1.:

Tangential diameter length (L): Width of *PS* parallel to the driving direction, m

Normal diameter length (W): Width of *PS* perpendicular to the driving direction, m

Depth (D): Height difference between road surface and the innermost of the *PS*, m

Center distance (m_c): Distance between the entrance and the innermost of the *PS*. According to the driving direction, it can be divided into two categories, one is approach center distance (m_c), the other is depart center distance (m_g).

Driving modes on *PS* road section

There are three stages if drivers' discover of the *PS*s: Recognition, Judgment and Execution. According to wheel pathes, driving modes can be classified into three types, shown as fig.2:

Mode 1: Drivers failed to notice *PS* or drivers continued their original driving route. This phenomenon results from following factors:

(1) Drivers' neglect of *PS*s

(2) Discover the *PS*，drivers predicated that tires won't run into *PS*s along original driving route

(3) Discover the *PS* and the fact that tires may run into *PS* along original driving route, drivers determined to pass through *PS*s by means of deceleration.

Mode 2: Drivers discover the *PS*s and its badly influence, so they turned the steering wheel and altered their driving route. Because of the interference of vehicles adjacent sides, it may be impossible to merge into adjacent lanes or perhaps it is not necessary to alter lanes, drivers still drive along original lane or occupied a little part of adjacent lane after slight swing of driving direction, and then back to normal. It may lead to two kinds of consequences as follows:

(1) The distance to the *PS*s may be too short for drivers to adjust driving direction dramatically, or, traffic densities on both sides are too high for drivers to merge into adjacent lanes. Therefore vehicles still run into *PS*s after altering directions.

(2) Vehicles changing direction, and then pass through the road section without running into *PS*s.

Mode 3: Drivers discover the *PS*s which influence badly on driving, and it is available to merge into nearby lanes, drivers merge into adjacent lanes and then came back to normal driving as before.

(1) The distance to the *PS*s may be too short for drivers to adjust driving direction dramatically vehicles may still run into *PS*s at the time of changing lanes or after merging into adjacent lanes

(2) After changing lane vehicles pass though the road section smoothly instead of running into *PS*s.

Research and analysis based on wheel path

We choose 10 *PS*s located in different streets in Harbin for field measurement, which include Huashan Rd. (3),Caiyi Str.(3),Huanghe Rd.(1), Ganshui Rd., Xidazhi Rd.(1) and Zhujiang Rd.(1) and the influence on the road traffic operation was recorded on video. State indicators of investigated *PS* are shown in table1.

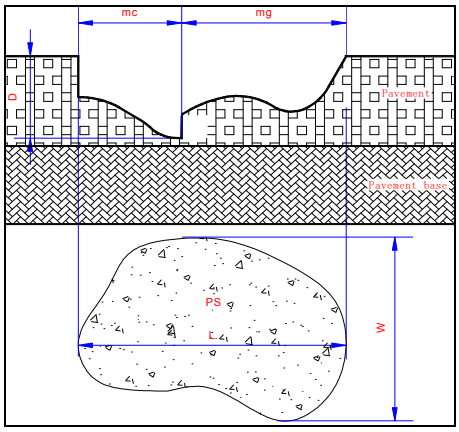

Fig.1 Schematic plot of *PS* pavement

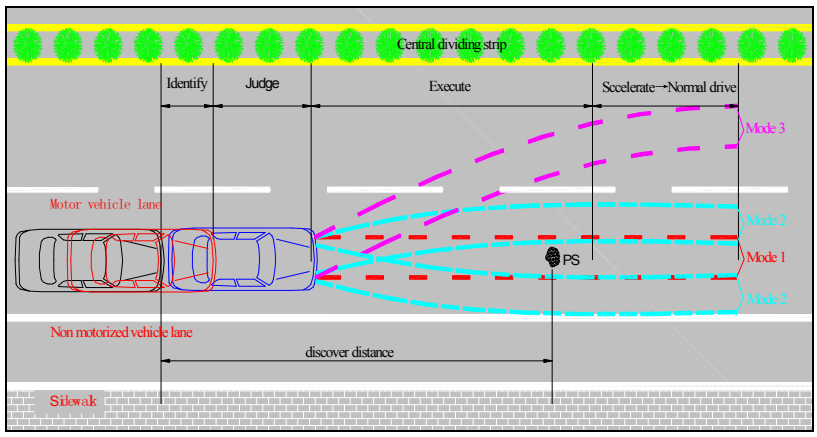

Fig.2 Wheel path of each Driving mode

Table1 State indicators of investigated *PS*

No.	Location	Lane No.	Direction	L (m)	W (m)	D (m)	m_c (m)	m_g (m)
1	Huashan Rd., 40m to the north of Pujiang Rd.	6	North	0.72	1.25	0.06	0.35	0.37
2	Huanghe Rd.,50m to the west of Huashan Rd.	6	West	3.75	0.83	0.03	1.12	2.63
3	Xidazhi Rd., 50m to the south of Jiaohua Str.	6	North	0.68	0.40	0.07	0.35	0.33
4	Xuanqing Str.,30m to the south of Pinggong Str.	6	North	0.22	0.38	0.04	0.10	0.12
5	Huanshan Rd.,80m to the south of Huanghe Rd.	6	North	0.82	0.86	0.05	0.34	0.48
6	Caiyi Str.,30m to the north of Liushun Str.	2	South	1.38	3.22	0.09	0.70	0.68
7	Caiyi Str.,50m to the south of Liushun Str.	2	South	0.42	0.58	0.12	0.23	0.19
8	Caiyi Str.,150m to the north of Gongbin Rd.	2	North	0.15	0.35	0.08	0.08	0.07
9	Ganshui Rd.,30m to the west of Tianshun Str.	4	East	0.48	0.35	0.08	0.20	0.28
10	Zhujiang Rd.,200m to the west of Songshan Rd.	4	West	0.88	0.82	0.02	0.38	0.50

(2) Traffic survey on *PS* pavement

We adopt AutoScope-2004 video detection system aided by artificial judging to investigate in the surveyed road section. And we acquired information including traffic volume, lane occupation ratio, vehicle types, speed, headway, vehicle density and so on. The survey result is shown as table2.

Table2 The Traffic & Speed in each mode

NO.	Traffic(pcu/h)					Average Speed (km/h) At the SP spot				S_l(%)
	M1	M2	M3	Totol	Original	M1	M2	M3	Totol	
1	75	177	130	382	33	16.41	24.97	28.88	24.62	24.62
2	71	197	112	380	43	14.29	36.20	40.40	33.34	33.34
3	103	190	84	377	36	28.70	32.17	32.37	31.26	31.26
4	76	84	9	169	35	28.28	29.58	30.25	29.03	29.03
5	57	246	27	330	24	15.97	18.05	21.49	17.97	17.97
6	2	26	75	103	22	8.88	9.89	16.05	14.36	14.36
7	14	59	35	108	20	14.14	16.27	17.95	16.54	16.54
8	33	60	14	107	26	20.40	23.09	23.76	22.35	22.35
9	22	108	14	144	21	15.60	16.77	17.41	16.65	16.65
10	56	180	34	270	28	11.21	20.64	22.74	18.95	18.95

Note: Where M_i is mode i; Traffic is only the traffic on the *PS* lane in an hour; S_l is the rate of decrease speed, $S_l = 1 - V_o / V_a$ Where V_o is the original speed; All cars average speed at the *PS* spot V_a is: $V_a = \sum_{i=1}^{n} T_i * V_i \Big/ \sum_{i=1}^{n} T_i$, T_i is traffic about mode i; V_i is average speed about mode i at the *PS* spot, n is the mode number.

Judging from the driving mode, *PS*s significantly influenced the variation of vehicle trajectory. Almost 78.5 percent of the vehicles altered their driving direction, and 56% drivers chose slightly altering as mode 2 while 22.5% drivers chose changing lanes as mode 3.

As to the decrease of speed,we found that *PS*s can obviously bring down the driving speed whose average rate of descent reached 22.2%.In practical terms, speed descents for mode 1 ,whose rate of descent reached 50.3%, are more distinct than the rest two modes, while relatively the rates of descent for mode 2 and 3 are only 24.3% and 12.5%.Through observation, we made a conclusion on the cause of speed descent, that is a great many vehicles ran into *PS*s and drivers slowed down to ease the turbulence occurring at the same time, and there are still plenty of drivers decelerated for fear of running into *PS*s; Percentage of vehicles running into *PS*s are relatively low for mode 2 and 3 and most vehicles kept larger safety space between the wheels and the *PS*s.

Judging from the relation between characterization index and driving mode along with speed，the influence of *PS*s on vehicle operation can't be determined simply by characterization index, it's the comprehensive reaction of various aspects such as figures and location of the *PS*s, driving speed, driver characteristics, etc. From the curves of each single factor and speed descent, we concluded that there exist significant differences between each curve, while curves of normal diameter length and speed descent are most similar to each other, which indicates that normal diameter length is the most important factors for speed descent on condition that there are slight differences in other factors. The conclusion is shown in fig.3.

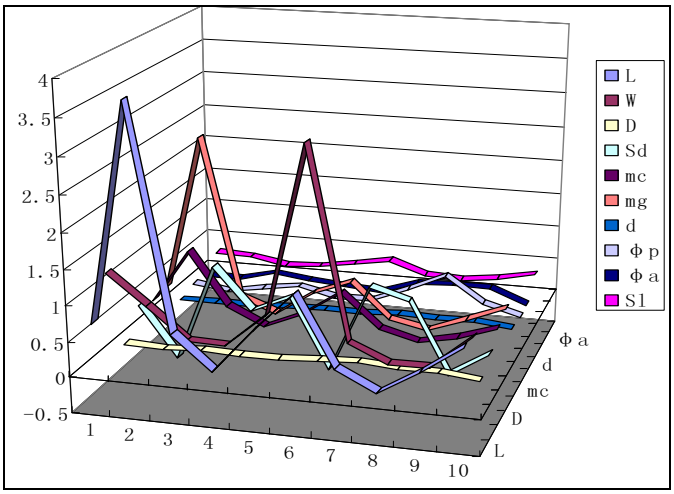

Fig.3 Curves of factors and speed descent rate

Research and analysis based on speed

At the different speed, the vehicle's driving mode is distinguishing. As the speed rising, the traffic in mode1 and mode2 cut down, and the vehicle driving in mode4 rise, which is shown in Table3 and fig.4, and dashed lines in figure 4 are trendlines of M1, M2 and M3.

The reasons are (1) The car running in branch road has lower speed, and the most branch road only has 2 lanes, if its driver discovers the *PS* and he wants to change driving lane, he has to stem against, and if the retrorse lane is busy, there is no choice to driving in mode 3; (2) the car gets across the *PS* running in low speed is more comfortable than high speed.

Conclusions

(1) *PS*s significantly influenced the variation of vehicle trajectory, 78.5 percent of the vehicles altered their driving direction, and 56% drivers slightly altered driving direction while 22.5% drivers changed lanes, and the average rate of speed descent is over 20%.

(2) *PS*s can obviously bring down the driving speed whose average rate of descent is more than 20%, and speed descent in mode 1 is the most obvious of three modes.

(3) The influence of *PS*s on vehicle operation can't be determined simply by characterization index, it's the comprehensive reaction of various aspects such as figures and location of the *PS*s, driving speed, driver characteristics, etc. Relatively speaking, normal diameter length can be the most important factors for speed descent.
(4) The relationship between driving speed and driving mode choosing is correlative tightly, the main driving mode choosing influence factor are lane number, driving speed, traffic and the PS' size and figure.

Table3 The relation between speed and mode choosing

NO.	Speed Original (km/h)	Totol(veh)	Traffic in each Mode					
			M1		M2		M3	
			Traffic(veh)	Rate(%)	Traffic(veh)	Rate(%)	Traffic(veh)	Rate(%)
1	0-20	324	83	25.6	193	59.6	48	14.8
2	20-40	892	265	29.7	421	47.2	206	23.1
3	40-60	765	168	22.0	356	46.5	241	31.5
4	60-80	341	72	21.1	176	51.6	93	27.3
5	>80	48	9	18.8	19	39.6	20	41.7

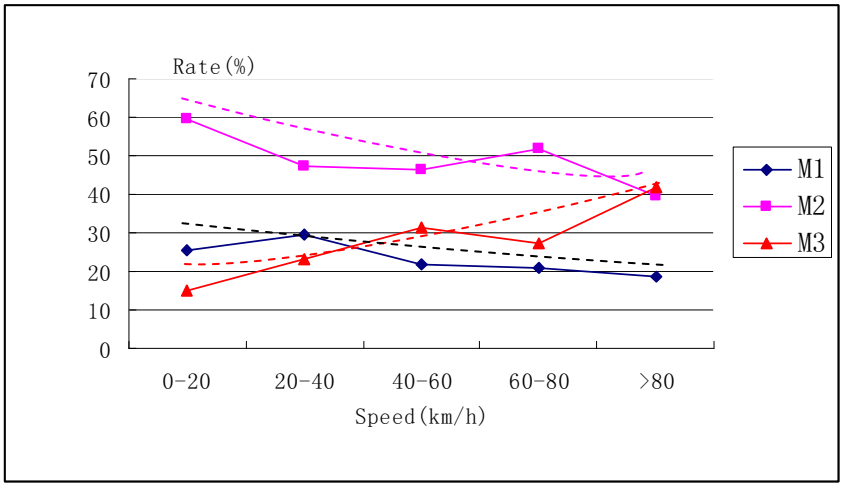

Fig.4 The relationship between Speed and mode choosing

Acknowledgements

This work was financially supported by the National Natural Science Foundation of China (Grant No.51078113 & Grant No.51178149) and National Key Technologies R & D Program of China during the 11th Five-Year Plan Period (2006BAJ18B03-05).

References

[1] Sutter Lawrence Leo. An approach to characterizing materials related distress in portland cement concrete pavements[D]. Michigan Technological University. 2001

[2] Koubaa Amir. A new methodology for assessing the frost resistance of concrete aggregates. University of Minnesota. 1997

[3] Xu Qinghua.Repair Techniques of the Asphalt's Potholes and Simulate Analysis of Computer[D]. Chang'an University.2009

[4] CJJ36-2006.Urban road maintenance technical specifications.2006

doi:10.4028/www.scientific.net/AEF.5.82

Equilibrium model of urban taxi service network based on the integrated service modes

ZHU BAI[1,a], JIAN WANG[2,b]

[1]School of Transportation Science and Engineering, Harbin Institute of Technology, Harbin, China

[2] School of Transportation Science and Engineering, Harbin Institute of Technology, Harbin, China

[a]baizhu1979@yahoo.com.cn, [b]wang_jian@hit.edu.cn

Keywords: taxi service; network equilibrium; cruising taxi mode; dispatch taxi mode

Abstract. This paper proposes an equilibrium model of urban taxi services on network to present the impact of the integrated service modes and the influence of the elastic customer demand distribution on taxi network equilibrium. Based on the cruising service mode, the model can describe how occupied taxis and vacant taxis cruise on network to provide services and search for customers by considering both the expected time cost and ride revenue and the elastic distribution characteristic of customer demand. At the same time, the dispatch service equilibrium problem by researching trip mode choice behavior is also considered. The model can then establish the relationship between customer waiting time and taxi search/waiting time by introducing a taxi-customer meeting function. And moreover, in supply-demand equilibrium, a number of performance measures of the taxis market can be obtained, such as the number of cruising taxis, the number of dispatch taxis and the average customer waiting time.

Introduction

As the urbanization speeds up, people have increasingly paid attention to the trip mode of taxi which is regarded as the important supplementary mode of public transit due to a flexible and speedy service offered by taxi. Especially with the frequent fluctuation of gas price, the increasing attention to environmental protection and the constant occurrence of the supply-demand unbalance problem, it is very important to research the taxi traffic system and advance its operational level.

The research achievements could be divided into two types of model and they were aggregated models and equilibrium models. The relevant researches of aggregated models were that: Douglas (1972) was the precursor of the first studies. He considered a taxi market where taxi service was the cruising one and the fares were scheduled by management department and the entry is free [1]. The relevant researches of equilibrium models based on the network structure were that: Yang and Wong presented a series of models during the years 1997-2011 studying the taxi market in the network of Hong Kong [2].

At present, the literatures published are almost based on a single taxi service mode, either cruising mode or dispatch mode. No models have integrated them at the same time. However, with the advancement of taxis installed GPS, the application of dispatch mode becomes more and more frequently so that the integrated service mode considering the existence of cruising and dispatch modes will be the future development trend.

Based on this, this paper is structured as the followed chapters: the second chapter analyzes the characteristic of the integrated taxi service mode and establishes the probability model of trip mode choice for traveler. The third chapter describes the supply-demand equilibrium state with the elastic customer demand in the taxi market and constructs a equilibrium model of taxi on network. The

next chapter presents the relationship function between the passage waiting time and taxi search/waiting time. The fifth chapter gives the detailed steps of the algorithm to solve taxi model. Finally, the last chapter contains the conclusion and proposes the future extension in taxi field.

The trip mode choice model

Suppose that there are the cruising service mode and the dispatch one existing in the taxi market at the same time. If the total number of taxis on network is Num and the proposition of taxis installed GPS is α, the number of taxis for the cruising service is $Num*(1-\alpha)$ and the number of taxis installed GPS is $Num*\alpha$. The taxis installed GPS can provide not only the dispatch service but also the cruising service.

Suppose that there are two taxi service modes and there is other public transit to be alternative mode chosen by customers on network at the same time.

According to the trip mode choice of travelers, the probability that reflects the split rate of cruising taxi service and dispatch taxi service and other transit modes is followed as:

$$P_{ij}^{rc}=\frac{\exp\{-\theta^{'}h_{ij}^{rc}\}}{\exp(-\theta^{'}h_{ij})+\sum_{r=1.2}\exp(-\theta^{'}h_{ij}^{rc})},i\in I,j\in J. \tag{1}$$

Where P_{ij}^{rc} is the probability to choose a given taxi service mode from zone i to zone j; $r\in R,R=\{1,2\}$, $r=1$ is the cruising taxi service chosen by customer, $r=2$ is the dispatch taxi service chosen by customer; h_{ij}^{1c} is the full travel cost of the customer who chooses the cruising taxi service from zone i to zone j; h_{ij}^{2c} is the full travel cost of the customer who chooses the dispatch taxi service from zone i to zone j; h_{ij} is the full travel cost of the customer who chooses the other transit modes from zone i to zone j, and the structure of h_{ij} used here is from[3]; the value of parameter $\theta^{'}$ reflects the degree of uncertainty in customer demand and taxi services from the perspective of customers.

Here, the full travel cost function of customer who chooses the cruising taxi service is followed as:

$$h_{ij}^{1c}=F_0+\pi t_{ij}+\lambda_1 t_{ij}+\lambda_2 w^{1c} \tag{2}$$

Where F_0 is the taxi flag-drop charge and π is the variable charge per unit ride time; t_{ij} is the travel time via the shortest route from origin zone i to destination zone j; $F_0+\pi t_{ij}$ is the fare of a taxi ride from zone i to zone j; λ_1 and λ_2 are the customers' monetary values of unit in-vehicle time and waiting time respectively; w^{1c} is the waiting time of customer who chooses the cruising service; $\lambda_1 t_{ij}$ and $\lambda_2 w^{1c}$ are the in-vehicle travel cost and waiting cost for the cruising taxi service respectively.

Here, the full travel cost function of customer who chooses the dispatch taxi service is followed as:

$$h_{ij}^{2c}=F_0+\pi t_{ij}+\lambda_1 t_{ij}+\lambda_2 w^{2c}+u \tag{3}$$

Where $F_0 + \pi t_{ij}$ is the taxi ride fare of dispatch taxi service and the same as the one of cruising service; λ_1 and λ_2 are the same as the above explanation; w^{2c} is the waiting time of customer who chooses the dispatch service; u is the communication cost which is used to dial to book the dispatch taxi service.

Therefore, the total customer demand choosing cruising service is given by

$$\sum_{i\in I}\sum_{j\in J} Q_{ij}^{1c} = \sum_{i\in I}\sum_{j\in J} Q_{ij}^{c} P_{ij}^{1c} \tag{4}$$

Where Q_{ij}^{c} is the total customer demand on network.

At the same time, the total customer demand choosing dispatch service is given by

$$\sum_{i\in I}\sum_{j\in J} Q_{ij}^{2c} = \sum_{i\in I}\sum_{j\in J} Q_{ij}^{c} P_{ij}^{2c} \tag{5}$$

The equilibrium model of taxi on network

(1) Introduction of model variables

Assume that there is a road network $G(V, A)$, where V is the set of nodes and A is the set of links on network. Suppose that the demand-supply equilibrium exists on network. In any given hour, the number of customers who choose the taxi travel from origin zone i to destination zone j is $\sum_{i\in I}\sum_{j\in J} Q_{ij}^{1c} + \sum_{i\in I}\sum_{j\in J} Q_{ij}^{2c}$ （person/h） and the customer demand is elastic. I and J are the sets of customer origin and destination zones respectively. $t_a(v_a)$ is the travel time on link $a \in A$ .The total traffic flow v_a includes both the number of taxis and normal traffic volume. t_{ij}^{k} is the travel time on route $k \in R_{ij}$, $t_{ij}^{k} = \sum_{a\in A} t_a(v_a)\delta_{ij}^{ak}$,where R_{ij} is the set of routes between O-D pair(i , j)and $\delta_{ij}^{ak} = 1$ if route k uses link a and 0 otherwise. $t_{ij} = \min(t_{ij}^{k}, k \in R_{ij})$ .The time fraction is an hour, and congestion on network isn't considered here, and a trip is that a taxi is only occupied by a customer.

(2) Taxi service time relationship

Suppose that there are N^1 cruising taxis traveling on network and consider one unit period (1h). The customer demand is obtained by the above trip mode choice model. The total taxi service time include the occupied time and the unoccupied time. The total occupied time T^{ot} （veh • h） is the taxi-hours required to complete all cruising trips for all taxis and is given by:

$$T^{ot} = \sum_{i\in I}\sum_{j\in J} T_{ij}^{ot} t_{ij} \tag{6}$$

Where T_{ij}^{ot} is the occupied taxi movement (veh/h) from zone $i \in I$ to zone $j \in J$ along the shortest route; t_{ij} is explained in Eq.2.

The total unoccupied time T^{vt} （veh • h） consists of the search times of vacant taxis from zone to zone and waiting times within zones and is followed as:

$$T^{vt} = \sum_{i\in I}\sum_{j\in J} T_{ji}^{vt}(t_{ji} + w_i^t) \tag{7}$$

Where T_{ji}^{vt} is the vacant taxi movement (veh/h) from zone $j \in J$ to zone $i \in I$ along the shortest route; w_i^t is the taxi search/waiting time within zone $i \in I$; t_{ij} is explained in Eq.2.

Therefore, the relationship between the total taxi service time and the total number of taxis in terms of the 1-h period is given by:

$$\sum_{i\in I}\sum_{j\in J} T_{ij}^{ot} t_{ij} + \sum_{j\in J}\sum_{i\in I} T_{ji}^{vt}(t_{ji} + w_i^t) = N^1 * 1 \tag{8}$$

Where N^1 is the total number of cruising taxi (veh).

(3)Route choice behavior of taxi drivers

Suppose that once a customer ride is completed at a destination zone $j \in J$, the taxi driver could either stay in the same zone or move to other zones to find a next customer. Based on this, each driver tries to minimize his expected search time to meet the next customer, and the expected search time is a random variable due to variations in perceptions and the random arrival of customers. This random variable is assumed to be identically distributed with a Gumbel density function [4, 5]. Thus the probability that a vacant taxis meeting a customer eventually in zone $i \in I$ is given by

$$P_{i/j} = \frac{\exp\left\{-\theta''(t_{ji} + w_i^t)\right\}}{\sum_{m\in I}\exp\left\{-\theta''(t_{jm} + w_m^t)\right\}} \quad i \in I \;\; j \in J \tag{9}$$

Where $P_{i/j}$ is the probability of taxi that searches and meets the next customer in zone $i \in I$ after taking a customer to zone $j \in J$; θ'' is a nonnegative parameter and its value reflects the degree of uncertainty on customer demand and taxi services from the perspective of individual taxi drivers, which is explained in [6].

(4)The supply-demand equilibrium relationship

In a stationary equilibrium state, in terms of cruising taxi service, the movements of vacant taxis on network should meet the customer demands at all origin zones, or every customer will eventually receive taxi service after waiting. In the equilibrium state, the supply-demand relationship of vacant taxi for cruising service is followed as:

$$\sum_{i\in I} T_{ji}^{vt} = \sum_{i\in I} Q_{ij}^{1c} = Q_j^{1c}, j \in J \tag{10}$$

$$\sum_{j\in J} T_{ji}^{vt} = \sum_{j\in J} Q_j^{1c} P_{i/j} = Q_i^{1c}, i \in I \tag{11}$$

In the equilibrium state, the supply-demand relationship of occupied taxi for cruising service is followed as:

$$\sum_{i\in I}\sum_{j\in J} T_{ij}^{ot} t_{ij} = \sum_{i\in I}\sum_{j\in J} Q_{ij}^{1c} t_{ij} \tag{12}$$

In the equilibrium state, the supply-demand relationship for dispatch service is followed as:

$$N^2 = \sum_{i\in I}\sum_{j\in J} Q_{ij}^{2c} = \sum_{i\in I}\sum_{j\in J} Q_{ij}^{c} P_{ij}^{2c} \tag{13}$$

Where N^2 is the number of taxis which provide dispatch service.

Therefore, the total number of taxis which provides cruising service is given by:

$$N^1 = Num - N^2 \tag{14}$$

(5)A combined trip distribution and assignment UE model with elastic demand

As far as the cruising taxi service is concerned, the taxi movement on network is described by using a combined trip distribution and assignment UE model with elastic demand Q_{ij}^{1c}.This mathematical programming model is given by:

$$\min Z = \sum_{a\in A}\int_0^{v_a} t_a(w)\,dw + \frac{1}{\theta''}\sum_{j\in J}\sum_{i\in I} T_{ji}^{vt}(\ln T_{ji}^{vt} - 1) - \sum_{i\in I}\sum_{j\in J}\int_0^{Q_{ij}^{1c}} Q_{ij}^{-1}(w)dw \tag{15a}$$

$$subject\quad to: \sum_{i\in I} T_{ji}^{vt} = \sum_{i} Q_{ij}^{1c} \tag{15b}$$

$$\sum_{j\in J} T_{ji}^{vt} = \sum_{j} Q_{ij}^{1c} \tag{15c}$$

$$\sum_{k\in R_{ij}} f_{ij}^{k} = T_{ij}^{n} + T_{ij}^{ot} + T_{ij}^{vt} \tag{15d}$$

$$v_a = \sum_{i\in I}\sum_{j\in J}\sum_{k\in R_{ij}} \delta_{ij}^{ak} f_{ij}^{k} \tag{15e}$$

$$f_{ij}^{k} \geq 0 \tag{15f}$$

$$T_{ji}^{vt} > 0 \tag{15g}$$

Where T_{ji}^{vt} is explained by Eq.(7); T_{ij}^{ot} is explained by Eq.(6); T_{ij}^{nt} is normal traffic movements from origin zone $i \in I$ to destination zone $j \in J$ (veh/h); f_{ij}^{k} is traffic flow on route k from zone $i \in I$ to zone $j \in J$; Q_{ij}^{-1} is the inverse function of demand function.

(6)Taxi search/waiting time

Based on the calculated T_{ji}^{vt} and the completed iterative balancing factors A_i and B_j form [6], taxi search/waiting time is obtained by using Eq.16 and Eq.17. The detailed deduction of Eq.16 and Eq. 17 is from [3]. They are necessarily improved here and are given by:

$$f = \exp\{\frac{-\theta''(Num - N^2 - \sum_{i\in I}\sum_{j\in J} Q_{ij}^{1c} t_{ij} - \sum_{i\in I}\sum_{j\in J} T_{ji}^{vt} t_{ji}) - \sum_{i\in I}\sum_{j\in J} Q_{ij}^{1c}\ln A_i}{\sum_{i\in I}\sum_{j\in J} Q_{ij}^{1c}}\} \tag{16}$$

Taxi waiting times can then be obtained as

$$w_i^t = -\frac{\ln(fA_i)}{\theta''} \tag{17}$$

Customer waiting time at demand-supply equilibrium state

According to [3], the function relationship between the passage waiting time and taxi search/waiting time is obtained by introducing the Cobb-Douglas type of customer-taxi meeting function into the model, and that is given by

$$W_i^c = \frac{1}{D_i \sum_{j\in J} Q_{ij}^{1c} w_i^t} \tag{18}$$

Where W_i^c is the passage waiting time (h); D_i is the location-dependent constant. If the meeting between customer and taxi occur at fixed taxi stands (point meeting), the corresponding D_i is assumed to have a large value, such as D_i=10^4 （1/veh·h）; if it is the residential zones, D_i is 0.01 （1/veh·h）; if it is the commercial zones, D_i is 0.1（1/veh·h）.

The solution algorithm of equilibrium model

The general procedure is set out below:

Step 1.Initialization: set an initial set of customer-waiting times, $W_i^{c(0)}$, $i \in I$, let $n := 1$.

Step2.Customer demand of different trip modes updating: update $Q_{ij}^{rc(n)} = Q_{ij}^{c} P_{ij}^{rc(n)}$, $i \in I$, $j \in J$, $r \in R$, where $P_{ij}^{rc(n)}$ is given by Eq.1.

Step3.A equilibrium model of taxi on network: solve the equilibrium model of taxi on network for given $Q_{ij}^{rc(n)}$, $i \in I$, $j \in J$, $r \in R$ by the iterative balancing method and thus obtain a set of taxi searching/waiting times, $w_i^{t(n)}$, $i \in I$.

Step4.Updating customer-waiting time: update $W_i^{c(n)}$, $i \in I$ with $w_i^{t(n)}$, $i \in I$ according to Eq.18.

Step5.Convergence criterion: if convergence is attained according to Eq.19, then stop. Otherwise, let $n := n+1$ and go to step 2.

$$\left| \frac{W_i^{c(n)} - W_i^{c(n-1)}}{W_i^{c(n-1)}} \right| \le \varepsilon \tag{19}$$

Conclusions

This paper established an equilibrium model of taxi service on network. This model reflected the existence of integrated service modes including cruising and dispatch modes and considered the influence of elastic demand distribution. Based on these, in supply-demand equilibrium, a number of performance measures such as taxi search/waiting time and customer waiting time were obtained, which can examine the level of taxi service on network and further provide the meaningful references and theoretical support for advancing the operation level of taxi market. With the proposed equilibrium model of taxi on network, this model could be usefully extended in the regulation policies of taxi market based on the integrated service modes, especially the pricing and the entry number of taxi market.

References

[1] Douglas G. Price Regulation and optimal service standards. The taxicab industry,1972.
[2] Josep Maria Salanova et.al.A review of the modeling of taxi services[J].Procedia Social and Behavioral Sciences 20 (2011) 150-161.
[3] Yang H., Cowina W.Y.Leung, et al. Equilibria of bilateral taxi-customer searching and meeting on networks[J]. Transportation Research: Part B, 2010, 44: 1067~1083.
[4] Bian Yang, Wan Jian, Lu Jian. equilibrium model of urban taxi service network[J].Journal of traffic and transportation engineering, 2007.2, 7(1):93~98.
[5] Luo Ruigao, Shifeng. A taxi service network equilibrium model with the influenced of demand distribution[J].Journal of railway science and engineering, 2009.2,6(1):87~91.
[6] Yang H.and Wong S.C. A network model of urban taxi services. Transport Research B, 1998,Vol.32,No.4,pp235-246.

doi:10.4028/www.scientific.net/AEF.5.88

Study on the Characteristic of Eye During Traffic Operation

Xu Hui-zhi[1,a], Wang Yu-ping[2,b], Wu Chong[1], Cheng Guo-zhu[3], Pei Yu-long[3]

[1] Post-doctoral Station of Management science and engineering, Harbin Institute of Technology, Harbin 150001, China,[2] Harbin Metro Group Corporation Ltd, Harbin 150000, China, [3] School of Transportation Science and Engineering, Harbin Institute of Technology, Harbin 150090, China

[a] 353812396@qq.com, [b] rock510@163.com

Key words: Traffic Operation; Driver; Characteristic of Eye; Experiment

Abstract. To design vehicle auxiliary equipment, it need master the characteristic of eyes. The paper adopted iView X HED as equipment to get the characteristic of eye during traffic operation, results could be treat as experiment research. The paper collected text data of eye, and adopted location, during, blink time, blink frequency, and transient of eye focus as parameters to study the characteristic of eye, and given a measurable value to them. It was a foundation to further research of driver's characteristic. The result showed that: the location mainly focus in ahead, the average value of time and blink was 0.3098s and 0.231s. Frequency of blink was respond to traffic condition, the mainly direction of transient was left and right.

Introduction

Traffic flow could produce traffic conflict. Mainly reason was the drivers got inadequate information about traffic environment. ITS proposed a concept of assistance system to driver, but need to know the characteristic of drivers, especially to the characteristic of driver's eye [1,2].Then, it could design an equipment of information collection and dangers warning [3,4]. Such, the paper design a test to study the characteristic of eye, via by collected data of location, during, blink time, blink frequency, transient of eye focus, to quantitative study to characteristic of eye in traffic [5;6].

Fig1. Investigate scenes1

Fig2. Investigate scenes2

The equipment of information collection was iiView X HED. Principle of work was got the eye’s image by infrared camera, and to track the trajectory of eye’s focus. Real-time computing the time , distance and speed of eye in Horizontal and vertical direction , and computing the location and diameter of pupils. Sampling rate was 50/60Hz, Tracking resolution was 0.1°, Monitor accuracy of recording was 0.5 ~ 1° , and the weight of helmet was 450g. The connection had two method: Wired and wireless (wireless connection was Bluetooth, the max control distance was 300m). Fig1 and fig2 was the special scene in traffic survey. Cross was the calibrated point and the circle was the location of driver’s view-point in traffic survey scene [7,8].

Location and During of View-point

During the driving, drivers transit their view-point corresponding to the change of traffic environment. In the proceeding, the view-point would remain in a stable point, and collected the information of traffic environment and to make a judgment, then, to decide the operating characteristic in next step. It could get from the traffic survey; the parameter of view-point during reflected the capacity of driver to concept and deal information. The average during of view-point was 700.4s. The mount of simple was 1233.

Location of View-point. Distribute of view-point location were shown in fig3 when driving in city road. So, it could get the conclusion: the distributed of view-point was mainly in the center of the field view-area.

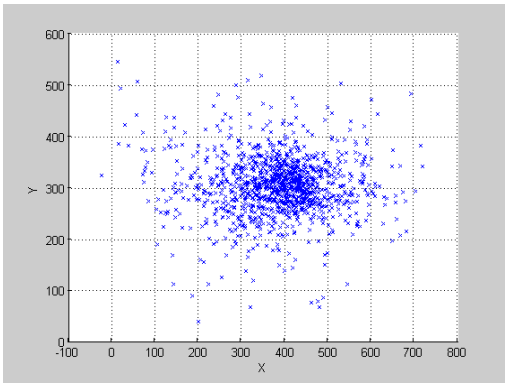

Fig3. Distribution of the view-focus location

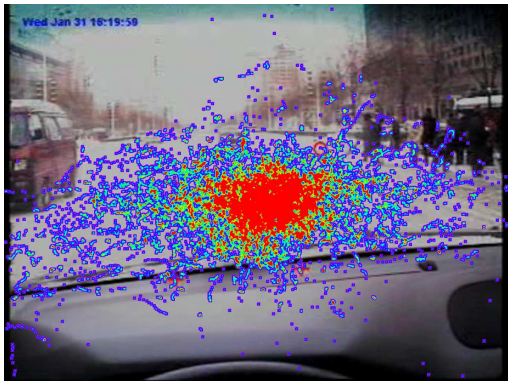

Fig4. Heat of the view-focus location

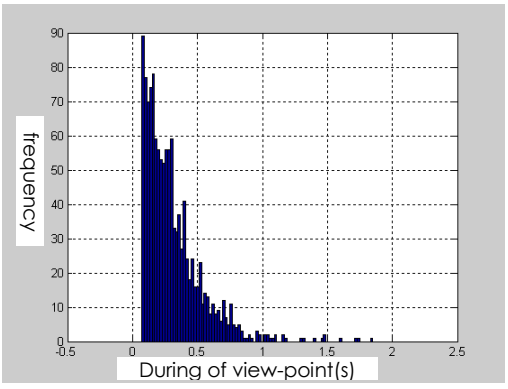

Fig5. Frequency of the viewpoint residence time

During of View-point. It divides the collection data of view-point during into 0.02s groups, then to draw the frequency chat shown in fig5. The max value was 1.840s, the min value was 0.078s, and the average value was 0.3098s. The frequency was 89 in the interval (0.07s, 0.09 s], 77 in the interval (0.09s, 0.11s], and 70 in the interval (0.11s, 0.13s]. Overall, the frequency of view-point during reduced corresponds to the increased of operation time.

Blink time and Blink Frequency

Blink time and blink frequency were indicators which reflect the physiological characteristic of drivers. It could get the capacity of drivers to receiving and processing information. The length of survey dada was 700.4s, and got 1413 simples of blink.

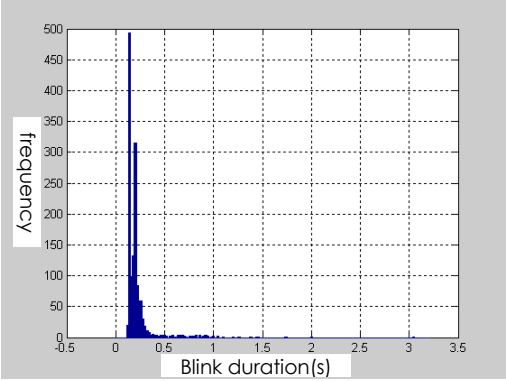

Fig6. Distribution frequency of blink duration

Blink Time. Blink time of drivers distribute in the interval [0.02s, 3.04s], the average value was 0.231s. It divide the blink time in several groups, the interval was 0.02s, draw the frequency chat shown as fig5.

The frequency was 493 in the interval (0.13s, 0.15s], it was the first peak about the blink. The frequency was 315 in the interval (0.19s, 0.21s], it was the second peak about the blink.

It could get the result that the frequency nearly equivalent in the interval [0.35s, 1.05s], the frequency value in the interval [1, 4], the value was 0 or 1 in the interval (1.05s, ∞). Blink time mainly concentrated in the interval [0.11s, 0.33s].

Blink Frequency. The blink frequency was real time change during operation. Operation time and environment were main reason to change the blink frequency. Thus, it could get the fatigue characteristic of drivers though the parameter of blink frequency.

It got the statistics table via by survey data, as shown in fig 1, and take parameters such as average value, max value, min value, Mean square error. Average value reflected the number of blink, max value reflected the strength of blink, and Mean square error reflected the dispersion of blink. Min blink frequency was 0 times/10s, average was 2.213 times/10s.

Tab.1 Descriptive statistical indicators of blink data (10s)

index	value
average value	2.165
max value	11.000
min value	0.000
Mean square error	2.213

It could get the result though analysis the statistical data: the driver need often blink to ease the fatigue witch cause by continued driving. On the other side, it also proves the correct that adopted blink frequency as the evaluated parameter to visual adaptability.

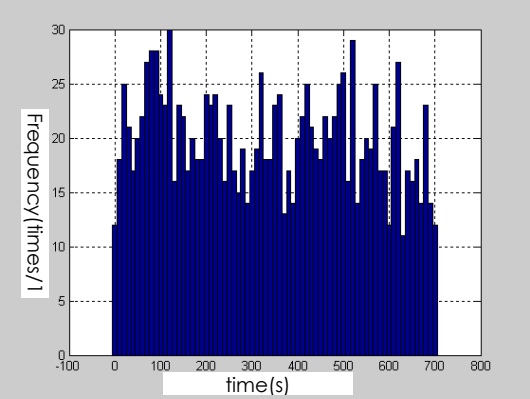

Fig7. Blink frequency

Transient of Eye Focus

The survey got 374 group data about transient of eye focus. It could draw a transient chat by the survey data in view field, as shown in fig9. Arrow direction reflected the direction of transient, Arrow size reflected the speed of transient. The transient of eye focus mainly occur in the center of view, but the transient speed was slowly relative to around field. The traffic environment and object continued change during driving, the drivers need to change location of view-point to collection the information. So, to study the regular pattern of eye focus transient could reflect the characteristic of driver correspond to the traffic change and urgent condition. In order to analysis the transient of eye focus, Enlarge the fig 9, and shown in fig10, fig11, fig12, fig13, fig14.

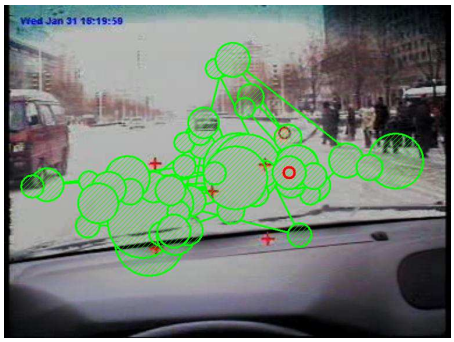

Fig8. Viewpoint stay and transfer

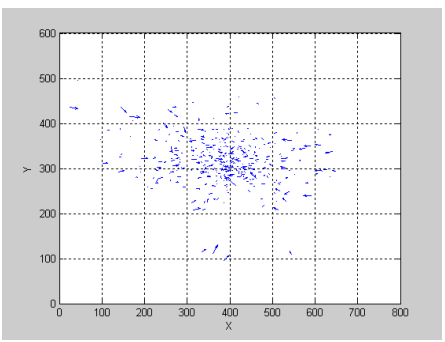

Fig9. Viewpoint quickly transfers

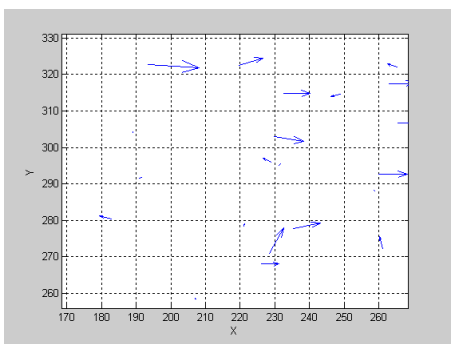

Fig10. Partial view of the left

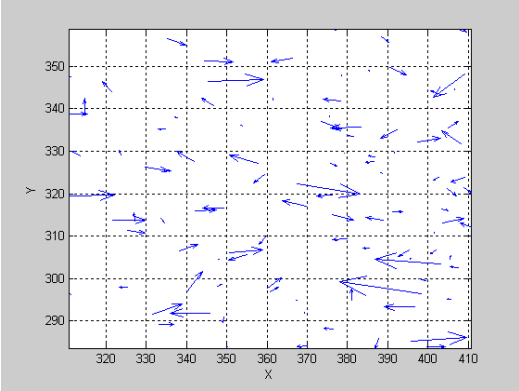

Fig11. Partial view of the center

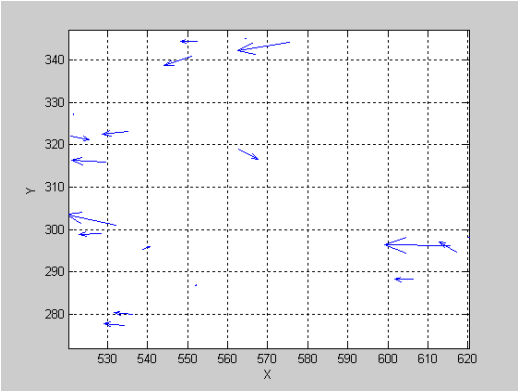

Fig12. Partial view of the right

It could know from fig10, the main direction of eye focus transient was right in left view field. In order to get the information in center and right area when eye focus in left, the speed of transient became fast, and more left, more fast.

It could know from fig11, the main direction of eye focus transient was left and right in center view field. Direction of up and down seldom appears. It transit became more frequency in the center view field.

It could know from fig12, the main direction of eye focus transient was left in right view field. The characteristic of eye focus transient was opposite to the left view field.

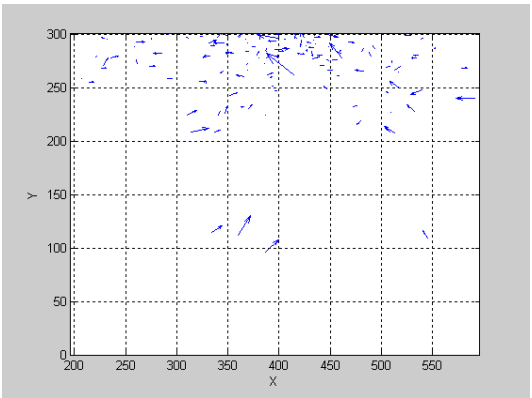

Fig13. Partial view of the lower

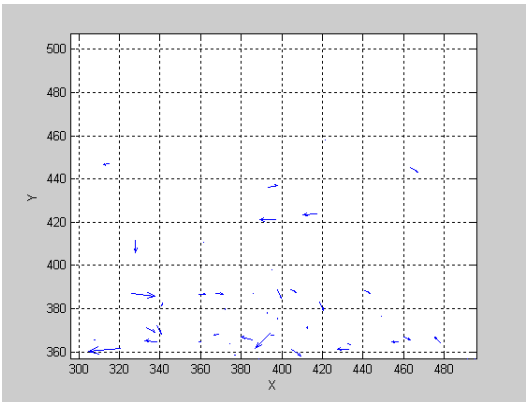

Fig14. Partial view on the side

It could know from fig13, the main direction of eye focus transient was down, left, right in up view field. The drivers though up view field to get the information in distant, the survey was city road, the average velocity was 20km/h, the eye focus of driver was in 30～40m ahead. The change in distant could not cause the rapid reflect, so, the characteristic of eye focus transient was less. In order to get the information in center and right area when eye focus in left, the speed of transient became fast, and more left, more fast.

It could know from fig14, the main direction of eye focus transient was up, left, right in down view field. The drivers though up view field to get the information in nearby, the driver was less attention to the information. The main direction was up, it reflect the characteristic that the driver transient his eye focus into center field when got the traffic information.

So, it could get the conclusions: the direction of eye focus transient was left and right. The more away to center field, the transient became more fast.

Conclusion

It adopted the characteristic of eyes as study object, Quantitative analysis the parameters of location, during, blink time, blink frequency, transient of eye focus. The result shown that: the location of eye focus mainly in ahead, the average value of time and blink was 0.3098s and 0.231s, frequency of blink was respond to traffic condition, the mainly direction of transient was left and right.

Acknowledgements

This work was financially supported by National Natural Science Foundation of China(51108137) and China Postdoctoral Science Foundation(2012M511499). Thanks for the sponsoring of the Fundamental Re-search Funds for the Central Universities (Grant No. HIT. NSRIF. 201150),and China Postdoctoral Science Foundation(20110491090).

References:

[1] M. J. Henning. Preparation for lane change manoeuvres: Behavioural indicators and underlying cognitive processes[D]. Ph.D. dissertation Fakultät Human und Sozialwissenschaften, TU Chemnitz, 2009.

[2] Dario D., Salvucci, Andrew Liu. The time course of lane change: Driver control and eye-movement behavior[J]. Transportation Research Part F 5, 2002, 5(2): 123-133.

[3] Hiroshi Ohno. Analysis and modeling of human driving behaviors using adaptive cruise control[C]. Applied Soft Computing , 2001, 1(3): 237-243.

[4] Yasushi Nishida. Driving characteristics of the elderly: risk compensation of the elderly driving from the viewpoint of reaction behavior[J]. JSAE Review, 1999, 20(3): 375-380.

[5] Ioannis Golias, Mstthew G., Karlaftis. An international comparative study of self-report driver behavior[J]. Transportation Research Part F, 2002, 4(4): 243-246.

[6] Nakaho Numata, Hiroki Kitajima, Yoshihiro Goi, Keiichi Yamamoto. Analysis of driver's behavior before and after crashes in simulated expressway driving to predict sleeping levels for doze alarm activation[J]. JSAE Review, 1998, 19: 269-275.

[7] Jerry L. Deffenbacher, David M. Deffenbacher, Rebekah S., Lynch. Anger, aggression, and risky behavior: a comparison of high and low anger drivers[J]. Behavior Reach and Therapy, 2003, 41(6): 701-718.

[8] Mohamed A., Abdel-Aty, A., Essam Radwan. Model traffic accident occurrence and involvement[J]. Accident Analysis and Prevention, 2000, 32(5): 633-642.

doi:10.4028/www.scientific.net/AEF.5.94

Layout Optimization of Integrated Transfer Hub of Metropolis

Man Sun[1,a], Shi An[2,b]

[1]School of Transportation Science and Engineering, Harbin Institute of Technology, 73 Huanghe Road, Harbin, China, 150090

[2]School of Transportation Science and Engineering, Harbin Institute of Technology, 73 Huanghe Road, Harbin, China, 150090

[a]sunman_hit@yahoo.com.cn, [b]anshi@hit.edu.cn

Key words: Integrated Transfer Hub; Demand Forecasting; Layout Optimization; Scheme Evaluation

Abstract. Integrated transfer hubs are the important transportation infrastructures and the passenger distributing center places, they play a very important role in promoting the development of transportation system. While domestic integrated transfer hubs exist some problems as not playing enough attention to the layout planning. The spatial layout and facility layout are reasonable and imperfect, what making low transfer efficiency, traffic bottlenecks and waste of resources. Therefore layout optimization of integrated transfer hub is a problem urgently to be solved.

Combine with features and running states of transit hubs in our country, passenger transport demand is forecasted and the combination forecasting model is constructed based on quadratic. In layout optimization of integrated transfer hub, the optimization model of facility layout is also put forward with minimum average cost as the object, making layout of hub effectively optimized. While proposing the optimization method, system evaluation are proposed aiming at the method, and internal benefits, social benefit and environmental benefit are used to evaluate the optimized system.

1. Introduction

Along with the fast development of our national economy, the transport industry in China entered a period of comprehensive progress. Building and improving our comprehensive transportation system becomes urgent need to develop the economy[1]. Comprehensive transport hub is a important constituent of a country or region's comprehensive transportation system. It involves in the transport industry in various technical processes, and it is the main base of various modes of transportation to converge. Integrated transfer hubs play an important role in promoting the function of comprehensive transport system, even in promoting the city development[2]. How to play a prominent role of integrated transfer hub in the city traffic network and regional integrated transport network effectively, to enhance the order of supply or demand, and to improve completeness of network structure, is the major problem that needs to solve urgently[3].

Based on our country transportation hub station features and running states, we can find that, our country's integrated transfer hubs exist some problems as attaching importance on line construction while despising hub layout. Hub planning didn't get enough attention, what resulting in a distributed transfer and affecting the efficiency and benefit [4]. Unreasonable layout of interior hub made passengers walking very long distance to transit and resources utilized inadequately, so that to affect the efficiency of transportation system directly.

Foreign countries paid great attention to the study in construction of integrated transfer hubs. Research in hub plan, hub design and policy formulation had been carried out since 1950s. Many experiences and methods of hub design that fit city features were explored, which obtained good results[5-6]. In recent years, in full recognition of the importance of transfer hub construction, domestic scholars had conducted many studies. Some metropolis constructed some integrated transfer hubs, such as Beijing South Railway Station Hub, Shanghai Hongqiao Hub and Shenzhen Futian Hub.

2. Influence factors and principles of integrated transfer hub layout

2.1 Influence factors of integrated transfer hub

Integrated transfer hub layout planning is affected by many factors. It's an important step to analyze the layout factors for hub planning. The main factors can be summarized as follows.

(1)Social and economic factors

Social economic development impacts the hub design mainly in two aspects, the scale and the layout. In the scale of station, the more developed economic grown and more population in region, the more passenger demand generated. With the development of economy and the improvement of people's living standard, safety, convenience and other requirements have also been strengthened. In the layout of station, change of passenger demand and increase of travel frequency also affect the hub layout. Transfer hub layout should meet not only the downtown residents' needs, but also the suburbs' and the development zone residents'[7].

(2) Traffic conditions

①City road network condition. Different road network layout forms get different traffic characteristics. Layout of hub should give full consideration to the coordination and cohesion of city road network, so that to get smaller effects.

②External network connection. Integrated transfer hub design should plan station layout according to the different nature of road traffic, and get better convergence of the external road network. Making full use of existing resources can also reduce the impact on the city traffic.

③Modes of transportation development. Integrated transfer hub involves multiple transportation modes. Each different development traffic mode affects hub layout distinctly. Developed and mature traffic mode gets lager transfer passengers and assumes heavier transfer task, so it impacts the hub layout greater.

④Reachability of hubs. Different distribution of function area and traffic flow cause different time to achieve hub vary greatly. Reasonable hubs layout can reduce the transfer time of the passengers and the pressure on urban transport[8].

(3) Urban layout factors

Development morphology and development function of cities affect nature of city, function region and development direction of cities. Each form has the own characteristics, which along with residents travel, economic activities and cultural activities determine the hub layout.

(4) Passenger travel factors

As passengers travel preferences and travel habits becoming increasingly important factor of the impact of layout, transfer hub meet needs of passengers at different levels and provide excellent transportation services is wise activity.

2.2 Principles of integrated transfer hub

Hub layout reasonable or not relate to the implementation of benefit and fulfilling of functions. Integrated hubs layout planning should follow the following principles.

(1)Meet the needs of regional transport development. Integrated hubs should not only meet the needs of the regional socio-economic and transport development planning, but also fully embodies the economic characteristics of the region to adapt to the needs of regional development[7].

(2)Coordinate with the overall city layout planning. Spatial distribution structure and traffic flow should be given full consideration to. As the same time, future direction of urban development, resource distribution and population structure should also be considered to coordinate with other urban infrastructure and meet the needs of sustainable urban development.

(3)Coordinate with the development of road transport planning and integrated passenger transport network. Adapting to the road network development objective and matching with the main highway network can achieve the convenience of transport and give full play of advantages in the integrated transport.

(4)Make full use of the existing station resource and save the construction investment. On full study of the existing passenger transport hub, combined with the existing terminal condition, rational distribution can be conducted an resources can be made full use of.

(5) Reduce the impact on the environment and the surrounding urban residents. Passengers and vehicles with frequent activities within hub would make on air pollution an noise pollution to the surrounding environment. Hub layout should consider the negative impact on the surrounding environment to reduce environmental interference.

3. External transport passenger forecast

There are many similarities between the hubs transfer amount forecast and traffic distribution forecast. Drawing on the traffic distribution $f(C_{ij})$ forecast methods can help analyze passenger sharing. Construct an impedance function with the combination of power and exponent function, which choosing time, fee, comfort level and security level as the most significant factors to affect transfer behavior. There is the linear combination function[9] .

$$C_i = C_0 + k_{1i} \cdot C_{1i} + k_{2i} \cdot C_{2i} + k_{3i} \cdot C_{3i} + k_{4i} \cdot C_{4i} \tag{3-1}$$

C_i ——generalized travel costs of transport mode i

C_{1i}， C_{2i}， C_{3i}， C_{4i} —transfer time, cost, comfort level, security level of transport mode i

C_0 ——other factors that influence transport i

k_{1i}， k_{2i}， k_{3i}， k_{4i} ——corresponding coefficient

So the hub transfer passenger forecasting model is as follow:

$$q_{ij} = a_i b_j O_i D_j f\left(C_{ij}\right) \tag{3-2}$$

$$a_i = \frac{1}{\sum_j b_i D_i \left(C_{ij}\right)} \tag{3-3}$$

$$b_j = \frac{1}{\sum_i b_j D_j \left(C_{ij}\right)} \tag{3-4}$$

$$f(C_{ij}) = C_{ij}^{-\gamma} \cdot e^{-\beta C_{ij}} \tag{3-5}$$

4. Layout optimization of integrated transfer hub

The goal to establish the transportation function layout mode in hub is to minimize the average transfer cost of all modes. There are some assumptions.

(1)There is one dominant mode, and subsidiary modes are m. k=1，2，…m.

(2)Alternative point of the subsidiary modes are n. i=1，2，…n，and n ≥m

(3)Only one functional area which to construct proposed

(4)Alternative points get area restrictions[10]

Decision variables:

$$X_{ik} = \begin{cases} 1, & alternative\ piont\ i\ is\ seleced\ as\ functional\ area\ k \\ 0, & alternative\ piont\ i\ is\ not\ seleced \end{cases}$$

The objective function mainly purpose to minimize the average transfer cost of all modes. Two parts need to be considered when calculating the total transfer cost. First, the transportation costs C_1 between the dominant mode and the subsidiary mode. Second, the transportation costs C_2 between subsidiary modes. C_0 is cost caused by other factors such as the construction cost-sharing and operation cost-sharing.

$$\overline{C} = \frac{C}{N} = \frac{C_1 + C_2 + C_0}{N} \tag{4-1}$$

$$C_1 = \sum_{i=1}^{n}\sum_{k=1}^{m}\left(N_k + N_k'\right)X_{ik}\cdot c_i \tag{4-2}$$

$$C_2 = \sum_{i=1}^{n}\sum_{j=1}^{n}\sum_{k=1}^{m}\sum_{l=1}^{m} N_{kl}X_{ik}X_{jl}\cdot c_{ij} \tag{4-3}$$

$$N = \sum_{k=1}^{m}\left(N_k + N_k'\right) + \sum_{k=1}^{m}\sum_{l=1}^{m} N_{kl} \tag{4-4}$$

The objective function:

$$\min \overline{C} = \frac{\sum_{i=1}^{n}\sum_{k=1}^{m}\left(N_k + N_k'\right)X_{ik}\cdot c_i + \sum_{i=1}^{n}\sum_{j=1}^{n}\sum_{k=1}^{m}\sum_{l=1}^{m} N_{kl}X_{ik}X_{jl}\cdot c_{ij} + C_0}{\sum_{k=1}^{m}\left(N_k + N_k'\right) + \sum_{k=1}^{m}\sum_{l=1}^{m} N_{kl}} \tag{4-5}$$

Constraints are as follows:

$$\sum_{k=1}^{m} f\left(N_{k0}\right)\cdot X_{ik} \le S_i \qquad i = 1,2,\cdots n \tag{4-6}$$

$$\sum_{k=1}^{m} X_{ik} \le 1 \qquad i = 1,2,\cdots n \tag{4-7}$$

$$\sum_{i=1}^{n} X_{ik} = 1 \qquad k = 1,2,\cdots m \tag{4-8}$$

$$\sum_{k=1}^{m} X_{ik}e_k \le E \qquad k = 1,2,\cdots m \tag{4-9}$$

N_k ——transfer amount from the dominant mode to subsidiary mode k

N_k' ——transfer amount from subsidiary mode k to the dominant mode

N_{kl} ——transfer amount from subsidiary mode k to t subsidiary mode l

N_{k0} ——total traffic flow of subsidiary mode k

c_i ——generalized transfer cost from alternative site i to the dominant mode

c_{ij} ——generalized transfer cost from alternative site i to alternative site j

C_0 ——fixed cost sharing

S_i ——available area of alternative site i

e_k ——construction cost of transportation mode k

E——total investment

In the mode: formula (4-5) is the objective function, meaning the minimum average transfer cost; formula (4-6) means meeting the area restriction when the alternative site is selected; formula (4-7) means each alternative site can only be constructed to one traffic functional region; formula (4-8) means each traffic functional region only choose one alternative site; formula (4-9) is the investment restriction.

The model above is nonlinear 0-1 integer programming model, which can be solved by heuristic algorithm. With the implicit enumeration in operations research and with computer programming, optimal solution in model can be obtained.

5. Evaluation of integrated hubs layout

(1) Internal benefit

Optimization layout of hub improve the level of convergence of the various modes of transportation and the transfer efficiency. It shortens transfer time, attract more passenger traffic and reduce the transfer cost. With the transfer time, transportation management fees, hub attracting capacity and traffic accident reduction as the indicators to measure the internal benefit.

(2) Social benefit

Service range is expanded because of layout optimization, it makes the social benefits increasing combined with the urban transport system. Transfer hub contacts various modes of transportation, so that optimization of hub layout is the key to transportation modes convergence and external traffic distribution[11]. With the the congestion reduced efficiency, hub service range, degree of coordination with other hub and promotion of social development as the indicators to measure the social benefit.

(3) Environmental benefit

Layout optimization of urban external hubs can effectively reduce congestion, distribute traffic reasonably and reduce environmental pollution. It minimizes interference and impact on the surrounding environment and residents living. With the congestion reduction, environmental pollution effects, road service area reduction amount and the coordination degree with surrounding environment as the indicators to measure the environmental benefit.

Conclusion

Layout optimization of urban external integrated transport hub is a problem worthy of study. On the basis of passenger demand forecasting and distribution, the model was established with the minimum average transfer cost as the objective. Integrated transfer hub was optimized and evaluated from three aspects.

References

[1] Yuan Hong, Lu Huapu. Study on model and method of comprehensive transportation terminal. Journal Of Highway And Transportation Research And Development. 2001.03

[2] Peng Hui. Research on integrated transportation hub layout. Master degree thesis of Chang'an University. 2006

[3] Feng Wei. Theoretical Research on Key Problems of City's External Traffic Comprehensive Transfer Hubs System. Doctoral dissertation of Southwest Jiaotong University. 2010.

[4] Wang Jiancong. Key Issues on Transfer Organization of City Passenger Traffic Hubs. Doctoral dissertation of Beijing Jiaotong University.

[5] Marianov, V.and Serra, D.Loeation of hubs in a competitive environment. European Journal of Operational Resear c h, 114.1999, 3:63-71

[6] Mark C. Walkek. Planning and designing of on street light rail transit stations. Transportation Research Record 1361:3-9

[7] Zhou Li. The Study on Layout Method of Urban Highway Passenger Transport Hub. Master degree thesis of Beijing Jiaotong University. 2008

[8] Hu Along. Study on the Layout of Urban External Traffic Transfer Hubs. Master degree thesis of Southwest Jiaotong University. 2005.

[9] Luo Xia, Fang Dahong. Research on demand prediction of integrated transportation hub. Railway Transport and Economy.2009

[10] Jiang Lingyu. Study on Facility Layout Optimization of Integrated Passenger Transportation Hub. Master degree thesis of Southwest Jiaotong University. 2007

[11] Xie Tao. Study on Locating the Urban Transfer Terminals and Integrating the Traffic Resources. Master degree thesis of Dalian University of Technology. 2005.

doi:10.4028/www.scientific.net/AEF.5.99

NL Model on Traffic Mode Split among High-density Town Cluster

Shimei Wu[1, a], Yulong Pei[1, b]

[1] School of Transportation Science and Engineering, Harbin Institute of Technology, Harbin 150090, China
[1] DongGuan Development and Reform Bureau, DongGuan 523888, China
[2] School of Transportation Science and Engineering, Harbin Institute of Technology, Harbin 150090, China
[a]email: s0825r@qq.com, [b]email: yulongp@263.net

Keywords: transportation planning; high-density town cluster; traffic travel mode; NL model; multi-mode rail transit

Abstract: With urbanization process acceleration in China, traffic travel among cities becomes increasing, and traffic mode split is the key link of traffic passenger flow forecast among cities. In this paper, the concept of high-density town cluster was proposed to analyze the characteristics of development, population composition, and traffic facilities among high-density town cluster. Based on applicability analysis of aggregate model and disaggregate model, survey content of revealed preference (RP) and stared preference (SP), and traffic mode hierarchical division according to average speed, then NL disaggregate model among high-density town cluster was constructed. NL model which was parameter calibrated and validated with DongGuan citizen travel investigation data in 2009 was used to analyze the trend of traffic mode split. The result shows that high-density town cluster, such as DongGuan, are establishing a three-dimensional travel mode set, including high-speed rail, intercity rail, suburban rail, urban rail transit, intercity express bus, car, taxi, and common public transport. With the network of multi-mode rail transit further improving, ratio on choosing the traffic mode of multi-mode rail transit, such as high-speed rail, intercity rail, suburban rail, urban rail transit, increases dramatically.

Introduction

Recently years, with the number of traveling among cities, such as Pearl River Delta Area, Yangtze River Delta Area, Bohai Area, and so on, increased dramatically, and the travelers require that the transportation should be rapid, comfortable, and safe. However, traditional train, bus, and taxi don't meet the requirement mentioned before. On this condition, the planning and construction of high speed train, intercity rail transit, and suburb railway accelerate dramatically. However, passenger traffic forecasting which plays an important role in the planning and construction of rail transit is not well carried out, or be a mere formality. Therefore, passenger traffic forecasting cannot suit for the development of transportation among cities, strengthening the research on passenger traffic forecasting is very necessary and urgent.

Definition of High-density Town Cluster

At present, China has formed some high-density town clusters, such as Pearl River Delta Area, Yangtze River Delta Area, Beijing-Tianjin-Hebei region, Changsha-Zhuzhou-Xiangtan region, West coast, Liaoning province coastal belt, and so on.

Like the term of high-density town cluster, there are still other terms, such as urban agglomeration, big city belt, urban development region, urban high-density area, and so on. Domestic scholars have studied and analyzed these terms (Li X. J, 2008). According to these terms' definition, the high-density town cluster is defined in this paper.

Based on development pattern and space distance, high-density town cluster is defined of region where cities and towns rapid develop simultaneously, distances among the centers of cities are less than 100 kilometers, travel time by freeway among the centers of cities are less than one hour, distances between adjoin towns are less than 10 kilometers, travel time by urban aerial roads between adjoin towns are less than 10 minutes, are formed by different town clusters, the functions of which are related to each other, and connect frequently.

Forecasting Model Choice

The forecasting model can be divided into aggregate models and disaggregate models. Aggregate models are based on the traditional "Four-stage method" (Lu H. P., 1998).

Aggregate models are based on the traditional "Four-stage method". Disaggregate models attempt to analyze these problems, like whether the individual of traffic behavior decision-maker unit travel or not, where to go, use what mode of transportation, and choose which path, and so on. Modeling and summation of each traveler how to choose the best selection branches, then total traffic demand can be calculated. Disaggregate model which is discrete choice model based on maximum effect theory includes Logit model (MNL model), Probit model, NL model, Mixed Logit model, and some other models like that (Kenneth, 2003; Guan, 2004).

NL model overcomes the problem of mutual independence of non-related options for MNL model. What's more, NL model solution is much easier than Probit model, expresses the relevance of options in some extent at the same time (Hensher, et al., 2002). Therefore, NL model is chosen to establish the mode of intercity travel mode choice in high-density town cluster.

Model Established

Resident travel investigation (revealed preference, RP) and resident travel intention survey (stared preference, SP) were conducted in 2009 for the development and planning of rail transits network in Dongguan. Survey content includes personal socio-economic characteristics (gender, age, profession, educational background, income), household socio-economic characteristics (home address, family members, household income, household car and number of bicycles), activities chain investigation data (activity purpose, start time, travel distance, travel mode, travel fee, whether transfer the transport) and resident travel intention survey on the presume that multiple modes rail transits network is built; stations are set; and the ticket prices are difference. All these survey data provide the necessary foundation for confirming the option branches and selecting the variables in RP model and SP model.

Determining of Choice Branch

In the RP investigation, intercity traffic modes which resident can choose in Dongguan include suburb rail, intercity rapid bus, intercity bus, taxi, car, however, walk and bicycle are not considered due to travel distance. Choice branches are confirmed by the main travel way during the process of modeling. For instance, if one travel way includes walk, bus, and intercity rapid bus, and the choice branch is intercity rapid bus; if one travel way includes car and intercity railway, and the choice branch is intercity railway. In the SP survey, intercity travel modes for Dongguan resident choosing have increased high speed railway, intercity rail transit, and urban rail transit.

MNL model

Options of MNL model can be divided into multiple layers by relevance, each layer is one model, and every two layers can be connected by logarithm of the lower layer total utility. The theoretical foundation of MNL model is that traveler chooses the maximum utility project under the special choice condition. MNL model can be expressed as following (Zhang, et al., 2008).

$$U_{i,n} = V_{i,n} + \xi_{i,n} \tag{1}$$

$$P_{i,n} = \frac{\exp(\lambda V_{i,n})}{\sum_{i=1}^{N} \exp(\lambda V_{i,n})} \tag{2}$$

Where, $U_{i,n}$ is the utility function when traveler n chooses the i travel project. parameter $V_{i,n}$ is constant variable, and $\xi_{i,n}$ is probability. MNL model assumes that $\xi_{i,n}$ subject to the double exponential distribution, and all variables are pair wise independent. $P_{i,n}$ is the probability of traveler n chooses the i travel project. N is the number of travel projects for choosing. RP model and SP model can be established owing to the difference of survey mode and content. SP model presumes that both the probability of SP and RP have the same distribution.

Influence Factor Model of Utility Value

There are many factors which influence residents in high-density town cluster travel. Travel time, travel fee, household income, and the qualitative variables constituted by convenience, comfort, and security are chosen to as the model variables.

Utility functions include linear function, logarithmic function, and so on. The linear function is widely used, and its expression is intuitive, and easy to solve. Which is shown as following

$$V_{in} = \sum_{k=1}^{K} \theta_k X_{ink} \tag{3}$$

Utility function of high-density town cluster resident for intercity traveling is expressed.

$$V_{in} = \theta_1 T + \theta_2 F + \theta_3 S + \theta_4 R \tag{4}$$

Where, T indicates travel time, including transport travel time, transport connected run time, waiting time, transferring time, and so on; F indicates travel fee, including ticket price, parking fee, tolls, fuel cost, and so on; S is household income, which is related to other influence factors; R is qualitative variable, including convenience, comfort, security, and so on; According to the quantitative methods researched by home and abroad scholars, the service level of different traffic modes can be divided into highest, higher, common, low four grades, and the value range is (4,0), which is chosen by travelers.

Traffic Mode Hierarchical Division

In the Dongguan investigation, residents pay close attention to the travel time when they choose the intercity travel traffic mode, and travel time is closely related to operation speed of transport. Hence, traffic mode hierarchical division is based on operation speed of the main transport.

Virtual mode 1: travel mode which its average operation speed is up to over 200 km/h is high speed railway.

Virtual mode 2: travel modes which their average operation speeds are between 100 km/h and 200 km/h are intercity rail transit and suburb railway.

Virtual mode 3: travel modes which their average operation speeds are between 60 km/h and 100 km/h are urban rail transit, urban rapid bus, private vehicle, officer vehicle, and taxi.

Virtual mode 4: travel modes which their average operation speeds are amount to under 60 km/h are intercity common bus, individual vehicles for short distance travel, such as private vehicle, officer vehicle, and taxi.

Therefore, probability calculation formula for variety of traffic modes is expressed as.

$$P_{A_{in}} = P_{(i|A)n} P_{An} \tag{5}$$

Where, A_{in} is the i choice branch under virtual mode A; $P_{A_{in}}$ is the probability of traveler n choosing mode A_i; $P_{(i|A)n}$ is the probability of traveler n choosing mode i based on virtual mode A; P_{An} is the probability of traveler n choosing virtual mode A.

Parameter Calibration

Parameters $\theta_1 \sim \theta_4$ are calibrated by maximum likelihood estimation method. Choice result is defined as constant term, and when the traveler n chooses mode i, constant term is 1; or not, constant term is 0. Estimation methods of parameter $\theta_1 \sim \theta_4$ include N-R, D-F-P, and H-J, which will not detailed discuss (An, 2004).

Mode Validation and Trend Analysis

RP and RP surveys were conducted in Dongguan in 2009 and relevant data with ESS(effective sample size) of 6000 were collected，which distributed in 32 towns and streets in the whole city. Those data were organized and applied in *Rail Transit Network Planning and Adjustment for Dongguan.* we chose Multi-Logit module in SPSS.

Mode Validation

Table 1 Parameters for Different Intercity Trip Modes in Dongguan in 2012

Trip Mode	θ_1	*t* statistic	θ_2	*t* statistic	θ_3	*t* statistic	θ_4	*t* statistic
High-speed railway	-0.1354	2.35	-0.1632	3.22	0.1090	2.87	0.0624	3.11
Guangzhou-Shenzhen bullet train	-0.1583	3.21	-0.0936	2.33	0.0959	2.57	0.0663	2.89
Intercity rail transit	/	/	/	/	/	/	/	/
Urban rail transit	/	/	/	/	/	/	/	/
Intercity rapid bus	-0.1061	1.99	-0.2071	4.35	-0.0245	3.79	0.0482	4.13
Private cars	-0.1873	2.05	-0.1104	3.88	0.1433	2.89	0.0457	3.57
Taxi	-0.2232	5.34	-0.0874	2.19	0.1123	2.67	0.0087	6.28
Official vehicles	-0.2466	4.26	-0.0017	2.87	0.0029	3.36	0.0454	3.33
Intercity Bus	-0.0252	2.65	-0.2853	3.26	-0.1784	4.38	0.0026	2.68
Short distance vehicles	-0.0133	3.11	-0.0204	2.77	-0.1328	3.25	0.0011	4.36

Generally, we use t statistic and ρ^2 in Statistics & Probability to validate a mode by conducting t test on single variable. If $|t| \geq 1.96$, it can be said that t test pass muster，as for ρ^2,if it is between 0.2 to 0.4,we can conclude that the mode fits well.

From the data collected in the survey in Dongguan in 2012, we got various parameters for different travel modes which are shown in table 1.

It can be seen from the table that each t statistics of parameters for different intercity trip modes meet the request that $|t| \geq 1.96$, which means relevant parameters meet requirement.Predicted value of the mode for 2005 and 2009 can be calculated by SPSS, which can be seen in table 2.

Table 2 Comparison of predicted value with survey value of proportion of different intercity trip modes in Dongguan

Year	A1	A2		A3					A4	
	High -speed railway	Guangzhou -Shenzhen bullet train	Intercity rail transit	Urban rail transit	Intercity rapid bus	Private cars	Taxi	Official vehicles	Intercity bus	Short distance vehicles
2005	0	0.196	0	0	0.457	0.174	0.088	0.031	0.033	0.021
survey value	0	0.187	0	0	0.462	0.180	0.082	0.033	0.035	0.021
Error	0	4.81%	0	0	-1.08%	-3.33%	7.32%	-6.06%	-5.71%	0%
2009	0	0.188	0	0	0.473	0.162	0.094	0.035	0.031	0.017
survey value	0	0.193	0	0	0.480	0.157	0.089	0.032	0.030	0.019
Error	0	-2.59%	0	0	1.46%	3.18%	5.62%	9.38%	3.33%	10.53%

It can be seen from the table that errors of predicted value compared to survey value are small and prediction results of trip modes which accounted for a larger proportion such as Guangzhou-Shenzhen Bullet Train, Inter-city Rapid Bus transit; Private Cars and Taxi are more accurate. And ρ^2 value of this mode is 0.338 which means the mode fits well.

Trend Analysis

Guangzhou-Shenzhen Bullet Train in Dongguan will be formally opened to public in 2012. Intercity rail transit of Guangzhou-Dongguan-Shenzhen and Dongguan-Huizhou and Urban Rail Transit R2 is still under construction while Foshan-Dongguan Intercity rail transit is still under planning.Intercity travel modes proportions in Dongguan among 2009, 2012, 2015, and 2020 are shown in table3.

Table 3 Intercity travel modes proportion in Dongguan

Year	A1	A2		A3					A4	
	High -speed railway	Guangzhou -Shenzhen bullet train	Intercity rail transit	Urban rail transit	Intercity rapid bus	Private cars	Taxi	Official vehicles	Intercity bus	Short distance vehicles
2009	0	0.188	0	0	0.473	0.162	0.094	0.035	0.031	0.017
2012	0.063	0.166	0	0	0.467	0.139	0.085	0.034	0.030	0.016
2015	0.075	0.138	0.103	0.078	0.372	0.094	0.063	0.033	0.028	0.016
2020	0.077	0.112	0.175	0.145	0.278	0.082	0.059	0.033	0.025	0.014

We can see from the forecast result, intercity travel mode structure will change, with the rapid construction and operation of Dongguan passenger traffic facilities over the year of 2009, 2012, 2015, and 2020. With the further improvement of high speed railway and intercity railway network,

choice proportions of multiple rail transits composed by high speed railway, intercity railway, suburb railway, and urban rail transit will dramatically increase, ranging from 0.188 in the year of 2009 to 0.229 in the year of 2012, and ascending from 0.394 in the year of 2015 to 0.509 in the year of 2020, while that of intercity rapid bus, private cars, and taxi will gradually decrease. However, the choice proportions of official vehicles, intercity bus, and short distance vehicles will remain the same level.

Conclusion

Nowadays, planning and construction of high speed railway, intercity rail transit, and urban rail transit are in the period of accelerate development, passenger flow forecasting is significant for determining the construction projects and scales, and travel mode choice is an important step of passenger flow forecasting. Study on NL model of travel mode choice in high-density town cluster will play a reference role in the process of similar cities or regions planning.

References

[1] X. J. Li. Town high-density area and town cluster planning-practices and understanding. Journal of Urban Planning, (2008) 1-7.

[2] H. P. Lu. Theory and method in transportation planning. Tsing Hua University Press. 1998, pp. 56-73.

[3] Kenneth E Train. Discrete choice methods with simulation. Cambridge University Press, 2003, pp. 45-62.

[4] H. Z. Guan. Disaggregate Model-Traffic Behavior Analysis Tools. China Communications Press, 2004, pp. 27-42.

[5] H. R. Zhu. Study on traffic behavior characteristics and traffic mode choice based on activity analysis. Tongji University, (2005) 32-36.

[6] Hensher D, Greene W. Specification and estimation of the nested logit model: Alternative Normalizations. Transportation Research B, 36 (2002) 3-15.

[7] H. R. Zhang, G. Ren, W. Wang. Application of discrete choice model in trip mode structure forecasting. Journal of Transportation Systems Engineering and Information Technology, 5 (2008) 44-49.

[8] A. Jin. On methodology of parameter estimation in logit model. Journal of Transportation Systems Engineering and Information Technology, 4 (2004) 71-75.

[9] W. T. Zhang. SPSS 11 Statistical Analysis Course. Beijing, 2002.

doi:10.4028/www.scientific.net/AEF.5.105

Practice Analysis of Road Traffic Crashes Accident of a City in China

Liwei Hu[1,a], Jian xiong[2,b]

[1]Faculty of Transportation Engineering, Kunming University of Science and Technology, Kunming 650500, P.R.China; School of Transportation Science and Engineering, Harbin Institute of Technology, Harbin 150090, P.R.China.
[2]Faculty of Transportation Engineering, Kunming University of Science and Technology, Kunming 650500, P.R.China.

[a]liweihukm@sina.com, [b]xjebox@qq.com

Keywords: traffic accidents; crash features; contributory factor; crash type

Abstract. Many studies focused on the development of crash analysis approaches have resulted in aggregate practices and experiences to quantify the safety effects of human, geometric, traffic and environmental factors on the expected number of deaths, injuries, and/or property damage crashes at specific locations. Traffic crashes on roads are a major cause of road crashes in the metropolitan area of Xi'an. In an attempt to identify causes and consequences, reported traffic crashes for six years in Xi'an were analyzed using a sample of 2038 reports. The main types of information from such reports were extracted, coded, and statistically analyzed. Important results were obtained from frequency analyses as well as multiple contributory factors related to traffic crashes, including crash severity, time and location of occurrence, geometry of the road, AADT and *v*/*c*. This paper presents the results of such analyses and provides some recommendations to improve traffic safety and further studies to analyze potential crash locations.

Introduction

Worldwide deaths, disabilities, and injuries from road accidents, a major concern all over the world, have reached epidemic proportions. In 2002, more than 1.18 million people died in road crashes, and approximately fifteen million are injured annually (Source: World report on road traffic injury prevention: summary, 2004). In Europe, the sharp increase in accidents related to urban traffic costs more than two billion dollars during recent years. In Britain, around 3,500 people are killed each year and around 33,000 people are injured in road accidents. There were nearly 6,420,000 auto accidents reported to the police in the United States in 2005, and 2.9 million people were injured and 42,636 people killed, in which talking on a cell phone caused nearly 25% of accidents (Source: http://www.griefspeaks.com/id114.html). In New York City, specifically, the review of 2010 traffic accident database found: 1) 269 traffic deaths of all types and a 34 percent increase in auto fatalities; 2) 18 and 152 fatalities from bicycle accidents and pedestrian accidents, respectively (Source: http://www.lawfitz.com/new-york-city-traffic-accident-deaths-rise-slightly-in-2010). Nowadays, China has also witnessed a substantial rise in the number of traffic crashes, injuries and fatalities, especially since 1998 [1].

In response to these issues, various studies have recently examined aspects of motorcycle safety, in combination with available influencing variables and causes information. Typically, researchers employ statistical techniques (i.e., Poisson, negative binomial and regression models, etc.) in these types of studies [2]. Over the past years, numerous investigations have looked at the age and gender of drivers as risk factors, and younger and older drivers are more prone to be involved in a serious accident than median-aged ones [3]. Road geometric type, lightness, weather condition and other environmental factors (e.g., the time of the day, traffic volume, etc.) also play an important role when analyzing the aspects of accident crashes and injuries [4].

To provide a broad overview, numerous statistical researches have been conducted in order to understand the relations between influence factors and crash features via types of models [5]. Another class of studies utilize time series techniques for identifying the change of accident counts and

accident rates at a given time, analyzing the effects of potential factors on accident occurrence, and developing a statistical model for forecasting future trends of crashes and injuries such as in references [6], and so on. Actually, each crash is a unique event that is caused or influenced by combinations of variables that may not even be observable [7]. Furthermore, reaching such conclusions that a set of variables can be identified as the causes of traffic crash is almost impossible.

This study follows an earlier work on the analysis of traffic accidents at intersections [8] and aims to identify the multiple crash features in Xi'an city. Several potential factors including district, human, vehicle, time, traffic volume, environmental and site factors are considered. Statistical analyses of multiple vehicle traffic accidents are conducted using the crash data in Xi'an city over the time of 2004~2009. The corresponding safety improvement measures are suggested so as to enhance the safety performance of road traffic and decrease the probability of crash occurrence in China's metropolitan regions.

Crash Features

Analyses were performed on the data collected from the General Administration of Transportation in the form of accident reports. The analyses included frequency, cross-classification tabulation, and construction of crash spot maps.

Temporal-Spatial Patterns

Xi'an is at the top of list of cities with alarmingly high traffic crash fatality rates in China. A summary of crash type statistics for the year 2004~2009 for each district is presented in Table 1. More than 85% of crashes were vehicle collisions/crashes. About 53.8% of the total accidents occurred in the Yata district and Beilin district.

Table 1 Number of crashes and injuries by districts

Districts	Crash Type				Injuries				Deaths
	Collision	Running over	Overturning	Drugs	Total	Minor	Major	Total	
Yanta	587	24	32	19	662	70	36	105	38
Beilin	509	12	23	4	548	54	15	68	36
Lianhu	274	15	24	13	326	79	42	121	45
Weiyang	92	21	18	3	134	61	30	91	57
Xincheng	171	14	31	23	239	69	26	95	60
Baqiao	101	11	9	7	128	75	19	94	17
Total	1734	97	137	69	2038	407	167	574	253

Around 318 fatalities occurred in the year 2009 with a decreasing trend. However, the overwhelmingly high proportion of younger drivers involved in traffic crashes has become a serious new concern. Over 60% of the fatalities for 2009 were in the age group of 18-40, though Xi'an had implemented new and stricter penalties under the new national traffic laws in May 2008 in order to minimize traffic crashes. The statistics show that the main cause of crashes is careless driving (e.g., mobile phone use while driving, fatigue, obsessive behavior, etc.) and speeding, which represent about 43% and 26% of the total crashes, respectively. The second main cause of crashes is drunk driving representing about 14%. The rest of the reasons together represent about 17% of total crashes due to facilities, weather and other effects. Therefore, all but a few crashes can be blamed on careless driving, and other factors also play important roles.

Statistics also demonstrate that the safety situation in Xi'an was still serious as shown by the numbers of reported crashes during the years 2004~2009, which are presented in Table 2. The number of crashes increased steadily during the years 2004~2006, and following this period began to decrease. Collisions represented the larger proportion of the total number of crashes. However, the crash rate was still at a high rate. The average number of crashes per day increased from 0.91 in 2004 to 1.06 in

2006 and then decreased to 0.85 in 2009. Crashes involving personal injuries fluctuated between a daily average of 0.15 to 0.4 and, fatal crashes which included at least one death occurred at a daily average of about 0.13, which meant perhaps one life was lost weekly because of road crashes.

Table 2 Statistics of traffic crashes over the year 2004-2009

Year	2004	2005	2006	2007	2008	2009
Total number of crashes	332	346	387	345	317	311
Collision crashes	270	284	324	291	262	259
Crash of overrun/overturning/drugs/others	62	61	64	54	55	52
Total injuries	113	73	102	146	86	54
Minor injuries	76	48	68	107	60	38
Major injuries	37	25	34	39	26	16
Fatal crashes	41	41	37	39	46	49
Average no. of crashes per day	0.91	0.95	1.06	0.95	0.87	0.85
Average no. of injuries per day	0.31	0.20	0.28	0.40	0.24	0.15
Average no. of fatalities per day	0.11	0.11	0.10	0.11	0.13	0.13

Frequency in Age and Weather

Frequency analysis was performed for the following variables: time, day, weather, road surface condition, crash type, crash location, number of lanes, road type, car movement, crash type (general crash, rear end side collision), and severity.

Table 3 presents the injuries and deaths involved in crashes. Clearly, the number of male persons related to crashes was about three times of that of females and about a half of the injuries and deaths were drivers, which also confirmed the importance of educating the safe driving program. Moreover, the percentage of motorcyclists was up to 15.79%, an alarming number among all the injuries and deaths. It was also noticed that 70.77% of injuries and deaths involved persons aging 25~60, especially those between 31~40, a group with higher driving risk. However, we found that the crash involvement rate of younger and older drivers was significant higher than that of medium aged ones.

Table 3 Injury and death categories involved in crashes

Persons	Male	Female	Driver	Passenger	Pedestrian	Motorcycler	Bicycler
Percent/%	74.86	25.14	46.17	13.43	13.45	15.79	11.16
Age	< 16	16-24	25-30	31-40	41-50	51-60	> 61
Percent/%	9.34	11.54	15.93	18.89	19.24	16.71	8.35

Table 4 shows the effects of weather and brightness on crash occurrence. Obviously, the weather has a significant effect on crash occurrence and more than two third of observations occurred on bad weather days including cloudy, rainy, foggy, snowy, and heavily windy ones. Brightness also affects the frequency of crashes through affecting driving behavior of drivers, and we can see that as high as 17.94% of crashes during darkness, with street lamps.

Table 4 Crash distribution by weather and bright effect

Weather	Sunny	Cloudy	Rainy	Foggy	Snowy	Heavy windy
Percent/%	31.73	13.79	17.38	11.17	17.48	8.45
Brightness	Dawn	Daylight	Twilight	Dark with street lamp	Dark without street lamp	Entrance and exit to urban tunnel
Percent/%	1.33	63.74	6.15	17.94	9.97	0.87

Location Specification

Crash distributions according to road type are shown in Table 5. It can be noticed that 33.46% of crashes were in arterial roads. Cumulative percentage shows that 45.09% of crashes occurred on expressways and arterials. This is because of high speeds and high traffic volumes on these two types

of roads, and more frequent entrances and exits on such type of roads also contributed to the occurrence of crashes. The second highest incidence rate was in the sub-arterials category, with 19.72% of crashes occurring on them, due partially to the lack of effective safety facilities. Significantly, unsignalized intersections is a typical black spot prone to traffic crashes.

Table 5 Crash distribution by road type and crash location

Road Type	Percent/%	Position	Percent/%
Expressway	11.63	Roundabout	2.49
Arterial	33.46	Bridge	0.65
Sub-arterial	19.72	Tunnel	0.87
Branch and minor roads	10.12	Unsignalized intersection	12.43
Residential Street	2.36	Signalized intersection	6.27

Table 6 shows the cross tabulation of crash types and districts. It can be noticed from the results that car collision which had the highest percentage of crash occurrence had its highest percentage of 21.8% in Beilin district. This may be attributed to the high traffic volume and low speeds in these districts. The other types are noticed to have their highest percentage of occurrence in Weiyang and Baqiao. Unfortunately, truck-involved crashes made up a large percentage pattern in the crash reports, and this is particularly true for outlying or peripheral areas [10]. Roadside barriers, light poles, even trees and other stationary objects sometimes are prone to cause serious secondary collisions and severe injuries.

Table 6 Crash percentage in types on districts

Crash type	Yanta	Beilin	Lianhu	Weiyang	Xincheng	Baqiao
Car collision	18.8	21.8	19	12.5	14.5	13.4
Collision into stationary objects	12.6	12.6	12.1	23.5	19.8	19.4
Collision into pedestrians	14.7	19.5	17.1	13.9	21.7	13.1
Overturning	18.9	15.1	22.5	13.3	11.9	18.3
Falling down	17.3	11.5	16.1	22.9	9.5	22.7
Others	17.7	19.5	13.2	13.9	22.6	13.1

Potential Causes

As a result of reviewing the crash reports, crashes caused by sudden stop were observed statistically as the most frequent types, responsible for 32.3% of the total records. These usually occurred in traffic congestions where vehicles were moving slowly and traffic was mainly in stop-and-go situations, and drivers usually did not keep enough space between themselves and other vehicles [11]. Actually, traffic safety performance function (SPF), has a statistical relationship with congestion on urban freeways and observed safety, measured in the number of crashes over a unit of given time [crashes per kilometer per year (CPKPY)] and it varies with traffic exposure, measured in annual average daily traffic (AADT). Six years of data were used to analyze such effects on selected multi-type urban road segments. Figure 1 presents a pattern of total observed CPKPYs as the AADT increases for expressway and arterial segments. It should be pointed out that such a function for branch and minor streets was neglected due to a lack of crash records.

In Figure 1, traffic density at 34,000 AADT is a critical point and can be viewed as a critical density (point A), beyond which notably higher crash rates are observed with AADT changes, and the portion of the left of this critical density can thus be considered as a sub-critical zone, as AADT increasing from 8,000 to 34,000 induces the increase of traffic density by 3.5 times [from 5.7pcu per kilometer per lane to 25.8 pcu/(km·ln)], while traveling speed remains almost the same (62 km/h to 55 km/h). The portion to the right of point B can be viewed as a super-critical zone and the portion between

sub-critical and super-critical densities can be viewed as a transitional zone, featuring an increase in CPKPY from 21 to 52, compared with 8-21 from point C to point A. Further examination of SPF reflects that passing an AADT of 34,000, the number of crashes increases at a much faster rate with an increase in AADT.

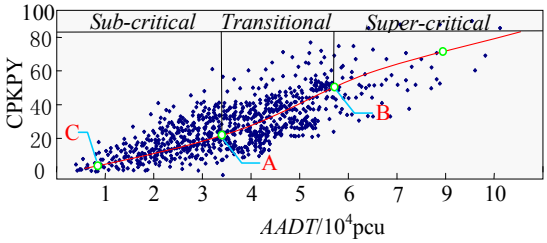

Figure 1 Statistical changes in segment crashes with AADT

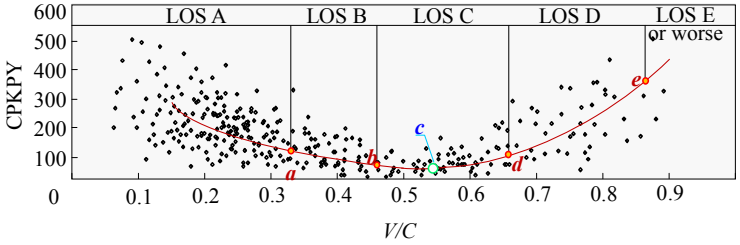

Figure 2 Statistical relation of crash rate and *v/c*

In actuality, the crash rate changes with traffic volume, and SPF reflects how these changes take place. Lower rates within equal SPF mean higher safety rather than higher rates. However, numerous research reports have shown that predictive models that use traffic volume as the only explanatory variable may not adequately characterize the crash process on freeway segments [12]. Functional forms that incorporate density and v/c ratio offer a richer description of crashes occurring on these facilities, whether they are located in a rural or urban environment [13].

Figure 2 shows the relation between traffic crash rates measured in crashes per 100 million vehicle kilometers travelled and volume to capacity ratio (v/c). Obviously, the operation ranging 0.5~0.6 under LOS C meets the lowest level of crash rate and we yield the lowest 45 crashes with respective to moderate v/c (0.54). Such a V regression mode also shows that free traffic flow usually brings serious rear-end or other types of crashes due to drivers' low vigilance of danger. Furthermore, more congested flow under LOS D or worse improves the likelihood of minor crashes.

Nevertheless, separate predictive models for single- and multi-vehicle crashes should be developed rather than one common model for all crash types [14]. Different variables (i.e., type of roads, barriers, etc.), for example, all have varying effects on the occurrence of crashes and statistical rates. Individual analysis may help find potential causes and effective measures to deal with the particular locations or long term safety improvement programs.

Summary

The presented study is designed to be a first step towards analyzing traffic crashes in Xi'an city. Crash features related to time, position, type of roads and type of crashes, etc., and exposure effects involving AADT and v/c analyses provide many important types of information that are required by engineers and decision-makers to improve safety for the driving public in this western metropolis of China. Such analyses must be performed regularly (annually) for long-term traffic safety environment consideration [8].

During the review process of crash reports, some recommendations were suggested. Road geometry in Xi'an should be checked on the national level and improvements should be made at many locations that are not up to standards, for example improving sight distances at intersections and roundabouts; checking the appropriateness of (and redesign if necessary) the acceleration and deceleration lanes to and from arterials and sub-arterials [15], etc. Moreover, it is also recommended to increase awareness of traffic signals ahead by installing warning signs before intersections and to provide enough pedestrian crossings and overpasses, especially at heavy traffic intersections and commercial regions [16]. Sufficient traffic safety education is also necessary not only for drivers but also for voluntary participants (i.e., pedestrians, bicyclists, et al). For scientific research demand, crash messages need to be more accurately identified in order to construct more accurate crash database using available GPS technology [17].

Acknowledgments

This work was financially supported by the National Natural Science Foundation of China (Grant No. 51108137).

References

[1] D. D. Clarke, P. Ward, C. Bartle, et al, "Killer crashes: Fatal road traffic crashes in the UK", Accident Analysis and Prevention, 42(2), 2010, pp. 764–770.

[2] S. Mitra, "Spatial autocorrelation and Bayesian spatial statistical method for analyzing intersections Prone to injury crashes", Transportation Research Record, 2136, 2009, pp. 92–100.

[3] B. Falk, H. Montgomery, "Developing traffic safety interventions from conceptions of risks and accidents", Transportation Research Part F: Traffic Psychology and Behaviour, 10(5), 2007, pp. 414–427.

[4] T. F. Golob, W. W. Recker, "Relationships among urban freeway accidents, traffic flow, weather, and lighting conditions", Journal of Transportation Engineering, 129(4), 2003, pp. 342–353.

[5] X. S. Wang, A. A. Mohamed, P. A. Brady, "Crash estimation at signalized intersections significant factors and temporal effect", Transportation Research Record, 1953, 2006, pp. 10–20.

[6] X. Ye, R. M. Pendyala, S. P. Washington, "A simultaneous equations model of crash frequency by collision type for rural intersections", Safety Science, 47(3), 2009, pp. 443–452.

[7] Y. G. Wang, K. M. Chen, Y. L. Pei, et al, "Integrating before and after crash features into measuring the effectiveness of intersection safety improvement project in Harbin", Transport, 26(1), 2011, pp. 112–121.

[8] H. Zhu, K. K. Dixon, S. Washington, et al, "Predicting single-vehicle fatal crashes for two-lane rural highways in Southeastern United States", Transportation Research Record, 2147, 2010, 88–96.

[9] X. P. Yan, M. Ma, Ming, H. L. Huang, et al, "Motor vehicle-bicycle crashes in Beijing: Irregular maneuvers, crash patterns, and injury severity", Accident Analysis and Prevention, 43(5), 2011, pp. 1751–1758.

[10] K. Ratkeviciute, "Model for the Substantiation of road safety improvement measures on the roads of Lithuania", Baltic Journal of Road and Bridge Engineering, 5(2), 2010, pp. 116–123.

[11] I. Fi, J. Galuska, "Recommendations for new capacity values on freeways", Periodic Polytechnica: Civil Engineering, 54(2), 2010, pp. 127–136.

[12] J. Kononov, B. Bailey, B. K. Allery, "Relationships between safety and both congestion and number of lanes on urban freeways", Transportation Research Record, 2083, 2009, pp. 26–39.

[13] L. D. Zhong, X. D. Sun, Y. S. Chen, et al, "Research on the relationship between V/C and crash rate on freeway", Journal of Beijing University of Technology, 33(1), 2007, pp. 37–40.

[14] S. R. Geedipally, D. Lord, "Investigating the effect of modeling single-vehicle and multi-vehicle crashes separately on confidence intervals of Poisson-gamma models", Accident Analysis and Prevention, 42(4), 2010, pp. 1273–1282.

[15] A. Pande, M. Abdel-Aty, A. Das, "A classification tree based modeling approach for segment related crashes on multilane highways", Journal of Safety Research, 41(5), 2010, pp. 391–397.

[16] O. Prentkovskis, E. Sokolovskij, V. Bartulis, "Investigating traffic accidents: a collision of two motor vehicles", Transport, 25(2), 2010, pp. 105–115.

[17] S. S. Durduran, "A decision making system to automatic recognize of traffic accidents on the basis of a GIS platform", Expert Systems with Applications, 37(12), 2010, pp. 7729–7736.

doi:10.4028/www.scientific.net/AEF.5.111

Influence of High-Grade Highway Construction on Industry-Economic Belt in Heilongjiang Province

Li Shuxia[1], Qin Shihuan[2]

[1] School of Humanities and Social Sciences, Harbin Institute of Technology, Harbin, 150090, China

[2] Shenzhen Graduate school, Harbin Institute of Technology,Shenzhen,518055,China.

E-mail:602373072@qq.com

Keywords: High-grade Highways; Industry-Economic Belt; "Point-Axis-Facet" Theory; Harbin-Daqing-Qiqihar Industrial Corridor

Abstract

With the victory of “Three-year decisive battle”of road construction in Heilongjiang Province and the formation of high-grade highway network, high-grade highways gradually have profound effects on promoting economic and social development and enhancing the public life level, as well as meeting the traffic demands in Heilongjiang province. The influence of the highway construction on industrial-economic belt in Heilongjiang province was analyzed. As an example, by forecasting various index of Harbin-Daqing-Qiqihar Industrial Corridor, we confirmed that the construction of high-grade highways in Heilongjiang play positive roles in industrial-economic belt.

0 Introduction

In the process of building a moderately prosperous society and accelerating modernization, Heilongjiang Province highway transportation needs to achieve leapfrog development in the new environment which is full of great opportunities and severe challenges. In order to promote better and faster development of social economy, the government of Heilongjiang province introduced the Implement compendium of *three- year showdown of the highway construction in Heilongjiang Province* [1] in August 2008, in which they plan to use more than three years to build freeways of 3042 kilometers and highways of grade 1 or 2 of 3355 kilometers and rural highways of,60,799 kilometers as well as to open up the national and provincial trunk highway, the main highway in the province all the completion of two or more roads. Academia and all levels of government continue to recognize the social and economic benefits of highway and recognition, high-grade highway industry in national economic development strategy, the status of the regional industrial layout and structural adjustment has improved significantly. Therefore, the highway industry-economic belt has gradually become the focus question of the transport of Economic Research.

In our previous evaluation research in high-grade highways[2], high-grade highways in provinces such as Hebei, Hubei, Zhejiang, Anhui,etc,can not only bring good economic benefits, but also contribute more than 3% on gross domestic product (GDP) of the same period. And the concept of "*Industrial economic belt of high-grade highways*" was introduced in the General Introduction of Industrial-economic belt of high-grade highways and development along the Yangtze River in Jiangsu Province [3], and its specific function and role profiles of was discussed, and on this basis, a number of targeted recommendations has been made for future development of Industrial-economic belt along the Yangtze River in Jiangsu Province with practice.

For better description of the influence of the construction of high-grade highways on the development of *Industrial-economic*, we carried on research on four aspects，that is the introduction of the theory, the evolution mode, the "point - axis - side" theory and the contribution of Harbin-Daqing freeway to the Harbin-Daqing-Qiqihar Industrial Corridor.

1 High-grade highways industrial-economic belt theory

High-grade highway industry-economic belt refers to the stripe regional economic system which treat the development of high-grade highway as development spindle and the town or city cluster closely linked to each other on the spindle or in its close attract area (about 50 ~ 80 kilometers).

And the high-grade highway industry economic belt has the following characteristics [4]: firstly, it's a system of high-capacity, high-speed and high efficiency; Secondly, there exist full-featured towns of various scales in the region; Thirdly, industries in this region are concentrated, the scale of the economy is considerable and the growth speed is great; Fourthly, different towns in the area have different division of labor and the industry have a pattern of diffusion in ladder shape along the highway.

In view of this, and combined with the general characteristics of Traffic Economic Belt, the meaning of the high-grade highways industrial economy should be a stripe regional economic system built on high-grade highways and the transport networks they formed, which is based on the features of high-grade highways, which rely on the large and medium-sized cities along the high-grade highways, which treat the import and export and crossroads of the high-grade as growth poles and treat the high-grade highway network and other linear infrastructure (mainly supporting highways, and other communications lines) as the development axis as well, and which is dominated by the development of efficient agriculture, high-tech industries and tourism, information and other emerging industry-led regional economic sustainable development objectives for the constraints of a ribbon, which is the inevitable product of the industrialized societies and is a contemporary space economy form one of the most typical and most common form.

2 Formation and evolution mode of high-grade highways industrial-economy belt in Heilongjiang

The constructions of high-grade highways strike the regional economic system which is at low level balance thus inducing the imbalance of regional development. The gathering effect was enhanced and the economic development was accelerated at the exit or the intersection of high-grade highways while economic developments of many other areas are stagnated due to the negative impact of high-grade highways [5]. High-grade highways continue to act on the legions along the highways, the general level of economic development in the region are improved, and the extent of the impact of high-grade highways reached equilibrium. Logistics, people, technology flow and the flow of information in the region exchanged freely, level of economic development in each "point" was significantly higher than adjacent areas, and the structure of the economy as a whole space achieved a high grade of balance, then the economic belt of high-grade highway industry has basically taken shape.

Generally speaking, the formation of highway industry-economic belt goes through three phases with significantly different characteristics; following is the elaboration on the formation of the Harbin-Daqing freeway industry-economic belt.

1) Prototype stage

In the early stage after Harbin-Daqing freeway was built, poor economic development regions away from the exit subject to a greater negative impact which reduce the rate of economic growth. At this stage，the decrease in the number of geographical latent region was taken as the principal thing ,the amount of the regions was considerable and started decreasing, growing region began to appear and the number of diffusion regions kept the same.

2) Growth Stage

Since Harbin-Daqing freeway opened to Public，agricultural industry structure of the towns along it has undergone tremendous changes. Efficient agriculture, aging, agriculture, and agricultural production area of specialization has been through great development; internal industry structure of industry and the tertiary industry has increased. The number and the strength of the

towns were rapidly expanded and enhanced, and population kept gathering to the areas along the freeway, polarization effect was further enhanced, and the core - the edge of the dual space structure has become increasingly evident.

3) Maturation Stage

At this stage, Harbin-Daqing freeway economic belt has been expanded rapidly, economic belt within the urban division of functions and linkages became more explicit, satellite towns of cities kept emerging, and the local section of Megalopolis began to appear, the influence basin of the economic belt received more expansion. The main features of this stage is the appearance of the diffusion region and the disappearance of latent types, as well as the decrease or even the disappearance of the output types, and teemed with a large number of growth types whose rate of increase slows down.

If they continued to developing new development axis after the mature of certain industry-economic belt (such as new high grade highway or high-grade railway), then the formation and development of the industrial-economic belt with a new development axis began with a new round of circulation.

3 Point, axis, facet of industrial-economy belt of high-grade highways in Heilongjiang Province

3.1 The "point" of the High-grade highway

The so-called point means that any one region is starting with some points on the start, then develop along the axis between each point, and interwoven into the economic network, which is the starting point of a regional development. Economic belt of high-grade highways are mainly divided into two types: one is the existing town, the other is located in the town the highway intersection.

There gradually formed the LongYun, New XiangFang, Ha Dong the SongBei four logistics parks which located separately in the south, east, and north in Harbin. And there formed freight market with integrated logistics center as a platform, exhibition and trade hall, Container Yard and logistics trading sector with Daqing Wanbao petrochemical logistics center as a platform, processing area and storage area in Daqing. While there exit formation of three major logistics markets the Nanyuan Logistics Base, the Beiyuan logistics base, and the North Warehouse Logistics Center.

3.2 The "axis" of the High-grade highway

Concentration and diffusion of regional economic activities are not in disorder, it has a trend of longitudinal diffusion along the high-grade highway. Attract and diffusion force along the highway will have an important impact on the economic development. It can be predicted that construction of high-grade highway in the three-year showdown will undoubtedly become the axis of future economic development of Heilongjiang.

The direct distance of axis of high-grade highways to attract logistics facilities in the area is about 10 km. Diffusion distance and the distribution range of Logistics center depends on their own skills and the quality of the existing transportation infrastructure, and the travel time along the axis of the high-grade highways. The results show that the logistics facilities located within 5 km accounting for 75.5%, and 10 km or less accounting for 97.1%.

Result of advantages survey in freeway interchange near the entrance location shows that it can be helpful for transportation between the cities (51.2% of investigators), avoiding traffic jam (50.9%), operation of the oversize vehicles (36.8%), and convenient joints to the port and airport (9.9%).

3.3 The “facet” of the High-grade highway

High-grade highway economic industry belt is the result of the point-shaft spread, the result of the development is the expansion of gathering center and increase of extreme center, and the further development at this time can form organically contacted urban agglomeration or metropolitan areas with high grade highways as axises, all sorts of cluster center for support, composed of different levels of transportation network within the given areas. Taking Harbin-Daqing freeway as an example, the industrial economy of Harbin-Daqing highway took Harbin and Daqing as developing

centers, relying on scale economies in the two core cities, whose development pattern is “points and axises”. Cities along the highway such as Zhaodong and Anda developed gradually into organic connection part of Harbin and Daqing.

4 Contribution of Harbin-Daqing freeway on the Harbin-Daqing-Qiqihar Industrial Corridor

Construction of Harbin-Daqing-Qiqihar Industrial Corridor project, which is located in the southwest of Heilongjiang Province, began in August 2005.The provincial capital city of Harbin, the oil city of Daqing, heavy equipment, industrial city of Qiqihar and cities along the freeway like Zhao Dong and Anda are included in the Corridor, and the total planned area is 921 km2, the actual start area was 62.4 km2 by the end of 2009[6]. Industries prioritized in the cities along Harbin-Daqing-Qiqihar industrial corridor are shown in the table below.

Table 1 Industries prioritized in the cities along Harbin-Daqing-Qiqihar industrial corridor

City	Industries prioritized
Harbin	Focus on the development of high-tech such as the leading automotive, aerospace, mechanical and electrical industry, pharmaceutical industry, environmental protection industry, information industry, green food industry and modern logistics industry.
Daqing	Focus on developing alternative industries with high additional value, such as petrochemical, natural gas chemical industry, and substitute industries like agricultural and sideline products deep processing, textiles, new materials, machinery manufacturing, electronic information,etc.
Qiqihar	Focus on making the equipment industry, expanding the green food industry and kerosene chemical industry bigger and stronger, developing the electronic information, environmental protection, energy, paper, metallurgy, building materials industry vigorously.
Zhaodong	Focus on the development of the biotechnology industry and agricultural products, grain deep-based Chinese herbal medicine deep processing industry.
Anda	Focus on the development of dairy-based agricultural and sideline products and fine chemicals and taking on the petroleum products processing industry under the radiation of Daqing.

It can be seen from Table 1, the development of the industry in the cities along the Harbin-Daqing-Qiqihar Industrial Corridor are inseparable from the fast and efficient support of the Harbin-Daqing freeway, it can be concluded that Harbin-Daqing freeway provides a strong support for development of the cities along it. What can be specifically reflected is that it promotes the economic development of the Harbin-Daqing-Qiqihar Industrial Corridor; the social development of the cities in the area of Harbin-Daqing-Qiqihar Industrial Corridor; and the commodity circulation of the Harbin-Daqing-Qiqihar Industrial Corridor; as well as the development of tourism resources along it.

4.1 Promotion of Harbin-Daqing freeway on the economic development of the Harbin-Daqing-Qiqihar Industrial Corridor

Harbin-Daqing freeway provides a good investment environment for Harbin-Daqing-Qiqihar Industrial Corridor; promotes the vigorous development of the export-oriented economy of the Harbin-Daqing-Qiqihar Industrial Corridor and the rapid development of utilization of foreign captivate in the region. Changes of gross industrial production from 2006 to2010 along Harbin-Daqing-Qiqihar Industry Corridor and in the project area are shown in Figure 1.

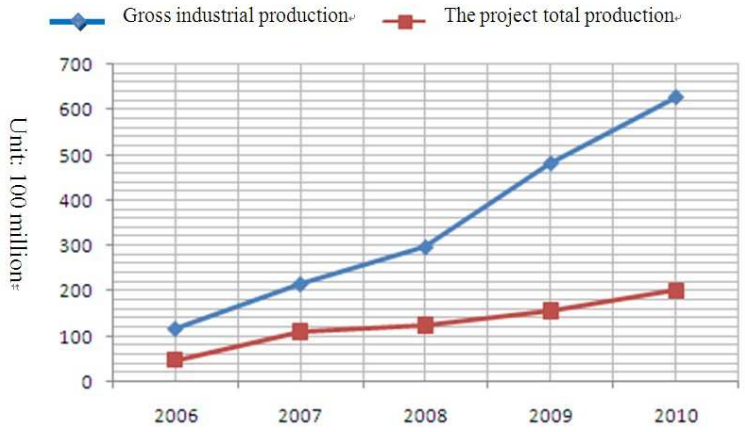

Figure 1 Changes of gross industrial production along Harbin-Daqing-Qiqihar Industry Corridor and in the project area

It can be seen from Figure 1, since the construction of Harbin-Daqing-Qiqihar Industry Corridor the number of enterprises relying on convenient transportation conditions provided by Harbin-Daqing freeway increased with continuous expansion of the construction scale. From 2006 to 2010, GDP in the Harbin-Daqing-Qiqihar Industrial Corridor received rapid development, from 11.7 billions in 2006 to 62.67 billion in 2010.

4.2 Promotion of Harbin-Daqing freeway on the social development the cities in the area of Harbin-Daqing-Qiqihar Industrial Corridor

Harbin-Daqing freeway promotes the economic development of Harbin-Daqing-Qiqihar Industrial Corridor as well as the social development of areas along it. The following table shows how the cities along Harbin-Daqing-Qiqihar Industrial Corridor developed in 2010.

Table 2 Development of the cities along the Harbin-Daqing-Qiqihar Industrial Corridor in 2010

Item \ City	Harbin	Qiqihar	Daqing	Zhaodong and Anda
The total planning area of the project (km^2)	287	128	340.0	217
Gross industrial production (100 million)	192.5	133.5	231.2	69.5
Total production of the project (100 million)	63.3	43.9	71.7	22.2

It can be seen from Table 2, the total planning area of the project in Daqing is the biggest and followed by Harbin and Qiqihar. Industrial output value of Daqing ranges the first, which is 23.12 billion Yuan, followed by Harbin, Qiqihar, Zhaodong and Anda. Since the project is still in the stage of rapid construction and development, it is reasonable to believe that the rapid development of industrial output value of Harbin, Daqing and Qiqihar will continue.

Gross industrial output value of Harbin and Daqing accounted for more than 70% of the total output value of Harbin-Daqing-Qiqihar Industrial Corridor, thus Harbin and Daqing becoming two key development supporting points of Harbin-Daqing- Qiqihar Industrial Corridor, which play a decisive role in the development of Harbin-Daqing-Qiqihar Industrial Corridor. As it were, development of cities along the Harbin-Daqing freeway leading the development of Harbin-Daqing-Qiqihar Industrial Corridor.

4.3 Promotion of Harbin-Daqing freeway on the circulation of commodities of the Harbin-Daqing-Qiqihar Industrial Corridor

Due to the construction of Harbin-Daqing freeway, time of the goods in transit is shortened; the economical efficiency of transportation increase and the circulation of commodities in Harbin-Daqing-Qiqihar industrial corridor and the development of urban and rural trade are promoted. At present, Harbin-Daqing-Qiqihar Industrial Corridor is relying on the advantages of the highway to speed up the circulation of commodities and develop to a deeper and wider field with the idea of bigger market and bigger circulation.

The following table shows the proportion of Harbin-Daqing-Qiqihar Industrial Corridor accounted for the province's freight. It can be seen that freight volume of the cities along Harbin-Daqing-Qiqihar industrial corridor accounted for a large proportion of over 30% of that in Heilongjiang from 2006 to 2009, among which freight volume of Harbin and Daqing contributed 20% or more.

Table 3 Proportion of freight volume in Harbin-Daqing-Qiqihar industrial corridor in the total freight volume of the province

Years	total freight volume(10000 tons)	Contribution rate of Harbin-Daqing-Qiqihar Industrial Corridor (%)	Contribution rate of Harbin - Daqing (%)
2006	48389	34.36	22.86
2007	51996	32.86	21.81
2008	35424	51.35	34.31
2009	36486	45.09	27.02

Recently, the comprehensive economic strength and quality of Heilongjiang Province kept springing and the economic attractiveness of the surrounding areas is enhanced, thus providing a broader space for the development and expansion of Harbin-Daqing-Qiqihar Industrial Corridor. The total GDP of the cities along Harbin-Daqing-Qiqihar Industrial Corridor has always been in a steady upward trend. The following table shows GDP and the growth of it in Harbin-Daqing-Qiqihar Industrial Corridor from 2003 to 2010.

Table 4 GDP and its growth in Harbin-Daqing-Qiqihar industrial corridor in 2003-2010

Project	2003	2004	2005	2006	2007	2008	2009	2010
GDP (100 million)	4057	4750	5511	6216	7077	7912	8885	9996
Growth Rate (%)	10.2	11.7	11.6	12.0	12.1	11.8	12.3	12.5

4.4 Promotion of Harbin-Daqing freeway on tourism resource development

There are rich tourism resources along Harbin-Daqing-Qiqihar Industrial Corridor. People's travel speed is speed up, travel time is shortened and the comfortableness，convenience and continuity of the travel are improved because of the freeway. And the development and effective utilization of tourism resources along the Corridor are promoted.

Highway volumes of passenger traffic in Heilongjiang from 2000 to 2010 are shown in Figure 1-2. Domestic tourist arrivals and tourism revenues of Heilongjiang increased year by year from 2005 to 2010. Convenience of Harbin-Daqing freeway greatly promoted the tourism development of the cities along Harbin-Daqing-Qiqihar Industrial Corridor and the growth of tourism income in Heilongjiang.

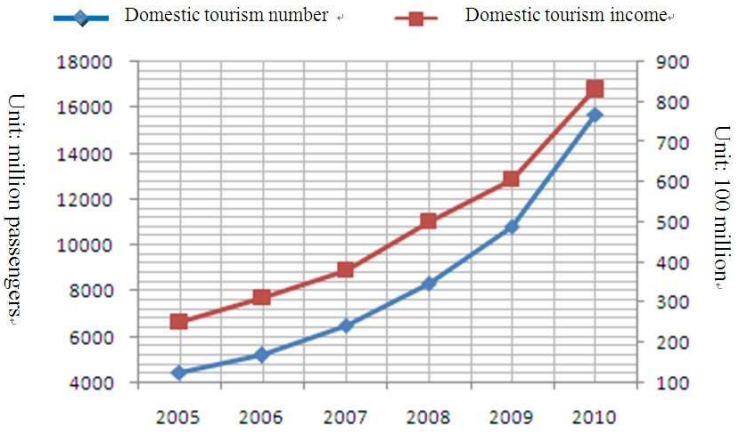

Figure 2 Variation trends of domestic tourist arrivals and tourism revenue in Heilongjiang from 2005 to 2010

5 Conclusions

This article describes the evolution of high-grade highways industrial economic belt, which has gone through three stages of the prototype stage, growth and maturity. Four aspects of contributions of Harbin-Daqing Freeway on the Harbin-Daqing-Qiqihar Industrial Corridor were illustrated, that is the promotion on economic development of Harbin-Daqing-Qiqihar Industrial Corridor, the promotion of social development of the cities along Harbin-Daqing-Qiqihar Industrial Corridor, the promotion on the circulation of commodities of Harbin-Daqing-Qiqihar industrial corridor, and the promotion on the development of tourism resources along it.

6 References

[1]Wang Qingyun. Optimize the structure: grasp the adaptability of the transportation and economic development [J]. Integrated transport,2009,(5):20-22.

[2]Shang Jie, Tong Guang Ji.The rapid development of new ways of rural economy [M]. Harbin: Northeast Forestry University Press, 2004, (6)74-83.

[3]Guo Chen, Ming-Hua Yang. Jiangsu Province along the Yangtze River development and the highway industrial economy with Summary [J]. Southeast University of Economics and Management, 2007, (9):05-10.

[4]Nan Liu. The highway's impact on regional economic development --- Zhejiang Province, Hangzhou-Ningbo Expressway [J]. China Soft Science, 2002,(11): 98-101.

[5]HAN Zeng-lin, etc. Highway economic belt formation and evolution mechanism and layout planning method are discussed [J]. Geography, 2001, (4): 471-478.

[6]Harbin-Daqing-Qiqihar Industrial Corridor overall industrial layout planning[R]. Heilongjiang Province Development and Reform Commission, 2005, (8): 11-16..

doi:10.4028/www.scientific.net/AEF.5.118

Modeling for Driver Decision-Making Behavior during Amber Signal Time at Intersection

Qi Weiwei[1, a], Pei Yulong[1, b], Song Mo[1, c]

[1]School of Transportation Science and Engineering, Harbin Institute of Technology, Harbin 150090, China

[a]qwwhit@163.com, [b]yulongp@263.net, [c]07smhit@163.com

Keywords: amber light; red clearance; amber interval dilemma; game theory model; traffic safety

Abstract. Current traffic lights are composed of red, amber, and green, and the drivers' behavior choices and the content of the relevant laws & regulations during the amber light are disputed. For current signal intersections, the amber light time and the red clearance aren't differentiate from each other, and most of the time ,the amber light time acts as red clearance. It will not improve the traffic operating efficiency of the intersection, but bring more traffic conflicts, if the role of the amber light returns to academic definition, in which the amber is a warning signal. In this paper, the process that the drivers choose stopping by slowing down or passing by maintaining the speed during amber time is analyzed through studying the vehicle dynamic characteristics. The generalized amber interval dilemma is defined to establish the mixed-strategy game theory model, which reveals the utility of the driver and signal manager during the amber interval, and the research in algorithm of Nash Equilibrium point is also a focus. According to Nash Equilibrium, the optimal solution of the game theory model is (acceleration, amber setting) or (deceleration, amber canceling).

Introduction

Method of amber timing plays a significant role in the safety and efficiency of intersections. However, the purpose of amber interval in a signal cycle is not clearly defined in current traffic regulations. The lack of uniform design method for amber light causes lots of confusions in traffic operation and enforcement in China [1]. The driver characteristics include brake-response time for first-to-stop vehicles, deceleration rates for first-to-stop vehicles, distinguishing characteristics and predictions of first-to-stop versus last-to-go events, and distinguishing characteristics and predictions of red-light-running events [2]. Statistical analyses were used to investigate the effects of the time to stop line, gender, age group, and grade on the average deceleration rates. Results demonstrate that male drivers appear to show slightly higher rates of deceleration than female drivers. This difference increases as the trigger time to stop line decreases. Younger drivers (younger than 40 years old) and older drivers (60 years of age or older) exhibit greater deceleration rates when compared with drivers in the age group from 40 to 59 [3]. The models that characterize driver brake perception–reaction time (PRT), brake time, and stop–go decisions at the onset of an amber indication at a high-speed signalized intersection approach [4]. Many scholars devoted themselves to the optimization amber light time, and the results are applied to the field of urban traffic management and control [5, 6]. Driver characteristics during amber interval are important for aspects such as intersection safety evaluation, signal timing design and so on. Driver behavior model is proposed based on logistic regression method, and the model is tested by receiver operating characteristic curve [7, 8].

Amber Interval Dilemma

The first type of dilemma zone occurs at locations where amber times are not long enough. This causes a situation, in which some drivers can't stop in time for the red indication without uncomfortable braking, but also can't enter the intersection before the red indication without considerable accelerating. The upping condition represents a traditional definition of dilemma zone,

which referenced by most traffic engineering textbooks and guides. This situation can be improved with amber intervals that are sufficiently long. ITE (Institute of Transportation Engineers) recommends the following equations for timing the amber interval to eliminate the dilemma zone:

The amber lights up, if the driver decides to brake, then relevant Stopping Distance (s_H) will be consist of Response Distance (s_{Re}) and Braking Distance (s_B), which is shown as follows [1]:

$$s_H = s_{\mathrm{Re}} + s_B \tag{1}$$

According to dynamic characteristics of the vehicles, design formula for s_{Re} and s_B are shown as follows [1]:

$$s_{\mathrm{Re}} = vt_{\mathrm{Re}} \tag{2}$$

$$s_B = v^2 / 2b_v \tag{3}$$

Where, v represents driving speed of the vehicles/ ($\mathrm{m \cdot s^{-1}}$);

b_v represents braking deceleration of the vehicles/ ($\mathrm{m \cdot s^{-2}}$).

The amber lights up, if the vehicle runs at a relatively high speed and has already approached the stopping line, then in premise of keeping previous speed, the driver should take decision to pass through, that is passing through the stopping line before the red light starts. Then the vehicle will steer in a distance of s_F at previous speed during the time of amber light, whose formula is as follows [1]:

$$s_F = vt_A \tag{4}$$

Where, s_F represents the distance that the vehicle runs at previous speed during the time of amber light/ (m); t_A represents the time of amber light/ (s).

Parking curve and passing curve for the vehicle at time of amber light can be pictured separately from formula (1) and formula (4), which is shown in figure 1. The dash area in the figure 1 represents amber interval dilemma. The diver can neither stop at the stopping line safely, nor pass though the stopping line without acceleration at the amber interval dilemma.

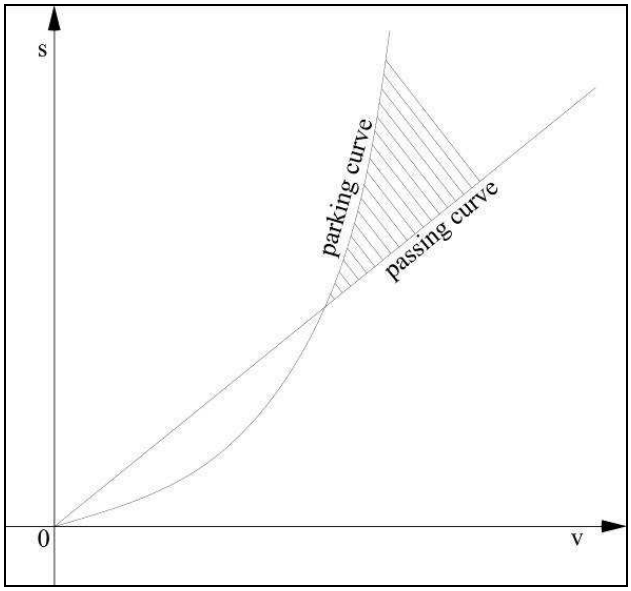

Figure 1 Decision Curve for Drivers

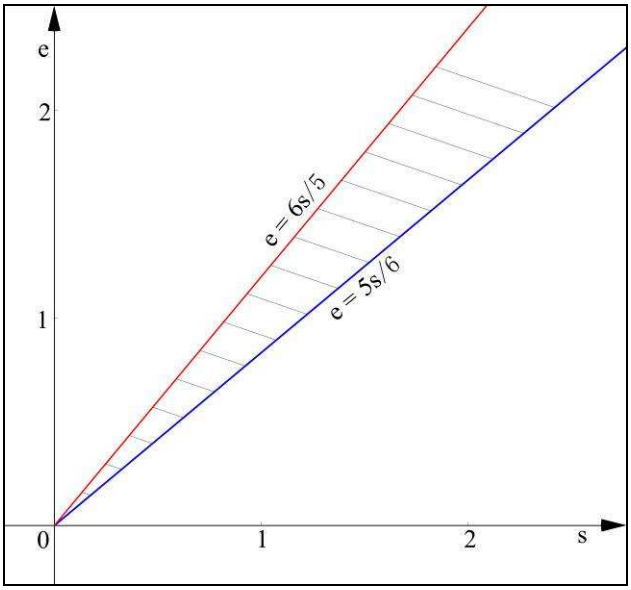

Figure 2 Game Theory Curve for Drivers

The decision-making behaviors of the drivers in the amber light time of the signal-controlled junctions are established under the driver's absolute obedience to road traffic specification. In reality, the drivers, each of whom has a selfish side, often don't comply with the relevant specifications in amber light period, and to accelerate through the intersection, which leads to serious conflicts. Thus, the next section demonstrates the game theory model between the drivers and managers based on the driver's absolutely rational within the amber light time at signalized intersections.

Game Theory Model

A. Game Theory Model for Pure Strategy

The amber light problem is related to traffic efficiency and driving safety, which can evolve into the game theory model between the driver and signal manager.

(1) Assume that the driver only concerns about traffic efficiency, and signal manager only concerns about driving safety in the amber light time, then the game theory model can be established as payoff matrix 1. According to Nash Equilibrium, the optimal solution of the game theory model is (acceleration, amber setting).

payoff matrix 1		manager	
		amber setting	amber canceling
driver	acceleration	u, $-u$	$2u$, $-2u$
	deceleration	$-2u$, $2u$	$-u$, u

(2) Assume that the driver only concerns about driving safety, and signal manager only concerns about traffic efficiency in the amber light time, then the game theory model can be established as payoff matrix 2. According to Nash Equilibrium, the optimal solution of the game theory model is (deceleration, amber canceling).

payoff matrix 2		manager	
		amber setting	amber canceling
driver	acceleration	$-u$, u	$-2u$, $2u$
	deceleration	$2u$, $-2u$	u, $-u$

The analysis result shows that the process of decision-making behavior for the driver and signal manager is concerned about the tendency closely to traffic efficiency or driving safety, which affects the driver's behavior in the amber light significantly. Both traffic efficiency and driving safety should be considered in the research, and a mixed strategy game model will be established to describe the relationship between the driver and signal manager.

B. Game Theory Model for Mixed Strategy

Drivers' selection is single in the matrix 1 and matrix 2, but it is not stationary that drivers select acceleration or deceleration. They select one of the two acts with a certain probability. Assuming p is the probability for drivers to select acceleration, and $(1-p)$ is the probability to select deceleration. Assuming q is the probability for managers to select amber setting, and then $(1-q)$ is the probability to select amber canceling. The game theory model can be established as payoff matrix 3. The payoff for driver and manager can be expressed as function $\Omega(p,q)$, and according to Nash Equilibrium, the optimal solution of the game theory model is calculated through formula (5) and (6).

payoff matrix 3			manager	
			amber setting	amber canceling
			q	$1-q$
driver	acceleration	P	$e-s/2$, $s-e/2$	$2e-2s$, $-2s+2e$
	deceleration	$1-P$	$-2e+2s$, $2s-2e$	$-e/2+s$, $-s/2+e$

$$\Omega_{driver}(p,q) = pq(e - s/2) + p(1-q)(2e - 2s) + (1-p)q(-2e + 2s) + (1-p)(1-q)(-e/2 + s) \quad (5)$$

$$\Omega_{manager}(p,q) = pq(s - e/2) + p(1-q)(-2s + 2e) + (1-p)q(2s - 2e) + (1-p)(1-q)(-s/2 + e) \quad (6)$$

A first-order differential condition of formula (5) and (6) is as follows:

$$\begin{cases} \frac{\partial \Omega_{driver}}{\partial p} = (\frac{1}{2}e + \frac{1}{2}s)q + (\frac{5}{2}e - 3s) = 0 \\ \frac{\partial \Omega_{manager}}{\partial q} = (\frac{1}{2}s + \frac{1}{2}e)p + (\frac{5}{2}s - 3e) = 0 \end{cases} \quad (7)$$

From formula (7), the Nash Equilibrium (p^*, q^*) can be calculated as follows:

$$\begin{cases} p^* = \frac{3e - 2.5s}{0.5e + 0.5s} \\ q^* = \frac{3s - 2.5e}{0.5s + 0.5e} \end{cases} \quad (8)$$

Next section, the solution of equation (8) is discussed according to the relation between *e* (value of traffic efficiency) and *s* (value of driving safety).

Discussion for Game Theory Model

The $0 \le p^* \le 1$ and $0 \le q^* \le 1$ are the objective conditions of probability function variables, so inequality can be expressed as follows based on the equations (8).

$$\begin{cases} 0 \le \frac{3e - 2.5s}{0.5e + 0.5s} \le 1 \\ 0 \le \frac{3s - 2.5e}{0.5s + 0.5e} \le 1 \end{cases} \quad (9)$$

Based on formula (9), it can be calculated as formula (10).

$$\begin{cases} \frac{5}{6}s \le e \le \frac{6}{5}s \\ \frac{5}{6}e \le s \le \frac{6}{5}e \end{cases} \quad (10)$$

So, Discussion is extended as follows:

1) When $e = \frac{5}{6}s$ and $s = \frac{6}{5}e$, then $p^* = 0$ and $q^* = 1$

2) When, $e = \frac{6}{5}s$ and $s = \frac{5}{6}e$, then $p^* = 1$ and $q^* = 0$

This inequality (10) can be represented as a shaded area in the two-dimensional axis, which is shown in figure 2. Thus, the condition $e = s$ is a special condition, and the payoff matrix 3 can be updated as payoff matrix 4, in which, we assume $e = s = 1$. According to Nash Equilibrium, the optimal solution of the game model is ($p^* = 0.5$, $q^* = 0.5$). The results show that drivers will make choice from acceleration or deceleration with probability of 0.5.

payoff matrix 4			manager	
			amber setting	amber canceling
			q	$1 - q$
driver	acceleration	P	1/2 , 1/2	0 , 0
	deceleration	$1 - P$	0 , 0	1/2 , 1/2

Conclusions

In summary, the optimal solution of the game theory model for pure strategy and mixed strategy is similar, and the following conclusions can be got.

1) The drivers and mangers pay attention to both traffic efficiency and driving safety, and the probability they select which acts is closed with the relation between e and s.

2) The drivers who have the selfish side often don't comply with the relevant specifications in amber light period, because that (acceleration, amber setting) is one of the optimal choices in the model for pure strategy.

3) It is rational that the mangers improve traffic operation level by prohibiting passing the stop line in amber light period, because that (deceleration, amber canceling) is one of the optimal choices in the model for pure strategy.

Acknowledgments

The study was supported by the National Natural Science Foundation of China (51178149).

References

[1] K. P. Li, P. K. Yang, Y. Ni. Amber Interval Design at Urban Signalized Intersections. Urban Transport of China, July 2010, 8(4): 67-72

[2] T. J. Gates, D. A. Noyce, L. Laracuente, and E. V. Nordheim. Analysis of Driver Behavior in Dilemma Zones at Signalized Intersections. Transportation Research Board of the National Academies, Washington, D. C., 2007, pp. 29-39

[3] I. E. Shawarby, H. Rakha, V. W. Inman, and G. W. Davis. Evaluation of Driver Deceleration Behavior at Signalized Intersections. Transportation Research Board of the National Academies, Washington, D. C., 2007, pp. 29-35

[4] H. Rakha, A. Amer, and I. E. Shawarby. Modeling Driver Behavior within a Signalized Intersection Approach Decision–Dilemma Zone. Transportation Research Board of the National Academies, Washington, D. C., 2008, pp. 16-25

[5] L. G. Zhang, J. D. Fan, J. K. Zhang. The Optimal Model of Chang Interval for the Signalized Intersection. Technology & Economy in Areas of Communications, 2009, 53(3): 16-18

[6] H. Retzko, M. Boltze. Timing of Inter-green Periods at Signalized Intersections: the German Method. ITE Journal, 1987, 7(1): 23-26

[7] K. J. Long, L. R. He, L. D. Han. Driver Behavior at Signalized Intersection during Yellow Interval. Systems Engineering, 2010, 28(12): 117-120

[8] Papaioannou P. Driver behavior, dilemma zone and safety effects at urban signalized intersections in Greece. Accident Analysis and Prevention, 2007, 39: 147-158

doi:10.4028/www.scientific.net/AEF.5.123

Evaluation Index System on Relationship between Urban Mass Rail Transit and Its Surrounding Land Use Based on TOD Mode

Chuan Ding[1, a], Yaowu Wang[1, b], Binglei Xie[1, c] and Yaoyu Lin[1, d]

[1]Shenzhen Graduate School, Harbin Institute of Technology, Shenzhen, 518055, China

[a]dingchuan@126.com, [b]wyw@hitsz.edu.cn, [c]xiebinglei@126.com, [d]linyy@hitsz.edu.cn

Keywords: Mass Rail Transit, Land Use, Relationship, TOD Mode, DEA Model

Abstract: To establish the evaluation index system on relationship between urban mass rail transit and its surrounding land use based on transit oriented development (TOD) mode, the suitable methods and principles of evaluation index system were analyzed. An evaluation procedure frame was proposed based on data envelopment analysis (DEA) model. Then the evaluation indexes from urban mass rail transit system and land use system selected based on interactive relations between urban mass rail transit and land use under TOD mode.

Introduction

There is complex interaction between urban transport and land use. Urban transport improves the accessibility to different regions, and makes a significant effect on land use, while land use is derived from the transportation generation[1]. Total transportation demand, with distribution of main traffic direction can be determined by land-use pattern and function layout[2].

Currently, mass transit rail has become a sustainable mode in the face of more serious traffic congestion, energy consumption and traffic environment problems, etc. Many cities in China are constructing mass transit rail. Large-capacity, rapid-speed, and low-pollution rail transit meets not only the urban traffic demand, but also strengthens commerce, employment activities in the central city, therefore stimulates the formation of outskirts development along the rail route. In order to achieve the coordinated development between urban rail transit and its surrounding land use, a scientific and rational evaluation index system should be firstly built, and then coordinated development status can be determined, which can provide a theoretical basis on planning and construction adjustment for operational management.

Many scholars have done some researches on the relationship between transportation and land use. Chu constructed macro evaluation index system considering the characteristics of Beijing, where indexes were selected from three aspects, land intensive degree, efficiency and service level of transport system, and environmental quality[3]. Yang analyzed coordination of urban transportation and land use in 16 typical cities of China, and proposed a simply evaluation indexes based on TOD, however, the index system didn't embody the interactive relationship between transportation and land use, just considering them as input and output of the system separately[4]. University of North Carolina and Curtis established a evaluation system on coordinated relationship between transportation and land use regarding to the distributed and low-density development mode for some large cities in U.S. That is helpful reference to construct the evaluation index system between rail transit and its surrounding land use in high-density cities of China[5-6]. In conclusion, the current studies on relationship evaluation between urban transportation and land use are concentrated on the macro level, so coordinated development discussion of urban rail transit and land use are mainly qualitative analysis[7-8].

In the implementation stage, TOD programs may not carried out strictly accordance with the standard planning scheme, and deviated from the coordinated planning of rail transportation and land use due to different benefits of government, real estate developers and other departments. In reality, it turns to be a transit related development (TRD), rather than transit oriented development. In different stages of construction period, tracking survey on implementation effects is necessary for

coordination evaluation. In this paper, micro evaluation on coordination relationship between mass rail transit and its surrounding land use has some theoretical and practical significance. The urban mass rail transit and land use based on TOD are shown in Fig. 1.

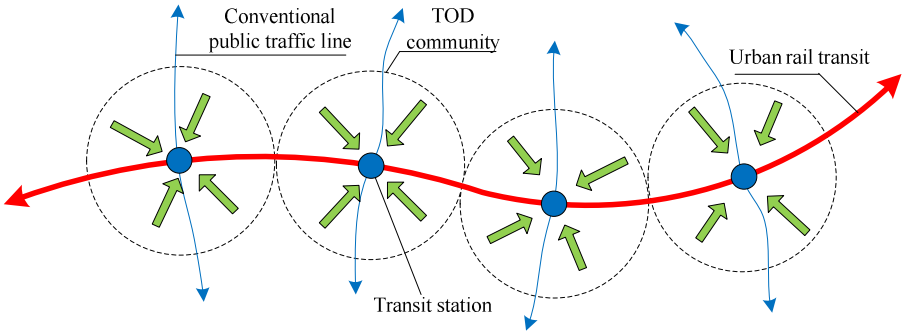

Fig. 1 Urban mass rail transit and TOD area land-use

Evaluation methods selection and principles

Evaluation object selected in this paper are the urban rail transit and its surrounding land use named TOD community along the route. Land development is guided by the mass rail transit. Therefore, mass rail transit is considered as a system input, land use of the TOD community as a system output, and validity of the system input-output is the extent of the coordinated degree between urban rail transit and land use of TOD community. Firstly, representative indexes are selected from the two systems to establish the evaluation index system. The input-output relationship between mass rail transit and land use is described in Fig. 2.

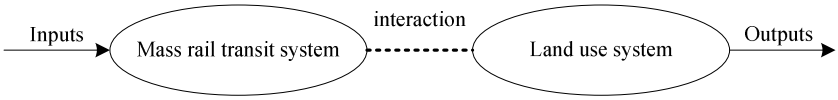

Fig. 2 Urban mass rail transit and TOD area land use

Evaluation methods selection

There are analytic hierarchy process, fuzzy comprehensive evaluation method, value function method and data envelopment analysis in multi-objective decision making to assess a complex system. Data envelopment analysis was proposed by Charnes, Coopor and Rhodes in 1978. The principle of the method considers every evaluation object as a decision making units (*DMU*), maintains input or output of *DMU* unchanged, and get the overall analysis of the ratio of input to output. Linear programming technique can be employed to determine the relatively valid production frontier, and then the individual *DMU* are projected onto valid frontier. Finally, the relatively validity of *DMU* is determined according to distance of the *DMU* deviated from the valid frontier.

There are four reasons for DEA method selected in this paper. Firstly, it can adapt to the evaluation index system which has a multiple input and output on the comprehensive validity evaluation. Especially, it has an absolute advantage since it can access validity of multi-objective decision-making of complex system. Secondly, making index being dimensionless of input and output data are not needed in DEA method. Consequently, it cannot be affected by different measurement units of the indexes, and thus more accurate. Thirdly, the model itself can calculate the weight. It does not require a pre-given weight of the input and output indexes, excluding a lot of subjective factors. It has irreplaceable advantages compared with traditional method, and improves the accuracy of evaluation results greatly. Last, DEA method can not only judge the validity of *DMU*, but also further analyze the cause of the *DMU* invalid, and obtain countermeasures using DEA projection principle.

The evaluation procedure frame of coordinated relationship between mass rail transit and TOD communities based on DEA method is proposed in Fig. 3.

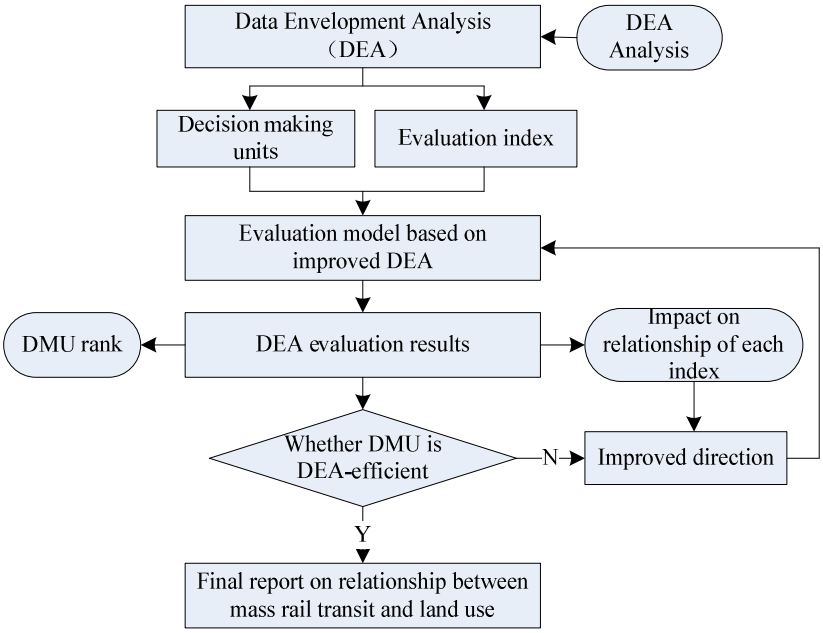

Fig. 3 Evaluation procedure frame of coordinated relationship

Principles of establishing evaluation index system

The TOD mode is a key way to achieve sustainable development between urban rail transit and land use though integrating them. According to the features of urban rail transit and TOD communities along the route, the selection of the evaluation indexes should follow there principles. Firstly, the indexes selected should be representative. Although there are many indexes to characterize urban rail transit system and land use of TOD community system, those factors which has a deeper impact, and close to the coordinated development should be emphasized. Meanwhile, factors should be able to fully reflect the degree of implementation of land use based on TOD mode, in order to determine whether the land use of TOD community along the route is adapted to the rail transit system, or coordinated development is achieved, that is to avoid the waste of rail transport resources due to inadequate development, and prevent from exceeding the supply of rail transit because of excessive development. Secondly, DEA method does not take into account interaction among the indexes. Because ignoring the correlation among the indexes will reduce the accuracy of the evaluation results. Thus, diversity of the evaluation indexes should be ensured, at the same time, strong correlation of the internal indexes in rail transit system and the TOD community land use system should be avoided[9]. Last, we should ensure that the index data is available and able to be quantified which is also important.

Selection of evaluation indexes

The evaluation indexes are selected based on the principles that can be seen from Tab.1. There are six indexes from mass rail transit system and five indexes from land use of TOD community selected in the evaluation index system at last.

Urban mass rail transit system

1) Average transfer time is used for the evaluation of transfer efficiency between rail transit and bus transit. Mass rail transit and bus are the main trip modes for TOD community residents. Coordinated development of between the rail and bus should have a highly efficient transfer to reduce residents time-consuming. 2) The average time for the TOD residents travelling from home to the transit station is used for evaluating the convenience of transit service facilities in TOD community. The coordinated TOD communities should have perfect slow transport system where residents can quickly and easily reach the transit station by foot or bicycle. 3) Utilization rate of the transit station capacity which is the ratio of the average transit flow per hour to the passenger capacity of transit station is used for evaluating usage of transit resources which are used by TOD community residents. Coordinated bus resource utilization rate is high and does not exceed the

passenger bearing capacity of the station. 4) Split rate of bus trips is for the evaluation of TOD resident's choice to travel by bus. Coordinated TOD community should have a higher transit split rate, because public transport should be the first choice of TOD community residents. 5) Vehicle kilometers travelled (VKT) per capita is used to evaluate impact of car trips in TOD community on environment. Residents of TOD community under the coordination state will choose low-carbon environmentally friendly transit trip instead of being dependent on vehicles. 6) Trip distance per capita is used to evaluate the mixed land use effect on residents' trip of TOD community. On the coordinated state, commercial, residential, official and different properties of lands are aggregated, and some trips are within TOD community, thus reducing the total traffic demand.

Tab.1 Evaluation Index System of Coordinated Relationship

System	Coordinated performance	Index
Urban mass rail transit	Efficient transfer between mass rail transit and buses	Average transfer time (min)
	Convenient path from home to transit station in TOD community	Average time from houses to stations (min)
	No wasting public transport resources and no more than the passenger capacity of transit station	Utilization rate of the transit station capacity (%)
	Encourage public transit ridership	Split ratio of bus trips (%)
	Reduce emissions from cars to protect the environment	Vehicle kilometers travelled per capita (*km* per capita)
	Reduce unnecessary trips to control the total traffic demand	Trip distance per capita (*km* per capita)
Land use of TOD community	Make full use of land resources to prevent the spread in a low density	Population density (*people* per square kilometers)
	Jobs-Housing balance	Jobs-housing ratio (%)
	High density development	FAR (floor area ratio)
	Comfortable environment for walking and bicycle	Non-motor lane area ratio (%)
	Mixed land use to layout different function land	Non-residential land area ratio (%)

Land use system

1) Population density is population size in the unit area. It can reflect the intensive use of the limited land resources. TOD community under coordinated status is a vibrant gathering place with a high population density, which can inhibit disordered extension of low density land use effectively. 2) Jobs-housing ratio refers to the proportion of the number of working positions taking the total number of residents in the community. It is used to evaluate whether the employment and house have achieved a balance. Coordinated TOD community has a higher ratio to reduce long-distance traffic demand, hence alleviate traffic congestion effectively. 3) Floor area ratio (FAR) refers to the rate of total floor area to the TOD community land area. It is used to evaluate the degree of land development. Coordinated TOD community should show the high-density, high-strength characteristics. It provides adequate bus traffic for passengers and does not exceed the traffic supply capacity of the urban main line of bus transit. 4) Non-motor lane area ratio is used for evaluating the construction of walking lane, bicycle lane and other slow traffic system in the TOD community. Coordinated TOD community has perfect walking lane, bicycle lane to access the bus station in order to facilitate the residents taking the bus. 5) Non-residential land area ratio can reflect the

degree of mixed land use in the TOD community. On the coordination state, TOD community should make a mixed development of commercial, residential, office and other functional properties land. It is to avoid living in a single land use pattern, resulting in residents only working or shopping in the central area and living in the community.

Conclusions

Through analyzing the suitable methods and principles of evaluation index system on relationship between urban rail transit and land use based on TOD mode, an evaluation procedure frame was proposed based on DEA model, and the evaluation index system was set up. The whole research hadn't taken into an actual case to verify the evaluation index system, so further research is needed.

Acknowledgments

This work was partially supported by National Science Foundation of China (Project Nos. 71173061, 70903018 and 51008002), State Key Laboratory of Subtropical Building Science South China University of Technology (Project Nos. 2011KB20) and Scientific Research Innovation Foundation in Harbin Institute of Technology (HIT. NSFIR. 2011126).

References

[1] Waddell P, Ulfarsson G F, Franklin J P, et al. Transportation Research Part A. 2007, 41: 382-410.
[2] Yim K K , Wong S C, Anthony Chen, et al. Transportation Research Part C. 2011, 19: 351-362.
[3] Chu Haoran, Wang Jiangyan, Zhou Yanhu, et al. Urban Transport of China. 2008, 6(5): 30-35. (in Chinese)
[4] Yang Liya, Shao Chunfu, Nie Wei, et al. Journal of Beijing Jiaotong University. 2007, 31(3): 6-9. (in Chinese)
[5] University of North Carolina. Report on the Theory and Practice of Integrated Land Use and Urban Transportation. 2006.
[6] Carey Curtis. Planning Practice and Research. 2008, 23(3): 285-302.
[7] Chiu Y H, Huang C W, Ma C M. European Journal of Operational Research. 2011, 209(2): 95-103.
[8] Chuan Ding. Harbin Institute of Technology Thesis for the Mater Degree of Engineering. 2011. (in Chinese)
[9] Zhang Junrong, Guo Yaohuang. Systems Engineering-Theory Methodology Application. 2004, 13(6): 520-523. (in Chinese)

doi:10.4028/www.scientific.net/AEF.5.128

Dynamic Network Selection in Vehicular Heterogeneous Wireless Networks

Lang Gaiping[1, a], Xu Yubin[1, b] and Ma Lin[1, c]

[1]School of Electronic and Information Engineering, Harbin Institute of Technology, Harbin 150008, China

[a]langgaiping@163.com, [b]ybxu@hit.edu.cn, [c]malin@hit.edu.cn

Keywords: Intelligent Transportation Systems (ITS); LTE; WLAN; Radio Resource

Abstract. Three general types of applications, safety applications, traffic applications and non-safety applications, are developed over vehicular networks. Different usage frequency may occur for different applications in vehicular networks. Most of current researches only focus on the safety applications, traffic applications or non-safety applications. Actually, these applications are used by one vehicular according to his dynamic requirements. So, this paper takes these applications together into account, and corresponding access policy is proposed.

Introduction

In the past, cars embedded with advanced materials and sensors to strengthen safety. In recent years, with the development of wireless communication technologies, cars are equipped with radio interfaces. Using these radio interfaces, they can not only obtain safe guarantee but also enjoy other new applications. Three general types of applications are developed over vehicular networks. Safety applications improve the safety of the passengers on the roads through sending warning information to their neighboring vehicles about accident, slippery road and emergency vehicle warning and so on. Traffic applications provide drivers with the traffic situation and road information to avoid congestion. Non-safety applications include many types of services, such as video conference, web browning, map and weather information downloading and so on.

Nowadays, various wireless access technologies, such as Wireless Local Access Networks (WLAN) and cellular networks (3G, LTE), are coexisting. In this heterogeneous environment, different networks have different characteristics, and can meet diverse quality of service (QoS) demands of end users. None of these networks, however, satisfies all the required services and applications. If these networks with compensatory characteristics can cooperate, users with multiple radio interfaces may experience satisfied services at anytime and anywhere. Meanwhile, cooperative use of the multiple radios enhances the performance of the heterogeneous system in the sense that the network resources can be used efficiently. So, in this paper we use heterogeneous framework to develop Intelligent Transportation Systems (ITS).

Related Works

Recently, researches about vehicular heterogeneous networks are emerging to enhance the vehicle communication quality. Generally, member networks include WLAN, cellular network, and WiMAX and so on. Heterogeneous vehicular network architecture was introduced, and a mobility pattern aware routing protocol was proposed to provide the reliable route path for V2V communication [1]. Emergency services and road safety evolves with the development of vehicular communication networks [2]. Most of the researches about vehicular communications and vehicular networks only deal with a single type of application, such as only emergency services or only safety application. Drivers may need to use various applications, and single type of networks cannot meet all applications' requirements at the same time [3]. So heterogeneous vehicular network is needed, another reason is that WLAN's coverage area is relatively small and not available in every place. In heterogeneous vehicular networks, group handover may occur frequently, passengers travelling by bus or train experience similar channel condition and they are close to each other. If they make

decision individually, they may select the same network to handover. This may result in congestion and user even may be dropped. Considering characters of vehicular networks, such as high speed, mobility pattern, and topology restrictions, group users are enabled to select network from the point view of the whole system based on mobility prediction [4]. Mobility prediction is an important problem in handover decision, and it can provide useful information for user position and users distribution.

Problem Formulation

Motivation. A key motivation of considering heterogeneous vehicular network is that WLAN will only be effective when it is ubiquitously deployed and vehicles' speed are relatively low, but this will not happen in these years. Therefore, nowadays a heterogeneous platform is the best way forward. In fact, LTE is a type of wide area network, and WLAN is deployed only in the hotspot. They are complementary in the data rate and coverage area and so on. So for LTE and WLAN, cooperating to provide all kinds of applications for vehicles is a reasonable choice.

Network Architecture. Here, a simple scenario is presented in fig. 1, and heterogeneous networks are composed of WLAN and LTE. We assumed that only one direction of vehicles is considered.

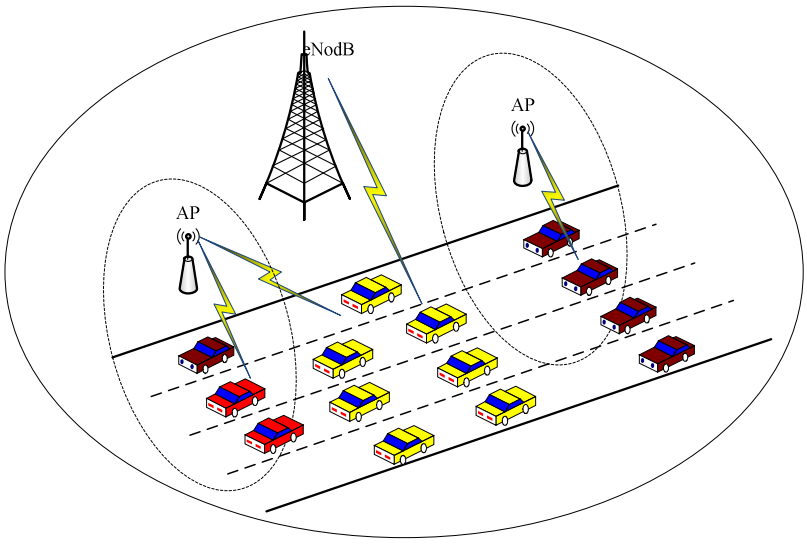

Fig. 1 Network architecture

Access Policy. We consider a highway vehicular communication scenario, where without loss of generality we can confine our analysis in spatial domain to the direction of moving vehicles. 802.11e (WLAN) has two access mechanisms [5], EDCA and HCCA. HCCA has higher priority than EDCA. So, if one vehicle is using WLAN now, he will choose appropriate access mechanism according to the application on use. If he needs to send or receive the safety message, he will use HCCA to compete for channel using. V2R communication is only suit for low speed condition or static environment. V2V is an optional communication. The ability of LTE supporting safety application is poor, but the ability supporting infotainment applications are stronger than WLAN. Because of small coverage area of WLAN, high speed vehicle will encounter frequent handover, which induces more overhead and waste valuable resource. Therefore, on the condition of safety guarantee, satisfying vehicles maximally is a promising issue.

Overview of LTE and WLAN Technology

LTE. LTE is a standard for wireless data communications technology and an evolution of the GSM/UMTS standards. E-UTRAN is radio network of LTE. It consists of eNBs, providing the E-UTRA user plane and control plane protocol terminations towards the UE. The eNBs are interconnected with each other by means of the X2 interface. The eNBs are also connected by means of the S1 interface to the EPC (Evolved Packet Core), more specifically to the MME (Mobility

Management Entity) by means of the S1-MME interface and to the Serving Gateway (S-GW) by means of the S1-U interface. The S1 interface supports a many-to-many relation between MMEs / Serving Gateways and eNBs [6]. LTE architecture is in fig. 2.

WLAN. IEEE 802.11 specifies two medium access control mechanisms: the mandatory distributed coordination function (DCF) and the optional point coordination function (PCF) [7]. To enhance QoS support in 802.11, IEEE 802.11e is introduced, and his MAC mechanism is the hybrid coordination function (HCF). The HCF includes two medium access mechanisms: contention-based channel access and controlled channel access, providing prioritized and parameterized QoS access to the wireless medium. The contention-based access method of HCF is the enhanced distributed channel access (EDCA). The EDCA provides QoS support using different access categories (ACs) with their independent back-off entities. The controlled channel access is HCF controlled channel access (HCCA). HCCA provides polled access to the wireless medium.

An AC uses three parameters to indicate his contention process. They are AIFSD[AC], CWmin[AC], and CWmax[AC]. CW parameter takes an initial value of CWmin[AC], and his maximum is CWmax[AC]. Different AC have different these three parameters. AIFSD[AC] is calculated as

$$\text{AIFSD[AC]} = \text{SIFS} + \text{AIFS[AC]} \cdot \text{SlotTime}. \tag{1}$$

AIFS[AC] is an integer greater than zero. SIFS is Short Inter Frame Space. SlotTime is time units in WLAN.

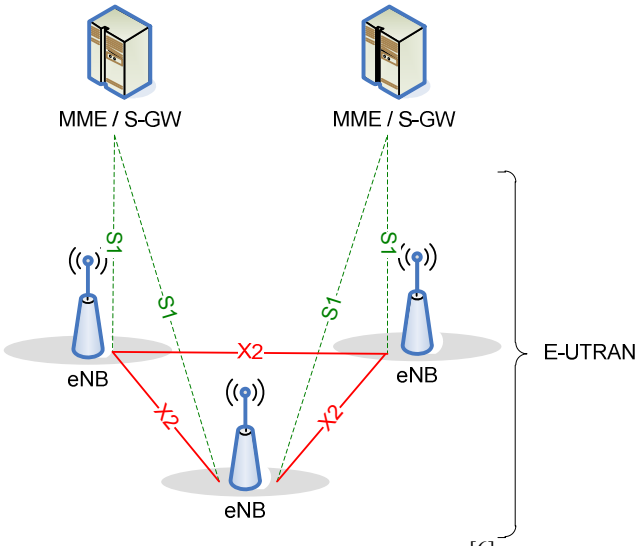

Fig. 2 LTE architecture[6]

Communication Process

In this paper, vehicles select different networks to access according to their speed and application type on use. Through properly selection, drivers can achieve satisfied service. From the discussion of previous section, we present a new network selection way. A vehicle needs to know available networks at any time in order to make decision about whether handover or not. Then according to the current network condition and vehicle's own status, he can start selection process. General process is shown in fig. 3.

For the decision of an available network, vehicle checks received signal strength (RSS), if RSS is higher than RSS threshold, available bandwidth is estimated. If available bandwidth is larger than requirement, this network is considered available. Available bandwidth is calculated

$$BW = B_0 - L\frac{NAV}{T_n + 0.5T_{n,c}(N-1)} \tag{2}$$

Where B_0 is total bandwidth of system, L is mean frame length, T_n is NAV duration of a successful transmission, N is retransmission times [8].

If the number of available networks is larger than one, the problem can be divided into two sides. If the speed of vehicle is higher than the threshold V_{th}, it need to handover to LTE network, or keep in original network if it is in the LTE network at last moment. If the speed of vehicle is lower than the threshold V_{th}, the vehicle is accessed to WLAN network. But which access mechanism is used is judged according to application type of the vehicle, if it is safety application, HCCA is used, otherwise EDCA is used.

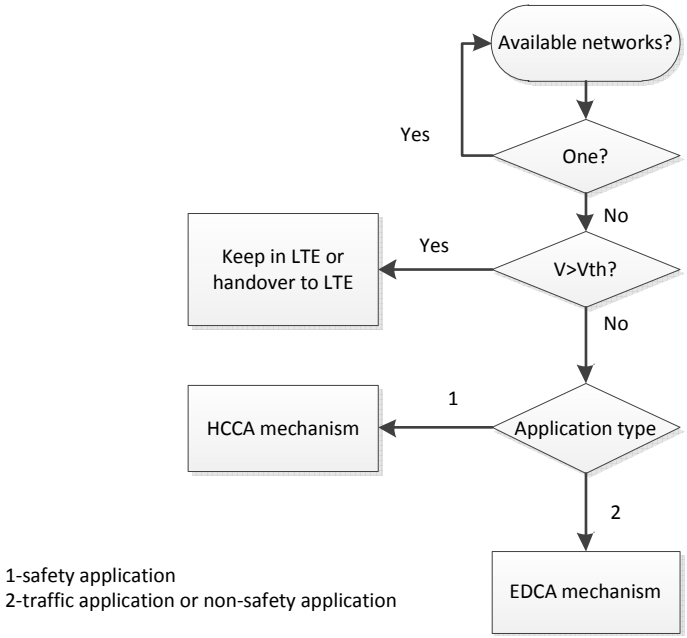

Fig. 3 Flowchart of network selection

Conclusions

Throughout previous analysis, we can know that vehicles achieved satisfied experience by accessing different networks which are cooperative heterogeneous system composed of WLAN and LTE. Using this network selection algorithm, all applications are considered and correctly processed. Furthermore, system resource is utilized efficiently. Meanwhile, drivers not only achieve safety information in time, but also they can experience good time on the road.

References

[1] C. C. Hung, H. Chan, and E. H. K. Wu, Mobility pattern aware routing for heterogeneous ve hicular networks, Wireless Communications and Networking Conference (WCNC), Apr. 2008, pp. 2200-2205.

[2] F. J. Martinez, C.K. Toh, J.C. Cano, C. T. Calafate, and P. Manzoni, Emergency Services in Future Intelligent Transportation Systems based on Vehicular Communication Networks, IEEE Intelligent Transportation Systems Magazine, 2010, pp. 6-20.

[3] E. Hossain, G. Chow, V. C. Leung, R. McLeod, J. Misic, V. W. wong, and O. Yang, Vehicular telematics over heterogeneous wireless networks: A survey, Computer Communications, vol. 33, 2010, pp. 775-793.

[4] G.X. Zhang, F.Q. Liu, an Auction Approach to Group Handover with Mobility Prediction in Heterogeneous Vehicular Networks, 11th International Conference on ITS Telecommunications, 2010, pp. 584-589

[5] IEEE 802.11e, Part 11: Wireless Medium Access Control (MAC) and Physical Layer (PHY) Speci fi cations: Medium Access Control (MAC) Quality of Service Enhancements, IEEE Std. 802.11e-2005, 2005.
[6] 3GPP TS 36.300 Tech. Spec., Evolved Universal Terrestrial Radio Access (E-UTRA) and Evolved Universal Terrestrial Radio Access Network (E-UTRAN) work in progress, June 2011.
[7] IEEE Std. 802.11, "Wireless LAN Medium Access Control (MAC) and Physi-cal Layer (PHY) Specifications," 2012.
[8] Dong Ma, Student Member, IEEE, and Maode Ma, Senior Member, IEEE, "A QoS Oriented Vertical Handoff Scheme for WiMAX/WLAN Overlay Networks", IEEE Transactions on Parallel and Distributed Systems, VOL. 23, NO. 4, APRIL 2012, pp. 598-606.

doi:10.4028/www.scientific.net/AEF.5.133

Two-Stage Data Mining Based Vehicle Navigation Algorithm in Urban Traffic Network

Xiantong Li[1,a], Shi An[1,b]

[1]No.73, Huanghe Street, School of Transportation Science and Engineering, Harbin Institute of Technology, Harbin, China

[a]lxt@hit.edu.cn, [b]anshi@hit.edu.cn

Keywords: Urban traffic network, data mining, vehicle navigation, traffic information

Abstract. Along with the development of Intelligent Transportation System, traffic detectors collect numerous transportation state data in information databases and accumulate. Such data is greatly meaningful to the vehicle navigation. In this paper, we propose a noble two-stage algorithm about vehicle navigation by using data mining methods on the historical and current transportation dataset. This algorithm begins with picking sensitive data about start and end point in an urban traffic network, and data from related (or nearest) road fragments. Referring to current time and season, the algorithm gives an evaluation to every related road fragments and outputs a most reasonable route between start and end point. The experimental and theoretical analyzes show that this algorithm can form an efficient and effective route in reasonable time.

Introduction

Urban traffic navigation algorithms are greatly based on traffic information datasets, which can be get from detectors of ITS (Intelligent Transformation System). But, after the ITS occurred, a huge number of detectors were spread into traffic network to monitor the partial or total transportation system situation. In such situation today, mass data is formed more and more quickly than before, on which introduces new problem into traffic information analysis.

According to such situation, analysis methods *cannot* just be the regular ones, such as association rules mining, data fusion, and data classification, in order to simulate the nearest future about traffic condition. These methods have inherently functionally insufficient problem. *For example*, association rules mining may evaluates single road segments in a route separately, without considering the structure or substructure of the urban traffic network. When a road segment between start and end point is used frequently, it might have highly related with the new route. Obviously, this segment happens to have nothing to do with the new route when it is a one-way street, or a recently broken one.

Focusing on graph datasets, which records data and relationships between data at the same time, graph mining is a meaningful branch of data mining to solve such problems, especially in vehicle navigation. For a single graph data, it has two parts, which are vertices and edges. Vertices represent data, and edges stand for relationships. *For example*, in chemical dataset, vertices are atoms, and edges are compound keys between atoms. In urban traffic network, vertices are separate street segments, and edges are traffic crosses. When analysis applies on urban traffic network graph dataset, the results bring out some interesting knowledge behind the mass dataset.

Unfortunately, graph mining algorithms are the high time-complexity class. The algorithms on such problems have to bare the complexity because the subgraph isomorphism is NP-complete [1,2]. Today, there are several algorithms proposed to solve graph mining problems. On chemical dataset, the algorithms are based on depth first visiting method to mining frequent substructures to achieve high performance [3-5]. But, in traffic datasets, it is very different from chemical datasets, where the size of graphs is much bigger than chemical datasets. When the algorithms in chemical dataset graph mining are introduced into traffic datasets, they should not work well, or have limited efficiency.

When a vehicle navigation algorithm combined with the thinking of graph mining, it considers not only the frequency of road segments, but also the substructures of traffic network. Most existing navigation algorithms are founded on shortest path in a directed graph. Shortest path in a directed

graph [6] is an effective algorithm to find out whether vertex *B* is reachable from vertex *A*, though it does not consider the usage of an edge between them, or the situations of substructures of a traffic graph. In paper [6], H. Gonzalez proposed an algorithm based on urban traffic graph to find out the efficient route between start and end points. This algorithm sets transportation data as references to calculate the route, but it is works only on current transportation dataset.

In this paper, a noble urban traffic navigation algorithm is introduced, which is based on graph mining and association rules mining. It has two stages to fulfill the target of data analysis when the user picks start and end vertices in the traffic graph. In the first stage, association rules mining algorithm is implemented to produce a set of frequent edges in the graph. After this, it gives the function to evaluate every single edge. In the second stage, graph mining method carries out to form frequent subgraph based on these edges according to the historical traffic network graph and current transportation dataset. In Evaluation and Results part, this algorithm shows that it can give a more efficient and effective route than exit ones.

Methodology

Transportation network can be translated into graph data, which vertices are road segments and edges are road crosses. This translation keeps the traffic signals and road conditions more greatly than other methods. In figure 1, it is a part of an urban traffic network a), and it is translated in the way above c). Also, it can be translated by another method, which is that the vertices are road crossed and edges are road segments (c). It is clear that this translation loses some information in the original traffic network.

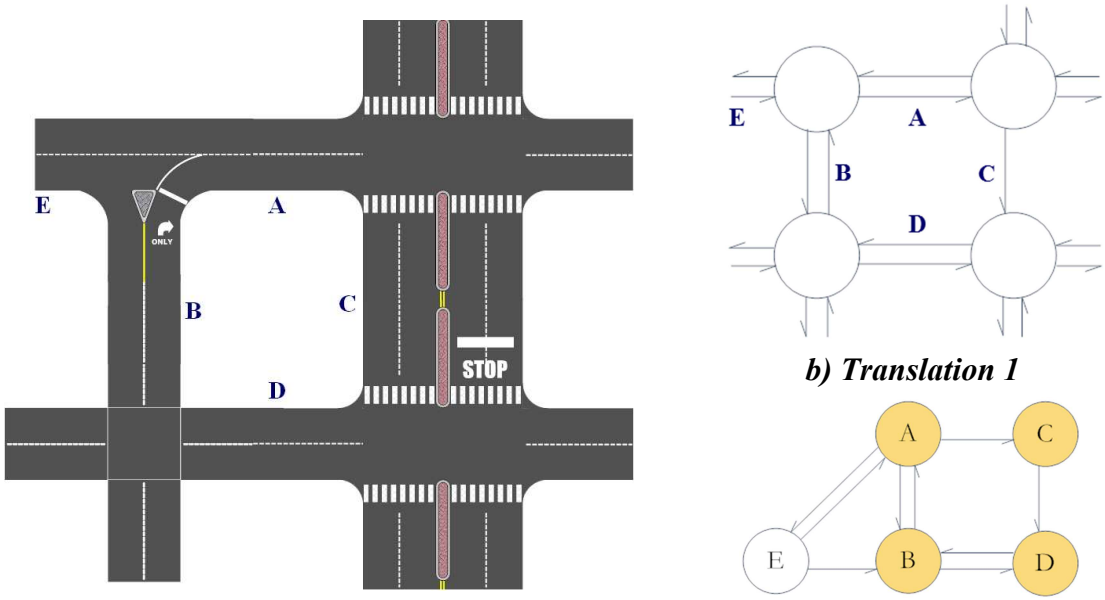

a) Traffic Network *b) Translation 1* *c) Translation 2*

Figure 1. The mapping between traffic network and directed graph.

The transportation dataset can be divided into two parts. The first part is historical records, nearest or furthest. And the second part is current records. In this paper, the algorithm is founded on such historical and current data. For the same urban traffic network, it has many snapshots in the dataset for different time stamp.

Definition 1 (Traffic Graph Data). A traffic graph data is a directed graph, which is a 6-tuple, $G = \{V, E, \Sigma, L, D, \omega\}$. Here, V is vertex set, E is edge set, Σ is label set of vertices and edges. L is a mapping between V and E to Σ, which represents $V \rightarrow \Sigma$ and $E \rightarrow \Sigma$. D is another mapping which represents the edges directions between two vertices, D: $v_1 \rightarrow v_2$. ω is a weighting function which calculates the traffic conditions affected by other elements.

ω is a set which contains several elements about environment, such as whether, rush hours or not, special days, safety, and others. By such set, a definition can be made to weight the vertices and edges in a traffic graph data. Different interests make different functions. This should be defined by users.

In this algorithm, we focus on frequent edges and frequent substructures in urban traffic graph. For this target, the algorithm can be divided into two stages. In the first stage, it calculates the frequent edges between start and end points in the graph. It discovers the frequent substructures above these frequent edges in the second stage. The growth of frequent substructures accords to the depth first method. When one of those substructures is large enough to cover the start and end vertices, it will contain the efficient route of this trip. After all, the algorithm deploys another depth first visiting to find out such route.

Frequent Directed Edges Mining. There are many graphs in an urban traffic dataset. It can be drawn from one urban traffic network at different timestamps. For all these induced graphs, the first thing to do is to give the beginning vertex A and ending vertex B of a trip. Then it begins to form the frequent directed edge set in the graphs according to the Edge Picking Algorithm (EPA) bellow.

When the beginning vertex A and ending vertex B are given, EPA analyzes current transportation records to collect related information. Then it launches to query the historical records to collect graphs in urban traffic dataset which have the nearest situation to current one, which named G_h. Afterwards, EPA carries out a frequent edges mining step to discover the most frequently used edges e_f between A and B. As the result, the frequent edge set E_f is returned to the up layer of the algorithm to form the final route.

Here, the most frequently used edge e_f is such edge. It is used mostly in the same situation like current. It considers not only transportation system effectives, but also other conditions like weather, rush hours, and so on. Different user should define different functions about thus procedure. When a trip is highly related about safety like chemical transportation, it should adjust the weight of an edge more leaning to safe. In the evaluation and results part, we will show an example about the adjustment of such function.

Enlargement of Frequent Edges. After the algorithm EPA returns the frequent edge set E_f, it evolves into the second step of mining.

The second stage is a graph mining algorithm indeed which is called Edge eXpands Algorithm (EXA).

In EXA, it first sorts the frequent edges in E_f by descending order. Then, it picks out the most first edge in E_f as current edge e_c. EXA queries frequent edges in G_h to add it into e_c's vertices to form a larger path or substructure. The query method is depth first visiting. After EXA adds edges to every edge in E_f, it checks whether these paths or substructures can joint together to cover vertices A and B. If it does, EXA returns that path or substructure and ends running. If it does not, EXA adds new frequent edges in G_f to those paths or substructures in E_f until it satisfied the ending condition.

When EXA forms a path or a substructure that covers vertices A and B, it visiting the traffic network graph by such path or a path in the substructure to check out whether it is an answer. After all, if there are more than one answers returned, EXA should give out the evaluation of all these paths to the user.

Evaluation and Results

The evaluation environment is Window 7 Ultimate running on i7 CPU, which has 4GB RAM and a 160SSD hard disk. All primary code was writing in gcc 3.4.4 under CodeBlocks.

We used real road maps from areas of the United States in all of our experiments. The map we used is San Francisco Bay area (90 by 125 miles) with 175,343 nodes, and 223,606 edges. We simulated different traffic conditions using the Network-based Generator of Moving Objects by Thomas Brinkhoff [8], which is a well-known traffic simulator.

The most important parameter of this algorithm is the weight function. Here, we use the Standard Deviation to reduce its complexity. If there are N parameters in this function, the equation (1) is the weight function in the algorithm.

$$\Delta = \frac{1}{N}\sum_{k=1}^{N} \mu_k p_k \quad (1)$$

Here, μ_k means the k^{th} parameter's ratio, and p_k means the value of the k^{th} parameter.

The results of experiments are shown in figure 2. Figure 2 a) shows the average internal between our algorithm and realistic data, which is a real ride in the dataset. In this part, we chose 5 couples of vertices in the traffic network as beginning and ending vertices. Each couple has 10 tests to generate the average data. It is clear that our algorithm is much efficient than real ride. Figure 2 b) shows the effective from our weighting function. As it shown in figure, the more complicated, the more time consumed.

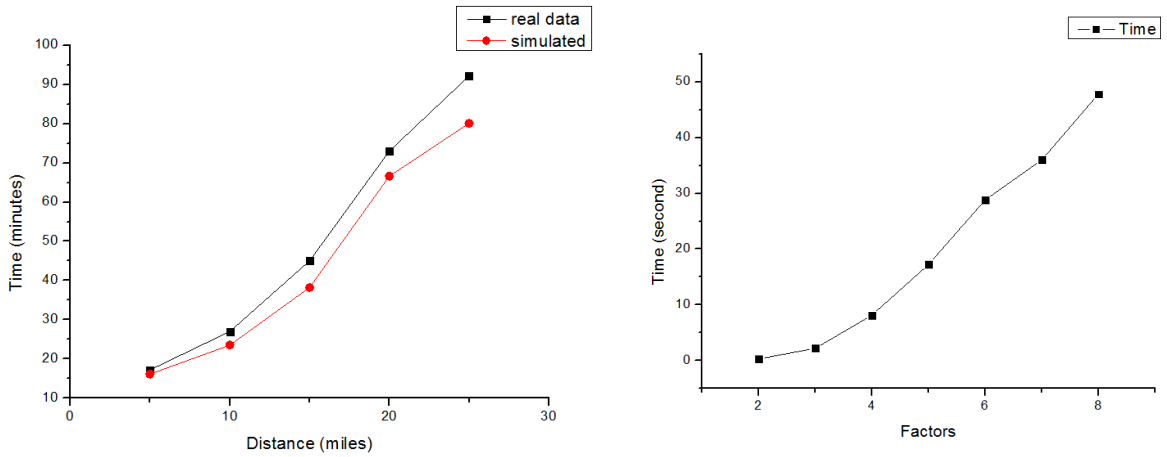

a) Algorithm and Realistic Data *b) The Effectiveness of Algorithm*

Figure 2. Experimental Results

This two-stage data mining based navigation algorithm can give an efficient route in a specified time, with considering the traffic impact factors. Unless other navigation algorithms, it combines historical dataset and current dataset together to avoid the efficient route just in theory.

Conclusion

In this paper, we propose a two-stage algorithm to calculate the route for a vehicle in an urban traffic network. Unlike existing navigation algorithms, this algorithm based not only on the traffic network map, but also considers the transprotation datasets. According to the two parts of transportation dataset, named as historical dataset and current dataset, this algorithm can be divided into two stage to generate the route, which is EPA and EXA. It combines association rules mining and graph mining into an integrated one to simulate the most efficient route between beginning and edge vertices at current situation. Evaluation and results shows that this algorithm can discover such route based on historical dataset and save time in travel.

Acknowledgements

This research was sponsored in part by the Creative and Developing Foundation of Harbin Institute of Technology under grant HIT.NSRIF.2010036 and part supported by the 863 Foundation of China under grant No. SS2012AA112310. The views and conclusions contained herein are those of the authors and should not be interpreted as representing the official policies, either expressed or implied, of the P.R.C. Government. The P.R.C. Government is authorized to reproduce and distribute reprints for Government purposes notwithstanding any copyright notice herein.

References

[1] M. Garey, D. Johnson. Computers and Intractability: A Guide to the Theory of Np-completeness. W. H. Freeman and Company, 1979.

[2] G. Yang. The Complexity of Mining Maximal Frequent Itemsets and Maximal Frequent Patterns. 10th ACM SIGKDD International Conference on Knowledge Discovery and Data Mining. Seattle, WA, USA, 2004:344–353.

[3] X. Yan, J. Han. gSpan: Graph-based Substructure Pattern Mining. IEEE International Conference on Data Mining (ICDM). Maebashi City, Japan, 2002:548–551.

[4] J. Huan, W. Wang, J. Prins. Efficient Mining of Frequent Subgraphs in the Presence of Isomorphism. IEEE International Conference on Data Mining (ICDM). Melbourne, Florida, USA, 2003:549–552

[5] S. Yang, X. Yan, B. Zong, A. Khan. Towards Effective Partition Management for Large Graphs. SIGMOD'12 (Proc. 2012 Int. Conf. on Management of Data), Jun 2012.

[6] Hector Gonzalez, Jiawei Han, Xiaolei Li, Margaret Myslinska, John Paul Sondag. Adaptive Fastest Path Computation on a Road Network: A Traffic Mining Approach. Very Large Databases 2007 (VLDB ’07), September 23-28: 794-805.

[7] Thomas H. Cormen, Charles E. Leiserson, Ronald L. Rivest, and Clifford Stein. Introduction to Algorithms, Second Edition. MIT Press and McGraw-Hill, 2001. ISBN 0-262-03293-7. Section 24.3: Dijkstra's algorithm, pp. 595–601.

[8] T. Brinkhoff. Network-based generator of moving objects. Technical report, IAPG, http://www.fh-oow.de/institute/iapg/personen/brinkhoff/generator/.

doi:10.4028/www.scientific.net/AEF.5.138

Analysis on Driver's Physiological and Eye Movement Characteristics under Alcohol Effect

Chuanyun Fu[1,a], Yulong Pei[2,b]

[1]School of Transportation Science and Engineering, Harbin Institute of Technology, Harbin 150090, China

[2]School of Transportation Science and Engineering, Harbin Institute of Technology, Harbin 150090, China

[a]email: fuchuanyunhao@163.com, [b]email: yulongp@263.net

Keywords: Alcohol Effect; Driver's Physiological Characteristics; Driver's Eye Movement Characteristics; Elimination Time

Abstract: Drinking-driving significantly impacts on road traffic safety. Characteristics indicators of driver's physiological and eye movement were screened to conduct driving experimental test, this study comparable analyzed the drivers' variation of skin electricity under different alcohol intake, also uncovered the heart rate change law over drinking different bottles of beer by establishing the Poincare section. Variation of fixation number, average pupil diameter, saccade number, saccade speed peak, blink number, and average blink duration time under different alcohol intake were revealed. According to experimental test and analysis of drivers' physiological and eye movement characteristics indices recovery after drinking, this paper gave the alcohol effect elimination time. Results show that alcohol effect elimination time can be determined by analyzing driver's physiological and eye movement characteristics indices, which is useful for mastering the reasonable driving time after drunk.

Introduction

The phenomenon of drinking driving exists generally in China, which is prohibited gradually by strengthening legal responsibility in recent years. Although it is a fact that drunk driving can cause the serious traffic accidents, whether drinking a small amount of alcohol would influence road traffic accident or not, and how to determine the extent of alcohol impact on safety driving. These problems arouse that lots of experts and scholars have different viewpoints (Holubowycz, 2007). Therefore, it is necessary to conduct the experimental study on the relationship between the alcohol effect and characteristics of drivers' physiological and eye movement, analyze the variation of indices screened from the physiological and eye movement characteristics, uncover the intrinsic reasons for alcohol influence the driver. Which is useful to enhance the consciousness of self awareness, and is great significance of improving road traffic safety.

Experiment Design

(1) Experimental Equipment

Experimental car: Santana 2000 era superman series. Clean appearance, good condition, and good engine performance.

Multi channel physiological instrument: Nexus-10 Multi channel physiological instrument, which mainly consists of laptop computer, sensors, wireless Bluetooth, and software BioTrace +.

Helmet type eye tracker: I View X HED, storage analysis of image data, real-time calculation of time, displacement, speed and pupil diameter, gaze position of eyes movement.

(2) Test Sample

According to the experimental project, considering driving safety after drunken, sample representativeness, time, economic and other factors, three drivers are chosen to be the test sample.

(3) Test Location

Considering the legal requirements and driving safety, driving test location is selected in a new built road without opening, which its traffic signs and markings are clear, can meet the test requirements.

(3) Indices Screening

Owing to test purpose, test condition, and indices characteristics, skin electric and heart rate are chosen to be the physiological characteristics indices; gaze, saccade, and blink are chosen to be the eye movement characteristics indices.

(4) Test Plan

In the process of actual driving, multichannel physiological instrument and helmet type eye movement apparatus are applied for testing drunk drivers' physiological and eye movement characteristics indices. The experiment was divided into the following two stages.

The first stage: Physiological and eye movement characteristics indices of three drivers without drinking are static tested. During the process of experiment, physiological characteristics indices are tested 5 minutes, and eye movement characteristics indices are tested 3 minutes.

The second stage: Physiological and eye movement characteristics indices of three drunk drivers are dynamic tested. Firstly, the driver should be familiar with road environment, and adjust the driving state of mind during the period of 20 minutes driving. Secondly, physiological and eye movement characteristics indices of driver without drinking are tested in the process of 20 minutes driving. Lastly, physiological and eye movement characteristics indices of driver, after who drinks the first bottle of 500ml and 11 degrees bottled Harbin beer (cumulative alcohol consumption 500ml), the second bottle of beer (cumulative alcohol consumption 1000ml), the third bottle of beer (cumulative alcohol consumption 1500ml), the fourth bottle of beer (cumulative alcohol consumption 2000ml), are tested respectively in the process of 20 minutes driving. When the driver finishes one experiment, he will rest 10 minutes, then conduct another experiment.

Analysis of Driver's Physiological Characteristics under Alcohol Effect

Skin Electric

Multi-channel physiological instrument records skin electrical values for the electrical resistance of the skin, its unit is k ohm. Skin electrical values are related to the drivers' mood change when they are driving after drinking. Under the following two different drinking states, driver skin electrical indexes are the specific analyzed. As it can be seen from the result, in normal driving state, the skin electrical values are relatively high, and skin electrical fluctuations are also obviously over time changing. Driving after drinking, the skin electrical values have significantly declined, skin electrical fluctuations over time has become relatively flat, with increased alcohol consumption, skin electrical values begin to gradually decline, down to the rate of relatively stable, skin electrical fluctuations over time are comparable small. Both driver 1 and driver 2 after drinking 2000ml, their skin electrical curve remains a straight line over time changing. Indicating that driving after drinking the mood of people is affected, secretion of sweat and skin conductivity ascends with alcohol consumption increasing.

Heart Rate

Poincare section is an effective means of heart rate analysis, it puts all the adjacent heart rate data markers in a Cartesian coordinate system (Song, 2007), the formation of regular scatter plots. Poincare section can not only reflect the overall characteristics of heart rate, but also show intuitively the beat-to-beat changes in the moment, so it can reveal the heart rate variability with nonlinear characteristics. On the various drinking condition, heart rate data of driver are statistical analyzed, drawing on Poincare section, as shown in Figure 1.

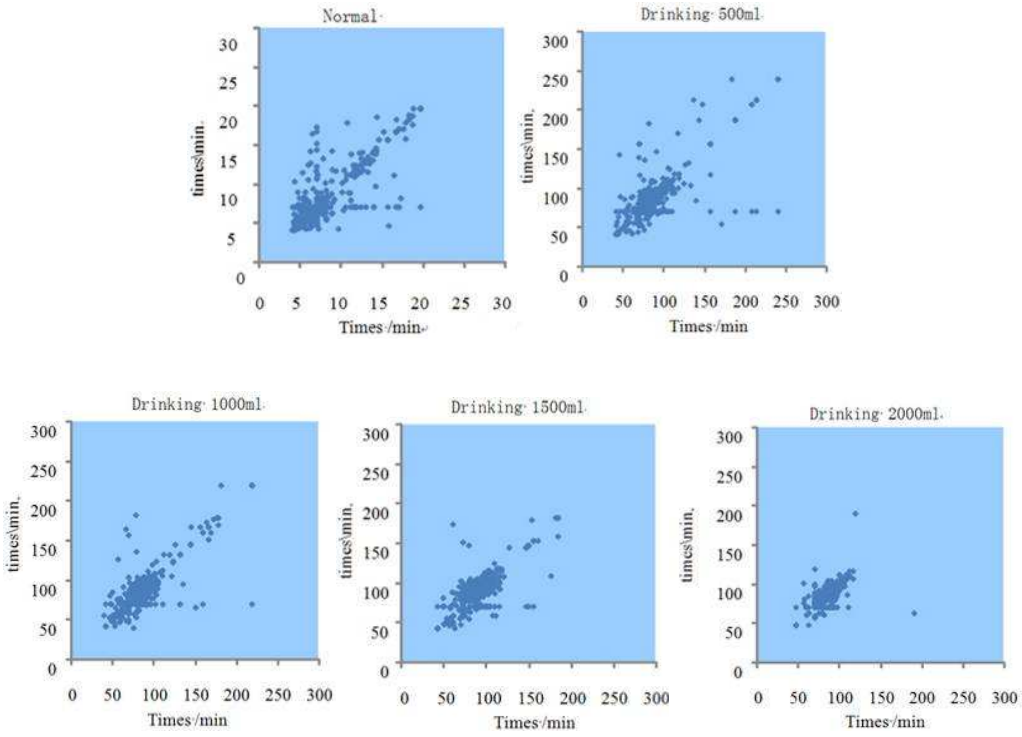

Fig.1 The driver's heart rate on Poincare section

As can be seen from the graph, in normal driving state, most of the scatter is concentrated in the angle of 45 degrees which is close to a straight line, but there are also many scattered distribution from the angle of 45 degrees with straight sides. It shows a kind of sinus arrhythmia phenomenon, and the heart rate the degree of symmetry, changes in heart rate speed. After drinking 500ml, scatter in the direction of 45 DEG distribution distance is longer than that of the normal state, and heart rate changes degree becomes large. After continuous drinking, heart rate variation is small, suggesting that started drinking, alcohol causes central nervous excited, accentuates the burden on the heart, but as the alcohol content increasing, central nervous is restrained; with alcohol consumption increasing, scatter in the direction of 45 DEG distribution distance becomes short, description of heart rate variation amplitude decreases, scatter more and more closely, the heart rate still remain the same level.

Analysis on Driver's Eye Movement Characteristics under Alcohol Effect

Fixation

With the view point number, the information handled, and regions of interest increasing, the fixation point number will also increase (Guo, et al., 2006). It can be seen that the number of fixation decreased with the alcohol consumption increasing, which is shown in Figure 2. The mean

pupil diameter is defined over a period of time the driver all pupil diameter average, can reflect the driver drive in the process of the degree of tension. Figure 3 shows that the average pupil diameter increases gradually after drinking different alcohol.

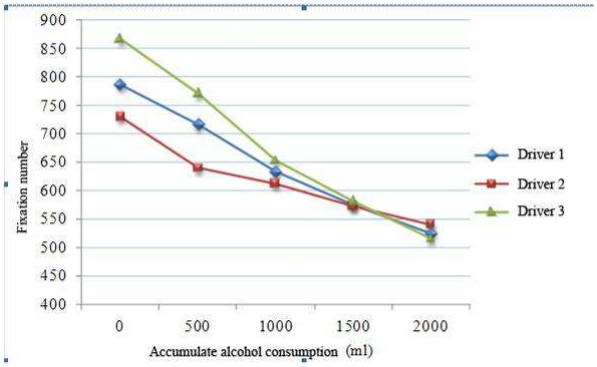

Fig.2 Fixation point number changes under the condition of different alcohol consumption

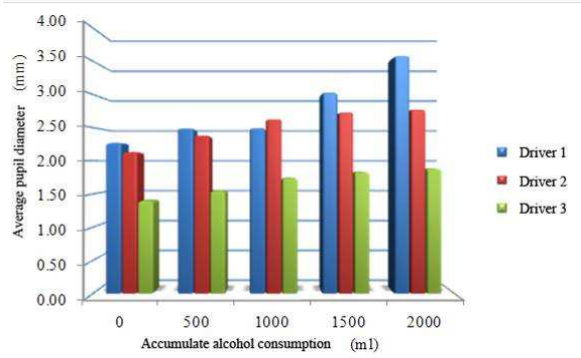

Fig.3 Average pupil diameter under the condition of different alcohol consumption

Saccade

The number of saccade can reflects the driver drive in the process of concentration. Figure 4 shows that the saccade frequency decreases with the alcohol consumption increasing. Saccade eye movement is a variable of motion and saccadic speed peak value is defined in a successive saccades during saccadic speed maximum, can reflect the driver to obtain information on speed. Figure 5 shows that saccade velocity peak value decreases with the alcohol consumption increasing.

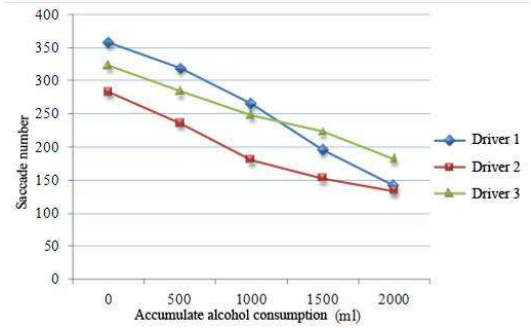

Fig.4 Saccade frequency changes under the condition of different alcohol consumption

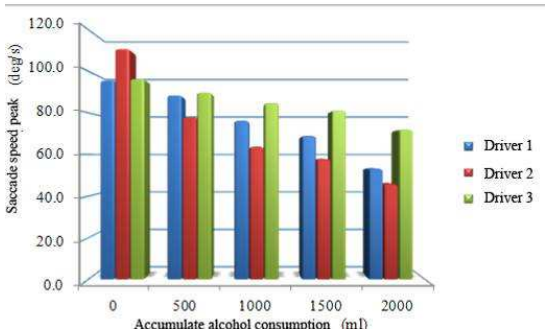

Fig.5 Saccade speed peak changes under the condition of different alcohol consumption

Blink

Under normal circumstances, when the tension of blink frequency will have more concentrate one's attention on blink, number of blink will decrease (Yuan, 2008). With the alcohol consumption increasing, the number of blink dramatically reduces, which is shown in figure 6. Average blink duration refers to a period of time the driver all blink time average, can reflect the driver's fatigue degree. Figure 7 shows that the average blink duration time increases gradually, with the alcohol consumption increasing.

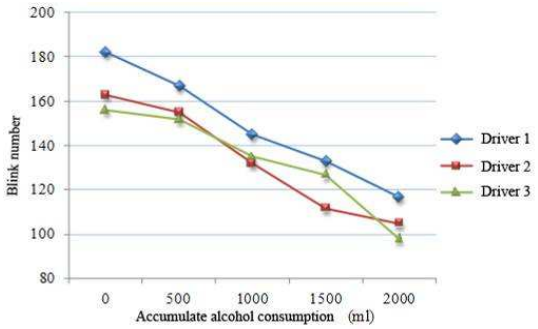

Fig.6 Number of blink changes under the condition of different alcohol consumption

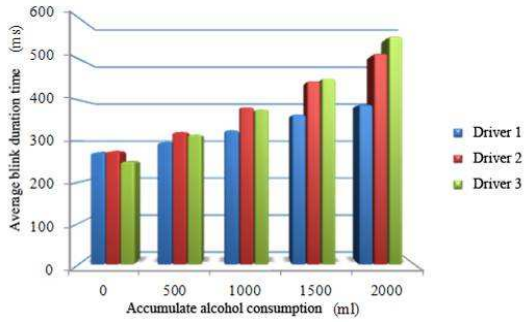

Fig.7 Average blink duration time changes under the condition of different alcohol consumption

Alcohol Effect Elimination Time Analysis

With time going, alcohol effect will be eliminated gradually, and the driver's physiological and eye movement characteristics will also gradually recover. Taken 500ml alcohol for an example, based on the physiological characteristics, alcohol effect elimination time is analyzed.

After each driver drinking 500ml beer, in the 1h, 2h, 3h, 4h, 5h and 6h 6 stages, the physiological characteristics indices are tested separately, the results are shown in Table 1.

Table 1 Recovery test results of driver's physiological indices after drinking 500ml alcohol

Time after drinking	Skin electrical (kΩ)	Heart rate(number/min)
1h	3.624	104.17
2h	4.254	102.35
3h	5.583	100.98
4h	6.631	98.47
5h	7.236	96.26
6h	7.690	95.33
Normal($\bar{x} \pm s$)	7.500±0.500	95.00±5.00

In order to analyze the variation of driver's physiological indices over time going after drinking 500ml alcohol, the relationship model between alcohol effect elimination time and skin electric indicator can be expressed as follows by regression analysis.

$$f_1 = -0.0674t^2 + 1.3384t + 2.1746 \quad (R^2=0.9864) \tag{1}$$

where, f_1 is driver's skin electrical, kΩ; t denotes alcohol effect elimination time, h. The relationship model between alcohol effect elimination time and heart rate indicator is expressed.

$$f_2 = -1.8566t + 106.09 \quad (R^2=0.9886) \tag{2}$$

where, f_2 is driver's heart rate, kΩ; t denotes effect of alcohol elimination time, h.

In formula (1), when F1 = 7, reasonable solution is selected to meet the requirements, t > 4.73. Hence, when it amounts to 4.73h after drinking, driver's skin electrical can return to normal. In the formula (2), when F2 = 100, then t =3.28. Likewise, when it amounts to 3.28h after drinking, driver's heart rate can return to normal. The maximum of above two physiological indicators recovery respectively time is recognized as the alcohol effect elimination time. For instance, if the driver drinks 500ml alcohol, and alcohol effect elimination time is 4.73h.

According to the above method, under alcohol consumption of 500ml, 1000ml, 1500ml and 2000ml, alcohol effect elimination time based on physiological characteristics and eye movement indexes can also be calculated, as shown in Table 2.

Table 2 Alcohol effect elimination time based on physiological and eye movement indexes

Alcohol consumption (ml)	500	1000	1500	2000
Physiological indicators	4.73	7.96	12.13	14.45
Eye movement indexes	4.51	8.27	10.73	12.32

Conclusion

Under the influence of alcohol, the driver's physiological and eye movement characteristics indices are analyzed in this paper. Skin electric and heart rate are chosen to be driver's physiological characteristics indices, and fixation, saccade, and blink are chosen to be the driver's eye movement characteristics indices for studying under different alcohol consumption condition. Research shows that in the process of driving after drinking, alcohol results in that driver's galvanic skin decreases, heart rate climbs, number of fixation goes down, the average fixation duration increases, the average pupil diameter becomes larger, saccade frequency reduces, the average saccade amplitude declines, saccadic speed peak and blink number drops, average blink duration time ascends. In addition, a small amount of alcohol can make drivers nervous excited, and may improve parasympathetic nervous system function of some motorists. In the light of recovery time calculation of driver's physiological and eye movement indices, alcohol effect elimination time can be determined, which is the guiding meaningful for driver grasping driving time after drunk.

References

[1] Holubowycz OT, Kloeden, CN. .Usual drinking and drink driving behavior of injured male drivers and riders: a comparison between those with zero and high blood alcohol concentrations. Proceedings of the Australasian Drink-Drive Conference, 2007: 121-130.
[2] C. Z. Song. Studies of driver's physiological loads based on HRV. Hohhot: Inner Mongolia Agricultural University, 2007: 32-47.
[3] Y. S. Guo, R. Fu, J. F. Zhang, W. Yuan. Fixation distribution of driver while driving through passageways with different widths. Journal of traffic and Transportation Engineering, 2006, 16(12): 51-54.
[4] W. Yuan. Study on car driver's dynamic visual characters test on city road. Xi'an: Chang'an University, 2008: 62-75.

doi:10.4028/www.scientific.net/AEF.5.144

Research on Route Selection Model of Road Network Emergency Evacuation under Ice and Snow

Zhang Yaping[1,a], Song Chengju[1,2,b], Yang Zhichao[1,c], Zhang Wei[1,a]

[1]School of Transportation Science and Engineering, Harbin Institute of Technology, 73 Huanghe Road, Harbin 150090, China

[2]School of Automotive and Transportation Engineering, Heilongjiang Institute of Technology, 999 Hongqi Street, Harbin, 150050, China

[a]zxlt0905@163.com, [b]songchengju@sohu.com, [c]hit-yangzhichao@163.com

Keywords: Ice and Snow Condition; Emergency Evacuation; Route Selection; Network Optimization

Abstract: The route selection of road network emergency evacuation is of great practical significance for possible emergencies in future. Based on analyzing the principles of emergency path selection, the paper takes the traffic capacity, intersection density and vehicle delays in the intersection into consideration, and establishes the route selection model of road network emergency evacuation under ice and snow.

Introduction

Urban road network is one of the Infrastructures exposed to the natural conditions, the influence of adverse weather conditions or disaster weather on the urban road network is generally serious[1], northern cities in winter suffer more snow and ice, the traffic in Beijing and Shenyang have been disordered and even paused caused by snow storm. Some southern cities have also suffered the freezing rain and snow weather. In order to effectively resist the influence of snow and ice on the urban road traffic, reduce the impact on urban emergency evacuation, it is necessary to study In-depth on the route selection problem of emergency evacuation under ice and snow[2].When an emergency takes place in cities, it is necessary to evacuate and transfer persons in large scale[3], due to the sharp increasing of traffic flow and the change of traffic operating conditions in the short time, the running balance of the road network must be broken, the road network traffic in entire city will be re-allocated, therefore, it is of great significance for guiding future possible emergency to establish the route selection module based on the emergency evacuation conditions[4].

The Initial Selection of emergency evacuation route

Evacuation route would depend on the existing road network, but not the full use, therefore, for the route selection, it is necessary to conduct route initial selection for the final optimal results [5]. When the route is selected, the safety and efficiency of emergency evacuation routes should be fully considered, to conduct initial selection on candidate routes. The main selected parameters include:

Road condition. The basic condition of the road influence comfort of drivers and evacuees directly, and better conditions could ensure the safety of vehicles. In addition, from the evacuation demand and the road design, the urban roads on high level have better performance in road capacity and road stability [6], and meet the evacuation needs better avoid traffic congestion in large scale caused by the evacuation.

The emergency lane and the shoulder setting.

When emergencies happen and emergency evacuation is needed, evacuation vehicles are mostly large vehicles, and it is possible for mechanical accidents and the possibility of misuse to take place under emergency conditions. Therefore, it is necessary for vehicles to park on the emergency lane so as not to affect others emergency vehicles, otherwise it will cause the traffic congestion and slow down the progress of emergency evacuation.

The connecting roads quantity and intersection density.

"Connecting road" refers to the link road between the public roads and residential main road in the foreign definition, and the link road between the two adjacent signalized intersections in emergency evacuation, as well as other minor roads or the import and export of everyday life and commercial services. If the number of connection is too much, it is bound to affect the evacuation efficiency of vehicles on the main roads. The high density of intersections will also aggravate the vehicles intertwined exacerbate.

Traffic control methods and information level.

In the existing urban road traffic conditions, the information level will directly influence the evacuation efficiency and the enforcement of evacuation plan in the process of emergency evacuation. Intelligent transportation facilities could transmit information of all sections in road network to the control and command center, and transmit the corresponding guidance and decision-making information back to the road users, so that real-time monitoring and induction for the evacuation in site could be realized.

Regional climate conditions.

In the existed study on emergency routes selection, the premise is normal weather conditions. It is needed to take the extreme climatic conditions into consideration for establishing and selection emergency evacuation routes. According to the weather conditions, it will determine the number of evacuation routes, the performance of evacuation vehicle, and the equipment of vehicle ancillary facilities and so on.

Emergency Evacuation Network Optimization

After the initial selection of evacuation routes, the selected evacuation routes are generally irregular, and the actual evacuation capability needs to be verified. The capacity of evacuation networks is calculated as follows:

$$C_p = C \times N \times f_w \times f_S \times f_B \times f_D \times f_V \times f_P \tag{1}$$

Where, C_p is possible capacity (pcu/l/h), N is the lanes number of One-way road, f_w is the capacity correction factor by Lane width and lateral clear width, f_s is the capacity correction factor by snow and ice conditions, f_B is the capacity correction factor by bus, f_D is the capacity correction factor by driver conditions in Emergency situation, f_V is the capacity correction factor by Fault vehicle, f_p is the capacity correction factor by interference of pedestrian and bicycle .

On the existing urban roads, buses occupy a certain proportion. When the bus is in and out of temporary stops, it will inevitably lead to the reduction of road capacity. The urban road network capacity will be reduced in different snow conditions, and with snow at a different level, the reduce extent of capacity is different.

Emergency evacuation route selection model

The basic selected steps of emergencies route in the snow and ice conditions is: firstly, determine urban roads which meet certain basic conditions as an evacuation road objects by initial selection, and then in accordance with the evacuation route selection model, evacuate from the

shortest time and vehicle flow reasonable allocation point of view, and take the traffic capacity, intersection density and vehicle delays in the intersection into consideration to determine a reasonable evacuation route.

The influence of different evacuation routes on evacuation time.

In the actual evacuation, the evacuation route is divided into series route, parallel route or mixing route, and the series route is divided into series route with same lanes or not. Evacuation route is the series route of single-path: in order to analyze and calculate conveniently, the paper refers to the concept of evacuation time in unit road length, known as the "equivalent evacuation time". The formula is as follows:

$$t_{0,ij} = t_{0,ij}^{0}[1 + \alpha_{ij}(\frac{q}{c_{ij}^{n}})^{\beta_{ij}}] \tag{2}$$

$$t_{0,ij}^{0} = \frac{l_d}{v_{f,ij}} \tag{3}$$

Where, $t_{0,ij}$ is travel time per unit length of i kinds of road in j kinds of weather conditions, l_d is length of sections , $V_{f,ij}$ is free speed of i kinds of road in j kinds of weather conditions, q is traffic of sections ; C^{n}_{ij} is capacity under the condition, $\alpha_{ij,}$ β_{ij} is lock coefficient of the road and snow conditions respectively, it is shown as follows in Fig.1.

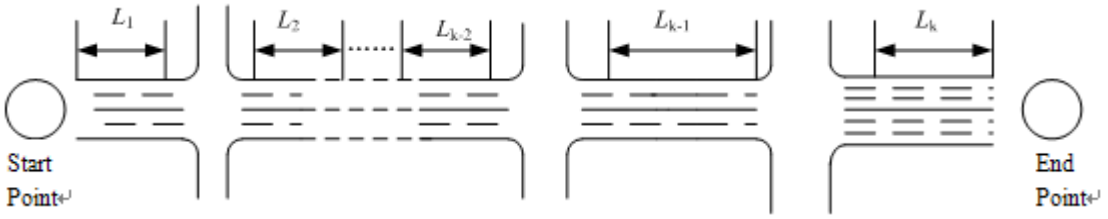

Fig. 1. Schematic diagram of series evacuation route travel time (excluding the intersection)

Therefore, when the evacuation route is connected by multi-path with different lanes, the total travel time for the evacuation section is that:

$$T = \sum_{k=1}^{k} L_k t_{0,ij} \tag{4}$$

Where, T is total evacuation time of series route, L_k is the length of k-th route, $t_{k,ij}$ is unit travel time of k-th route in corresponding climate condition and road types.

Evacuation route is the parallel multi-path: In parallel route, the simplest case is two parallel roads; it is shown as follows in Fig.2:

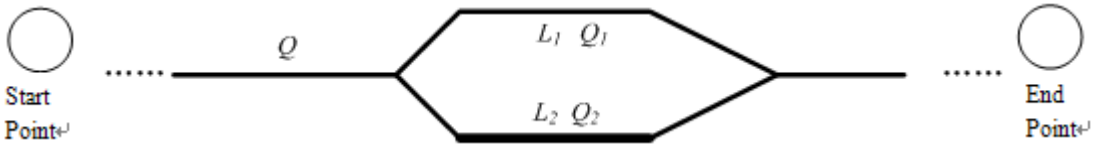

Fig.2. Schematic diagram of Parallel evacuation route Travel time

It can be seen from the above figure:

$$\begin{cases} Q = Q_1 + Q_2 \\ T(L_1) = T(L_2) \end{cases} \tag{5}$$

The solution of this equation could be obtained by equation 5 and 3, in order to obtain the travel time of two evacuation slip. Similarly, when the evacuation route is multiple parallel routes, the calculation method is similar:

$$\begin{cases} Q=Q_1+Q_2+.....+Q_n \\ T(L_1)=T(L_2)=T(L_3)...=T(L_n) \end{cases} \tag{6}$$

When the candidate routes are the combination of several parallel roads, evacuation the route with the gross shortest vehicle traveling time is optimal.When the drawn route is the combination of series and parallel ones, which is shown as equation 7:

$$T=\sum_{k=1}^{k} L_k t_{0,ij}+\sum_{n=1}^{m} T(L_n) \tag{7}$$

Where, m is the number of parallel routes, $T(L_n)$ is the road blocking function value of n-th parallel sections, the remaining parameters are the same meaning as above.

If the evacuation route is the combination of series and parallels, it needs to calculate the evacuation time of the connections. Respectively, the total evacuation travel time of entire routes could be obtained by the sum of the the evacuation time of sub-sections. The optimal route is the route with shortest evacuation time.

The influence of evacuation intersection on the evacuation time: under different weather conditions, the main reason for the vehicles delay in signal intersection is the vehicles interleaving of the different direction. According to the above analysis and existing reference, it is known that N junctions in an evacuation path, its total delay is:

$$D=\sum_{k=1}^{n} d_k \tag{8}$$

$$d_k=\frac{a_j C_k(1-\lambda_k)^2}{1-Y}+b_j x_k^2[(x_k-1)+\sqrt{(x_k-1)^2+\frac{16x_k}{Q_k}}] \tag{9}$$

Where, d_k is average delays per vehicle of k-th intersection, C_k is the cycle length of k-th intersection (S), X_k is the imported Road saturation of k-th intersection = qC/sG, λ_k is G/C, Q_K is capacity (pcu/hr), y is $\lambda_k X$.

In the reference [7], the ITS setting is considered as an impact factor on emergency evacuation of urban road network. According to the ITS setting of the evacuation routes, the impact factor is divided into three levels and take use of direct correction factor to standardize the emergency evacuation route selection model. This study considers the impact factor that ITS setting impact on emergency evacuation as 1 during the process of model standardizing, and that is no impact on emergency evacuation selection.

Selection Model of emergency evacuation route.

The emergency evacuation route selection process in the paper is divided into sections and intersection. The sections part should establish travel time impedance function in different snow and road grade conditions; while in the intersection, vehicles delays model in different snow conditions should be established. Through the combination and calculation of these two parts, the optimal evacuation route selection model based on a single OD points could be drawn. The formula is as follows:

$$T=\min(T_j)=\min[T_{Tj}+T_{Dj}], i=1,2,...n \tag{10}$$

Where, T_j is the evacuation time of the j-th route, T_{Tj} is the evacuation time of the j-th route in the consideration of capacity, T_{Dj} is the total intersection delays of the j-th evacuation route.

In summary, the optimal evacuation route selection model based on single OD points in different snow conditions can be obtained. Assuming that in an OD points, there are n routes, each route with m sections and l signalized intersections. The optimal evacuation routes selection model in different weather conditions is calculated as follows:

$$T = \min(T_i) = \min[\sum_{k=1}^{m} L_k t_{0,ij} + \sum_{k=1}^{l} d_k], i = 1,2,...n \tag{11}$$

$$t_{0,ij} = \frac{l_d}{v_{f,ij}}[1 + \alpha_{ij}(\frac{q}{c_{ij}^n})^{\beta_{ij}}] \tag{12}$$

$$d_k = \frac{a_j C_k (1-\lambda_k)^2}{1-Y} + b_j x_k^2[(x_k - 1) + \sqrt{(x_k - 1)^2 + \frac{16 x_k}{Q_k}}] \tag{13}$$

Where, m is the number of evacuation routes, n is the number of candidate routes, l_d is the length of single section, $V_{f,ij}$ is the free speed of i kinds of road in j kinds of weather conditions, q is the volume of section, α_{ij}、β_{ij} is the travel time parameters in section in the corresponding road and snow conditions, c^n_{ij} is the section capacity i kinds of road in j kinds of weather conditions; a_j,b_j is the parameters in different snow and ice condition, Q_k is capacity (pcu/hr), Ck is the cycle length of k-th intersection (S), y is $\lambda_k X_k$, X_k is the imported Road saturation of k-th intersection =qC/sG; λ_k is G/C.

For emergency evacuation, the evacuation purposes is to transfer evacuate personnel to a safe region quickly[8]. In general, the selected routes are many or more. The sort of evacuation routes by the evacuation route selection model could not effectively determine to meet the evacuation requirements or not, and the number of vehicles needed to allocate on road is not sure. So according to the characteristics of emergency evacuation, based on traffic emergency evacuation traffic allocation, multiple routes could be obtained by the emergency evacuation route selection model. It determines the number of emergency evacuation route selection and the flow on each route for minimizing the total evacuation time.

Conclusion

This paper determines the steps of the emergency evacuation route selection by analyzing the emergency evacuation route selection principle. Through the initial selection of the emergency evacuation route, it analyzes the influence of different evacuation routes on the evacuation time, and network optimization. Ultimately it establishes the emergency evacuation route selection model.

Acknowledgements

This research is funded by Heilongjiang Province Natural Science Foundation of China（Grant No. E200940）

Reference

[1] Lam, Hu Shao, Agachai. ‘Modeling impacts of adverse weather conditions on a road network with uncertainties in demand and supply’. Transportation Research Part B 2008, 42: 890–910.

[2] National Climatologic Data Center. 2002. United States Snow Climatology. National Climatologic Data Center, NOAA, United States Department of Commerce, http://lwf.ncdc.noaa.gov/oa/climate/monitoring/snowclim/mainpage.html.

[3] Yang H, Zhang X. The multi-class network toll design problem with social and spatial equity constraints .Journal of Transportation Engineering, 2007,128, 128 :420-428.

[4] Perry, A.H., and Symons, L.J. Highway Metrology, University of Wales, Swansea, Wales, United Kingdom, 1991.

[5] National Climatologic Data Center. 2008. United States Snow Climatology. National Climatologic Data Center, NOAA, United States Department of Commerce.

[6] Khattak A J, Knapp K K, Giese K L and Smithson L D. Safety implications of snowstorms on interstate highways. Presented at the Annual Meeting of the Transportation Research Board, January, Washington, D. C., 2000.

[7] Traffic research center, Beijing University of Technology. Olympic transportation planning [R]. Beijing university of technology.2004.(In Chinese)

[8] Benjamin F Zhan. Three Fastest Shortest Path Algorithms on Real Road Networks: Data Structures and Procedures .Journal of Geographic Information and Decision Analysis, 1998,11, 1(1) :69-82.

doi:10.4028/www.scientific.net/AEF.5.150

Modeling and Simulation of Bus Priority Oriented Urban Road Network Elastic Equilibrium

Lihua Liu[1, 2, a], Yaping Zhang[1, b] and Yu Wei[1, c]

[1]School of Transportation Science and Engineering, Harbin Institute of Technology, Harbin 150090, China

[2]Department of Transportation Engineering, Henan University of Urban Construction, Pingdingshan, 467044, China

[a]liulihuaalicia@126.com, [b]zxlt0905@163.com, [c]weixiaoyu8899@163.com

Keywords: Bus Priority. Elastic Equilibrium. ABC Classification. Bi-Level Programming. VISSIM.

Abstract. Influenced from economy, population and many other factors, rail transit and elevated road have poor applicability in small and medium sized city. Maximizing application of available road resources and bus facilities, reducing the environmental pollution is the critical issue faced by current situation of urban transportation development in China. Guided by Bus Priority Oriented, utilized comprehensive techniques, such as ABC classification, bi-level programming model, sensitivity analysis, this paper constructed a theoretical frame of elastic equilibrium based on system optimization. Taking time and environment as optimized objectives, this paper established the Bi-Level multi-objective programming model based on travel time, and programmed with MATLAB for the calculation. Finally, the case study is illustrated. The software VISSIM was adopted to realize the simulation of the volume before and after the implementation of elastic plan in urban areas of PingDingshan. The simulation results showed the validity and feasibility of the modeling and simulation of Bus Priority Oriented urban road network elastic equilibrium.

1. Introduction

The elastic traffic is a great interesting topic of research at present and also the direction of future traffic development. Based on the Bus Priority Theory, the elastic traffic has all the strategic merits of the bus priority, is the allocation of resources, an effective way to solve the traffic jam problem in cities, will contribute to the solution of problems such as "energy emergency" and"environmental pollution" as well.

Many measures had been taken on trip during peak hours currently, they focused on questions for the moment. It is urgent to establish the theory system of elastic traffic to alleviate and improve urban transportation.

2. Bi-Level multi-objective programming model based on travel time

From the application of relative theories, the final optimization results of system can be reflected in the following three aspects.

(1)Minimum of total service time

Targeting at optimization of density, maximization of volume and idealization of speed under elastic equilibrium, model will reaches the anticipated goal of the minimum of total service time.

(2) Maximum of environmental benefits

(3) Minimum of users' travel time

This study divides influence factors into three categories--A (subjective measures), B (objective macrography) and C (others, such as economy ,planning). Class C was not discussed for its uncertainty.

The model can satisfy user and system optimal, formulated as follows[1]:

$$\text{(U1) } \min T(x_a,y_a)=\sum\sum r_i d_{rs} B_a^i(x_a(y),y_a) \tag{1}$$

$$\text{(U2) } \min E=\alpha\sum F(x_a(y),y_a)+\beta\sum P(x_a(y),y_a) \tag{2}$$

$$\text{s.t. } y_a \geqq 0 \tag{3}$$

Parameters above can be solved by the functions belows:

$$\text{(L1) } \min Z(x)=\sum\sum\int_0^{x_a(y)} B_a^i(x_a(y),y_a)dx^i \tag{4}$$

$$\text{s.t. } \sum\sum\sum \delta_{rs}^{ak} f_{rs}^{ik} = x_a(y),\ a\in A \tag{5}$$

$$f_{rs}^{ik} \geqq 0,\ i=1,2,...,I,\ k\in P_{rs},\ rs\in RS \tag{6}$$

$$\sum f_{rs}^{ik} = r_i d_{rs},\ rs\in RS,\ i=1,2,...,I \tag{7}$$

$$\sum r_i = 1 \tag{8}$$

where, N——set of all nodes.

A—— set of all sections.

R——set of all origins.

S——set of all destinations.

P——set of all paths.

a——one section.

r——one origin.

s——one destination.

k——one path.

i——classification of travelers: i=1 bus, i=2 compact car, i=3 non-motor.

r_i——proportion of trip mode.

x_a——volume of section a.

q——OD demand on section.

d_{rs}——traffic demand of OD (r-s).

f_{rs}^{ik}——volume on path k of trip mode i for OD (r-s).

$x_a(y)$——corresponding volume when designed capacity increment changes.

y_i——vector of the of designed capacity increment for section i, the decision variable in the bi-level programming model.

$B_a^i(x_a(y),y_a)$——travel-time of traveler i on section a.

P_{rs}——set of sections for all OD.

$F(x_a)$——fuel consumption for volume of section a.

$P(x_a)$——emission for volume of section a.

E——environmental optimal value.

α, β——coefficient.

δ_{rs}^{ik}——relation between path and section, if section a on path k δ_{rs}^{ik} =1, otherwise δ_{rs}^{ik} =0.

x——column vector $(\ldots, x_a, \ldots)^T$, $a\in A$.

Upper question has two objective functions, U1 is the network design of elastic equilibrium, which analysis of elastic demand and measures were conducted. U2 is the design of environmental optimizing.

Lower question L1 is users' equilibrium assignment. The travelers' behavior conform to user optimum principle based on the travel time budget.

The steps of Algorithm based on sensitivity is as follows[2]:

Step 1: Set initial solution y^0, the capacity increment, and set iterations n=0.

Step 2: Solve lower question according to given y^n, obtain the OD demand q^n.

OD demand.

Step 4: Substitute the formula $q_{rs} \approx q_{rs}(y^*)+\sum[\partial q_{rs}(y)/\partial y_a]_{y=y^*}(y_a-y_a^*)$ to the upper objective functions, obtain new capacity increment y^{n+1}.

Step 5: If $\max|y_a^{n+1}-y_a^n| \leq \varepsilon$ stop, Where ε is the iterative precision. Or set $n=n+1$,back to step 2.

Algorithm ends.

3. Case Analysis

The elastic equilibrium of bi-level programming model was validated by public transportation system in PingDingshan (CBD).

Combined with the current situation of PingDingshan, trip mode was divided as follow: A (public transportation), B (compact car) and C (non-motor vehicle).

Bus OD demand in 2016 was Predicted by Growth Factor Method according to the survey data of current travel demand of public transportation. The result was shown as table 1.

Table 1 Bus OD demand in 2016

D O	Beidu Town	Railway station	ZhanHe District	Central Plaza	Dawu Intersection
Beidu Town	3114	7898	5103	10926	1785
Railway Station	7512	8640	9152	19885	5192
ZhanHe District	5435	10178	4015	15604	4143
Central Plaza	10752	20359	14589	23431	10380
Dawu Intersection	2205	6499	4837	12676	3553

This study discussed scene one (only B takes effect) and scene two (A and B).

In view of current traffic of PingDingshan (1, Zhongxing road north section. 2, Jianshe road west section. 3, Zhongxing road south section. 4, Jianshe road east section), the scheme was expressed as follows:

(1) Increase the departure frequency

Compared to 10 minutes before, add up the departure frequency to 3 minutes.

(2) Temporary bus lane

JianShe Road and ZhongXing Road during the morning and evening peak hour.

(3) Linear control

Optimize the signal control system of JianShe Road.

(4) LED screen

Set up LED screen near the edge of the central area.

(5) prohibiting left turn, bus exclusive-use signal and bus left-turn waiting zone.

Now considering the five kinds of measures above as the influencing factors of A only, apply the given conditions to the bi-level programming model, build raw data network as table 2 shown. Where t_1 signifies original runtime of the bus on sections for the whole network, t_2 signifies original runtime of the compact car on sections for the whole network, T signifies total runtime for whole system[3,4].

Table 2 Raw data in the tested network

section	t_1 (s)	t_2 (s)	T (s)
1	157.7	113.8	1980314.39
2	414.3	338.8	
3	173.5	123.4	
4	308.1	270.1	

The optimized in the road network is shown as table 3. Where: t_1' signifies improved runtime of the bus on sections for the whole network, t_2' improved signifies original runtime of the compact car on sections for the whole network, T' signifies improved the total runtime for whole system, $T-T'$ signifies decrement of total time.

Table 3 Results of design optimization in the tested network

section	$t_1^{'}$ (s)	$t_2^{'}$ (s)	$T^{'}$ (s)	T-$T^{'}$ (s)
1	129.8	77.7	1008346.30	971968.09
2	174.5	150.0		
3	163.9	81.8		
4	187.6	226.6		

Be seen from the chart, travel time of compact car user decreases 0~3 minutes averagely, 0~2 minutes to bus.

Then consider the second objective environmental optimum in upper model. The result was shown as table 4 via calculation, where F signifies the decrement of energy, units by L/(km×h). P signifies the decrement of pollution, namely the emissions of every ton standard coal, units by t/(km×h)[5].

Table 4 Results of environmental optimizing

section	Decrement of F L/km	Decrement of P t/km	variation of volume		E
			Compact car	bus	
1	2.26	0.73	-185	+14	1.88
2	21.14	1.41	-349	+20	15.21
3	5.68	0.68	-168	+9	4.43
4	25.36	1.41	-336	+11	19.37

Through the contrast and statistical analysis, it can be found that after those Elastic Equilibrium measures, the traffic congestion gets relief, the amount of compact car effectively decreases, the amount of large-capacity traffic tools increases “Bus Priority” promotes, the energy consumption and emissions of pollutant caused by traffic congestion both decrease, system achieves equilibrium.

4. Results and Discussion

The summary of innovations in this dissertation is as following:

1) Application of ABC classification, trip mode and the influence factors were split by ABC classification, to divide of elastic equilibrium and discuss respectively according to the specific situations.

2) The optimization of time and environment. The minimum of system time and environmental optimization as the upper objective functions of bi-level programming model, and minimum of users time as the lower.

3)Application of “Elastic Equilibrium”. “Elastic Equilibrium” is defined as the new balanced subjected to some elastic factors. The study builds elastic equilibrium system of the urban traffic oriented to “Bus Priority” and showed the expected effect through modeling and simulation.

4)VISSIM simulation. The software VISSIM was adopted to realize the simulation of the volume before and after the implementation of elastic plan in urban areas of PingDingshan.

References:

[1] Yang Hai. Sensitivity Analysis for the Elastic-Demand Network Equilibrium Problem with Applications[R]. Transportation Research, 1997, 31 (1):55-70

[2] Ben-Ayed O, Blair Ce. Computational difficulties of Bilevel linear Programming[J]. Operations Research,1990,38 (1):556-559

[3] Ren Gang. Traffic Distribution Model and Algorithm under the Control of Management[M]. Southeast University Press, 2007

[4] Teng Chunsheng, Li Zhihui. Theory and Application of Bi-Level Planning[M]. Science Press, 2002

[5] Pei Yulong, Zhang Yaping. Modeling and Simulation of Traffic System[M]. China Communications Press, 2004

CHAPTER 2:

Bridge Monitoring, Safety and Maintenance

doi:10.4028/www.scientific.net/AEF.5.157

A New Combination Method of Temperature and Vehicle Load Effects Based on SHM Data

Wang Zijiang[1, a], Hu Rongpan[1,b] and Li Shunlong[2,c]

[1]Key Laboratory of Advanced Material & Intelligent Control Technology on Transportation Safety, Harbin Institute of Technology, Harbin, China

[2] School of Transportation Science and Engineering, Harbin Institute of Technology, 150090, Harbin, China

[a]wangzijian1987@163.com, [b]rongpan.hu@gmail.com, [c]lishunlong@hit.edu.cn

Keywords: Load Effects Combination, Stochastic Process, Structural Health Monitoring.

Abstract. When more than one load act on a structure, the combination of the load effects should be considered, especially for which are variant in time and in space. A new method to calculate the combination of two different loads effects as well as to predict the extreme value distributions in the subsequent service life is proposed. The loads discussed in this paper are two main loads acting on the cable-stayed bridge: the temperature and vehicle load, which can be modeled as rectangular pulse process and filtered Poisson process respectively. Firstly, truncated distributions of the two load effects are depicted using the monitoring data of Nanjing 3rd Yangtze River Bridge. The generalized Pareto distribution fits well to the upper tails of the vehicle load effect and the mean values of the temperature load effect in an hour follows a two weighted normal distribution. Then the combination of the two load effects as well as the prediction of extreme values in the subsequent service life can be calculated. In the end, the results obtained through the proposed method are compared with the observed value of the bridge.

Introduction

Load effects are important concerns in structure design and structural safety analysis. As a structure is usually subjected to several different kinds of loads simultaneously, the combination of the load effects should be considered. Structural loads, which vary in time (e.g., wind load, vehicle load, seismic load, temperature load, etc.) and in space are usually modeled as stochastic process. To find a method to combine these stochastic loads accurately and conveniently has always been a concern for many scholars.

Turkstra's rule commonly adopted to estimate the combination of several stochastic loads because of its simplicity [1]. However, the estimation is non-conservative as it ignores the possibility that different load processes might attain the maximum values simultaneously [2]. Ferry-Borges and Castanheta method is simply and widely used. It ignores the short-term temporal fluctuation and correlation [3]. Wen proposed load coincidence method based on the model of Poisson process [4]. The exceed probability of the combination can be estimated according to the incidence ratio of load combination. Larrabee and Cornell [5] developed a point crossing formula applicable to the linear combination of stable and independent stochastic load processes. Yasuhiro Mori and Takahiro Kato [6] developed a theoretical expression of the combination of a Poisson square wave process and a Poisson impulse process.

This paper presents the theoretical expression of the cumulative distribution function (cdf) of the combination of two stochastic load effects commonly concerned in bridges. These two loads refer to the temperature load and the vehicle load which cause the deck stress of the long span cable-stayed bridges. The real-time data of these load effects, collected by the structural health monitoring system which is permanently installed on Nanjing 3rd Yangtze River Bridge will be used for the analysis of the next section.

Identification of vehicle load effect and temperature load effect

As temperature load effect varies significantly in different seasons, the monitoring data are expected to include every month to guarantee an accurate evaluation of the temperature load effects distribution properties. The deck stress time history in 278 days collected by the No.13 sensor during 2006.1~2011.12 has been selected for the analysis in the following section.

Moving average method obtains a series of average values to reflect the trend of the time-variant sequence, as shown in Fig. 1.

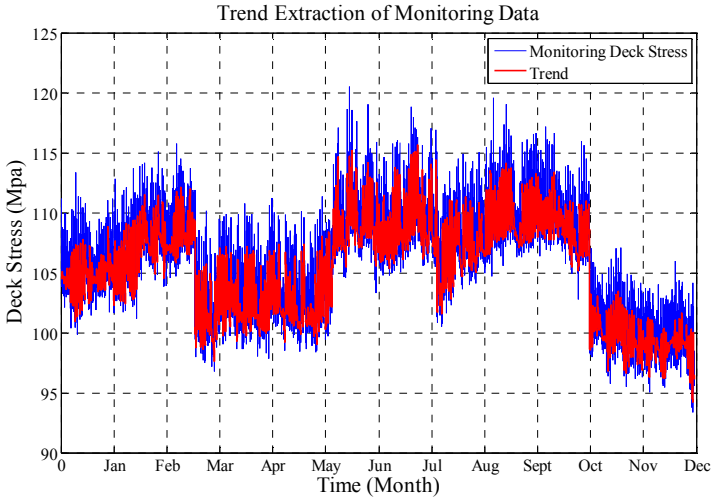

Fig. 1 Trend extraction from deck stress time history

Removing the mean from the trend, the deck stress time history can be categorized into three parts: vehicle stress (shown in Fig. 2), temperature stress (shown in Fig. 3) and constant load stress (105.3471 MPa).

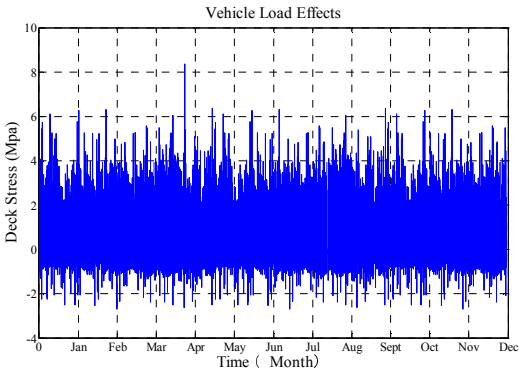

Fig. 2 Vehicle stress time history

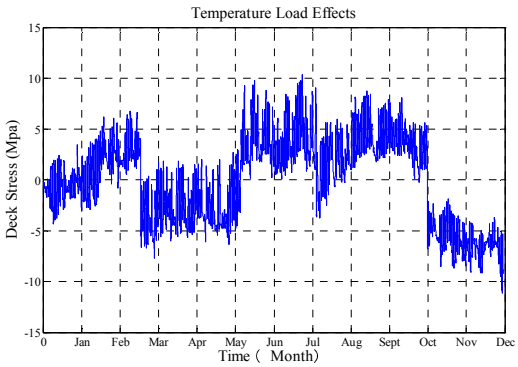

Fig. 3 Temperature stress time history

In the extreme value distribution estimation, the tail part of the stress would be points of interest. generalized Pareto distribution is employed to fit the upper tail of vehicle load effects, where the threshold is chosen as 1 MPa.

$$F_L(x) = 1 - (1 - \frac{0.0807(x-1)}{0.8640})^{1/0.0807}. \quad (1)$$

As the vehicle load effect can be modeled as filtered Poisson process, cdf of the extreme value distribution can be expressed as:

$$F_{L\max}(x) = \exp\{-\lambda T_s (1 - F_L(x))\}. \quad (2)$$

where λ means the parameter of the Poisson process, T_s denotes the subsequent service life and $F_L(x)$ represents the cdf of truncated vehicle load effect.

Monte-Carlo simulation provides an effective way to obtain the pdf of different service life. Statistical results indicate that the pdf of hourly mean temperature load effect can be fitted by two weighted normal distribution. The fitting equation can be expressed as:

$$F_{T(x)} = 0.6369\Phi(\frac{x-2.463}{1.3756}) + 0.3631\Phi(\frac{x+4.671}{1.1861}). \quad (3)$$

Combination of two stochastic load effects

The vehicle load effect can be described approximately as filtered Poisson process as shown in Fig. 4 and the temperature load effect can be modeled as rectangular pulse process with the duration time μ_d being 3600 seconds as shown in Fig. 5.

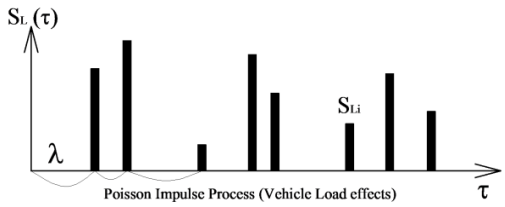

Fig. 4 Filtered Poisson process

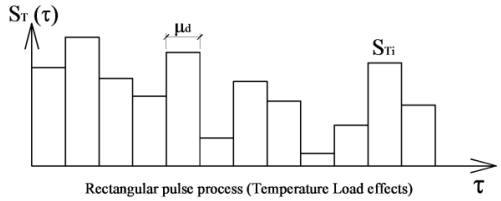

Fig. 5 Rectangular pulse process

The cdf of the maximum intensity of Z_{dmax} in the subsequent service life T_s can be expressed as (4) [6]:

$$F_{Zd\max}(z) = \left[\int_0^{\infty} \exp\{-\lambda\mu_d [1 - F_{S_L}(z - z_T)]\} f_{z_T}(z_T) dz_T\right]^{T_s}. \quad (4)$$

Numerical integration is applied to calculate the values of $F_{zdmax}(z)$ in different subsequent service life and the curves are plotted in Fig. 6. The pdf (shown in Fig. 7) of daily extreme value is also calculated by Monte-Carlo simulation from the corresponding curve in Fig. 6.

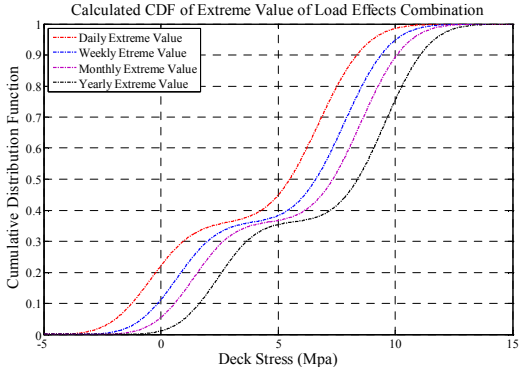

Fig. 6 Calculated cdf of combination

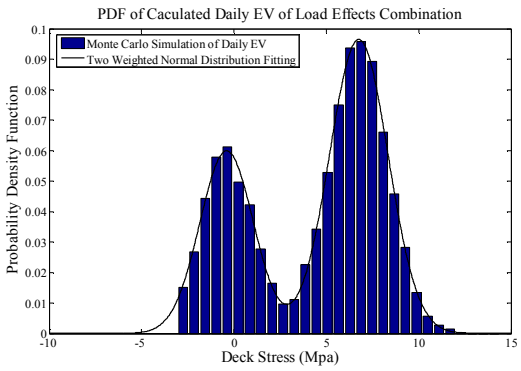

Fig. 7 Calculated pdf of combination

To certify the effectiveness of this combination method, a comparison has been made between the proposed method and other rules(e.g. the Turkstra's rule and the Borges' rule). The calculated pdfs of hourly maximum load effect are shown in Fig.8.

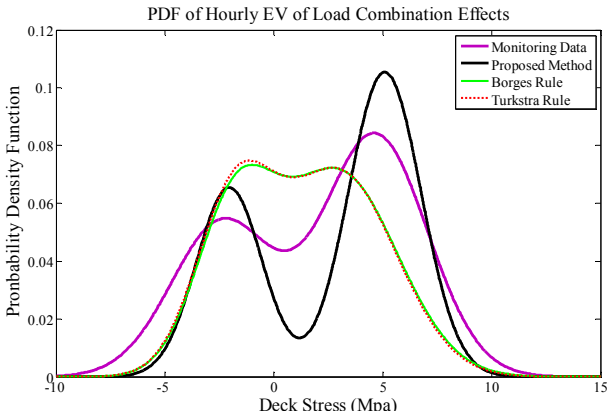

Fig. 8 Comparison between different combination methods

The overlapping areas between calculated pdf curves and the empirical pdf curve are calculated and shown in Table 1.The result indicates the validity of the proposed combination method .

Table 1 Result of calculated overlapping areas

Different combination method	Overlapping area
Turkstra's rule	0.7100
Borges' rule	0.7107
Proposed method	0.7275

Conclusion

This paper reviews the development of the combination rules of several stochastic loads and proposes a method of combining two stochastic loads which can be modeled as rectangular process and filtered Poisson impulse process respectively. The analysis of the vehicle and temperature load effects is based on the real-time data collected through the SHM system which accurately reflect the real condition of the bridge. To describe the combination of load effects, the truncated distribution of two stochastic processes is discussed firstly. The generalized Pareto distribution is applied to fit the upper tail of the vehicle load effect while the temperature load effect follows two weighted normal distribution. Then numerical integration is applied to calculate the cdf of combination and the prediction of maximum stress can be obtained from calculated cdf by means of the Monte-Carlo simulation. In the end, a comparison is made between the proposed method and other combination rules. Result of the comparison proves the validity and accuracy of the proposed method.

References

[1] Turkstra C.J., Theory of structural design decision, Solid Mechanics Division, Study NO. 2, University of Waterloo , Waterloo, Ont , 1970.

[2] Howard T. Pearce, Y. K. Wen, Stochastic Combination of Load Effects, J. Struct. Eng, ASCE, 110 (1984)1613-1629.

[3] J. Ferry-Borges, M. Castenheta, Structural Safety, Laboratoria Nacional de Engenhera Civil, Lisbon,1971.

[4] Wen Y.K., Statistical combination of extreme loads, J. Struct. Div, ASCE, 103(1977)1079–1093.
[5] Larrabee R.D., Cornell C.A. Combination of various load processes, J. Struct. Div, ASCE, 107(1981)223–239.
[6] Yasuhiro Mori, Takahiro Kato, Kazuko Murai, Probability models of combinations of stochastic loads for limit state design, Structural Safety 25 (2003) 69-97.

doi:10.4028/www.scientific.net/AEF.5.162

Reinforcing the Bridges in Tunnel Excavation Region by Using a Method Combining Jacking Superstructure and Grouting Substructure

Bao Jin[1, 2, a],Yang Liu[1,b]

[1]School of Transportation Science and Engineering, Harbin Institute of Technology, Harbin, China, 150090

[2]Jinan Urban Construction Group Co., Ltd, Jinan, China, 250000

[a] jin-_bao@163.com, [b] ly7628@hit.edu.cn

Keywords: Bridge engineering, tunnel engineering, bridge reinforcement, jack-up technique, grouting technique

Abstract It is crucial to alleviate the effect of construction of underground transportation on the safety of the bridges in tunnel excavation region since it is inevitable for the tunnel to go across the city viaduct. To solve above problem, a technique of bridge reinforcement was proposed, which combines the jacking superstructure of bridges and grouting substructure. With this technique, the uneven settlement of the bridge foundation could be controlled as well as the change of the upper structure of bridges could be limited in a reasonable interval. Finally, the effectiveness of proposed method is demonstrated by reinforcing a real bridge in the region of subway construction in Guangzhou, China.

1. Introduction

It is impossible to avoid the effect of the construction of underground transportation on the safety of bridges located in the same road network since the city subway network are always accordance with the road network. Especially, the effect of subway tunnel excavation on bridges could not be ignored. The reason is that the subway tunnel excavation construction causes the disturbance of surrounding soils, which may reduce the ability of resisting load of the soil layer [1,2]. Meanwhile, the soil disturbance causes the loss of groundwater in a certain amount, which is the direct reason for uneven settlement of bridge foundation [3,4]. Therefore, it is important to alleviate uneven settlement of bridge foundation caused by the construction of subway and to ensure the ability of resisting load.

This paper proposed a method for reinforcing the bridge foundation by combining the jacking superstructure and grouting substructure of bridge. The basic idea of this method is that, on one hand, the change of the upper structure of bridge could be controlled in a safety limit, and, on the other hand, the uneven settlement of bridge foundation could be alleviated in a safety interval. Need to point out that the proposed technique only can be applied to the bridges with continuous girder or the simply supported beam, but not to continuous rigid frame bridges.

2. Bridge foundation reinforcement by using the combination between jacking superstructure and grouting substructure

2.1 Introduction of Bridge foundation reinforcement by using the combination between jacking superstructure and grouting substructure

The procedure of proposed method is described as follows: start → tunnel excavation → close the working platform temporarily → jacking the superstructure of bridges → drill and set up grouting pipe at the working face → drill and set up grouting pipe for side work face → grouting

the sleeve valve tube → soil consolidation → tunnel excavation → construction monitoring → repeating grouting……→ the tunnel goes through the bridge foundation → construction monitoring → sealing grouting pipe → end

2.2 Implement of Bridge foundation reinforcement by using the combination between jacking superstructure and grouting substructure

2.2.1 Implement of jacking superstructure of bridge

(i) Set up the scaffold platform

(ii) Placement of Jack

When the superstructure of bridges are jacked, different types of jack could be selected according to the actual situation between the pier and girder, e.g., two types of jack are popular, i.e. 320 tons and 180 tons of ultra-thin jacks.

(iii) Jacking the superstructure of bridge

The success or failure of jacking directly influence the safety of the bridge, so it is necessary to take some effective measures to ensure that the bridge jacking would be completed in the shortest time. Initial lifting force of jack should be about 50% of the controlling values, and then the load will be implemented by additional 5% for each time. When the jacking goes to the design position, replacing the bolt on the support by steel plates and unloading slow.

(iv) Construction monitoring

Here, the displacement of girder should be monitored during the process of jacking. The sensors could be fixed at four standpoints on the top of pier.

2.2.2 Implement of grouting substructure of bridge

(i) Drilling

The DTH drill can be applied and the drill could be selected according to the diameter of the hole. After drilling, the high quality thin slurry supporting could be utilized. In case for the collapse of the hole, drive pipe could be applied to reinforce the structure of hole. When the casting materials are injected into the holes, the drive pipe should be taken out.

(ii) Set up sleeve valve tube, pour casting materials

When the design depth is obtained, casting materials (clay slurry) and grouting scope of material will be poured into the hole in order to prevent sleeve valve grouting pipe to be distorted or damaged. According to the grouting requirements, type B grouting pipe should be poured into grouting part.

(iii) Solidification

The grouting need to wait until the slurry near orifice is solidified. The time for solidification should be controlled about three days.

(iv) Ring opening grouting

In the early period of the grouting stage, the slurry (or water) is applied to increased pressure. During the process of pressuring, the open loop would be realized if the pressure dropping dramatically or the pulps increase rapidly. To ensure the safety of grouting, the right order should be obeyed.

(v) Construction monitoring

During the grouting process, the effect of grouting pressure may cause the ground to go up, which may make damage the surface of concrete road or tunnel primary support. Therefore, the settlement of bridge foundation shall be monitored in order to guide the construction safety.

3. Practical application of proposed method

3.1 Introduction of practical example

The proposed method is applied to reinforce the bridges in the tunnel excavation region. This project is located at the intersection between west road and sai wan road, Guangzhou, China. The inner loop viaduct is up on the station, the left line consists of 3×22m+24m+3×22m continuous rigid frame bridge and 26 m + 40 m + 26 m prestressed concrete continuous girder, adn the right line consists of 3×22m+3×24m continuous rigid frame and 26 m + 40 m + 26 m prestressed concrete continuous girder. The inner loop viaduct takes use of Φ1200, Φ1500, Φ1800 of bored piles, the pile foundations are end-bearing pile and friction pile. During the construction process, 25 foundation (XJ25) and 34 foundation (XJ34) occurs larger settlement, as shown in Fig.1.

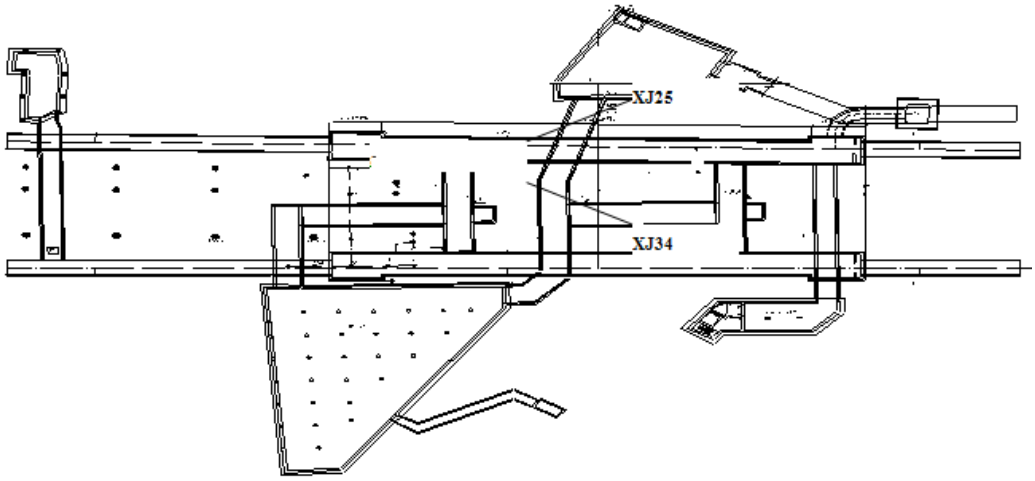

Figure 1 Tunnel and pile foundation position schemes

3.2 Application of proposed method

The No.25 and No.34 bridge foundation were reinforced by using the proposed method. Each bridge foundation was jacked twice, and the process of settlement of foundation is shown in Fig. 2.

According to the design code of bridge of China [5], the theoretical settlement of No. 25 and No. 34 pier go to 27.74 mm and 80.16 mm respectively. Comparing with the results in Fig.2, both settlements of two piers after reinforcement by using proposed method belong to the allowed interval. Therefore, the effectiveness of proposed method was verified.

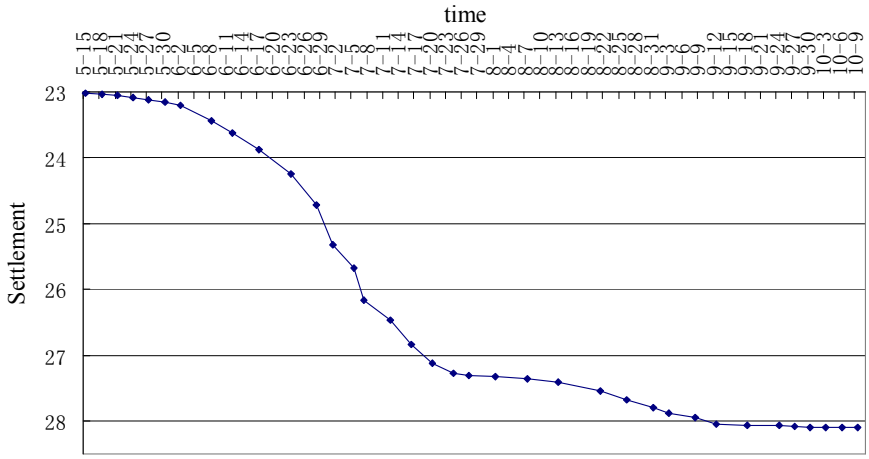

(a) XJ25 foundation jacking and grouting

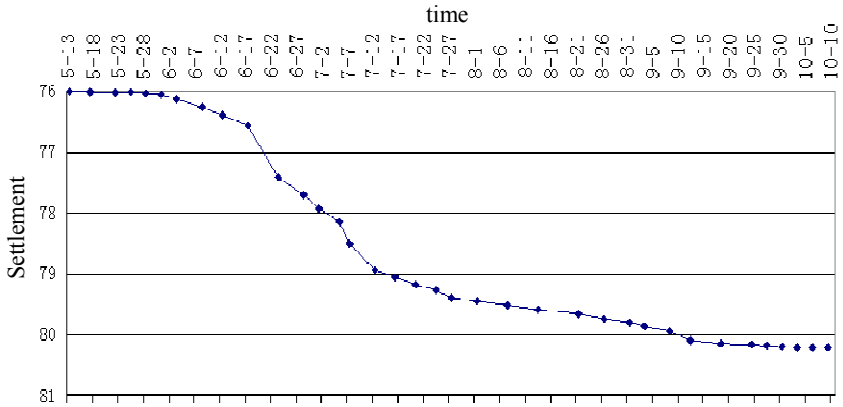

(b) XJ34 foundation jacking and grouting

Figure 2 Settlement of bridge foundation during construction

4. Conclusion

A method combining the jacking and grouting was proposed to reinforce the foundation of bridges that are located in the tunnel excavation region. The basic idea of proposed method is to solve the reinforcement of bridge foundation caused by tunnel excavation in both sides, i.e., jacking the superstructure and grouting the substructure of bridges. With the proposed method, the uneven settlement of the bridge foundation could be controlled as well as the change of the upper structure of bridges could be limited in a reasonable interval. The proposed method account on the advantages of both jacking and grouting technology, and this method overcome the disadvantages of traditional method, such as the complex procedure of implementing, long cycle of construction, damage of surroundings and traffic interruption. According to rough statistic, each blade foundation reinforcement can save construction costs 100,000￥.

ACKNOWLEDGEMENT

This research is financially supported by National Science Foundation of China (Grant Nos. 51008097).

References

[1] G.Q. Sun, Down through the tunnel building protection scheme selection and grouting test plan, Journal of railway engineering, 2010,144 (9):35-40. (in Chinese)

[2] L. Li, The protection scheme discusses of the building foundation subway tunnel through, Tunnel construction, 2008, 28 (6):720-723. (in Chinese)

[3] Z.M. Zhang, Q.Q. Zhang, The test research about post-grouting compressive pile mechanical properties, Journal of rock mechanics and engineering, 2009, 28 (3): 476-482. (in Chinese)

[4] F.R. Xu, Q.Q. Li, The application of sleeve valve barrel grouting consolidation in the viaduct pile foundation of the protection, Modern urban rail traffic, 2010:33-37. (in Chinese)

[5] JGJ 94-2008, Building pile foundation technical specifications, Beijing, 2008. (in Chinese)

doi:10.4028/www.scientific.net/AEF.5.167

The Effect Analysis of Wind Load on Vehicle-Bridge Coupled Dynamic Behavior

LI Yan[1,a] and SUN Hang[1,b]

[1]School of Transportation Science and Engineering, Harbin Institute of Technology, Harbin, China

[a]liyan_2007@126.com, [b]bridge_hit@126.com

Keywords: Vehicle-Bridge Coupled Vibration; Mode Integration Theory; Wind Load; Buffeting.

Abstract. A computer simulation method of solving vehicle-bridge system vibration response considering wind load is presented based on mode integration theory. Vehicle model and fluctuating wind load model are established, corresponding vehicle stiffness and damping matrix is educed in the method. A practical cable-stayed bridge dynamic analysis is completed successfully by programming with fore mentioned method. Wind load have a great influence on bridge vibration acceleration under low wind velocity. Vehicle vertical dynamic response is influenced evidently by wind induced bridge vibration, its lateral response is controlled by wind load and bridge response. The effect on system dynamic response of wind load is remarkable. For other type large span bridges the method also can be referred and have important application value in interrelated research. The accuracy of calculation is high enough for practical purposes.

Introduction

Long span cable-stayed bridges mostly were used crossed large river and channel, where hurricane usually happened. Hurricane-induced strong winds have been greatly threatening the safety of vehicles on the bridge. Currently, decisions on driving speed limits and closing of transportation on bridges and highways in windy environments are mostly based on intuition or subjective experience [1]. Durative strong wind load also affect the structural durability and safety of bridge. A rational prediction of the performance of vehicle-bridge system under strong winds is of utmost importance to ensure transportation efficiency and safety [2].

Recently the study on vehicle-bridge vibration under strong wind is rarely carried out [2]. Hence the research for vehicle-bridge system dynamic response under strong wind is indispensable for guaranteeing bridge operation security and transportation safety.

The present study put forward a vehicle-bridge dynamic response analysis method considering dynamic wind load based on the mode integration theory. Dynamic equilibrium equation derivation of vehicle model and wind load model are given in the paper. The project example analysis shows that the method is suitable for the interrelated analysis of similar engineering and project appliance.

1 Simulation of stochastic wind field

The vehicle-bridge coupling vibration system dynamic response is analyzed in time domain for its obvious time-varying characteristic. Simulation of stochastic wind field is first step to compute vehicle-bridge vibration under wind circumstance. In the study spectral representation method is used to simulate of stochastic wind field. Supposed wind speed and wind spectrum along bridge length direction are invariable, bridge deck heights are in is uniform, the distance of two closed wind speed simulate point is same. Impulsive wind load of the j point can be generated with:

$$f_j(t) = 2\sqrt{\Delta\omega}\sum_{m=1}^{j}\sum_{l=1}^{N}\left|H_{jm}\omega_{ml}\right|\cos(\omega_{ml}t-\theta_{jm}(\omega_{ml})+\phi_{ml}),\qquad (j=1,2,\cdots,m) \tag{1}$$

where $\Delta\omega=(\omega_{\max}-\omega_{\min})/N, \omega_l=\omega_{\min}+(l-1/2)\Delta\omega$, N is frequency interval， $\omega_{\max},\omega_{\min}$ are maximal and minimal frequency limited value, ϕ_{ml} is a random variable uniformly distributed between 0 and 2π; S is cross-spectral density matrix of wind spectrum, H is Cholesky decomposition matrix of S. H_{jm} is the lower triangular matrix of (j,m) subdeterminant of H :

$$\theta_{jm}(\omega_{ml}) = \tan^{-1}\left(\frac{\mathrm{Im}\,H_{jm}(\omega_{ml})}{\mathrm{Re}\,H_{jm}(\omega_{ml})}\right) \tag{2}$$

Simu spectrum is used in simulating wind load in lateral and along bridge directions, Lumley-Panofsky spectrum is used in vertical, defined equations can be found in [3]. The author completed simulation stochastic wind field of the long span cable-stayed bridge with self-compiling computing program.

2 Dynamic analysis of vehicle-bridge system under strong wind

2.1 Vehicle model

In the present study, a vehicle is modeled as a combination of several rigid bodies connected by several axle mass blocks, springs, and damping devices (Fig.1). The bridge deck and the tires of the vehicles are assumed to be point-contact without separation. Vehicle body owns four DOF: vertical displacement, lateral displacement, pitching displacement and rolling displacement; each wheel owns vertical and lateral displacement; the whole vehicle model includes 12 DOFs.

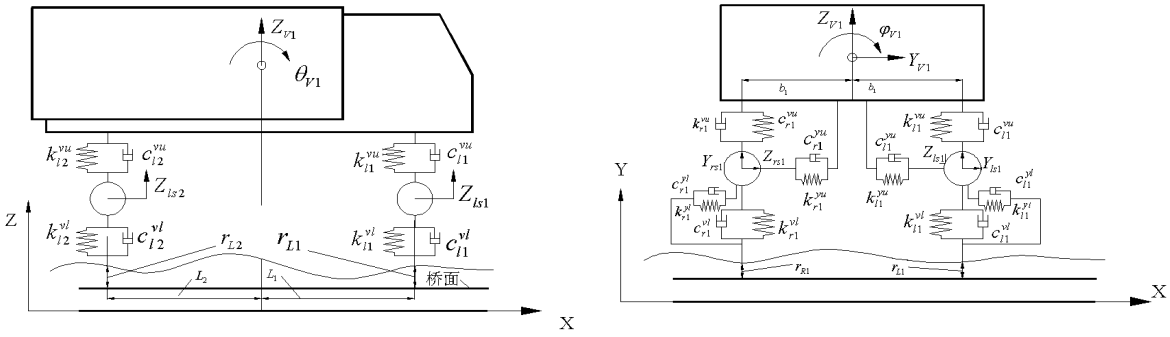

Fig .1 Vehicle model

The vehicle stiffness matrix K_v is detruded by stiffness integration method. Both the stiffness and damping matrix are symmetrical. K_v and C_v have same form, C_v can be gotten by displacing k with c. Vehicle stiffness matrix are listed in reference [6]

2.2 Bridge model

The long span and complexion of factual bridge structure make compute vehicle-bridge system vibration difficulty and calculate cost. The study shows that dynamic response of complex bridge structure is controlled by its several low order mode. The structure dynamic analysis accuracy can arrive engineering requirements by considering several low order modes. In the present study mode integration theory is applied in vehicle-bridge vibration analysis. At first cable-stayed bridge FEM is built, construction mode and frequency can be attained by modal analysis. Motions in three directions including vertical, lateral, and torsion of the bridge are expressed with the mode superposition technique as:

where $\phi_h^n(x), \phi_\theta^n(x), \phi_v^n(x)$ respectively are the components in the three directions (lateral, vertical and torsion) for the nth mode shape; N_b is the total number of modes for the bridge under consideration; q_n is the generalized coordinates of the bridge. All the mode shapes are standardized by generalized mass equaling 1. The displacement of bridge can be showed as:

$$Y_b(x)=\sum_{n=1}^{N_b} q_n \phi_h^n(x), \theta_b(x)=\sum_{n=1}^{N_b} q_n \phi_\theta^n(x), \quad Z_b(x)=\sum_{n=1}^{N_b} q_n \phi_v^n(x) \tag{3}$$

2.3 Vehicle-bridge system motion equation under strong wind load

The wind effects on vehicle-bridge system consist of lift force, drag force and rolling moment, each component includes static force, aeroelastic self-excited forces induced by interaction between wind and bridge or vehicle, and turbulent buffeting forces. It is usually assumed that the analysis begins with the static equilibrium position of the bridge under self-weight and static wind force action. Only aeroelastic self-excited forces and turbulent buffeting forces on the bridge, static wind and turbulent buffeting forces on the vehicle are considered in the dynamic analysis of the bridge.

The motion equations of vehicle-bridge system under wind load are:

$$\begin{bmatrix} M_{vv} & 0 \\ 0 & M_{bb} \end{bmatrix}\begin{Bmatrix} \ddot{X}_v \\ \ddot{X}_b \end{Bmatrix}+\begin{bmatrix} C_{vv} & C_{vb} \\ C_{bv} & C_{bb} \end{bmatrix}\begin{Bmatrix} \dot{X}_v \\ \dot{X}_b \end{Bmatrix}+\begin{bmatrix} K_{vv} & K_{vb} \\ K_{bv} & K_{bb} \end{bmatrix}\begin{Bmatrix} X_v \\ X_b \end{Bmatrix}=\begin{Bmatrix} F_{vb} \\ F_{bv} \end{Bmatrix}+\begin{Bmatrix} F_v^{st}+F_y^{bf} \\ \tilde{F}_b^{bf}+\tilde{F}_b^{se} \end{Bmatrix} \tag{4}$$

where M, K, C respectively represent for mass, stiffness and damping matrix; $X, \dot{X}, \ddot{X}$ represent for displacement, velocity and acceleration respectively; superscripts of "v" refer to vehicle, "b" refer to bridge, "vb" and "bv" refer to the vehicles-bridge coupled terms; F_v^{st}, F_v^{bf} represent for static and turbulent buffeting forces on the vehicles respectively; $\tilde{F}_b^{bf}, \tilde{F}_b^{se}$ represent for modal turbulent buffeting forces and self-excited forces on the bridge respectively. The matrix form of vehicles-bridge interaction can be found in [4]. Newmark-βmethod is used to solve the system motion equations. The wind load on the vehicles-bridge system is discussed in the following section.

2.4 Wind load on the vehicles-bridge system

2.4.1 Wind load on bridge

(1) Buffeting forces

The buffeting forces on the ith point of the bridge is expressed as:

$$F_{bi}^{bf}=[f_{Di}^{bf}, f_{Mi}^{bf}, f_{Li}^{bf}]^T \tag{5}$$

$$\text{where: } \begin{matrix} f_{Di}^{bf}=0.5\rho\bar{U}^2BL_i\left[2C_{Di}u_i(t)+C'_{Di}w_i(t)\right], f_{Mi}^{bf}=0.5\rho\bar{U}B^2L_i\left[2C_{Mi}u_i(t)+C'_{Mi}w_i(t)\right] \\ f_{Li}^{bf}=0.5\rho\bar{U}BL_i\left[2C_{Li}u_i(t)+(C'_{Li}+C_{Di})w_i(t)\right] \end{matrix} \tag{6}$$

where $u_i(t), w_i(t)$ represent horizontal and vertical component of turbulent wind respectively; $f_{Di}^{bf}, f_{Mi}^{bf}, f_{Li}^{bf}$ are buffeting drag force, torsion moment and lift force on the i th point of the bridge; ρ is air dense; $\bar{U}$ refer to mean wind velocity; B_i, L_i represent section width and height of the i th girder section; C_L, C_M, C_D and C'_L, C'_M, C'_D refer to aerodynamic coefficient and corresponding Derivatives.

(2) Self-excited forces on the bridge

The self-excited forces can be expressed as product of displacement and impulse response function of the bridge in the time domain, the impulse response function are educed by the function of flutter derivative from wind tunnel experiment[5]. The self-excited force on the ith point of bridge is expressed as:

$$\begin{aligned} f_{Li}^{se}(t)=&\frac{1}{2}\rho\bar{U}_i^2B_iL_i\left\{A_{Da1}a_i(t)+A_{Da2}\left(\frac{B_i}{\bar{U}_i}\right)\dot{a}_i(t)+A_{Da3}\left(\frac{B_i}{\bar{U}_i}\right)^2\ddot{a}_i(t)\ +\sum_{k=1}^{m}A_{Dak+3}\int_{-\infty}^{t}\dot{a}_i(\tau)\exp[-\frac{d_{Dak}}{B_i}(t-\tau)]d\tau\right\} \\ &+\frac{1}{2}\rho\bar{U}_i^2L_i\left\{A_{Dh1}h_i(t)+A_{Dh2}\left(\frac{B_i}{\bar{U}_i}\right)\dot{h}_i(t)+A_{Dh3}\left(\frac{B_i}{\bar{U}_i}\right)^2\ddot{h}_i(t)\ +\sum_{k=1}^{m}A_{Dhk+3}\int_{-\infty}^{t}\dot{h}_i(\tau)\exp[-\frac{d_{Dhk}}{B_i}(t-\tau)]d\tau\right\} \\ &+\frac{1}{2}\rho\bar{U}_i^2L_i\left\{A_{Dp1}p_i(t)+A_{Dp2}\left(\frac{B_i}{\bar{U}_i}\right)\dot{p}_i(t)+A_{Dp3}\left(\frac{B_i}{\bar{U}_i}\right)^2\ddot{p}_i(t)\ +\sum_{k=1}^{m}A_{Dpk+3}\int_{-\infty}^{t}\dot{p}_i(\tau)\exp[-\frac{d_{Dpk}}{B_i}(t-\tau)]d\tau\right\} \end{aligned} \tag{7}$$

Where $p_i(t), a_i(t), h_i(t)$ refer to lateral, torsional and vertical displacement of the i th point of bridge respectively; $A_{Daj}, A_{Dpj}, A_{Dhj}(j=1,\cdots,3+m)$ and $d_{Dak}, d_{Dak}, d_{Dak}(k=1,2,\cdots,m)$ are nondimensional coefficient which are irrespective with frequency and can be obtained by least squares method based on actual measured flutter derivative under different reduced frequency. m usually equate 2. Self-excited lift force and torsional moment expression can be gotten by the same method.

2.4.2 Wind load on the vehicle

Showed in fig.2, mean wind speed on bridge is U_m, the driving speed of vehicle is U_v ,the relative wind speed can be expressed as:

$$U_R = \sqrt{[\bar{U} + u(x,t)]^2 + U_V^2}, \varphi = arctg[\frac{\bar{U} + u(x,t)}{U_V}] \tag{8}$$

Where $u(x,t)$ represents turbulent wind speed component on the vehicle, which can be simulated by the same method with bridge. The static wind and buffering force on the vehicles are expressed as:

$$\begin{aligned} &F_x = 0.5\rho U_R C_D(\varphi) A_f; F_y = 0.5\rho U_R^2 C_S(\varphi) A_f; F_z = 0.5\rho U_R^2 C_L(\varphi) A_f; \\ &M_x = 0.5\rho U_R^2 C_R(\varphi) A_f h_v; M_y = 0.5\rho U_R^2 C_P(\varphi) A_f h_v; M_z = 0.5\rho U_R^2 C_Y(\varphi) A_f h_v; \end{aligned} \tag{9}$$

where A_f is the frontal area of the vehicle; h_v is the distance from the gravity center of the vehicle to the road surface; $C_D, C_S, C_L, C_R, C_P, C_Y$ are the coefficients of drag force, side force, lift force, rolling moment, pitching moment and yawing moment for the vehicle.

3 Numerical example

The cable-stayed bridge of the 2nd Changjiang river bridge of Nanjing has a main span 628m and total length 1238m, its tower height is 195.41m. The FEM of the bridge is shown in fig.3. The dynamic response of vehicles-bridge system under strong wind for the bridge is studied by self-compiling program in Matlab. Dynamic characteristic calculation can be found in [6].

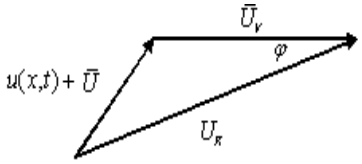

Fig .2 Relative wind velocity on the vehicle

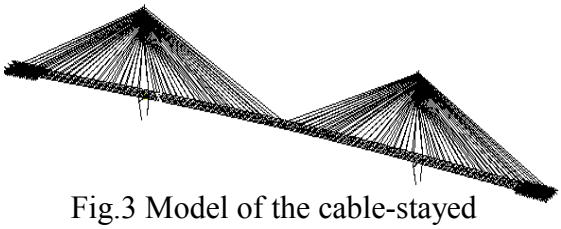

Fig.3 Model of the cable-stayed bridge

In the dynamic analysis 20 low order modes is considered to meet computing accuracy requirement. The damping ratio of the bridge is defined as 0.5% on the dynamic field test. The total weight 300kN vehicle model is used in the present study. The model parameter and aerodynamic parameter are listed in the reference [7]. Take the road surface roughness as "good" level, roughness coefficient is 0.62×10^{-6}m^3/cycle. The design wind speed is 40m/s on the girder height, the earth's surface roughness type is I level, the coherence function of wind spectrum is defined with Davenport

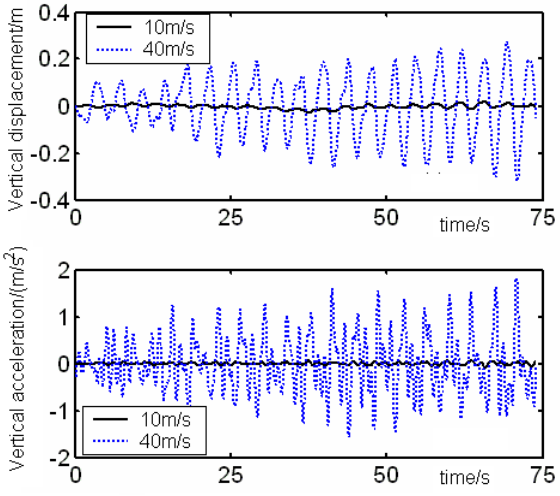

Fig.4 Vertical dynamic response of cable-stayed bridge in mid span

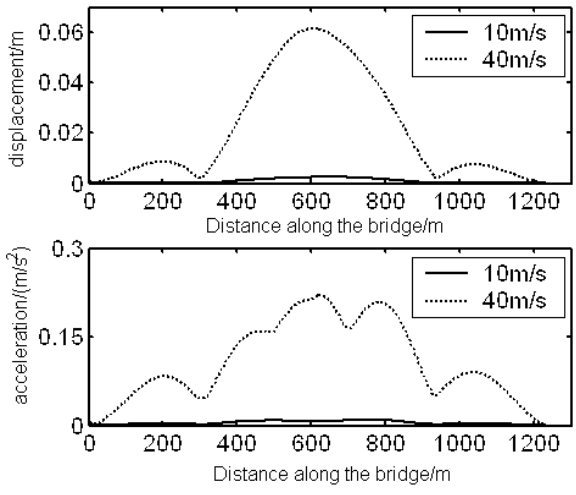

Fig.5 Vertical peak value response of the bridge along span

form [1], dimensionless deamplification factor is 7，the distance of simulation points is 15.475m, aerodynamic parameters are attained by tunnel test [8]. Vehicle speed is 60km/h，integral time length is 0.025s. In the study vehicle-bridge system dynamic response of the cable-stayed bridge is computed under $\bar{U}=10m/s$ and $\bar{U}=40m/s$ respectively. The analysis results are shown in Fig.4 to Fig.9.

Lateral response of the bridge is showed in Fig.6 and Fig.7. It is suggested that wind load is main factor on lateral response of the bridge under strong wind, the point is validated as Fig.7.

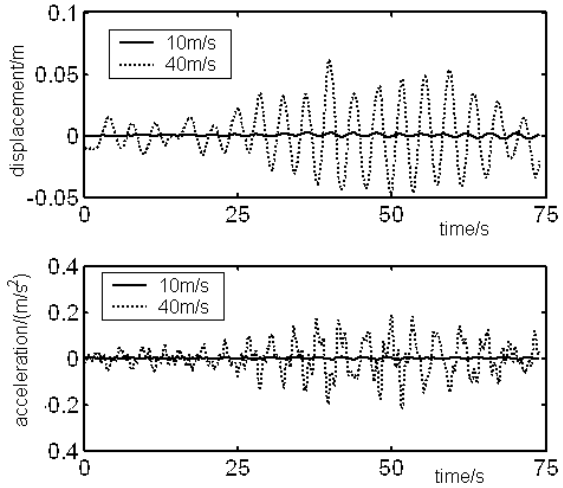

Fig. 6 Lateral response time history of in mid span

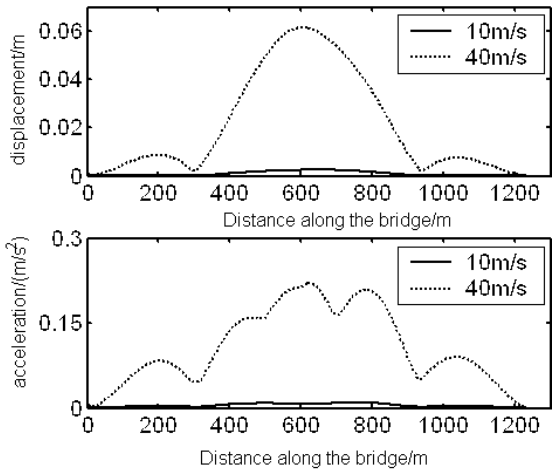

Fig. 7 Lateral peak value response along span

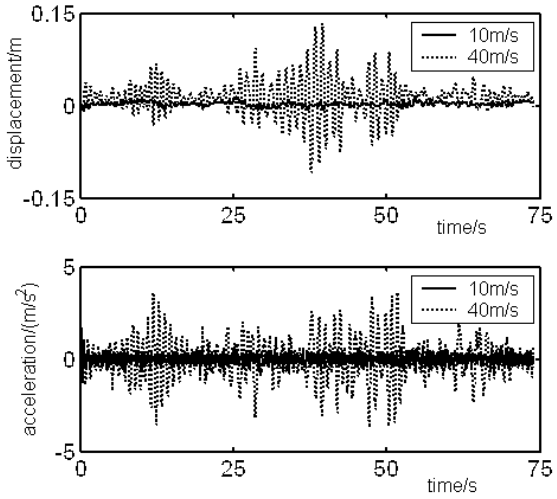

Fig. 8 Vertical response histories of vehicle body

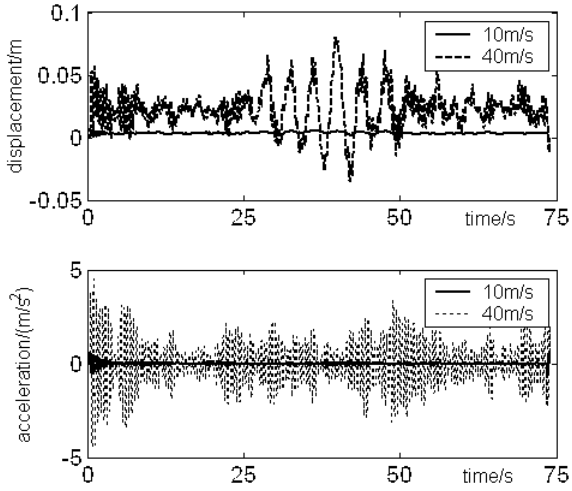

Fig.9 Lateral response histories of vehicle body

The displacement and acceleration time history in mid span of the bridge under two cases is shown in Fig.4. The vertical displacement and acceleration in mid span is controlled with wind load (wind speed 40m/s); under relatively low wind speed (10m/s), the peak vertical displacement appears when vehicles driving through the mid of bridge, the acceleration has the same trend with displacement response, that indicates response is mainly affected by vehicle; The entire bridge displacement and acceleration peak appears peak when the vehicle is driven through the near mid of bridge, which indicates that the influence response comparison is showed in Fig.5, that indicates that wind load is the controlling factor for the vertical response of the bridge replacing vehicles under strong wind.

The vehicle response is showed in Fig.8 and Fig.9. Vertical displacement and acceleration of vehicle of bridge vibration on vertical dynamic response of vehicle is remarkable. As showed in Fig.9, the influence of instantaneous wind on vehicle response is greater when vehicle driving in the bridge. Vehicle displacement appears peak when it pass the middle of the bridge and then attenuate gently, the peak is caused by interaction of lateral vibration of the bridge in mid span and vehicle. It is observed that lateral dynamic response of vehicle is controlled with wind load by comparing results of relatively low and high wind speed cases.

4 Conclusion

(1) The vehicle-bridge system dynamic response analysis model considering fluctuating wind is brought forward based on the mode integration theory. This method can be used for the relevant dynamic analysis of other types of long-span bridges.

(2) Analysis results showed that: the vertical displacement response of the bridge under strong winds was affected significantly by wind load, lateral displacement response was controlled by the wind load; under low wind speed (10m/s) the acceleration of the bridge was greater impacted by wind load, the effluence of bridge vibration on vertical displacement and acceleration response of the vehicle was obvious caused by wind load. The study showed that the safety of vehicle and bridge would be threaten under the strong wind conditions. Carrying out dynamic response study of vehicles-bridge under wind circumstance is very necessary.

(3) The study provides useful referring information and laid the initial foundation for related researches, including the further fatigue damage analysis of cable-stayed bridge under traffic and wind loads, vehicles safety driving on the bridge under disastrous wind load, and etc.

5 Acknowledgements

This research is financially supported by National Science Foundation of China (Grant Nos. 51108132) and Fundamental Research Funds for the Central Universities National Science Foundation of China (HIT.NSRIF.2012059).

References

[1] Z.X. Li, T.H.T. Chan and J.M. Ko: Fatigue Damage Model for Bridge under Traffic Loading: Application Made to Tsing Ma Bridge. Theoretical and Applied Fracture Mechanics, 2001, 35(3): 81-91.

[2] C.S. Cai, S.R. Chen. Framework of Vehicle-bridge-wind Dynamic Analysis. Journal of Wind Engineering and Industrial Aerodynamics, 2004, 92(2): 579-607.

[3] Li Yong-le, Zhou Shu-hua, Qiang Shi-zhong. Simulation of Three-dimensional Fluctuating Wind Field for Large Span Cable-stayed Bridge. China Civil Engineering Journal, 2003,36(10):60-65.

[4] W. H. GUO, Y. L. XU. Fully Computerized Approach to Study Cable-stayed Bridge-Vehicle Interaction. Journal of Sound and Vibration, 2001, 248(4): 745-761.

[5] Chen. X. Z, Matsumoto M, Kareem A. Time Domain Flutter and Buffeting Response Analysis of Bridges. Engineering Mechanics, ASCE, 2000, 126(1): 7-16.

[6] Li Yan. Wind-vehicle-bridge Dynamic Response and Fatigue Reliability of Cables of Long Span Cable-stayed Bridges. Ph.D dissertation, Harbin, Harbin Institute of Technology, 2008

[7] Sheng Guo-gang, Li Chuan-xi, Zhao Bing. Dynamic Analysis of A Simply-supported Beam Subjected to Moving Vehicles. Engineering Mechanics, 2006, 22(12):154-158.

[8] Wind Tunnel Laboratory of Tongji University. Wind Tunnel Experiment Report of the 2nd Nanjing Changjiang River Bridge. 1998

doi:10.4028/www.scientific.net/AEF.5.173

Error Analysis and Amendment Technology of Vibration Wire Strain Sensors

Zhonglong Li[1,2,a], Xiaodi Zhu[3,b] , Zhenyu Liu[1] , Dejian Xu[1]

[1]School of Transportation Science and Engineering, Harbin Institute of Technology, Key Laboratory of traffic safety, specialty materials and intelligent control technology transportation industry Harbin 150090, China;

[2]Postdoctoral Station of Mechanics, Harbin Institute of Technology, Harbin 150090, China;

[3]The Communications Research Institute of Liaoning Province, Shenyang 110015, China

[a]lizhonglong@hit.edu.cn or lizhonglong2004@126.com, [b] hongjianggu@163.com

Keyword: Vibration Wire Strain Sensors, Error Analysis, Amendment Technology

Abstract: With good stability and high reliability, vibration wire strain sensors were extensively applied in many momentous projects. In the paper, the basic principle and working characters of vibration wire strain sensors were introduced. Also, error caused by working principle, structural bending deformation and temperature were analyzed. In the end, amendment technology was provided for improving measurement accuracy of structural strain.

Introduction

Vibration wire strain sensor is a kind of non-electric quantity measuring sensor, which is extensively applied in the world. It has advantages of simply structured, good durability, strong anti-interference ability, reliable and stable measured values, high accuracy and easy operation. Comparing with resistance strain sensor, it is more easily for data collection, transmission, processing and storage. Its usage may realize automatic tests with high accuracy. Therefore, vibration wire strain sensors are widely used in the environment of poor working conditions and high monitoring technical requirements such as civil engineering, harbor engineering, mechanical ship, reservoir, dam, etc. Now, it has turned to be an indispensable gauging tool for industry and scientific research. It is believed to have a great future of application and development.

In the paper, the working principle of vibration wire strain sensor is analyzed. Also, error analysis and amendment formulas through aspects of working principle structural bending deformation and temperature fields are discussed. Experiments were carried out to prove the correction of theoretical analysis.

Working Principle

Vibration wire strain sensor is mainly composed of diaphragm, vibration wire, clamp holder, vibrator and vibration pickup. The force requiring measurement will change the string tension through diaphragm. Then, vibrator will supply string excitation force to make the sting vibrate. Vibration pickup will convert the mechanical vibrations into the same frequency signal output. Therefore, the change of natural frequency is responded by change of electrical signal.

Based on vibration theory and relationship between string vibration and tension, the function of vibration frequency and structural strain may be obtained.

Relationship BetweenString Tension and Natural Frequence. Based on string vibration theory, considering the influence of string stiffness and ignoring its sag impact, the string differential equation of motion is obtained as following:

$$EI\frac{\partial^4 y}{\partial x^4} - T\frac{\partial^2 y}{\partial x^2} + m\frac{\partial^2 y}{\partial t^2} = 0 \tag{1}$$

where y is transverse vibration displacement (perpendicular to the string length) , x is vertical coordinates, T is string tension increment caused by vibration, EI is the flexural rigidity and m is linear density.

Similar to simply supported beam bearing axial force with hinges at both ends, the boundary condition is $y(0)=0, y''(0)=0, y(L)=0, y''(L)=0$. The equation of equivalent expressions is:

$$\sin \alpha l = 0 \tag{2}$$

where $\alpha^4 = \frac{\omega^2 m}{EI}$.

The solution of Eq.2 is $\alpha_n l = n\pi \ (n=1,2,3,\cdots)$. The equation of string n-order natural is:

$$\omega_n = \frac{n\pi}{l}\sqrt{\frac{T_n}{m}(1+\frac{n^2\pi^2}{l^2}\frac{EI}{T_n})} \tag{3}$$

The equation of string tension T_n is:

$$T_n = \frac{m\omega_n^2 l^2}{n^2\pi^2} - EI(\frac{n\pi}{l})^2 \tag{4}$$

The natural frequency of vibration is $\omega_n = (\frac{n\pi}{l})^2\sqrt{\frac{EI}{m}}$. Using the relationship of $\omega = 2\pi f$, the function between string tension and natural frequency can be obtained as $T_n = Af_n^2$, where $A = (\frac{l^2}{n^2}-\pi^2)4mf_n^2$, $T_n = (\frac{l^2}{n^2\pi^2}-1)m\omega_n^2 = (\frac{l^2}{n^2}-\pi^2)4mf_n^2$.

If ignoring the impact of string flexural rigidity, Eq.3 can be changed as following:

$$f_n = \frac{n}{2l}\sqrt{\frac{T_n}{m}} \tag{5}$$

Eq.5 reflects the relationship between natural frequency f_n and string tension T_n.

Calculation Model. In fact, stress increment is what actual test really cares about. Therefore, if begin frequency is f_0 and the end frequency is f_n, the increment is $\Delta T_n = A(f_n^2 - f_0^2)$. This equation can be used to calculate stress.

1. Error Analysis and amendment Technology

Each kind of sensor has its characteristics including using conditions and environment. The error reasons are analyzed with considering the characteristics of working principle, structural bending deformation and temperature field. Further more, the amendment function is provided.

Amendment Technology Based on Working Principle. Based on vibration theory, the proportional relationship between string tension and 2-order natural frequency is derived. This equation shows sensor has nonlinear characteristic. However, in practice, linear relationship is expected for convenience of calibration and data processing. Therefore, in this paper, natural frequency difference is used to amend the equation:

$$\Delta T_n = A(f_n^2 - f_0^2) + B(f_n - f_0) \tag{6}$$

Where coefficient *A* and *B* can be obtained by least squares curve fitting.

Amendment Technology Based on Structural Bending Deformation

Because the theory of vibration wire strain sensor is based on string theory, it is accurate when only under axial tension or stress. However, this state is rare in test of real project. Generally, structures are under bending force, which means it is necessary to study application condition and amendment of vibration wire strain sensor based on structural bending deformation.

The element force state of structure under bending deformation is shown as Fig.1. The relationship between real test strain and theory one is shown as following:

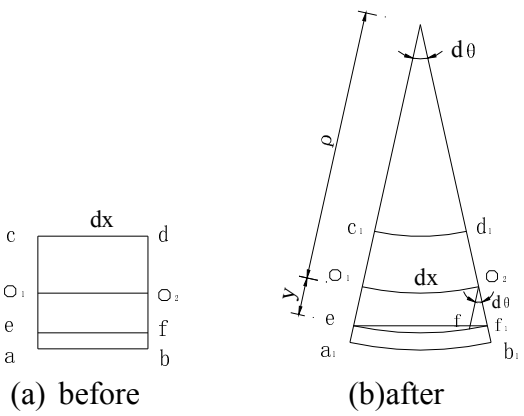

Fig.1-1 Element deformation under bending deformation

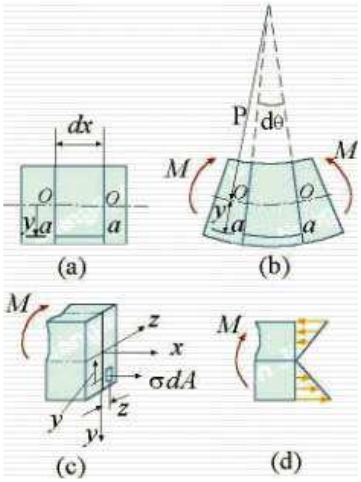

Fig.1-2 Element strain under bending

Theory of Strain. Based on mechanics of material, the theory value of strain can be obtained as following:

$$\varepsilon_l = \frac{ff_1^{\frown}}{ef^{\frown}} = \frac{(\rho + y)d\theta - \rho d\theta}{\rho d\theta} = \frac{y}{\rho} \tag{7}$$

which may be expressed shortly as : $\varepsilon = \frac{y}{\rho}$.

Real Test Value of Strain. During working, the output of vibration wire strain sensor is actually due to string tension to vary degrees of frequency difference. Therefore, what it measures actually is the increment of string-length instead of increment of the arc-length, which causes error. The equation of real test value of strain is

$$\varepsilon_c = \frac{\Delta l}{l} = \frac{ef_1 - ef^{\frown}}{ef^{\frown}} = \frac{2(\rho + y)\sin(d\theta / 2) - \rho d\theta}{\rho d\theta} \tag{8}$$

When $d\theta \in [0,0.5]$, the relative error of $\sin(d\theta)$ and $d\theta$ is lower than 5%, which may consider $\sin(d\theta) = d\theta$. After equivalent transformation, the equation above is the same as the theory one. When $d\theta$ is bigger than 0.5 rad, real test value should be amended.

Amendment Technology. Using geometric relation $\varepsilon = y/\rho$, physical relation $\sigma = E\varepsilon$ and static equilibrium relation $M = EI_z/\rho$, the relationship between neutral layer structure curvature and bending moments may be expressed as $1/\rho = M/EI_z$. In practice, *dx* is standard distance of sensor. For a given sensor, *dx* is a constant value. The theory value and test value are:

theory value $\varepsilon_l = \frac{y}{\rho} = \frac{My}{EI_z}$

test value $\varepsilon_c = \frac{2(\rho + y)\sin(d\theta/2) - \rho d\theta}{\rho d\theta} = \frac{2(\frac{EI_z}{M} + y)\sin(\frac{Mdx}{2EI_z}) - dx}{dx}$.

Therefore, $\frac{\varepsilon_l}{\varepsilon_c} = k = (\frac{My}{EI_z}) / (\frac{2(\frac{EI_z}{M} + y)\sin(\frac{Mdx}{2EI_z}) - dx}{dx}) = (\frac{M^2 y}{2EI_z[(EI_z + My)\sin(\frac{Mdx}{2EI_z}) - Mdx]})$.

The parameters in the above equation are known, which means the test value may be amended.

Amendment Technology Based on Temperature Field

When using vibration wire strain sensor to measure concrete structural strain, it is necessary to remove the section temperature strain of concrete and temperature deformation caused by test point.

Assuming both concrete section temperature and temperature of steel string of vibration wire strain sensor increase a same value of Δt, the test value of strain is made up of two parts: free expansion deformation of concrete structure and steel string deformation caused by temperature variations.

Assuming test value is ε_t, free expansion deformation of concrete structure is ε_{h}, steel string deformation caused by temperature variations is ε_g, so:

$$\varepsilon_h = \alpha_h \Delta t, \quad \varepsilon_{\mathrm{g}} = \alpha_{\mathrm{g}} \Delta t$$

Where α_h and α_{g} are respectively the coefficient of linear expansion of concrete and steel string. Then,

$$\varepsilon_{\mathrm{t}} = (\varepsilon_h - \varepsilon_{\mathrm{g}}) = (\alpha_h - \alpha_{\mathrm{g}})\Delta t$$

When the temperature change of concrete section is uniform, change of test value is caused by difference of coefficient of linear expansion of concrete and steel string.

Therefore, when using vibration wire strain sensor to measure strain, it is important to pay attention to the difference of coefficient of linear expansion of concrete and steel string, which causes test error.

Conclusion

Each kind of sensor has its characteristics including using conditions and environment. It is necessary to ensure the respectively amendment technology based on vibration wire strain sensor's working principle, real force state and environment. In the paper, errors and respectively amendment technology are discussed. The amendment equation improves the accuracy of sensor in the measurement, becoming more accuracy to evaluate structural stress level and may be useful to scientific experiment and practical industry.

Reference

[1] F. Yu, N. Gupta. An Efficient Model for Improving Performance of Vibrating-Wire Instruments, J. Measurement, Vol.37 (2005) No.3, p.278-283.

[2] T.L. Bai, Z.L. Deng, J. Xie and F.P. Hu: Accurate Mathematical Model of Vibrating Wire Sensors and its Application, J. Rock Mechanics and Engineering, Vol. 52 (2005) No.24, p.5966-5969.

[3] R.S. Zhang and T.M. Wang: *Mechanics of Materials* (China Building Industry Press, China 1997).

[4] Y.L. Chui, Y.M. Liu and F. Yu: Resonant Sensor Theory Formula Correction Method and its Application, J. Test and Measurement Technology, Vol. 10(1996), No.1, p.17-22.

[5] T.L. Deng, S.L. Zhao, Z.Y. Zhao and S.M. Zhao: Research on High Accuracy Vibrating Wire senor, J. Journal of Shandong University of Science and Technology, Vol. 29(2010), No.1, p.52-56.

doi:10.4028/www.scientific.net/AEF.5.177

Modified Formula of Estimating Fundamental Frequency of Girder Bridge with Uniform Cross-section

Gao Qing-fei[a], Wang Zong-lin[b], Liu Yang[c], Guo Bin-qiang[d]

School of Transportation Science and Engineering, Harbin Institute of Technology, Harbin 150090, China

[a]Email: gaoqingfei_1986@163.com, [b]Email: wangzonglin@vip.163.com,
[c]Email: ly7628@hit.edu.cn, [d]Email: guobinqianglove@163.com

Keywords: Girder Bridge; Estimation of Fundamental Frequency; Natural Vibration

Abstract: Based on present research, there is a big difference between the estimation of the first frequency of Girder Bridge obtained by the design code of bridges, issued by department of transportation of China in 2004, and the theoretical value in some cases. To overcome above issue, theoretical analysis combined with numerical simulation was applied to estimate the fundamental frequency of Girder Bridge with uniform cross-section. The effect of the ratio between side span and central span on the estimating fundamental frequency was discussed in detail. Finally, an improved method was proposed to estimate the first frequency of Girder Bridge, and the effectiveness of the proposed method was verified.

1 Introduction

Most bridges are designed using a static analysis, adjusted by the impact factor which is a function of the natural frequency [1]. According to *General Code for Design of Highway Bridges and Culverts*, the impact factor of simple-supported girder bridge is bound up with the first flexural frequency of the bridge while it is related to the first two natural frequencies for continuous girder bridge. Thus, the estimated accuracy of natural frequencies is particularly significant.

In the above-mentioned Code, estimated formulas of simply supported girder bridge and continuous girder bridge are suggested as follows [2].

For simply supported girder bridge,

$$f_1=\frac{\pi}{2l^2}\sqrt{\frac{EI_c}{m_c}}. \tag{1}$$

For continuous girder bridge,

$$f_1=\frac{13.616}{2\pi l^2}\sqrt{\frac{EI_c}{m_c}}, \qquad f_2=\frac{23.651}{2\pi l^2}\sqrt{\frac{EI_c}{m_c}}. \tag{2}$$

Where, f_1 — the first natural frequency, f_2 — the second natural frequency, E — Young's modulus, I_c — second moment of area of mid-span cross-section, m_c — mass of mid-span per unit length, and l — span length.

Obviously, the existing estimated formulas have the following defects:

- For multi-spans continuous girder bridge, the meaning and selection of span length l are not clear (the length of central span or side span).
- For multi-spans continuous girder bridge, the number of spans and the ratio of side span and central span are not considered in formula (2).

Shortly, it has an urgent need to study the influence of every parameter and to get a more rational formula of estimating fundamental frequency of Girder Bridge with uniform cross-section.

2 Theoretical Analysis

Based on mechanical concepts, simply supported girder bridge is statically determinate structure while continuous girder bridge is statically indeterminate structure. In this section we develop the equation governing the transverse vibration of a straight girder without damping subjected to external force. D' Alembert principle, Lagrange equation, and Hamilton principle were applied to found the equation of girder bridge vibration [3].

Fig.1a shows such a girder with flexural $EI(x)$ and mass $m(x)$ per unit length, both of which may vary with position x. The external forces $p(x,t)$, which may vary with position and time, cause motion of the girder described by the transverse displacement $y(x,t)$(Fig.1b). The equation of motion to be developed will be valid for support conditions other than the simple supports shown and for girders with intermediate supports.

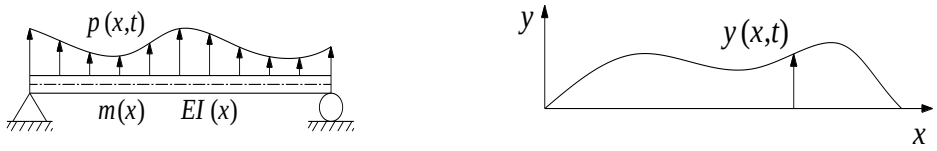

(a) girder and applied force (b) displacement

Fig. 1 System with distributed mass and elasticity

$$m(x)\ddot{y}+\frac{\partial^2}{\partial x^2}\left[EI(x)\frac{\partial^2 y}{\partial x^2}\right]=p(x,t). \tag{3}$$

2.1 Simply supported girder

Setting $p(x,t)=0$ gives the differential equation governing free vibration of the system, which for systems with constant $EI(x)$ and $m(x)$ specializes to

$$m\ddot{y}+EI\frac{\partial^4 y}{\partial x^4}=0. \tag{4}$$

We attempt a solution of the form

$$y(x,t)=\varphi(x)q(t). \tag{5}$$

Substituting Eq.(5) in Eq.(4) gives

$$\frac{m}{EI}\frac{\ddot{q}(t)}{q(t)}+\frac{\varphi^{(4)}(x)}{\varphi(x)}=0. \tag{6}$$

The first part of equation (6) is a function of t only and the second part depends on x. For equation (6) to be valid for all values of x and t, the two parts must therefor be constant.

$$\frac{\varphi^{(4)}(x)}{\varphi(x)}=C=-\frac{m}{EI}\frac{\ddot{q}(t)}{q(t)}. \tag{7}$$

Setting $C=\alpha^4$, thus equation (7) becomes two ordinary differential equations, one governing the spatial function $\varphi(x)$ and the other governing the time function $q(t)$.

$$\begin{cases}\dfrac{\mathrm{d}^4\varphi(x)}{\mathrm{d}x^4}-\alpha^4\varphi(x)=0.\\ \ddot{q}(t)+\omega^2 q(t)=0.\end{cases} \tag{8}$$

where

$$\omega^2=\alpha^4\frac{EI}{m}. \tag{9}$$

Setting $\varphi(x)=Be^{rx}$, substituting which in the first one of equation (8) gives

$$(r^4-\alpha^4)Be^{rx}=0. \tag{10}$$

Then

$$r_{1,2}=\pm\alpha,\quad r_{3,4}=\pm i\alpha\,. \tag{11}$$

Substituting Eq.(11) in $\varphi(x)=Be^{rx}$ leads to

$$\varphi(x)=B_1e^{\alpha x}+B_2e^{-\alpha x}+B_3e^{i\alpha x}+B_4e^{-i\alpha x}. \tag{12}$$

So

$$\varphi(x)=A_1\sin\alpha x+A_2\cos\alpha x+A_3\sinh\alpha x+A_4\cosh\alpha x. \tag{13}$$

These four constants $A_i(i=1,2,3,4)$ depends on the boundary conditions of the girder.

The boundary conditions of simplified Euler-Bernoulli beam shown in Fig.1(a) are listed as follows:

$$\varphi(0)=0,\ \varphi''(0)=0,\ \varphi(l)=0,\ \varphi''(l)=0. \tag{14}$$

From Eq.(13)

$$\varphi''(x)=\alpha^2(-A_1\sin\alpha x-A_2\cos\alpha x+A_3\sinh\alpha x+A_4\cosh\alpha x). \tag{15}$$

Combining Eqs.(13), (14) and (15), we obtain the frequency equation:

$$\sin\alpha l=0. \tag{16}$$

Hence the solution is

$$\alpha_n l=n\pi\quad (n=1,2,3,\ldots\ldots). \tag{17}$$

Then, from Eqs.(9) and (17)

$$\omega_n=\alpha_n^2\sqrt{\frac{EI}{m}}=\left(\frac{n\pi}{l}\right)^2\sqrt{\frac{EI}{m}}\qquad (n=1,2,3,\ldots\ldots). \tag{18}$$

And, for the natural frequencies of simplified girder

$$f_n=\frac{\omega_n}{2\pi}=\frac{n^2\pi}{2l^2}\sqrt{\frac{EI}{m}}\qquad (n=1,2,3,\ldots\ldots). \tag{19}$$

2.2 Continuous girder

For common continuous girder bridges, the cross-section is uniform when the span of bridge is small and the cross-section is variable when the span of bridge is large. The continuous girder bridges with variable cross-section are more complicated, and it is difficult to analysis by theoretical methods. Then the continuous girder bridges with uniform cross-section are theoretical analyzed in this paper.

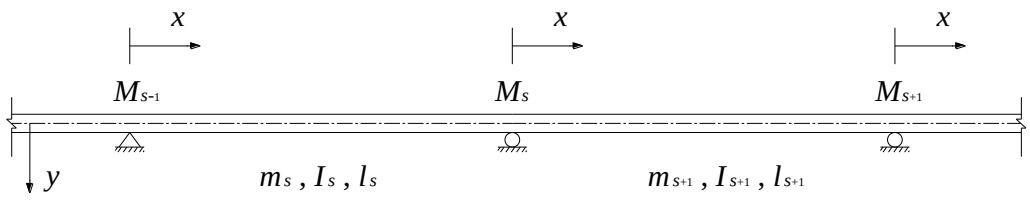

Fig. 2 Symbol conventions of continuous girder

For the continuous girder bridges with uniform cross-section, the distribution of mass and stiffness are equal in every span. The function of the *n*th natural vibration mode in the *s*th span can be expressed as follows.

$$\varphi_{ns}(x)=A_{ns}\sin\alpha_{ns}x+B_{ns}\cos\alpha_{ns}x+C_{ns}\sinh\alpha_{ns}x+D_{ns}\cosh\alpha_{ns}x. \tag{20}$$

These four constants (A_{ns}, B_{ns}, C_{ns} and D_{ns}) depends on the boundary conditions of the continuous girder. where

$$\omega_n^2=\alpha_{ns}\frac{EI_s}{m_s}. \tag{21}$$

The boundary conditions and the continuity of deflection and slope and the compatibility of the forces and moments in the s-span continuous Euler-Bernoulli girder shown in Fig.2 are listed as follows:

$$\begin{cases}\varphi_{ns}(0)=0.\\ \varphi_{ns}(l_s)=0.\\ \varphi'_{ns}(l_s)=\varphi'_{n(s+1)}(0).\\ EI_s\varphi''_{ns}(l_s)=EI_{s+1}\varphi''_{n(s+1)}(0)=-M_{ns}.\\ \varphi_{n(s+1)}(0)=0.\end{cases} \tag{22}$$

From Eq.(20)

$$\varphi'_{ns}(x)=\alpha_{ns}(A_{ns}\cos\alpha_{ns}x-B_{ns}\sin\alpha_{ns}x+C_{ns}\cosh\alpha_{ns}x+D_{ns}\sinh\alpha_{ns}x). \tag{23}$$

$$\varphi''_{ns}(x)=\alpha_{ns}^2(-A_{ns}\sin\alpha_{ns}x-B_{ns}\cos\alpha_{ns}x+C_{ns}\sinh\alpha_{ns}x+D_{ns}\cosh\alpha_{ns}x). \tag{24}$$

Combining Eqs.(20), (22), (23) and (24), we obtain the frequency equation:

$$M_{n(s-1)}\frac{H_{ns}l_s}{\alpha_{ns}l_sI_s}-M_{ns}\left[\frac{G_{ns}l_s}{\alpha_{ns}l_sI_s}+\frac{G_{n(s+1)}l_{s+1}}{\alpha_{n(s+1)}l_{s+1}I_{s+1}}\right]+M_{n(s+1)}\frac{H_{n(s+1)}l_{s+1}}{\alpha_{n(s+1)}l_{s+1}I_{s+1}}=0. \tag{25}$$

where

$$\left.\begin{aligned}G_{ns}&=\frac{\cosh\partial_{ns}l_{ns}}{\sinh\partial_{ns}l_{ns}}-\frac{\cos\partial_{ns}l_{ns}}{\sin\partial_{ns}l_{ns}}\\ H_{ns}&=\frac{1}{\sinh\partial_{ns}l_{ns}}-\frac{1}{\sin\partial_{ns}l_{ns}}\end{aligned}\right\} \tag{26}$$

From equation (25), A equation can be gained in every support of the continuous girder bridges. And all these equations can be listed as a group. According to set the coefficient determinant of $\{M\}$ as zero, natural frequency equations can be obtained.

For common continuous girder bridges transferred from simply supported girder bridges, the distribution of mass and stiffness are equal in every span. Then the frequency equations can be listed as follows.

1) Two-spans continuous girder:

$$G_{n1}+G_{n2}=0. \tag{27}$$

2) Three-spans continuous girder:

$$4G_{ns}^2-H_{ns}^2=0 \quad (s=1,2,3). \tag{28}$$

3) Four-spans continuous girder:

$$2G_{ns}^2-H_{ns}^2=0 \quad (s=1,2,3,4). \tag{29}$$

3 Parametric Study

As we know, the natural frequencies reflect the distribution of the mass and stiffness of the bridge. The influence of the natural frequencies of Girder Bridge with uniform cross-section consists of the following parameters: the number of spans, the length of central span, the ratio of side span and central span, the properties of mid-span cross-section, and the material properties.

Taking common continuous girder bridges transferred from simply supported girder as an example, finite element models were made using ANSYS.

Symbol account: k – the ratio of side span and central span, λ– the fundamental frequency ratio of bridge with unequal span to bridge with equal span which equal to central span.

Table 1 Physical parameters of finite element model

Physical parameters	Value	Physical parameters	Value
Length of main span	l=40m	Height of section	h=2.00m
Area of section	A=1.3017m^2	Density	ρ=2600kg/m^3
Moment of inertia	Ix=0.6346m^4	Modulus of elasticity	E=3.45e10Pa

Table 2 Vertical natural frequency of Girder Bridge with constant section (Hz)

Vertical mode order	Simply supported girder bridges	Continuous girder bridges			
		Two-spans	Three-spans	Four-spans	Five-spans
1	**2.493**	**2.493**	**2.493**	**2.493**	**2.493**
2	**9.928**	3.894	3.195	2.908	2.766
3		**9.928**	4.664	3.894	3.458
4			**9.928**	5.030	4.355
5				**9.928**	5.229
6					**9.928**

Table 3 Fundamental frequency of Girder Bridge with constant section

Bridge(m)	k	f_1(Hz)	Bridge(m)	k	f_1(Hz)	Bridge(m)	k	f_1(Hz)
20+40+20	0.500	3.894	20+35+20	0.571	4.883	20+30+20	0.667	6.251
25+40+25	0.625	3.620	25+35+25	0.714	4.438	25+30+25	0.833	5.415
30+40+30	0.750	3.302	30+35+30	0.857	3.881	30+30+30	1.000	4.427
35+40+35	0.875	2.914	35+35+35	1.000	3.255	20+25+20	0.800	8.053
40+40+40	1.000	2.493				25+25+25	1.000	6.368

Table 4 k and λ of Girder Bridge with constant section

k	0.500	0.571	0.625	0.667	0.714	0.750	0.800	0.833	0.857	0.875	1.000
λ	1.562	1.500	1.452	1.412	1.363	1.325	1.265	1.223	1.192	1.169	1.000

4 Results and Discussion

Table 2 shows that the fundamental frequency of continuous girder bridge is the same as the simplified supported girder bridge, the length of which is equal to the main span of the continuous girder bridge. In other words, the number of spans has no influence on the fundamental frequency of Girder Bridge with equal span and constant section.

Table 3 shows the fundamental frequency of various Girder Bridge with different span arrangement. As we can see, the fundamental frequency decreases with the increasing of the main-span length when the side-span length is constant. And the fundamental frequency increases with the decreasing of the side-span length when the main-span length is constant.

Table 4 shows the influence by introducing two parameters (k and λ). The modified factor λ decreases with the increasing of the ratio k. A regression equation between k and λ can be found by statistical analysis as follows.

$$\lambda = -0.675k^2 - 0.113k + 1.787 \ (0< k\leq 1.0) \ (R^2=0.9999\approx 1.0). \tag{30}$$

And now

$$f_1=\lambda \frac{\pi}{2l^2}\sqrt{\frac{EI_c}{m_c}}. \tag{31}$$

5 Conclusions

The theoretical analysis combined with numerical simulation was applied to estimate the fundamental frequency of Girder Bridge with uniform cross-section in this paper. The results showed that the number of spans has no effect on the estimation of fundamental frequency of Girder Bridge with equal span and constant section. Based on this result, a improved estimation of the first frequency of Girder Bridge was proposed and the effectiveness was verified.

References

[1] T.J. Memory, D.P. Thambiratnam, G.H. Brameld, Free vibration analysis of bridges, J. Engineering Structure. 17(1995) 705-713.

[2] Department of the transport of P R China, General code for design of highway bridges and culverts, S. China Communication Press, Beijing, 2004, pp. 83-84.

[3] Anil K. Chopra, Dynamics of Structures — Theory and Applications to Earthquake Engineering (third edition), M. Tsinghua University Press, Beijing, 2009, pp. 629-630.

doi:10.4028/www.scientific.net/AEF.5.183

Dynamic Characteristics and Seismic Response Analysis of Self-anchored Suspension Bridge

Zhang Lianzhen[1,a], Chen Tianliang[1,b]

[1]School of Transportation Science and Engineering, Harbin Institute of Technology, Harbin City, China, 150090

[a]email:Zhanglianzhen79@163.com, [b]email:tzunchan@gmial.com

Keywords: Self-anchored suspension bridge, Dynamic characteristics, Time-integration analysis, Geometry nonlinear effect, Seismic response.

Abstract: Self-anchored suspension bridge is widely used in Chinese City bridge engineering for the past few years. Because the anchorage system of main cable has been changed from anchorage blocks to the ends of the girder, its' dynamic mechanics behavior is greatly distinguished with the traditional earth anchored suspension bridge. This paper studies the dynamic characteristics and seismic response of one large-span self-anchored suspension bridge which is located in China/Shenyang city. Using a spatial dynamic analysis finite element mode, the dynamic characteristics are calculated out. An artificial seismic wave is adopted as the ground motion input which is fitted with acceleration response spectrum according to the Chinese bridge anti-seismic design code. Time-integration method is used to get the seismic time-history response. Geometry nonlinear effect is considered during the time-history analysis. At last, the dynamic characteristics and the behavior of earthquake response of this type bridge structure are discussed clearly. The research results can be used as the reference of seismic response analysis and anti-seismic design for the same type of bridge.

Introduction

Self-anchored suspension bridge is widely used in Chinese City bridge engineering in recent years. The first one of this type bridge was constructed in 2000 in China mainland. In the following ten years, there are at least thirty self-anchored suspension bridges which are finished in China. Because of its' esthetics performance and good mechanics behavior, Self-anchored suspension bridge has become new favorite structure for bridge design engineer[1].

The mechanical behavior of self-anchored suspension bridge is different from that of the traditional earth anchored suspension bridge because the anchorage system of main cable has been changed from anchorage blocks to the ends of the girder[2]. Considering the characteristic of this type bridge, the girder is subjected to bending moment as well as axial force which is the huge horizontal component of the cable force. This mechanical character of the girder will bring the P-delta nonlinear effects which can reduce the bending stiffness of the bridge contrast to traditional earth anchored suspension bridge, which will enlarge the natural period of vibration of the self-anchored suspension. Besides, to balance the up-vertical component of the cable force, the huge additional mass block will be placed in the range of girder ends. The huge additional mass block also has an impact on the dynamic characteristics of self-anchored suspension bridge. Therefore, it is very necessary to study the dynamic characteristics of this type bridge.

To understand the seismic response pattern of self-anchored suspension bridge is also important, especially for those bridges which are located in strong seismic region. Self-anchored suspension bridge is a self balance structure system. That is to say, the girder have weaker constrain boundary

condition to satisfy the longitudinal movement induced by temperature and compress deflection. When the earthquake occurs, the girder will create longitudinal floating movement, the tower will bear huge horizontal earthquake force.

In this paper, taking one large-span self-anchored suspension bridge engineering as a case, the author study the dynamic characteristics and seismic response of this type bridge structure. Using a spatial dynamic analysis finite element mode, the dynamic characteristics are calculated out. An artificial seismic wave is adopted as the ground motion input which is fitted with acceleration response spectrum according to the Chinese bridge anti-seismic design code. Time-integration method is used to get the seismic time-history response. Geometry nonlinear effect is considered during the time-history analysis. At last, the dynamic characteristics and the behavior of earthquake response of this type bridge structure are discussed clearly.

Project overview and finite element model

The object bridge is located in China/Shenyang City, which is a component of ring way crossing Hunhe River. The bridge is a single-pylon self-anchored suspension bridge. Its' span arrangement is 48m+2×180m+48 m. The main girder is a steel box girder with a height of 4m and a width of 42.5m. The pylon has height of 90.969m from the top of pile caps to the tip of the pylon. Fig.1 shows the architectural effect figure of the bridge.

Fig.1 Architectural effect figure of the Bridge

To simulate the structural stiffness and mass distribution accurately and perform the dynamic analysis, a three-dimensional model of the bridge was built in SAP2000 software. Frame type elements are used to model the girder, pylons. Cable type elements are used to model the main cables and hangers. Respectively, the inter-force of final bridge balance state is integrated into the geometric stiffness matrix as initial conditions.

Dynamic characteristics analysis of the bridge

On the basis of finite element model, subspace iteration method is applied to perform the modal analysis. The preliminary 500 step frequencies and the modes of vibration have been calculated. As space is limited, only the front 10 step modes are enumerated in Table 1 below.

Owing to the small lateral stiffness of the pylon, the transverse bending of the pylon becomes the first vibration mode. Therefore, the response of pylon under horizontal earthquake should be key consideration during the anti-seismic design.

In the light of the front 50 step modes, it can be found that the structure frequency distribution range is closely space. There are 7 step modes in a frequency range from 0Hz to 1Hz, and 11 step modes with an extensive coverage of frequency from 1Hz to 2Hz. That is to say, coupling effect between the adjacent vibration modes is very prominent. Therefore, many modes can be aroused simultaneously in all probability. The shapes of main vibration modes are showed in Table 2.

Table 1 The natural frequency and corresponding vibration mode of the bridge

Mode no.	Frequency[Hz]	Mode description
1	0.455	Lateral bending mode of the pylon
2	0.660	Vertical asymmetric bending mode of the deck
3	0.798	Vertical symmetric bending mode of the deck
4	0.812	Lateral asymmetric sway mode of the two span cables
5	0.813	Lateral sway mode of the right span cables
6	0.813	Lateral sway mode of the left span cables
7	0.835	Lateral symmetric sway mode of the two span cables
8	1.396	Lateral asymmetric sway mode of the two span cables
9	1.397	Lateral sway mode of the right span cables
10	1.397	Lateral sway mode of the left span cables

Table 2 Shapes of main vibration modes

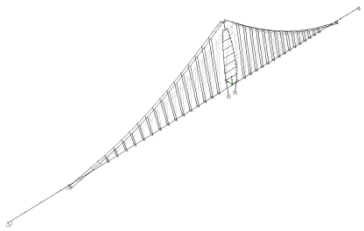

Mode 1 f=0.455Hz

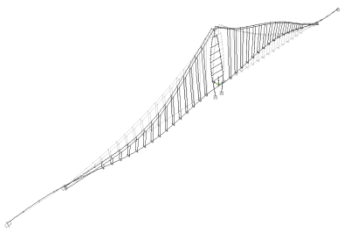

Mode 2 f=0.660 Hz

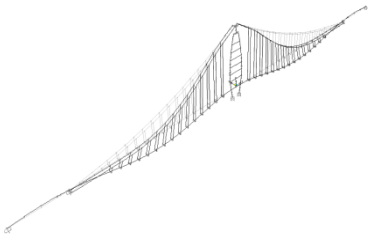

Mode 3 f=0.798 Hz

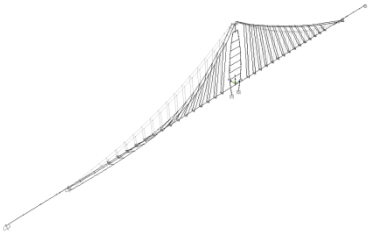

Mode 4 f=0.812 Hz

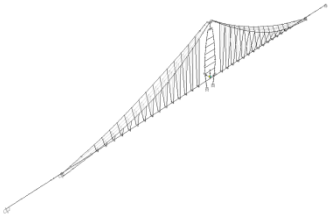

Mode 5 f=0.813 Hz

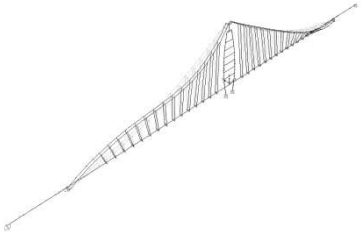

Mode 8 f=1.396 Hz

Seismic response analysis based on time history method

During time history analysis, Rayleigh damping was used to model the damping of the bridge[3]. In Eq. 1, the orthogonal scale factors of Rayleigh damping are: α=0.07278 and β=0.00798, [M] and [K] is mass matrix and stiffness matrix respectively.

$$[C] = \alpha[M] + \beta[K] \tag{1}$$

According to Seismic ground motion parameter zonation map of China and Guidelines for Seismic Design of Highway Bridges[4], the design acceleration response spectrum parameters of this bridge can be checked out and the peak acceleration of the design ground motion is 0.4452g. An artificial seismic wave as shown in Fig.2 is generated to fit the true response spectrum via trigonometric superposition method.

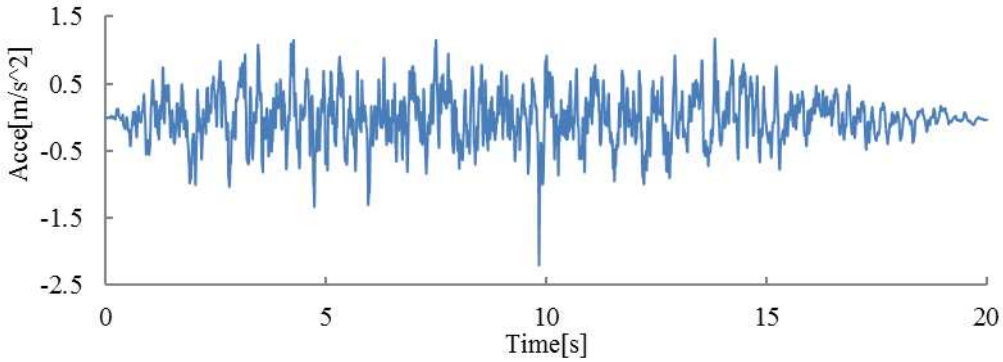

Fig.2 Artificial earthquake wave(EW)

Using the artificial earthquake wave as the ground motion input, including geometry nonlinear effect, seismic response of self anchored suspension bridge is calculated. The EW inputs consider longitudinal, transverse and vertical direction respectively[5]. The calculation result is the following.

EW input in longitudinal direction. The calculation result is list in Table 3 and Table 4. From Table 3 and Table 4, we can draw a conclusion. In this case, performances of longitudinal and vertical vibration are excited observably. However transverse displacements of any points along with the vertical displacements of pylon are negligible.

It can be seen that the maximum absolute moment response of pylon appears at the root from the above Table s. Thence, the root of pylon is the control section of this load case.

Table 3 The peak value of moment in plane of control section

Position	Min[kN·m]	Time[s]	Max[kN·m]	Time[s]
Intersection of G and P	-63880	4.65	55740	11.60
Root section of pylon	-105500	4.65	112600	9.95
Mid span of girder	-21590	5.30	17940	13.80

Where: G is short for girder, and P is short for pylon.

Table 4 The peak value of displacement of control section

Position	Min[m]	Time[s]	Max[m]	Time[s]
Pylon top(Longitudinal)	-0.027	9.25	0.029	13.05
Girder ends(Longitudinal)	-5.680E-03	10.10	5.897E-03	10.25
Midpoint of main span(Vertical)	-0.024	13.80	0.027	5.35

EW input in transverse direction. In this case, the seismic response result is list in Table 5 and Table 6. Under the transverse EW, the lateral vibration is prime performance of the bridge vibration. It's clear that the root of pylon is the control section from Table 5 and Table 6. And also, the moment of pylon root section in this case is bigger than that in longitudinal direction input case. The displacement of pylon top point is up to 0.14m.

Table 5 The peak value of moment out of plane of control section

Position	Min[kN·m]	Time[s]	Max[kN·m]	Time[s]
Intersection of G and P	-167900	10.35	154800	10.15
Root section of pylon	-127600	14.25	119100	17.85
Mid-third-point of girder	-126100	10.15	136100	4.85

Table 6 The peak value of displacement of control section

Position	Min[m]	Time[s]	Max[m]	Time[s]
Pylon top(Lateral)	-0.128	16.75	0.140	17.85
Girder end(Lateral)	-8.687-E03	4.85	7.957E-03	5.05
Midpoint of main span(Lateral)	-6.843E-03	10.15	6.661E-03	4.85

EW input in vertical direction. In this case, the aforesaid EW is multiplied by 0.65 as the ground motion input. The calculation result shows that the seismic response presents the vertical and longitudinal vibration of girder. And the response of pylon is very weak. Above all, in this case, all the response is small, so the result is not list in this paper.

EW input in three directions simultaneously. In this case, earthquake wave is input to analysis seismic response simultaneously. The scale factor of wave in three direction is 1:1:0.65 (longitudinal: transverse: vertical). Fig.3 shows the envelope of moment of girder and pylon (out of plane). Fig.4 shows the envelope of moment of girder and pylon (in plane). Fig.5 shows the time history curve of lateral and longitudinal displacement at the top of pylon. Taking these results to be compared with the above results which are calculated separately, it has no obvious change in peak value. That is to say, for this type bridge. The spatial coupled vibration in three dimension is not obviously.

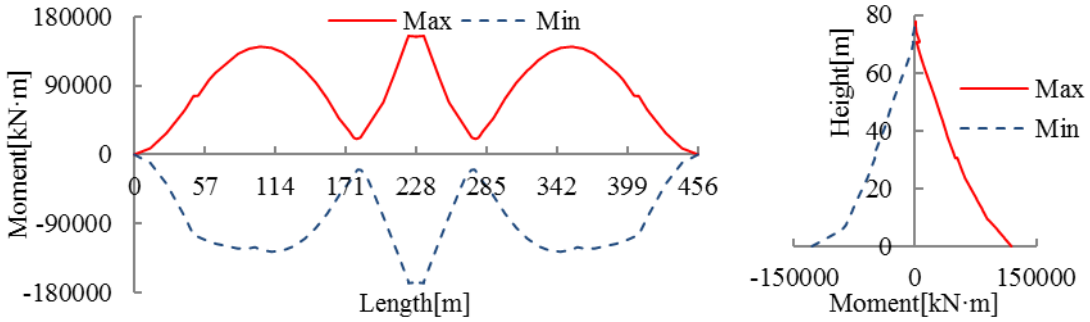

(a) girder (b) pylon

Fig.3 The envelope of moment of girder and pylon (out of plane)

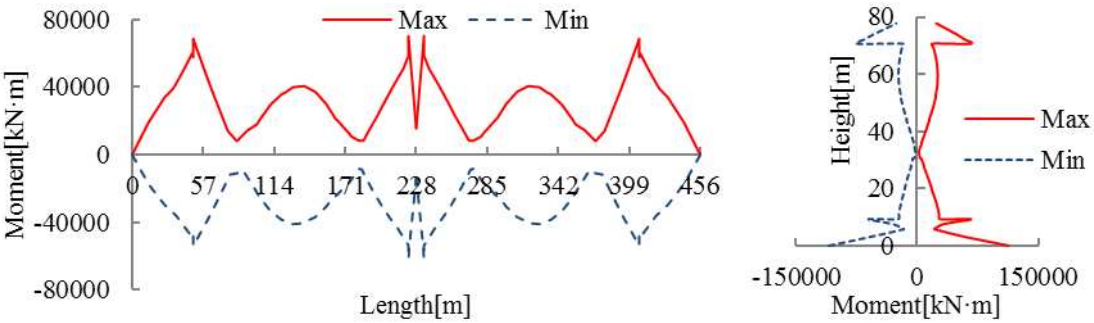

(a) girder (b) pylon

Fig.4 The envelope of moment of girder and pylon (in plane)

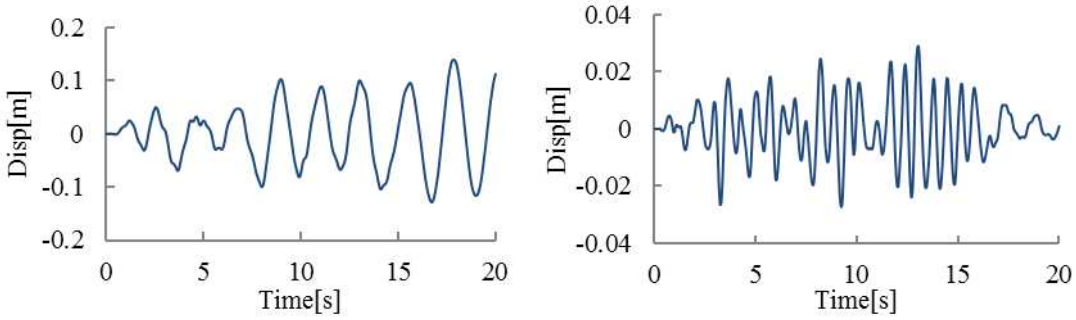

(a) Lateral displacement (b) longitudinal displacement

Fig.5 The time history curve of lateral and longitudinal displacement at the top of pylon

Summary

By studying the seismic performance and dynamic characteristics of the self-anchored suspension bridge, the following conclusions can be drawn:

The performance of lateral sway mode of the pylon for the first mode, which demonstrates the small lateral stiffness of the pylon, is noticeable to be controlled seismic design.

Under the longitudinal earthquake excitation, the longitudinal displacement of pylon is controlled object for this load case. The bottom of the pylon is the most dangerous position with large moment in plane excited by earthquake. Under the transverse earthquake excitation, the lateral displacement of pylon is controlled object for this load case. The bottom of the pylon and midpoint of main span are the most dangerous position with large moment out of plane. Although the internal force and displacement of pylon is relatively small under vertical seismic excitation, it can't be ignored in spatial seismic analysis which include EW input in in three directions since that the vertical load case affects a noticeable impact on girder.

The spatial coupling vibration effect of single tower self-anchored suspension bridge is not obvious. It reached the conclusion that the seismic analysis can be performed under unidirectional EW respectively.

References

[1] Shi lei, Zhang zhe, Design and mechanical performance analyses of concrete self-anchored suspension bridge, Journal of Dalian University of Technology, March 2003, v43, n2, pp. 202-206.

[2] Li Jianhui , Spatial structural analysis of main saddle for single tower spatial cable self-anchored suspension bridge, Journal of Southeast University, September 2009, v 25, n 3, pp. 372-375.

[3] Ray W. Clough, DYNAMICS OF STRUCTURES, Third Edition, Computers & Structures, Inc., Berkeley, 2003, pp.234-237.

[4] Transportation Ministry of China, Guidelines for Seismic Design of Highway Bridges (JTJG/T B02-01-2008), 2008, pp.33-40.

[5] Xie Xu, Seismic reponse and earthquake resistant design of bridges, China Communications press, Beijing, 2005, pp.137-139.

doi:10.4028/www.scientific.net/AEF.5.189

Study on Suspender's Fatigue Performance of Half-through CFST Arch Bridge Due to Vehicular Loads

Hang Sun[1, a], Jun Ma[1,b], Bo Yu[2]

[1]School of Transportation Science and Engineering, Harbin Institute of Technology, Harbin, China, 150090

[2]Research Institute of Highway Ministry of Transport, Beijing, China, 100082

[a] bridge_hit@163.com, [b] mjlxd@163.com

Keywords: CFST arch bridge; deck type; fatigue performance of suspender; The frequency value chart of vehicle load

Abstract: Due to the repeated action of vehicular loads, fatigue failure of suspenders of half-through arch bridge is main failure type. Usually the stress history of suspender is relevant with the vehicle load, dynamic property of structure and so on. In this paper, the traffic load spectrum investigation of Ha-Tong road is constructed through a 24-hour traffic flow investigation; And the space FEM established to get the stress response； Assume the fatigue performance of suspender as stochastic variable, the stress history of suspender is a stochastic process which changes with time, fatigue reliability analysis model is suggested based on accumulated damage model； Taking YIlan bridge as an example, the study on the effect of suspenders' length and deck type are carried out. The research method and results can be referenced while designing or evaluating the same bridge type。

1. Introduction

Concrete filled steel tube arch (CFST) bridge is a kind of popular bridge in mainland of China, and most of them are half –through CFST bridges. The parallel single suspender is usually applied in this kind of bridges. However, the investigation shows that the half-through suspender may be dangerous owing to its structural system. A common example is the Jinshanjiang Bridge in Yibin, China. The shortest pair of suspenders of north side of this bridge were damaged, and then another three pairs of suspenders were cracked after couples of minutes. Finally, almost of the whole bridge fell into the river[1 2]. Another example goes to Shouchun Road Bridge in China. 28 suspenders had to be replaced since the shortage of protection after working about 10 years[3].

Combining the designing work of Liuwu bridge in Lhasa, Chen Bing studied the fatigue performance of suspender[4], and found that fatigue damage is the main reason for the suspenders' failure. And the analysis of a half-through arch bridge carried by Gu An-bang[5] showed that the dynamic load impact effect on shorter suspenders is much larger than that on longer suspenders.

The study on suspenders' performance has received more attention, but not reaching explicit conclusions. above reasons has hindered the development of half-through CFST arch bridge.

2. Fatigue Cumulative Damage Rule

The fatigue failure of structure is an accumulation process of structure interior damage, with the increase of cycle number, the fatigue damage increases monotonously, hence the structure resistance declines. If define the accumulative damage as D(n), then the limit state equation is[6]:

$$D(n) - D_c \le 0 \tag{1}$$

where D(n) is the cumulative damage,which is a stochastic process and increase monotonously with the cycle number n； Dc is the critical damage value and also a stochastic process。When formula holds,the members are safe.

Usually fatigue damage D(n) is defined in Miner rule, because Miner rule can predict the mean life of structure due to stochastic loading more easier, which can be expressed as following equation:

$$D(n) = \sum_{i=1}^{n} \Delta D_i = \sum_{i=1}^{n} \frac{1}{N_i} \tag{2}$$

Where N_i is the corresponding fatigue life of stress amplitude, considering the S—N curve equation, then:

$$D(n) = \sum_{i=1}^{n} \frac{\Delta\sigma_i^m}{C} = \frac{nE(\Delta\sigma^m)}{C} \tag{3}$$

Then the limit fatigue state equationcan be obtained:

$$\frac{nE(\Delta\sigma^m)}{C} - D_c = 0 \tag{4}$$

Where C, $\Delta\sigma$ and D_c are stochastic variables。Material parameter C obeys lognormal distribution, the mean value of logarithm and const logarithmic standard deviation can be obtained from fatigue testing with constant amplitude. And as a critical damage value, D_c is a stochastic variable in general case, which obeys lognormal distribution, and the mean value is 1.0, the standard deviation is 0.3.

3. The Fatigue Reliability Analysis of Suspenders

3.1 The Space Finite Element Model

Yilan Mudanjiang Bridge is located on the west of old city zone of Yilan country, the main arch rib includes two separation types which is composed of triangle steel tube truss, and the transverse braces were cancelled in design. The arch axis of main arch is catenary, the arch-axis coefficient m=1.756, the net span L0=100m, the net vector height f_0=25m,the net rise-span ratio is 1/4. The spacing of suspenders is 6m, the bridge deck is 6m T beam.

The finite element calculation in this paper is finished by ANSYS. The main arch rib is modeled by linear space beam unit of three nodes. The suspenders are the connecting components between arch rib and suspension member transversal girder, using the tensioned-only bar elements, of which the influence of initial strain should be considered. The suspension member transversal girder, the column of cross beam and wind bracing can all be simplified into general beam structure, which can be modeled by linear space beam unit of two nodes. The floor system can be modeled by shell element of four nodes, the style of which has a great influence on the lining structure static

behavior and fatigue. The FEM is shown in figure 2. The force properties of the suspenders are compared between the longitudinal beam of continuous girder and of simply supported-continuous. In order to distinguish, the longitudinal beam of continuous girder is called the floor system of A style, and the simply supported-continuous is called B style.

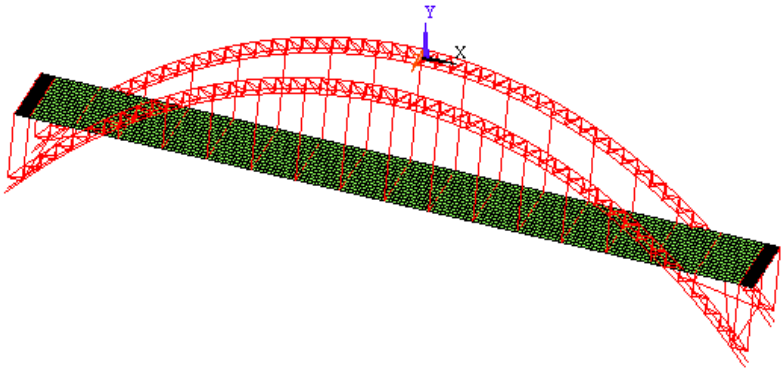

Fig. 2 The space finite element model of Yilan bridge

3.3 Stress History of Suspenders

In fact, the stress amplitudes are variable to different suspenders, under the same live load M1. The stress amplitude is reduced from 1# to 7#. Because of the longitudinal rigidity of the floor system, the force of the structure that M1 acts on should be distributed by the relative stiffness. The distribution of the force is related to the longitudinal rigidity of the floor system, the longitudinal rigidity of the suspenders and the in-plane stiffness of arch rib. Therefore, the shorter suspender is distributed to a larger axial force, and so as the stress amplitudes. So comparing to other suspenders, the shorter one is under the dangerous state and the fatigue reliability is lower. Under loads effect at all levels, the maximum amplitude of the suspenders' stresses are shown in figure 3.

Fig.3 The stress amplitude of suspenders to all levels loading

From figure 3, we can find that the stress amplitude of $1^{\#}$ is much larger than that of other suspenders, and the increase amplitude decay rapidly from $1^{\#}$ to $3^{\#}$. In general, the difference of stress amplitude is obvious between $1^{\#}$ and $2^{\#}$,That is , the short suspender effect is restricted to the shortest two suspenders, and other short suspenders do not exist this problem.

3.4 Stress History of Suspenders to different deck type

From the point of fatigue reliability, analysis was carried out aiming to different deck types, the result is shown in figure 4.

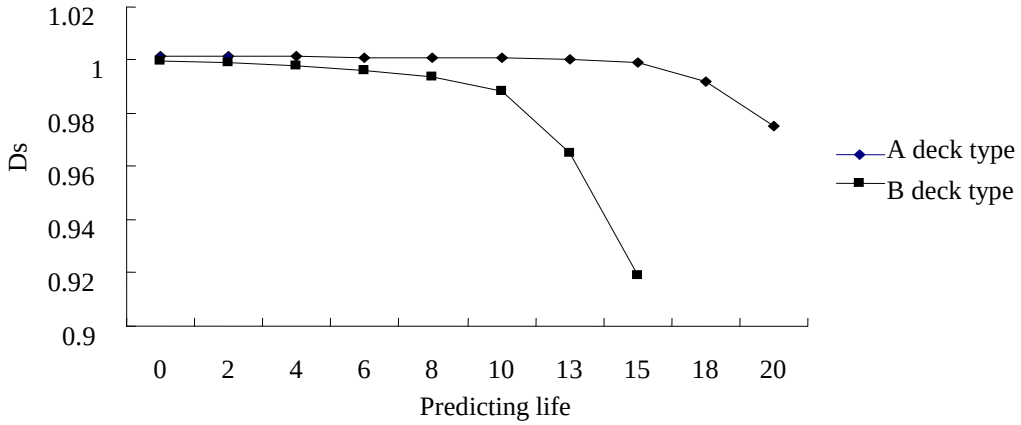

Fig. 4 Comparison of predictive DS value

It can be seen from figure 4, the remaining fatigue performance index of suspenders of A deck type is smaller than that of B deck type. Also with the the increase of service life, the difference increases.

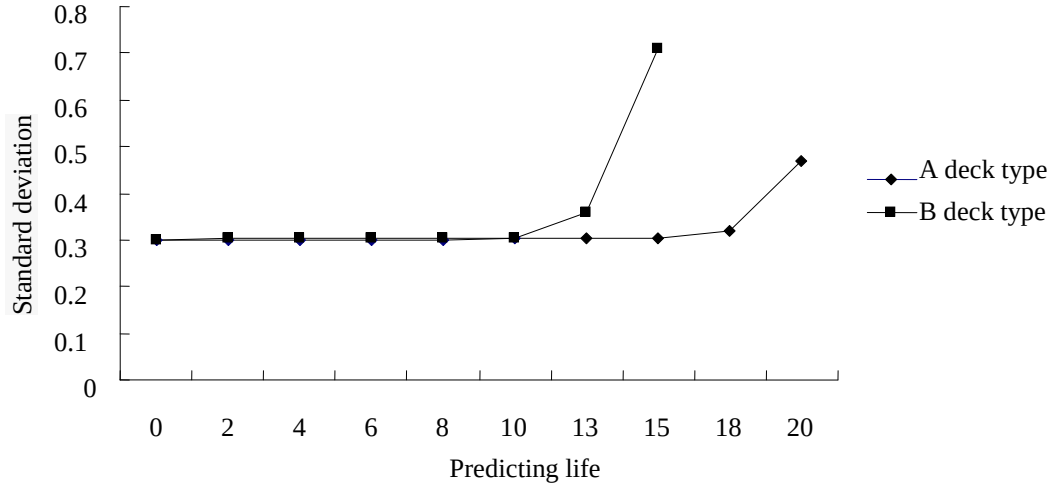

Fig. 5 Comparison of predictive value of DS standard deviation

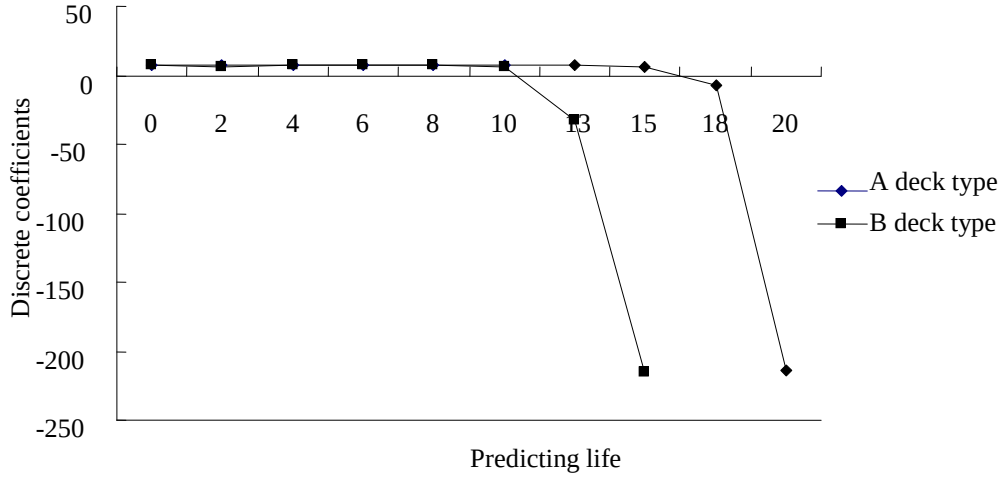

Fig. 6 Comparison of predictive value of DS discrete coefficients

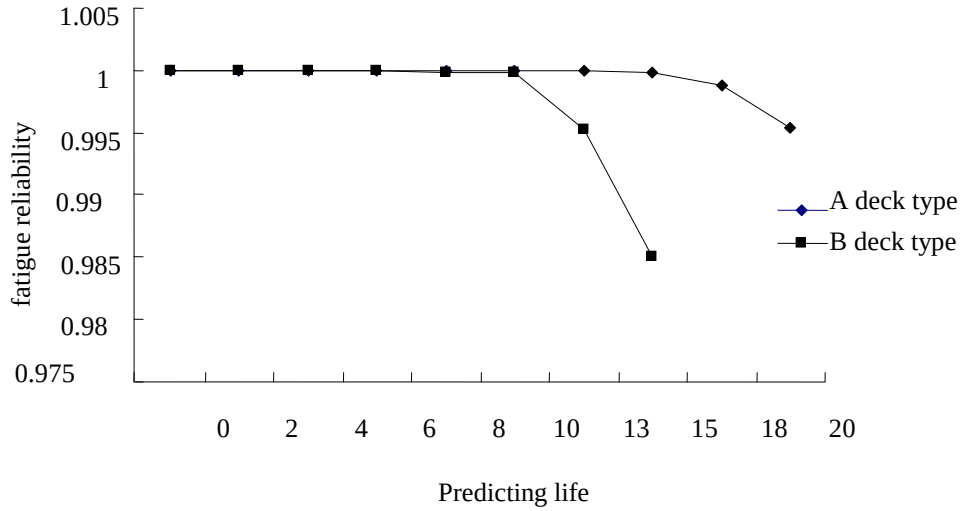

Fig. 7 Comparison of predictive fatigue reliability of suspenders to different deck types

From figure 5to6, we can find that the standard deviation of the retention fatigue index value DS of the prediction of A style's suspenders is more than that of B style, under the same service life and same application conditions. With the increasing of the service years, this difference is increased gradually. The standard deviation of the predict retention fatigue index value DS of A style's suspenders in the 22th year is basically the same as that of B style at the 27th year. And from figure 7, we can find that the fatigue reliability of the suspenders of A style is less than that of B, under the same service life and same application conditions. With the increasing of service lives, this difference is increased gradually. The fatigue reliability of the suspenders of A style in the 22^{th} year is less than that of B style at the 27^{th} year. Therefore, the floor system of B style should be preferred to use for the half -through type or through arch bridges (longitudinal beams are simply supported-continuous), from the point of fatigue reliability.

5 Conclusions

The simplified load frequency spectrum of Ha-Tong Road is provided by traffic volume investigation, based on the principle of equivalent fatigue damage. In this paper, the load of the suspender is taken as stochastic process, and the fatigue strength of the suspender is considered as random variable, thus, the analysis model of dynamic fatigue reliability based on the cumulative damage model is given. Also, this article establishes a finite element model of an arch model, studies the short suspender effect, and concludes that the short suspender effect is restricted to the shortest two suspenders comparable to the different influence of fatigue reliability of different floor system forms. At the same time, the deck system of simply supported-continuous longitudinal beams can reduce the stress amplitude of all suspenders' live load, and then improve the fatigue reliability of the suspenders. In short, this deck type is suggested under the consideration of suspenders' fatigue reliability.

References

[1] JGJ 94-2008, Building pile foundation technical specifications, Beijing, 2008. (in Chinese)
[2] Baochun, Chen. Concrete Filled Steel Tube Arch Bridges. People's Communications Publishing House, 1999:50~58[In Chinese]
[3] Baochun, Chen. Concrete Filled Steel Tube Arch Bridges Engineering Examples. People's Communications Publishing House, 2002:11~28[In Chinese]
[4] Code for Design of Highway Bridges and Culverts(JTG D60-2004), People's Communications Publishing House, 2004. [In Chinese]
[5] Ruqing Zhang, Xuegang Yin and Ming Dong, computational structural dynamics. Chongqing University Publishing House, 1987:41~109. [In Chinese]

doi:10.4028/www.scientific.net/AEF.5.195

State-of- the Art and practice of Concrete Structures Reinforced with FRP Bars

Zhang Lianzhen[1,a], Xiong wei[1,b]

[1]School of Transportation Science and Engineering, Harbin Institute of Technology, Harbin City, China, 150090

[a]email:Zhanglianzhen79@163.com, [b]email:xfd1991@gmial.com

Key words: FRP Bars, Concrete structure, Bond Performance, Shear Resistance, Flexural Behavior, Ductility.

Abstract: Fiber reinforced polymer (FRP) bars have been widely used in civil engineering used as a substitute for steel reinforcement because it has many advantage such as high strength, light weight and no corrosion. Moreover, the productive technology becomes more and more mature and industrialized so that FRP has become one economic and competitive structure material. Based on the recent researches, this paper mainly introduces progress in the studies on concrete structures reinforced with FRP bars. These contents in this paper include the bond performance of FRP bars in concrete, shear resistance, flexural behavior and ductility of concrete structure reinforced with FRP bars in the past few years in the world.

Introduction

Infrastructure deterioration owing to corrosion of steel reinforcement is one of the major challenges. The use of concrete structures reinforced with FRP composite materials has been growing to overcome the common problems caused by corrosion of steel reinforcement. The application of FRP bars in civil engineering can be divided into two classes. One is to substitute steel bars in concrete structures, and the other one is to maintain and strengthen old structures. In the past few years, with the development of FRP material technique, more and more scholar began to focus on the application research work on FRP. This paper mainly introduces progress in the studies on concrete structures reinforced with FRP bars. These contents in this paper include the bond performance of FRP bars in concrete, shear resistance, flexural behavior and ductility of concrete structure reinforced with FRP bars in the past few years in the world.

Bond performance of FRP bars in concrete

The development length of FRP bars The bond performance of FRP bars in concrete, which is the basic mechanical behavior, is the main factor of the mechanical performance, failure mode, serviceability, crack width, deformation and structure analyses and design. The bond performance of 82 concrete specimens with FRP bars are investigated by GAO et al. [1], and the development length and modified coefficient are presented. Ehsani et al. [2] did extensive research on both straight and hooked embedded GFRP bars of 102 specimens, and the constraint coefficient considering the concrete cover depth and the position of FRP bars is suggested. The results from these studies were used to compile the constants for use in the ACI440.1R-03 [3] equation for development length of a straight embedded FRP bar in concrete. Nathan Newman et al. [4] collected the database set of 48 test specimens from the open literature and emulated a specific bar

size and embedment length for various scenarios, and a refined design equation for development length of FRP bars was resulted. The following equation 1 of development length is recommended by ACI440.1R-03:

$$l_{bf} = \frac{A_{f,bar} f_{fu}}{\pi d \mu_f} \tag{1}$$

Where, $l_{bf}, d, A_{f,bar}, f_{fu}$ is the development length, diameter, area, ultimate strength stress of FRP bar respectively.μ_f is the average bond stress in the interface between FRP bar and concrete.

Bond strength and its factors The mechanics of bond stress transfer between FRP reinforcement and concrete has been investigated extensively. Bond stress is the shearing stress whose direction is parallel to the interface plane of FRP bars and concrete. The bond of an embedded bar, regardless of material, resists pull-out via three main mechanisms. The first is chemical adhesion between the two materials at their interface. The second is the friction bond which is due to coarseness in the surface of the bar. The third mechanism contributing towards the bond is mechanical bearing, such as that generated from the lugs on reinforcing bars upon the surrounding concrete [4]. Based on the studies on concrete reinforced with FRP bars, the factors that influence the bond strength can be divided to several classes below:

The strength of concrete 130 pull-out specimens were tested by Zenon et al[5]. In this experiment, different strength of concrete was adopted, and the results presented that concrete strength influenced the failure mode of concrete specimen reinforced with FRP bars. When the strength is higher than 30MPa, the interface of bond failure occurs on the surface of FRP bars, and the bond strength of FRP bars is independent on the strength of concrete. When the strength is around 15MPa, the bond failure mode changes, and that is to say, concrete strength influences directly the bond performance of FRP bars. Pull-out test of normal-strength concrete and high-strength concrete was performed by Gao et al[6], and the results show that the conclusion that bond strength of concrete reinforced with FRP bars is linear to the square root of compressive strength of concrete is hard to determine. The new ACI 440.1R-06 guidelines [7] use a different approach that relies on the equilibrium equation of anchored bars and an empirically derived expression for average bond stress normalized with respect to the square root of the compressive strength of the concrete.

Embedded length of FRP bars Pull-out tests were performed by Zenon et al. [5], and the results presented that if the diameter remain constant, the larger the embedded length of the FRP bars in the specimens are, the less uniform the distribution of bond stress, and the ratio of the average bond stress to the actual maximum bond stress when the specimen fails, that is to say, the bond strength of the specimens increases with the increase of embedded length. Therefore, the embedded length of FRP bars has great influence on bond strength of concrete with FRP bars. The new ACI 440.1R-06 guidelines [7] recommends embedded length of 5db to study the average bond strength of FRP bars and design the development length of FRP bars.

Diameter of FRP bars The studies on bond performance of FRP bars in concrete present that when the embedded length of FRP bars remain constant, the bond strength decreases with the increase of the diameter of FRP bars. During the pull-out test, the peak bond stress moves gradually from the loaded end towards the unloaded end of the bar, while the bond stress value at the loaded end decreases considerably, having a nonlinear distribution of stresses along the bar. Tighiouart et al. [8] held the view that larger bar diameters develop bigger gaps between the concrete and FRP bars, and these gaps could induce the decrease of bond strength of FRP bars in the concrete. Tastani

[9] did an experiment of 30 directly pull-out test, and the variables include surface treatments, diameter and relative bond area of FRP bars, and induced the modified equation of bond-slip model based on the test results.

Types and surface treatments of FRP bars Javier [10] investigated the bond behaviors of GFRP bars of four types which have different surface treatments. The study presented that formula recommended by ACI 440 seems to be very conservative. Furthermore, the bond strength increase with the increase of the transverse constraint, and in the same condition of constraint, the bond strength of normal steel bar and concrete is a little larger than that of FRP bars and concrete. B. Benmokrane et al. [11] did experiments on the mechanical properties and bond strength of carbon fiber fiber reinforced polymer on the mechanical properties and bond strength of new generation of carbon fiber reinforced polymer (CFRP) reinforcing bars used as nonprestressed reinforcement for concrete structures. Two types of CFRP reinforcing bars, namely, 9-mm-diameter CFRP ribbed bars and 9.5-mm-diameter CFRP sand-coated bars, were investigated. Both types of the CFRP bars exhibited almost the same bond strength to concrete similar to steel bars. The minimum bond development length for the two types of CFRP bars seemed to be equal to about 20db for the sand-coated bars and 30db for the ribbed bars.

Analytical modeling of bond behavior

When concrete structures with FRP bars are analyzed numerically, the bond-slip relation should be considered. However, a general bond-slip law has not been proposed up to now because of the many factors that exert an influence, including the different behaviors and mechanisms involved in the different types of rebar. Currently, several bond-slip models including BPE model, modified BPE model [12], Malvar [13] model and CMR [12] model and continuous curve mathematical model have been proposed and modified BPE model has been applied to the analysis of concrete structure reinforced with FRP bars. The double branch model, proposed in Cosenza et al. [13] as a modification of the BPE model [12], consists of an ascending and a softening branch for the pre- and post-peak bond behavior, respectively. These two branches are given by the following equations:

$$\frac{\tau}{\tau_{\max}} = (\frac{s}{s_1})^{\alpha} \tag{2}$$

$$\frac{\tau}{\tau_{\max}} = 1 - \frac{p \cdot (s - s_1)}{s_1} \tag{3}$$

Where α is a curve fitting parameter that must be no larger than 1 to be physically meaningful, s_1 is the slip at peak bond stress, and p is a parameter based on curve-fitting of experiment data.

Shear resistance of RC beams with FRP bars

As FRP bars are linearly elastic material and the transverse serviceability and elastic modulus are lower, the shear strength of FRP-reinforced concrete beams is different from that of steel bar RC beams. M. Guadagnini et al [14] investigated the shear behavior of 6 beams with FRP bars. The results of this study showed that the approaches of current proposal by the ACI and the Institution of Structural Engineers of U.K underestimate the contribution of the concrete and the shear reinforcement to the total shear capacity of FRP RC beams. El-Sayed et al [15] compared five methods, including ACI 440.1R-06, CSA-S806-02, ISIS-M03-07, the British Institution of

Structural Engineers guidelines and mendation of the Japan Society of Civil Engineers. A modified compression field theory approach was compared with the experiment database obtained from the literature. Islam [16] investigated the shear strength contribution of carbon fiber reinforced polymer (CFRP) bars attached with concrete beams using a near surface mounted (NSM) technique. Four concrete beam were cast with regular steel reinforcement in flexure. The performance of the NSM technique was found to be very effective with no occurrence of delamination, debonding or fracture of FRP. A new formula to calculate the nominal shear strength provided by NSM CFRP bars has also been proposed by Islam as follows equation.

$$V_n = V_c + V_s + V_f \tag{4}$$

Where Vn stands for shear capacity of RC beam, *Vc* stands for the nominal shear strength provided by concrete, and *Vs* and V_f stand for the nominal shear strength provided by steel and FRP bars, respectively.

Flexural behavior of RC beams with FRP bars

*Nonprestressed concrete structur*e Alsayed et al. [17] investigated flexural behaviors of FRP reinforcement RC beams and normal RC beams and compared the results of both. The test results show that the structural behaviors of FRP reinforced concrete are similar to normal RC in many aspects. However, with the low elastic modulus of FRP, the deflection of FRP reinforcement RC beam increases immediately after the beam starts to crack. To the concrete beams with the same size and ultimate flexural serviceability, the deflection of FRP bars RC beams is 2-4 times as the steel RC beams. Currently there are two calculating models to calculate the deflection of FRP RC structure. The first model is to utilize the effective moment of inertia. Different methods used to calculate the effective moment of inertia were presented by Issa [18]. The general idea is to combine the uncracked moment of inertia and cracked moment of inertia and calculate the deflection of the bended structure through elastic analysis. The second model is to consider the interaction between FRP bars and concrete.

Prestressed concrete(PC) structure Due to the low elastic modulus of FRP bars, the deflection and crack width of FRP RC beams are too large for nonprestressed concrete structure, and the high strength of FRP could not be fully utilized. One effective way to solve this problem is to use FRP bars as prestressed bars. The flexural behavior is the basic character of prestressed concrete structure reinforced with FRP bars, and a lot of studies have been investigated by many researchers. Based on the position of FRP bars in concrete beams, the PC beams can be classified into three types, which include internal bonding, internal unbonded, external PC structure. To internal bonding FRP bars PC beams, the prestress is mainly provided by the bond between FRP bars and concrete. The flexural strength can be calculated. Since 1992, Luc R et al. [19] started to study the feasibility to use GFRP bars in PC structure, and three 2-meter long GFRP bar PC beams and one 20-meter PC beam were tested. The results demonstrated that the load-deflection relationship of FRP bars PC beams is linear before the crack and doublely linear after the crack, as the stiffness of the beams decrease. To unbonded PC beams, the prestress is mainly provided by the anchorage at the ends of FRP bars. As the FRP bars can move relatively against concrete beams, the relative deflection of FRP PC beams is larger and the serviceability is lower. Xue [20] and Zhang [21] did researches on internal unbonded PC beams reinforced with FRP bars, and the results demonstrated that the effective prestress and crack width can be calculated by current design code. Compared to internal unbonded FRP bars PC beams, external PC beams can produce quadratic effect as the

effective eccentricity decreases with the change of the deflection after the beams are bent. Robert [22] did experiments on strengthening behavior and the results pointed out that the strengthed beams got great improvement on crack moment, deflection and ultimate serviceability.

Ductility

Due to the linear elastic brittle behavior of FRP bars, the flexural behavior of FRP-reinforced concrete beam exhibits no ductility. In order to improve the ductility of such composite systems, it is proposed to add a certain amount of steel rebars in FRPRC systems such that the brittleness of FRP rebars can be compensated by the ductile nature of the additional steel reinforcement. Lau [23] did experiments on 12 specimens consisting of plain concrete beams, steel-reinforced concrete (SRC) beams, pure FRPRC beams and hybrid FRPRC beams, and the test results showed the hybrid FRPRC beams behave in a more ductile manner when compared with the pure FRPRC beams. Also, it is pointed out that a higher degree of over-reinforcement in the beam specimen resulted in a more ductile FRPRC beams; that is to say, over-reinforcement is a preferred approach in the design of FRPRC members. Xu et al. [24] did research on bending resistance of reinforced concrete beam strengthened with near-surface mounted FRP bars. The test results presented that the bearing capacity of structure reinforced with near-surface mounted FRP depend on the adhesive property between concrete and phenol-formaldehyde resin, and edge distance and separation distance influence the mode of failure and bearing capacity. In addition, the bearing capacity increases with the increase of the anchorage length.

Summary

With 20 years' studies on the mechanical behaviors of FRP bars RC structure, great progress has been made, and lots of design codes have been published worldwide. However, there are still a lot of problems to be solved, especially the over-large deflection. Hybrid FRP bars are fabricated and might be an effective method. In the same time, the bond behaviors of FRP bars and concrete still need to be investigated as it affects the failure modes, serviceability, crack width and deflection of FRP bars RC beams, and it is the main factor in the structure analysis and design. A general bond-slip law has not been proposed up to now. Therefore, studies are still needed to be investigated on the FRP bars RC structures, especially bond behaviors.

Reference

[1] G Danying, B.Brahim, Bonding mechanism and calculating method for embedded length of fiber reinforced polymer rebars in concrete, Journal of Hydraulic Engineering. (2000)

[2] Ehsani M R. Saadatmanesh H.Tao S, Design recommendation for bond of GFRP rebars to concrete, Journal of structural engineering. (1996):247-254.

[3] ACI Committee 440. (2003), "Guide for the design and construction of concrete reinforced with FRP bars." ACI 440.1R-03, American Concrete Institute, Farmington Hills, MI, 42

[4] Nathan Newman, Ashraf Ayoub, Abdeldjelil Belarbi, Development Length of Straight FRP Composite Bars Embedded in Concrete, Journal of Reinforced Plastics and Composites.

[5] Zenon Achillides, Kypros Pilakoutas, Bond behavior of fiber reinforced polymer bars under direct pullout conditions, Journal of composites for constructure.

[6] G Danying, B. Brahim, Influential factors of bond properties between fiber reinforced polymer (FRP) rebars and concrete, Industrial Construction. (2001).

[7] ACI Committee 440. (2006), "Guide for the design and construction of concrete reinforced with FRP bars." ACI 440.1R-06, American Concrete Institute, Farmington Hills, MI, 44

[8] B. Benmokrane, B. Tighiouart, O. Chaallal, Bond strength and load distribution of composite GFRP reinforcing bars in concrete, ACI materials journal, (1996), 93(3):246-253.

[9] S. P. Tastani, S. J. Pantazopoulou, M. ASCE: Bond of GFRP bars in concrete:experimental study and analytical interpretation,Journal of composites for construction, (2006), 10(5): 381-391.

[10] Javier malvar L, Tensile and bond properties of GFRP reinforcing bars. ACI, (1995).

[11] B. Benmokrane, B. Zhang, K. Laoubi, B. Tighiouart, I. Lord, Mechanical and bond properties of new generation of carbon fibre reinforced polymer reinforcing bars for concrete structures. Can. J. Civ. Eng. 29:338-343 (2002).

[12] Cosenza E, Manfredi G, Realfonzo R, Behavior and modeling of bond of FRP rebars to concrete, ASCE Journal of Composite Constructure (1997)

[13] Malvar L. J, Bond stress-slip characteristic of FRP rebar. (Report TR-2013-SHR. Nacal facilities engineering service center, port hueneme, California, 1994).

[14] M. Guadagnini, K. Pilakoutas, P. Waldron, Shear resistance of FRP RC beams: experimental study, Journal of composites for construction. (2006).

[15] A K. El-Sayed, Khaled Soudki, Shear design equations of concrete beam with FRP reinforcement, Journal of composites for construction. (2011)

[16] A.K.M. Anwarul Islam, Effective methods of using CFRP bars in shear strengthening of concrete girders, Engineering Structures. (2009)

[17] Alsayed S H, Flexural behavior of concrete beams reinforced with GFRP bars, Cement and concrete composites. (1998)

[18] M S. Issa, I M. Metwally, S M. Elzeiny, Influence of fibers on flexural behavior and ductility of concrete beams reinforced with GFRP rebars, Engineering Structures. (2011)

[19] T. Luc R, Lambotte H, Hans-Joarchim Miesseler, Loading tests on concrete beams prestressed with glass fiber tendons, PCI Journal, (1992)

[20] Xue Wei-chen, Experimental studies and FEM analysis of concrete beams prestressed with new-type FRP rebars, Journal of the China railway society, (2003), (in Chinese).

[21] Zhang peng, Deny yu, Wei Shuying, Zhu Jian, Experimental study on behavior of unbonded prestressed concrete beam reinforced with carbon fiber reinforced plastics bars, Industure Construction. (2004).

[22] Robert A. Tjandra, Kiang Hwee Tan, Strengthening of RC continuous beams with external CFRP tendons. (Fifth International Conference on Fiber-Reinforced Plastics for Reinforced concrete. London, 2001)

[23] Denvid Lau, Hoat Joen Pam, Experimental study of hybrid FRP reinforced concrete beams, Engineering Structures. (2010).

[24] Y XU, H Wang, R Guo, X Fan, Research on bending resistance of reinforced concrete beam strengthened with near-surface mounted FRP bar. (Electric Technology and Civil Engineering, 2011 International Conference, Lushan, 2011).

doi:10.4028/www.scientific.net/AEF.5.201

Dynamic Response Analysis of Half-through CFST Arch Bridges Affected by Crossbeams Setting

Jun Ma[1, a], Yan Li[2,b]

[1]School of Transportation Science and Engineering, Harbin Institute of Technology, China

[2]School of Transportation Science and Engineering, Harbin Institute of Technology, China

[a]majunlxd@163.com, [b]liyan_2007@126.com

Keywords: bridge engineering; half-through CFST arch bridges; FEM; dynamic response; crossbeams

Abstract. As one of the most important components of CFST arch bridges, the cross beams should affect the bridges' dynamic performance and response magnificently by means of affecting these three factors mentioned above. Based on the Maocaojie Bridge, its FEM models of half-through CFST arch bridges with different settings of cross beams are built. The different seismic responses of six operating conditions are calculated with three dimensional earthquake waves input. The internal force and displacement envelope diagrams of arch ribs are extracted and analyzed in situations of in-plane moment, out-plane moment, vertical displacement and transverse displacement. It can conclude that the joint section between arch rib and bridge deck should be designed carefully because of its large displacement and internal force, and the cross beams should be optimized to safety the arch bridge dynamic response considering lateral rigidity. The conclusions may be useful to the seismic design and strengthening treatment of CFST arch bridges. To strengthen the joint section between arch rib and bridge deck or optimize the setting of cross beams will increase the ductility of half-through CFST arch bridge and decrease the damages caused by large earthquake.

Introduction

For half-through CFST (concrete filled steel tube) arch bridges, its main components are arch, cross beams, deck, suspenders, tied bar (especially to the tied arch bridge) and etc. every component would affect the bridge's dynamical character obviously.

As one of these components, cross beams can not only strengthen the transverse stability but also enhance the transverse stiffness and mass which cause the increasing response of arch rib under transverse earthquake wave especially to half-through and through type arch bridge. Since the transverse stability calculating method and seismic design method for CFST arch bridge are not perfect, some designers use over-strengthened cross beams to avoid lateral buckling. These treatments will cause waste and go against seismic safety especially to the bridges which locate at earthquake region[1]. References [2-4] analyzed the affection to the half-through CFST arch bridges' general mechanical behaviors which include the dynamic behavior by the setting of cross beams. These analysis paid more attention to the affection to arch bridges' natural frequency by the settings. The affections by deck, suspenders and tied bars are also being analyzed in Reference [5-6].

The dynamic time-history analysis method is often used in bridge structure dynamic analysis. This method is based on the D'Alembert principle which can indicate as dynamic equation below:

$$[M]\{\ddot{\delta}\}+[C]\{\dot{\delta}\}+[K]\{\delta\}=-[M]\{I_x\}\ddot{\delta}_g(t) \tag{1}$$

where： $[M]$, $[C]$ and $[K]$ as structure's mass, damp and stiffness matrix， $\{\delta\}$ and $\ddot{\delta}_g(t)$ as time-history vector of structure node's displacement and ground acceleration.

From the equation, it can figure out that there are three main factors which affect the structure's dynamic performance, the mass matrix, the stiffness matrix and the damp matrix. The cross beams, as one of the most important component of half-through CFST arch bridge, would affect the stiffness matrix and the mass matrix obviously. It is necessary to research the cross beams' setting and optimal design based on dynamic analysis.

1. FEM Models of Different Crossbeam Settings

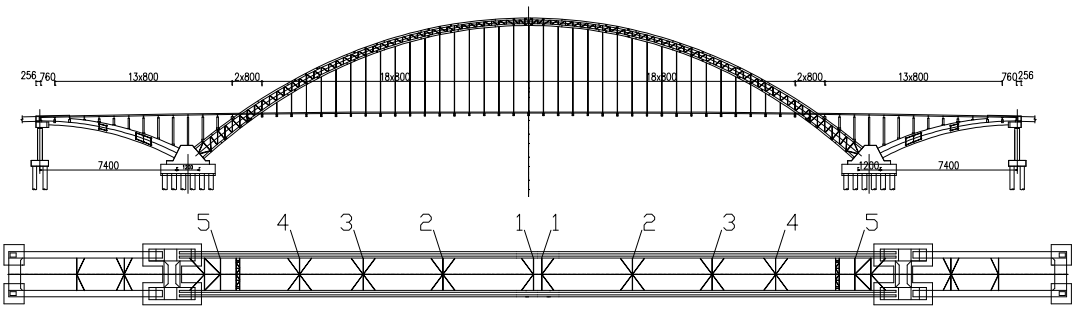

Fig. 1. Layout of *Maocaojie* Bridge and settings of cross beams

As a typical example, *Maocaojie* Bridge (showed in Figure 1) is a tied half-though CFST arch bridge with three spans (80m+368m+80m), catenary arch axis, 1/5 as its rise-span ratio, and 1.543 as its arch-axis coefficient. The bridge has ten cross beams in shape of K type and X type (showed in Figure 1). According to this, the calculating analysis has four operating conditions (showed in Table 1). The 5# cross beam is under the deck and near the skewback. Its effect to dynamic response is not obvious because of the large stiffness of skewback, so the calculating analysis is mainly on the 1#-4# cross beams.

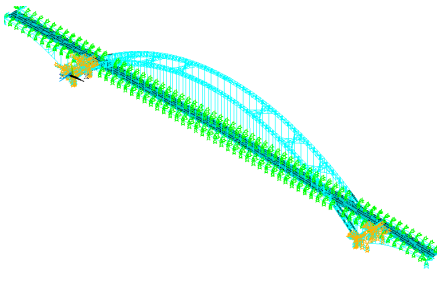

(a) Model of operating condition I

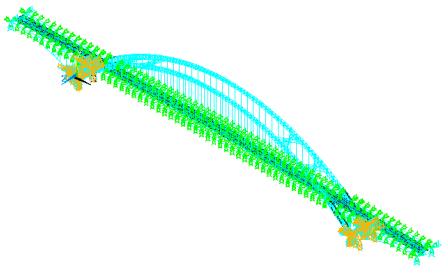

(b) Model of operating condition II

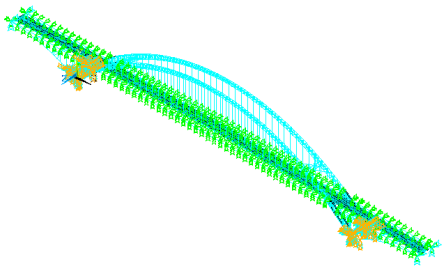

(c) Model of operating condition III

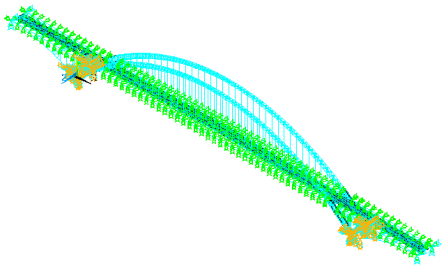

(d) Model of operating condition IV

Fig. 2 FEM models of *Maocaojie* Bridge

The FEM model of *Maocaojie* Bridge is built with general FEM program ANSYS. The arch elements are built with Beam 189 which is 3-D Quadratic Finite Strain Beam with user-defined cross section. The suspenders and tie bars are built with Link 10 which is Tension-only or

Compression-only Spar. The decks are built with Shell 63 which is Elastic Shell. The other components are built with Beam 4 which is 3-D Elastic Beam. The model has 5325 elements and 2431 nodes totally.

Table 1 Operating conditions for *Maocaojie* Bridge's analysis

Operating condition	Description
1	Model without 1# cross beam
2	Model without 1# and 2# cross beams
3	Model without 1# - 3# cross beams
4	Model without 1# - 4# cross beams

To verify the model, the static and modal analyses are carried on. The calculating results and those from Reference [7-9] are compared in Table 2 and 3.

Table 2 Results contrast of lower chord deflection in vault Unit (mm)

Operating conditions (In Chinese Standard of Bridge Design)		Finished dead state	Serviceability limit state	Ultimate limit state
Displacement	Calculating Results of the Model	0.173	0.201	0.24
	Calculating Results of Ref. 7	0.172	0.206	0.238
	Test Results of Ref. 7	0.189	0.193	0.252

Table 3 Results of modal analysis

Order of modal shape		1	2	3	4	5	6	7	8
Frequency (Hz)	Calculating Results of the Model	0.240	0.325	0.450	0.524	0.726	0.841	0.849	1.167
	Calculating Results of Ref. 8	0.240	0.367	0.446	0.467	0.660	0.790	0.820	0.940
	Calculating Results of Ref. 9	0.234	0.325	0.364	0.459	0.565	0.784	0.842	0.962

The static and modal analyses results inosculate with those in Reference [7-9] well. The FEM model is reliable.

2. Earthquake Wave Input

The El Centro wave is selected to calculate the time-history response of arch structure. The time interval is 0.02s, and load duration is 40 seconds. The peak values of accelerations are 0.313g at NS, 0.199g at WE and 0.205g at UD (1g=9.8m/s^2). The earthquake wave is inputted at three directions at same time to simulate the real condition.

3. Analysis of Calculating Results

The models of the four operating conditions are achieved by the program's the birth and death capability. The results of the four operating conditions are carried on with complicated FEM calculations. The Envelope diagram of moments and displacements in arch ribs are extracted to indicate the dynamic response of the bridge structures with different cross beam settings.

3.1 In-plane Moment（M_y）

It can conclude from Fig.3 that the four envelope diagrams of in-plane moment are nearly same in shape. With the reduction of cross beams, the maximum moments between 50m and 150m of arch rib are decreased, and the wave peaks are decreased from four to one. The biggest maximum moment of four conditions is operating condition 2 (without cross beam 1 and 2). The 2# cross beam effect the in-plane moment relatively larger than the others. It is 48m away from arch crown which is 1/7.25 of arch length.

3.2 Out-plane Moment（M_z）

It can conclude from Fig.4 that the four envelope diagrams of out-plane moment are nearly same in shape. With the reduction of cross beams, the maximum moments appear between 50m and 150m of arch rib. The maximum value appears at 44m away from skewback. The moments of operating condition 3 are larger than the moments of other conditions shows that the 3# cross beam is important to the out-plane moment response. It is 88m away from arch crown which is 1/4.386 of arch length.

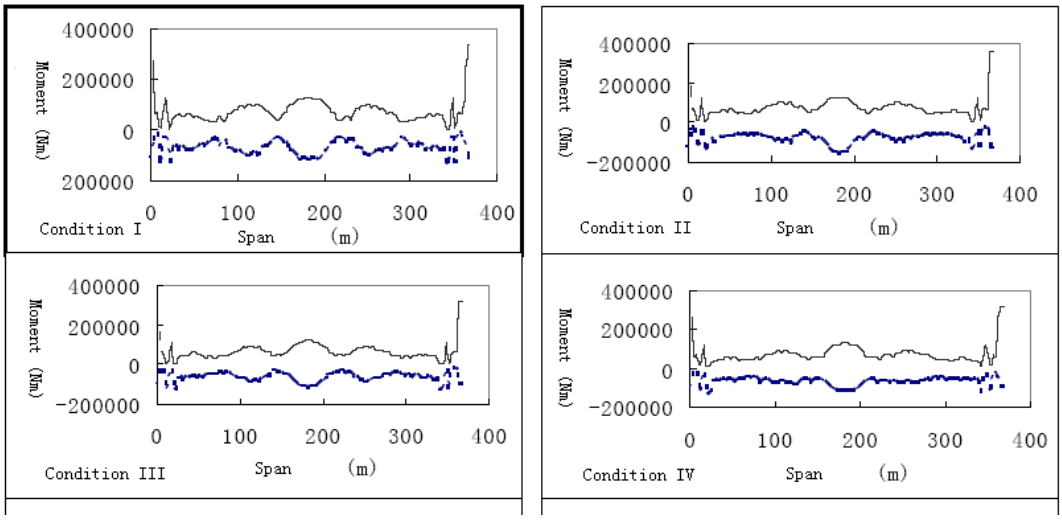

Fig. 3 Envelope diagram of in-plane moment

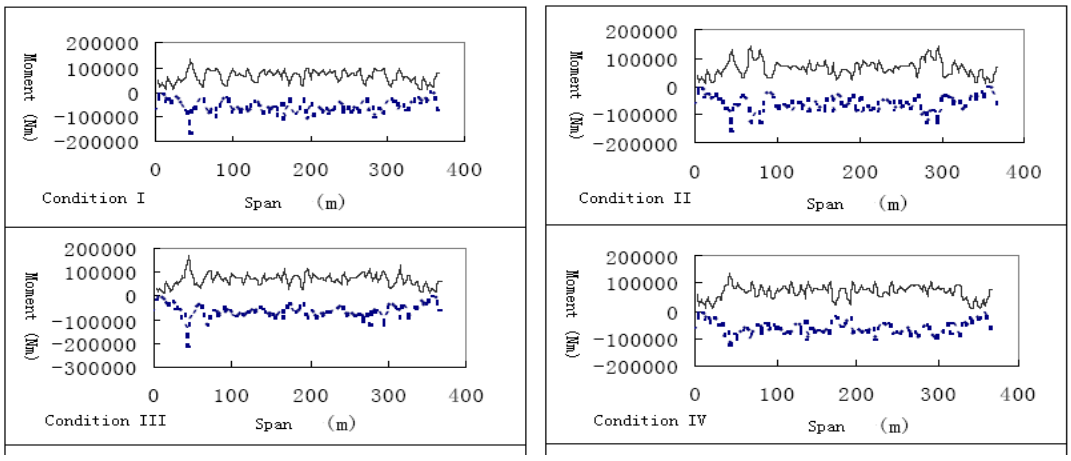

Fig. 4 Envelope diagram of out-plane moment

3.3 Vertical Displacement（Y-Direction）

It can conclude from Fig.5 that the four envelope diagrams of out-plane moment are changed regularly. The diagrams are symmetrical and the maximum displacement is about 0.03m which appears at arch crown. In operating condition 1, there are two wave peaks beside the arch crown. As

the decrease of cross beams, the peaks are abated. The maximum displacement is 0.307m which appears in operating condition 2 shows that the 2# cross beam is effect the vertical displacement relatively larger than the others.

3.4 Transverse Displacement（Z-Direction）

It can conclude from Fig.6 that the four envelope diagrams of out-plane moment are changed regularly. The diagrams are symmetrical and the maximum displacement is about 0.018m which appears at arch crown. As the decrease of cross beams, the transverse displacements are reduced and two wave peaks appear beside the arch crown. The cross beams strengthen the transverse stiffness, but cause the transverse displacement increased.

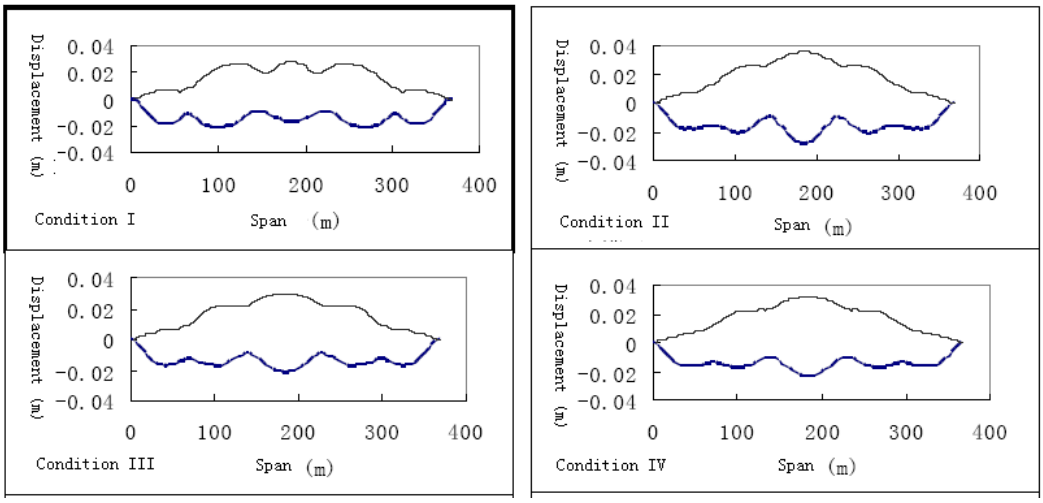

Fig. 5 Envelope diagram of Y-axial displacement

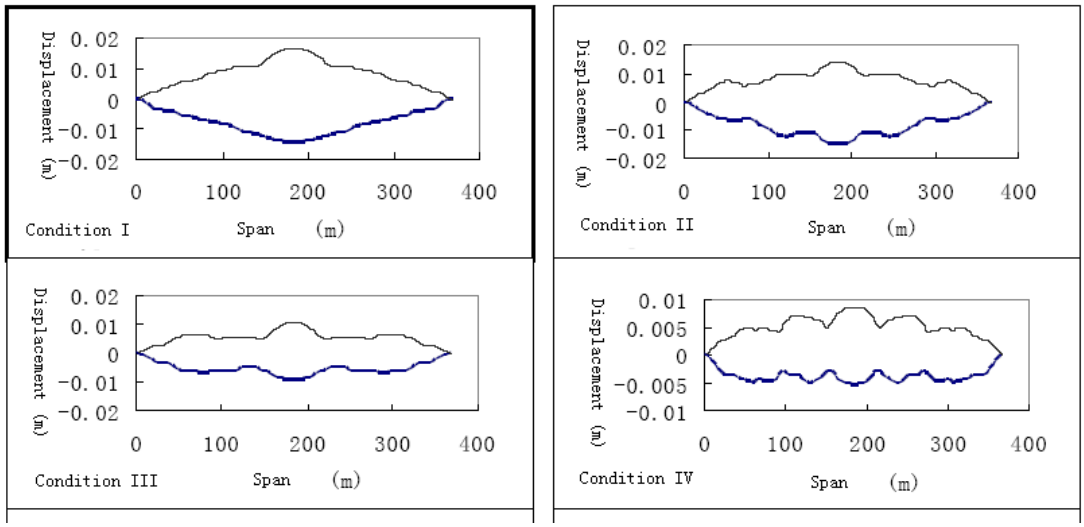

Fig. 6 Envelope diagram of Z-axial displacement

4. Conclusion

(1) The cross beams at 1/4 span effect the out-plane dynamic response obviously and the one at 1/8 span effect the in-plane dynamic response.

(2) The joint section between arch rib and bridge deck should be designed carefully because of its large displacement and internal force.

(3) For the half-through CFST arch bridge, the cross beams mainly effect the out-plane dynamic response. With the cancellation of cross beams one by one, the arch crown displacement reduces step by step and the displacements between deck and arch crown increase step by step. The existence of cross beams has both sides effect on arch general seismic capability. Optimizing the setting of cross beams will increase the ductility of half-through CFST arch bridge and decrease the damages caused by large earthquake.

References

[1] Chen Baochun, Design discussion of CFST arch constructrues[C]. Proceedings of the 14th national conference on bridge structure, Nanjing, 2000, pp505-510

[2] Yun Di, Zhang Sumei, Influence of transverse braces arrangement on dynamic characteristics of half-through CFST arch bridge. Journal of Harbin Institute of Technology, 2003(sup): 259-262

[3] Wen Feng, Shou-ying, Liu Mu-guang, Duan Shu-jin, Effects of Transverse Brace Arrangements on the Dynamic Characteristics of CFST Arch Bridges, Traffic Engineering and Technology for National Defence(2007) 43-45

[4] Zhao Yueyu, Jin Bo, Lao Wenquan, Influence of transverse braces arrangement on mechanical characteristics of CFST arch bridge, Hunan Communication Science and Technology, 2006, 32(3): 100-102

[5] Zhou Shui-xing, Hu Mian-yi, Zhou Xian-ying, Mechanics Analysis of Half-through CFST Arch Bridges with Different Bridge Deck Types, Journal of Highway and Transportation Research and Development, 2005, 22(4):57-60

[6] Hu Mianyi, Zhou Shuixing, Zhou Xianying, Analysis of the Best Bridge Deck s Relative Position for Long-span Half-through CFST Arch Bridge,. Journal of Highway and Transportation Research and Development, 2005, 22(6):82-84

[7] ZHANG Yang, SHAO Xu-dong and etc. Spatial Nonlinear Finite Element Analysis for Long-Span Trussed CFST Arch Bridge, China Journal of Highway and Transport, 2006, 19(4): 65-70

[8] WANG Yijun, QIAO Jiandong, Statics and dynamic annly sis of maocaojie bridge, Technological Development of Enterprise, 2003, 10: 7-8

[9] WANG Hao, QIAO Jiandong and etc. Seismic Response Spectrum Analysis of Maocaojie Bridge. Journal of Seismology, 2003, 23(3): 62-65

doi:10.4028/www.scientific.net/AEF.5.207

Review of studying on Fatigue Damage of Concrete Bridge

Lihui Yin[1,a], Zonglin Wang[2,b]

[1] School of Transportation Science and Engineering, Harbin Institute of Technology, China

[1] Institute of Architecture and Engineering, HeiLongJiang University, China

[2] School of Transportation Science and Engineering, Harbin Institute of Technology, China

[a] yinlihui666@126.com, [b] wangzonglin@vip.163.com

Keywords: concrete bridge; fatigue damage; repeated load

Abstract. In this paper, it systematically reviews the research status of fatigue damage of concrete bridges on the basis of previous studies and the problems for further research are discussed. From the bridge component materials perspective, the paper analyses the status and the development direction of the dynamic constitutive models. At the same time, the paper summarizes the fatigue cumulative damage theory and analyses the advantages and disadvantages of the various theories. The main contents of this paper include: the research history and status of fatigue damage of concrete bridges, the damage variable selection, the fatigue cumulative damage theory, the problems for further research on the fatigue damage of concrete bridge.

1 Introduction

In 1829, German engineer Albert studied the hoist hinge fatigue strength. From then on, people began to pay attention to the fatigue damage of metallic materials. In 19th century end, the fatigue characteristics of concrete materials began to be studied. In 1898, Considere and Dejoly launched an in-depeh study on the fatigue characteristics of the mortar and concrete, and it can be said that this is the beginning of concrete fatigue characteristic research. At the beginning of 20th century, along with the development of highway, railroad and aviation industry in the word, people paid more and more attention to the research on the fatigue damage properties[1,2,3,4,5,6,7,8].

Especially as the highway traffic infrastructure engineering, highway bridge plays a cruial role in highway transportation system. Under the action of various factors, the bridge will be vibrated in vertical, longitudinal, transverse. If the dynamic response is too large, it will cause the structural fatigue accumulation. Because the bridge materials used are not homogeneous and continuous, in fact, there are many tiny defects. Under cyclic load, these mocro-defects will gradually develop, combined injury. If these micro-defects are not effectively controlled, it is very likely to arouse the brittle fracture of materials and structures. It will lead to the operational performance of bridge and structural safety of recession. Early fatigue damage is often not easy to be detected, but the consequences could be disastrous.

2 The research status of fatigue damage of concrete bridges

In 1958, CDM was proposed by Kachanov. Subsequently, Rabotnov introduced the damage variable. Since nineteen eighties, damage mechanics theory in the field of concrete material behavior modeling has been widely applied. Fatigue is the decay process of the structure stress performance under the action of repeated load. The fatigue essence is the material fatigue damage

accumulation process along with the increase in the number of fatigue loading. Correctly understanding the damage generated and accumulated in the process is very important, because it is the basis of building damage equation, analyzing fatigue damage process of the material and predicting the fatigue life.

2.1 The damage variable selection

Under fatigue load, the material properties will deteriorate. The physical quantity, used to describe the material mechanical property deterioration, is named as the damage variable.

In 1938 and 1955, Kommers[9] and Henry [10] took the chang of fatigue limit as the measurement of damage.

In 1988, Lemaitre[11] used the sectional area reduction as the damage index:

$$D=1-A_1/A \tag{1}$$

In this formula, "A_1" is the sectional area after cracking, "A" is the sectional area before cracking.

In 1993, Miroslaw[12] regarded the fatigue failure as the process of energy release based on the principle of conservation of energy. So he defined the energy dissipation as the damage variable:

$$D=E/Etot \tag{2}$$

In this formula, "E_{tot}" is the the total energy dissipation capacity, "E" is the dissipation of energy.

In 1996, Ravindra[13] defined the Splitting tensile strength attenuation as the damage variable:

$$D=1-\sigma_t/f_t \tag{3}$$

In this formula, "σ_t" is the residual splitting tensile strength, "f_t" is the initial split tensile strength.

2.2 The fatigue cumulative damage theory

The reasonable damage accumulation model is the basis of describing cumulative damage development process of structures or members under cyclic loading.

2.2.1 Linear cumulative damage theory

Linear cumulative damage theory[14] is that "the relationship between fatigue damage and load cycling is linear under cyclic load. The fatigue damage can accumulate linearly. All stress is independent and unrelated. When the accumulated damage reaches a certain value, specimens or components will induce fatigue failure.

$$D=n/N \tag{4}$$

In this formula, "n" is the stress cycle and "N" is the fatigue life of material. When the structure is destroyed, D=1.

Because of its simple features, it has been widely used in engineering. But there are insufficient in miner theory, such as damage independent of the load status and cumulative damage independent of the load order.

2.2.2 Nonlinear cumulative damage theory

Many experiments showed that Fatigue cumulative damage law presented the characteristics of the nonlinear damage. Therefore the domestic and foreign scholars proposed a nonlinear fatigue damage cumulative model[15,16,17,18,19,20,21,22].

The model of Freudenthal-Heller considered the interaction effect between loads, so it is more widely used in engineering.

$$D = nm^{c}r^{d} \tag{5}$$

In this formula, “n” is the stress cycle , “m” is the material injury nuclear number, “r” is the damage evolution rate, “c” and “d” are the material constant .When the structure is destroyed, $D=N_1m_1^cr^d$.

3 The main problems of research of fatigue cumulative damage theory

Because of the complexity of concrete structure, the existing research results also exist the following problems:

(1) Fatigue load on bridge structure fatigue research is very important, but our country has not stipulated relevant specification. Most researchers use the vehicle load spectrum as the fatigue load, rather than the form of standard fatigue vehicle, which causes the research of the vehicle bridge coupling vibration great difficulty.

(2) Most damage model is built on the common concrete structure, but most of the current concrete bridge structures use the high strength concrete. Using common concrete dynamic damage model to simulate fatigue damage behavior of high strength concrete is obviously not suitable.

(3) At present, most of the research has focused on the fatigue damage of earthquake. They have the important theory value for the structure under earthquake effect on fatigue damage. Most damage models give the definition of structural damage in macroscopical angle, but most of the existing models don’t measure structure damage scales from the material deterioration scale.

(4) Most damage model rarely considered the bonding performance degradation law between steel bar and concrete in material level. In fact, the cause of actual bridge structure damage may be damaged in the joint surface between the reinforcement and concrete.

4 Conclusions

For concrete bridge, moving vehicle load is the main form of load. In order to better study the fatigue damage, firstly, we must study the standard form of fatigue load the vehicle. Secondly, we must study the material fatigue damage constitutive model. Finally , based on the vehicle bridge coupling vibration, we can study the mechanism of fatigue damage of concrete bridge.

References:

[1] Considere.M, Influence des armatures metalligues les proprietes des mortiera et betons, Compt Rendu de 1’ academie Des Sciences.127(1898)992-995.

[2] Van O.J.L, Fatigue of concrete, Transactions, ASCE. 58(1907)294-320.

[3] Graf O., Brenner, Experiments for investigating the resistance of concrete under often repeated compression loads, Bulletin, Deutscher Ausschuss fur Stahlbeton. 83(1936)45-53.

[4] Clemmer H. E., Fatigue of concrete, Proceedings, ASTM. 22(1922)408-419.

[5] D. J. Cook and P. Chindaprasirt, Influence of loading history upon the tensile properties of concrete, Magazine of Concrete Research.116(1981)154-160.

[6] Traina L A., Jeragh A.A., Fatigue of plain concrete subjected to biaxial cyclical loading, ACI Publication.75(1982)154-160.

[7] Eric C.M.Su, Thomas T.C.Hsu, Biaxial Compression fatigue and discontinuity of concrete, ACI Materials Journal. 3(1988)178-188.

[8] Kolluru V. Subramaniam, Fatigue of concrete subjected to biaxial loading in the tension region, Ph. D. Dissertation, Northwestern University.12(1999)20-32.

[9] Kommers J B, The effect of overstressing and understressing in fatigue, Amerrica Socoiety Testing and Materials. 38(1938)249-268.

[10] Henry D L, A theory of fatigue damage accumulation in steel, Transation of the ASME. 77(1955)913-918.

[11] Lemaitre J, A Continuous Damage Mechanics Model for Ductile Fracture, ASEM，Journal of Engineering Materials and Technology. 3(1988)83-89.

[12] Miroslaw Grzybowski, Christian Meyer, Damage accumulation in concrete with and without fiber reinforcement, ACI Materials Journal.6(1999)594-604.

[13] Ravindra Gettu, Antonio Aguado, Marcel 0.F.0liveira, Damage in high-strength concrete due to monotonic and cyclic compression-a study based on splitting tensile strength, ACI Materials Journal. 6(1996)519-523.

[14] Miner M A, Cumulative damage in fatigue, J Appl Mech. 12(1945)159-164.

[15] Marco S M, Starkey W L, A concept of fatigue damage, Transaction of the ASME, 75 (1954) 627-632.

[16] Manson S S, Halford G R. Practical implementation of the double linear damage rule and damage curve approach for treating cumulative fatigue damage, Int J.Fract.2(1981)169-192.

[17] Freudenthal A M, Heller R A, On stress interaction in fatigue and cumulative damage rule, Journal of the Aerospace Science.7(1959)431-442.

[18] Halford G R, The energy required for fatigue, Journal of Materials.1(1966)3-8.

[19] Niu X, Li G X, Lee H, Hardening law and fatigue damage of a cyclic hardening metal, Engineering Fracture Mechanics.2(1987)163-170.

[20] Chaboche J L, Lesene P M, A non-linear continuous fatigue damage model, Fatigue and Fracture of Engineering Materials and Structures.1(1988)1-7.

[21] Freudenthal A M, Heller R A, On stress interaction in fatigue and cumulative damage rule, Journal of the Aerospace Science.7(1959)431-442.

CHAPTER 3:

Advanced Technique in Road Engineering and Material Science

doi:10.4028/www.scientific.net/AEF.5.213

Evaluation of Warm-Mix Asphalt Compaction Performance by Variable-Temperature Gyratory Compaction

Liming WANG [1,2,a], Yiqiu TAN [1,b]

[1]School of Transportation Science and Engineering, Harbin Institute of Technology, Harbin 150090, China

[2]College of Civil Engineering, Northeast Forestry University, Harbin 150040,China

[a]wlmdxx@126.com, [b]yiqiutan@163.com

Keywords: compactibility, optimum compaction temperature, Warm-Mix Asphalt, gyratory compaction, variable-temperature

Abstract: For dynamic changes of viscosity reducing mechanism of different types of additives in after mixing mixture, the Warm-Mix Asphalt would present different compaction performance development with the change of paving temperature and time. The authors employed an improved variable-temperature gyratory compaction experiment to evaluate different mixtures' compaction performance. In the research, specimen preparation were tried to imitate natural cooling process of paving construction, and the development of construction energy index and the optimum compaction temperature were two ways to carry out qualitative and quantitative evaluation respectively . The authors proposed an equidensity –temperature method which based on analogous principle to determine the optimum compaction temperature of Warm-Mix Asphalt indirectly, this method fit for those mixture that their optimum compaction temperature can not be predicted by binder directly, and can also avoid defects of the direct methods by mixture. According to the experiment results, there is significant difference in the compactibility and the optimum compaction temperature to different Warm-Mix Asphalt. The overall evaluation information of Warm-Mix Asphalt compaction performance could be get by the combination used of the variable-temperature gyratory compaction and the evaluation methods in the paper.

Introduction

Background and Objective. Compared with Hot-Mix Asphalt(HMA), Warm-Mix Asphalt(WMA) can be mixed at a relative lower temperature by reducing viscosity of binder or cohesive strength of aggregate surface at high temperature. The residual viscosity reducing mechanism in after mixing mixture make WMA have warm pave performance[1].

At present, there are about four typical ways to produce WMA: ①Reducing binder's viscosity by asphalt foaming; ②Coating emulsified asphalt on hot aggregates; ③Adding high melting point of organic additives; ④Diluting binders with solvent. After mixing, the residue of viscosity reducing effect in different WMA will change with paving time and temperature significantly, and thus the compaction performance of different WMA will be distinct.

The compaction performance of mixture contains two indexes: compactibility and OCT (Optimum Compaction Temperature). The compactibility presents the workability at certain temperature. The OCT presents neither slippage -upheaval nor cracking when compacted at this temperature range. Those two indexes, especially the latter, are important indicator of the construction control.

Evaluation Methods of the Compactibility By Gyratory Compaction. Compactibility evaluation is the estimate of the density growth law in compaction process. The SGC (Superpave Gyratory Compacter) collect compaction height continuously, facilitates the analysis of density-energy relationship. Compactibility evaluation by *CEI* (Construction Energy Index) computed base on SGC compaction curves is shown in Fig.1.

The *CEI* is a energy index which the mixture density was compacted from certain low to high degree in the paving process[2,3]. As many specifications and guides require that the pavement should be compacted to G_{mm}=92~93% (G_{mm}-Grade of Maximum Theoretical Density), the area under the compaction curve from loose (0 compaction times) to a given density represents the

energy that the pavers and rollers woke done during the construction. This index is written as $CEI_{loose\text{-}92/93}$. In variable-temperature test, the mixture would attain to different loose density underwent 0 times compaction at different temperatures, and the value would have big random error when only compacted at static pressure. The authors employed $CEI_{88\text{-}93}$ which describes the compactibility of after initial compaction as index, it has better accuracy than $CEI_{loose\text{-}92/93}$ in theory. The smaller the *CEI*, the easier the mixture be compacted.

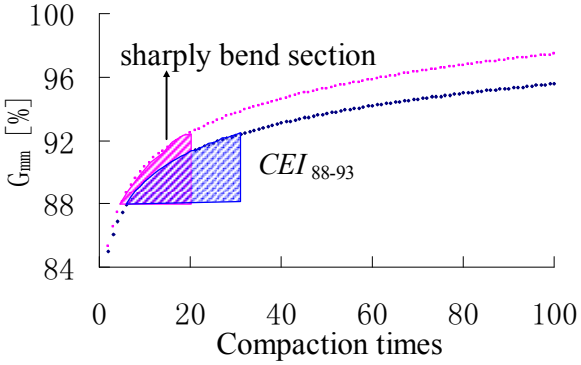

Fig. 1 The $CEI_{88\text{-}93}$ of different mixture

Determine Method of the OCT. If WMA were produced base on the mechanisms of foregoing ①, ② and ④, the composition and effect of viscosity reducing in after mixing mixture would change dynamically, not only change with paving temperature and paving time, but also change with the mixing temperature and mixing time. Those WMA OCT can't be determined directly with binder's equiviscosity-temperature method according to the ASTM D2493. If WMA was produced base on the mechanism of foregoing ③, there are also research showed that the OCT which estimated by asphalt directly would have not matched the actual project performance[4]. At the same time, the equiviscosity-temperature method would not applicable to WMA with polymer modified asphalt. For above reasons, The OCT of WMA should be determined through the mixture.

At present, the OCT determined direct method though variable-temperature compaction is commonly used. If use unmodified asphalt, test would set a target density like in reference [5], and then to find OCT in compaction curves. If polymer modified asphalt was used, similar to the reference [6], there might be a density peak at high temperature stages, and could be used as density standard of the OCT. Whichever direct methods are used, there are four defects: ①Different compaction methods or mixture types have different target densities, assumed standard is difficult to determine; ②Even if modified asphalt had been used, the density peak is almost impossible appear under WMA mixing temperature; ③Some asphalt's viscosity is sensitive to shear rate, when compaction shear rate different from laboratory to in site roller work, directly determined OCT may not be suitable for the construction; ④The final density of standard compaction will not sensitive to temperature change if the compaction energy is too large or the compaction temperature is too high.

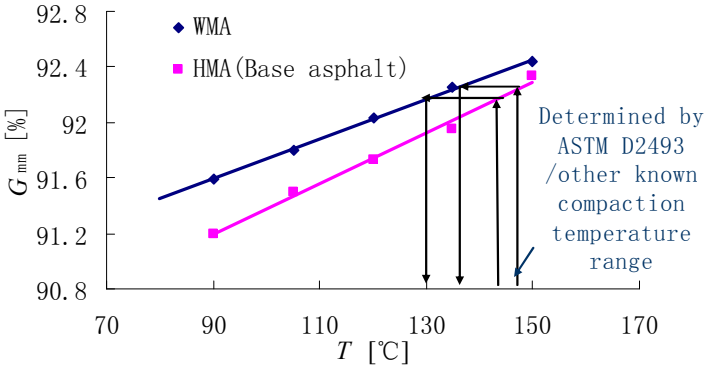

Fig.2 Theoretical process of the equidensity-temperature method

From above analysis, it is an ideal method that analogy is employed to avoid first three defects in the above paragraph. This method compares variable-temperature compaction density-temperature curves of WMA with others which its/their compaction temperature have been known. This method is called equidensity-temperature method, its theoretical process shown in Fig.2. In the paper, basic

HMA with unmodified asphalt was used as an analog object, the OCT of HMA was determined by ASTM D2493 which employed Brookfield viscometer. In the process of analogy, the density in energy sensitive areas in compaction curves was chosen as the analogy index.

Experimental Design of Variable-Temperature Gyratory Compaction

Basic Mixture. As experiment mixture should reflect the effect of asphalt film on shearing process of compaction as far as possible, a soft and fine dense-graded HMA was chosen as the basic mix proportion deliberately. Its optimum asphalt content is 4.5%, and the gradation distribution is listed in Table 1.

Table 1 Gradation distribution of basic dense-graded HMA

Mesh size [mm]	0.075	0.15	0.3	0.6	1.18	2.36	4.75	9.5	13.2	16
Passrate [%]	6	9	13	19	18	41	59	80	93	100

Performance parameters of the base asphalt used for test are listed in Table 2.

Table 2 Performance parameters of asphalt

Penetration [25℃, 0.01mm]	Softening point [℃]	Ductility [cm]	Penetration index	Compaction temperature [℃]
81	42.7	153	-1.5	134~138

Notes: JTG E20-2011 test standard

In the experiment, the authors prepare a basic HMA and four kinds of WMA, different WMA use different additives, and Table 3 is the description of the additives .

Table 3 Description of the test additives

Name	Basic chemical composition	Dosage	Usage
A	synthetic zeolite powder with crystal water	0.3% (mixture)	add in with filler
B	dilute emulsifier with water	10%(binder)	add in the asphalt just before mix
C	high melting point paraffin wax	3.5%(binder)	add in the asphalt in advance
D	composite liquid organic solvent	3.5% (binder)	add in the asphalt just before mix

Those WMA with different additives are called WMA(A),WMA(B),WMA(C) and WMA(D) respectively. Because of the small additives residual dose in after mixed mixture, the mix proportion need not to be changed.

Specimen Preparation Process. In order to unify test condition, All WMA were mixed at 145℃ uniformly according to the instructions of additives' producer, whiles the HMA was mixed at 155℃. Some WMA, such as those production mechanism are based on the foaming, emulsification and dilution, are not suitable for controlling the temperature slowly in the oven. In the research, mixtures temperature had been controlled after placed into molds. The detailed specimen preparation method is a three-steps process: first, the after mixing mixtures were weighed accurately and placed into mold with heat preservation cover as quick as possible, second, pre-compacted to $G_{mm}\approx 80\%$ by static pressure, at last, specimens were gradually cooled to test temperature at room temperature similar to paving process . The process of specimen preparation is shown in Fig 3.

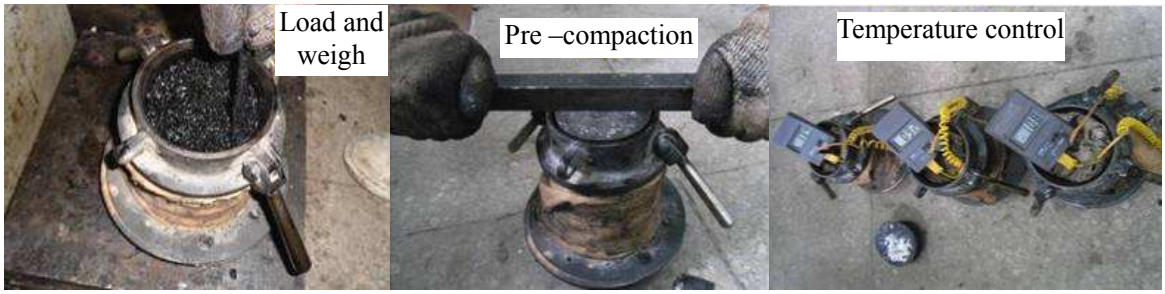

Fig.3 The process of specimen preparation

Compaction Conditions Control. The study use an old standard SGC, its rotation angle is 1.25°, compaction load is 600kPa. The compaction temperature from 135℃ to 90℃ interval 15℃. At every temperature, one experiment set was conducted and each set has twice parallel test, the basic HMA was added a set at 150°C.

Results and Discussion

According to the experimental conditions control of above, the authors get five set of different whole process compaction curves, all of them were plotted in Fig.4.

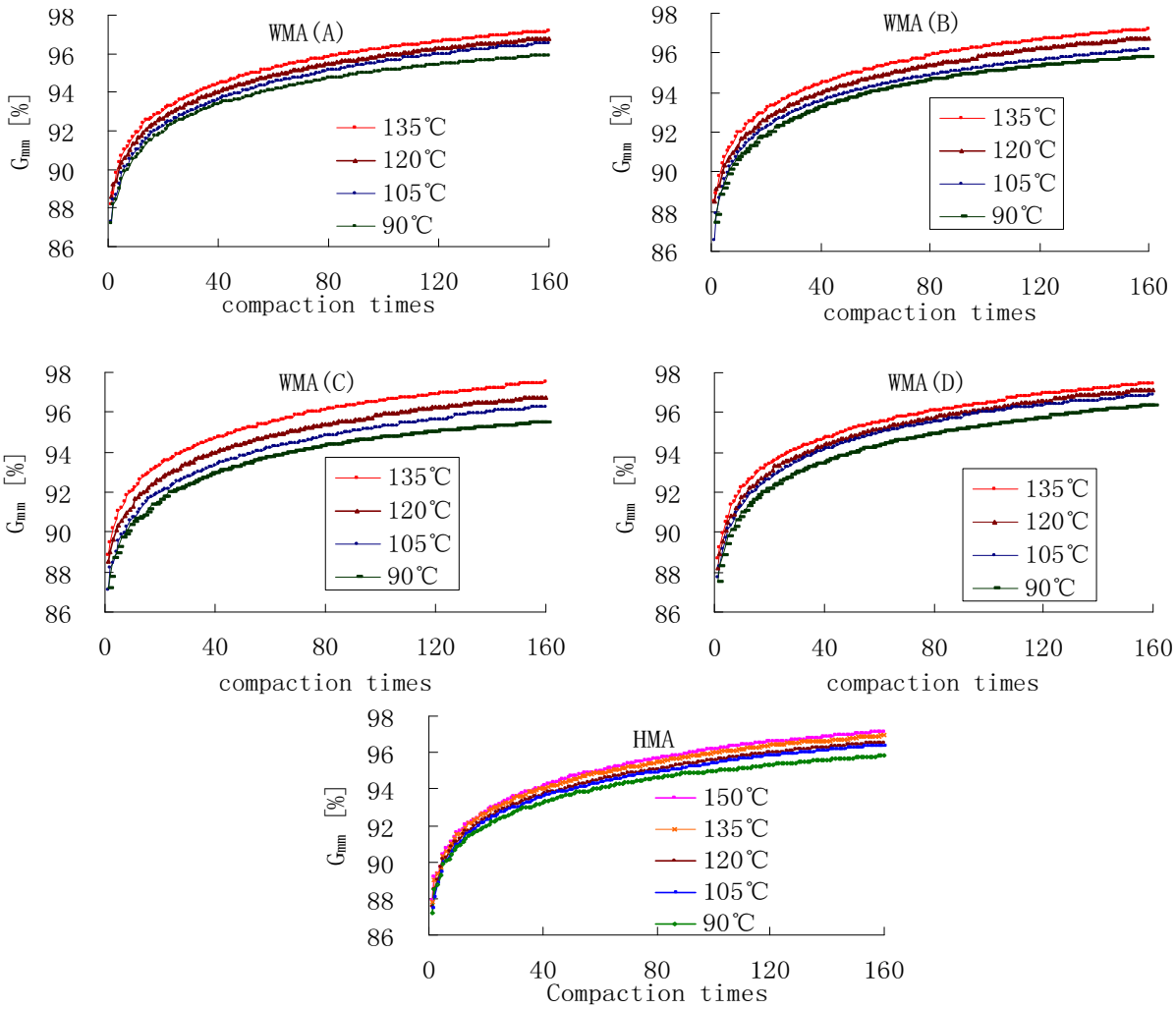

Fig.4 Compaction curves of variable-temperature experiment

Compactibility Evaluation of WMA. According to evaluation index described in Fig.1, the $CEI_{88\text{-}93}$ of different WMA at different temperatures were computed and plotted in Fig.5.

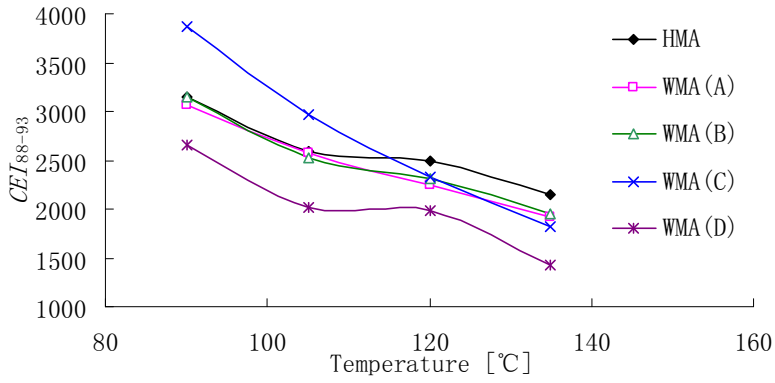

Fig. 5 $CEI_{88\text{-}93}$ of different WMA at different temperatures

In the Fig.5, the $CEI_{88\text{-}93}$ of all types of WMA obvious lower than that of the HMA at 135℃, this indicates that all types of WMA have warm-pave performance. But, when the variation of the $CEI_{88\text{-}93}$ are concerned, different WMA presents different development trends. WMA (A) and WMA (B) shows similar trends, their $CEI_{88\text{-}93}$ lower than that of the HMA over 105℃, it means that

those two WMA easy to compact over the temperature, while with the temperature decreases, this effect fades away and the compactibility approach to HMA under 105℃gradually. WMA (C) significantly reduce the compaction power at 135℃, but if the compaction temperature decreases to under 105℃, the $CEI_{88\text{-}93}$ would higher than HMA. This appearance might be related to the about 100℃ melting point of the additives, when the temperature is lower than 100℃, hardening additives no longer has help effect to compaction, but increases compaction difficult. At any compaction temperature, the $CEI_{88\text{-}93}$ of WMA (D) is the smallest, and its development trend like that of the HMA. This low shows that WMA (D) has the best warm-pave performance.

When $CEI_{88\text{-}93}$ at 135℃(conventional paving temperature) is used as apples-to-apples evaluation criteria, the order of different mixtures' compactibility is WMA(D)>WMA(C)>WMA (B)≈WMA(A)>HMA.

The OCT of WMA. All G_{mm} of a certain compaction times in Fig.4 were collected and paired plotted in Fig.6 accordance with the manner of Fig.2. The certain compaction times should lies in the certain curve range that its G_{mm} has clear difference and sensitive to compaction temperature, this range is the sharply bend section of a compaction curve. In the paper, 30 times were selected.

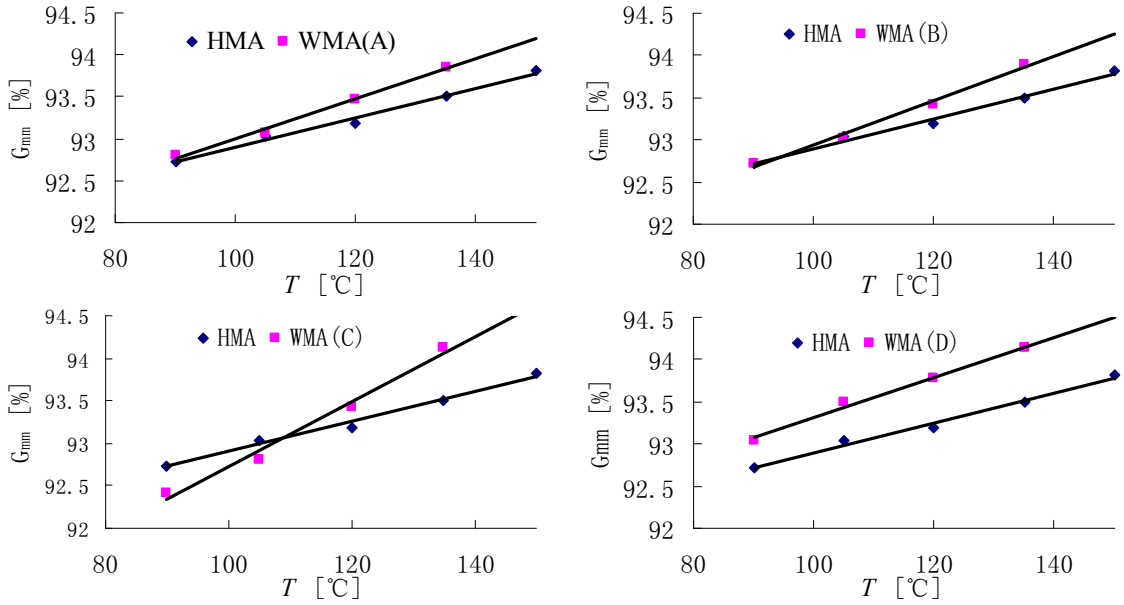

Fig.6 Temperature-density paired drawings of 30 compaction times

According to the equidensity-temperature method in Fig.2, the OCT of different WMA were determined and listed in Table 4.

Table 4 OCT of different WMA

Mix type	OCT[℃]	Mix type	OCT[℃]
WMA(A)	121~124	WMA(B)	122~124
WMA(C)	121~123	WMA(D)	108~111

Compared with HMA, the OCT reduction of WMA(A),WMA(B) and WMA(C) in Table.4 are close, it is about 12~15℃, while the reduction of WMA(D) reaches to 26~27℃. Above data are far less than advertise of additives producers, the reason is that producer' data are commonly compared with the limit of actual construction. In addition, due to the difference of additives' property, additives' dose, binder's property and test condition control which used in different research, the absolute reduction of WMA compaction temperature is difficult to quantify.

OCT ranges of all WMA in Table.4 look narrower than that of the basic HMA, In fact, it's the result that limited number of data is fitted to straight line. If small steps were used in variable-temperature test, the experimenter can get a high related coefficient fitted curve which their middle section may flatter than HMA, then a wider range might be get. Nevertheless, if parameter level is less, the linear fitting should be priority.

Overall Evaluation of Different WMA Compaction Performance. Compared with the basic HMA, the compactibility and the OCT reduction of WMA(A) and WMA(B) are similar, with the cooling of mixtures, two additives effect to compaction performance gradually reduced and closer

to disappear. The WMA(C) has similar OCT reduction to WMA(A) and WMA(B) at high temperature, while its compactibility obvious lower than that of the first two under 105℃. The compactibility of WMA(D) significantly higher than others, and its OCT reduction reaches to 26~27℃. Such compaction performance as WMA(D) is beneficial to extending the effective compaction time under low temperature, but may affect the opening time to traffic and the early high temperature stability, in other words, WMA(D) is not Warm-Mix Asphalt to a certain extent.

Conclusion

ⅰ.For dynamic changes of viscosity reducing mechanism of WMA additives in after mixing mixture, the condition control of variable-temperature gyratory compaction experiment needs to be improved. The specimen preparation method in the paper make its cooling process approach to actual construction condition.

ⅱ. The analysis of $CEI_{88\text{-}93}$ based on variable-temperature gyratory compaction experiment can qualitative evaluate WMA's compactibility and their development with the temperature change. At 135℃, the order of different mixtures' compactibility is WMA (D)>WMA(C)>WMA (B)≈ WMA(A)>HMA, while with the decrease of compaction temperature, different types of WMA shows a distinct difference. The compactibility of WMA (A) and WMA(B) gradually reduced and closer to disappear when temperature decreases. The compactibility of WMA (C) lower than that of the basic HMA under 105℃. At any compaction temperature, the $CEI_{88\text{-}93}$ of WMA (D) is the smallest and its compactibility higher than any mixture consistently.

ⅲ. The equidensity-temperature method is an indirect way based on analogous principle to determine the OCT of asphalt mixture that unsuited to be predicted by binder directly, and can also effectively avoid defects of the direct methods by mixture. By means of the equidensity-temperature method, the OCT reduction of WMA(A),WMA(B) and WMA(C) are similar and about 12~15℃, while the reduction of WMA(D) reaches to 26~27℃.

ⅳ. The overall evaluation information of Warm-Mix Asphalt compaction performance could be get by the combination used of the variable-temperature gyratory compaction and the evaluation methods in the paper.But, as dynamic residual of viscosity reducing mechanism of most of WMA additives, not only relate to the compaction temperature and time, but also relate to the mixing temperature, the condition control of variable-temperature experiment has great effect on experimental results. Therefore, to those kinds of mix, the evaluation of compaction performance is relative rather than absolute.

References

[1]ZHANG Zhen,SUN Li-jun. The Control Indicates Research of Evotherm Warm-Mix Asphalt, J. Journal of Wuhan University of Technology. 2009,31(8) 29-32

[2]ZHANG Zheng-qi,YUAN Ying-jie,WANG Bing-Gang. Information of Gyratory Compaction Densification Curve of Asphalt Mixture and Its Application, J. China Journal of Highway and T ransport. .2005,18（3）:1-6

[3]LI Yu-shi,YANG Rui-hua,SHAO la-geng,LI Chuang-min. Compactness Analysis of Asphalt Mixture, J. Journal of Highway and Transportation research and Development. 2005,22 (3) 28-34

[4]ZHOU Yan,CHEN Suan-fa,ZHENG Mu lian ZHANG kai. Research on Mixing and Compaction Property of Warm Mix Asphalt., J. Journal of Wuhan University of Technology. 2010,32(1)61-64

[5]WU Chao-fan,ZENG Meng-lan, WANG Mao-wen,XIA Yang. Determination of the Mixing and Compaction Temperatures for Warm Mix Asphalt with Sasobit, J. Journal of Hunan University(Natural Sciences), 2010 ,37(8) 1-5

[6]LI Ning-li, LI Tie-hu, CHEN Hua-xin,ZHANG Zheng-qi. Mixing and Compaction Temperatures of Modified Asphalt Mixture, J. China Journal of Highway And Transportation , 2007, 20(2)40-44

doi:10.4028/www.scientific.net/AEF.5.219

Laboratory Study on Properties of Tire Crumb Rubber Modified Bituminous Mixture

Yuming Dong [1,a], Yiqiu Tan [2,b]

[1]School of Transportation Science & Engineering, Harbin Institute of Technology, Harbin, China 150090.

[2]School of Transportation Science & Engineering, Harbin Institute of Technology, Harbin, China 150090.

[a]dongdym@163.com, [b]yiqiutan@163.com

Key words: Crumb rubber, Mixture, Rutting resistance, Cracking resistance.

Abstract: This paper investigates the laboratory properties of tire crumb rubber modified (CRM) bitumen mixture. Two types of mixtures containing two binders (pen90 bitumen; CRM bitumen) were used to produce Marshall Sample and determine optimum content. Mechanical performances of bituminous mixtures were evaluated by Chinese wheel rutting test (WRT), 3point beam bending test (3P-BBT) at low temperature, indirect tensile Strength test (ITST) at freezing-thawing cycles. Superpave gyratory compactor (SGC) specimens also were prepared for modulus test. Resilient modulus (*E*) data were obtained by unconfined uni-axial compression test according to the specification of China. Dynamic modulus (*E**) data were obtained by Simple Performance Test (SPT). Two temperatures were used at dynamic modulus test. The results indicate that CRM bituminous mixture performs better than referenced bituminous mixture on viscoelastic behavior, rutting resistance, cracking resistance and moisture stability.

Introduction

In recent years, crumb rubber modification within a wide range of contents and sizes has been done to improve asphalt performance at pavement service temperatures. The ability of crumb rubber to improve the mix properties depends on many factors, including the incorporation technology, nature of the rubber, size of the rubber particles, and the percentage of rubber in the mix and its reaction time with asphalt. Field studies have shown that crumb rubber modification of asphalts can improve the asphalt pavement performance [1, 2, 3, 4]. The use of crumb rubber modifiers with asphalt binders seems to enhance the fatigue resistance, as illustrated in a number of studies [5, 6, 7, 8]. The improved performance of asphalt rubber pavements compared with conventional asphalt pavements has partly resulted from improved rheological properties of the asphalt–rubber binder. However, optimum crumb rubber content still needs to be determined for different crumb rubber contents. Moreover, the viscoelastic properties of CRM asphalt mixture also are investigated by SPT.

Design of Mixture

Marshall Method still is used for mix design of the crumb rubber modified (CRM) asphalt mixture. For this method, mix design includes materials selection, gradations selection, optimum asphalt contents, and verification of performance.

Properties of original materials

The base binder pen 90# is used to modify asphalt with tire scrap crumb rubber. The mixing processing over 45 min at 180℃ is adopted in the laboratory. According to *the construction technical specification for asphalt pavement of highway* (JTG F40-2004) in China, the technical parameters of 90# pen base asphalt meet to its specification. The parameters of CRM asphalt is shown in table1.

Table1 Testing parameters of CRM bitumen

Test Item	CRM bitumen	requirement	methods
Penetration@25℃ (0.1mm)	64.5	40-80	T0604
Ductility@5℃ （cm）	17.4	>10	T0605
Softening Point($T_{R\&B}$) (℃)	57.6	>47	T0606
Elastic Recovery （%）	81.1	>55	T0662
Br. Viscosity@180℃ （Pa·s）	2.44	1.0-4.0	T0611
Thin Film Oven Test (TFOT)			
Mass Loss (%)	-0.23	<0.4	T0610
Penetration Ratio (%)	88.9	>80	T0604
Ductility Ratio@5℃ (%)	64.8	>40	T0605
Softening Point Ratio（%）	101.2	<110	T0606

The addition of tire crumb rubber improves the properties of virgin bitumen. The limestone coarse aggregate is adopted, and must be clean, hard, the lower F&E and the manufactured fine aggregate is adopted, and must be clean, higher S.E; the low silica stone is made for the filler to be fine enough, clean and the lower plastic index.

Gradation Design

The different grades are used for the CRM asphalt mixture and the usual asphalt mixture in this study, and the nominal maximum aggregate size (NMAS) is 13.2mm. Considering rubber grains distributed in CRM binder, the two mixtures are different from the passing percent of 4.75mm sieve size. The one of CRM-AC-13 is 30%, and the one of AC-13 is 45%. The rubber grain can be a fine aggregate in the CRM mixture. The passing percentages of sieves in the two mixtures are shown the following table.

Table2 Passing percentage of mineral mixtures (%)

Sieve Sizes(mm)	13.2	9.5	4.75	2.36	0.075
CRM-AC	95	65.6	30	23.5	7
AC	95	70	45	30	5

The gap grade based on the skeleton compact theory with multi-filling state is adopted to improve the rutting resistance in this study. Thus the rutting resistance, the thermo-cracking resistance and the water resistance must be considered for mix design in Beijing.

Selection of optimum bitumen content

Based on predicting asphalt content, the distance of 0.5% is adopted, and five contents are selected for Marshall Specimens with 75 hammers dual sides. Based on the volumetric method, the void content is a main parameter for determining asphalt content. Generally, the objective void air content is considered as 4%, and the void mineral aggregate (VMA) is more than 15% for the NMAS 13.2mm mixture. In theory, the crumb rubber is beneficial to extend pavement life, however this make the construction of HMA difficult. Thus CRM asphalt mixture need the higher mixing

temperature for good workability. The characteristics of two mixtures, including rutting resistance, cracking resistance, moisture stability, static modulus, and dynamic modulus, were investigated in this study.

Properties of CRM Mixture

The performances of CRM asphalt mixture also include the rutting resistance at high temperature condition, the cracking resistance at low temperature condition, moisture sensitivity at humid regions, and mechanical strength. Marshall Test, wheel tracking test, 3 point beam bending test (3P BBT), and Indirect Tensile Strength Test are adopted for evaluating performances.

Stability at the high temperature

The high temperature properties are evaluated by Marshall Stability test and wheel tracking test for mixture in China. As the following table shows, rutting resistance of CRM mixture is higher than AC, especially dynamic stability.

Table3 Results of high temperature properties

Test Parameter	AC	CRM-AC
MS/kN	8.6	8.8
FV/mm	2.1	2.9
DS@60℃/(cycles/mm)	1290	3810

The Marshall Stability (MS) and the Flow Value (FV) have no obvious differences for two mixes.

Cracking resistance at the low temperature

The 3 point beam bending test is used to evaluating the cracking resistance of bituminous mixture in China. The maximum bending strain of two mixtures is respectively 2200με and 3568με over the 2000με standard value. The crumb rubber modifier effectively improves the low temperature property of bituminous mixture.

Moisture sensitivity

The residue stability (RS) of Marshall Test and the tensile strength ratio (TSR) of indirect tensile strength test (ITST) are used to evaluating the moisture resistance for bituminous mixture in China.

Table4 Results of moisture sensitivity

Test Parameter	AC	CRM-AC
RS/%	81.3	92.3
TSR/%	78.8	82.5

The above test results show that adding of crumb rubber is beneficial to the moisture resistance.

Resilient modulus

Static resilient modulus of road material is the most important input parameter in designing asphalt pavement structure in China, based on multi-layer elastic system theory. The resilient modulus was measured and its elastic mechanical characteristic was investigated.

Resilient modulus test uses the diameter φ100 mm and height 100 mm samples, and these samples are made by gyratory compactor. Axial compression load is applied on unconfined specimen by sequence at 20℃ condition. Six recycles of loading and unloading are applied on specimens after the first stage of steady compressing, and the peak value of every recycle of loading and unloading is 0.1-0.6 times as the strength. After stress and strain are determined, the resilient modulus may be calculated. The samples of CRM-AC and reference asphalt mixture AC are prepared for resilient modulus test. Testing data of resilient modulus are shown in the following table after statistically processing.

Table5 Resilient Modulus and Strength @20℃(MPa)

Mixture types	AC	CRM-AC
Resilient Modulus (MPa)	1198	1587
Axial Strength (MPa)	3.44	6.03

Obviously, the resilient moduli and the axial strengths of three CRM mixtures are higher than reference mixture. This result demonstrates that the tire scrap crumb rubber is very beneficial to improve stiffness of asphalt mixture. In unconfined compression load, the more mastic fluidized structure is weaker than the more aggregate skeleton structure.

Dynamic modulus

Dynamic moduli of pavement material can perform the real behavior under the traffic load. The dynamic moduli of CRM-AC and AC are tested in this study. Dynamic moduli at the two testing temperature are determined by AMPT. The complex modulus and phase angle are obtained.

The following tables show the parameters achieved by for CRM-AC and usual AC. Dynamic moduli of CRM-AC are higher than the one of AC at the same temperature. As the data at 40℃ shows, E* of CRM mixture is 3154Mpa and E* of AC mixture is 2127Mpa under 25Hz frequency; E of CRM mixture is 1146 MPa and E of usual mixture is 480Mpa under 0.1Hz frequency.

Table6 Results of CRM-AC and AC@ the lower temperature

CRM-AC						
Loading frequency (Hz)	25	10	5	1	0.5	0.1
Dynamic modulus (MPa)	10823	8598	7289	4682	3889	2370
Phase angle (°)	23.8	26.0	28.0	30.5	30.9	31.1
AC						
Dynamic modulus (MPa)	10554	7572	6285	3838	3145	1942
Phase angle (°)	20.2	22.3	23.5	26.2	26.5	27.6

Table7 Results of CRM-AC and AC@ the higher temperature

CRM-AC						
Loading frequency (Hz)	25	10	5	1	0.5	0.1
Dynamic modulus (MPa)	3154	2463	2058	1504	1378	1146
Phase angle (°)	28.6	26.1	24.7	19.9	18.4	17.5
AC						
Dynamic modulus (MPa)	2127	1436	1115	691	605	480
Phase angle (°)	36.7	33.9	32.4	26.9	23.1	18.8

Generally, based on dynamic modulus and phase angle, storage modulus $E^{'}$ and loss modulus $E^{''}$ can be calculated by the formula: $E^{'}=|E^*|\ \sin\delta$, $E^{''}=|E^*|\ \cos\delta$, as the above table shows. For rheological material, the storage modulus represents elastic characteristic and the loss modulus represents viscoelastic characteristic. For $E^{'}$ and $E^{''}$ at the same temperature, ones of CRM-AC are higher than ones of AC.

For the further study on the rutting resistance and the fatigue resistance of CRM asphalt mixture, the rutting factor ($E^*/\sin\delta$) and the fatigue factor ($E^*\cdot\cos\delta$) are achieved by SHRP calculation method based on dynamic modulus and phase angle. At 21.1℃, the rutting factor has no obvious distinguish between CRM-AC and AC, but the fatigue factor of CRM-AC is evidently higher than AC. It indicates that at usual temperature condition, the rutting resistance of CRM-AC is close to AC, but the fatigue resistance of f CRM-AC is superior to AC.

The crumb rubber is very beneficial to improve the fatigue resistance of asphalt mixture with usual temperature state. However, the rutting factor of CRM asphalt mixture is obviously higher than AC at 40℃.

Conclusions

After finished the blending design of CRM mixture, the rutting resistance, cracking resistance, moisture sensitivity, resilient modulus and dynamic modulus of tire crumb modified asphalt mixture are systematically investigated in this paper, and the following conclusions can be drawn:

1) Bituminous mixtures with tire crumb rubber have the better performance of pavement, including rutting resistance, cracking resistance, and moisture sensitivity.
2) However, the gradation of rubber particles needs to be considered in blending design of CRM mixture. And the properties vary with the different crumb rubber content.
3) Moduli test results also indicate that the addition of crumb rubber to asphalt binder generally increased the binder viscosity and improved the resistance of rutting at the higher temperature and the fatigue resistance at the ordinary temperature.

Acknowledgements

The authors acknowledge the Beijing Road Bureau for financial support of this project. Thanks are expressed to P.E. Hao Liu and Liying Yang for helpful discussions. Thanks are also expressed to Mr. Jianguo Wang and Qian Wang of R&D center in Beijing municipal R&B building Material Corporation for specimens' preparation and measurement.

References

[1] Brown, D. R., Jared, D., Jones, C., and Watson, D. (1997). "Georgia's experience with crumb rubber in hot-mix asphalt." *Transportation Research Record*. *1583*, Transportation Research Board, National Research Council, Washington, D.C., 45-51.

[2] Stroup-Gardiner, M., Chadbourn, B. C., and Newcomb, D. E. (1996). "Babbitt, Minnesota: Case study of pretreated crumb rubber modified asphalt concrete. *Transportation Research Record*. *1530*, Transportation Research Board, National Research Council, Washington, D.C., 34-42.

[3] Maupin, G. W., Jr. (1996). "Hot-mix asphalt rubber applications in Virginia." *Transportation Research Record*. *1530*, Transportation Research Board, National Research Council, Washington, D.C., 18-24.

[4] Charania, E., Cano, J. O., and Schnormeier, R. H. (1991). "Twenty-year study of asphalt rubber pavements in Phoenix, Arizona." *Transportation Research Record*. *1307*, Transportation Research Board, National Research Council, Washington, D.C., 29-38.

[5] Raad, L., and Saboundjian, S. (1998). "Fatigue behavior of rubber modified pavements." *Transportation Research Record*. *1639*, Transportation Research Board, National Research Council, Washington, D.C., 73-82.

[6] Soleymani, H. R., Zhai, H., and Bahia, H. (2004). "Role of modified binders in rheology and damage resistance behavior of asphalt mixtures." *Proc., 83rd Annual Meeting of the Transportation Research Board*, Washington, D.C., Paper No. 04-3974.

[7] McGennis, R. B. (1995). "Evaluation of physical properties of fine crumb rubber-modified asphalt binders." *Transportation Research Record*. *1488*, Transportation Research Board, National Research Council, Washington, D.C., 62-71.

[8] Billiter, T. C., Davison, R. R., Glover, C. J., and Bullin, J. A. (1997). "Physical properties of asphalt rubber binder." *Pet. Sci. Technol.*, 15(3-4), 205-236.

doi:10.4028/www.scientific.net/AEF.5.224

Carbon Fibre/Silicon Composite Sensors for Concrete Structural Health Monitoring in Compression

Lili Yang[a], Yongquan Zhang[b], Yong Ge[c,*], Qinghua Zhu[d], and Ce Zhang[e]

School of Transportation Science and Engineering, Harbin Institute of Technology, Harbin 150090, P.R. China

[a]liliyang@hit.edu.cn, [b]zyqzygzs@126.com, [c,*]hitbm@163.com, [d]qinghuazhu2005@126.com
[e]roronoazoroshx@126.com

Keywords: Structural Health Monitoring; Concrete; Carbon Fibre/Silicon Composite; Compression

Abstract. Structural health monitoring of concrete infrastructures has attracted enormous attention due to the brittle nature of concrete. In this research, we report the carbon fibre/silicon rubber composite sensors and their excellent monitoring in concrete's compression. It is shown that the electric resistance change synchronously with the mechanical deformation of concrete during the compression process. With the increase of carbon fibre fraction, the sensitivity decreases and the numerical equations to predict the structural change are also obtained. The experimental results reported here highlight the potential application of CF/silicon composites as an effective, real-time structural monitoring sensor with low-cost and long life.

Introduction

Structural health monitoring (SHM) and damage detection tools have been urgently needed for civil infrastructures/systems due to the increased awareness of economic and social effects of deterioration resulting from the coupling effect of long-term, fatigue and mutation [1-3]. Among the conventional materials for infrastructures, cement-based concrete is of typical brittle materials and there are large number of randomly distributed micro-cracks and micro voids inside. Under the external force, the micro-crack will continue to expand and finally link to each other [4, 5]. Compared with other kinds of SHM sensors such as optical fibre or piezoelectric materials [6, 7], conductive polymer composites (CPC) are of increasing importance and show promising properties for a wide range of sensor principles. The major reason is the possibility to tailor the material properties very precisely and they also show outstanding flexibility, low cost, high durability and great compatibility with structural materials [8-10]. Among these materials, composites with carbon fibers as dopants have been intensely studied due to their excellent electric and mechanical properties. Carbon fibre/silicon rubber composites as structural health monitoring sensors were studied in our group and it has been proved that the composites have stable electric resistance-time characteristic, wide working temperature range and large deformation [11]. In this work, their real-time structural monitoring in concrete's compression was further studied. Results show that they have excellent sensing performance.

Experimental

Preparation of CF/silicon rubber composites. Short carbon fibres (CF) were chosen with conductivity of 5.6×10^4 S/m and length of 3 mm. They were cleaned with acetone and kept in the oven. As the matrix, silicon rubber was diluted with hexane. The composite sensors were prepared by room temperature melt mixing method [11]. Carbon fibres were added into the diluted solution and mixed manually and then under the ultrasonic device. Four weight fractions of 0.6%, 0.75%, 0.8% and 0.9% were chosen, which corresponds to the volume fraction of 0.84%, 1.05%, 1.13% and 1.26%. The residual air in the mixture could be removed through evacuating device. Organotin and

tetraethoxysilica (TEOS) were added under mixing which were used as the catalytic and crosslinking agent, respectively. After 24h room temperature curing in a mold, the composites were obtained with a size of 150 mm × 150 mm × 3mm.

Characterizations. Samples were coated with platinum and observed on a QUANTA 200F (FEI, America) at an accelerating voltage of 20kV. The sensitivity tests of composites were characterized by the real-time combination of mechanical and electronic performance. Concretes doped with polymer were chosen as the study goal. The four-electrode method was used in the resistance tests which were carried on a digital multimeter (UT805, Uni-Trend Group Limited). The strain and stress results were obtained with the help of CSS-88000 series electronic universal testing machine.

Results and Discussion

Morphologies of composites. Fig. 1 shows the typical pictures of composites with low and high fraction of carbon fibres. It indicates that carbon fibres after treatments are uniformly distributed in the silicon rubber. Moreover, with the increase of carbon fibres, the bridging points between fibres increase which form the channels for electron transport in the whole composites.

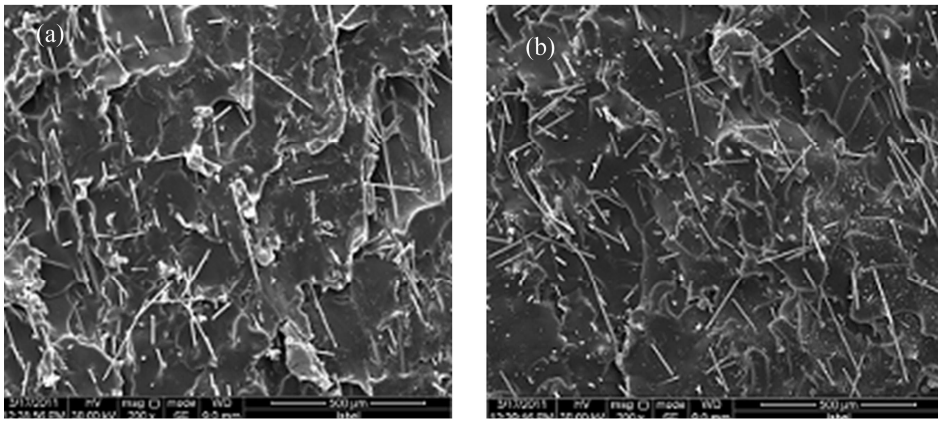

Fig. 1 Typical SEM images of carbon fiber/silicon composites with doped fraction of 0.84% (a) and 1.26% (b)

The electrical property of CF/silicon rubber composites is firstly studied before the sensing performance. Fig. 2 shows the current-potential curves of composites. It is obvious that the composites agree with the Ohm's law when the potential is smaller than 8V, which is similar with some metallic conductors. However, the conductivity is slightly increased due to the decrease of CF's resistance as the temperature rises during the electric process. As a matter of fact, the composites will expand simultaneously which increase the distance between fibres and decrease the conductivity of composites. According to the results from Fig. 2, it represents that the latter effect is not obvious here.

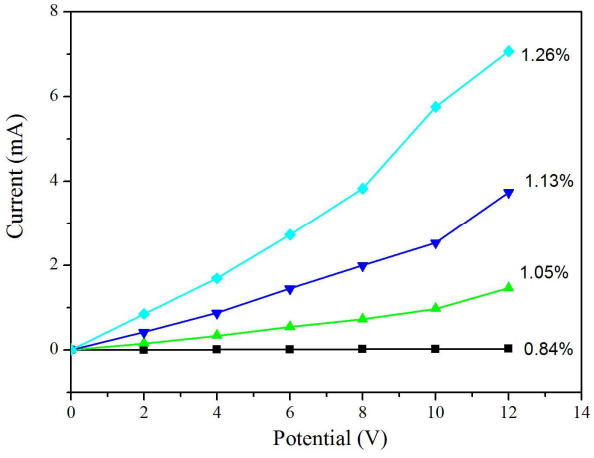

Fig. 2 The current-potential curves of CF/silicon composites with different volume fraction of CF

Structural monitoring properties. The composites were bonded to the concrete using the post-yield epoxy. Electrical contacts are established by drying colloidal silver paste over single-strand wire to form a two-probe measurement setup as shown in Fig. 3. After a 6h drying period, the structural monitoring of CF/silicon rubber sensors during concrete's compression is conducted by combination of compressive load tests and electric characterization.

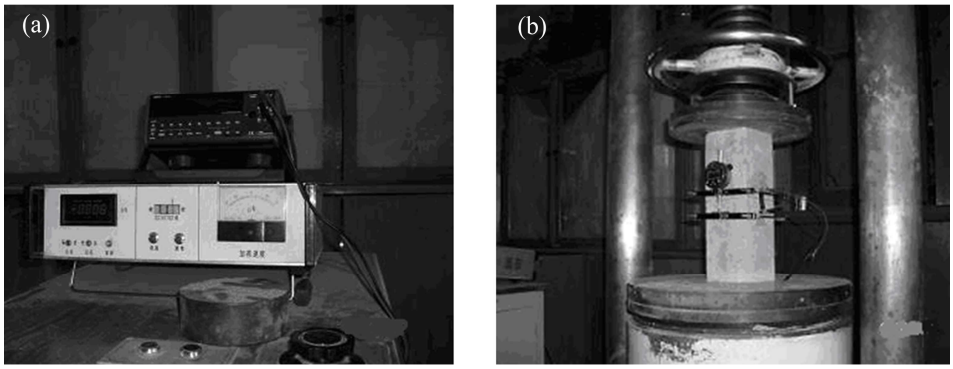

Fig. 3 Equipments (a) and testing (b) images of CF/silicon sensors monitoring the concrete compression

The compressive strain, stress of concrete and the electric resistance of composites were collected until the failure of concrete. It is observed that the four side faces of concretes expand due to the longitudinal compression and the sensors were tensed. Fig. 4 shows the experimental results of concrete and composites with different factions. It is shown that stress-strain curves of concretes could be divided into two phases, namely the elastic (OA) and plastic (AB) phase. Meanwhile the electric resistance curves are also divided into two periods (OA_1 and A_1B) followed along with stress-strain curve. In the first phase, the stress and electric resistance change ratio linearly increase with the strain. But the resistance changes not greatly in this period. During the second phase, the resistance changes frequently and nonlinearly. The micro-cracks expand inside the concrete until the failure of concrete. The results here indicate that the CF/silicon rubber composite sensors could monitor the structural change during the compression process.

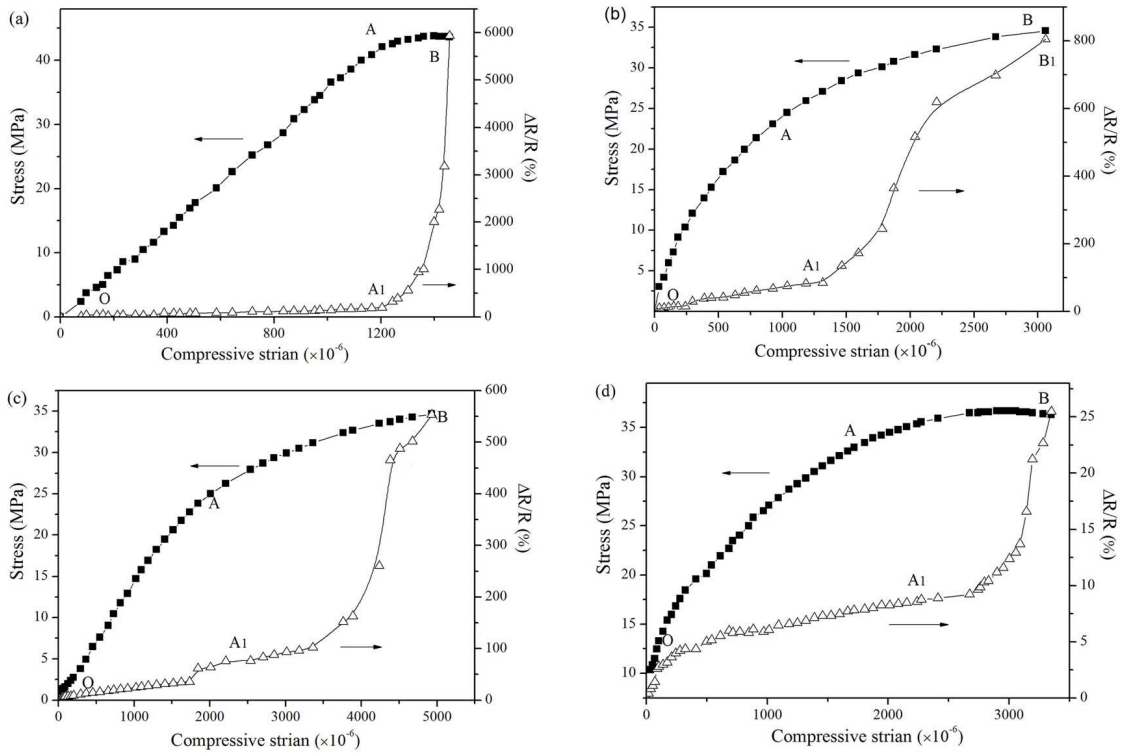

Fig. 4 Sensing curves of composites with different CF fraction 0.84% (a), 1.05% (b), 1.13% (c) and 1.26% (d)

Numerical studies of sensing performation. In order to further describe the sensitivity of CF/silicon rubber composite numerically, the resistance change curves at two phases are fitted seperately. It is obvious that a linear relationship could be established for the first phase and an exponential curve is appropriate for the second phase. The first equation is described as:

$$\Delta R/R=A\varepsilon \quad (0<\varepsilon\leq\varepsilon_0) \tag{1}$$

where A is the coeffiency or the slope of the fitted lines. Fig. 5 shows the fitted curves for the first phase. It is observed that the slope decreases with the increase of fraction of carbon fibre.

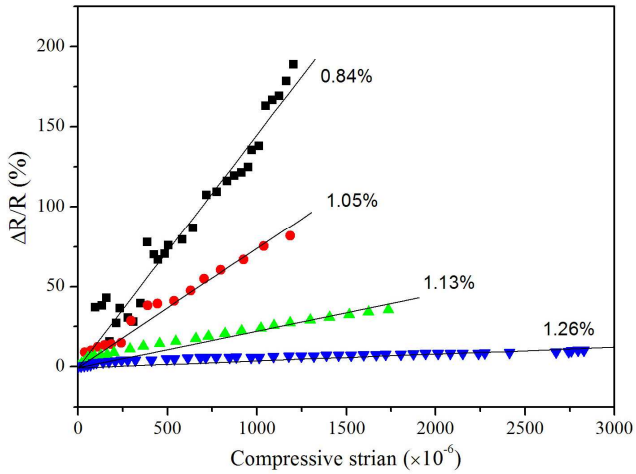

Fig. 5 The experimental and fitted curves about resistance change ratio and compressive strain of composites during the first phase

For the structural health monitoring sensors, one of the most important factors is the strain sensitivity which is expressed as [12]:

$$S_R=\frac{\Delta R/R}{\varepsilon} \tag{2}$$

Thus $S_R=A$ here which means A represents the strain sensitivity. Table 1 shows the calculated results. The sensitivity decreases by two orders of magnitude of composites with the increase of carbon fibre.

Table1 Related fitted parameter during the first phase

Concentration of CF (vol%)	Parameter A	Coefficient of correlation R^2
0.84	1.40×10^5	0.96
1.05	7.06×10^4	0.98
1.13	2.28×10^4	0.98
1.26	3.90×10^3	0.89

For the second phase, the fitted equation could be described as:

$$\Delta R/R=C+D\exp(E\varepsilon) \quad (\varepsilon_0<\varepsilon<\varepsilon_{max}) \tag{3}$$

where C, D and E are coefficients for the exponential curves. Fig. 6 reveals the fitted results and Table 2 shows the calculated factors for the equations. It is demonstrated that the mechanical formation of concrete during compression could be predicted from these equations easily.

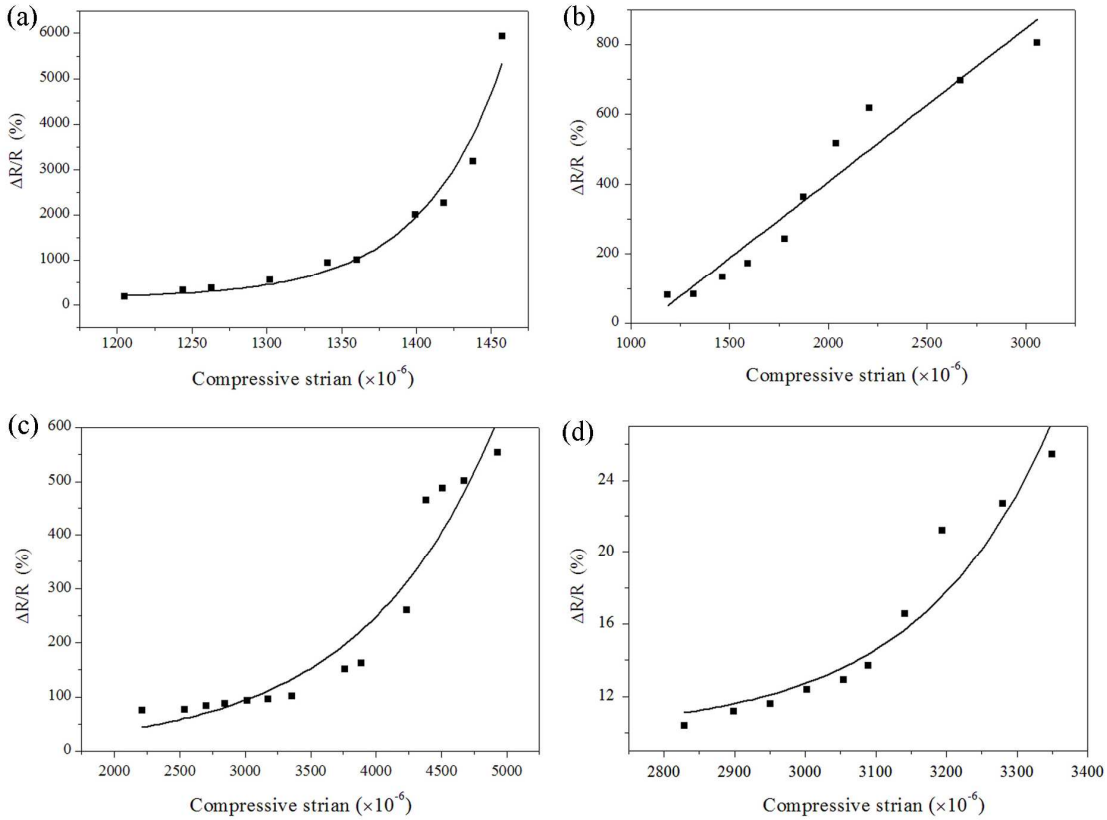

Fig. 6 The experimental and fitted curves of composites with different CF fraction 0.84% (a), 1.05% (b), 1.13% (c) and 1.26% (d) during the second phase

Comparing with these two phases, the monitoring of the latter one is more important due to the heavier destruction. Thus the broad range at second phase is good for the structural health monitoring. According to the results shown in Fig. 4, the optimal fraction of carbon fibre is about 1.10vol%. Based on the relationship between the conductivity of composites and their CF fraction, the percolation threshold is 0.80vol% [11]. The sensing performance shown here proves that CF/silicon rubber composites have excellent structural monitoring properties during concrete compression.

Table 2 Related fitted parameters during the second phase

Concentration of CF (vol%)	C	D	E	Coefficient of correlation R^2
0.84	152.49	1.33×10^{-8}	1.83×10^{4}	0.97
1.05	1.58×10^{6}	-1.58×10^{6}	-0.28	0.94
1.13	1.25	4.884	9.81×10^{2}	0.93
1.26	10.03	3.06×10^{-7}	5.33×10^{3}	0.92

Summary

In this work, the carbon fibre reinforced silicon composites were prepared and their structural health monitoring of concrete in compression was studied. Results show that the electric conductivity of carbon fibre/silicon rubber composites has the synchronous change with the compressive

deformation of concrete. The fitted equations in order to predict the structural change are obtained through segmentation fitting. With the increase of carbon fibre fraction, the sensitivity decreases but the monitoring range expands. The optimal fraction is about 1.10vol% of carbon fibre.

References

[1] P.C. Chang, A. Flatau, S.C. Liu, Review paper: health monitoring of civil infrastructure, Struct. Health Monit. 2 (2003) 257-267.

[2] M. Majumder, T.K. Gangopadhyay, A.K. Chakraborty, K. Dasgupta, D.K. Bhattcharya, Fibre Bragg gratings in structural health monitoring-Present status and applications, Sens. Actuators, A 147 (2008) 150-164.

[3] N.D. Alexopoulos, C. Bartholome, P. Poulin, Z. Marioli-Riga, Structural health monitoring of glass fiber reinforced composites using embedded carbon nanotube (CNT) fibers, Comp Sci. Tech. 70 (2010) 260-271.

[4] H. He, P. Stroeven, M. Sroeven, L.J. Sluys, Influence of particle packing on elastic properties of concrete, Mag. Concrete Res. 64(2) (2012) 163-175.

[5] P. Li, H.C. Gu, G.B. Song, R. Zheng, Y.L. Mo, Concrete structural health monitoring using piezoceramic-based wireless sensor networks, Smart Struct. Syst. 6 (2010) 731-748.

[6] H. Inada, Y. Okuhara, H. Kumagai, Health monitoring of concrete structures using self-diagosis materials, Civ. Struct. Health Monit. 4 (2005) 239-248.

[7] G. Song, Y.L. Mo, K. Otero, H. Gu, Health monitoring and rehabilitation of a concrete structure using intelligent materials, Smart Mater. Struct. 15 (2006) 309-314.

[8] M. Wolf, R. Schmittgens, A. Nocke, D. Hecker, M. Liepelt, E. Schulthei, Plasma deposition of conductive polymer composites for strain sensor applications, Prcedia Chem. 1 (2009) 879-882.

[9] C. Cedric, K. Vladan, L. Maryline, Design and development of a flexible strain sensor for texitile structures based on a conductive polymer composite, Sensors 7 (2007) 473-492.

[10] N. Hu, Y. Karube, M. Arai, T. Watanabe, C. Yan, Y. Li, Y. Liu, Investigation on sensitivity of a polymer/carbon nanotube composite strain sensor, Carbon 48 (2010) 680-687.

[11] L.L. Yang, Y. Ge, Q.H. Zhu, C. Zhang, Z.P. Wang, P.H. Liu, Experimental and numerical studies on the sensitivity of carbon fibre/silicone rubber composite sensors, Smart Mater. Struct. 21 (2012) 035011(5pp).

[12] K.J. Loh, J. Kim, J.P. Lynch, N.W.S. Kam, N.A. Kotov, Multifunctional layer-by-layer carbon nanotube-polyelectrolyte thin films for strain and corrosion sensing, Smart Mater. Struct. 16 (2007) 429-438.

doi:10.4028/www.scientific.net/AEF.5.230

Investigation of the responses of asphalt pavement structure considering load - Poisson's ratio relation

Zhang Lei[1, a], Tan Yi-qiu[2, b*], OuYang Jian[3, c],Gong Xiang-bing[4,d]

[1]School of Transportation Science and Engineering, Harbin Institute of Technology, Harbin 150090, China

[2]School of Transportation Science and Engineering, Harbin Institute of Technology, Harbin 150090, China Corresponding Author.

[3]School of Transportation Science and Engineering, Harbin Institute of Technology, Harbin 150090, China

[4]School of Transportation Science and Engineering, Harbin Institute of Technology, Harbin 150090, China

[a]hit.andy@foxmail.com, [b]tanyiqiu@hit.edu.cn, [c]yijianpiaoqian@126.com, [c]gongxiangbing@126.com

Keywords: asphalt mixture; deformation properties; Poisson's ratio; response of the structure;

Abstract. Poisson's ratio is one of the important parameters that can be used to reflect the deformation characteristics of solid materials. To further understand the mechanical behaviors of materials and improve the accuracy of the finite element simulation results, the Poisson's ratio must be defined accurately. In this paper, DIC technology is employed to investigate the Poisson's ratios of asphalt mixtures under the different gradation and different compaction conditions. It is found that the Poisson's ratios of different asphalt mixture are quite different and the number of compaction had a greater influence on Poisson's ratio. It also showed that Poisson's ratio of asphalt mixture was not a constant under the 25℃ temperature condition, but varied with load. The experiment data suggested that the curve of the load - Poisson's ratio could be divided into three sections through the observation of the graph and it also could be used to investigate the properties of asphalt mixtures deformation resistance. General-purpose finite element software is used to simulate the different contact pressure and Poisson's ratio under dynamic loading condition, in order to find the response of asphalt pavement structure based on the relationship between load and Poisson's ratio. It was found that the relationship of load - Poisson's ratio significantly affected the response of asphalt pavement. It meant that the relationship of load - Poisson's ratio should be considered when designing the asphalt pavement to improve the asphalt pavement service life.

1. Background

Poisson's ratio (μ) and elasticity modulus (E) are the two important parameters that characterize the material properties in the elastic theory analysis. In the design of pavement structure, the modulus values of asphalt mixture varies with temperature, however, the value of Poisson's ratio is always taken as a constant, without considering the effect of variation of Poisson's ratio on the response of asphalt pavement structure. Some researchers [1, 2] have found that Poisson's ratio increases with the rise of temperature and the content of asphalt. Therefore, it is very important to determine Poisson's ratio under different experimental conditions, such as different temperatures, different kinds of asphalt mixture, to improve the accuracy of the mechanical analysis. To achieve this purpose, the deformation of asphalt mixture should be measured accurately. In most of tests, the deformations of materials are measured by the resistance strain gage or LVDT. Such techniques require a large specimen for strain gage placement and impose tight geometry tolerances to minimize variations of strain at the gage location [3], which make it difficult to prepare the specimens, and hardly to address complex mechanical behavior with just a global stress– strain curve obtained by the classic

measurement techniques, especially for some heterogeneous materials. Asphalt mixture is a kind of heterogeneous material, wherein its fracture behavior is complicated and difficult to quantify the deformation parameters because of the difficulties of the observation of the fracture process, especially when the cracks first initiate, they are tiny and random occurrence because of the irregularly shaped and randomly oriented aggregate particles and mastic[4, 5].

To obtain more experimental information, such as microscopic information of the asphalt mixture deformation processes to improve the identification procedures for this type of material, a high resolution and full-field measurement methods are required. One of them is the Digital Image Correlation (DIC) technique [6, 7], an optical and noncontact measurement technique, which is based on a comparative analysis of digital images of the structural member captured at different deformation states. This technique has been applied successfully to various classes of mechanical and civil engineering materials and structural problems [8-11]. There are also some applications to asphalt mixture. Arasan et al.[12]quantified the morphological characteristics of coarse aggregates with digital image processing approach. Kim et al.[13]found that typical dense-graded asphalt mixtures could be characterized for their material properties with an approximate RVE size of 60 mm with the help of DIC technique. Montepara et al. [14] and Birgisson et al. [8]investigated the cracking behavior of HMA mixtures with DIC system and demonstrated the DIC technique overcome the shortcomings of traditional on-specimen strain measurement devices achieving satisfactory accuracy compared to strain gauges.

In this paper, DIC method is introduced to determinate the full-field strain produced by IDT (indirect tension test) to obtained load- Poisson's ratio relation of different asphalt mixtures, and then, the responses of asphalt pavement structure considering load- Poisson's ratio relation will be analyzed by general-purpose finite element software.

2 Materials and experiments

2.1 Materials used

2.1.1 Asphalt and grading

The basic properties of the binder used in this study as per Chinese specifications (JTJ052-2000) are shown in Table 1.

Table 1 The Basic Properties of Asphalts

Evaluation index	Unit	Technical requirements	Test results	Test method (JTJ052-2000)
Penetration (25℃，100g，5s)	0.1mm	60~80	66	T0604-2000
Softening Point ($T_{R\&B}$)	℃	≮55	69.2	T0606-2000
Ductility 5℃ (5cm/min)	cm	≮30	33.9	T0605-1993
Elastic Recovery (25℃，5cm/min，1h)	%	≮65	92.7	T0662-2000
Storage Stability	℃	≯2.5	1.2	T0661-2000

The gradations used in this research are shown in Table 2.

Table 2 Passing percentage of mineral mixtures (%)

Sieve Sizes(mm)	16	13.2	9.5	4.75	2.36	1.18	0.6	0.3	0.075
AC-16	88.7	72.8	45.3	30.8	21.0	15.4	11.8	8.0	6.0
AC-13	95.9	75.3	46.0	31.5	21.0	15.4	11.8	8.0	6.0

The filler used is limestone powder passed through a 200 sieve and the specific gravity of it is 2.740. The polyester fiber (BoniFibers®) content added in the designed asphalt mixture is 0.3% by weight.

2.1.2 Mixture design

The mix design procedures for AC-16 and AC-13 in this paper are determined as per the Chinese specification JTJ052-2000 (T0703-1993). Locally available materials that meet the normal AC-16 and AC-13 specifications are used to produce the mixes. With the asphalt and gradation mentioned

above, five kinds of asphalt mixture (A, B, C, D and E) are made by gyrat ory compaction under the condition of optimal asphalt content to maintain consistency through the study. The results are shown in the following Table 3.

Table 3 The Category of Asphalt Mixtures

Mixture type	The number of gyratory compaction	Asphalt content (%)	Mixture ID
AC-13	90	5.2	A
	125	5.2	B
	205	5.2	C
AC-16	125	4.7	D
	205	4.7	E

2.2 Experimental part

2.2.1 Method of loading

Indirect tension test (IDT) is one of methods widely used in engineering practice to evaluate the mechanical performance of mixture samples under loading [15, 16], which is employed in this research. Laboratory specimens are prepared using Superpave Gyratory Compactor. The specimens are placed in a temperature chamber set to 25℃ for 12h prior to the IDT test, and the test is done using Materials Testing System (MTS-810). The tests are conducted at 25℃ temperature, 10mm/min loading rate to monitor the deformation behavior of mixes with DIC technology.

2.2.2 Method of measuring deformation

In this research, Vic-3D 2010 produced by Correlated Solutions, Inc. was employed. This system is a complete, turn-key system for measuring the shape, displacement and strain of surfaces in three dimensions [17]. The optics adopted at maximum magnification allows 0.01 per pixel resolution. The camera was set up at a distance away from the specimen so that the resulting imaging window was focused on the whole surface of specimen, where Region Of Interest (ROI) is. Once the image sequence of the fracture test has been acquired, the features on the specimen surface are tracked along the sequence to obtain image coordinates.

3 Results and discussion

3.1 Poisson's ratio test results and discussion

Poisson's ratio is one of the fundamental properties of any engineering material. Knowing the value of Poisson's ratio of asphalt mixture is important for evaluation and simulations.

3.1.1 Poisson's Ratio of different asphalt mixture

The ratio between transverse strain ε_x and longitudinal strain ε_y is defined as Poisson's ratio =- $\varepsilon_x/\varepsilon_y$. From DIC test, ε_x and ε_y can be obtained, and then the can be calculated as per above formulation. The results are shown in Fig. 1 and Fig. 2 [18].

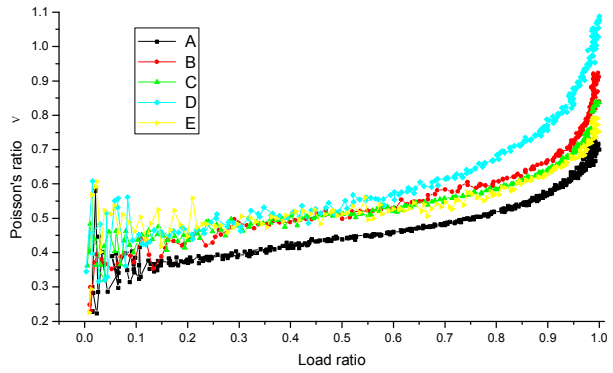

- Load ration=P/P_{max}.

Fig. 1 Curve of Load ration-Poisson's ration

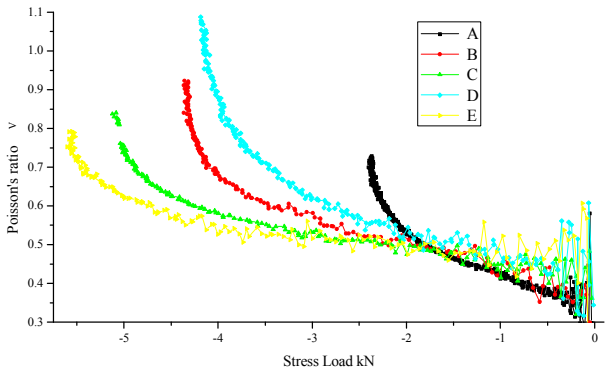

Fig. 2 Curve of Load -Poisson's ration

From Fig.s 1 and 2 it can be found that all the Poisson's ratio of mixture in the initial load are unstable, because of compression process; With the load increasing, Poisson's ratio tends to a stable and linear growth; When the load (or load ratio) exceed a certain point, the Poisson's ratio increases rapidly, eventually leading to destruction of the specimen. Therefore, the load - Poisson's ratio curve can be divided into three phases: initial compression phase, stable development phase and critical limit phase. It is also can be concluded from Fig. 1 and 2 that the Poisson's ration is not a constant for asphalt mixture at 25℃, it is related with the load magnitude.

From Fig. 1 and 2, it can be found that gyratory compaction time has a great influence on Poisson's ration. The fewer gyratory compaction times, the shorter second phase of the load - Poisson's ratio curve and the higher growth rate; it is adverse to mixture performance.

3.1.2 Modeling Poisson's Ratio of different asphalt mixture

It can be known that the Poisson's ration is not a constant from the above result, to improve the computer simulations results, the relationship between Poisson's ration and load should be investigated. In this research, Burges model y=1/[1/a+x/m+1/b*(1-exp(-x*b/n))] is employed to evaluate the relationship of them, the curves are fitted by Origin® 8.1 software. To eliminate the negative effects of the first phase, the fitting starts at -0.5kN. The results are shown in Table 4.

Table 4 Fitting results

Asphalt mixture type	Fitting Function: y=1/[1/a+x/m+1/b*(1-exp(-x*b/n))] Fitting Parameter				R^2
	a	m	b	n	
A	3.0159	-11.0824	-4085034.05	-728566.80	0.99
B	2.5961	-16.9402	-123754201.91	-31285823.93	0.98
C	2.3988	-26.9984	-1151465.34	-480636.92	0.99
D	2.5207	-13.8309	-1467960.42	-466329.25	0.99
E	2.28933	-36.8260	-1765410.79	-778828.82	0.98

It is can be found that Burges model can fit load - Poisson's ratio curve well, and correlation coefficients are all above 0.98.

3.2 Finite element simulation results and discussion

To further investigate the effect of load - Poisson's ratio on the responses of asphalt pavement structure, general-purpose finite element software is employed in this part.

3.2.1 The establishment of finite element model

3.2.1.1 Establishment of the model

Studies have shown when the size of the pavement structure model is greater than 5m × 5m × 5m, structural size has little effect on the calculation results. In this paper, the model size is 6m×5m×5m. The structure of pavement is shown in Table 5.

Table 5 Structure of pavement

Thickness	Possition	Material parameters
4cm	AC-16	E=1200Mpa,
6cm	AC-20	E=1200Mpa
8cm	AC-25	E=1100Mpa, μ=0.35
36cm	Cement-stabilized crushed stones	E=1500Mpa, μ=0.25
20cm	Cement-stabilized gravel	E=2000Mpa, μ=0.30
--	Subgrade	E=50Mpa, μ=0.40

All materials are considered as the elastic material, each structural layer of the pavement is completely continuous contact; the model around boundary is restricted to generate Longitudinal, horizontal and normal displacement, but it can rotate about the normal axis, the bottom cannot move vertically. The element type of FEM model is reduced integrated quadratic three dimensional octahedrons (C3D8R). Then apply more seeds on the area of wheel loading and asphalt mix layers.

Calling subroutine written by FORTRAN through Dload port Abaqus to apply dual-wheeled uniform moving load on model. To eliminate the edge effect and shorten the computation time, the longitudinal end of model on both sides of 0.5m is not applied load, only applying load on the middle of model. The region of load is shown in Fig. 3.

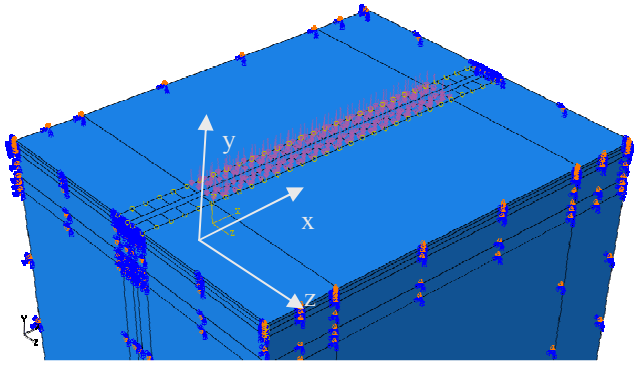

Fig. 3 The region of load

3.2.1.2 Study cases

To study the effect of load- Poisson's ratio relation on the responses of asphalt pavement structure qualitatively, according to the above test results, six cases are determined, they are shown in Table 6 and Table 7.

Table 6 Load and material parameters in different cases

Case		1	2	3	4	5	6
Pressure (Mpa)		0.7	0.9	0.9	1.1	1.1	0.7
Poisson's ratio	Top surface	0.35	0.35	0.40	0.45	0.35	0.40
	Mid surface	0.35	0.35	0.38	0.40	0.35	0.38

Table 7 Material parameters in other layers

Materials	Lower surface	Top base	Lower base	Earth subgrade
Poisson's ratio	0.35	0.25	0.30	0.40

3.2.1.3 Determination of observation position

Studies have shown that the point directly below the wheel load is the most adverse point under static loads. So in this paper, the stress and strain of this point are investigated.

3.2.2 Results and analysis

3.2.2.1 The structural response in various pressures and Poisson's ratio

In this section, Case 1 and Case 6 are selected. The simulation results are shown in Fig. 4.

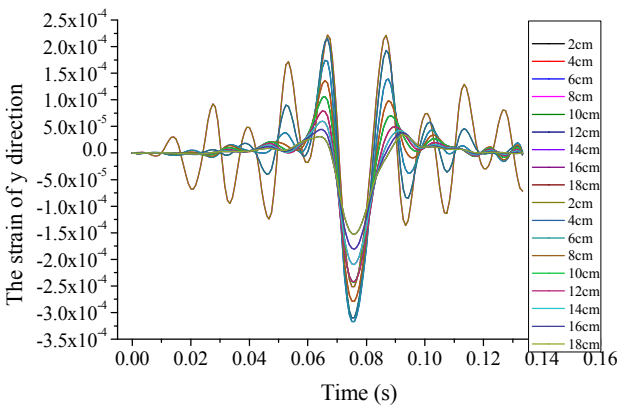

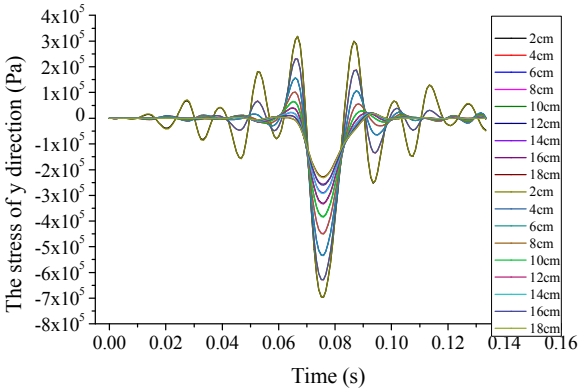

(b)

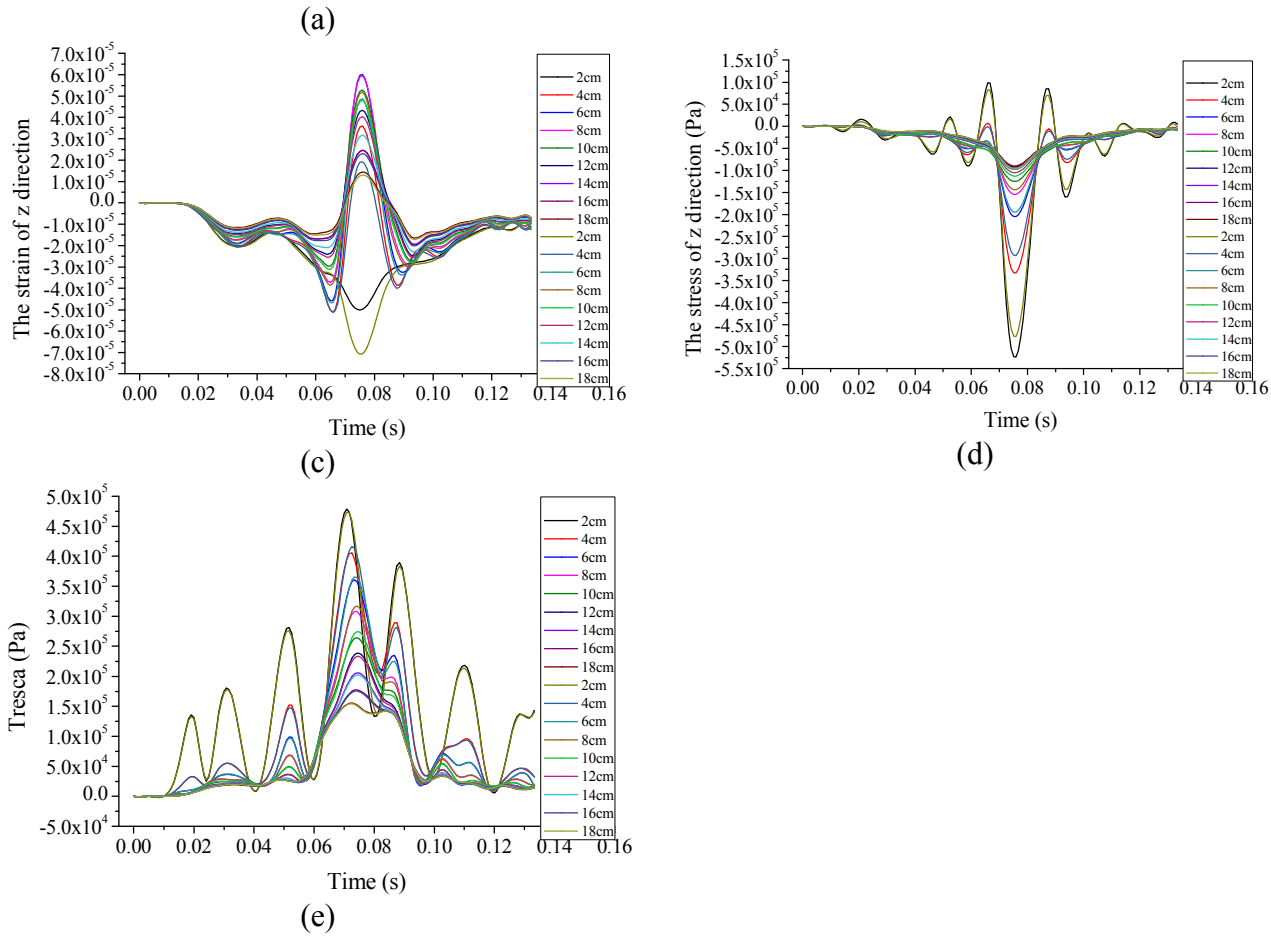

Fig. 4 The simulation results of Case 1 and Case 5

It can be inferred from Fig. 4 that with the load close to the observation point there is a slight stress and strain response; and when the load on the observation point, the response amplitude of structure is max. The stress-strain responses of different depths have the same trend, but different amplitude. From Fig. 4-a and Fig. 4-b it can be found that when the load moves to the observation points, the state of these points are not only the process of compressive stress (compressive strain) formation and dissipation; these points subject to tensile stress before the compressive stress (compressive strain). It means that when load passing, the pavement will subject the compression and shear process. From Fig. 4-c it can be found that when the load on the observation point, there is tensile strain in the direction of z. It also can be inferred from Fig. 4 that when Poisson's ratio changed, the amplitude of responses will be effect, but the laws of responses will be the same.

There is the same law between Case 2 and Case 3and between Case 4 and Case 5, whose results are not shown in this paper.

3.2.2.2 The asphalt pavement structural response considering load- Poisson's ratio relation

To study the effect of load- Poisson's ratio relation on pavement structural response, the strain of z direction at the depth of 6cm in Case 1, 2, 3, 4 and 5 are plotted in Fig. 5.

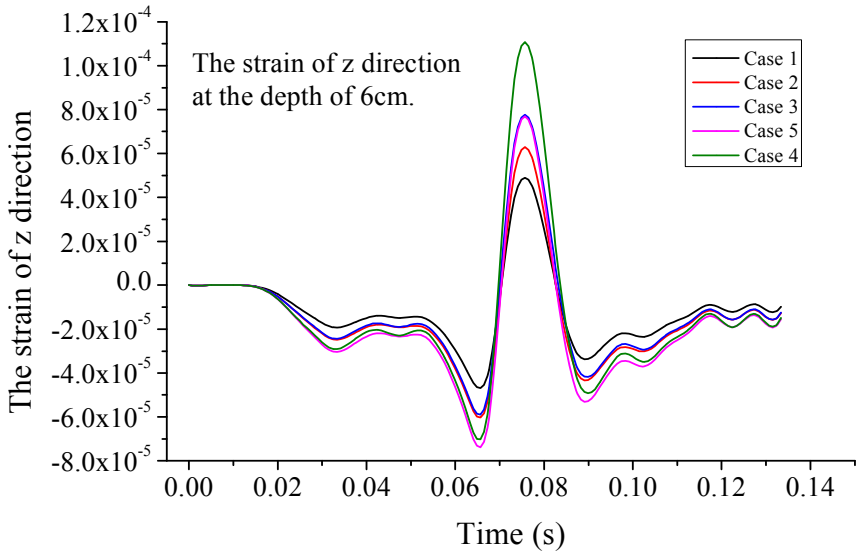

Fig. 5 The strain of z direction under different Cases.

From Fig. 5 it can be found that whether or not to consider the load- Poisson's ratio relation, the strain of z direction at the depth of 6cm will be increased varied with the increase of the load. When without considering the load- Poisson's ratio relation, the increase of transverse deformation is 29.5% when the load increases from 0.7Mpa to 0.9Mpa; when the load increases from 0.7Mpa to 1.1Mpa, the increase of transverse deformation is57.6%. However, when considering the load- Poisson's ratio relation, the increase of transverse deformation is 59.6% when the load increases from 0.7Mpa to 0.9Mpa; when the load increases from 0.7Mpa to 1.1Mpa, the increase of transverse deformation is127.5%. It means that the load- Poisson's ratio relation has the significant effect on the transverse deformation of asphalt pavement. The greater load, the more significant effect.

Excessive transverse deformation would lead to transverse flow, which is one of the reasons that lead to rut. Therefore, the load- Poisson's ratio relation should be considered when designing the asphalt pavement, especially in heavy-load and overload pavement, to ensure the pavement life.

4 Conclusions

Based on the testing and analysis presented herein, the conclusions of the study are summarized as follows:

(1) The load - Poisson's ratio curve can be divided into three phases and the Poisson's ratio is not a constant for asphalt mixture at 25℃, it is related with the load magnitude; The number of gyratory compaction has the great effect on the deformation properties of asphalt mixture, the more number of gyratory compaction, the better deformation resistance.

(2) When load passing, the pavement will subject the compression and shear process. When the load is on the observation point, there is tensile strain in the direction of z. It also can be inferred from Fig. 6 that when Poisson's ratio changed, the amplitude of responses will be effect, but the laws of responses will be the same.

(3) Whether or not to consider the load- Poisson's ratio relation, the strain of z direction at the depth of 6cm will be increased varied with the increase of the load, but the load- Poisson's ratio relation has the significant effect on the transverse deformation of asphalt pavement. The greater load, the more significant effect.

(4) Excessive transverse deformation would lead to transverse flow, which is one of the reasons that lead to rut. Therefore, the load- Poisson's ratio relation should be considered when designing the asphalt pavement, especially in heavy-load and overload pavement, to ensure the pavement life.

Acknowledgement

The authors are grateful to the financial support by National Natural Science Foundation of China (50808058 & 51101138), and many thanks should be given to Guo Meng for his help.

References:

[1] Palit, S.K., Reddy, K.S.,Pandey, B.B. Laboratory evaluation of crumb rubber modified asphalt mixes. J Journal Of Materials In Civil Engineering, 2004, 16(1), 45-53.
[2] SHAO, X., SHAO, M., BI, Y.,SUN, L. Testing Method of Asphalt Mixture Poisson Ratio. J Journal of Tongji University(Natural Science), 2006(11), 1470-1474.
[3] Makeev, A., Ignatius, C., He, Y.H.,Shonkwiler, B. A Test Method for Assessment of Shear Properties of Thick Composites. J Journal Of Composite Materials, 2009, 43(25), 3091-3105.
[4] Kim, H., Wagoner, M.P.,Buttlar, W.G. Micromechanical fracture modeling of asphalt concrete using a single-edge notched beam test. J Materials And Structures, 2009, 42(5), 677-689.
[5] Issa, M.A., Islam, M.S.,Chudnovsky, A. Size effects in concrete fracture - Part II: Analysis of test results. J International Journal Of Fracture, 2000, 102(1), 25-42.
[6] Pan, B., Wang, Z.,Xie, H. Generalized spatial-gradient-based digital image correlation for displacement and shape measurement with subpixel accuracy. J Journal Of Strain Analysis For Engineering Design, 2009, 44(8), 659-669.
[7] Sutton, M.A., Wolters, W.J., Peters, W.H., Ranson, W.F.,McNeill, S.R. DETERMINATION OF DISPLACEMENTS USING AN IMPROVED DIGITAL CORRELATION METHOD. J Image And Vision Computing, 1983, 1(3), 133-139.
[8] Birgisson, B., Montepara, A., Romeo, E., Roncella, R., Roque, R.,Tebaldi, G. An optical strain measurement system for asphalt mixtures. J Materials And Structures, 2009, 42(4), 427-441.
[9] Birgisson, B., Montepara, A., Romeo, E., Roque, R.,Tebaldi, G. Influence of Mixture Properties on Fracture Mechanisms in Asphalt Mixtures. J Road Materials and Pavement Design, 2010, 11, 61-88.
[10] Toussaint, E., Destrebecq, J.F.,Ferrier, E. Analysis of Cracks and Deformations in a Full Scale Reinforced Concrete Beam Using a Digital Image Correlation Technique. J Experimental Mechanics, 2011, 51(6), 879-890.
[11] Jolin, M., Kuntz, M., Bastien, J., Perez, F.,Hild, F. Digital image correlation analysis of crack behavior in a reinforced concrete beam during a load test. J Canadian Journal Of Civil Engineering, 2006, 33(11), 1418-1425.
[12] Arasan, S., Yenera, E., Hattatoglu, F., Hinislioglua, S.,Akbuluta, S. Correlation between Shape of Aggregate and Mechanical Properties of Asphalt Concrete Digital Image Processing Approach. J Road Materials and Pavement Design, 2011, 12(2), 239-262.
[13] Kim, Y., Lee, J.,Lutif, J.E.S. Geometrical Evaluation and Experimental Verification to Determine Representative Volume Elements of Heterogeneous Asphalt Mixtures. J Journal Of Testing And Evaluation, 2010, 38(6), 660-666.
[14] Montepara, A., Romeo, E., Birgisson, B.,Tebaldi, G. Strain Localization and Damage Distribution in SBS Polymer Modified Asphalt Mixtures. J Road Materials and Pavement Design, 2010, 11(4), 899-915.
[15] Lytton, R.L., J. Uzan, E.G.F., R. Roque, D.H.,Stoffels., S. Development and Validation of Performance Prediction Models and Specifications for Asphalt Binders and Paving Mixtures. J Report SHRP-A-357, Strategic Highway Research Program, Washington D.C., USA, 1993.
[16] Buttlar, W.G.,Roque., R. Development and Evaluation of the Strategic Highway Research Program Measurement and Analysis System for Indirect Tensile Testing at Low Temperature. J Report TRB1454, Transportation Research Board, Washington, D.C. USA., 1994.
[17] http://www.correlatedsolutions.com/index.php/products/vic-3d-2010.
[18] Tan Yi-qiu, Zhang Lei, Guo Meng, Shan Li-yan and Zhang Kui. Investigation of the deformation properties of asphalt mixtures with DIC technique. J Construction and Building Materials, 2012.

doi:10.4028/www.scientific.net/AEF.5.238

The Freeze-Thaw Resistance of Concrete Control Structure for Debris Flow on Tianshan Highway

HUANG- Yong[1,2,a], XU Huining*[3,b], CHEN-Hongkai[4,c]

[1]State Key Laboratory of Geological Hazard Prevention and Geological Environment Protection, Chengdu University of Technology, Chengdu 610059, China;

[2]Xinjiang Traffic Science Institute of Communication, Urumqi 830000, China;

[3]Harbin Institute of Technology, Nangang District, 92 Xidazhi Street, Harbin 150001, China;

[4]Chongqing Jiaotong University, 66 Xuefu Avenue, Chongqing 400074, China

[a]476786514@qq.com, [b]email: xhn1983@163.com, [c]chk99@163.com

*Corresponding author : XU Huining

Key Words: Tianshan Highway; Debris Flows; Concrete Structure; Freeze-Thaw

Abstract: The extreme climate in Tianshan area has a significant impact on the freeze-thaw resistance of concrete control structure for debris flow. This paper describes a fiber reinforced concrete designed for Tianshan area. The impact factors on the freeze-thaw resistance of concrete are analyzed. The optimal composition for concrete control structure is discussed. And the engineering economic of such material is compared with that of Portland cement concrete. Research results shows fiber reinforced concrete can greatly improve the freeze-thaw resistance of concrete, and significantly extend its life with a great of practical value.

Introduction

Tianshan Mountains located in the Northwest of China, belongs to warm areas and boreal-arid areas, poor relief, the temperature changes. Polar minimum temperature is up to -35℃, the average winter temperature is -12.2℃, and the winter period will last as long as 4 to 6 months. As the long cold winter season, it brought a lot of problems for the project construction. After freezing and thawing, concrete often happens internal cracking, surface sapling, its quality and intensity decreased significantly; seriously affect the structure of using safety reduction its serviceable life. Thus, study on the corresponding concrete debris flow control structures in the area of anti-freeze-thaw performance and enhance its anti-freeze-thaw method of performance have also become a highway construction and maintenance of a key issue.

1 Research ideas

Antifreeze is able the concrete to harden in the negative temperature, and achieve the desired performance under the provided conditions. The affection of freeze-thaw on concrete is strong, because of the specificity environment on Tianshan area. Freeze-thaw resistance, anti-cracking performance and its dense closely related fibers crack resistance. The study plans to use to add fly ash, fiber, antifreeze and other ways to improve the concrete of the antifreeze. By comparing the ordinary cement concrete, freeze-thaw resistance of different fibers and antifreeze amount concrete, and drawn the affection of concrete for freeze-thaw resistance from fibers antifreeze content and the relations between amount content and anti-freeze-thaw concrete ,finally the conclusion that the amount fibers and antifreeze optimal mix.

2 Construction of test model

2.1 Raw material selection

Necessary indicators of raw materials for the tests are as follows: ① cement (C): P325 ordinary Portland cement; ② natural sand (S): ③ middle sand, fineness modulus 2.7; ④ gravel (G): diameter 5mm ~ 20mm , well-graded; ⑤ antifreeze: FJW-14 composite antifreeze; ⑥ super plasticizer: with the series of antifreeze super plasticizer, by the same water rate and antifreeze; ⑦ Fiber: polypropylene fiber, length of 12mm; ⑧ Fly: Ⅱ-class fly ash.

2.2 Test Options

According to “Design Manual of Concrete Mix" select raw materials and mix design, combined with the control structures features of debris flow on Tianshan highway, selecting the design strength grade of concrete is C30, each group shown in Table 1.

Table 1 Ratio of concrete specimen

Test ID	Cement [kg]	Sand [kg]	Lithotripsy [kg]	Water [kg]	Fly Ash [kg]	Cryoprotectants [%]	Fiber [%]	Super plasticizer [%]
S	313	595	1264	162	66	/	/	1
A1	313	595	1264	162	66	4	0.3	/
B1	313	595	1264	162	66	4	0.4	/
C1	313	595	1264	162	66	4	0.6	/
A2	313	595	1264	162	66	5	0.3	/
B2	313	595	1264	162	66	5	0.4	/
C2	313	595	1264	162	66	5	0.6	/
A3	313	595	1264	162	66	6	0.3	/
B3	313	595	1264	162	66	6	0.4	/
C3	313	595	1264	162	66	6	0.6	/

The sample size is 100mm × 100mm × 100mm, each group has 3 samples, a total of 30 group specimens. Using artificial mixing produces concrete specimen, the mixing concrete put into steel, vibration molding, add standard conservation.

2.3 Experimental study on freeze-thaw resistance of concrete

2.3.1 Test program of freeze-thaw resistance

According to the "ordinary concrete long-term performance and durability testing methods" (GBJ82-1985) implementation, using slow freezing and thawing froze Act. During the trial test is divided into three aspects: (1) All samples of the compressive strength of the standard conservation 28d; (2) freeze-thaw samples before freezing and thawing, after freezing and thawing 25 times the sample quality and strength; (3) the compressive strength of freezing and thawing test pieces.

2.3.2 Analysis of test data

(1)Benchmark specimen strength of 28d

28d compressive strength of concrete was measured in each group (Table 2).

Table 2 Specimen baseline strength test for 28d

Specimen No	Compressive strength [MPa]			The representative value [MPa]
S	31.7	32.6	33.4	32.57
A1	32.9	34.6	33.8	33.77
A2	34.7	33.7	36.2	34.87
A3	34.8	33.8	35.4	34.67
B1	35.8	33.0	30.9	33.23
B2	33.2	35.8	30.4	33.13
B3	31.9	31.3	29.2	30.80
C1	29.4	29.9	30.1	29.80
C2	30.5	31.4	30.6	30.83
C3	26.5	32.6	31.4	31.40

Concrete compressive strength is the trend of downward. Apart from individual points (4 ‰fiber content 6% antifreeze), other points of strength with the volume change antifreeze range small, amount of antifreeze can be seen for a relatively small impact on the strength of concrete. Antifreeze content of 6%, the concrete compressive strength of a larger magnitude of changes, trends vary uncertainties more.

Different fiber content of the larger changes in the strength of concrete, up to 4mpa, therefore, the impact of fiber on the compressive strength of concrete is significant. Fiber content is 3 ‰, antifreeze content is 5%, the compressive strength of concrete is the highest, antifreeze content is 6%, its strength is in a slightly lower intensity; fiber content is 4 ‰, compressive of concrete volume is in the antifreeze 4%,obtain the maximum intensity is 6% ,it may be in a larger attenuation; fiber content in the 5 ‰, the compressive strength of concrete in the antifreeze content of 6% ,obtain the maximum, minimum 4% Department, and three The difference between values is not great. When the fiber content is up to 5 ‰, compressive strength is far less than other samples, and observes the specimen, fiber distributed unevenly, and the fiber content unsuitable 5 ‰.

(2)Strength loss rate of freeze-thaw specimen

By 25 times of freeze-thaw cycle, the freeze-thaw test piece, the test items of compressive strength is in Table 3. This shows that the number for the S concrete strength loss rate of 14.72 % of all samples of the maximum intensity of the loss, mixing fibers and antifreeze can significantly improve the performance of concrete antifreeze. ΔF_{cmax}= 14.72 %, far less than 25%, indicating that the sample can withstand repeated freeze-thaw cycles.

Table 3 The record of loss rate for freeze-thaw cycles 25 times about strength

Specimen No.	After the freeze-thaw [MPa]	Before the freeze-thaw [MPa]	Strength loss rate [%]
S	30.87	36.20	14.72
A1	32.2	36.93	12.81
A2	32.47	36.87	11.93
A3	32.77	35.43	7.51
B1	33.13	37.67	12.05
B2	32.87	36.86	10.82
B3	32.60	34.50	5.51
C1	32.03	35.77	10.46
C2	32.37	35.80	9.58
C3	34.10	35.90	5.01

When the fiber content certain, the strength of concrete with antifreeze loss rate showed a significant increase in volume decline. Fiber content is 3 ‰, the antifreeze content is 4%, when the intensity of the biggest losses, 5% loss of slightly lower intensity, 6% dropped, when the intensity of the loss; fiber content is 4 ‰, the antifreeze content is 4 % to obtain the maximum intensity of 6% when the smallest loss; fiber content is 5 ‰, the antifreeze content is 4% to get a maximum, minimum 6 percent. With the freeze-thaw damage and lower fiber content an increase that is doped fiber strength loss of concrete freezing and thawing significantly weaken the role. Curve similar to the three parallel, and antifreeze content from 5% to 6%, when the mass loss of a significant reduction of compressive strength attenuation lesser extent, different fiber content of freeze-thaw loss of strength followed by size: 3 ‰> 4 ‰ > 5 ‰.The results show that the fiber content has an important effect on the strength of concrete undergoing the freeze-thaw cycle. The main reason is the combined effects of fiber reinforced flexible network skeleton.

Maintaining the same amount of antifreeze, fiber content increase by 3 ‰, 4 ‰, 5 ‰, the strength of concrete increases ,when the fiber content loss. Fiber content unchanged, antifreeze content will grow from 5% to 6%, the strength of concrete will fall in a sharp losses. With the increasing amount of antifreeze compound, concrete primer gas also increased, these bubbles uniformly distributed in concrete and isolated and cut off the pores road, slowing the expansion of concrete when cold changes, thereby ,it will improve the concrete of frost resistance significantly . Antifreeze content is 6%, the strength of concrete loss lower than 4%, 5%, different content of freeze-thaw about intensity of antifreeze followed by the size of the loss rate: 4%> 5%> 6%.

(3)Mass loss rate of freeze-thaw specimen

Concrete due to freeze-thaw erosion by frost heave pressure cracking, spilling produce mass loss, while structural damage of strength reduction is to speed up, it seriously affects the use of structures security. Through the analysis of freezing and thawing frozen samples before and after the quality, mass loss is from the maximum value for the S group of concrete (0.32%), far less than 5% .All the concrete mix can withstand many freeze-thaw cycle times (Table 4).

Table 4 The mass loss rate and freeze-thaw specimen

No.	①			②			③			Loss rate [%]
	Original Quality	Freezing Quality	Loss	Original Quality	Freezing Quality	Loss	Original Quality	Freezing Quality	Loss	
S	2.446	2.438	0.008	2.47	2.461	0.009	2.476	2.469	0.007	0.32
A1	2.435	2.445	10	2.435	2.429	0.006	2.475	2.485	10	0.25
A2	2.445	2.443	0.002	2.47	2.461	0.009	2.475	2.508	33	0.22
A3	2.426	2.42	0.006	2.388	2.385	0.003	2.427	2.425	0.002	0.15
B1	2.545	2.559	14	2.485	2.479	0.006	2.41	2.42	10	0.24
B2	2.41	2.404	0.006	2.418	2.416	0.005	2.384	2.4	16	0.23
B3	2.38	2.377	0.003	2.47	2.464	0.006	2.368	2.365	0.003	0.17
C1	2.473	2.471	0.002	2.4	2.395	0.005	2.373	2.367	0.006	0.18
C2	2.42	2.418	0.002	2.444	2.454	10	2.395	2.387	0.008	0.21
C3	2.453	2.45	0.003	2.49	2.485	0.005	2.486	2.482	0.004	0.16

When fiber content decreases; antifreeze content is 6%, the mass loss of the maximum value appears in 4 ‰, and the minimum value is still achieved in 5 ‰. Mass rate of concrete will Loss, when the fiber content increases. Fiber content for is 4 ‰, 5 ‰, the mass loss of concrete changes are uniform, and fiber content is 5 ‰, the concrete mass loss much lower than the other two contents. And antifreeze content is 6%, it increases after the mass loss reduction, quality, larger changes, the laws of different fiber content in the quality of 3 ‰ for the loss and the other two points of a large margin. After analysis, we can see that the role of antifreeze bleed air caused by uneven and fiber content.

Concrete mass loss, when the fiber content reduces. Fiber volume is 3 ‰, 4 ‰ hours, the volume increase in antifreeze, concrete specimen mass loss rate of decline and antifreeze which content 4%, 5% will change in a small range. The fiber content of the 5 ‰, the mass loss rate is the smallest.

(4)Comprehensive analysis

In summary, select 6‰ antifreeze and 5 ‰ fiber consumption, when the concrete frost resistance for the best. At the same time, according to analysis of relevant data, we can see that fiber content for the 5 ‰ (C1, C2, C3) and B3 Group compressive strength of concrete for 28d is lower, it is difficult to ensure that the structural strength of concrete to meet the requirements. While the remaining groups of concrete benchmarks strength for 28d, freezing and thawing of concrete specimen strength and mass loss in Table 5 as below.

Table 5 Concrete benchmarks strength, strength loss rate and mass loss rate of 28d

Specimen No.	28d baseline intensity [MPa]	Strength loss rate [%]	Mass loss rate [%]	Options
A1	33.77	12.81	0.25	
A2	34.87	11.93	0.22	Program I
A3	34.67	7.51	0.15	Program II
B1	33.23	12.05	0.24	
B2	33.13	10.82	0.23	Program III

According to Table 5, it can be determined three options:

Program I, fiber content is 3 ‰ and antifreeze volume is 5% (A2); Program II, fiber content is 3 ‰ and antifreeze volume is 6% (A3); Program III, fiber content is 4 ‰ and antifreeze content is 4% (B2). We can see that the program I is the best program.

3 Development of freeze-thaw resistance materials for the control structure of debris flow and mix design

Through comparison and contrast the compressive strength of concrete specimen and mass loss, before or after freezing and thawing, we received two add admixture groups' higher performance. Because of large sections project along the Tianshan highway, requires large quantity of raw materials, which must be from the perspective of economic analysis and sets of programs on the feasibility and applicability (Table 6). After comparison and contrast, the second program of prices is more cost-effective for choice. If the special sections need for high strength concrete, we selected the first group program.

Table 6 Material price list of selection program

Material	Cement (C)	Natural sand (S)	Lithotripsy (G)	Antifreeze	Super plasticizer	Fiber	Fly Ash	Total [Yuan]
Program1	86	46	80	45	0	42.55	60	317.003
Program2	86	46	80	36	0	42.55	60	308.003
Plain concrete	86	46	80	0	9.5	0	60	281.503

(Note: This price is based on Urumqi prices; even each cubic of raw materials prices is the total sum)

4 Conclusions

In the high-altitude and high cold of Tianshan areas, it assumes ordinary concrete life cycle is 6 years, According to the relevant conclusions of the pilot project, the freeze-thaw resistance of control structure (Program1) for debris flow about life cycle is 9 years, but the freeze-thaw resistance of control structure for ((Program1) debris flow control structure of the life cycle is 13.2 years. If control structure of debris flow need total volume of concrete for 9000m3, According to a period of 25 years calculated, ordinary concrete needs 6,776,250 Yuan, but the freeze-thaw resistance of control structure concrete ((Program1) need for 6.75 million Yuan, the freeze-thaw resistance of control structure concrete ((Program2) need 4,815,341 Yuan, if add the construction and other costs, the total cost of freeze-thaw resistance of concrete were significantly less than the ordinary concrete (ordinary concrete has a short life cycle, need more cycle construction costs and other building maintenance costs).

References:

[1] N. Qian, Z. H. Wan. Sediment Movement Mechanics [M]. Beijing: China Science Press .1983
[2] H. K. CHen, H. M. Tang, Y. T. Ma. Research and Prevention of Highway Debris flow [M]. Beijing: China Communication Press .2004
[3] H. K. Chen, H. M. Tang, Y. T. Ma. Research and new prevention concept of large highway debris flow [J]. Highway . 2(2004)
[4] B. X. Tang, S. C. Zhang. Debris Flow Study [J]. Journal of Chinese Academy of Sciences Institute.1992, (2):119-123
[5] J. S. Wu, L. H. Tian. Study on the Debris Flow [J]. Mountain Research, 1996, 14 (2):26-33
[6] G. X. Chen,J. K. Wang. Debris Flow Control [M]. Beijing: China Railway Publishing House .1983:30-48

doi:10.4028/www.scientific.net/AEF.5.243

Dynamic Characteristics of Rubber Powder Modified Cement Asphalt Mortar

LI Yunliang[1,2,a], OU Yangjian[1,b] ,TAN Yiqiu[1,c] ,LU Mingyu[3,d]

[1]School of Transportation Science and Engineering, Harbin Institute of Technology, Harbin 150090, P.R.China

[2]Post-doctoral Research Center in Civil Engineering, Harbin Institute of Technology, Harbin 150090, P.R.China

[3]Department of Mechanical Engineering, The Hong Kong Polytechnic University, Hong Kong, China

[a]liyl-hit@163.com, [b]yijianpiaoqian@126.com, [c]yiqiutan@163.com, [d]lmyhaerbin@yahoo.com.cn

Keywords: cement asphalt mortar (CA), rubber powder, natural frequency, damping

Abstract. Cement asphalt mortar (CA) is mainly applied in track system of high-speed railways for vibration attenuation. The impact on dynamics performance of CA with the admixture of rubber powder was studied. The beam specimen made of CA was manufactured for analyzing its vibration frequency and damping characteristics by free attenuation vibration tests. Results showed that there was no big change for fundamental frequency after admixture of rubber powder. However, high order frequency and structural damping increased with the increase of admixture amount. Damping ratio of CA was increased by admixing rubber powder, which can be better for energy absorption and vibration attenuation.

Introduction

Cement asphalt mortar (CA) is the key engineering material in the slab track system of high-speed railways. It is a kind of inorganicorganic composite material consisting of Portland cement, asphalt emulsion, water, fine aggregates, and other admixtures. It is a semi-rigid composite material of which, the matrix is formed by cement hydration and emulsified asphalt breaking. CA is injected in between the track slab and concrete roadbed (Fig.1), and it is an essential supporting and force transmission component, which can provide adequate rigidity and toughness for the track[1,2].

During the last decade, research has mainly focused on various aspects of CA, such as formulation, construction technology, mechanical properties and durability [3-7].Vibration attenuation effect on CA has been less involved in recent research. High-speed trains have a great impact on sub-rail foundation under operation. The existence of CA can consume the energy produced during impact procedure, making vibration and impact effect be reduced to ensure train operation stable and comfortable. CA can also decrease force impact on sub-rail foundation and reduce maintenance and repair costs to keep the whole line in an outstanding service performance for a long time. Thus vibration attenuation effect is considered as one of the most important functions of CA. The vibration attenuation function was improved by admixing rubber powder into CA and the CA beam specimen was applied to evaluate the vibration frequency and damping characteristics by free attenuation vibration tests. The impact on dynamics performance of CA with the admixture of rubber powder was analyzed and estimated.

Materials and experimental investigation

Materials. Cement(C): were ordinary portland cements P.I 42.5, The properties of the three cements were listed in Table 1. Asphalt emulsion(A): anion slow-breaking emulsion asphalt. The properties of the three asphalt emulsion were listed in Table 2. Sand(S) is graded sand blended by two single size

sand of 0.15~0.3mm(S1), 0.3~0.6mm(S2). Water(W) was tap water. Water reducing agent(WT) is polycarboxylic type superplasticizer. Defoamer(D) is tributyl phosphate. Fineness of rubber powder (RP) can be divided into three groups as 30~50 mesh, 50~100 mesh and 100~200 mesh.

Table 1 Physical properties of cements

Surface density (g/cm^3)	Setting sime(min)		Compressive strength(MPa)		
	Initial set	Final set	3d	7d	28d
3.05	135	180	15	21.5	46.9

Table 2 Properties of anion asphalt emulsion

Density (g/cm^3)	Storage stability 5d (%)	Sieve test (%)	Penetration (25)	Solid content (%)
1.01	0.1	0.02	79	60

Preparation of CA. Ratio of raw materials for CA takes cement as benchmark and other materials are provided according to mass ratio of cement. Rubber powder was added into raw materials instead of the same mass asphalt to make sure the total mass of raw materials is a constant. Dosage of sand was reduced to keep the volume of raw materials as a constant. (mix proportions of cement mortar was listed in Table 3). To simulate the mixing sequence in the field, raw materials were weighed and homogenously mixed according to the mixing sequence in Fig.2. Fresh mortar was then cast into 403403160 mm^3 molds. Specimens were demoulded after 1 day and cured at 60±5% relative humility and 20±2°C temperature until the age of 28 days.

Table 3 Mix proportions of CA

C	A+RP	S	W	RP	WT	D	AI
1	0.22	1.6	0.4	0.03,0.06,0.09	0.012	0.001	0.00004

[a]All mass ratios are relative to cement. Ratio for total mass of asphalt and rubber to cement is 0.22, rubber instead of asphalt with the same mass.
[b] Water in the asphalt emulsion is counted into the calculation of W/C.

Experimental methods

Natural frequency and damping ratio of specimen were obtained by free attenuation vibration tests. One end of the beam was fixed as boundary condition. Excitation was applied using modal force hammer. Structural responses were measured by acceleration transducers. Data were collected and analyzed by model recognition software to obtain natural frequency and damping ratio of specimen.

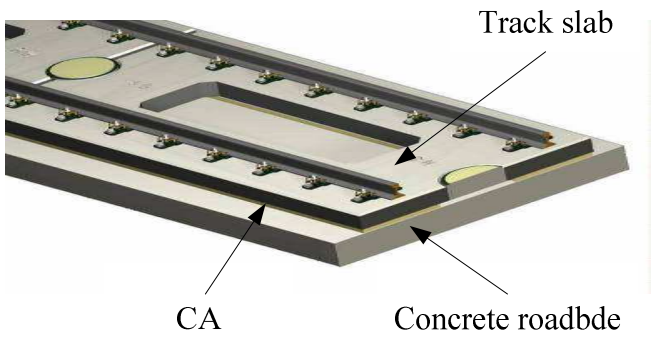

Fig.1 Structure of slab track

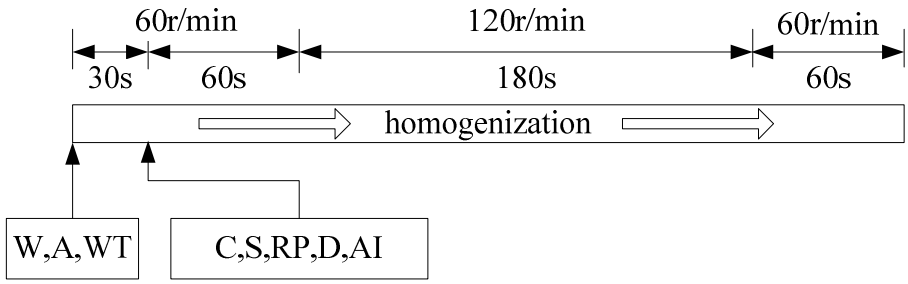

Fig.2 Mixing sequence of CA

Results and discussions

Effect of rubber powder on natural frequency of CA. Figures 3 to 5 show effects of different rubber powder quantities on structural vibration frequency. Quantities of rubber powder are 0, 0.03, 0.06 and 0.09 (mass ratio to cement), respectively. Effects due to different degrees of rubber powder particles (30-50 mesh, 50-100 mesh and 100-200 mesh) were considered. Experimental results indicate that the first three order natural frequencies without rubber powder are 152Hz, 197Hz and 225Hz. First order frequency varies from148 Hz to 156 Hz after admixture of rubber powder. Maximal change is only 3.9% in first order frequency which indicates that rubber powder in different thick degrees have little effect on first order frequency. Quantity of rubber powder has big effects on second and third natural frequencies of structure with 8.6% increase in second order frequency and 33.3% increase in third order frequency. With the increase of rubber powder amount, second and third order frequencies generally increase and, the thicker the rubber particle, the more effect on frequency.

Effect of rubber powder on CA damping. Figure 6 is a curve showing effect of rubber powder amount on structure damping. Structural damping increases with the increase of rubber powder amount. The damping is 2.75% without rubber powder and increases to 3.5% (27.3% change) when rubber powder amount is 0.09. The thinner the rubber powder, the more effect on structure damping. Thus introducing thinner rubber powder can effectively increase structure damping to enhance energy absorption and vibration attenuation functions of CA.

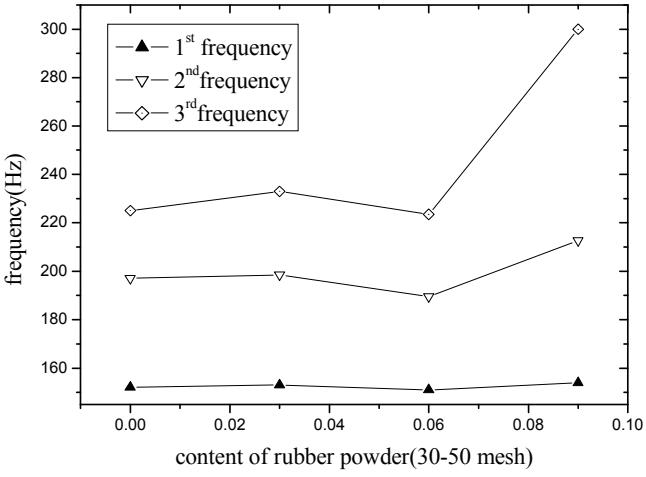

Fig.3 Effect of rubber powder onfrequencies(30-50 mesh)

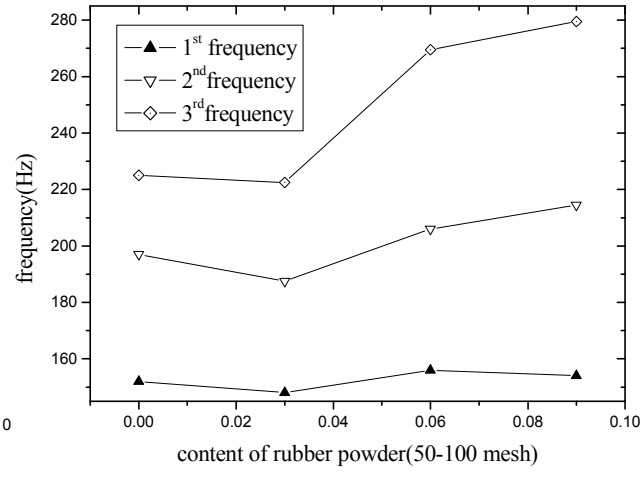

Fig.4 Effect of rubber powder on frequencies (50-100 mesh)

Rubber is a kind of high elastic damping material. Elastic deformation performance of CA mortar is increased after admixture of rubber powder to absorb more energy and increase structure damping, which has little effect on structural fundamental frequency simultaneously.

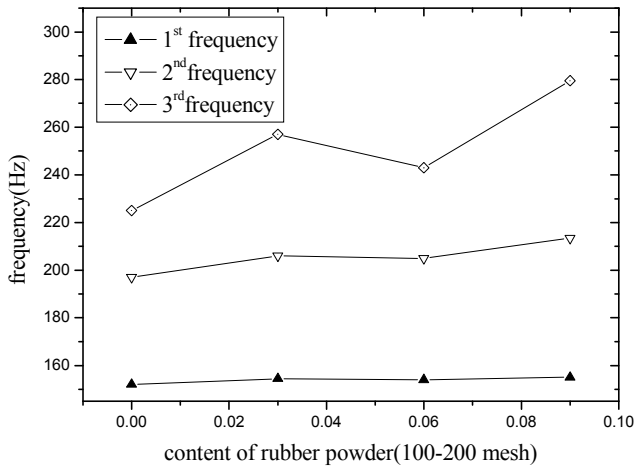

Fig.5 Effect of rubber powder on frequencies (100-200 mesh)

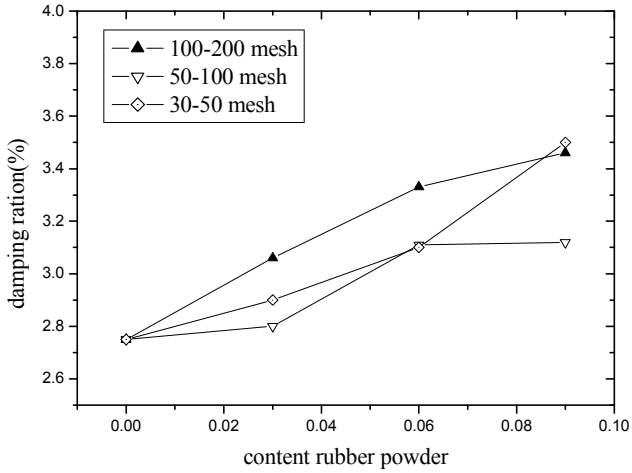

Fig.6 Effect of rubber powder on damping (50-100 mesh)

Conclusions

Natural frequency and damping characteristics of cantilever beam specimen made by CA with different admixtures of rubber powder were analyzed using free attenuation vibration tests. Experimental results indicated that there was no big change in fundamental frequency after admixture of rubber powder in CA, but great effects existed on high order frequencies. Damping ratio of beam specimen increased with the increase of rubber powder amount. Rubber powder can improve damping performance of CA for better usage in energy absorption and vibration attenuation.

Acknowledgements

Research support by the National Natural Science Foundation of China(NO.51078114) and Research Fund for the Doctoral Program of Higher Education of China(NO.20102302120058) is gratefully acknowledged.

References

[1] Huawu He. The technology of ballastless track. Beijing: China railway publishing house, 2005 (Chinese)

[2] Wang Fazhou, Liu Zhichao, Wang Tao. A novel method to evaluate the setting process of cement and asphalt emulsion in CA mortar. Mater Struct , 2008,41:643-649

[3] Liu YL, Kong XM, Zou Y, Yan PY. Static and dynamic mechanical behavior of cement asphalt mortars. J Railway Sci Eng, 2009,6(3):1-7 [Chinese].

[4] Yang JB, Yan PY, Kong XM, Li X. Study on the hardening mechanism of cement asphalt binder. Sci Chin: Technol Sci, 2010,53(5):1406-1417

[5] Hu SG, Wang T, Wang FZ, Liu ZC, Gao T, et al. Influence factors on freezing and thawing durability of cement asphalt mortar. J Wuhan Univ Technol, 2008,30(8):30-32 [Chinese]

[6] Yanrong Zhang, Xiangming Kong, Shanshan Hou, Yongliang Liu, Song Han. Study on the rheological properties of fresh cement asphalt paste. Construction and Building Materials, 2012,27:534-544

[7] Shuguang Hu, Yunhua Zhang, Fazhou Wang. Effect of temperature and pressure on the degradation of cement asphalt mortar exposed to water. Construction and Building Materials, 2012,34:570-574

doi:10.4028/www.scientific.net/AEF.5.247

The Research on Equipment for Detecting Strength of Shallow Asphalt Pavement under Ice Frozen

Zhao Maocai[1a], Ji Lun[1b], Gao Shixian[1c]

[1]School of Transportation Science and Engineering, Harbin Institute of Technology, Harbin, China, 150090

[a]Zhao_maocai@126.com, [b]jilun@hit.edu.cn, [c]gaoshixian0424@163.com

Keywords: Asphalt pavement; Penetrating Strength Detector of Shallow Pavement; Falling distance; Penetrator Probe

Abstract: Aiming at detection of strength of shallow asphalt pavement under ice frozen, this thesis has developed the Penetrating Strength Detector of Shallow Pavement through finite element numerical simulation, whose theory is based on evaluating strength of asphalt pavement by penetrating depth of the penetrator impacting into asphalt pavement.

Introduction

The ice frozen phenomenon has generally occurred to the pavements in the moist plateau district of southwest China, which has tended to get worse in recent years. The freeze-thawing effect due to ice frozen phenomenon has led to weakness and destruction of the shallow asphalt pavement, and then diseases such as cataclasm, stripping, pit slot, loosening etc. turn up. How to evaluate ice frozen effect to the strength of asphalt pavement accurately is of great actual significance for establishment of deuteric maintenance and repair plan.

Nowadays, relevant non-destructive inspection methods to evaluate strength of asphalt pavement on spot conclude Benkelman Beam, Falling Weight Deflectometer(FWD), Rolling Dynamic Deflectometer(RDD), Traffic Speed Deflectometer(TSD) etc, which own a common feature that the measurement index is deflection, while deflection is defined as reflection of the combined strength of pavement structure layers under loading points, and the strength value of asphalt shallow pavement remains unavailable[1-4].

The thesis has developed the Penetrating Strength Detector of Shallow Pavement through finite element numerical simulation, whose theory is based on evaluating strength of asphalt pavement by penetration depth of the penetrator impacting into asphalt pavement. This new-style instrument is able to evaluate strength of shallow asphalt pavement quickly, possessing extensive applicability and wide prospect.

Design principle of Penetrating Strength Detector of Shallow Pavement

The thesis draws lessons from the operating principle of Dynamic Cone Penetrator (DCP)[5]. Falling hammers of certain sizes will be designed and made to fall free from a certain height, generating impact force that can inject the penetrator into pavement with a certain depth. The whole working process will be simulated by finite element method to confirm the specification of the detector.

Selection of instrumental components based on finite element analysis

Three types of falling hammers are drafted initially for the instrument, according to hammering energy, divided as 5kg, 10kg, and 15 kg. Falling distance of hammers sets as 0.5-0.8m; there're also 4 types of penetrators with the height of 120mm, according to diameter, divided as 12mm, 10mm, 8mm and 6mm.

The thesis has simplified the impacting and penetrating simulation and only established a penetrator-pavement model instead, while function from falling hammer to penetrator is simply to impacting load upon the penetrator. Considering the size of penetrator is relatively small to pavement structure and the detection aim is strength of pavement surface layer, a pavement model by length*width*height=1.0m*1.0m*0.15m is sufficient for accuracy requirement. The penetrating depth is setting as about 10cm.

Considering the process of penetrator impacting into pavement has a significant effect only to a small region around the penetrator and the actual situation of the chosen pavement model, boundaries and underside of the model are totally fixed， that is U1=U2=U3=UR1=UR2=UR3=0; and symmetry planes adopt symmetrical boundary condition, that is U3=UR1=UR2=0 and U1=UR2=UR3=0; top surface remains free. The boundary condition is shown in Figure 1[6].

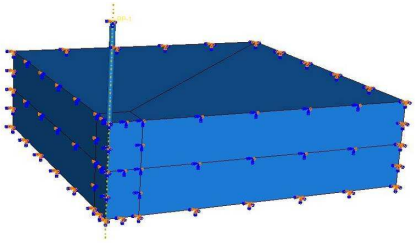

Figure 1. Boundary condition of finite element model

The thesis has conducted grids division to the asphalt pavement model in numerical simulation. We choose 8-node solid element C3D8R of reduced integration as pavement element and explicit linear three dimensional stress elements C3D4 as penetrator model [7]. In order to improve the accuracy of simulation and calculation, the region of pavement structure affected by penetrator has been divided to grids as shown in Figure 2.

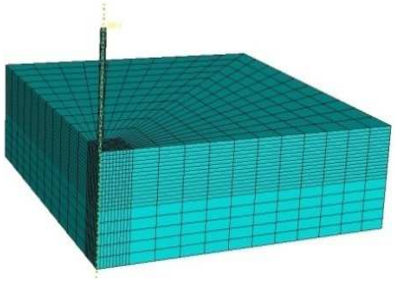

Figure 2. Grids division of finite element model

Considering the force applied to asphalt pavement is instantaneous impact load, we can ignore the viscous effect to material and assume that asphalt concrete only presents elastoplasticity, therefore the D-P Model is chosen to simulate asphalt concrete. The material parameters of finite model are shown as Table 1, 2 and 3.

Table 1. Material parameters of pavement model

Elastic modulus (MPa)	Poisson's ratio	Density (kg/cm^3)	Damping
13400	0.25	2.4	0.9

Table 2. Parameters of D-P model

Angle of friction	Flow stress ratio	Dilation angle
30°	1	30°

Table 3. Material parameters of penetrator model

Elastic modulus (MPa)	Poisson's ratio	Density (kg/cm3)
210000	0.3	7.85

The instantaneous impacting force of penetrator F varying with time t is a half-sine relationship: $F=F_0 \sin wt$. According to momentum theorem, the impacting load from falling hammer to penetrator can be calculated by $\int_0^{0.0004} F_0 \sin \omega t dt = \Delta mv$ as Table 4 shows. Falling distance chooses 0.5m.

Table 4. Impact load

Hammer weight(kg)	5kg	10kg	15kg
Impacting load(N)	6146.7	12293.4	18440.1

We can get 4 series of relationship as follows by software calculating:

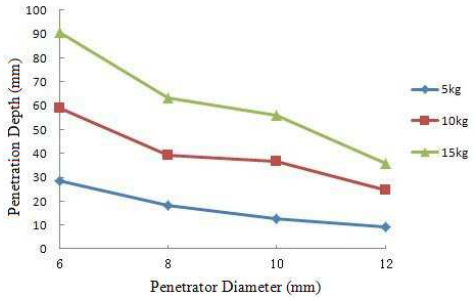

Figure 3. Relationship between penetration depth and penetrator diameter

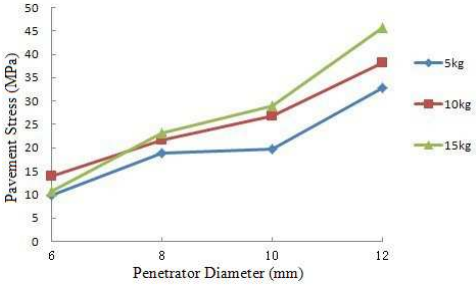

Figure 4. Relationship between pavement stress and penetrator diameter

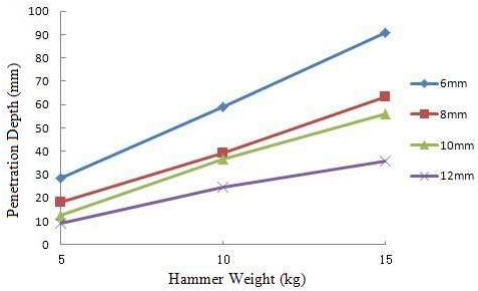

Figure 5. Relationship between penetration depth and hammer weight

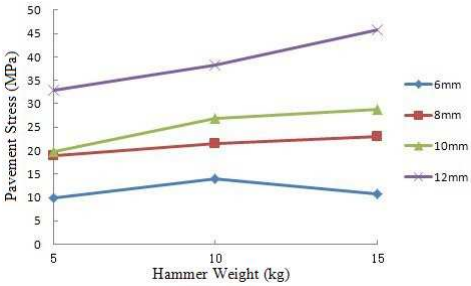

Figure 6. Relationship between pavement stresses and hammer weight

Analyzing the data from 4 pairs of relationship above, the penetrator with diameter of 12mm and the falling hammer weighing 15kg will generate oversized stress to pavement and result in destruction; while stress and penetration depth of the 6mm-diameter penetrator and the falling hammer weighing 5kg will make the reference standard lose the relevant part of high pavement strength in follow-up research, which is uncompleted.

In summary, the penetrators with diameter of 8mm and 10mm as well as hammer weighing 10kg are determined to be the main instrumental components.

Design of the Penetrating Strength Detector of Shallow Pavement

The Penetrating Strength Detector of Shallow Pavement is mainly consisted of 4 parts as whole supporting structure, guide bar, falling hammer and penetrator, shown in Figure 7.

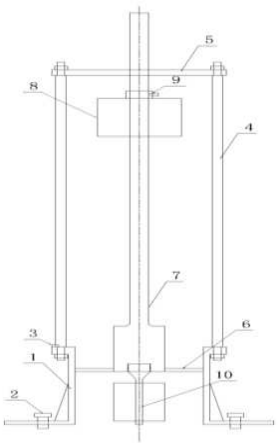

Figure 7. Design chart of Penetrating Strength Detector of Shallow Pavement

1.Bottom fixed barrel; 2.Leveling bolt; 3.Leveling bubble; 4.Fixed bar; 5.Top guide disc;

6. Bottom guide disc; 7.Guide bar; 8.Falling hammer; 9.Block button; 10. Penetrator probe.

The entitative structure of the Penetrating Strength Detector of Shallow Pavement is shown in Figure 8.

Figure 8. Penetrating Strength Detector of Shallow Pavement

After the establishment of reference standard through comparison with other indoor experiment results, this detector can conduct impacting penetration experiments to evaluate strength of pavement indirectly after suffering ice frozen damage, which is characterized by simple operation, convenient application, clarity and accuracy of data collecting, etc.

Conclusion

According to analyzing and calculating results, conclusions can be figured out as follows:

The design range of falling hammers of the Penetrating Strength Detector of Shallow Pavement is 5kg, 10kg and 15kg, and the hammer weighing 10kg is chosen as main instrumental component.

The design range of falling distance of the Penetrating Strength Detector of Shallow Pavement is 0.5-0.8m.

The penetrator height of the Penetrating Strength Detector of Shallow Pavement is 120mm. There’re 4 types of penetrators classified by diameter as 12mm, 10mm, 8mm and 6mm. The depth of measurement can reach 100mm.

The thesis has developed the entitative structure of the Penetrating Strength Detector of Shallow Pavement.

The determination of corresponding reference standard between falling distances, diameter of penetrator, penetration depth and pavement strength about the Penetrating Strength Detector of Shallow Pavement will get further demonstration in other thesis.

Summary

This research is Sponsored by the department of China science ministry No: 2008BAG10B02.

References:

[1] Wang Wenming. Preliminary Studies on Detection of Pavement Deflection[J]. Liaoning Traffic Technology, 1999, 22(5):14-15.

[2] Li Jianhua. Application of Falling Weight Deflectometer in Road Construction Control[J]. Journal of Changsha University(Engineering and Technology Edition), 2002(2):10.

[3] J A Bay, K H Stokoe. Project Sunmary Report 1422-3F, Development of a Rolling Dynamic Deflectometer for continuous Deflection Testing of Pavements[R]. Center for Transportation Research, Bureau of Engineering Research, The University of Texas at Austin, 1998: 24-28.

[4] Abdel-Khalek, Ahmed Moustafa. Pavement Structural Evaluation Using the Rolling Wheel Defectometer[D]. Louisiana State University, M D. 2011,11.

[5] Kleyn E G, Van Van Zyl G D. Application of the Dynamic Cone Penetrometer(DCP) to Light Pavement Design[J]. Proceedings of First International Symposium on Penetration Testing. Orlando Florida. A. A. Balkema Publishers, Rotterdam, Netherlands. 1988: 435-444.

[6] R I Macckie. Object oriented Programming of the finite element method[J]. International Journal for Numerical Methods in Engineering, 1992, 35(2): 425-436.

[7] Hibbit, Karlsson, Sorensen. ABAQUS Theory Manual[R], Pawtucket: America ABAQUS Inc, 2001.

doi:10.4028/www.scientific.net/AEF.5.253

Experimental Study on Factors Affecting Interlayer Shear Strength of Fiber Seal

CAO Peng[1,a], FENG Decheng[2,b] GONG Chunwei[3,c] and ZHAO Yin[4,d]

[1]School of Transportation Science and Engineering, Harbin Institute of Technology, Harbin, China

[2]School of Transportation Science and Engineering, Harbin Institute of Technology, Harbin, China

[3]School of Transportation Science and Engineering, Harbin Institute of Technology, Harbin, China

[4]CCCC Second Highway Consultants Co. Ltd. Wuhan, China

[a]caopeng518888@126.com, [b]fdcgxy@vip.sina.com,

[c] gcw1988@gmail.com, [d]zhaoyin.hit@gmail.com

Keywords: Fiber Seal; Orthogonal Test; Grey Relational Analysis

Abstract: In order to study influence of different factors on interlayer shear strength of fiber seal, an orthogonal experiment about four factors, respectively, test temperature, fiber content, asphalt content and gravel coverage, and three levels are developed with bevel shear test. The influence rules are evaluated by range analysis method. The result demonstrated that fiber content is the most correlative influencing factor. Thus provides a basis for the selection of material and performance of the fiber seal.

Introduction

Fiber seal, which can be used as wearing course and stress absorbing layer [1], composes with hierarchically sprinkling asphalt, fiber and gravel. The structure of fiber seal is shown in Fig.1. Intensive work had been carried out during the past decades worldwide. Ball et al explored the factors affecting multiple chip seal layer instability[2]. Lee and Richard Kim presented a method to determine the optimal protocol for rolling chip seals based on aggregate retention performance and aggregate embedment depth, a third-scale model mobile loading simulator (MMLS3) were employed[3]. Huurman developed a 3D meso-mechanical FE model of a seal and obtained stresses and strains that developed in the various relevant structural components of the seal[4]. Fiber seal has been significantly applied in a series of projects since introduced into China in 2007[5,6] because of its superior performance in waterproof, stress absorbing and bonding properties[7]. Practical application indicated that the capacity of bonding with pavement layer was a key property of fiber seal[8]. However, due to no thorough and systematic studies on the influencing factors, there is a lack of clear guiding ideology for material selection and performance evaluation of fiber seal.

The bonding capacity of fiber seal varies with variable parameters. In this article, shear strength is taken as a evaluation index, four parameters, *A*- fiber content, *B*- asphalt content, *C*- gravel coverage and *D*- test temperature, are selected as influence factors. Meanwhile, three typical levels of each factor are selected according to engineering practice to design orthogonal test, then evaluating the influence rules on the test index with rang analysis and grey correlation analysis (GRA) method. This research could provide theory basis for the material selection of fiber seal.

Interlayer Shear Strength Experiment

Experiment Principle

Bevel shear test is a better way to simulate the stress state of pavement under load compared to direct shear test [9]. The principle of bevel shear test is shown in Fig.1. Two same forces appear on parallel and perpendicular cross sections under the load *T*. T_h is the shearing action on interface what makes specimen failed.

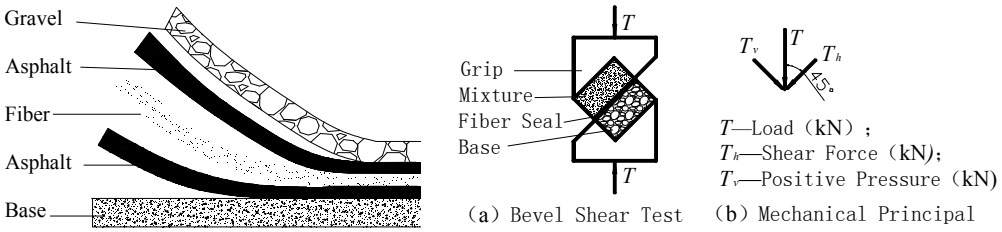

Fig.1. Structure of Fiber Seal and Schematic Diagram of Bevel Shear Test

Material Composition and Performance

Anda 90# road petroleum asphalt is used as binder of fiber seal (SHRP-H-355, 1993), technical specifications are listed in Table 1.

Table 1. Anda 90# Road Petroleum Asphalt Technical Specifications

Test parameters	Penetration (25℃,100g,5s)	Ductility (15℃,5cm/min)	Softing point $T_{R\&B}$	Density (15℃)
Units	[0.1mm]	[cm]	[℃]	[g/cm^3]
Test result	90	＞150	45.0	1.015

Particle size of 3~5mm granite gravel is chosen as aggregates of fiber seal, graduation of gravel is listed in Table 2. Specifications of gravel and polyester fiber are recorded in Table 3 and Table 4, respectively.

Table 2. Graduation of Gravel

sieve size [mm]	16	9.5	4.75	2.36
percent of pass [%]	100	100	7.5	0

Table 3. Technical Specification of Fiber Seal Aggregate

Test projects	Crushing value [%]	Water absorption [%]	Apparent density [g/cm^3]	Adhesion of asphalt
Test result	10.5	0.51	2.81	5 grade
standard	≤14	≤2.0	≥2.60	≥4 grade

Table 4. Technical Indicators of Polyester Fiber

Test projects	Density [g/cm^3]	Oil absorption rate[%]	Moisture content [%]
Result	1.36	350	0.2

Specimen Molding Method

The size of specimen is 150 mm×150mm×150mm , of which the height of semi-rigid base and asphalt mixture is 70mm respectively. Fiber seal is made between the base and upper layer. To match the actual construction process better[2], the technological process of fiber seal in laboratory is described as follows:

(1) Preparing semi-rigid base; (2) Heating the asphalt and gravel to 170℃ ± 5℃ and then spreading a certain quality of asphalt onto base surface; (3) Spreading fiber and compacting; (4) Spreading another layer of asphalt; (5) Spreading gravel and compacting; (6) Shaping asphalt mixture as upper layer on top of fiber seal. The technological process of fiber seal is shown in Fig.2.

a.Prepare base b.1st layer of asphalt c. fiber d. 2nd layer of aspha e. spread gravel

Fig. 1. Process of Laboratory Production

The experiment was conducted per material test system (MTS 810) after the specimens cured 7d, loading in strain control mode, at a speed of 3.5mm/min [10], collecting the failure loads T and converting into shear strength.

Orthogonal Test

Fiber content (*A*), asphalt content (*B*), gravel coverage (*C*) and test temperature (*D*) are the factors to be observed, there are three levels of every factor, as shown in Table 5.

Table 5. Experiment Factor Levels

Level	Factors			
	A	*B*	*C*	*D*
1	40	1.3	35	5
2	60	1.6	50	20
3	80	1.9	70	35

Table $L_9(3^4)$ was chosen in the orthogonal test and 9 groups of samples were tested based on Table 6, in which homologus shear strength is also listed.

Table 6. L_9 (3^4) Orthogonal Test and Result

No.	*A*	*B*	*C*	*D*	Shear Strength [MPa]
1	1 (40)	1 (1.3)	1 (35)	1 (5)	0.38
2	1	2 (1.6)	2 (50)	2 (20)	0.73
3	1	3 (1.9)	3 (70)	3 (35)	0.48
4	2 (60)	1	2	3	0.82
5	2	2	3	1	1.04
6	2	3	1	2	0.93
7	3 (80)	1	3	2	0.25
8	3	2	1	3	0.44
9	3	3	2	1	0.78

Range Analysis

In range analysis, range *R* typifies the influence degree on experiment index of every factor, the result is shown in Table 7. Fig.3 reflects the change trend of shear strength with influence factors.

Conclusions can be drawn from Table 7 and Fig.3:

(1) Fiber content is the most important factor affecting the shear strength of fiber seal, next are asphalt content and gravel coverage, test temperature is the smallest factor.

(2) According to the range value, to take account of getting higher shear strength, the suggested composition is $A_2B_2C_2D_1$, namely, fiber content is 60g/cm^2, asphalt content 1. 6g/cm^2, gravel coverage 50% and test temperature 5℃.

(3) With fiber content increasing, shear strength improves firstly and then reduces. Shear strength meet peak when fiber content reaches 60%. This phenomenon indicates the appropriate amount of fiber can improve the bonding performance of fiber seal, while excessive amounts leads to poor bonding strength. Gravel coverage has similar rule.

(4) Shear strength increases firstly and obtains the maximum value when asphalt content attains 1.6 g/cm^2, then grows down smoothly with increasing in asphalt content, with the increment of temperature, shear strength decreases monotonically.

Table 7. Visual Analysis of Result

Parameter	Result of visual analysis of shear strength			
	A	*B*	*C*	*D*
k_1	0.53	0.48	0.58	0.73
k_2	0.93	0.74	0.78	0.64
k_3	0.49	0.73	0.59	0.58
Range *R*	0.44	0.25	0.19	0.15
Order of factors	*A*>*B*>*C*>*D*			
Optimal level	60	1.6	50	5
Optimal composition	$A_2B_2C_2D_1$			

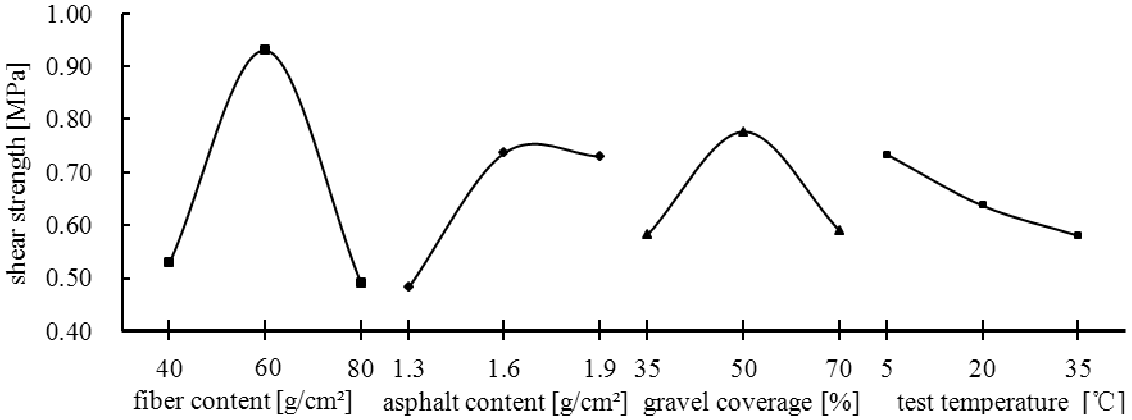

Fig.3. Relationship of Index with Influencing Factors

Grey Relational Analysis

GRA is used to analyze correlativity of influencing factors taking grey correlation degree (GCD) as estimating indexes [11]. Studies have shown that GRA is an effective means to deal with the orthogonal test result [12,13]. The steps of GRA include: (1) Establishing the comparative sequence and the referenced sequence; (2) Initializing the data because of the different dimensions or units of each factor; (3) Obtaining absolute difference of the comparative sequence and the referenced sequence; (4) Seeking for the extremums among absolute difference; (5) Calculating coefficient in GRA and GCD; (6) Arranging and analyzing grey correlations. GCD is shown in Table 8.

Table 8. Grey Relational Coefficient and GCD

No.	Influencing factors			
	Fiber content	Asphalt content	Gravel coverage	Temperature
1	1.000	1.000	1.000	1.000
2	0.760	0.809	0.833	0.584
3	0.917	0.936	0.879	0.337
4	0.816	0.716	0.780	0.376
5	0.703	0.660	0.732	0.627
6	0.755	0.748	0.669	0.653
7	0.685	0.895	0.743	0.466
8	0.776	0.976	0.949	0.333
9	0.982	0.832	0.802	0.735
GCD	0.822	0.841	0.821	0.568

The influence of each comparative sequence on a reference sequence will be clear from the arrangement of grey correlation degree. The conclusion draw from Table 8 is that the factors can be arranged in the order of effecting scale on shear strength as follows: asphalt content >fiber content > gravel coverage > temperature.

Conclusion

In this paper, an orthogonal test was developed to explore the factors affecting interlayer shear strength of fiber seal, and the conclusions can be drawn as follows:

(1)Visual analysis shows that the shear strength of fiber seal increases firstly, and then decreases with the increment of material content, while decreases monotonically with the increment of temperature.

(2) To get the maximum of shear strength, the suggested composition is that fiber content is 60g/cm^2, asphalt content 1.6g/cm^2, gravel coverage 50% and temperature 5℃.

(3) Both the results of range analysis and GRA demonstrate that the fiber content is the most correlative influencing factor, next is asphalt content, which means it's important to control fiber and asphalt content in selection of materials.

References

[1] F.J.Benson, and B.M.Galoway, Retention of cover stone by asphalt surface treatments. bulletin 133, Texas Engineering Experiment Station, Texas A&M University System, College Station, Texas, 1953.

[2] G.F.A.Ball, J.E.Patrick and P.R.Herrington, Factors affecting multiple chip seal layer instability. Land Transport New Zealand Research Report, (2005), No. 278.

[3] J.Lee and Y.R.Kim, Determination of the optimal number of coverages for the rolling of chip seals. Can. J. Civ. Eng. 37 (2010) 54-65.

[4] SHRP-H-355, Innovative Materials Development and Testing Volume4: Joint Seal Repair. Strategic Highway Research Program National Research Council, Washington, D.C. (1993) 31-52.

[5] X.H.Yan, J.C.Yu and J.G,Wang, Introduction and application of fiber seal. Northern Communications, 8 (2008) 50-53.

[6] Z.H.Zhang, A new technology of highway construction and maintenance, Petroleum asphalt, 22 (6) (2008) 41-43.

[7] D.D.Gransberg and D.M.B.James, Chip seal best practices. National Cooperative Highway Research Program Report Synthesis 342, Transportation Research Board, National Research Council, Washington, D.C., 2005.

[8] Committee of State Road Authorities, Surfacing seals for rural and urban roads, Technical Recommendations for Highways, RSA Department of Transport, South Africa, 1986.

[9] ASTM, Standard test method for sweep test of bituminous emulsion surface treatment specimen, ASTM D 7000-04, American Society for Testing and Materials, West Conshohocken, Pa (2004).

[10] D.C.Feng and Y.Song, Study of test and evaluation method on interfacial combining state of asphalt pavement. Journal of Harbin Institute of Technology, 39 (4) (2007) 627-631.

[11] J.L.Deng, Basic method of grey system. Wuhan: Huazhong Uinversity of Science and Technology Press, (1987) 17-42.

[12] Z.Y.Lei, Grey Correlation Analysis on Logistics Energy Consumption, ICCTP, (2009) 3216-3221.

[13] C.L.Zhang, Q.Y.Meng and S.Han, Analysis of Influence Factors of Modified Asphalts Performance Based on Orthogonal Design and Grey Relation Degree Theory, Highway, 11 (11) (2009) 191-195.

doi:10.4028/www.scientific.net/AEF.5.259

Mechanics and pavement properties research of nanomaterial modified asphalt

CHEN Shang-jiang[1, a], ZHANG Xiao-ning[2, b]

[1] School of Transportation science and engineering, Harbin institute of technology, Harbin 150001, China; Guizhou Transportation Planning Survey & Design Academe Co., Ltd, Guiyang 550001, China

[2] School of Transportation science and engineering, Harbin institute of technology, Harbin 150001, China

[a] email：553075780@qq.com, [b] email：prozxn@163.com

Key Words: Road engineering, nanomaterial modified asphalt, nano powdered rubber, mechanics performance

Abstract: Nanomaterials (nano powdered rubber VP401, VP501 and sepiolite and $CaCo_3$ composites) were selected to improve the high-temperature and low-temperature performance of asphalt binder. Nanomaterial modified asphalt was prepared using the high shear machine. Laboratory experiments of asphalt binder and asphalt mixture were conducted to evaluate the properties of modified asphalt binder, including the penetration, ductility, softening point, viscosity, and etc. Also, asphalt mixture tests were carried out, such as the cleavage strength test, resilient modulus test, rutting test, water stability test and etc. Based on the test results, asphalt binder modified by 1% nano powdered rubber VP401 has better performance resistance to low temperature crack and rutting, compared to other nanomaterial modified asphalt binder.

Introduction

Transportation infrastructure construction, especially the highway and rural highway construction, makes communication among the areas more easily, also makes the national travel more convenient. The time required in the trip becomes shorter than before. At the same time, it is good for improving the investment environment, attracting and gathering funds, technology and talents together. These advantages accelerate the regional economic development and regional progress. During the service years, asphalt pavement diseases were come out and emphasized, such as cracking and rutting [1]. In order to delay the asphalt aging time and extend the service life of the asphalt pavement, asphalt modification research is significant from the material standpoint.

Numerous research work of modified asphalt has been done in China. Luan, et al presented the low temperature performance evaluation results of SBS modified asphalt binder [2]. Three kinds of base asphalt binder and five kinds of SBS modified asphalt binder were prepared to be analyzed. Results showed the low temperature performance of SBS modified asphalt was better through the BBR test analysis, and the low temperature property of linear SBS modified asphalt was better than the star SBS modified asphalt. Tan, et al [3] studied the low temperature cracking performance of diatomite asphalt binder and mixture, and analyzed the control asphalt and three kinds of modified asphalt using differential scanning calorimetry (DSC) and temperature-stress analysis. From the results of low temperature bending test, low temperature compression test and shrinkage test, that low temperature of diatomite modified asphalt binder is better than control asphalt binder was concluded. Liu, et al [4] tested the properties of nano calcium carbonate modified asphalt binder and mixture, and test results showed the high temperature performance of 8% calcium carbonate modified asphalt mixture was improved. In this paper, the three kinds of nanomaterials (VP401, VP501, and composite of nano sepiolite and calcium carbonate) were selected to modify the control asphalt binder. Several dosages of nanomaterials were used by weight in the asphalt modification, and mixing processing was conducted in the high shear machine. The Marshall Binder tests (penetration, softening point, ductility and viscosity) were carried out to evaluate the performance

of modified asphalt binder. Through the comparison and analysis of test results, the optimum content of nanomaterials was determined. Furthermore, the mechanical and pavement performance tests were used to evaluate the overall properties of nano-modified asphalt mixture. Finally, Test results show the 1% nano powdered rubber VP401 modified asphalt binder and mixture has better performance compared to the control and other modified asphalt binders and mixtures. Nano-modified asphalt binder also is the hot research direction for asphalt modification in the world. The test work in the paper would show some advices for future research.

Nanomaterials and performance test plan of asphalt mixture

Modifiers

Nanomaterials have some special characteristics, such as small size effect, surface effect, and quantum tunneling effect. In the macro physical properties, it can produce the mutation properties of materials, such as making an insulator into a conductor and the conductor into an insulator, magical photoluminescence, photocatalytic sterilization effect, high strength and high toughness. In the past several years, nanotechnology has been gradually applied into pavement material field. Nanomaterials (organic, metal or inorganic non-metallic) were introduced to modify the asphalt binder, and the purpose is to utilize the magic nano-effect to improve the asphalt binder performance. Nano-modified asphalt binder was different from other modified asphalt, because the nanomaterials would have the potential to change the microstructure of modified asphalt binder. However, micro-structure of asphalt determines the macro performance of asphalt binder. So the nanomaterial might fundamentally improve the asphalt performance, also it is a good way to modify the base asphalt. Thus, nano-modified asphalt research would be the hot spot in the research area.

(1) The nano powdered rubber is obtained from irradiating and sulfuring rubber latex particles in dry process. Nano powdered rubber VP401 is a super fine butadiene powdered sulfide rubber, Narpow Nitrile-Butadiene UFPR (ultrafine full-vulcanized powdered rubber), and nano powdered rubber VP501 is a super fine butadiene powdered sulfide rubber, Narpow Carboxylic Nitrile-Butadiene UFPR. Two main functions of the materials are for toughening nylon and modifying the friction materials, such as the polarity plastic and sulfide thermoplastic elastomer materials [5]. The test samples in the study (Narpow nano powdered rubbers) were provided by Beijing chemical institute.

(2) Sepiolite and calcium carbonate: sepiolite clay, gray or grey, low density and the dry powder can float on the surface of water. It has a strong suction, and high absorption rate in the water. It is also like a paste and strong sticky clay. Sepiolite is rich in Mg fibrous mineral and silicate clay, palygorskites-sepiolite, and has the 2-1 type chains and layers of transitional structure. From the scanning electron microscopy (SEM) images of the sepiolite clay, cross-sectional thickness of sepiolite fiber is only 0.1 μ m, and sepiolite is a kind of ideal nano clay mineral. Calcium carbonate is made from a mechanical method, and directly crushing natural calcite, limestone, and shell using high pressure grinding. Calcium carbonate, a white, odorless and tasteless powder, is almost insoluble in water at the absence of ammonium salt or iron trioxide. Heating results in the decomposition into CaO and carbon dioxide (CO2). It can be a filler for the production of rubber, plastic, paper, paint and ink industry, and widely used in organic synthesis, metallurgy, glass and asbestos and other fields. The test specimen in the study was obtained from Hunan Liuyang sepiolite field [6].

Preparation of nano-modified asphalt binder

This base asphalt binder (No. 70) was obtained from China national offshore oil corporation. The modified asphalt binder was prepared by the high shear machine at condition of 3000 rpm/min and around 150^{o}C. Firstly, nanomaterials (0.5%, 1%, 2%, and 3% nano powdered rubber VP401 and VP501, composites of 1% sepiolite and 0.5%, 1%, 2% calcium carbonate) were slowly added into the base asphalt binder, and mixed in the high shear machine for 60 min. The nano-modified asphalt binder was ready for performance testing.

Nano-modified asphalt binder and mixture tests

(1) Basic tests of nano-asphalt binder

Penetration test is often used to determine the asphalt consistency; Softening point test is the basic test of asphalt binder, and it is one of the three indexes which are most commonly used in China. It reflects the asphalt viscosity at high temperatures, directly expresses and relates to the deformation rate; The ductility of asphalt is the sum of deformation when the asphalt binder is stretched; Viscosity are commonly used to determine the mixing and compaction temperatures of asphalt mixture; Penetration, softening point, ductility and viscosity tests were followed by the test procedures (JTJ052-2000) [7].

(2) Mechanical and pavement performance test of nano-asphalt mixture

Cleavage strength test is used to determine the mechanics characteristic of asphalt mixture when the asphalt mixture is at condition of a specified temperature and a loading rate or an elastic fracturing stage. Meanwhile, it would be commonly used for determining the mechanical design parameters in the asphalt pavement structure design and evaluating the low temperature cracking performance of asphalt mixture. Resilience modulus is the mainly material parameters of asphalt mixture. Rutting test is to simulate the wheel loading on pavement and accumulate the deformation of the sample. It is used to evaluate the resistance ability to plastic flow deformation of asphalt mixture at the specific temperature. When the asphalt mixture is soaked in the water, the adhesion between the asphalt and aggregates would be reduced. The water stability of asphalt mixture was expressed by the physical and mechanical properties of asphalt mixture in the water. The residual stability of asphalt mixture in the water after 48 hours is one of evaluation indexes. Cleavage strength, resilience modulus, rutting, water stability tests of asphalt mixture were followed by the asphalt mixture test procedures (JTJ052-2000).

Test results and discussions

Nano powdered rubber modified asphalt binder

(1) VP501 modified asphalt binder

First of all, the nano powdered rubber VP501 was slowly added into the control asphalt at the various weight percentages. Then, the modified asphalt was mixed in the high shear machine and the nano-modified asphalt was formed. The performance tests of asphalt binder were conducted and the test results are shown in Table 1.

Table 1 Tests results of VP501 modified asphalt

Properties	Concentrations of VP501				
	Base asphalt	0.5%	1%	2%	3%
Softening point (^oC)	48.3	51.8	52.0	52.3	52.5
Penetration (dmm) at 5^oC	12	11	11	10	9
Penetration (dmm) at 15^oC	28	25	23	24	23
Penetration (dmm) at 25^oC	68	64	61	58	53
Penetration index (PI)	0.405	0.302	0.490	0.314	0.256
Equivalent softening point T_{800} (^oC)	53.500	53.911	55.513	54.870	55.423
Equivalent breaking point $T_{1.2}$ (^oC)	-21.472	-19.938	-20.405	-19.110	-17.922
Ductility (cm) at 5^oC, 5cm/min	5	9	9	9	7
Ductility (cm) at 25^oC, 5cm/min	>100	>100	>100	>100	85
Viscosity (Pa·s) at 135^oC	1.312	1.582	1.408	1.528	2.112

From Table 1, test results show the effect of nano powdered rubber VP501 on the performance improvement of modified asphalt binder. The softening point of modified asphalt was significantly improved compared to the base asphalt, even reach to 52.5^oC, and the softening point increased by increasing the concentration of nano powered rubber VP501. About the penetration and ductility of modified asphalt at 15^oC, they decreased with the content increase of VP501. Penetration index, equivalent softening point and equivalent breaking point of modified asphalt binder presented the

same trend. They showed that the overall property of 1% nano powered rubber VP501 was improved most, and the high temperature performance of 1% VP501 modified asphalt was significantly enhanced. However, the low temperature performance of modified asphalt might decrease. Therefore, 1% VP501 is the best content for the asphalt modification.

(2) VP401 modified asphalt binder

Similarly, the same dosages of nano powdered rubber VP401 were added into the base asphalt and the modified asphalt was mixed in the high shear machine. The test results are shown in Figure 2.

Table 2 Tests results of VP401 modified asphalt

Properties	Concentrations of VP401				
	Base asphalt	0.5%	1%	2%	3%
Softening point (^oC)	48.3	54.9	54.3	54.8	55.8
Penetration (dmm) at 5^oC	12	9	9	8	7
Penetration (dmm) at 15^oC	28	20	21	21	22
Penetration (dmm) at 25^oC	68	53	52	50	44
Penetration index (PI)	0.405	0.256	0.329	0.034	0.014
Equivalent softening point T_{800} (^oC)	53.500	55.948	56.280	55.081	55.736
Equivalent breaking point $T_{1.2}$ (^oC)	-21.472	-17.397	-17.862	-15.882	-15.607
Ductility (cm) at 5^oC, 5cm/min	5	8	8	8	7
Ductility (cm) at 25^oC, 5cm/min	>100	>100	>100	92	64

From Table 2, the test results exhibit the influence of nano powdered rubber VP401 on the performance improving of modified asphalt. The softening point of VP401 modified asphalt increased as increasing the VP401 content, and compared to the base asphalt, it was greatly improved. Ductility of VP401 modified asphalt at the temperatures of 15^oC and 5^oC decreased and the low temperature performance of modified asphalt might reduce. Penetration index, equivalent softening point and equivalent breaking point of VP401 modified asphalt had the similar trend, which showed that the temperature susceptibility of modified asphalt reduced, and 1% VP401 modified asphalt has the best overall performance. Thus, the high temperature performance of VP401 modified asphalt was greatly improved, and 1% nano powered rubber VP401 was the best concentration for the asphalt modification.

(3) Sepiolite and $CaCO_3$ modified asphalt binder

Sepiolite and calcium carbonate at certain weigh percentages were added into the base asphalt. The modified asphalt was mixed in the high shear machine and the binder tests were conducted. The experimental results are shown in Table 3.

Table 3 Tests results of Sepiolite and $CaCO_3$ modified asphalt

Properties	Concentrations of Sepiolite and $CaCO_3$			
	Base asphalt	1%S+0.5%C	1%S+1%C	1%S+2%C
Softening point (^oC)	48.3	48.0	46.8	46.2
Penetration (dmm) at 5^oC	12	11	10	9
Penetration (dmm) at 15^oC	28	24	23	21
Penetration (dmm) at 25^oC	68	65	63	62
Penetration index (PI)	0.405	0.243	0.005	-0.308
Equivalent softening point T_{800} (^oC)	53.500	53.666	52.933	51.910
Equivalent breaking point $T_{1.2}$ (^oC)	-21.472	-19.538	-17.723	-15.474
Ductility (cm) at 5^oC, 5cm/min	5	8	8	8
Ductility (cm) at 25^oC, 5cm/min	>100	>100	>100	>100

From Table 3, the test results showed that the overall performance of modified asphalt decreased compared to the base asphalt when the Sepiolite and calcium carbonate were added into the base asphalt. The low temperature performance of modified asphalt was significantly decreased,

and high temperature of modified asphalt might slightly increase. Penetration index, equivalent softening point, equivalent breaking point had a peak point at 1% sepiolite + 0.5% calcium carbonate modified asphalt. Thus, 1% sepiolite + 0.5% calcium carbonate relatively might be the best content for the asphalt modification from test results.

Mechanical and pavement test of modified asphalt mixture

Asphalt mixture has been widely used for the pavement construction, and asphalt mixture should be able to withstand the large traffic loading and natural environment changing. The strength of asphalt mixture directly influences the performance and service life of pavement, also relates to the pavement maintenance cost. At the low temperature the temperature shrinkage stress exceeds the range of asphalt mixture, and the pavement cracking would occur. At the high temperature, the shear stress of pavement would be out of range, the rutting would appear. The Strength of asphalt mixture is mainly determined by the bonding among aggregates and adhesion between asphalt and aggregates. Asphalt performance, aggregate gradation and characteristics are the key factors of asphalt pavement. The gradation of asphalt mixture in this study is AC-13. Cleavage strength of asphalt mixture was tested by the material testing machine at the condition of 15°C, 50 mm/min loading rate and 0.30 Poisson ratio. Resilient modulus of asphalt mixture was tested by the universal testing machine at the condition of 0.35 poisson ratio and 20°C. The automatic rutting test instrument was used for the rutting test. The testing temperature is 60°C±0.5°C, and the sample dimension is 30 cm × 30 cm × 5 cm. The water stability of asphalt mixture was measured by the Marshall residual stability, and test specimen was formed by the Marshall testing instrument. Test results of cleavage strength; resilient modulus, rutting, and water stability are shown from Figure 1 to Figure 3.

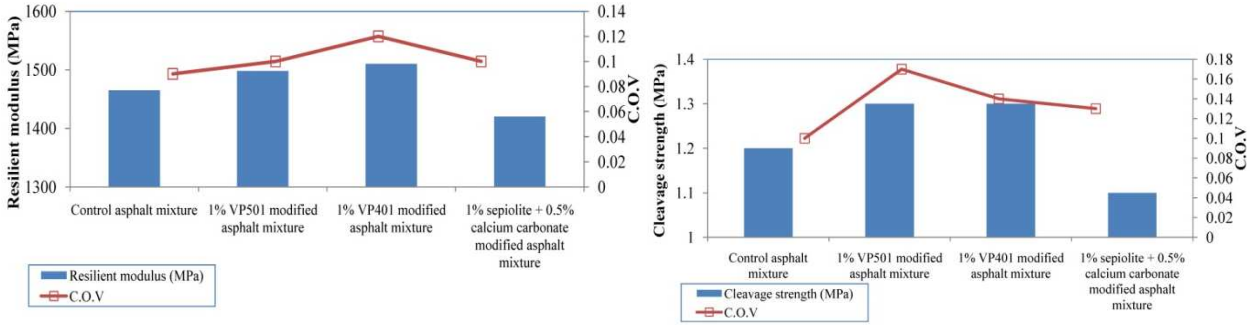

(a) Resilient modulus results (b) Cleavage strength results

Figure 1. Resilient modulus and cleavage strength and results of asphalt mixtures

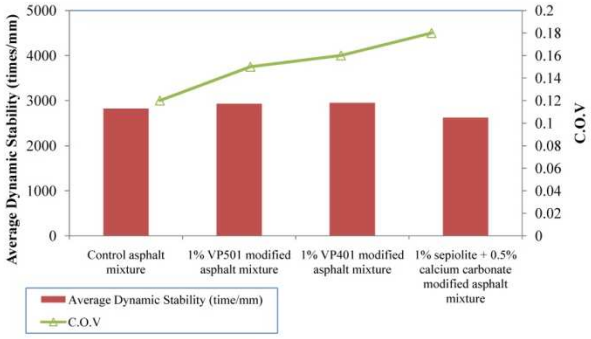

Figure 2. Rutting tests results of nano-materials modified asphalt mixtures

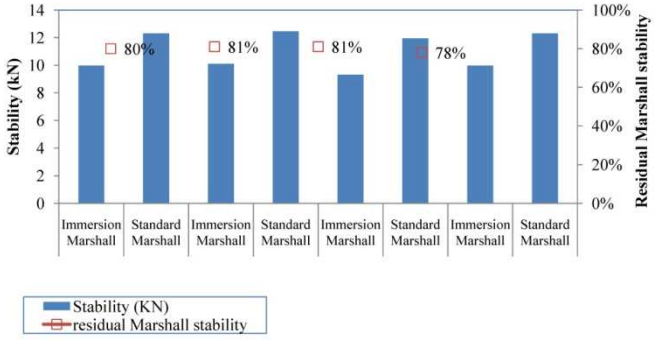

Figure 3. Water stability results of nano-materials modified asphalt mixtures

Conclusions

Based on the test results, the following conclusions can be drawn.

(1) The basic properties of nano-modified asphalt binders show that when the nano powdered rubbers VP401 and VP501, 1% sepiolite + 0.5% calcium carbonate were added into the base asphalt, the softening point and equivalent softening point were improved. Therefore, these kinds of nano-modified asphalt can improve the overall performance of asphalt pavement most, especially in the high temperature property.

(2) The test results show the 1% nano powered rubber VP401 and VP501 modified asphalt have high cleavage strength, high resilience modulus, good high temperature performance, good water stability compared to other asphalt mixtures. Therefore, nano powered rubber VP401 and VP501 would be the best modifier in this study.

In summary, from the test results, the 1% nano powered rubber VP401 and VP501 modified asphalt binder and mixture would have good performance to resist permanent deformation and prevent fatigue cracking.

References

[1] F. Ma. Research on performance of pavement and modification mechanism of Nano-CaCO3 modified asphalt. Xi'an: Chang'an University, 2004.

[2] Z. S. Luan, J. Q. Lei, Q.U. Pu and H. X. Chen. Evaluation methods of SBS Modified asphalt binders. Journal of Wuhan University of Technology, 2010, 32(2):15-18.

[3] TAN Yi-qiu, SHAN Li-yan, FANG Jun and ZHANG Xing-you. Anti-cracking mechanism of diatomite asphalt and diatomite asphalt mixture at low temperature. Journal of Southeast University (English Edition), 2009, 25(1):74-78.

[4] D. L. Liu, A. J. Yue and L. Chen. A study of the performance of Nano Calcium Carbonate modified asphalt and the mixture. Journal of Changsha Communications University, 2004, 20(4): 70-72.

[5] Y. Q. Liu, Z. Q. Fan, H.Y. Ma, Y. Tan and J. L. Qiao. Application of nano powdered rubber in friction materials. Wear, 2006, 261(2):225-229.

[6] E. Sabah, M. Majdan. Removal of phosphorous from vegetable oil by acid-activated sepiolite. Journal of Food Engineering, 2009, 91(3):423-427.

[7] L. Xiang, J. Cheng and G. H. Que. Microstructure and performance of crumb rubber modified asphalt. Construction and Building Materials, 2009, 23(12):3586-3590.

doi:10.4028/www.scientific.net/AEF.5.265

Site Monitoring on Temperature Field Distribution of Asphalt Pavement in Seasonal Frozen Soil Region

MA Hong-yan[1,a], FENG De-cheng[1,b], JING Ru-xin[1]

[1]School of Transportation Science and Engineering, Harbin Institute of Technology, Harbin,China

[a]mhyhit@163.com, [b]fdcgxy@vip.sina.com

Key words:Asphalt Pavement, Temperature Field, In-Site Monitoring, Seasonally Frozen Soil Region

ABSTRACT: As pavement bear the comprehensive effect of environment factors at the same time, its internal temperature field distribute complicatedly and difficult to be predicted. Due to the internal temperature field of pavement is the key of pavement performance and service durability, this paper improved the layout scheme of the temperature field, based on the previous test scheme of factual temperature field. Using the factual temperature field data of asphalt pavement, this paper studied on the temperature distribution characteristic of each layer, summed the temperature filed distribution rule of asphalt pavement and put forward the control points of pavement design low temperature.This paper verified the universality of low design temperature in SHRP (Strategic Highway Research Program) and pointed out some problems like the low temperature design temperature (T_{min}) had quite large safe factor.

Introduction

Analysis and research on the internal temperature field distribution of asphalt pavement can be helpful to structure design and material selection reasonably. Asphalt mixture with viscoelastic properties exhibits different mechanical properties and damage form on different environmental conditions.

Many domestic and foreign scholars have engaged in temperature field study of pavement and obtained lots of achievement.Barber[1] determined temperature field theory of pavement at first and used heat conduction equation to calculate the highest temperature of pavement.Straub[2] established temperature prediction model of pavement based on the factual temperature field in New York State. Christison and Anderson[3] proposed one-dimensional unsteady calculation method to analysis the low temperature field of pavement. On 1980s, Yan Zuo-ren[4] established temperature field prediction method of layered pavement with cyclic heat. On 1990s, Wu Gan-chang[5-6] proposed two-dimensional nonlinear unsteady temperature field calculation theory of semi-rigid asphalt pavement based on the analytical method.SHRP[7-8](Strategic Highway Research Program), LTPP[9] (Long Term Pavement Project) and C-SHRP[10] (Canada- Strategic Highway Research Program) put forward extreme temperature prediction model of pavement. Hermansson[11] proposed high temperature field prediction model of asphalt pavement.

Research work about temperature field of pavement mainly focused on theory, numerical simulation, field measurement, prediction model and so on. However, theoretical research is difficult and hard to guarantee calculation accuracy, the boundary conditions of numerical simulation is difficult to control and has difference with actual condition, and the applicability of

prediction model is bad. In contrast, field measurement can get more reliable temperature dates of each layer which is helpful to get the distribution and variation of asphalt pavement temperature field.

Based on this, this paper put forward a comprehensive field measurement method based on the temperature field measurement method study. Then after analysis on temperature field measurement date of asphalt pavement, the distribution law of asphalt pavement temperature field, which is verified by design temperature of asphalt pavement in SHRP, is obtained.

1. Temperature Field Measurement Design

According to the seasonal freezing climate in Heilongjiang, based on the highway engineering from Qiqihar to Tailai, the temperature field of pavement at different depths was observed in recent years thought paving typical asphalt test road and laid the temperature field monitoring equipment.

1.1 Experimental Conditions

Based on the weather station location, text conditions and natural environment and after investigate on natural conditions along Qi-Tai highway, a test area was selected on the east of pavement (150 meters away from pavement) at K129+900. This location which closes to the pavement with excellent ventilation and without shelter facilities can guarantee the environment and pavement at same level.

1.2 Emplacement Information Collection System Settings

The typical asphalt pavement was paved in test area. The plane sizes of test area were in Table 1and top view shown in Figure 1. The structure of pavement is as same as highway at K129+900, shown in Table 2.

Measuring points where buried temperature sensors were selected at road surface (0cm), middle of surface layer (6cm), top of base (12cm), top of cushion (27cm) and top of roadbed (42cm). The transverse position of sensors were around the central axis in turn 10cm which shown in Figure 3.

Figure 1 Resistance Temperature Detectors

In addition, in order to get accurate air temperature, some sensors which test air temperature were set. The practical method is set three stents which are 1.5 meter high[12], and a temperature sensor is fixed on the top of each stent. The mean value is treated as air temperature.

Table 1 Structural Combination of Asphalt Pavement

Structure Layer	Thickness	Material	Size
Upper Layer	4cm	AC-16	3.5m×3.5m
Lower Layer	8cm	AC-20	
Base	15cm	Cement Stabilized Macadam	3.8m×3.8m
Cushion	15cm	Natural Gravel	4.1m×4.1m
Roadbed	Compaction Degree＞95%	Silty Sand	4.7m×4.7m

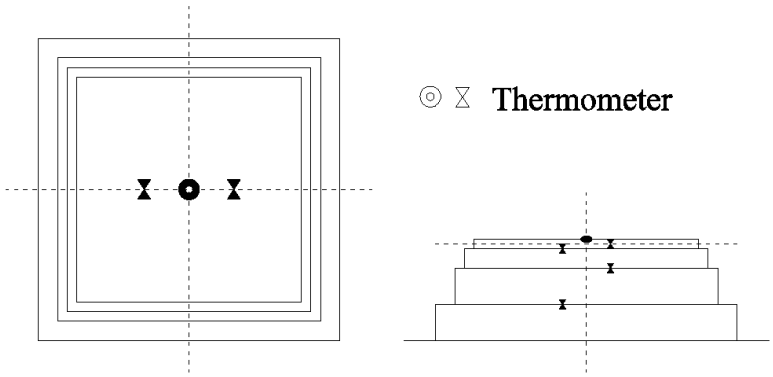

Figure 2 Layout of Sensor and Pavement Structure

After temperature sensors were laid completely, the signal lines, which connect to temperature collection and processing equipment, were put into collection room. 12 sensors all worked well through debug by wire transmission, then real-time monitor started by wireless transmission. The collection frequency was 1 time every 10 minutes. Remote control was realized by Transmission technology of mobile communication and internet. The date remote collection and wireless transmission was realized under the normal power supply.

2. Asphalt Pavement Temperature Field Distribution

This paper selected June 2010 to May 2011 as a cycle year. According to the meteorological date in this year, The extreme minimum temperature (-34.8℃) of Qiqihar appeared in January 14, 2011. And the extreme maximum temperature (37.7℃) appeared in June 24, 2010[13].

Therefore, by analyzing the temperature field data in the January 13~15th, 2010 and June 23~25th, 2011，the variation of each structural layer temperature of asphalt pavement with time and depth were obtained.

2.1. Each Layer Distribution Law

The temperature field data of the January 13~15th,2010 and June 23~25th,2011 which recorded the relationship of temperature of structural layer and air temperature was showed in picture 3~4. The analyses were as follows.

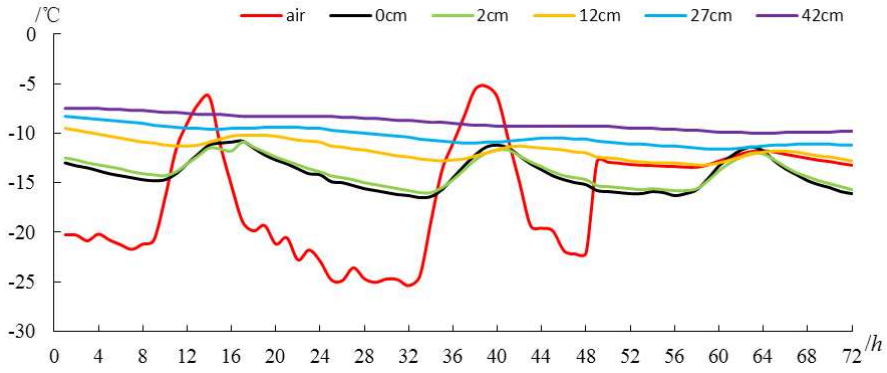

Figure 3 2011.01.13~15 The relationship between each layer structural temperature and air temperature

① The period of temperature range of middle course and upper layer middle layer are consistent, which illustrated that air temperature is the major influencing factor of road surface temperature.

② The gradient distribution of each layer temperature was differs according to different seasons. In the summer, with the increase of depth, the temperature of structural layer decreased, thus, the temperature of surface layer was the highest; in the winter, with the increase of depth, the temperature of structural layer increased, thus the temperature of surface layer was the lowest but

higher than air temperature. Namely, the temperature variation of the surface layer was the most sensitive, and the cracking which as the result of temperature shrinkage was from the top to the down might be the Top- Down cracking.

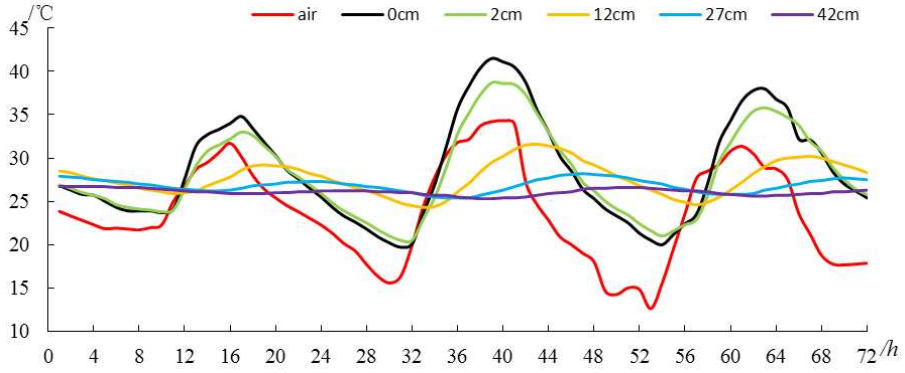

Figure 4 2011.06.23~25 The relationship between each layer structural temperature and air temperature

③ The day temperature range of the structure differed with different seasons and depth. With the increase of depth, the day temperature range decreased; meanwhile, the summer-time day temperature range was larger than that of winter-time. For the reason that the temperature of the base would be steadier when the day temperature range of surface layer was the highest, it was realized that when the pavement structure was higher than certain depth, the structural temperature of the base would be steady, this depth was called critical thickness.

2.2. Distribution Law Along Depth

The temperature data of 2am, 8am, 2pm, 8pm were selected to analysis the distribution characterization of the temperature field of different direction, which was showed in the figure 5~6.

The asphalt pavement temperature field distribution rule of different depths differed with different seasons[14]. In winter, the temperature of the base courses was the highest and that of the surface layer was the lowest; with the increase of air temperature, the temperature range of structure decreased gradually. In the summer, the temperature distribution of structure was rather complex, the highest temperature might occurred in the surface layer or the middle layer, and the day structural highest temperature was the surface layer temperature when the air temperature was the highest; the lowest temperature might occurred in the surface layer or the base courses; the day structural lowest temperature was the surface layer temperature when the air temperature was the lowest.

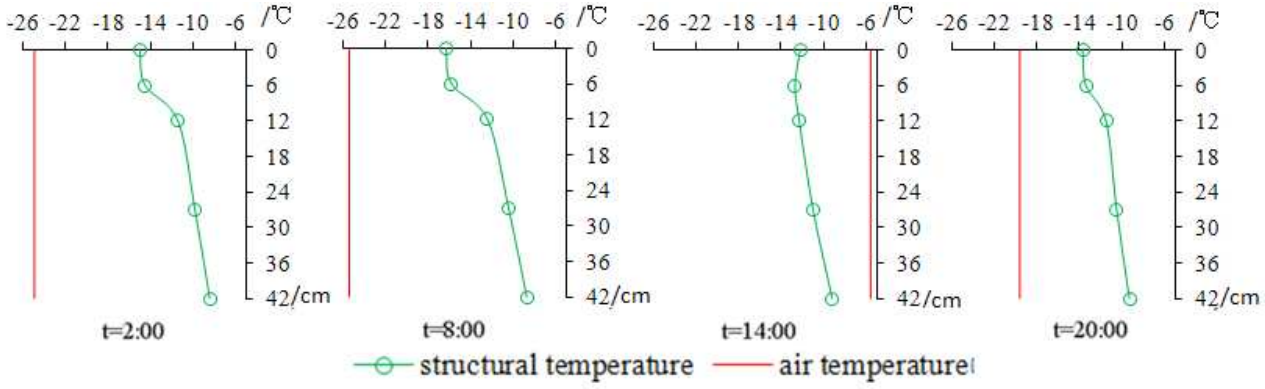

Figure 5 2011.01.14 Day representative moment temperature field distribution situations with different depths

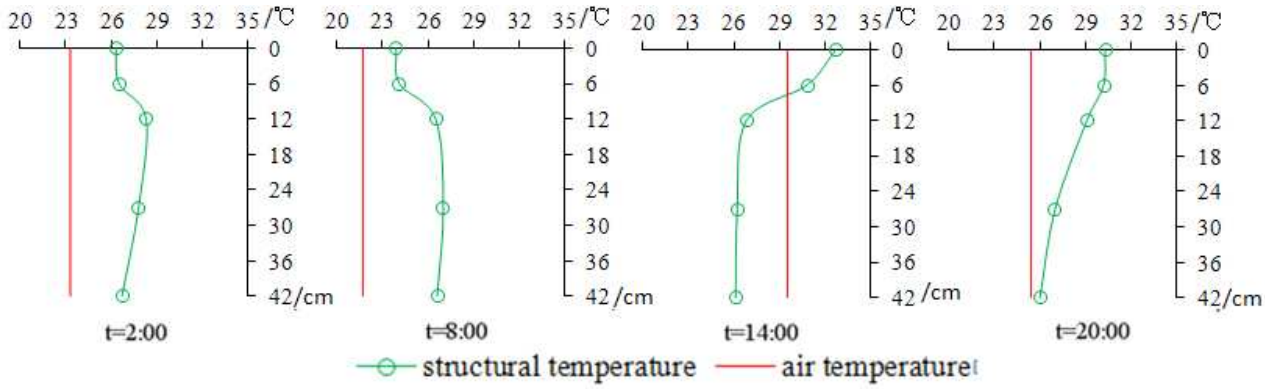

Figure 6 2010.06.24 Day representative moment temperature field distribution situations with different depths

This paper aimed at being as guidance for road design according to local extreme temperature. Namely, the guidance for the reasonable selection of materials and design of structure by handling the most unfavorable working state.

2.3 Discussion of SHRP Design Temperature

At present, the selection of asphalt materials in pavement design in the domestic is usually according to the PG grading method commended by AASHTO. The PG grading is determined according to the extreme temperature of local climate, so the relationship between the extreme temperature of the climate and pavement affects directly on the rationality and economy of the material selection.

The distribution of asphalt pavement temperature field shows: in the asphalt pavement structure, the minimum structure temperature is the temperature of pavement surface when the air temperature reaches the extreme minimum, which is higher than the extreme minimum air temperature.

$$T'_{min} > T_{air,min} \quad (1)$$

where

T'_{min} —pavement structure minimum temperature；

$T_{air,min}$—air extreme minimum temperature.

SHRP provides: the annual extreme minimum air temperature is adopted as the design minimum temperature. As see in the equation (2), the design minimum temperature value in SHRP is too conservative. The asphalt materials selection according to this method will increase the project cost because of the high low-temperature performance.

The temperature minimum design value of pavement surface according to SHRP does not apply to Heilongjiang region, so materials selection should not fully according to the SHRP standard.

3. Conclusion

① The temperature gradient of each structure layer has seasonal different property. In summer, the temperature of structure layer decreases with the depth increases, which is the opposite in winter.

② The day amplitude of structure temperature changes with the change of season and depth. The greater the depth, the smaller the day amplitude; and the day amplitude in summer is greater than in winter.

③ The distribution of the temperature field along the depth has seasonal difference. When the pavement structure reaches a certain thickness, the structure temperature at the pavement bottom tends to stabilizing, and the thickness is called critical thickness.

④ The minimum temperature adopted in SHRP Design standard is pointed out so conservative. The materials selection in practice is not appropriate to refer to this standard.

References

[1] Barber.E.S.Calculation of Maximum Pavement Temperatures from Weather Reports[A]. Washington D C:Highway Research Board,Bulletin 168,National Research Council,1957.

[2] Straub,A.L., H.N.Schenck Jr.,FE.. Przybycien.Bituminous Pavement Temperature Related to Climate[J]. Highway Research Record,1968,256:53-77.

[3] Christison,J.T,K.O.Anderson. The Response of Asphalt Pavement to Low Temperature climatic environment[A]. Proceeding of the 3rd International Conference on the Structure Design of Asphalt Pavement[C]. September 1972.

[4] Yan Zuo-ren. Analysis of the Temperature Field in Layered Pavement System [J].Journal of Tongji University (Natural Science),1984,(3).

[5] WU Gan-chang. Analysis of Semi-rigid Pavement Temperature Stress[M].Beijing:Science Press,1995.

[6] WU Gan-chang.The Analytic Theory of the Temper-ature Fields of Bituminous Pavement over Semi-rigid Road Base[J]. Applied Mathematics and Mechanics,1997,18(2):181-190.

[7] Huber.G.A..Weather Database for the SUPERPAVE Mix Design System[R]. Washington D C: Strategic Highway Research Program,National Research Council,1994.

[8] Kennedy.T.W.,GI.OZ..Superior Performing Asphalt Pavements(Superpave):The Product of the SHRP Asphalt Research Program[R]. Washington D C: Strategic Highway Research Program, National Research Council,1994.

[9] Mohsent.A,M.Symons.Improved AC Pavement Temperature Models from LTPP Seasonal Data [A]. Washington D C:Transportation Research Board 77th Annual Meeting,1998.

[10] Robertson.W.D..Determining the Winter Design Temperature for Asphalt Pavement [A]. Proceeding of Association of Asphalt Paving Technology,1997.

[11] Hermansson,Ake.Simulation Model for Calculating Pavement Temperature Including Maximum Temperature. Transportation Research Record,2000,1699:134-141.

[12] China Meteorological Administration. Rules About Ground Surface Meteorological Observation [M].Beijing: Meteorological Press,2003:6-10.

[13] China Meteorological Data Sharing Service System.SURF-CLI-CHN-MUL-YER-CES.(2002-09-10)[2011-03-28]:http://cdc.cma.gov.cn/shuju/search1.jsp?dsid=SURF_CLI_CHN_MUL_YER_CES&tpcat=SURF&type=table&pageid=3

[14] QIN Jian,SUN Li-jun.Study on Asphalt Pavement Temperature Field Distribution Pattern[J]. JournaI of Highway and Transportation Research and DeveIopment,2006,(8).

doi:10.4028/www.scientific.net/AEF.5.271

the Analysis, Discussion and Suggestions for the Mesh Reinforcement Technique of Polymer Mortar Wire Rope

Shuren Zhang[1,2,a], Zhonglong Li[1,2,b]

([1.] School of Transportation Science and Engineering, Harbin Institute of Technology, Key Laboratory of traffic safety, specialty materials and intelligent control technology transportation industry Harbin 150090, China;
[2.]Postdoctoral Station of Mechanics, Harbin Institute of Technology, Harbin 150090, China)

[a]18745059800@126.com, [b]lizhonglong2004@126.com

Keyword: Piece of steel wire rope course, Polymer mortar, Bonded prestress, Reinforcement

Abstract: The mesh reinforcement technique of polymer mortar wire rope is a new reinforcement technique used more in the domestic fittest reinforcement project recent years. Recently, there are no unified technical standards, the detailed practice is not same in practical work. There are big differences among the reinforcement effects. The key issue is whether or not to impose the prestressed steel wire rope and the prestressed size. The difference of the actual practice and reinforcement effect reflects the understanding gap polymer mortar wire rope of mesh reinforcement technique action principle of the designer. A correct understanding of polymer mortar wire rope of mesh reinforcement technique the mechanism and the objective analysis strengthening effect and actively explore research in engineering application problems have a practical significance to promote the healthy development of the structure strengthening technology.

Analysis of the polymer mortar reinforcement mechanism of wire rope nets

There are a lot of methods to reinforce the weak component in practical engineering, According to the mechanism, they can be reinforced two big kinds of passive reinforcement and active reinforcement [1] .

Passive reinforcement for the kind of direct reinforcement. Direct reinforcement reinforcement refers to adding tensile (or shear) reinforcing materials in the weak area of the tension in the component (or shear).Adding more strong material after the reinforcement method assume only live load and add after the internal cause constant load. Compared with the original beams reinforced, the following reinforcing materials should be strain lag. In Common Circumstances in the limit state, It should be less than the eed tensile strength limitation .The high tensile properties of the wire rope is unable to give full play to the role. It is a kind of great waste.

Prestressed reinforcement initiatively. Prestressed reinforcement initiatively refers to a prestressed concrete reinforcing system which adding reinforcing materials prestress in the tension zone (or shear weak area) where reinforced. Then spray note high-powered composite mortar, combine the reinforced beam body with the integration unbonded. When we reinforce the steel wire mesh in polymer mortar, if prestressed concrete to the wire rope, it also called polymer mortar prestressed reinforcement of mesh wire rope, This reinforcement method belongs to the active principle from strengthening category. The main purpose to add more material prestress is to solve reinforcing materials "strain lag" from the fundamental, improve the efficiency in the use of materials, after that , the original beams of the stress state is improved, the original beams of the bearing capacity and crack resistance is enhanced.

The application of the high-powered composite reinforcement fabric mortar (HPF) strengthening technology.

Liangtao Bu come up with the high-powered composite mortar proposed reinforcement fabric (HPF) strengthening technology in the book *the new technology of the high-powered composite mortar steel reinforced concrete structure (HPF),* using the ordinary hot rolling steel instead of the

high strength steel wire nets, The reinforcement effect is equal with no adding prestressed polymer mortar wire rope nets piece of reinforcement. But the structure is more simple, construction is more convenient, and the reinforcement cost also reduced [2].

Even though high-powered composite mortar (polymer mortar) steel reinforcement technique belongs to passive reinforcement category , it's plastic performance is good because the ordinary tensile strength the hot rolling steel used is relatively low. for strengthening the medium and small span of the reinforced concrete beam board which is little influenced by "add after reinforcing materials strain lag", The ultimate state reinforcing steel bar add after the stress basically can achieve (or close to) the tensile strength limit .it still can improve the bearing capacity and structure and rich the purpose of durability. High-powered composite mortar (polymer mortar) steel reinforcement technique especially suitable for the reinforcement of the reinforced concrete column. Axial force after strengthened beam of longitudinal reinforcement in the ultimate state of stress, can achieve the compressive strength of the design value. Furthermore, the reinforcement method has the characteristics of constraint reinforcement, it can limit the lateral deformation of the core concrete, then make concrete in a three stressed statement. Indirectly improved the structure of the concrete compressive strengthen, that can get the purpose of improving the structure of bearing capacity and durability double strengthening.

Rationality analysis for adopting the wire rope nets of prestressed reinforcement.

Theory of research and engineering practice shows that the prestressed reinforced used by prestressed concrete must use high strength reinforced whose stress relaxation smaller. General use of the high strength steel wire, steel strand and fine rolling steel rebar. Wire rope is a kind of high strength tensile materials with flexibility, it is mainly used for the engineering of lifting and raction. In recent years, it is a new attempt of the polymer mortar prestressed reinforcement technique of wire rope nets to wire rope for prestressed reinforcing the fittest reinforcement project. Its main advantage is: The anchor wire rope connection anchor structure is simple, (Put the wire rope end through a bolt of the ring at the end of the hole, fixed with the card after the enfoldment.) Wire rope has certain the flexibility so that it can adapt to the needs of different shape structure reinforcement. The main problem using the prestressed steel wire rope is still lack of necessary understanding to the wire rope stress relaxation performance. According to some manufacturers, the wire rope stress relaxation rate at 10%, the recent test results by Harbin Institute of Technology is similar to the numerical.

The test measuring the strain with the frequency method, the initial tension strain of wire rope1 turns to 6458 με,The corresponding tension control stress for 936.4 MPa . It equals 0.6 times the tensile strength standard values. the initial tension strain of wire rope 2 turns to 6458 με, The corresponding tension control stress for 1073.0MPa. It equals 0.7 times the tensile strength standard values. 77 days after the measurement of 1, the stress of wire rope loss rate is about 19.24%, the stress of wire rope 2 loss rate is about 20.62%.

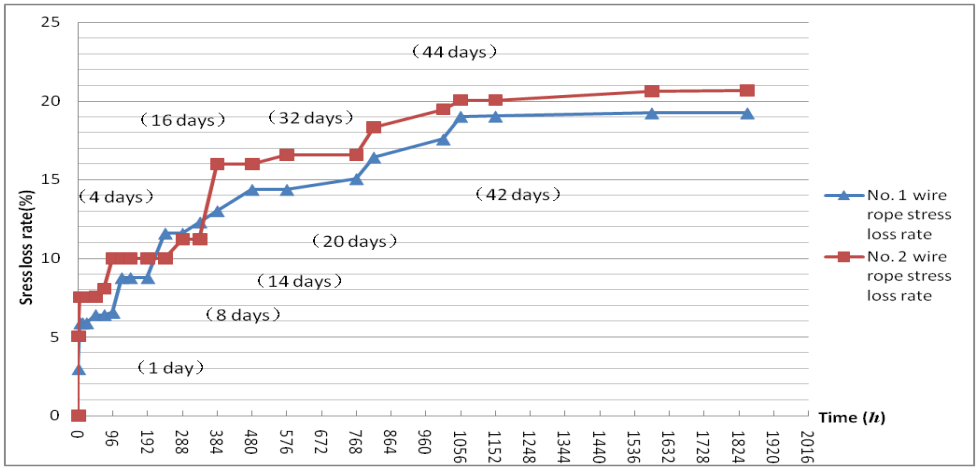

Fig.1 Curves between the wire rope stress losing and time

Fig. 1 shows for the wire rope stress and the relationship between the time loss rate curve, wire rope 2 shows 4 ~ 14 days of stress stable loss at around 10%. 14 days later the loss rate increase, 44 days later it basically stable, wire rope 1 shows 4 ~ 14 days of stress stable loss at around 8%, 8 days later the loss rate will suddenly increase,42 days later it basically stable.

There is something should be point out, The trial of measured stress losses including: The wire rope stress relaxation loss and card fixture sliding deformation loss in two parts, Among them what proportion of their respective is difficult to accurately dividing, it analyzed that 4~14days(or 5 ~ 8 days) trend to the stable10%, which is basically belongs to the stress relaxation loss, then rapid development of late stress losses reflect the characteristics of deformation sliding loss. The trial results are not accurate though stress relaxation of the loss of the value, But the conclusion through stress wire rope given by the test loss rate as high as 20% better reflect engineering used in the actual stress of wire rope net loss of the overall situation, The author thinks that the loss rate of stress as much as 20% of the prestressed steel wire rope for not be appropriate.

In addition, turn the wire rope into nets how exactly to carry on prestressed drawing work is also worth to discuss. Due to the limit by the construction equipment construction is only single (or a few root) partial tension, when push and pull in mesh nodes place it will produce friction which may cause the distortion of the node deformation or destroyed, These will affect the work of the structure performance after the effective and strengthening the tension of wire rope prestress value, The author thinks that we should put the view on the prestressed tendon layout and simplify construction. It is not necessary to take wire rope into nets in advance. the reinforcement of One way to force on both sides of the plate for normal section flexural strength just need in the longitudinal decorate wire rope, it according to decorate distribution reinforced In a horizontal structure requirement, when we make normal section flexural reinforcing to the stress of two-way four supporting board of the bearing capacity, should decorate wire rope in two directions, after wire rope tension, will the longitudinal and lateral wire rope nodes and locally, Wire rope tension after the first binding into nets can avoid node of the distortion of the influence of tension.

The key technology with the unbonded prestressed concrete reinforcement.

The system which the anchor in reinforced beam body on small diameter steel strand or ordinary hot rolling steel, beam on the strength of the body, then spray note high-performance tensile composite mortar is the author's new idea reinforcement design which summarized in 2004 in South Korea SRAP technology. The key techniques are tendons tension and anchoring and high strength compound the reasonable selection of mortar and injection.

The choice, tension and anchoring of prestressed reinforcing steel. There are many kinds of restressed reinforcing steelused for bonded prestressing tendons, In practical projects it should be based on strengthening the nature and structure of the force requirements, comprehensive considerate the environment of the structural use, conditions of the reinforcing construction, tension and anchored structure reinforcement cost, and other factors to choose the type of prestressed reinforcement.

Prestressed reinforcing steel used for bonded prestressing tendons can use small diameter and low relaxationsteel strand, fine rolling rebar and other domestic steel. Because of the old bridge reinforcement for prestressed tendon stress less loss of domestic steel, tension control stress is low, In some cases even can use small diameter of ordinary hot rolling steel (HRB400 or HRB335) and epoxy coating ordinary hot rolling steel (HRB400 or HRB335).The biggest advantage using common hot-rolled steel is can use welding anchor. Using the epoxy coatings hot-rolled steel with a certain ability of anticorrosive can reduce tensile strength requirement of the gush note composite mortar. The fixation of small diameter steel strand and fine rolling rebar prestressed anchor the load on the body of supporting angle steel, construction is simple, and the project cost is low.

Small diameter steel strand of the clip anchorage anchor to lower the project cost, using small jack to tension, Tension control stress could take f_{pk} from $\sigma_{con} = 0.5 \sim 0.6 f_{pk}$ as the prestressed tensile strength standard values. Small diameter fine rolling rebar adopt nuts anchor which from the

manufacturer. Using small hydraulic force measurement wrench to tension, Tension control stress can take $\sigma_{con} = (0.7 \sim 0.8) f_{pk}$,small diameter hot rolling steel (HRB400 or HRB335) welding connection anchor. Welding both ends of the steel to steel bar which is fixed in reinforced beam on the body. By adopting transverse taut deformation of tension, Tension control stress desirable and a period load the original beams reinforced stress to roughly the same level. Generally take $\sigma_{con} = (0.4 \sim 0.6) f_{pk}$.

The choice and injection of the high performance tensile composite mortar. The high performance tensile composite mortar injected with the depending on the unbonded prestressed concrete reinforcing system, prestressed reinforced beam body with a binding, it is the foundation to ensure they two work together that composite cement mortar high adhesive strength. The high tensile properties of composite cement mortar is the premise which can control structure anticrack , protect prestressed reinforced from corrosion.

Currently there is a lot of high performance domestic production composite mortar, There is still no uniform production standards. the performance indexes given by manufacturersare also different. The author suggested that the high performance concrete used for the inforcement composite mortar should meet the provisions of performance requirements in the table 1[3-4].

Table 1 The main performance requirements CMMR used for structure reinforcement

Mortar performance Points level	The standard values of the compressive strength [MPa]	Tensile strength standard values [MPa]	Surface bonding shear strength standard values [MPa]	Standard carbonation depth [mm]	Chloride permeability [the coulomb's]
Level 1	≮35	≮8	≮3	≯5	Very low(100-1000)
Level 2	≮30	≮6	≮2.5	≯8	Very low(100-1000)
Level 3	≮30	≮4	≮2	≯10	low(1000-2000)
Level 4	≮30	≮3	≮1.5	≯15	low(1000-2000)

The choice of composite mortar shall be comprehensive consideration of the structure of the use of the environment, the reinforcement design resistance requirements and strengthening the effects of the construction, the proposal to the following opinions treatment:

(1)Reinforced for cross-section bending in the bottom of the load in the tension zone.

①strengthen with the bonded prestressing of the small diameter steel strand, high strength steel wire and fine rolling steel rebar. In one, two kind of environment of the structure, can use level 2 compound mortar. In three, four categories of the environment of the structure appropriate USES level 1 composite mortar.

②Strengthen with the bonded prestressing in using common hot-rolled steel(HRB335,HRB400): In one, two kind of environment of the structure, can use level 3compound mortar. In three, four categories of the environment of the structure appropriate USES level 2 composite mortar.

(2)Reinforced for resisting shear used for webs (beam rib) the side inclined section.

Strengthen with the bonded prestressing in using common hot-rolled steel(HRB335,HRB400)can use level 3 compound mortar.

Composite mortar layer of protection of thickness(the distance from mortar surface to steel face) should be make sure according to the require of the durability based on the materials carbonation resistance and chemical resistance ability. Generally take 10~15(mm), the injection thickness of the composite cement mortar is related to the reinforced arrangement. Generally take 30~40(mm), Generally the sections which supporting angle for layout (anchor plate)have a large thickness ,so should be layered injection.

Reinforced concrete flexural members (beam or plate) should give priority to the bearing capacity of reinforcement is the unbonded prestressed concrete reinforcing scheme

With reinforced concrete beams reinforced for example, to have a discuss about the unbonded prestressed concrete reinforcement technique. Normal section flexural strength reinforcement appropriate uses 2 strands or 3 strands of steel strand and small diameter of fine rolling rebar unbonded prestressed concrete reinforcing scheme, The inclined-section shearing resistance reinforcement Appropriate uses the scheme of transverse tension of ordinary hot rolling steel or epoxy coating hot-rolled steel (HRB400 or HRB335) which have the unbonded prestressed concrete(Fig. 2).

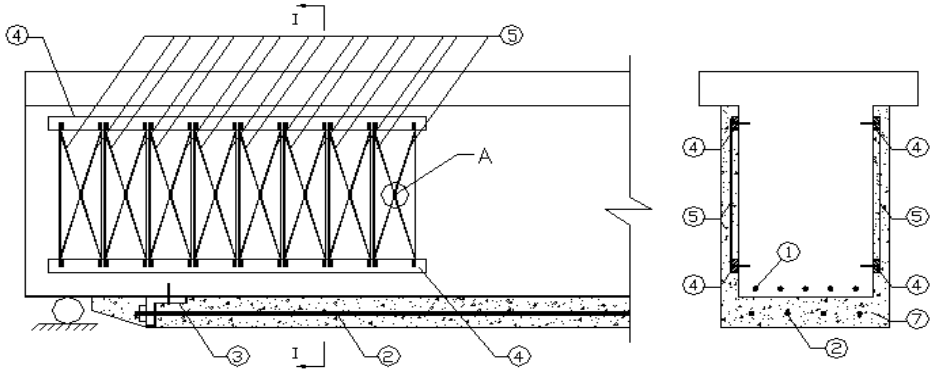

Fig. 2 The schematic drawing of the reinforced concrete beams reinforced bonded prestress structure

① The original beams of longitudinal reinforcement② Add after longitudinal tendons(3 strands of steel strand or small diameter fine rolling steel rebar) ③ Supporting anchor plate ④ Anchorage article steel plate⑤ add after transverse tension hot rolling steel vertical prestress (the dotted line shows the position before stretch-drawing, The solid line shows the position before stretch-drawing) ⑥ Horizontal card tight implement⑦ High-powered composite mortar injected finally

Normal section flexural reinforcement. In order to improve the flexural bearing capacity of the sorghum's normal section, add small diameter steel strand (or fine rolling steel rebar) tendons in the bridge bottom. The quantity required by force, Prestressed reinforcement length should be based on the require of the beam of each section flexural strength. After the introluces' strectch-draw inject high-performance tensile composite mortar in the bridge bottom. Bond the prestressed reinforcing steel and the reinforced beam body as one to constitute the reinforcing system of unbonded prestressed concrete. (Fig. 2)

The theoretical analysis and engineering practice shows that the strengthen of the unbonded prestressed concrete reinforcing system of reinforced concrete beam of normal section and may according to the structure stress requirements and greatly improve the bearing capacity of beams is cross-section bending .The composite mortar injected in the bottom of the beam Can protect tendons from corrosion , improve the durability of structures. In addition, the high performance tensile composite mortar which injected later increased the section size of the beam. Improve the bending stiffness of the structure. It is beneficial to solve live load deformation or excessive vibration problem.

Inclined section shear reinforcement. In order to improve the shear capacity of the beam inclined section, add the vertical tendons in both sides of the beam section beam, Vertical tendons with small diameter (6~12 mm) of ordinary hot rolling steel (or epoxy coating hot-rolled steel), Reinforced spacing inclined section should be based on the shear capacity required force, Generally take for 200~400mm. At both ends of the prestressed steel welding fixed in the anchorage article steel webs(steel plate of the article thickness should be not less than 5 mm), By adopting transverse taut deformation of tension, In the middle of the neighboring prestressed reinforcement two prestressed reinforcement on horizontal taut force , make prestressed taut hard dine in fixed Use

transverse card tight. And then jet 30 mm thick high-powered composite mortar In the web on both sides of the injection then bond the prestressed reinforcing steel and the reinforced beam body as one making up the reinforcement system of prestressing inclined section(Fig. 1).

When construction the measurement and calibration of the control stress for prestressing can according the transverse tension reinforced dip Angle (or reinforced the turning point coordinates). Suppose the anchorage of steel bar between points of two welding anchorage before tension is L_1, according to the reinforced dip angle after stretch-draw θ (or reinforced the turning point coordinates) Get the tension the total length of steel L_2.from this, we can get tension control stress(Eq. 1).

$$\sigma_{con} = \frac{L_2 - L_1}{L_1} E_P = (\frac{1}{\cos\theta} - 1) E_P \tag{1}$$

The theoretical analysis and engineering practice shows that the strengthen by adopting transverse tension ordinary hot rolling steel bonded prestressing reinforcing system for inclined section of the reinforced concrete beam, the structure is simple and it is convenient for construction, Can effectively improve the efficiency in the use of strengthening materials, Improve the shear capacity for inclined section, the high-performance tensile composite mortar

Injected on both sides of the injection increase the thickness so can not only reduce principal tensile stress but also protect the reinforcing steel bar from corrosion, improve the disability of the structure

Summing up

The main problems of polymer mortar strengthening technology application of wire rope nets is what there is no specific provision to whether the wire rope add prestressed or not , Reinforcement mechanism is not clear, concept of chaos.

During the reinforcement of steel wire mesh in polymer mortar, if the wire rope without prestressed, Its action principle is to belong to direct reinforcement kind of passive reinforcement category. under the circumstances, the high tensile properties of the wire rope is unable to give full play to the role.

In the reinforcement of the steel wire mesh in polymer mortar, If the wire rope with prestressed concrete, Also called polymer mortar prestressed reinforcement of mesh wire rope, Strengthening the construction of the external prestressing with characteristics, Later load have the unbonded prestressed concrete characteristics, From the principle of prestressed reinforcement belongs to the category of the initiative.

The theoretical analysis and engineering practice shows that the unbonded prestressed concrete reinforcing system will be the most competitive reinforcing scheme for the comprehensive technical and economic advantages of reinforcement effect significantly, prestressed anchor structure simple and tension construction is convenient and the low cost reinforcement.

References

[1] S.R. Zhang: *The eighth session of national building identification and strengthening academic exchange conference*(Harbin,China,2006). p.51.

[2] L.T. Bu: *the new technology of the high-powered composite mortar steel reinforced concrete structure* (China Building Industry Press,China,2006)

[3] S.R. Zhang: *The existing bridge reinforcement, reconstruction and evaluation of academic exchange and technical semina*(Jiangshu,China,2008). p.3.

[4] S.R. Zhang: Think twice about the design concept of bridge reinforcement, J. Bridge, (2008) No.1.

doi:10.4028/www.scientific.net/AEF.5.277

Load Transfer Characteristics and Durability Study of GFRP Dowels in Jointed Concrete Pavement

LI Luoke[1, a],TAN Yiqiu[1, b], GONG Xiangbing[1], LI Yunliang

[1] Harbin Institute of Technology, Institute of Transportation Science and Engineering,Harbin 150090 China

[a] llk217@126.com, [b] yiqiutan@163.com

Keywords: road engineering; concrete pavement; GFRP dowels; load transfer characteristics; ultimate bearing capacity; durability

Abstract: The corrosion of steel dowels in concrete pavement can compromise the load transfer capability of joints and lead to premature damage. To solve this problem, the non-corrosive glass fibre reinforced polymers (GFRP) bar has been used as dowels in concrete pavement instead of the steel dowels.This thesis demonstrates the Load Transfer Characteristics of a GFRP dowels with the help of a 3D finite-element model, and various evaluation method and index are studied as well, including: (1)efficiency of load transfer , (2)coefficient of shear transfer , (3) distribution ratio of shear transfer. An accelerated test is applied to examine the long-term performance of the GFRP dowel bars by using self-designed equipment.This study shows that GFRP dowels is a feasible alternative to steel dowels which can entirely meet the needs of road performance, and the research results will be useful in the design and application of GFRP dowels in jointed concrete pavements.

Introduction:

In a jointed concrete pavement, dowel bars are installed to transfer traffic wheel loads to the transverse joints without restricting the horizontal joint contraction and expansion. Dowel bars which are commonly used in jointed concrete pavement is made of steel.However, the steel dowels with the small diameter create high bearing stresses in the concrete surrounding, and cause the concrete to crush and spall locally under repeated wheel loads[1]. In addition, the corrosion of the steel dowels can reduce the load transfer efficiency of the joint and restrain vertical movement which compromise the performance of the pavement and lead to premature failure[2].To solve the problems of both corrosion and high bearing stress from conventional steel dowels,the large diameter GFRP dowel bars are now considered as a potential solution because of their resistance to the corrosive agents，high tensile strength and lower surface hardness.This paper researches the performance and feasibility of the GFRP dowel bars which are installed at the locations of transverse joints by the method of finite-element analysis together with experimental approach.

Load Transfer Characteristics of GFRP Dowels

Evaluation Indexes.In actual pavements, the displacement of the loaded slab edge and unloaded slab edge can be measured with a FED,therefore,the displacement–based load transfer efficiency (LTE_{δ}) has been widely used in actual engineering[3].This paper use the LTE_{δ} to directly assess the load transfer efficiency of a GFRP doweled joint and compare it with the steel dowels.,the parameter is calculated using the following equation:

$$\mathrm{LTE}_{\delta} = \frac{\omega_{\mathrm{UL}}}{\omega_{\mathrm{L}}} \times 100\% \tag{1}$$

where ω_{UL} =displacement of unloaded slab edge under the wheel load ; ω_{L} = displacement of loaded slab edge under the wheel load.

Shear force distribution shows the shear force transmitted by each dowel[4]. Shear force transfer ratio（SFTR）is defined as the amount of transferred load by the dowel group from shear force divided by the amount of applied wheel load as shown in the following equation:

$$SFTR = \frac{\sum_1^N Fs_I}{P} \times 100\% \tag{2}$$

Dowel shear ratio（DSR） gives the contribution of dowel bar system in transferring load across a joint by shear action[5]. That is s a calculation method of the relative contribution of dowels in the dowel group. That is

$$DSR = \frac{Fsi}{\sum_1^N Fsi} \times 100\% \tag{3}$$

In this paper,one dowel is considered as a engaged dowel in the load transfer system if the single DSR is larger than 1% of it.

Construction of 3D FE Model .3D Solid model has been chosen in this study,the design properties based on the Specifications of Cement Concrete Pavement Design for Highway[6]. The analysis software “ABAQUS” is used for this purpose,the structral and material detailed in Table 1.

Table 1 Structural and Material Parameters for Pavement

Layer	Dimension (m)	Elastic Modulus（Mpa）	Poisson Ratio	Density(Kg/m^3)
Concrete slab	5×4.5×0.26	30000	0.15	2400
Base	11.1×5.5×0.2	800	0.3	2000
Subgrade	11.1×5.5×2	150	0.35	2100
Steel bar	ϕ0.032	210000	0.3	7800
GFRP bar	ϕ0.032	30000	0.28	2600

Two concrete slab segments are supported by base and subgrade; a 5 mm wide joint is setted between the two concrete slabs for free expansion and contraction; a total of 15 dowels is included in this model with the spacing of 30cm, as illustrated in Figure 1.

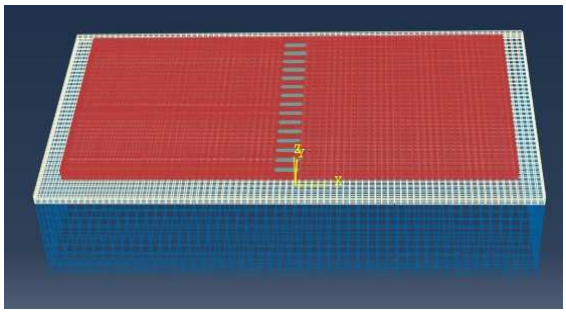

Figure 1 3-D FE Modeling of Dowel-Jointed Concrete Pavement

The concrete slab and the base layers are assumed to be frictional contact, and the slab-base friction value are considered as 0.05[7]; the base layers and the subgrade are assumed to be bound connection; all the dowels are setted as bound connection with the concrete slab in one side and setted frictional contact with the other concrete slab, the dowel-slab friction value considered as 0.1.

The standard axle load based on the current pavement design specifications is used as the model wheel load, and detailed in Table 2.

Table 2. Standard Axle Loading Data

Load case	Value
Single Wheel load (Kg)	5000
Tire pressure(MPa)	0.7
Tire Contact Shape	rectangular
Tire Contact Area (mm)	270×270

For the standard axle load analyse, two wheel loads are applied at the position as shown in Figure 2(a), a refined mesh zone is located at the edge of the joint[8], where wheel loads are applied, as shown in Figure 2(b).

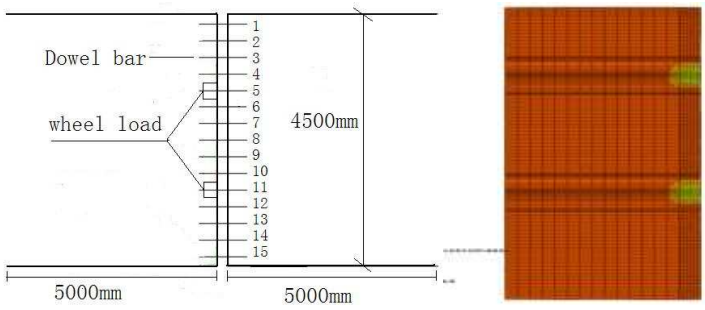

（a） (b)

Fig.2 Wheel Load position and dowel number for pavement model

Load Transfer Efficiency of GFRP Doweled Joint . This paper has been researching into four types of dowels, including a commonly used steel dowel with 32 mm diameter and three sizes of pultruded GFRP bars with the diameters of 32 mm ,40 mm and 54 mm. Figure 3 shows the joint face suffered from traffic load at the center of the joint.

Figure 3 The joint face of loaded slab suffered from traffic load

The LTEδ of the four types of doweled joint which is calculated according to the formula 1 are respectively 95.4%, 87.3%, 95.1% and 97.2%. It can be seen that the doweled joint,which uses the 32mm GFRP dowal bars,exhibits a significantly reduction in load transfer efficiency than the 32mm steel dowels.The LTEδ of the 40 mm doweled joint is almost the same as the 32mm steel dowels. The larger diameter, 54 mm GFRP doweled joint has the highest LTEδ in this study. That means GFRP bars have been introduced as a promising alternative material to the traditional steel dowels.

Load Transfer Behaviour of GFRP Dowels. Figure4 shows the shear force distribution of four types of dowels, and each marker shows the amount of shear force transferred by a dowel at transverse joint.

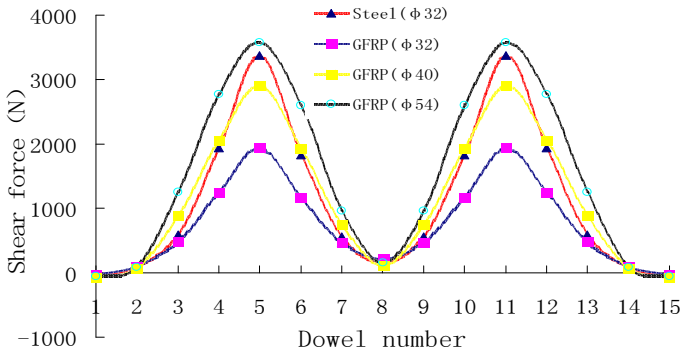

Fig.4 Shear force distribution of dowel at transverse joint

The SFTR of the four types of doweled joint which is calculated based on the formula 2 are respectively 16.8%,10.9%,17.1% and 22.5%. The SFTR of the four types of doweled joint is almost identical to the LTEδ of the joint. This ratio increases with the increase of diameter of GFRP dowels. The DSR of four types of dowels along the joint is shown in Table 3.

Table 3 DSR of four type dowel along the joint

Number	1	2	3	4	5	6	7	8
Steel（Φ32mm）	-0.3	0.5	3.5	11.5	21.9	10.9	3.4	0.9
GFRP（Φ32mm）	-0.3	0.5	4.4	11.4	17.7	10.6	4.3	1.9
GFRP（Φ40mm）	-0.5	0.6	5.2	12.1	17.0	11.3	3.3	1.7
GFRP（Φ54mm）	-0.2	0.7	5.5	12.3	15.8	11.6	2.9	1.8

From this diagram, one can clearly observe that eleven engaged dowels carry more than 99% of the transferred shear force in the dowel bar system. The contribution from the two end dowels (both sides) is inefficient no matter what type of dowels. In addition, the outer six dowels of both sides carried 7.4% shear force to the total amount of dowel bar system in the case of utilizing the 32-mm Steel dowel, 9.2% of 32-mm GFRP dowel case,10.6% of 40-mm GFRP dowel case and 12% of 54- mm GFRP dowel case. This phenomenon indicates that using the diameter of the GFRP dowel bar can increase the integrity of the doweled joint.

The results of numerical calculation in this study shows that the GFRP bars are a feasible alternative to commonly used steel dowels for using in jointed concrete pavements.The 40-mm GFRP dowels have been found to perform almost the same to the commonly used 32-mm steel dowels in load transfer efficiency of the doweled joint and load transfer behaviour of the dowel bar system. The large diameter GFRP dowels, especially the 54-mm bars, have been found to perform the best in this study.

Durability Study of GFRP Dowels

This study investigates the ultimate bearing capacity and long-term performance of the GFRP dowel bars under the condition of simulated vehicle axle loads.

Test Specimens. Four types of dowels are tested in this study, including a 32-mm steel dowel and three size of GFRP dowels with the diameters of 32mm,40mm and 54mm. All dowels are 500 mm in length and half of the lengh is embedded in a concrete slab with the dimensions of 300 mm x 400 mm x 260 mm which is the typical size standard based on the Specifications of Cement Concrete Pavement Design for Highway.The four types of dowel bars and specimen are shown in Fig.5.

Fig..5 Dowel bars and specimen

There are eight specimens for each type of dowels, four specimen are used for the static test, and the others for the long-term performance test.

Test Equipment. For all tests, the specimen is fixed under a rigid support beam to reduce the shake of the test machine during cyclic loading.The dowels are loaded in direct shear by a steel loading device to simulate the effect of the loaded panel transferring that load to an adjacent pane from the dowel bars by shear action as shown in Figure 6 below.

Fig.6 Test Equipment

Static test ..In the static test, the specimen are loaded to failure under step loading of 5KN/step by the loading device. The steel dowel reaches a maximum peak failure load of 45 kN, the failure pattern mainly is slipping pull crack as shown in Figure 7(a).The 32-mm GFRP dowel has a lower peak failure load of 30KN, the failure pattern is dowel bar broken as shown in Figure 7(b). The 40-mm and 54-mm GFRP dowels has peak failure loads of 42 kN and 55 kN respectively. The failure pattern is similar to the steel dowel specimen as shown in Figure 7(c).

(a) (b) (c)

Fig.7 Failure Pattern of Four Specimen

Test result shows that the larger diameter GFRP dowel bars are found to perform the best of ultimate load-carrying capacity.

Fatigue test . In order to research the durability of GRFP dowels , four types of specimens are conducted at fatigue loading at the frequency of 5 Hz for a total of 1,000,000 cycles at a level of 12KN. In order to simulate the amount of shear force transmitted by a dowel under treble the standard 100KN axle load calculated from FE model. The following experimental phenomena have been observed:(1) It can be seen that there is no indication of structural damage to any of the dowels or to the concrete pavement slab after the 1,000,000 cycle loading. (2) The dowel deflections are captured in fatigue experiment, the peak displacements are almost identical to the values measured in the static test provided earlier.(3) It is found a trifle debonding at the steel - concrete contact interface after the 1,000,000 cycle loading. At these locations, the concrete crushes subjected to high bearing stresses between steel dowel - concrete contact interface, which causes dowel looseness. The 40-mm and 54-mm GFRP dowels are not found any concrete crushed and dowel looseness after fatigue experiment because using of larger diameter GFRP dowel bars, even though a debonding phenomenon appears in the process.(4) The residual deflection of GFRP dowels after fatigue experiment is lower than the steel dowel, and then it recovers gradually within a day, which has better capability of fatigue resistance

Conclusions

The following major conclusions have been drawn from the present study:

(1) 3D finite element model has been chosen in this study,to investigate the load transfer characteristics of the GFRP dowels.The structural analysis package “ABAQUS” is used for this purpose. The results of numerical calculation in this study shows that the dowel shear ratio of GFRP bars is probably the same as commonly used steel dowels. The large diameter GFRP dowels, especially the 54-mm GFRP dowels, are found to perform the best in load transfer efficiency in this study.

(2) A experimental program including static and cyclic tests are carried out to study the performance of GFRP dowels.by using self-designed equipment. The static study shows that the using of larger diameter GFRP dowel bars can reduce the deflections， as well as bearing stress in the dowel-concrete contact interface. In addition, the using of larger diameter GFRP dowel could increasing the ultimate bearing capacity and durability of the doweled joint

(3) The recommendatory GFRP dowel is 20%-30% increase in diameter to traditional steel dowel because it should be more economical and reasonable in practical engineering.

Acknowledgments

The work described in this paper was fully supported by the National Natural Science Foundation of China (Grant No: 50808058) and Science and Technology Program of Heilongjiang Province (Grant No: 2010T0013-00).

References

[1] EDDIE D,SHALABY A,RIZKALLA S. Glass Fiber-Reinforced Polymer Dowels for Concrete Pavements[J]. American Concrete Institute Structural Journal,2001,98(2): 201-206.

[2] WANG Duan-yi,HU Chi-chun,RICHARD R.Assessment of Grouted Glass Fibber-Reinforced Polymer(GFRP) Tubes as Dowel Bar Alternatives[J].Highway, 2007(01):32-36.

[3] JIANG Ying-jun. Study of Conerete Pavement Materials and Strueture Under Heayv-load Transportation[D].Xi’an: Chang’an University,2005.

[4] ZHOU Zheng-feng,LING Jian-ming,YUAN Jie.3-D finite element analysis of the load transfer efficiency of joints of airport rigid pavement[J].China Civil Engineering Journal, 2009, 42(2): 112-118.

[5] SHIVA SRINIVASA. Characterization of stresses induced in doweled joints due to thermal and impact loads[D]. Morgantown，West Virginia: College of Engineering and Mineral Resources at West Virginia University,2001.

[6] FRIBERG B F. Design of Dowels in Transverse Joints of concrete Pavements[J]. American Society of Civil Engineering,1940,105(3):289-298.

[7]MURISON W S, Evaluation of Concrete-Filled GFRP Dowels For Jointed Concrete Pavements[Z]. Manitoba: University of Manitoba, 2004.

[8] ZHOU Zheng-feng,LING Jian-ming,YUAN Jie.3-D finite element analysis of the load transfer efficiency of joints of airport rigid pavement[J].China Civil Engineering Journal, 2009，42（2）：112-118.

doi:10.4028/www.scientific.net/AEF.5.283

Effect of Styrene Butadiene Rubber Latex on Mortar and Concrete Properties

Shuyi Yao [1, a], Yong Ge[2, b]

[1,2]School of Transportation Science and Engineering, Harbin Institute of Technology, Harbin 150090, China

[a]whx-lj2009@163.com, [b]hitbm@163.com

Keywords: SBR Modified Concrete; Mechanical Properties; Anti-Permeability.

Abstract: The use of styrene butadiene rubber (SBR) emulsions in concrete has been increasing in concrete construction and repair work due to its benefits to flexure strength, adhesion and impermeability. This research evaluated the influence of different contents (0%, 5%, 10%, 15%, and 20% by cement) of SBR on the mechanical properties and anti-permeability of the paste, mortar and concrete with the same water-to-cement ratio to analysis the SBR on the properties of them. For the mechanical properties, the compressive strength, flexure strength and elastic modulus were studied. The permeability was assessed by total charge-passed derived from rapid chloride permeability test (RCPT), all the samples were prepared and measured complying with the corresponding Chinese Industry Standard. Experimental results showed that the properties of the SBR modified concrete were associated with the corresponding properties of the SBR modified mortar and paste, and their properties changed in the same way with the incorporation of the SBR latex.

1. Introduction:

The use of high tensile strength materials such as fibers and rubbers to modify concrete is not new. Styrene butadiene rubber (SBR) latex, a type of high-polymer dispersion emulsion can be successfully bond to many materials, is widely used in engineering construction. A lot of researches have been done on the SBR latex modified cemented matrix. S. Natasha, M. Angelika etc. analyzed the SBR modified cement pasted and found that the polymer latex in the paste formed a continuous polymer network, and the compressive strength of latex modified paste was reduced, but the strain to failure was improved [1]. J. Schulze etc. found that the flexure strength of the mortar improved as the content of the SBR increased [2]. H Y Jiang found that SBR improved the water-proofing property of the mortar [3]. A. Mohsen analyzed the high-performance of fibrous polymer-modified concrete overlays and found that SBR polymer modified concrete could improve the toughness of the overlay concrete [4].The properties of the SBR modified paste, mortar and concrete have been researched, however, there are few researches analysis the influence of SBR on the concrete by comparing the properties of the SBR modified paste, mortar and concrete with the same water-cement ratio and polymer content. In this paper, the mechanical property and anti-permeability of the concrete influenced by the polymer content were studied, the comparison of 15% SBR modified concrete, mortar and paste with similar mix proportion were studied to analysis the SBR latex on the properties of the concrete. It is believed that the incorporation of SBR changed the properties of the paste in the concrete and enhanced the paste-aggregate bonding strength that resulted in the final properties of the SBR modified concrete. It is useful for simplifying the SBR

modified concrete research by analyzing the corresponding properties of the SBR modified mortar or paste. Also, it can be used to predicate the properties of the SBR modified concrete by the available SBR modified mortar properties.

2. Experimental Section

2.1 Materials

Cement used was grade 42.5 ordinary Portland cement produced by Ya Tai Cement Corp., complying with the Chinese Industry Standard GB 175-2007 with density of 3.10 g/cm^3. Coarse aggregate used was crushed limestone complying with the Chinese Industry Standard GB/T 14685-2001 with a gained size between 4.75mm~9.5mm. Sand used was river sand came from Songhua River complying with the Chinese Industry Standard GB/T14684-2001.

The admixtures used were SBR latex, high performance water reducer and anti-form agent. The SBR latex comes from Shandong Sheng De Corp. with solid content of 41±1% and pH of 9.0. The high performance water reducer used was UNF-5 Naphthalene water reducer came from Harbin Qiang Shi Corp. The anti-form agent used was DL-007 organ silicon air reducer came from Changzhou Zhen Tong Corp. All the admixtures used comply with the Chinese Industry Standard GB8076-2008.

2.2 Test method and specimens

For the experiment conducted, the test procedures followed the Chinese Industry Standard method showed in table 1. The slump and the air volume were controlled 15±3cm and2±1% separately by vary the content of super plasticizer and anti-form agent.

To eliminate the influence of the specimens' sizes, all the specimen of the paste, mortar and concrete were made with the same size dimensions. The specimens were made cube with dimensions of 100mm×100mm×100mm for compressive strength test and beam of dimensions of 100mm×100mm×300mm for elastic modulus test, 100mm×100mm×400mm for flexure strength test, and were cut into100mm×100mm×50mm for permeability test complying the corresponding standard separately. The conventional mortar and concrete specimens were cured in standard laboratory condition with temperature 20±2℃ and relative humidity more than 95%. The SBR modified specimens were cured in standard laboratory curing condition for the first 7 days, and then were air cured in 20±2℃ with the relative humidity of 60±5% for the rest 21days. The specimens were cured until 28d for test. For all test results discussed in this paper, Average of three specimens was used as the final experimental result.

When evaluating the anti-permeability of mortar and concrete, the total charge-passed of the paste were also tested. However, the permeability of conventional paste was so high that had beyond the range of the instrument, the permeability of the conventional paste was not discussed in this research.

Table 1 Test and test method standard

Test name	Method
Slump, Air volume	GB/T 50080-2002
Mechanical properties	GB/T 50081-2002
Total charge-passed(RCPT)	ASTM C1202-97

2.3 Mix proportions of concrete

Concrete with 0%, 5%, 10%, 15%, 20% of SBR were prepared with the water cement ratio of 0.34. The SBR contents were calculate by the solid quality of the SBR latex (i.e. the water in the latex was also included in the water cement ratio calculation). The same mix proportion of 15%

SBR modified paste, mortar and concrete were designed with differences in whether containing coarse or fine aggregate. All the experimental mixed proportions designed were summarized in Table 2.

Table 2 Mix proportion designed（kg/m^3）

Mix code	Cement	coarse	Sand	SBR latex	Water	Super plasticizer	anti-form agent
CP	450	0	0	0	153	5.4	0
MP	450	0	0	165	153	4.1	0.25
CM	450	0	780	0	153	5.4	0
MM	450	0	780	165	153	4.1	0.25
CC	450	975	780	0	153	5.4	0
MC5	450	975	780	55	121	4.9	0.06
MC10	450	975	780	110	88	4.5	0.11
MC15	450	975	780	165	56	4.1	0.25
MC20	450	975	780	220	23	3.6	0.44

3. Results and Discussion

3.1 Mechanical properties

3.1.1Compressive strength

The 28d compressive strength of different contents of SBR modified concrete was shown in Fig. 1. The compressive strength of the concrete decreased as the contents of the SBR improved. The compressive strength of the conventional concrete was 51.3MPa. As the SBR improved there was a slight reduction before the SBR content reached to 5 %(49.9MPa), then the compressive strength reduced sharply with the increase of SBR, and finally the reduction alleviated before the SBR content researched 20%. The result was consistent with R Wang [5] and A. Ali Abd Elkam [6] on their polymer modified mortar and polymer modified SCC research.

Fig. 2 compared the compressive strength of conventional and 15% SBR modified paste, mortar and concrete. Experimental results showed the compressive strength of 15% SBR modified paste, mortar and concrete were lower than the conventional. The compressive strength reduction of SBR modified concrete due to the fact that the incorporation of the SBR latex significantly reduced the compressive of the mortar and paste, the modified paste was only 52.7% of the conventional.

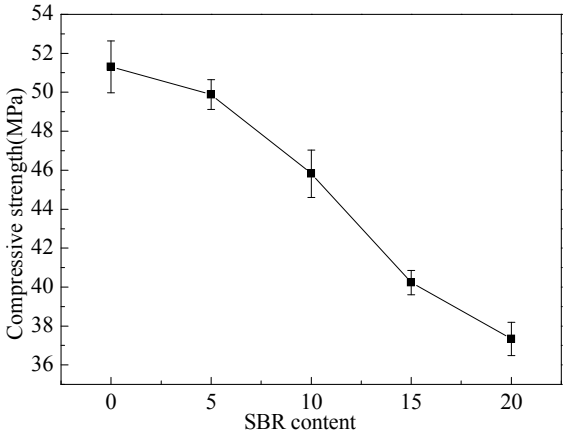

Fig.1. Influence of SBR latex on the 28d compressive strength of concrete

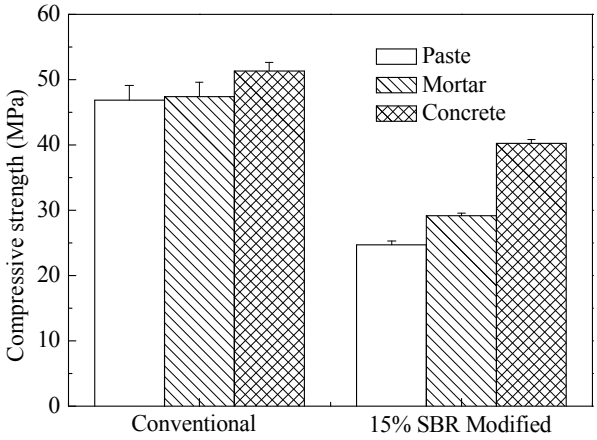

Fig.2. Compressive strength of the conventional and modified paste, mortar and concrete

3.1.2 Elastic modulus

The Elastic modulus properties of the SBR modified concrete showed a similar but sharper trend than that of the compressive strength. The elastic modulus of the concrete decreased as the content of the SBR increased, as shown in figure 3. The elastic modulus of the 20% SBR modified concrete was only 37% of the conventional concrete which was lower than that the compressive strength with the same SBR content with 73% of the conventional.

Fig 4 showed the elastic modulus of the conventional and 15% SBR modified paste, mortar and concrete. The experimental results explained the elastic modulus reduction. The incorporation of 15% SBR significantly reduced the elastic modulus of paste to its 33%, although the modified mortar and concrete gained similar growth as the fine and coarse aggregate added in, the final elastic modulus of the mortar and concrete were only 30% and 41% of the conventional one's.

The reduction in elastic modulus of the SBR modified concrete due to the incorporation of SBR polymer reduced that of the paste. The polymer in the paste acted as small pores [7] and continuous polymer network [1], the elastic modulus of hardened SBR was lower than the cement stone. It was easy to change its shape or disrupt under pressure. As a result, the resistance to press force and the elastic modulus reduced.

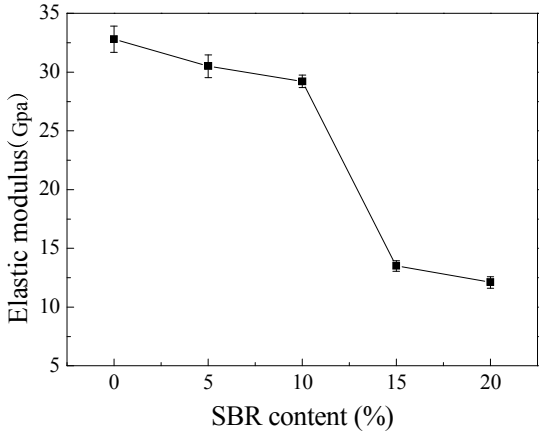

Fig. 3. Influence of SBR latex on the elastic modulus of concrete

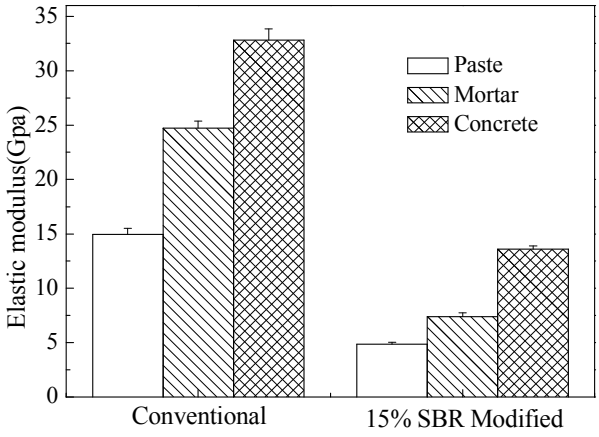

Fig. 4. Elastic modulus of conventional and modified paste, mortar and concrete

3.1.3 Flexure strength

Fig.5. showed the influence of SBR content on the flexure strength of the concrete. Experimental result showed that the flexure strength of the concrete increased consistently as the content of the polymer improved. It increased from 5.71MPa to 11.40MPa of 20% SBR content with an increment of 99.6%.

Fig 6 showed the flexure strength of the conventional and 15% SBR modified mortar and concrete. Experimental result showed that the flexure strength of the modified mortar was 8.55MPa, 66% higher than that of the conventional mortar of 5.15MPa. Compared with the conventional concrete gained little flexure strength improvement, the flexure strength of the modified concrete gained 29% increment from the modified mortar. The SBR modified concrete increased the flexure strength of the concrete with the following two reasons. The first one was that the SBR increased the flexure strength of the mortar, as shown in fig.6. The second reason was that SBR enhance the bonding of the interface of paste-aggregate of the interfacial transition zone (ITZ) between Portland cement paste and aggregate. This was accordance with the research of J. A. Rossignolo [8] which stated that SBR reduced the thickness of ITZ as the SBR reduced the quality of Ca^{2+} and the cent ration of water near the coarse aggregate.

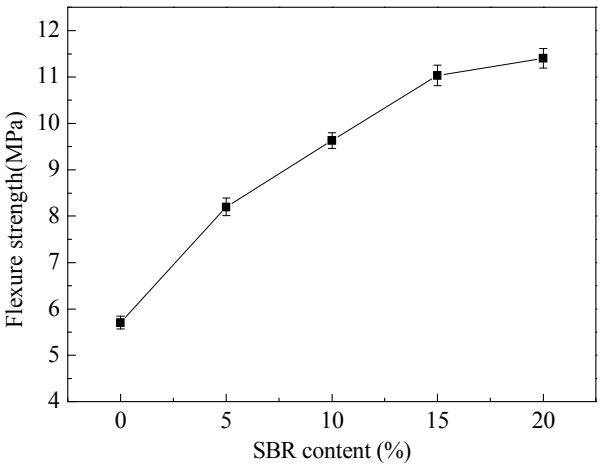

Fig. 5. Influence of SBR latex on the flexure strength of concrete

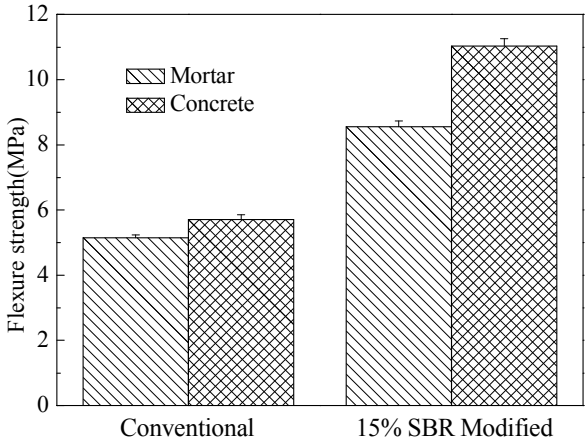

Fig. 6. Flexure strength of the conventional and modified mortar and concrete

3.2 Permeability

RCPT results are shown in Fig.7. The total change-passed of the conventional concrete was 1650C. The total change-passed of the concrete decreased sharply as the content of the SBR increased. The total charge-passed of the 20% SBR modified concrete reduced to 847C, about a half of that of the conventional. Experimental result showed that the anti-permeability of the concrete improved as the content of SBR increased.

Fig.9 compared the RCPT result of the conventional and modified mortar and concrete. The total charge-passed of the conventional mortar was 6766C of high permeability, while that of the 15% SBR was only less than one quarter with 1530C. The permeability of the both conventional and modified concrete were lower than the mortar. The total charge-passed were 2500C and 1101C separately. Experiment result showed that the SBR significantly reduced the permeability of the mortar, which was the main reason for the low permeability of the SBR modified concrete.

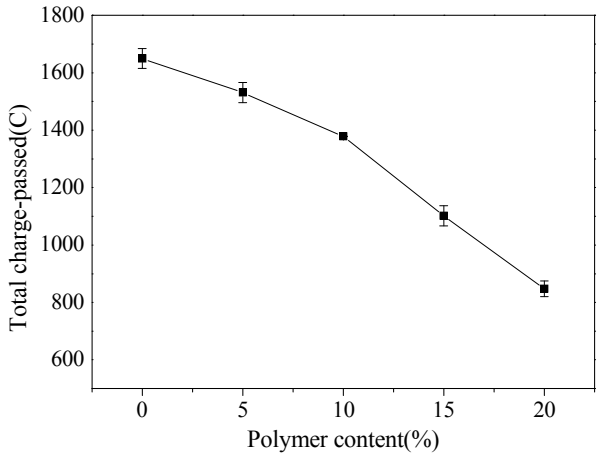

Fig. 7. RCPT results of different content of SBR modified concrete

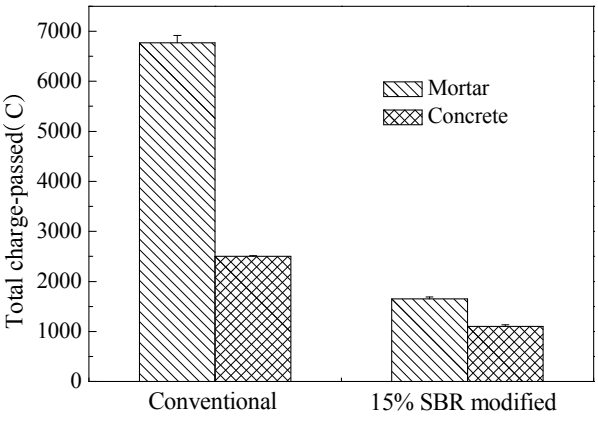

Fig. 8. RCPT result of 15% SBR conventional and modified mortar and concrete

The reduction in permeability was attributed to the fact that the SBR polymer particles were much smaller than the cement particles. They could be filled in the smaller voids of the paste and formed a monolithic film that surround the aggregates and cement particles. SBR modified mortar and concrete seldom bleeding which significantly affected the quantity of the continuous pores.

These effects both reduced the porosity and modified the pore structure [9]. Besides, the incorporation of SBR improves the tensile strength which prevented the micro-crack also improved the impermeability of the mortar and concrete.

4. Conclusions:

Based on the results and discussion presented in this paper, the following conclusions can be drawn:

The incorporation of SBR significantly changed the mechanical and permeability properties of the concrete. The compressive strength and elastic modulus of the SBR modified concrete were reduced, the flexure strength was improved and the anti-permeability of the concrete increased Obtained from the rapid chloride permeability test (RCPT) with the increase of SBR content.

The mechanical and permeability properties of paste, mortar and concrete changed in the same way with the incorporation of the SBR latex. The properties of the concrete containing SBR latex were determined by influence of SBR on the corresponding properties of the hardened paste and mortar.

The change in paste-aggregate of the interfacial transition zone (ITZ) between Portland cement paste and aggregate had great influence in the properties of the SBR modified concrete, especially for improvement of the flexure strength.

References:

[1] S. Natasha, M. Angelika, F. Gary P., B. Alexander, Polymerised high internal phase emulsion cement hybrids: Macroporous polymer scaffolds for setting cements, J. Cement and Concrete Research 41(2011)443-450.

[2] J. Schulze, Influence of water-cement ratio and cement content on the properties of polymer-modified mortars, J. Cement and Concrete Research, 1999，29-909.

[3] H. Y. Jiang, Z. X. Liu, Research of Polymer Cement Concrete, J．Journal of Wu Han University of Technology, 18 (1996): 37-38

[4] A. I. Mohsen, A. A. Mohammad, S. Hameed, High-Performance Plain and Fibrous Latex-Modified and Micro-silica Concrete Overlays, J. Journal of Materials in Civil Engineering 20(2008):742-752.

[5] R. Wang, P. M. Wang, X. G. Li. Physical and mechanical properties of styrene–butadiene rubber emulsion modified cement mortars, J. cement and concrete research 35(2005)900-906.

[6] A. Ali Abd Elkam, A. E. Abd Elmoaty, Experimental investigation on the properties of polymer modified SCC, J. Construction and Building Materials 34(2012)584-592.

[7] E. Sakai, J. Sugita, Composite mechanism of palmer modified cement, J. Cement and Concrete Research 25(1995)127–35.

[8] J. A. Rossignolo, Interfacial interactions in concretes with silica fume and SBR latex, J. Construction and Building Materials 23 (2009)817-821.

[9] M. Ramli, A. A. Tabassi. Effects of polymer modification on the permeability of cement mortars under different curing conditions: A correlational study that includes pore distributions, water absorption and compressive strength, J. Construction and Building Materials 28(2012)561-570.

doi:10.4028/www.scientific.net/AEF.5.289

The influence of admixtures on vibration viscosity coefficient of pavement concrete

Jishou Yu [1,a] Xiaoping Cai [2,b] Yong Ge [3,c] Zhigang Wu [4,d]

[1-3]School of Transportation Science and Engineering, Harbin Institute of Technology, Harbin 150090, China

[4] ZhongYe research institute of building

[a] hityu@sohu.com [b] chaicp@sina.com [c] hitbm@163.com [d] 388560@qq.com

Keywords: Pavement concrete, Vibration viscosity coefficient, Admixture

Abstract: In this paper, the influences of common admixtures including air entraining agent, superplasticizer, shrinkage-reducing agent, retarder, fly ash and slag on vibration viscosity coefficient of fresh concrete were analyzed. The results showed that the vibration viscosity coefficient of fresh concrete was markedly decreased when using UNF-5 naphthalene formaldehyde sulphonated superplasticizer. When SJ-2 air entraining agent, SZ103 shrinkage-reducing agent, retarder and slag were used, the vibration viscosity coefficient of fresh concrete was also reduced. But when fly ash was added, the vibration viscosity coefficient of fresh concrete was increased.

Introduction

Compared to other materials, cement concrete is suitable for pavement concrete because it has some special properties such as long service life, weather resistant, freezing resistant, wear resistance and anti-slide. Since 80s, cement concrete road has been rapidly developed. Slipform paving is one of the most advanced construction technology, it is an intelligent and automatic construction technology of pavement concrete. However, research data [1] showed that most advanced slipform pavers imported from developed country are idle because of the disappointed construction quality. The most serious problems are edge collapse and surface voids related to the workability of fresh concrete. And most research results showed that compared to slump, vibration viscosity coefficient is more suitable for evaluating the workability of fresh concrete when slipform paving is used. Both types and dosages of common admixture can influence the vibration viscosity coefficient of fresh concrete. Therefore, in order to guiding construction and improving the engineering quality, the influence law should be studied.

Materials and mix design

Cement of P·O 42.5 and class Ⅰ fly ash were used in all experiments. The fine aggregate used was river sand with the fineness module of 3.4. The coarse aggregate was crushed limestone rock with the maximum grain size of 26.5mm and crushing value of 4.5%. The slag is produced by Tong Guang Group with the specific surface area of 4800 cm^2/g. When studied the influence of additives on vibration viscosity coefficient, SJ-2 saponin air entraining agent, UNF-5 naphthalene formaldehyde sulphonated superplasticizer and SZ103 shrinkage-reducing agent were chose. Meanwhile, citric acid and sodium gluconate were chose as retarder.

According to “Test Method of Concrete vibration viscosity coefficient” which can be found in “Technical Specifications of Slipform Construction on Cement Concrete Pavement for Highway” (JTJ/T 037.1-2000), the experimental installation and experimental test method were chose.

The design philosophy was given by “Technical Specifications for Construction of Highway Cement Concrete Pavements” (JTG F30-2003). The base mix proportion is showed in table 1.

Table1 Mixture proportion of base concrete

Strength standard value [MPa]	*W/C*	Sand ratio [%]	Water [kg/m^3]	Cement [kg/m^3]	Sand [kg/m^3]	Coarse aggregate [kg/m^3]
4.0	0.40	34	144	360	670	1300

When studying on the influence of chemical admixtures on vibration viscosity coefficient, 15% cement was replaced by fly ash, and the substituted coefficient was 1.3. The dosages of superplasticizer were 0.6%, 0.8%, 1.0% and 1.2% respectively, and the dosages of air entraining agent and shrinkage-reducing agent were both from 0.1‰ to 0.6‰. When studying on the influence of mineral admixtures on vibration viscosity coefficient, the replacement ratio of fly ash and slag were both 10%, 20%, 30% and 40% respectively. When fly ash and slag were added together, fly ash occupied 30%.

Results and discussions

Effect of superplasticizer, shrinkage reducing agent and air entraining agent on vibration viscosity coefficient. Figure 1 showed that with the increasing of dosages of superplasticizer, the vibration viscosity coefficient of fresh concrete decreased. It is because of the lubrication action of superplasticizer. When adequate superplasticizer adsorbing on cement powder, there will be a stable solvation water film and steric hindrance will be produced by the film [2]. Because of the steric hindrance, the cement powders were separated from each other. At the same time, the slump of concrete also increased with the increasing of superplasticizer. But the most suitable slump for slipform pavers is 15～40mm[3]. Therefore the appropriate vibration viscosity coefficient can not be reached by only adjusting the dosages of superplasticizer.

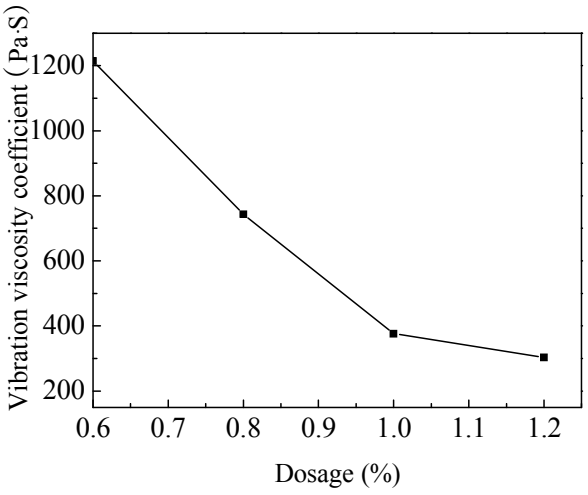

Figure 1 Relationship between dosages of superplasticizer and vibration viscosity coefficient

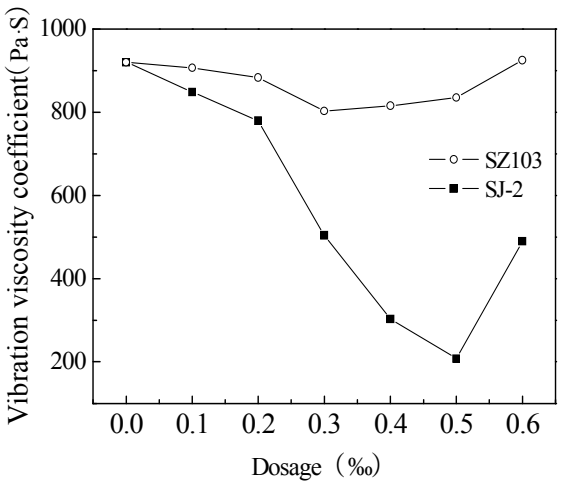

Figure 2 Effect of air-entraining agent and shrinkage reducing agent on vibration viscosity coefficient

It is can be found from figure 2, the vibration viscosity coefficient of fresh concrete was insensitivity with SZ103 shrinkage reducing agent. When the dosages of shrinkage reducing agent were changed from 0.1‰ to 0.6‰, the vibration viscosity coefficient almost remains unchanged.

Figure 2 also showed that when air entraining agent was used, the vibration viscosity coefficient of fresh concrete was sharply dropped to the lowest point, then it was increased, and the inflection point was 0.5‰. There are two mainly effects of air entraining agent. One is “miniature ball

bearing" effect, the other is surface effect. Numerous minification and individual air bubbles were brought into concrete by air entraining agent. The sliding friction between aggregate was changed into rolling friction by these air bubbles which have the same effect as balls. That means the friction drag becomes lower, and a better liquidity and a lower vibration viscosity coefficient of fresh concrete were reached. On the other hand, some air bubbles were absorbed by the surface of cement powders, which cause an increment of vibration viscosity coefficient. The two effects were concurrent, when the dosage of air entraining was under 0.5‰，the "miniature ball bearing" effect was the leading one, otherwise the surface effect was.

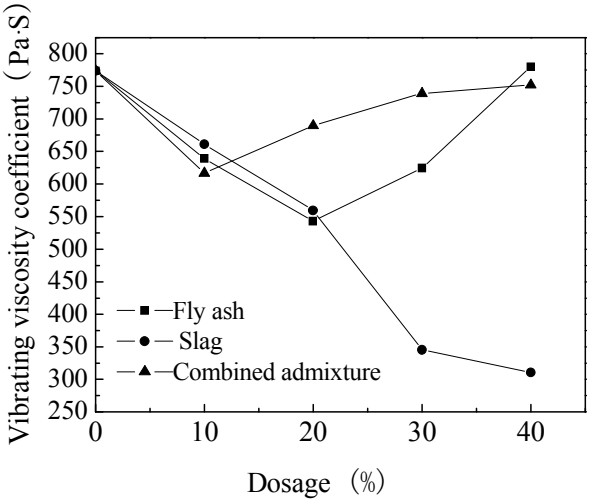

Figure 3 Effect of mineral admixtures on vibration viscosity coefficient

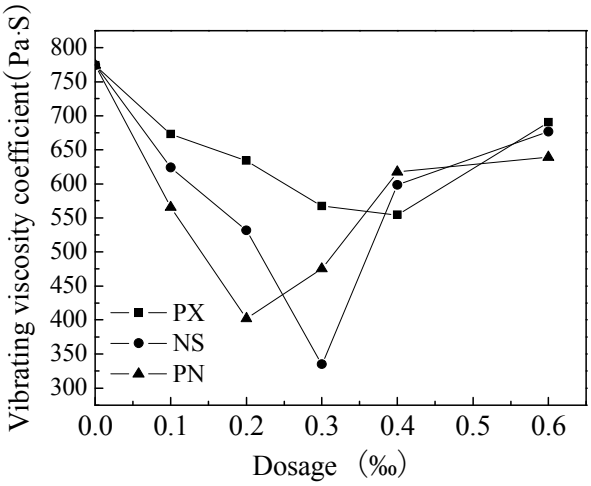

Figure 4 Effect of retarder and cellulose on vibration viscosity coefficient

Effect of mineral admixtures on vibration viscosity coefficient. It is can be seen from figure 3, when the dosages of slag increased, the vibration viscosity coefficient sharply decreased, because of its higher activity and lower water requirement. When adding fly ash or both of them, the two curves had inflexions, which were 20% and 10% respectively. Before the inflexion, vibration viscosity coefficient decreased with the increasing of dosages, and after the inflexion, vibration viscosity coefficient increased with the increasing of dosages. It is because of the effects of fly ash. Three effects of fly ash are volume effect, morphological effect and micro-aggregate effect. The main mineral compositions of fly ash are sponginess vitreous body and aluminosilicate glass microballoon. The sliding friction between binding material powder was changed into rolling friction by these spherical vitreous bodies [5]. Secondly, the adsorption force between fly ash and water is less than that between cement and water, and the dispersion of cement powders can be promoted by this character of fly ash. Therefore the vibration viscosity coefficient decreased. On the contrary, because of the low activity, hydration reaction of fly ash was stagnant during the early age, and the volume radio of water and binding materials would be increased. That means the liquidity of concrete mix decreased and the vibration viscosity coefficient increased. Consequently, when the dosages became higher, the vibration viscosity coefficient increased. In a word, the vibration viscosity coefficient decreased because of morphological effect and micro-aggregate effect, and increased because of volume effect. When both fly ash and slag were added, it would be a comprehensive effect.

Effect of other admixture on vibration viscosity coefficient. It is can be seen from figure 4 the vibration viscosity coefficients were decreased in different degree, when cellulose, sodium gluconate and citric acid were added into concrete. Take cellulose as an example, while the dosage

was 0.4‰, the vibration viscosity coefficient of fresh concrete was the lowest one. With the increasing of dosages, the vibration viscosity coefficient increased. However, the decrement causing by cellulose is not enough. Because the demand value of slipform paving is 300～500Pa·S, and the lowest vibration viscosity coefficient was above 550Pa·S when adding cellulose.

Sodium gluconate and citric acid are common retarders of concrete. After adding into concrete, some of them are absorbed by C_3A [6], others are dissolved in water and then absorbed by C_3S. Because of the absorption, the contact between water and cement powder were separated, and the hydration reaction was delayed. Therefore, the workability of concrete can be kept for a long time. When 0.2‰ sodium gluconate or 0.3‰ citric acid was added, the vibration viscosity coefficient were 400Pa·S and 350Pa·S respectively which were suitable for slipform paving. When the dosages increased, the vibration viscosity coefficient also increased. That means in this research, the best dosages of sodium gluconate and citric acid were around 0.2‰ to 0.3‰.

Conclusions

a. The vibration viscosity coefficient of fresh concrete decreased with the increasing dosages of superplasticizer. But the loss of slump was also increased. Therefore the appropriate vibration viscosity coefficient can not be reached by only adjusting superplasticizer.

b. The vibration viscosity coefficient of fresh concrete was insensitivity with SZ103 shrinkage reducing agent, but it was markedly affected by a certain dosage of air entraining agent.

c. With the dosages of slag increased, vibration viscosity coefficient of fresh concrete decreased. When the dosages of fly ash were under 20%, vibration viscosity coefficient of fresh concrete descended, and rose when the dosages were over 20%. The some results were obtained by combined mineral admixtures, and the inflection point was 10%.

d. The vibration viscosity coefficient of fresh concrete markedly decreased when adding retarders like citric acid and sodium gluconate.

References:

[1] Fu Zhi. Slip-form construction technique of pavement concrete[M]. Bei Jing: People Transport Press, 2000.

[2] Ge Zhaoming. Concrete admixture[M]. Bei Jing: Chemical Industry Press, 2005.

[3] Technical Specifications for Slipform Construction of Highway Cement Pavement Concrete. (JTJ/T037.1-2000).

[4] Xiong Dayu, Wang Xiaohong. Concrete admixture[M]. Bei Jing: Chemical Industry Press, 2002.

[5] Qian Jueshi. Fly ash characteristics and fly ash concrete [M]. Bei Jing: Science press.2002.

[6] Huang Shiyuan, Jiang Jiafen. Modern concrete technology[M]. Shan Xi: Science and Technology Press, 1998.

doi:10.4028/www.scientific.net/AEF.5.293

The Research on Tests for Detecting Strength of Shallow Asphalt Pavement under Ice Frozen

Zhao Maocai[1a], Gao Shixian[1b], Shi Dawei[2c], Huang Qishu[2d]

[1]School of Transportation Science and Engineering, Harbin Institute of Technology, Harbin, China

[2]Inspection Bureau of Guizhou province for traffic construction engineering quality, Guiyang, China

[a]zhao_maocai@126.com, [b]gaoshixian0424@163.com, [c]shidawei88@126.com, [d]huanqs@126.com

Keywords: Asphalt Pavement; Penetrating Strength Detector of Shallow Pavement; Void Ratio; Freeze-Thaw Cycle; Strength of Shallow Pavement

Abstract: The thesis utilizes the Penetrating Strength Detector of Shallow Pavement to conduct impacting penetration experiment, uniaxial compression test and diametral compression test to asphalt mixture of different void ratios and cycles of freezing and thawing, and then we've obtained the relationship between average penetration depth and compressive strength as well as tensile splitting strength of mixture, moreover, the initial reference standard of the Penetrating Strength Detector of Shallow Pavement is established. Afterwards, the thesis conducts impacting penetration test to the asphalt pavement cores from Chongzun freeway in Guizhou Province suffering from ice frozen damage. The effectiveness of the Penetrating Strength Detector of Shallow Pavement has been proved.

Introduction

Nowadays, the on-the-spot detective methods involving strength of shallow pavement conclude Benkelman Beam, Falling Weight Deflectometer(FWD), Ground Penetrating Radar, Ultrasonic wave method, WINDSOR method, Needle penetrating method of concrete (Penetrating resistance method and Detective needle pressing-in method of concrete strength) Rebound Apparatus, etc.; The methods in laboratory conclude CBR method, compression and tensile splitting tests of core samples, etc[1-3]. Generally speaking, the detected deflection is the comprehensive response of all structure layers under pavement surface to loading. Therefore, they can't detect the strength of a certain depth in pavement surface layer [4].

Ground Penetrating Radar is used to detect the thickness of highway surface course and defects. Because the damage from ice frozen to shallow pavement doesn't have obvious interface, it can not detect the strength of a certain depth in pavement surface layer, either [5-7]. Ultrasonic wave method is similar with Ground Penetrating Radar, which also can't detect the strength of a certain depth in surface layer [8].

What has Rebound Apparatus detected is a comprehensive value of concrete strength in a certain depth of concrete surface. The Rebound Apparatus can only obtain a overall evaluation instead of concrete strength of different depths [9].

WINDSOR method, as known as Needle penetrating method of concrete (Penetrating resistance method and Detective needle pressing-in method of concrete strength), is able to evaluate concrete strength with penetration depth or pressing-in depth according to corresponding relationship between penetration depth and concrete strength given by ASTM[10]. However, this method to evaluate the damage of shallow pavement under ice frozen still exist deficiencies as follows:

a. Auxiliary device to provide counterforce needs to be fixed on spot in advance, which is tedious and inconvenient;

b. The concrete strength of a defined depth can't be detected;

c. The penetration work can't be controlled. In most situations, after penetration work is fixed, the depth of penetrator injecting-in or pressing-in can't be controlled artificially (mainly affected by concrete strength and magnitude of penetration work—static pressure).

In consequence, the author has designed the Penetrating Strength Detector of Shallow Pavement which can overcome the detection deficiency above， aiming at resolving the detection and evaluation problem of shallow pavement under ice frozen. This detector is able to evaluate the strength of shallow pavement rapidly according to the relationship between detection data and multiple mechanical properties of pavement established by relevant experiments, possessing comprehensive applicability and extensive prospect.

The changing regularity about compressive strength and tensile splitting strength of the asphalt mixture in different void ratios

The experiment adopts similar materials and asphalt-aggregate ratio with Chongzun freeway pavement in Guizhou and molds several specimens through rotation compacting method according to Superpave specification, afterwards, the linear contrast relationship between void ratios and quality is obtained by fitting. Therefore, the specimen quality corresponding to design void ratios of 3%, 6%, 9% and 12% can be obtained, then we molds 36 specimens with 9 in each group corresponding to 4 void ratios according to the relationship above through rotation compacting method again.

We select 3 specimens from each group and put them in thermostatic water tank of 25℃ together for heat insulation of 4 hours, then the experiments are conducted on MTS material testing machine with loading speed of 2mm/min, afterwards the compressive strength and tensile splitting strength are obtained respectively.

The relationship that the compressive strength and tensile splitting strength obtained from experiments varies with void ratios is shown as Figure 1 and 2.

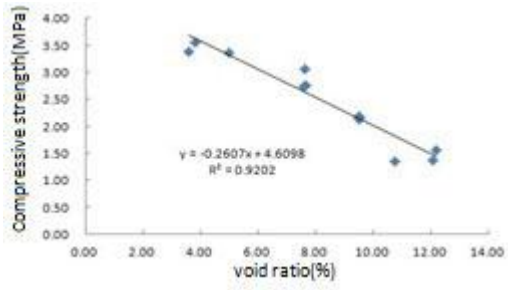

Figure 1. Change of compression strength with voidage

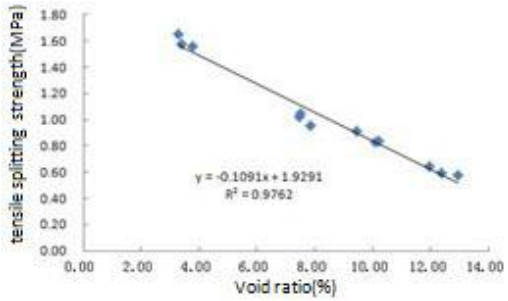

Figure 2. Change of splitting strength with voidage

As we can see from the two Figures above, the compressive strength and tensile splitting strength of asphalt mixture decrease as void ratio grows. The two pairs of relationship above own a great relativity by regression and the regression coefficient reaches 0.9209 and 0.9762 respectively. The slope of straight lines obtained by regression in the Figures is relatively large, which means that void ratio has great influence on strength of asphalt mixture.

The impacting penetration test to asphalt mixture of different void ratio

The experiment adopts the self-designed Penetrating Strength Detector of Shallow Pavement(10kg, 8mm) to conduct impacting penetration experiment under room temperature(25℃)， and testing targets are the remaining specimens molded. Because the testing specimens are independent without peripheral pressure, the thesis has manufactured a fixture of detecting asphalt mixture specimens to simulate the peripheral pressure.

The testing results of impacting penetration experiment to 12 specimens with different void ratios are shown as Figure 3 and 4.

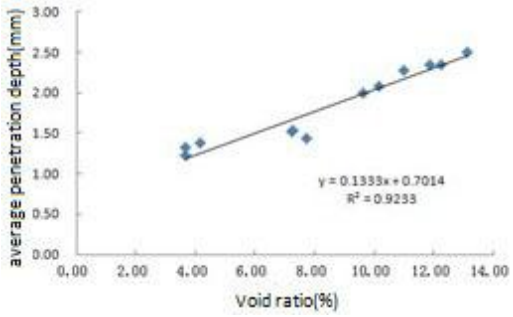

Figure 3. Change of peening times with voidage

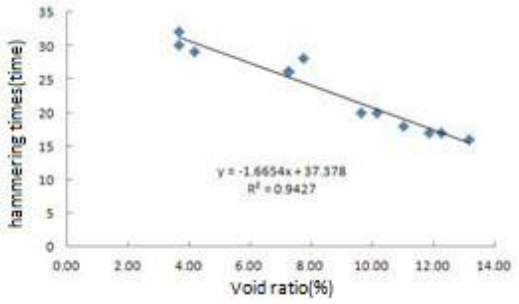

Figure 4. Change of peening times with voidage

The linear relationship between void ratio and average penetration depth as well as hammering times is good as the Figure4 have shown which enables us to contact the average penetration depth with the compressive strength and tensile splitting strength of asphalt mixture through the easily available and important index-void ratio.

The contrast analysis between impacting penetration experiment and compressive strength as well as tensile splitting strength of asphalt mixture

Firstly, we obtained the following equations through linear fitting to the experimental data:

$$Rc = -0.2607VV + 4.6098 \quad (1)$$

$$RT = -0.1091VV + 1.9291 \quad (2)$$

$$Da = 0.1333VV + 0.7014 \quad (3)$$

$$N = -1.6654VV + 37.378 \quad (4)$$

Where Rc is compressive strength,(MPa), RT is tensile splitting strength,(MPa), Da is average penetration depth,(mm), N is hammering times and VV is void ratio,(%).

We can obtain the relationships between compressive strength, tensile splitting strength as well as void ratio and average penetration depth as well as hammering times respectively according to the equations (1-4), which are shown as follows:

$$Rc= -1.9557Da+5.9816 \quad (5)$$

$$RT= -0.8185Da+2.5032 \quad (6)$$

$$VV= 7.5019Da-5.2618 \quad (7)$$

$$Rc= 0.1565N-1.2413 \quad (8)$$

$$RT= 0.0655N-0.5195 \quad (9)$$

$$VV= -0.6005N+22.4439 \quad (10)$$

Considering the uniformity of asphalt mixture specimens prepared in laboratory and the testing results of impacting penetration experiment, it's found that the average penetration depth shows linear change with the hammering times. Therefore, the thesis choose average penetration depth as the detection index of Penetrating Strength Detector of Shallow Pavement, while hammering times can only be the detection referenced index at the situation that total penetration depth is 10cm.

The changing regularity of asphalt mixture's tensile splitting strength in room temperature after freezing and thawing

Considering the climate features in Guizhou and existing conditions in laboratory, the thesis measures tensile splitting strength of the specimens, defining freezing for 8 hours and thawing for 16 hours as a freezing and thawing cycle, then 3 cycles as a small cycle.

We can obtain the relationship curve of tensile splitting strength of the asphalt mixture specimens changing with freezing and thawing cycles by tensile splitting strength experiment, which is shown in Figure 5.

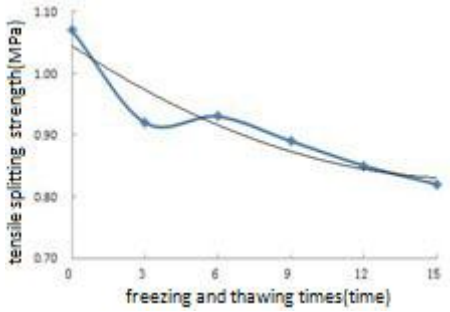

Figure 5. Change of tensile splitting strength after freeze-thaw cycles

As we can see from the Figure above, the tensile splitting strength of asphalt mixture in room temperature tends to decrease with freezing and thawing cycles grow. The tensile splitting strength varies obviously after 3 freezing and thawing cycles and then tends to ease up, the reason of which is the porosity characteristic of asphalt mixture. After vacuum water-saturated test, the inner void of mixture is filled with water, and then the void osmotic pressure and expansive force of ice are generated during water in voids turning into ice, which makes the void in specimens grow rapidly and tensile splitting strength of the first 3 freezing and thawing cycles decrease sharply. While after several cycles, the removal quantity of water during freezing process goes down gradually and the expansive force also tends to be steady, so the change of tensile splitting strength tends to ease up.

The impacting penetration experiment of asphalt mixture after freezing and thawing

In order to obtain the relationship between testing results of the Penetrating Strength Detector of Shallow Pavement and tensile splitting strength of asphalt mixture under different times of freezing and thawing cycles, the thesis conducts impacting penetration experiment to the same specimens molded and obtains the changing curve of average penetration depth varying with freezing and thawing times under different freezing and thawing damage, shown in Figure 6.

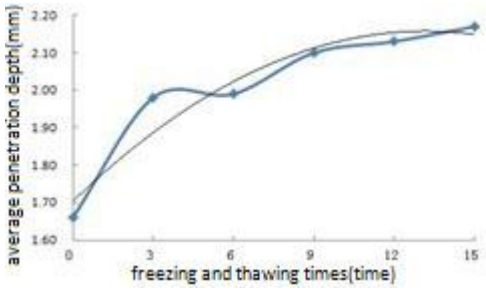

Figure 6. Change of average penetration depth with freeze-thaw cycles

As we can see from the Figure above, the average penetration depth tends to increase as the freezing and thawing times grow, and it also represents the behavior that the curve varies obviously in the first 3 freezing and thawing cycles and then tends to ease up afterwards, whose reason is almost the same with the former tensile splitting experiment.

The contrast analysis between impacting penetration experiment and tensile splitting strength experiment under freezing and thawing

After fitting analysis with the testing data, we can calculate to obtain the relationship between tensile splitting strength of asphalt mixture and average penetration depth of the Penetrating Strength Detector of Shallow Pavement, shown in Figure 7.

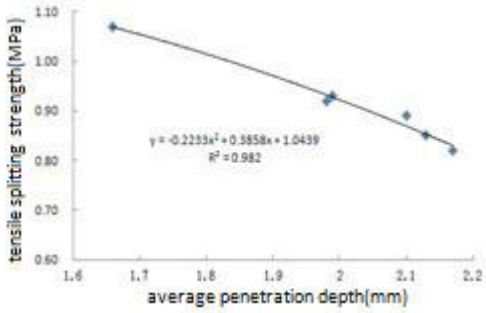

Figure 7. Relationship between tensile splitting strength and average penetration depth

The average penetration depth grows from 1.66mm to 2.17mm, while the tensile splitting strength decreases from 1.07MPa to 0.82MPa along with it. The regression parameter R2 can reach 0.9820 after fitting.

The evaluation to compressive strength and tensile splitting strength of the core samples

After analyzing the data above, the overall compressive strength level of core samples is relatively low and compressive strength of 60% core samples is below 3MPa. The tensile splitting strength mainly lies in the range of 0.6-1.5MPa, which can satisfy the specification requirement basically. The void ratio of nearly a half of core samples lies in 5%-9%, and some core samples' void ratio even reaches more than 13%. As the Technical Specification for Construction of Highway Asphalt Pavement has demanded, the void ratio shall be kept between 3%-5%. Therefore only 12%

of the core samples can meet the requirement of specification, which demonstrates that the asphalt pavement of Chongzun freeway has been damaged badly under long-term freezing and thawing and other complex conditions.

Conclusion

According to the actual testing contrast, the combination of falling hammer weighing 10kg and penetrator with diameter of 8mm is determined as detection components.

The changes of asphalt mixture specimens' mechanical property under different freezing and thawing times are controlled by designing different void ratios, and we conduct impacting penetration test, uniaxial compression test and tensile splitting test to the specimens and then obtained the conclusion that compressive strength and tensile splitting strength of asphalt mixture both decrease as average penetration depth in impacting penetration test increases, while void ratio increases as average penetration depth increases. We can establish the initial reference standard of the Penetrating Strength Detector of Shallow Pavement for detecting the void ratio, compressive strength and tensile splitting strength in room temperature by linear fitting.

The thesis conducts impacting penetration experiment to the core samples in asphalt pavement of Chongzun freeway in Guizhou Province under ice frozen damage, and then we obtained the void ratio, compressive strength and tensile splitting strength of the core samples in depth of 0-100mm by utilizing the detection reference standard established formerly. We have offered a great evaluation on the degree of the pavement suffering from ice frozen damage and also provided a reliable reference for the follow-up maintenance work.

Summary

This research is sponsored by the department of China science ministry No: 2008BAG10B02.

References:

[1] Liu Huaqing, Han Jiguang. Research on Nondestructive Detection Techniques of Freeway Pavement[J]. Journal of Highway and Transportation Research and Development, 2009,(1):49-50.

[2] Hu Xiaguang. The Present Status and Development of Rapid Detection Techniques of Pavement at Home and Abroad[J]. Journal of China and Foreign Highway, 2003, 23(6):95-99.

[3] Wang Zehua. Research on Nondestructive Detection Techniques of Pavement[J]. Journal of Anhui University Architecture, 2006, 14(2):22-24.

[4] ASTM. Standard Test Method for Measuring Deflections with a Light Weight Deflectometer (LWD) E2583 – 07[S] 2007.

[5] Samer Lahouar, Imad L.AI-Qadi. Automatic Detection of Multiple Pavement Layers from GPR Data[J]. NDT&E International 41(2008):69-81.

[6] Timo Saarenketo, Tom Scullion. Road Evaluation With Ground Penetrating Radar[J]. Journal of Applied Geophysics, 43_2000:119-138.

[7] C. Fauchard, X. De'robert, J. Cariou. GPR Performances for Thickness Calibration on Road Test Sites[J]. NDT&E International, 36 (2003) :67-75.

[8] Zhu Jinzhang, Luo Xin, Zhao Xiaolong. Supersonic Rebound Method to Evaluate the Compressive Strength of Freeze-thaw Concrete[J]. Low Temperature Architecture Technology, 2005(3):3-5.

[9] Natianal Standard of the People's Republic of China. Technical Specification for Inspection of Concrete Compressive Strength by Rebound Method[S]. JGJ/T23-2001.

[10] ASTM. Standard Test Method for Penetration Resistance of Hardened Concrete C803 / C803M - 03(2008) [S]; 2008.

doi:10.4028/www.scientific.net/AEF.5.299

Compacting Properties of Zeolite Based Warm Asphalt Mixture

Liying Yang[1,a], Yiqiu Tan[1,b]

[1]School of Transportation Science and Engineering, Harbin Institute of Technology, Haihe road 202#, Harbin, Heilongjiang, China 150090

[2]Beijing Municipal Road & Bridge Building Material Group Co.Ltd, West of Wanglizhuang Railway Bridge, Daxing District, Beijing, China, 102600

[a]yangliying_q@sina.com, [b]yiqiutan@163.com

Key words: Warm Asphalt Mix, Zeolite, Compaction Properties, Performance

Abstract. Warm asphalt mixture develops rapidly throughout the world in recent years. Zeolite based warm mix is one of the warm mixtures. In this paper, seven kinds of zeolites including six natural zeolites and one synthetic zeolite are selected. As warm mix additives, their physical properties such as density, water content and pore arrangements are tested respectively. To evaluate the compacting properties of zeolites based warm asphalt mixture, AC-20 mixture is designed and compaction is conducted. It shows that zeolites can reduce the compacting temperature for both Marshall and gyratory compaction. Temperature is the main factors which influence the compaction effect. Type of zeolite affects compaction to some extent. Marshall compaction is more sensitive to zeolite than gyratory compaction.

Introduction

Warm asphalt mixture is a new technology. It can reduce the mixing temperature for about 30℃ and thus decrease the energy consumption and lower the emission. The performance of the mixture is equivalent to its hot counterpart. There are four types of warm mix: Aspha-Min, WAM-Foam, organic additives and asphalt emulsion[1]. Aspha-min is a synthetic zeolite.

Zeolite is a group of alumino-silicates. Its unique character is the internal mineral skeleton which is a group of interconnected tetrahedrons. A silicon ion lies in the center which is surrounded by four oxygen atoms. The silicon-oxygen arrangement (SiO_4) forms a tetrahedron with four oxygen ions at the four top points. The silicon icon can be replaced by aluminum and an aluminum-oxygen tetrahedron forms. All these tetrahedrons interconnect, to form the zeolite skeleton. In the skeleton, there are many kinds of pores and tunnels with different size and shape. The porous zeolite contains certain amount of water of crystallization. The water will evaporate gradually with the increasing temperature, which leads to foaming in asphalt. The foams increase the binder volume and reduce the viscosity of the binder to improve the workability [2].

To evaluate the compacting properties of zeolite based warm mix, seven zeolites are selected and tested. AC-20 asphalt mixture is designed and the compacting behavior is researched.

Zeolites

Seven Zeolite samples including six natural zeolites and one synthetic zeolite are selected. The natural zeolites are taken from quarries of Heibei, Henan and Liaoning Provinces. The synthetic zeolite is Aspha-min.

Density. Density is the most fundamental property of mineral additives. Table 1 is the apparent density of zeolites. No.1 to No.6 is the 6 kinds of natural zeolites and No.7 is the synthetic product. The apparent density of all zeolites is far smaller than that of limestone filler. No.1 has the lowest density, while No. 6 has the highest. The density is mainly determined by their origin.

Table 1 Apparent density of zeolites and limestone filler

Zeolite	1	2	3	4	5	6	7	filler
Apparent density (g/cm^3)	2.127	2.375	2.145	2.294	2.223	2.623	2.297	2.811

Pore structure. Zeolite is a porous mineral. The large amount of pore provides enough space for water. With Mercury porosimetry test[3], the pore size and distribution of zeolites are tested and the result is listed in Table 2.

Table 2 Pore structure of zeolites

Zeolite	Median pore diameter （nm）	Average pore diameter （nm）	Porosity(%)
1	2311.5	97.0	58.69
2	6852.3	126.3	44.16
3	7725.8	72.7	46.44
4	6839.5	77.6	49.74
5	3951.3	317.8	50.46
6	22743.4	621.1	52.59
7	2172.9	1823.5	71.54

The pore character is quite different. To the seven kinds of zeolites, the synthetic zeolite has the largest amount of pores which are distributed uniformly.

Moisture content. There is some water among the pores of zeolites. In natural condition, the water stays stable, but it will evaporate if temperature increases gradually. The water content of zeolites differs a lot. To analyze the evaporation of water, five specific temperatures(105℃,120℃, 140℃, 160℃ and 180℃) are selected and the result is in Table 3.

Table 3 Water content of zeolites

Zeolite	Moisture loss under different temperature(%)				
	105℃	120℃	140℃	160℃	180℃
1	7.48	7.83	8.24	8.93	9.08
2	5.45	5.52	5.52	5.52	5.53
3	9.36	9.93	10.91	11.63	11.84
4	8.73	8.92	9.65	10.02	10.49
5	8.75	8.77	9.69	10.34	10.63
6	4.20	4.28	4.91	4.92	4.94
7	6.09	9.59	13.31	16.45	17.82
Mineral filler	0.43	0.43	0.43	0.44	0.44

The amount of water which evaporates at different temperatures is quite different to these zeolites. No.7 has the highest water loss while No. 6 has the lowest. But the water loss of zeolites is far more than limestone filler.

Asphalt mixture design

In AC-20 asphalt mixture, pen70 asphalt and limestone aggregates are used. In order to analyze the influence of zeolite on the properties of warm mix and to decrease the deviation of grading, all the aggregates are sieved in advance and then blended according to the target gradation of AC-20 mixture, which is in Table 4.

Table 4 Gradation of AC-20 asphalt mixture

Sieves(mm)	26.5	19	16	13.2	9.5	4.75	2.36	1.18	0.60	0.30	0.15	0.075
Passing (%)	100	95.0	83.0	72.0	57.0	38.0	26.0	18.0	13.0	9.0	6.5	5.0
Range (%)	100	90-100	76-90	64-80	50-64	33-43	21-31	13-23	9-17	6-12	4-9	3-7

Asphalt ratio. By volumetric analysis of the compacted Marshall specimens, the optimal asphalt ratio is 4.3%. To hot and warm mix, the asphalt ratio differs little.

Compacting properties of warm mixture

Compaction is the most critical means to improve the integrity and the stability of asphalt mixture. The composition of the mixture, the properties of the aggregates and the rheological characteristics of the binder influence the compacting[4,5,6]. As to warm mixture, it must exhibit satisfying compacting ability at relatively low temperature. In this paper, the compacting behaviors of all the seven zeolites mixture are investigated. Table 5 is the compacting results of Aspha-min warm mixture and Table 6 is the air void of Marshall specimens. Table 7 shows the gyratory compacting results of the mixtures.

Table 5 Marshall compacting results of Aspha-min mix

Type	Mixing temperature (℃)	Compacting temperature (℃)	VV(%)	VMA(%)	VFA(%)
Hot mix	160	150	3.9	14.0	72.1
Warm mix	150	140	4.1	14.1	71.0
	140	130	4.3	14.3	69.9
	130	120	4.3	14.3	70.0
	120	110	4.8	14.8	67.6
	110	100	5.6	15.5	64.0
	100	90	6.5	16.3	60.1
	90	80	7.1	16.9	57.9

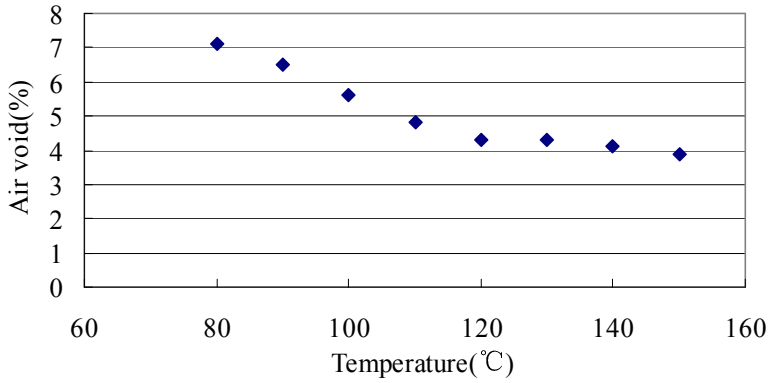

Figure1 Air void versus temperature

It is clear that to Aspha-min warm mixture, the air void of the mixture decreases with the increase of the compacting temperature as listed in Figure 1. There is a flat region in the compaction curve, which is between 120 to 140℃. In this temperature span, the mixture is compactable and the mixture is not sensitive to temperature. If the compacting temperature is below 120℃, the slope of the curve is steep and the mixture is sensitive to compacting temperature. It is suggested that to Aspha-min mixture, the compactable temperature is 120~140℃.

Table 6 Air voids of Marshall compacting mixtures (%)

Zeolite \ Compact temp(℃)	110	120	130	140
1	5.0	4.5	4.5	3.8
2	5.0	4.4	4.3	3.9
3	5.2	4.4	4.4	4.3
4	5.7	4.8	4.1	3.5
5	5.0	4.4	4.1	4.0
6	4.7	4.1	4.0	4.0
7	4.8	4.3	4.3	4.1

Table 7 Air voids of gyratory compacting mixtures (%)

Zeolite \ Compact temp (℃)	100	120	140
1	5.2	3.8	3.4
2	4.8	4.0	3.5
3	4.6	3.9	3.3
4	4.9	4.0	3.5
5	5.0	4.2	3.2
6	4.7	3.9	3.4
7	4.4	4.1	3.0
Hot mix	5.4	4.8	4.0

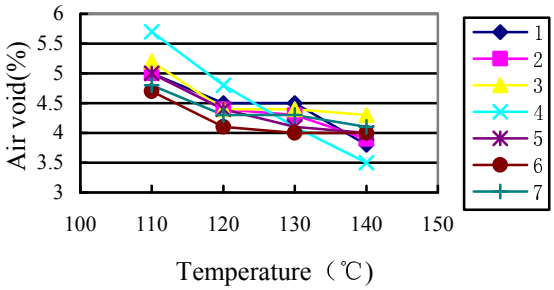

Figure 2 Air void of Marshall specimens

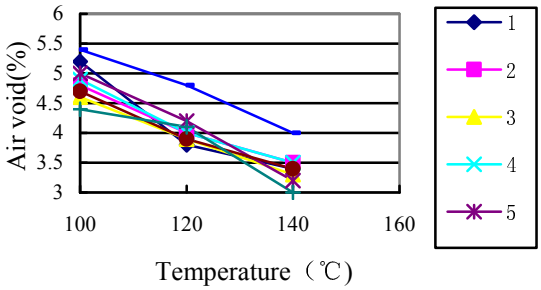

Figure 3 Air void of gyratory specimens

Marshall compaction result in Figure 2 shows that to different zeolites, the air void of the mixture is quite different. At the same temperature, No. 6 and No. 7 mixtures are easier to compact than the other five zeolites. No. 4 zeolite is most sensitive to temperature because the compacting curve is steep. Taking the pore structure into consideration, No.6 zeolite has the largest median pore diameter and No 7 has the largest average pore diameter. Pore diameter may influence the compacting effect. It is inferred that larger pores are helpful to the evaporation of the water and thus beneficial to the compaction.

The compacting curve of gyratory compacting specimens is Figure 3 and the comparison is Figure 4. Gyratory compaction specimens exhibit lower air voids. On the other hand, the air void of gyratory sample changes a little with the difference of zeolites, which means, gyratory compaction is less sensitive to the type of zeolites than Marshall compaction.

Hot mix is generally compacted at the temperature of 150℃, and the target air void is 4.0%. To keep the same level of air void, warm mix must be compacted no less than 120℃ to all these zeolites. Compared to hot mix, the compacting temperature of zeolite based warm mix decreases about 30℃.

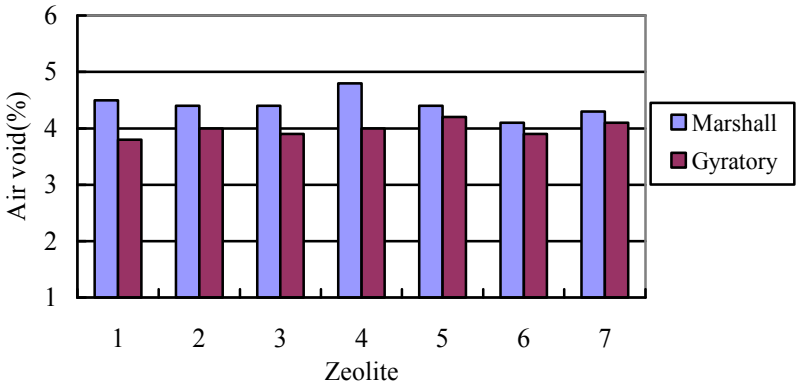

Figure 4 Air voids of Marshall and Gyratory specimens of 120℃

Conclusions

In this paper, the properties of zeolites are evaluated and analyzed. The compaction of asphalt mixture is conducted and the following conclusions can be drawn:

Zeolite has smaller density than limestone filler. It is porous and some amount of water stays in the pores. The water evaporation of zeolite makes it useful in warm mixture. The pore structure and water contend differs with different zeolites.

Temperature is the most important factor that influences compaction. With the increase of compacting temperature, the air void decreases. 120 ℃ is the critical compactable temperature for zeolite mixture.

It is inferred that the pore diameter is one of the factors that affect the compaction.

Marshall compaction is more sensitive to the type of zeolites than gyratory compaction.

Acknowledgements

The authors appreciate the support of the Ministry of Science and Technology on the Research project of "Cooperative Research on Green Manufacturing Technology for Asphalt Pavement" (2010DFB83490).

References

[1] Qin Yongchun, Huang Songchang. Warm Asphalt Pavement Technologies and latest Researches [J]. Petroleum Asphalt, 2006.8, Vol20(4): 18-20

[2] M. Carmen Rubio, Germán Martínez, Luis Baena, Fernando Moreno. Warm mix asphalt: an overview. Journal of Cleaner Production 24 (2012) 76~84

[3] LIU Yu xin. Measurement and Expression of Pore Structure of Particle Material. China Powder Science and Technology. 2000.8.Vol 6 No 4:1-27

[4] Shen Jin'an. Performance of Asphalt and Asphalt Mixture[M]. China Commnication Press, 2001.5

[5] Ji Jie. Performance Evaluation of Recycled Asphalt Mixture and Warm Asphalt Mixture [M]. China Communications Press, 2011.5

[6] ZHANG Jiu-peng, PEI Jian-zhong, XU Li, XING Xiang-yang. Gyratory compaction characteristic of SBS warm mixed asphalt mixture. Journal of Traffic and Transportation Engineering.Vol11(1).2011.2;1~6

[7] SUN Ji-shu, XIAO Tian, YANG Chun-feng, JIN Can-zhang.On Properties of Warm Mix Recycled Asphalt Mixture in Highway JOURNAL OF CHONGQING JIAOTONG UNIVERSITY(NATURAL SCIENCE). 2011.4. Vo.l 30(4).:259-253

[8] ZUO Feng, YE Fen. Evaluation on the technology and performances of warm mix asphalt mixture in foreign countries[J]. Chinese Journal of China & Foreign Highway.2007.27 (6): 164-168.

doi:10.4028/www.scientific.net/AEF.5.305

Study on Asphalt Pavement Temperature Field Distribution Law in Seasonally Frozen Regions

Rui Zhang [1,a] ,Yiqiu Tan [1, b] , Leyong Qu[2,c] ,Huining Xu[1,d]

[1] School of Transportation Science and Engineering, Harbin Institute of Technology, Harbin, Heilongjiang, 150090, China

[2]Beijing General Municipal Engineering Design &Research Institute, Beijing, 100082, China

[a] shanzhangrui@126.com, [b]yiqiutan@163.com,[c] 397978414@qq.com, [d]xhn1983@163.com

Keywords: Road Engineering, Asphalt Pavement, Temperature Field Distribution, Seasonally Frozen Regions

Abstract. Based on the temperature field data collected from a self-developed pavement system, asphalt pavement temperature field distribution law in seasonally frozen regions was studied in detail. Test data illustrated that: The atmospheric and pavement temperature shows cycle sine rule; Minimum and maximum values of pavement temperature occur at surface, In winter, pavement temperature gradually increases with increasing depth, but has contrary result in summer; As the increase of depth, the fluctuation range of pavement temperature decreases gradually, which lead to the appearance of daily and annual constant temperature point; The max freezing depth appeared at 120cm and there will be freezing core in spring in seasonally frozen regions.

Introduction

Road structure is exposed to the natural environment, in addition to bear the vehicle load, but also affected by environmental factors such as temperature, radiation, wind, rain, snow and so on[1,2]. So the pavement structure must not only meet the load requirements, but also to adapt to their environment. Only thus can guarantee its long-term performance, otherwise, the road structure is bound to have early damage [3,4].

Among environment factors, temperature has the greatest impact on the road structure [5]. According to statistics, 53.5% of the area in china belongs to seasonal frozen region, where torridity summer, frigid winter, great annual temperature difference are obvious features. Bearing capacity and service performance of pavement are sensitive to the change of temperature [6]. Therefore, it is necessary to develop the study on temperature distribution characteristic of asphalt pavement in seasonally frozen regions.

Brief Introduction of Typical Pavement Structure Model System

Currently,the experimental study on temperature field, mainly used building of typical test section in wild for long-term fixed point observation, and small indoor model test. The former need a long observation period, and consumes large amounts of human, material; the latter test could not impersonate the real working conditions of road structure because of small size, Therefore, this article adopts the common form road structure in China, builds outdoors test bench to simulate real-world conditions, and takes the study on variability and distribution of road structure temperature.

The seasonal frozen pavement structural model test bench has a total length of 5 meters, width of 2.1 meters, test-bed structure as shown in table 1:

Tab 1 Test-bed of Road Structures

structure layer	material	thickness /cm
surface layer	cmAC20+5cmAC20+7cmAC20	17
base	three-kinds ash	40
Subgrade	clay	—
Subgrade form	cutting	

The temperature sensors use semiconductor sensors of the WS-TS201, Measurement temperature range is -40~120℃, The measurement accuracy is ± 0.5℃. Sensor buried schematic as shown in Fig.1:

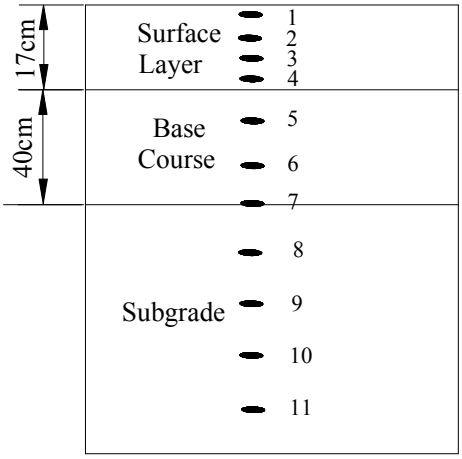

Sensor 1- depth 2cm Sensor 2- depth 5cm Sensor 3- depth 10cm Sensor 4- depth 17cm Sensor 5- depth 30cm Sensor 6- depth 43cm Sensor 7- depth 57cm Sensor 8- depth 90cm Sensor 9- depth 130cm Sensor 10- depth 170cm Sensor 11- depth 210cm

Fig.1: Sensor buried schematic

Daily Variation Law of Atmospheric Temperature

From the figure 2, we can know the daily variation law of atmospheric temperature:

The atmospheric temperature shows cycle sine rule. Heat up time is much shorter than the time to cool, so heating rate is greater than the cooling rate.

Minimum temperature occurred in 4:00-6:00 am, maximum temperature occurred in 14:00-15:00 pm.

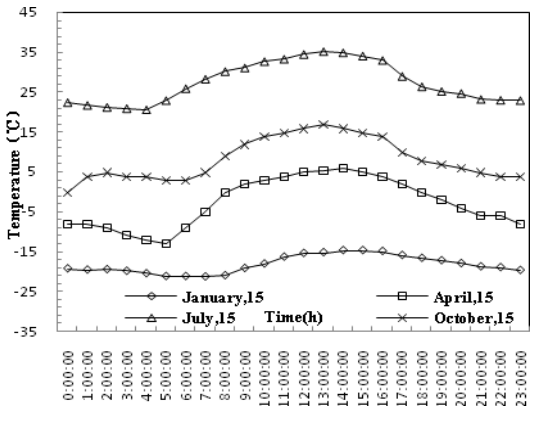

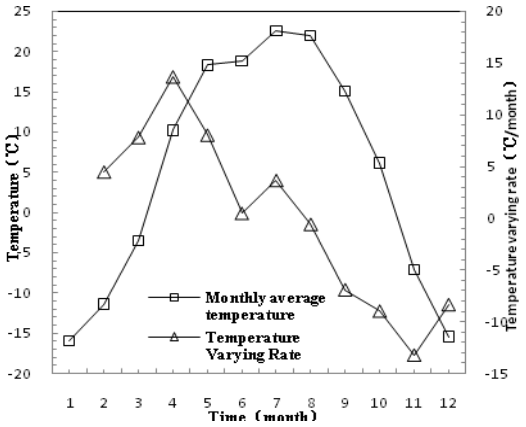

Fig.2: Daily atmospheric temperature in Harbin Fig. 3: Annual atmospheric temperature in Harbin

Annual Variation Law of Atmospheric Temperature

As known in Figure 3, the minimum average temperature occurred in January with -15℃, maximum average temperature occurred in July with 25℃.

Longer winter and summer, shorter spring and autumn, greater annual range of temperature are major features in Harbin.

Daily Variation Law of Pavement Temperature

The Figure 4 demonstrates the law as follows:

Pavement temperature has the similar variation law to atmospheric temperature, but lagging behind atmospheric, Minimum temperature occurred in 6:00-7:00 am, maximum temperature occurred in 14:00-15:00 pm.

Hysteretic nature gradually increases with increasing depth.

As increasing depth, the fluctuation range of pavement temperature decreases gradually, and tends to 0℃ at a certain depth, which can be called daily constant temperature point. Below daily constant temperature point, temperature a day can be represented by the temperature at any time, a daily cycle of temperature change can be instead by the annual cycle.

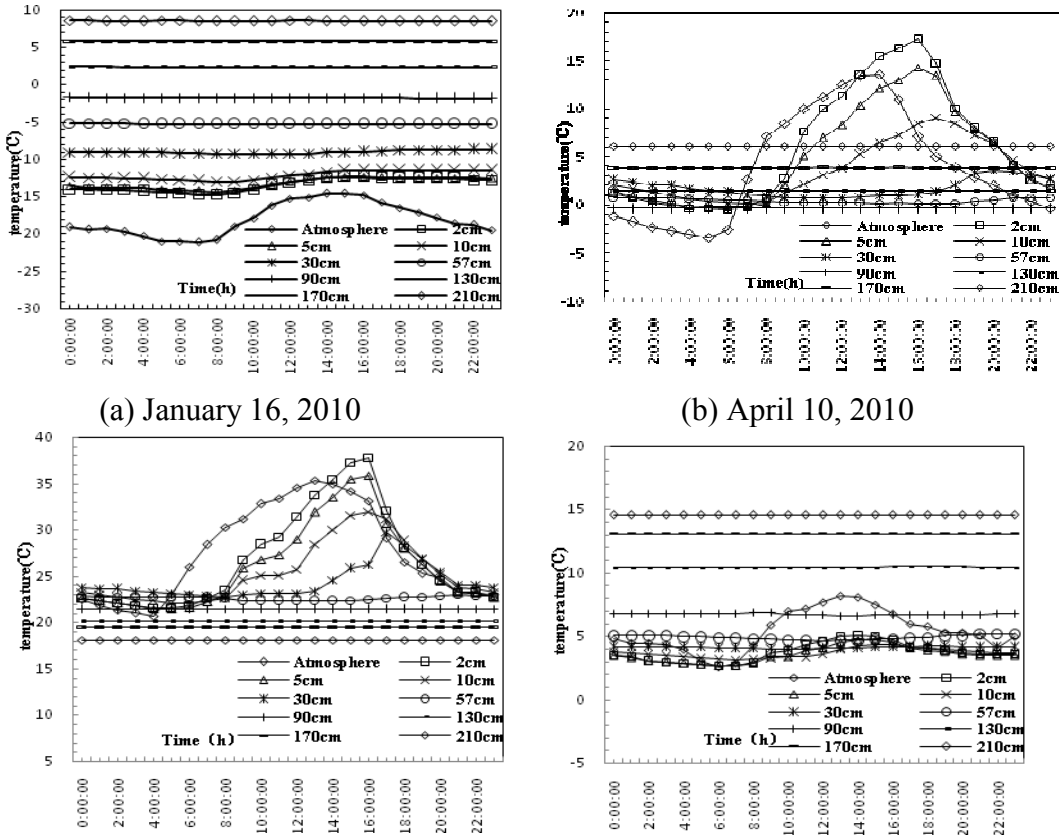

(a) January 16, 2010 (b) April 10, 2010

(c) July 27, 2010 (d) November5, 2010

Fig.4: Daily variation law of pavement temperature in Harbin

Annual Variation Law of Pavement Temperature

Figure 5 and Figure 6 illustrated that, the pavement temperature shows cycle sine rule with the period of a year, but has different extremum and phase.

In winter, pavement temperature gradually increases with increasing depth, but has contrary result in summer.

With the depth increasing, Hysteretic nature gradually increased and annual range of temperature difference gradually decreased. At a certain depth, the difference will tend to 0℃, where we can call the depth annual constant temperature point. Below the point, the structure will be constant temperature layer.

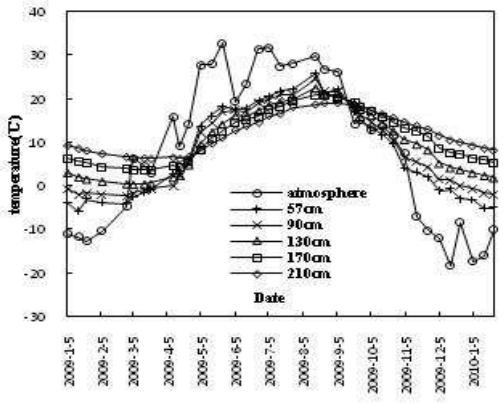

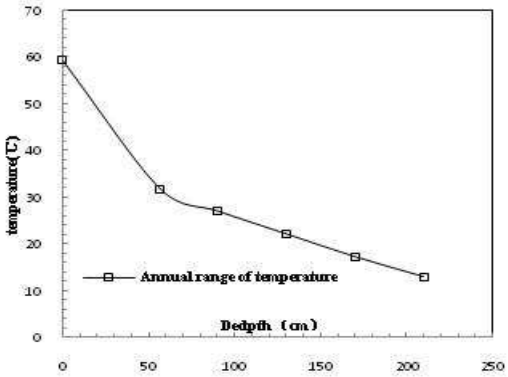

Fig.5: Annual variation law Fig.6: Annual range of temperature difference

Annual Change of Daily Constant Temperature Point

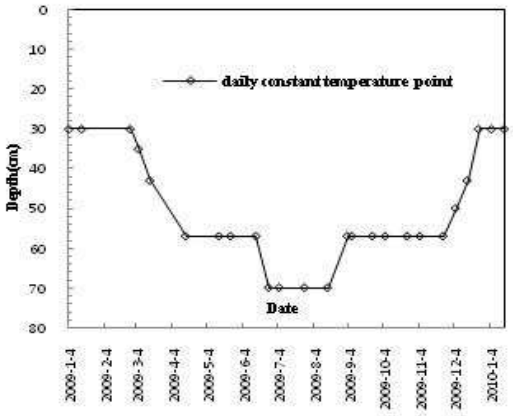

Fig.7: Daily constant temperature point

Figure7 shows the annual change of daily constant temperature point:
The curve is approximately symmetric. In winter, the daily constant temperature point has the minimum at 30 centimeter. And in summer, it has corresponding maximum at 70 centimeter. Moreover, there is sharply change in spring and autumn.

Freezing Depth Line

Figure 8 and Figure 9 shows that, the freezing depth line start in mid-November and reach maximum in late February with 120 cm. Subsequently, upper layer and lower layer start to melt synchronously in spring, which result in the appearance of freezing core. The freezing core is unique freezing phenomenon in seasonally frozen regions.

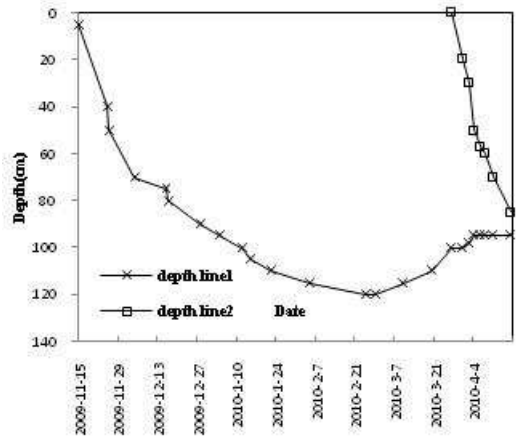

Fig.8: Freezing depth line in 2009~2010

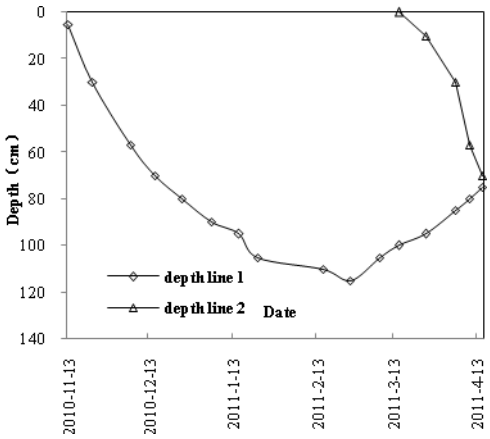

Fig.9: Freezing depth line in 2010~2011

Conclusions

The atmospheric and pavement temperature shows cycle sine rule. Heat up time is much shorter than the time to cool, so heating rate is greater than the cooling rate. As increasing depth, the fluctuation range of pavement temperature decreases gradually, which lead to the appearance of daily and annual constant temperature point. The max freezing depth appeared at 120 cm and there will be freezing core in spring in seasonally frozen regions.

References

[1] BARBER ES. Calculation of Maximum Pavement Temperatures from Weather Reports [A].Washington D C: Highway Research Board, Bulletin 168, National Research Council, 1957.

[2] ROBERTSON W D. Determining the Winter Design Temperature for Asphalt Pavement [A]. Proceeding of Association of Asphalt Paving Technology,1997.

[3] Zuoren Yan. Analysis of the Temperature Field in Layered Pavement System[J].Journal of TongjiUniversity,1984（3）：76-85 .（In Chinese）

[4] Ganchang Wu. The Analysis of Pavement Temperature Field of Multi-layer System[J]. China Journal of Highway and Transport,1992,5(4):17-25. （In Chinese）

[5] Lijun Sun, Jian Qin. Prediction Model on Temperature Field in Asphalt Pavement [J].Journal of Tongji University : Natural Science,2006,34(4):481-483. （In Chinese）

[6] Jian Qin, Lijun Sun. Study on Asphalt Pavement Temperature Field Distribution Pattern[J]. Journal of Highway and Transportation Research and Development,2006,23(8):18-21. （In Chinese）

doi:10.4028/www.scientific.net/AEF.5.310

Test Study on Road Performance of Soils Stabilized by Liquid Stabilizer in Seasonally Frozen Regions

CHEN Yao[1,2,a], TAN Yi-qiu[1,b]

[1]School of Transportation Science and Engineering, Harbin Institute of Technology, Harbin,China
[2]College of Architectural and Civil Engineering,Heilongjiang University, Harbin, China

[a]chenyao170105@126.com,[b] yiqiutan@163.com

Key words: stabilizer,soil, base course,performance,seasonally frozen region

ABSTRACT: In seasonally frozen regions, road construction often suffers from low strength,lack of durability, etc. Improving the typical clay's workability in Changchun with lime and the Base-Seal stabilizer (BS-100) shows promising results. A comprehensive investigation to assess the soil characteristics influence is undertaken, so as the lime and liquid stabilizer (BS-100) content on the physical properties of stabilized soils in seasonally frozen regions. The optimum mix proportions, unconfined compressive strength, splitting strength, modulus of resilience, freeze-thaw action, water resistance and penetration-resistance were outlined. By comparing with current specifications, the Base-Seal stabilized soil as base material has higher early strength, higher after-strength and better frost stability.The results can be applied in road construction in seasonally frozen regions.

Introduction

Adequate road network is an important factor to the socio-economic development in a country. However, the quantum of materials required for the construction is usually huge. Conventional materials such as cement, aggregates, steel are lacking and quite expensive[1]. As we all know, soil is the cheapest available material utilized by man for various construction-related purposes. Stabilization of soils with low-bearing capacity is an economical way for road construction. It can be used to form subase, road base and surface courses, a great deal of granular materials and cementious materials can be saved. So the solid wastes pollution and the consumption of natural resources will be reduced[2-5].

The natural durability and strength of the soil can be improved through the process of 'soil stabilization' using different types of stabilizers. The main methods[6-7] by which soils are stabilized for road purposes are:(1) mechanical or granular stabilization;(2) cement stabilization;(3) lime and lime-pozzolan stabilization[8]; (4) bituminous stabilization; and (5)stabilizer reinforced soil. In recent years, the use of cementitious material like Portland cement, hydraulic lime and lime-pozzolana mixes as stabilizer is quite common. But for these stabilized soils, their early strength is usually very low, and they have inadequate frost stability and water resistance[9].Therefore, a new type of lime-liquid stabilizer material is used as road base material in order to improve the typical clay's workability in seasonally frozen regions. The following sections present the experimental process and the results of various tests conducted on stabilized soils.

1. Experimental Process

1.1 Materials

Liquid stabilizer—'BS-100',it contains no acids or explosive materials and is environmentally safe, non-toxic, non-corrosive, non-flammable,non-allergenic.

Slake-lime—It is in line with the technical requirements for the Ⅲ grade with 55.3% reactive CaO+MgO.

Cement—C32.5 ordinary Portland cement.

Soil—The engineering properties of the original soil are presented in Table[1].

Table1 The engineering properties of the soil

ω_l(%)	ω_p (%)	I_P	ρ_{dmax}(g/cm^3)	ω_{op} (%)	Soil classification
38.1	23.0	15.1	1.92	12	MLS

1.2 Experimental design

Attempt to determine the optimum mix proportions, comprehensive series of laboratory tests were conducted with various percentage and combination of stabilizers. It consisted of standard proctor compaction and 7-day unconfined compression strength. The relative compaction of the test sample is 98%. The specimens were stored in curing room (20±2℃, 95±2%RH).Table[2] presents a summary of stabilized soil mixtures with various stabilizer combinations.

Table2 Stabilizer combination scheme for stabilized soils

Combination	Lime (%)	Cement (%)	BS-100(%)	ρ_{dmax} (g/cm^3)	ω_{op} (%)	7-UCS (Mpa)
1	3	0	0.25	1.85	12.5	0.93
2	3	0	0.28	1.85	12.5	1.03
3	3	0	0.32	1.85	12.5	1.06
4	5	0	0.25	1.84	12.8	1.62
5	5	0	0.28	1.84	12.8	1.79
6	5	0	0.32	1.84	12.8	1.69
7	7	0	0.25	1.83	13.0	1.78
8	7	0	0.28	1.83	13.0	1.67
9	7	0	0.32	1.83	13.0	1.60
10	0	2	0.28	1.92	12.1	0.74
11	0	2	0.32	1.92	12.1	0.60
12	0	4	0.28	1.91	12.3	1.33
13	0	4	0.32	1.91	12.3	1.40
14	0	6	0.28	1.90	12.6	1.66
15	0	6	0.32	1.90	12.6	1.68

1)The unconfined compressive and splitting strengths were determined on a hydraulic testing machine under strain-control at a loading speed of 1mm/min after curing for 28, 90,180 days.

2)The modulus of resilience was tested at 7,28 days. The specimens were soaked in the water with room temperature for 24h before the test.

3)Durability tests were conducted by studying the effect of water immersion on the unconfined compressive strength, freezing and thawing cycles on the strength and penetration-resistance.

Cylindrical specimens were examined for the effect of water immersion. The specimens were cured for 6 days, wrapped in plastic sheets in the curing room and then unwrapped from plastic sheets to put into water containers stored in the curing room until testing for soaked compressive strength (*S*s) at 1, 3 and 7 days[10].

The freezing and thawing tests were performed by a programmable freezing apparatus. The stabilized soil specimens were subjected to freezing and thawing tests in accordance with JTG D50-2006-A.2 and other testing methods[11].All specimens were cured for 27 days and soaked in the water with room temperature for 24h before the freezing and thawing cycles, and then placed in the freezing apparatus and conditioned at −35 °C for 24h. Then the specimens were transferred from the freezing apparatus into a test room at 20±2°C, 95±2%RH for 24h. This freezing and thawing cycle was repeated 5 times and then these specimens were subjected to the unconfined compressive strength tests.

4)The falling-head permeability tests were conducted at 7 and 28 days. The specimens were placed inside a cylindrical mold and then allowed to flow through the specimens. The test apparatus consists of a mold with lids and a standpipe 10mm in diameter and 130mm in length.

2. Results and Discussion

2.1. Standard proctor compaction tests

This test was used to determine the effect of stabilizers without BS-100 on maximum dry density and optimum moisture content. A summary of the results for the compaction tests on stabilized soils with various percentages of lime or cement is shown in Table[2]. We can see that the maximum dry density decreases and the optimum moisture content increases as lime content increases from 3% to 7%. The addition of lime raises the optimum moisture content. This is because the pozzolanic reaction of lime with the soil constituents tends to increase the optimum moisture content.

Similar behaviour was also observed in the case of cement stabilized soils when cement content is increased from 2 to 6%. But comparing with the lime, the increase in optimum moisture content with the addition of cement is attributed to the extra water required for cement hydration.

2.2. The optimum mix proportion

According to Table[2], lime stabilized soils have a higher unconfined compressive value after 7-day curing. This indicates that the combination of stabilizer and lime has a better stabilizing effect on the clayey soils in Changchun.

Table[2] also shows that when stabilizer dosage increases from 0.25% to 0.32% with 3% lime proportion, the 7-day unconfined compressive strength increases from0.93 MPa to 1.06 MPa. Although the strength keeps increasing, the increasing rate is far less than that when stabilizer dosage is relatively higher. When stabilizer dosage increases from 0.25% to 0.32% with 5% lime proportion, the curve of strength vs.mix formulation is a parabolic one. The strength curve has a declining tendency when stabilizer dosage increases from 0.25% to 0.32% with 7% lime proportion.

According to the above analysis, it can be noted: (1) a blind increase in mix proportion of stabilizer and lime cannot bring a strength increase. Instead, that makes the construction cost much higher; (2) with the mix proportion of 5% lime and 0.28% stabilizer, the peak value of the 7-day unconfined compressive strength (1.79MPa) can be achieved. A comparably higher value of 7-day strength (1.62 MPa) can also be obtained with 5% lime and 0.25% stabilizer.

Based on the above results and contrasts between the 7-day unconfined strength value and the required value in the Specification in China, it is decided that the optimum mix proportion is 5% lime and 0.25% stabilizer.

Table3 The data of unconfined compressive strength

The optimum mix proportion(%)		unconfined compressive strength(MPa)			
lime	BS-100	7d	28d	90d	180d
5	0.25	1.55	2.24	3.04	3.92

2.3 The unconfined compressive strength

As shown in Table[3], the 7-day moisture-laden unconfined compressive strength of BS-100 stabilized soils is 1.55MPa. According to the Specification of Asphalt Pavement Design for Highway of the Ministry of Communications of China, the 7-day strength of the lime fly ash road base material should be more than or equal to 0.8MPa. However, the 7-day strength value we get increases by 0.75MPa, higher than the required value.

The unconfined compressive strength of stabilized soils is increasing with the increase in age, and keeps a relatively higher increasing rate. The 28-day strength is 2.24MPa, which increases by 44.5% compared to the 7-day strength; the 90-day strength is 3.04Mpa, which increases by 35.71%, compared to the 28-day strength; the 180-day strength of stabilized soils is 3.92Mpa, 28.9% higher than the 90-day strength.Fig.1 presents the increasing tendency curve of the unconfined compressive strength of Base-Seal stabilized soils.

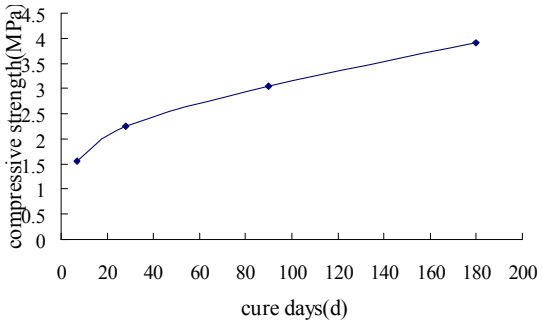

Fig1 The data of unconfined compressive strength

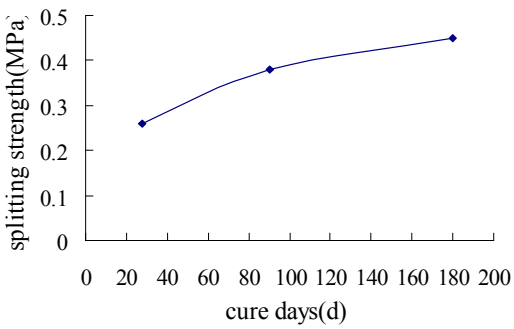

Fig2 The data of splitting strength

Table4 The data of splitting strength

mix proportion(%)		splitting strength(MPa)		
lime	BS-100	28d	90d	180d
5	0.25	0.26	0.38	0.45

Table5 The data of resilience modulus

mix proportion(%)		resilience modulus (MPa)	
lime	BS-100	7d	28d
5	0.25	262	447

2.4 The splitting strength

It is noted in Table[4] that the splitting strength of BS-100 stabilized soils is comparably higher in the early period. At the age of 28 days, the splitting strength is 0.26MPa. It keeps increasing with the increase in age. The 90-day splitting strength is 0.38 MPa, 46.2% higher than that of the 28-day stabilized soils; the 180-day splitting strength is 0.45MPa, 18.4% higher than that of the 90-day stabilized soils.Fig.2 is the increasing tendency curve for the splitting strength of BS-100 stabilized soils vs. age.

2.5 The resilience modulus

It is shown in Table[5] that the resilience modulus of BS-100 stabilized soils is 262MPa when the age is 7 days. With the increase in age, the 28-day resilience modulus is 70.6% higher than the 7-day modulus, reaching 447MPa. According to the Specification of Asphalt Pavement Design for Highway, it is suggested that the resilience modulus of the 180-day stabilized soils with lime mix proportion of 8%-12% should fall between 400MPa and 700MPa. However, the resilience modulus of the 28-day BS-100 stabilized soils is 447MPa, more than the minimum valuespecification required. It is certain that the resilience modulus will keep increasing with the increase in age until it remains constant.

2.6 The freezing and thawing resistance

Table[6] presents that the compressive strength of stabilized soils is gradually declining with the increase in freeze-thaw cycles. By observing the specimens, it is found that most specimens are complete although they go through 5 freeze-thaw cycles. Only several specimens get some inconspicuous transverse cracks. During the second time moisture-laden experiment, it is rare to find that the exteriors and edges of the specimens begin to peel. The average compressive strength of those specimens is 1.99 MPa, with loss strength of 11.16% and a freeze-thaw coefficient of 88.83%,which demonstrates a good effect of freezing and thawing resistance.

Table 6 The data of freeze-thaw cycle experiment

mix proportion(%)	cycle times	compare strength(MPa)	test strength(MPa)	loss strength(%)
5%lime +0.25%BS-100	5	2.24	1.99	11.16

2.7 The water stability

Table[7] shows the compressive strength development with water stability. The 1-day unconfined compressive strength of moisture-laden stabilized soils is 1.55MPa.The loss of strength is 26.54%, and the water stability coefficient is 73.46%; the 3-day unconfined compressive strength of moisture-laden stabilized soils is 1.46MPa,reducing by 0.09MPa compared to the 1-day strength. Referring to the control group specimens, it is found that the second group specimens have a loss of strength of 30.81%. The water stability coefficient is 69.19%. The loss of strength gradually increases with the increase in the soak time. Meanwhile, the 7-day unconfined compressive strength of moisture-laden stabilized soils is 1.59 MPa, 0.04 MPa higher and 0.13 MPa higher than the 1-day strength and the 3-day strength respectively. Its loss of strength is 24.64%. It can be seen that the water stability coefficient of BS-100 stabilized soils increases to 75.36%. Figure 3 demonstrates a comparison of the strength of BS-100 stabilized soils in terms of different water stability.

Table7 The data of water stability

mix proportion(%)	soaking age(d)	compare strength(MPa)	test strength(MPa)	loss strength(%)
5%lime +0.25%BS-100	1	2.11	1.55	26.54
	3	2.11	1.46	30.81
	7	2.11	1.59	24.64

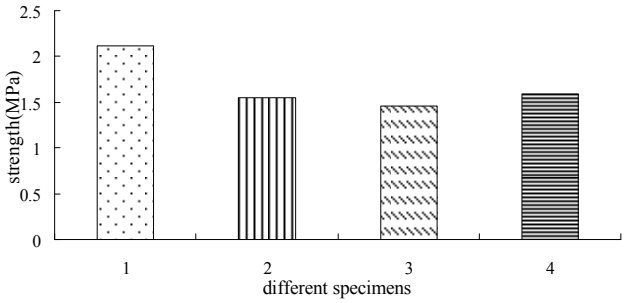

Fig.3 The strength contrast of water stability

Table 8 The data of penetration-resistance

mix proportion(%)		permeability coefficient (m/d)	
lime	BS-100	7d	28d
5	0.25	3.76×10^{-6}	2.83×10^{-6}

2.8 The penetration-resistance

According to the Technique Specification for Seepage Prevention Engineering on Canal, the penetration-resistant of earth materials (plain earth, lime, sand and stones) should be between $8.1\times10^{-5}$and 1.9×10^{-4}m/d. Table[8] shows that both permeability coefficients of the 7-day and 28-day BS-100 stabilized soils reached 10^{-6}. The permeability coefficient of the 7-day soils is 3.76×10^{-6}m/d, while that of the 28-day soils is 2.83×10^{-6}m/d which is 24.73% lower than that of the 7-day soils. Comparing with the suggested coefficient with the data we got from the experiment, we may find that the permeability coefficient of BS-100 stabilized soils is relatively lower.

3. Conclusion

On the basis of the test results, the following conclusions can be drawn:

1)The BS-100 stabilized soil has a high strength in the early period and its strength increases rapidly in the later period. This property helps shorten the stage of construction.

2)The BS-100 stabilized soil has a high splitting strength. With a high splitting strength, it can reduce the possibility of the occurrence of the cracks in the base course effectively.

3)The BS-100 stabilized soil has a remarkable effect on the increase of modulus of resilience. It can greatly enhance the load-bearing capacity of pavement structure.

4)The BS-100 stabilized soil has a remarkable frost resistant effect and better temperature stability. This is significant for the construction in seasonally frozen regions.

5)With the increase in soak time, the water stability coefficient is decreasing much slower and the loss of strength is reducing and finally keeps constant. When the loss of strength reaches the lowest peak, the unconfined compressive strength increases with curing period. However, due to moisture erosion, the strength increases much more slowly. Besides, there is also a better water stability without the occurrence of secondary muddiness.

6)Because of the limitation of curing period, only the 7-day and 28-day curing data of the relationship between permeability and age are obtained. Further tests and research should be done concerning the developing tendency of its permeability with the increase in age. However, the permeability coefficient will decrease with the increase of strength in the following period.

The results demonstrate the BS-100 stabilized soils have better impermeability and freeze-thaw resistance effects, which helps to prevent settlement, frost boil and other damages in seasonally frozen regions. The BS-100 stabilizer can be applied in road projects in Changchun and other areas with similar climate and soil properties.

References

[1]Bahar, R. (2004). “Performance of compacted cement-stabilized soil.” *Cement &Concrete Composites J.,* 26: 811–820

[2]Bo, P.(2001). “Research on liquid stabilizer reinforced soil.” *Journal of Xi’anHighway University J.,* 21(1): 15－18.

[3]Da-yan, W.(2005). “Physico-mechanical properties changes of Qinghai-Tibet clay due to cyclic freezing and thawing.” *Chinese Journal of Rock Mechanics and Engineering J.,* 24(23): 4 313－4 319.

[4]Feng-wu, L.(2003). “Application of soil solidify agent in road basic layer.”*Municipal Engineering Technology J.,* 21(5): 308－309.

[5]Jian-xiao, T. (2002). “Properties of S-soil solidified-agent for road performance.”*Journal of Chang’an University (Natural Science Edition) J.,* 22(5): 20－23.

[6]Shun-ni, L.(1998). “On the stabilizer for the soil with higher water content.” *Chinese Journal of Geotechnical Engineering J.,* 20(4): 83－86.

[7]Tong, L. (2003). “Study on indoor tests of fly ash and quick lime improving soft soils.” *Rock and Soil Mechanics J.,* 24(6): 1049－1052.

[8]Wei- rong, H.(2003). “Research on properties and application of road base materials stabilized by QJ-type soil-solidified agent.” *Highway J.,* (7): 156－159.

[9]Xiang-wei, F.(2006). “Study on engineering properties of improved soil by GT soil firming agent.” *Rock and Soil Mechanics J.,* 27(9): 1545－1548.

[10]Yi-min, W.(2006). “Pavement performances of dam embankment roads strengthened by ionic soil stabilizer.” *Journal of South China University of Technology(Natural Science Edition) J.,* 34(9): 56－61.

[11]Yi-ning, D.(2002). “Experimental study on strengthened soft clay with stabilizer ZDYT—2.” *China Civil Engineering Journal J.*, 35(3): 82－86.

doi:10.4028/www.scientific.net/AEF.5.316

Rutting Resistance Evaluation of Structural Combinations of Asphalt Pavement Subjected to Heavy Duty

Zejiao Dong[1,a], Xiangbing Gong[2,b], Guiqing Xiao[3,c], Teng Long[4,d]

[1] School of Transportation Science & Engineering, Harbin Institute of Technology, Harbin 150090, China

[2] School of Transportation Science & Engineering, Harbin Institute of Technology, Harbin 150090, China

[3] School of Transportation Science & Engineering, Harbin Institute of Technology, Harbin 150090, China

[4] School of Transportation Science & Engineering, Harbin Institute of Technology, Harbin 150090, China

[a]hitdzj@hit.edu.cn, [b]gongxiangbing@126.com, [c]wuxingxgq@sina.com, [d]lt328166958@163.com

Keywords: Asphalt pavement; rutting resistance; structural combination; heavy duty

Abstract. Rut, referred to as a common damage of asphalt pavement, is still a knotty problem to pavement researchers. Many reasons could cause rut, among which heavy duty, improper pavement structural combination design are two principal factors. As a result, three pavement structures and seven types of asphalt mixtures were used to evaluate the rutting resistance performance of different structural combinations. At first, through Marshall design method, the properties of asphalt mixtures were obtained such as gradation, asphalt content and so on. Based on the comparison of gradations and anti-rutting additives, the single layer rut was tested by wheel tracking test. Then, in order to consider the influence of pavement structural design on pavement rut, six types of structure combinations under identical heavy duty condition were designed to perform rutting test. It shows that anti-rutting gradation and anti-rutting additives can improve rutting resistance performance of single layer. Also, a proper structural design could provide a better bearing capacity of wheel load even for heavy duty. It is better to integrate the anti-rutting gradation and anti-rutting additives into structural design. In this paper the results provide some new insight into the relationship between rutting resistance and mixture gradation, anti-rutting additives, heavy duty and structural combination. The consideration of these factors will give a better pavement design.

Introduction

In recent years, as the axis load and tire press increase rapidly in most parts of China， as a consequence, rut becomes a common and difficult damage of asphalt pavement, also makes it hard to determine the index of pavement rehabilitation [1]. When rut depth grows to a certain value, it will be potential risk for drivers even meet a rainy day, because surface irregularities of road cross section easily results in vehicle drift. There are so many factors influence rut such as gradation, asphalt types, asphalt content, aggregate and climate, but even if these factors were known very well, it also has difficulties in finding the effective and economic control methods to reduce and avoid rut, so that many relative researches were in aims at some realm of pavement rut. As we all know that asphalt mixtures exhibit viscoelastic characteristic, whose property is relative with the rutting mechanism [2,3], the mechanism of pavement rut is always deemed that the shear stress in the road is bigger than shear strength of asphalt mixtures, especially in long and steep climbing sections of asphalt pavement [4], other researchers search the mechanism to reduce rut by geotextile [5]. Gradation is significant to asphalt mixtures, because of its direct relationship with various properties of mixtures; in addition, the increase of nominal maximum aggregate size (NMAZ) always results in improvement of rutting resistance [6]. Some kinds of additives can modify qualities of asphalt and the aggregate-asphalt interface then generate a strong mix in order to reduce rut [7]. Numerical analysis and pavement structural design are also used to determine what main reason of pavement rut is [8, 9].

To establish relevant between rut and gradation, anti-rutting additives, heavy duty, structural design, single layer and structure combination track board were applied into wheel tracking test of heavy tire press (1.1MPa), analyzed data of different experimental groups then come to a conclusion.

Marshall design method

This paper employed seven types of asphalt mixtures according to typical ones used in highway: KAC-16, KAC-20, ATB-25, KAC-25, AC-16, AC-20, AC-25, where K is mean anti-rutting gradation, shown in Tab.1. The different NMAZ and gradation were for the sake of considering the gradation's impact on pavement rut. Obviously, anti-rutting gradation's limitation is narrower than a normal one, Fig.1 shows that the aggregates' pass rate of KAC-20 is smaller than AC-20 except 9.5mm sieve, anti-rutting gradation is coarser than the normal one.

Tab.1 Seven types of asphalt mix gradation

Sieve size [mm]	Pass rate [%]												
	31.5	26.5	19	16	13.2	9.5	4.75	2.36	1.18	0.6	0.3	0.15	0.075
ATB-25	100	100	64.8	54.1	46.6	39.8	32	21.1	16	11.4	8.1	6.9	5.9
KAC-25	100	100	82.3	75.2	66.4	57.3	34.7	23.5	16	11.8	7.6	6.7	5.5
KAC-20	-	100	91.7	85.7	73.5	61.4	37.5	23.4	15.6	10.8	7.8	6.8	5.9
KAC-16	-	-	99.7	95.4	82.9	70.5	43.9	27.2	17.2	11.4	8.1	6.9	5.9
AC-25	100	100	88.7	78	69.6	54.2	37.5	28.5	21.4	15.7	11.4	7.2	5.7
AC-20	-	100	93.9	87.4	78.7	59.5	39.9	28.6	21.4	15.7	11.4	7.2	5.7
AC-16	-	-	100	94.1	86.7	67.2	40.9	29.3	22.3	16.4	11.7	9.5	6.8

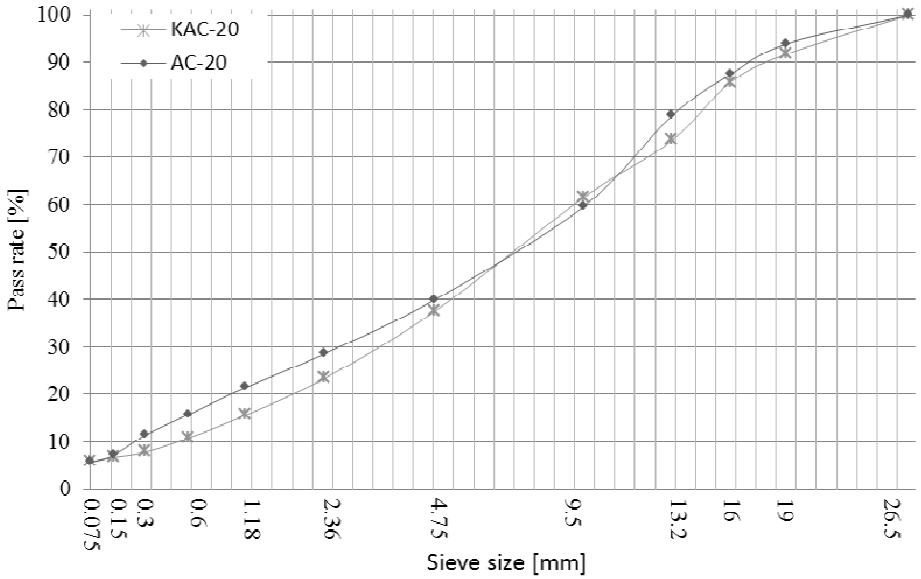

Fig.1 KAC-20 and AC-20 gradation curves

After gradations were determined, Marshall design method was applied to calculate the optimum asphalt content of seven mixtures, then obtained some volume indexes shown in Tab 2. All the data met requirements of *Enforceable Handbook of Technical Specifications for Construction of Highway Asphalt Pavements*.

Tab.2 Data of Marshall design method

Types	OAC [%]	γ_b [g/cm^3]	VV [%]	VFA[%]	MS [KN]	FL [mm]
ATB-25	3.8	2.537	4.0	60	11.3	2.32
KAC-25	4.1	2.400	4.5	62.9	10.5	2.90
KAC-20	4.9	2.500	4.8	67.0	12.1	3.70
KAC-16	5.1	2.467	3.6	73.8	11.8	2.90
AC-25	4.2	2.500	4.5	68.3	8.9	2.93
AC-20	4.7	2.495	4.4	69.0	15.5	3.70
AC-16	5.4	2.459	4.5	71.2	10.6	3.94

Single layer wheel tracking test

Based on data of the first section, gradation and asphalt content were applied into single layer wheel tracking test to estimate and check the property of anti-rutting resistance. According to *Standard Test Methods of Bitumen and Bituminous Mixtures for Highway Engineering*, wheel rolling equipment was used to shape experimental boards (300mm×300mm×50mm), wheel track testing was in 60℃ and remained 60 minutes at least until the curve reached stable. At last, the *DS* (Dynamical Stability) could be worked out by formula 1

$$DS = \frac{(t_2 - t_1) \times N}{d_2 - d_1} \times C_1 \times C_2 \tag{1}$$

Where t_1 and t_2 are the 45 minute and 60 minute from test began, d_1 and d_2 are corresponding deformation of t_1 and t_2, C_1 is correction factor of wheel tracking test equipment, in this test it is 1.5, C_2 is specimen coefficient depending on the size of tracking boards, it is 1.0 in this test, N is velocity of wheel tracking tire moving there and back, it is 42 round per minute.

In this section, took gradation and anti-rutting additives into consideration subjected to single layer test, but used normal tire press (0.7MPa). Aimed at finding how do these two factors effect rut, the results of these differently compared groups shown as follow.

Gradation. From Fig.2, it shows that anti-rutting gradation has a positive influence on improving the capacity to resist vehicle loads. The *DS* of KAC-20 increases by 17.4% comparing to AC-20, and the result of KAC-16 increases by 28.5% comparing to AC-16, while to KAC-25, it decreases by 3.4%, because when NMAZ reaches 26.5mm, the anti-rutting gradation seems similar with normal one when keeping a qualified VV. If just only increase the difference between two types of gradation, the anti-rutting one will be difficult to meet the regulation requirement such as a proper VV. But KAC-20 and KAC-16 do not have these problems, a wider selection in gradation than KAC-25. The maximum *DS* is exhibited in 19.5mm NMAZ either anti-rutting or normal gradation.

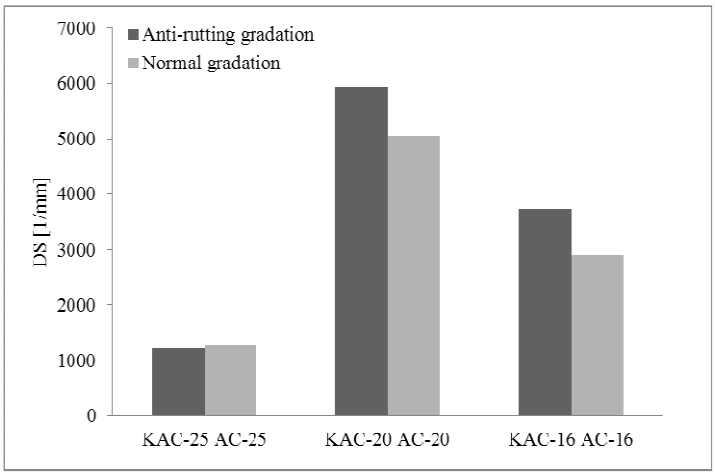

Fig.2 *DS* of different gradations

Anti-rutting additives. As a kind of modifiers, anti-rutting additive is playing a important role in modifying asphalt, it can improve cohesivness of asphalt and aggregate, also strenghen interface peeling resistance betweeen asphalt and aggregate. So this additive not only enhances anti-rutting capacity also improves low temperature cracking resistance. In this section, KTL additive was chosen because of its wide use in China and it has a good effectness, known as a kind of product of Beijing Tian Cheng KenTeiLai Technology Co., Ltd. Following recomment , dosage of admixture is 0.3%, and all gradations were chosen as anti-rutting gradation type, wheel tracking test results are illustrated in Fig.3, where + is added KTL anti-rutting additives into gradation.

It is obvious that KTL additive improves rut resistance. Comparing to KAC-16 and KAC-20, the KTL gradations' *DS* increase by 88.4% and 78.6%, which are siginificantly effectiver than anti-rutting gradtion. Then after combination of KTL additive and anti-gradation, it strenghened cappacity of rutting resistance, in addition, KTL additive is more cheaper than others.

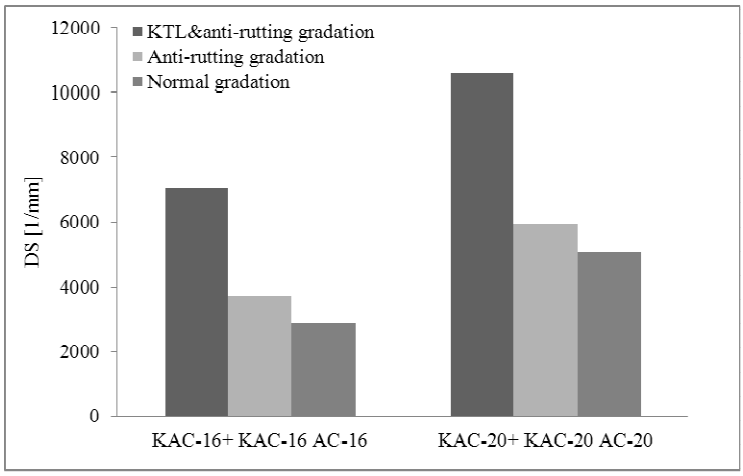

Fig.3 *DS* of different gradations and KTL additive

Combined structure boards wheel tracking test

Besides gradations and anti-rutting additives, pavement rut is always sensitive to pavement structural design, it could be proved that single layer wheel tracking test does not comfirm real high temperature performance of highways. In this section, two layer combined structure boards chosen among three pavement strucures of real projects were applied to simulate the real pavement structures, the boards and pavement structures are shown in Fig.4 and Tab.3.

Fig.4 Two layer combined structure boards

Tab.3 Three pavement structures

Layer	Structure 1	Structure 2	Strucure 3
Upper layer	5cm SBS AC-16	5cm SBS+KTL KAC-16	5cm SBS+KTL KAC-16
Middle layer	6cm SBS AC-20	6cm SBS+KTL KAC-20	6cm SBS+KTL KAC-20
Bottom layer	7cm AC-25	7cm KAC-25	7cm ATB-25

Heavy duty. Based on heavy duty investigation, the tire press of wheel track is 1.1MPa.

Combined structure design. Classification of combined structure is distinguished by different layer and structure combination, so that experimental groups' serial number is defined as H-K, when H is 1, which means that boards is combined by upper and middle layer, H is 2 means that middle and bottom layer, K is 1 means that structure 1, the rest can be done in the same manner. Then the wheel tracking test of heavy duty and combined structure were conducted, the results are shown in Fig.5.

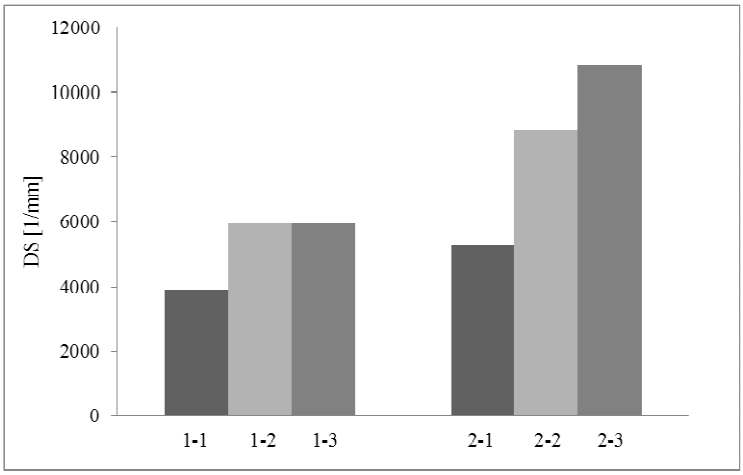

Fig.5 *DS* of different groups

Analyzed data of groups, comparing to single layer test results, combined structure boards could be more balanced, because the combination intergrates the difference bettween two kinds of single layers, such as 1-1, *DS* of AC-16 and AC-20 is 2907 and 5054, while the combined one is 3917, this phenomenon is same to other groups, which shows that combined strucure boards are similar to real pavement structures. For group 1 and group 2, the KTL additive and anti-rutting gradation are important to improve strutural rutting resistance, a substaintial increase shows in figure. What more, the combination of middle and bottom layers exhibilts a better anti-rutting capacity than one of upper and middle layers, as a result, these two layers play a significant role in bearing heavu duty. For group 2, the difference of 2-2 and 2-3 is diverse bottom layer, 2-2 is KAC-25 and 2-3 is ATB-25, the result of 2-3 increases by 22.7%, it is remarkable that a flexiabler layer such as ATB-25 can provide a more reseaonable strucure combination for rutting resistance, because flexiable layer can dissipate more vehicles moving energy.

Summary and conclusion

The major objective of the study presented in this paper is to find the relationship between rut and gradation, anti-rutting additives, structural design. The effort has provide different groups and experimental boards to evaluate the rut resistance of them, then got some conclusions as follow.

1. Anti-rutting gradation and anti-rutting additives can improve the capacity to avoid rut, however a coarse gradation has some limitation, and it is a kind of physical method. What more, additive has a advantage in enhancing properties of asphalt mixtures, its effectness is better than anti-rutting gradation.

2. Test results of single layer board based on diverse mixture are extremely various, combined strucure boards are similar to real pavement structures and *DS* of combined structure boards seem to be more balanced..

3. Combination of middle and bottom layer shows a stronger resistance than upper and middle layer combination, these two layers play a significant role in bearing heavu duty. What more, on the basis of comparation between 2-2 and 2-3 experimental groups, the result of 2-3 increases by 22.7%. A flexiabler layer such as ATB-25 might provide a properer structure combination for rutting resistance, because flexiable layer can dissipate more vehicles moving energy.

References

[1] Panagiotis Ch. Anastasopoulos, Fred L. Mannering, John E. Haddock, A Random Parameters Seemingly Unrelated Equations Approach to the Post-Rehabilitation Performance of Pavements, Journal of Materials in Civil Engineering (2012).

[2] Ronald Blab, John T. Harvey, Modeling Measured 3D Tire Contact Stresses in a Viscoelastic FE Pavement Model, The International Journal of Geomechanics vol.3 (3) (2002), p:271-290.

[3] Jaeseung Kim, Reynaldo Roque, Thomas Byron, Viscoelastic Analysis of Flexible Pavements and Its Effects on Top-Down Cracking, Journal of Material in Civil Engineering vol.21 (7) (2009), p:324-332.

[4] J. Z. Pei, Y. Chen, M. F. Chang, Mechanism of Rutting Formation in Long and Steep Climbing Sections of Asphalt Pavement, Proceedings of the Ninth International Conference of Chinese Transportation Professionals (2009), p:2179-2197.

[5] Yinghao Miao, Jinxi Zhang, Mechanism of Mitigating Shear-induced Rutting of Asphalt Pavement Using Geotextile, Airfield and Highway Pavement (2008), p:16-27.

[6] LIU Hong-ying, DAI Jing-liang, Effect of different gradations on asphalt mixture resistance to rut, Journal of Chang'an University (Natural Science Edition) vol.24 (5) (2004), p:11-15.(In Chinese)

[7] Elie Y. Hajj, Peter E. Sebaaly, Thileepan Sathanathan et al, Impact of Anti-strip Additives on Pavement Performance Using M-E Pavement Design Guide, Journal of Materials in Civil Engineering (2012).

[8] Zejiao Dong, Zongjie Sun, Xiangbing Gong et al, Mechanism Analysis of Rutting at Urban Intersections Based on Numerical Simulation under Moving Vehicle Loads, Advanced Materials Research vol.152-153 (2011), p:1192-1198.

[9] ZHANG Dongsheng, XU Xijuan, ZHANG Mingcheng et al, Semi-flexible Base's Material Properties and Pavement Structure Applicability, Proceedings of the Third International Conference on Transportation Engineering (2011), p:2139-2144.

doi:10.4028/www.scientific.net/AEF.5.322

Preparation of Latent Heat Materials Used in Asphalt Pavement and Theirs' Controlling Temperature Performance

Xin Bian[1,a],Yiqiu Tan[2,b], Jianfu Lv[3,c], Liyan Shan[4,d]

[1,2,3,4] School of Transportation Science and Engineering, Harbin Institute of Technology, Harbin 150090, China

[a]bianxin007@126.com,[b]yiqiutan@163.com, [c]lvjianfu@yahoo.cn,[d]myshanliyan@126.com

Keywords: Composite phase change materials; Temperature control; Rutting; Phase change asphalt mixture; Simulation experiment

Abstract: In order to solve rutting diseases of asphalt concrete pavement, latent heat materials for asphalt pavement were prepared and theirs' controlling temperature performance were studied. Phase change materials (PCM), which were fitted to thermal environment of road were selected, phase change asphalt, diatomite powder and pottery sand granular composite phase change materials (CPCM) were prepared by three kinds of import modes. The CPCM were chosen by comparing the performance of above mentioned materials. Latent heat asphalt mixture (LHAM) was made by replacing mineral powder and fine aggregate with CPCM. Its controlling temperature ability was tested by temperature monitor system. The results show that, comparing to general asphalt mixture, LHAM can reduce temperature to 8-10℃. Therefore, LHAM has a good effect on adjusting road temperature.

Introduction

The rutting problem of asphalt concrete pavement has bored road transport administrators in the past few years, it is urgent to seek scientific and effective methods to solve the problem. The asphalt mixture is a viscoelastic material, the main factors which affect its mechanical properties are loading and temperature. Loading conditions are not easy to control, so temperature becomes the dominant factor to solve rutting. For a long time, the researchers have focused on improving temperature stability of asphalt and asphalt mixture, asphalt modifing, adding fiber and optimizing gradation and so on measures have been put forward [1-2]. All methods have changed asphalt pavement's temperature passively. Although they have solved some problems in certain domain and condition, temperature-related diseases of asphalt pavement are still very serious. Therefore, the paper was from the angle of improving temperature status of asphalt pavement, latent heat materials used in asphalt pavement were prepared, theirs' temperature performance were tested. The organic phase change materials (OPCM) were imported into inorganic porous materials to prepare composite phase change materials (CPCM). The latent heat asphalt mixture (LHAM) was prepared by mixing CPCM into asphalt mixture through different channels. CPCM is used to absorb heat of pavement constantly. Because of appropriate phase change temperature and high phase change latent heat, its self-thermostat effect performance is great.

Preparation of Latent Heat Materials Used in Asphalt Pavement

Phase change materials selection The phase change materials (PCM) can change phase with temperature and provide phase change latent heat (PCLH). Phase change materials can be divided into four categories which are solid-solid, solid-liquid, solid-gas and liquid-gas [3-4].

The commonly used OPCM are waxes, paraffins, fatty acids, salts, alcohols and so on. Theirs solid forming are good. They are not prone to super cooling and phase separation[5]. The corrosivity of them are less. Theirs performance are more stable. Considering factors which like phase change temperature, phase change latent heat, thermal conductivity coefficient, volumetric change rate, volatility, boiling point and so on, myristic acid, palmitic acid, PEG 4000 are chosen and the thermal properties parameters are shown in Table 1. For example, latent heat materials the road used require phase change temperature 45 ~ 65 ° C. Latent heat and thermal conductivity are as much as possible. Volumetric change rate before and after phase change is as small as possible. Volatile temperature is greater than 180 ° C.

Tab.1 The Thermal Parameters of Organic Phase Change Materials

Sample	Phase change temperature (℃)	Phase change latent heat (J/g)	Thermal conductivity (w/m·k)
Myristic acid	49-51	141.48	0.159/0.162/0.165
Palmitic acid	61～64	164.79	0.159/0.162/0.165
PEG4000	51～54	143.56	0.300/0.500

Import modes and performance analysis of CPCM

Direct incorporation Asphalt is a viscoelastic material. The direct incorporation of the OPCM has a bad effect on its road performance. The three indicators of 10%, 20% and 30% three concentrations of phase change modified asphalt (PCMA) was determined, results show in Figures 1 to 3.

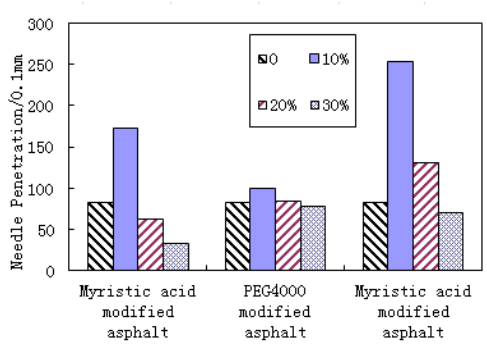

Fig.1 Needle Penetration of PCMA with Different Concentrations

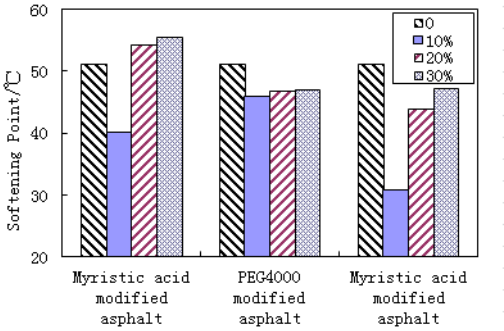

Fig.2 Softening Point of PCMA with Different Concentrations

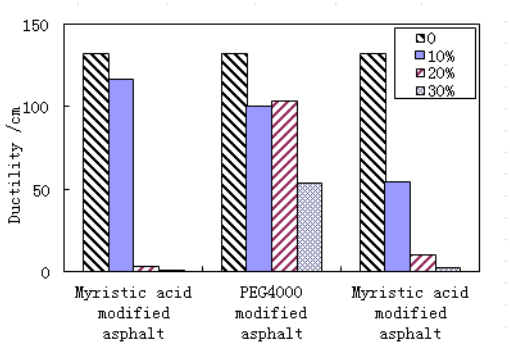

Fig.3 Ductility of PCMA with Different Concentrations

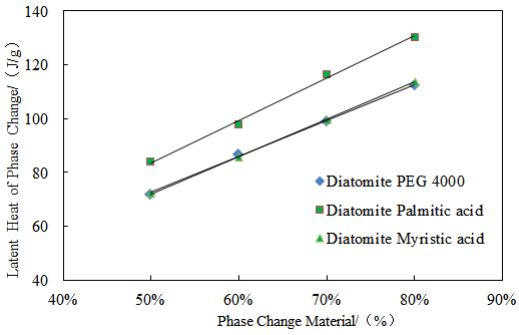

Fig. 4 Relationship Between PCLH and Import Volume of Power CPCM

Figures 1 to 3 indicate that, the direct incorporation of palmitic acid, PEG 4000 and myristic acid has a bad effect on the three indicators of asphalt, especially the ductility, The content of palmitic acid and myristic acid are 20% and 30% respectively, the ductility of PCMA are much lower, the

corresponding adhesion and toughness are poor. Comparatively speaking, the asphalt three indicators of PEG4000 PCMA has a less impact. However, the phase change temperature of PEG4000 is 51~54℃, it will turn into a liquid when reaches the temperature and lose viscoelasticity. Therefore, the import mode is abandoned.

Vacuum import The diatomite power composite phase change materials (CPCM) were prepared by vacuuming diatomite and importing OPCM into porous pore of it, the import uniformity was tested by DSC and the results are shown in Figure 4.

The results in Figure 4 indicate that the latent heat of diatomite power CPCM increases linearly with the increase import volume of OPCM, the uniformity is great. When the import volume of palmitic acid reachs critical value-60%, latent heat is 97.74J / g, phase change thermostat is good.

Vacuum import and encapsulation The pottery sand granular composite phase change materials (PSGCPCM) were prepared by vacuuming pottery sand and importing OPCM into porous pore of it. The import uniformity was tested by DSC and the results are shown in Figure 5.

The results indicate that the latent heat of PSGCPCM increases linearly with the increase import volume of OPCM, the uniformity is great. When the import mass ratio of palmitic acid reachs critical value-30%, latent heat is 50.93J / g, phase change thermostat is good.

The above analysis shows that the direct incorporation of OPCM reduces the pavement performance. In order to reduce the impact on the asphalt road performance, The OPCM is import into power diatomite and granular pottery sand, the import mode is very simple, inorganic porous material shields OPCM to some extent, and reduce the impact of the spill on the asphalt pavement performance, and phase change thermostat is good.

In order to guarantee asphalt mixture's pavement performance and has as much latent heat as possible, powder diatomite palmitic acid (PDPA) and granular pottery sand palmitic acid (GPSPA) CPCM were prepared, mineral powder and fine aggregate were replaced with the same volume, PDPA and GPSPA were mixed with asphalt mixture to prepare the latent heat of asphalt mixture.

Preparation of the latent heat asphalt mixture (LHAM)

For multi-layer pavement, rutting and other high temperature disease are generally caused by the deformation of the middle and underside layers[1]. the upper layer of asphalt concrete pavement get sunlight and contact with air directly[6-7], hence, The application of LHAM in the upper layer can be an effective protection for the middle and underside layers by maintaining temperature below the phase change temperature. Thus, the rutting could be effectively inhibited. Therefore, AC-16 which is commonly used in the upper layer was selected to prepare LHAM, the mixture gradation use gradation median. In the gradation, fine aggregate of 1.18mm and 0.6mm are substituted with the same volume by corresponding particle size pottery sand palmitic acid CPCM, meanwhile mineral power are also replaced with the same volume by powder diatomite palmitic acid CPCM.

Study of LHAM' Self-tune Temperature Effect

Laboratory and Field Temperature Testing Methods The rutting specimen were put at room temperature for 24h. They were demoulded and put into the solar thermal temperature controlling box. Each specimen was tiled 20mm thick earth soil and the gap was filled with earth soil and tamp. When the sensor displays both temperature are almost the same, dysprosium lamp [8] was opened and the temperature changes over time was recorded. The testing equipment is shown in Figure 7.

The asphalt mixture rutting specimen were put on the roof so that they could be directly exposed to sunlight. Sensor was used ditto, test and record the temperature changes over time, as shown in Figure 8.

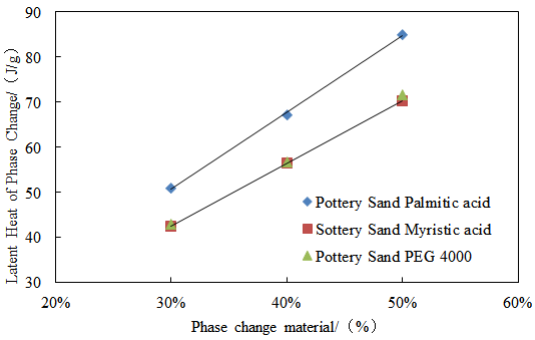

Fig.5 Relationship Between PCLH and Import Volume of Granular CPCM

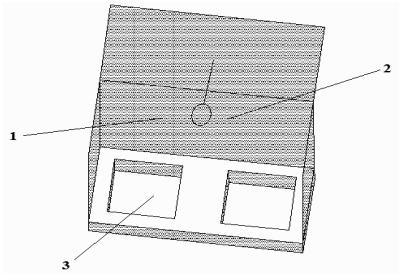

1-Insulation polystyrene board 2-Adjustable power dysprosium lamp 3-Rutting groove

Fig.6 Schematic Diagram of Solar Thermal Temperature Controlling Box

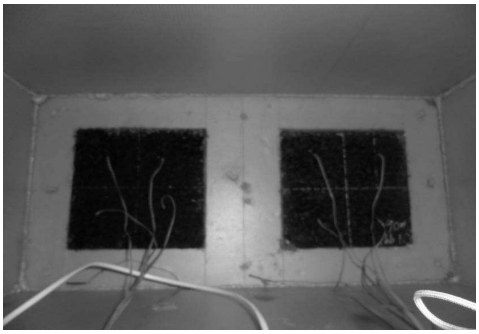

Fig.7 Laboratory Temperature Acquisition

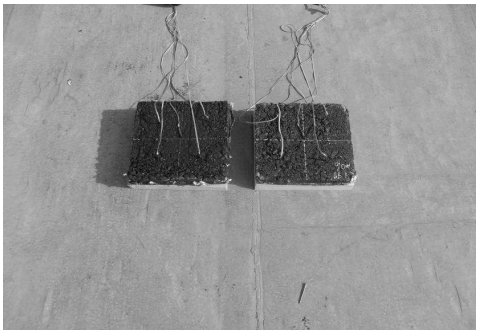

Fig.8 Field Temperature Acquisition

Evaluation of Laboratory and Field Thermostat Effect Figure 9 indicates that the temperature of asphalt mixture rutting specimen and PCAM rutting specimen increase with time, the temperature of the former is always higher than that of the latter one.

Figure 10 indicates that the temperature difference of the two rutting specimens increased constantly with time, at the time of 460min, the LHAM rutting specimen achieved the overall phase change temperature-59.1℃, and the temperature difference between the two specimens achieved the Maximum value-7.6℃. The results show that the CPCM in the latent heat asphalt mixture rutting specimen had been completely phase changed, fully absorbed heat and reached the saturation point. After that point, temperature difference between the two specimens decreased gradually.

Figure 11 indicates that PCAM rutting specimen's temperature rise rate is significantly less than the asphalt mixture rutting specimen's at the beginning of the period. When the overall temperature achieved the phase change temperature (PCT), temperature rise rate of PCAM rutting specimen instant mutated to be greater than asphalt mixture rutting specimen’s. After that point, both moved closer and tended to be equal at last. Analyze the reason, the latent heat asphalt mixture material rutting specimen achieve to the phase change temperature from the surface to the center. However, each time reach the temperature, the corresponding CHPM will instantly absorb a lot of heat, inhibit temperature rise. To start from the Macro-view, the performance appears that the temperature rise rate of latent heat asphalt mixture rutting specimen is significantly less than the asphalt mixture rutting specimen. When CPCM of LHAM rutting specimen entire happen phase change. Due to the overall temperature of LHAM rutting specimen are quite different from the air's, so the transient performance is that the temperature rise rate is greater than the asphalt mixture rutting specimen's. And then, with the temperature difference between LHAM and the air decreases, both temperature rise rate are gradually closer and tend to be equal at last.

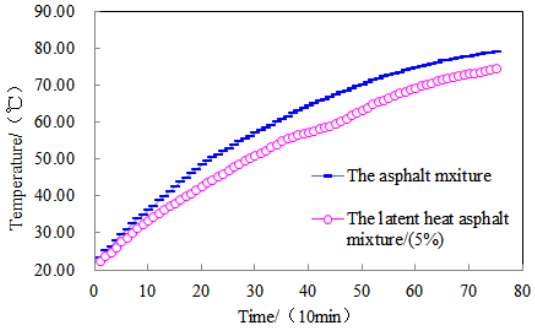

Fig.9 Laboratory Temperature-time Curve

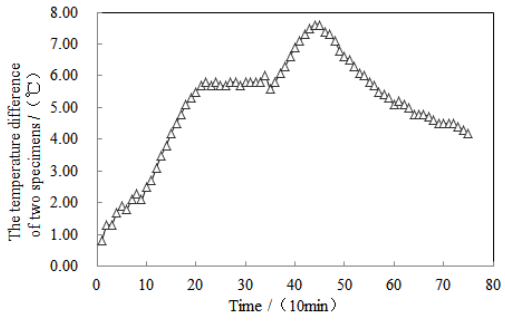

Fig.10 Laboratory Temperature difference-time Curve

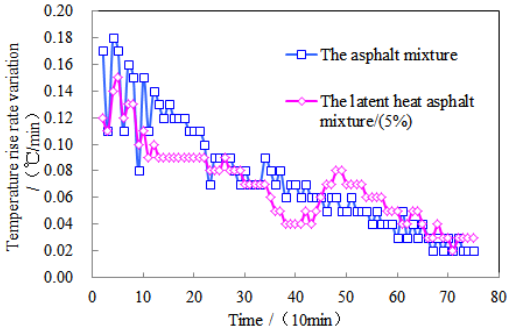

Fig.11 Laboratory Temperature Rise Rate Variation with Time

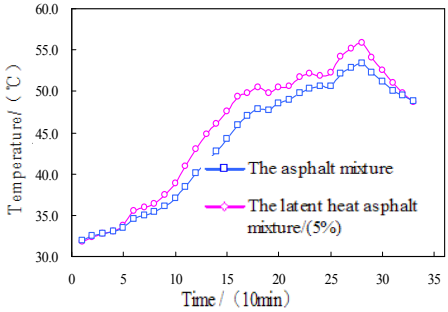

Fig.12 Field Temperature-time Curve

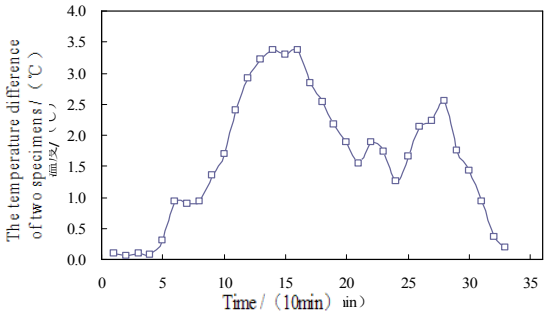

Fig.13 Field Temperature difference-time Curve

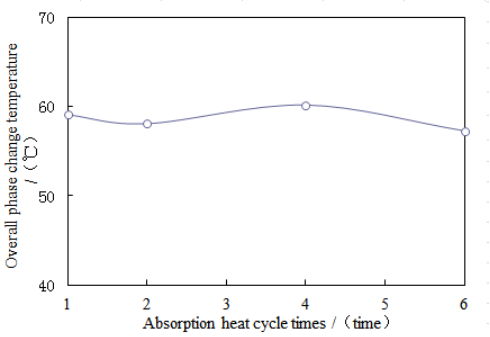

Fig.14 Relationship Between Laboratory PCT and Absorption Heat Cycle Time

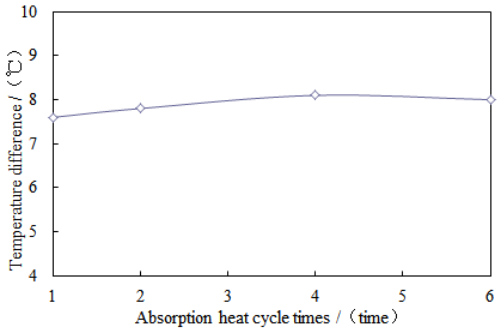

Fig.15 Relationship Between Laboratory Max-temperature Difference and Absorption Heat Cycle Times

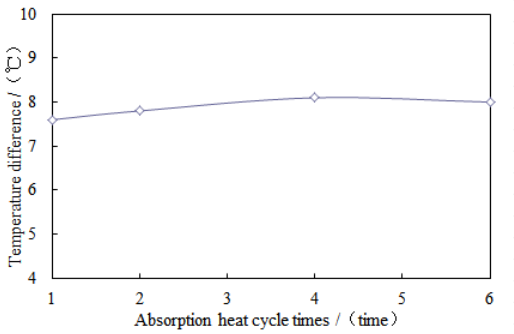

Fig.16 Relationship Between Field Maximum-temperature Difference and Absorption Heat Cycle Times

Evaluation of Laboratory and Field Thermostat Effect Figure 12 indicates that temperature of both specimens increase and then decrease with time, and temperature of the former is always greater than that of the latter one. But the curve has a big fluctuation. Analyze reasons, due to the changing of wind speed size and solar radiation intensity.

Figure 13 indicates that the temperature difference of asphalt mixture rutting specimen and PCAM rutting specimen increase constantly with time, and achieve to the maximum-3.4℃ at the time of 160 min. The effect of the phase change mixture on temperature is not good enough. Analyze reason, the asphalt mixture didn't achieve to overall phase change temperature (based on laboratory experiment it is 58.5~60.5℃), majority of CPCM phase change heat-absorbing potential has not been effectively carried out.

Laboratory and field phase change fatigue thermostat effect Figure 14 and 15 indicate that the change of the phase change temperature and the thermostat effect with the increase in absorption heat cycle is small. It shows that the phase change reversibility of LHAM is great.

Figure 16 indicates that the natural phase change fatigue of rutting specimen affect the results because of bad weather. The temperature didn't meet the overall phase change temperature range (58.5-60.5℃). So thermostat effect is poor and the maximum temperature difference is smaller.

Conclusions

When PCMA is at PCT or higher temperature range, the viscoelastic properties and corresponding road performance is deeply influenced, so the import mode is abandoned.

The OPCM is imported into inorganic porous material by using vacuum adsorption method and the powder and granular CPCM is prepared. The incorporation method have little impact on pavement performance of asphalt mixture. The incorporation is larger and thermostat is greater.

Laboratory simulation results indicate that when import mass ratio of OPCM was 5%, the maximum temperature difference of the PCAM and asphalt mixture was 7.6℃, the corresponding overall PCT was 59.1℃, At that time, the specimen show great slow temperature rise effect and good phase change reversibility.

The field experimental results indicate that the import mass ratio of OPCM is 5%, compare to the asphalt mixture, the maximum temperature difference was 3.4 ° C, the phase change reversibility is great.

The development of higher strength and greater porosity aggregate, importing of OPCM and packaging technology are further problems to be solved, meanwhile, the CPCM's long-term stability is also one problem to be considered.

References

[1]Hu Shu-guang, Li Qian, Huang Shao-long, et al. Highway, 2009,7(7):291-298.

[2]Rong Jian-guo. Study on Temperature Regulation Effect of Self-modulating Temperature Asphalt Mixture[D]Xian: Chang'an University,2009.

[3] R.Cox write.Xu Peng translate. Zhang Jian-chun check.Foreign Textile Technology, 2006,27(5):14-17.

[4]Zhang Ren-yuan,Xie Zhi-wei,Ke Xiu-fang,et al. Phase Change Materials and Phase Change Technology [M]. Beijing :Science Press,2009.

[5] Inaba H,TuP.Heat and Mass Transfer,1997,32(4):307-3.

[6] Qin Jian, Sun Li-jun. Journal of Highway and Transportation Research and Development, 2006,(23):19-20.

[7] Amonros E, Martin JL, Laumon B. Accident Analysis & Precention 2003, 35(4):537-547.

[8] Wang Yuan, Zhang Lin-hua. Acta Energies Solaris Sinica,2006,11(27)：1133-1135

doi:10.4028/www.scientific.net/AEF.5.328

Research on Alignment Consistency of Highways with the Basis of 85MSR

Xinglei Zhang[1, a], Xianghai Meng[2,b]

[1] School of Transportation Science and Engineering, Harbin Institute of Technology, Harbin, China

[2] School of Transportation Science and Engineering, Harbin Institute of Technology, Harbin, China

[a] zhang_xinglei321@126.com, [b]mengxianghai100@126.com

Keywords: traffic engineering; four-lane highways; alignment consistency; 85MSR.

Abstract. The alignment consistency of highways is an important guarantee for vehicle safety. In this thesis, by comparing the computing methods of ΔV_{85} and 85MSR, the author concludes that 85MSR is a more appropriate way to evaluate the highway alignment consistency. The author studies Ningfu section on Heda superhighway with 85MSR, pointing out the section with poor alignment consistency, and provides basic data for the analysis and prevention of this section and road improvement.

Introduction

Highway alignment, which dominates the planning, designing and constructing of highways, is the framework for highways. The alignment design has crucial influence on vehicle safety, comfort, economic performance, and traffic volume of highways. The alignment design includes horizontal design, longitudinal deign and combinatorial design. Criteria to measure a good design include reasonable selection of each parameter (e.g. sighting distance, superelevation, longitudinal slope and curve radius, etc.), following the principle of combinatorial design, harmony with environment and landscape along the highway so that drivers can visually see alignment consistency and mentally feel comfortable and safe[1].

Analysis in Alignment Consistency of Highways

Operating Speed

Operating speed refers to the 85th percentile speed measured on the characteristic point of a highway section when the traffic is in free flow and the weather is good [2]. The operating speed is proposed and applied in research by the United States, Germany and Australia, which ultimately reflects the smoothness and safety of horizontal and longitudinal alignment parameters.

With plenty of actual research, many countries use the operating speed as a basis for highway consistency design and adopt V_{85} as the operating speed to carry out alignment design so as to meet the basic requirement for coordinative dereferencing between each parameter and balanced alignment design. The followings are advantages of studying and solving highway alignment design on the basis of operating speed [3] :

(1) The blindness and non-concreteness, which is caused by using design speed as a fixed value in highway alignment design, can be avoided;

(2) The operating speed is determined from measured data and the elements for alignment design based on the operating speed can satisfy the running requirement and solve the compatibility problems between different design elements;

(3) Different factors, such as highway conditions, drivers, vehicles, natural landscape along the highways, and environment, affecting actual speed, are taken into consideration. So it is more scientific and comprehensive to study the highway alignment with operating speed;

(4) The principle of speed change control can guarantee the speed consistency on different sections without speed breakpoint so as to ensure that the highway alignment is successive.

The Traditional Evaluation Criteria for Alignment Consistency

Research shows that if highway alignment features are in conformity with driver expectations, operational errors will be obviously less than those happen when they are not in conformity. The highway alignment parameters, such as horizontal and longitudinal curve radius, longitudinal slope, superelevation, and widening, sight distance etc., are major factors that affect the operating speed, and whether the alignment elements are successive is reflected by the success of operating speed, so it is quite reliable to analyze the highway alignment condition with operating speed. The alignment consistency on a certain highway section can be analyzed by reasonable section division and measured actual operating speed.

Evaluation criteria for alignment consistency are of vital importance. Opposite conclusions may be reached if the alignment design quality on the same highway is evaluated with different criteria. And the same criterial is not applicable to all the countries due to different national conditions. Some countries started the alignment evaluation at early time and have made certain achievements. The USA is one of such countries; according to its research data, the operating speed difference between adjacent horizontal curve sections is closely related to safety conditions on the curve section [4], and the specific data are shown on the following Table1.

Table1 Relevance between Variability Trend in Operating Speed and Traffic Accident Rate

Gradient of Operating Speed [km/h]	Total Accidents in 3 Years	Accident Rate [time/million vehicle kilometers]
$\|\Delta V_{85}\|<10$	1483	0.46
$10\leq\|\Delta V_{85}\|\leq20$	217	1.44
$\|\Delta V_{85}\|>20$	47	2.76

On the basis of analyzing and tracing evaluation achievements of traffic safety made by America and European countries, and combining with the national conditions, China also deeply studies the relationships between traffic accident and highway geometrical parameters, traffic accident and operating speed, and highway geometrical parameters and operating speed. With gradual improvement of vehicle structures, size increased, power enhanced, the varibility capacity of operating speed to which vehicles can adapt is largely advanced, which calls for gradual improvement of highway alignment. But we cannot increase the operating speed by blindly improve alignment because it will result in a closed loop, so necessary traffic safety devices and legal approaches shall be supplemented. Combining research achievements of other countries and actual situation of China, $\Delta V85$, the difference between operating speed on adjacent section, is adopted as the evaluation index, and the evaluation criteria for alignment consistency provided in *Instruction* [2]is employed, as shown in Table 2.

Table 2 Evaluation Criteria for Alignment Consistency

Operating Speed Difference [km/h]	Alignment Consistency
$\|\Delta V_{85}\|<10$	Excellent
$10\leq\|\Delta V_{85}\|\leq20$	Good
$\|\Delta V_{85}\|>20$	Poor

The Proposition of 85MSR

According to the traditional calculating method ofΔV_{85}, speeds on two adjacent sections are supposed to be mutually independent, while the mutual influence of speeds on front and back alignments are not considered. The following Fig. 1 shows the speed variability when a vehicle runs on adjacent sections.

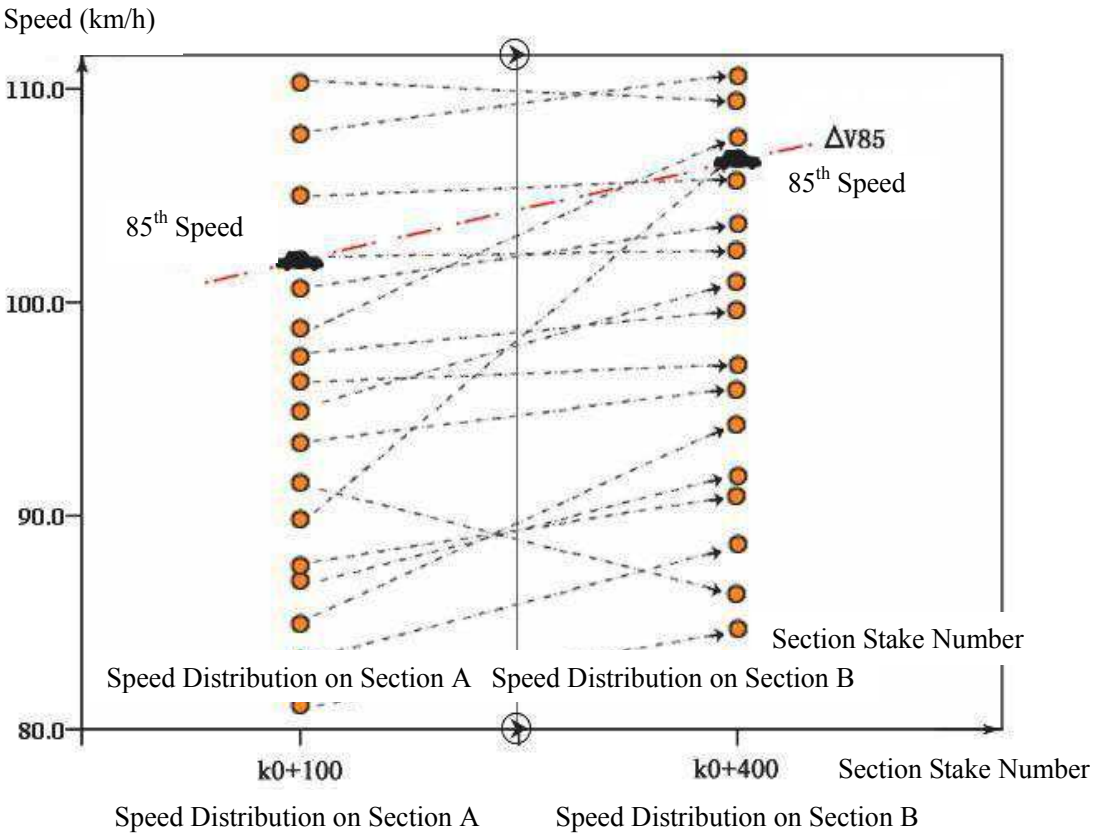

Fig. 1 Operating Speed Variability on Adjacent Sections

It can be seen from the above diagram that only the corresponding relation between two independent individuals is considered, which does not conform to actual situation because vehicle speed is not only related to gender, age, and driving behavior of a driver but also influenced by other vehicles in the process of running.

Because of the above consideration, speed difference of individual vehicles on adjacent sections shall be calculated separately, and then the value on 85% shall be obtained, so as to define as 85MSR.

This method takes the mutual influence of speeds on front and back alignments into consideration and eliminates the shortcoming of ΔV_{85} to a great extent, and the next step is to study the specific relationship between 85MSR and ΔV_{85} with mathematical methods [5,6].

It can be known from the calculation methods that ΔV_{85} studies the relationship between two individuals while 85MSR studies the group relationship, and ΔV_{85} assumes that speeds on front and back sections has no influence on each other while 85MSR takes the mutual influence into consideration.

The following is the calculation formula of ΔV_{85}[6]:

$$\Delta V_{85} = V_{(i)85} - V_{(i-1)85} = \overline{V_1} - \overline{V_2} + Z_{|85|}(\sigma_1 - \sigma_2) \tag{1}$$

Where, $\overline{V_1}$, $\overline{V_2}$ are Average speed on front and back sections; σ_1, σ_2 are Standard difference of speed on front and back sections; $Z_{|85|}$ is 85th value on standard normal analysis.

When mutual influence of speeds on front and back sections are considered, calculation formula of 85MSR is as follows[6]:

$$85MSR = (V_1 - V_2)_{|85|} = \left(\overline{V_1} - \overline{V_2}\right) + Z_{|85|}\sqrt{\sigma_1^2 + \sigma_2^2 - 2\mathrm{cov}(V_1, V_2)} \tag{2}$$

$$Var(V_1 - V_2) = \sigma_1^2 + \sigma_2^2 - 2\mathrm{cov}(V_1, V_2) \tag{3}$$

Where, $\text{cov}(V_1, V_2)$ is Covariance.

Suppose correlation coefficient of V_1, V_2 as $\rho = \dfrac{\text{cov}(V_1, V_2)}{\sigma_1 \sigma_2}$, on the basis of its quality, there is:

$$\left| \frac{\text{cov}(V_1, V_2)}{\sigma_1 \sigma_2} \right| \le 1 \quad \text{or} \quad -\sigma_1 \sigma_2 \le \text{cov}(V_1, V_2) \le \sigma_1 \sigma_2 \tag{4}$$

So the following relation always establishes:

$$\sqrt{\sigma_1^2 + \sigma_2^2 - 2\,\text{cov}(V_1, V_2)} \ge (\sigma_1 - \sigma_2) \tag{5}$$

Namely, 85MSR $\ge \Delta V_{85}$ always establishes, so the alignment consistency may be overestimated when it is evaluated with ΔV_{85} and the effect is not as good as 85MSR, so this thesis adopts 85MSR.

Analysis of Project Case

General Situation of the Inspected Section

All the data in this thesis come from the project named Evaluation of Alignment Adaptability and Research on Improvement Measures after First-Class Highway Becomes Superhighway supported by Department of Transport of Heilongjiang Province. Ningfu Section (at the border of Heilongjiang and Jilin) on Heda Superhighway is selected for the research, the design speed is 80km/h, and it is a dual four-lane highway with the roadbed width of 24.5m. The researched highway is on mountainous areas with complicated topography. 8 typical sections are selected from the project data; among them, some have certain evident single alignment parameter, e.g. high gradient value of small radius and some are sections with combination of horizontal and longitudinal features, which has great values for comparative analysis and are convenient for targeted research.

Data Analysis

In this thesis, V_{85} value is also used as the operating speed when analyzing the relationship between alignment and speed. The V_{85} value is from statistic method; the V_{85} value of each section can be obtained from curve chart for accumulated frequency distribution of speed. Please refer to Table 3.

Table 3 V_{85} Value of Oversize Vehicles on Researched Sections

Section Mileage Stake Number	V_{85} [km/h]	Section Mileage take Number	V_{85} [km/h]
k1+300~k1+400	79.57	k22+900~k23+100	72.50
k1+400~k1+500	83.11	k26+600~k26+700	59.34
k1+500~k1+600	68.93	k26+700~k26+800	64.64
k7+700~k8+000	92.33	k27+200~k27+400	82.00
k8+000~k8+100	50.94	k27+400~k27+600	77.15
k8+100~k8+200	50.63	k27+600~k27+800	81.61
k8+200~k8+300	51.42	k30+100~k30+300	99.41
k15+200~k15+400	73.66	k30+300~k30+500	101.66
k15+400~k15+600	68.76	k30+500~k30+700	92.60
k15+600~k15+700	59.07	k30+700~k30+900	77.53
k22+500~k22+700	99.70	k39+700~k40+000	84.36
k22+700~k22+900	92.81	K40+000~k40+400	86.69

The ΔV_{85} value on each section can be figured out according to the above operating speed, but the 85MSR value cannot be figured out. According to the formula [7]:

$$85MSR = 2.171 \Delta V_{85} + 4.0469 \tag{6}$$

Please refer to Table 4 for specific values:

Table 4 Corresponding Relation of ΔV_{85} and 85MSR on Each Section

Section Stake Number	ΔV_{85}	85MSR	Section Stake Number	ΔV_{85}	85MSR
K1+300~k1+600	3.54	11.73	k22+500~k23+100	6.89	19.01
	14.18	34.83		20.31	48.14
k7+700~k8+300	41.39	93.90	k27+200~k27+800	4.85	14.58
	0.31	4.72		3.46	11.56
	0.79	5.76	k30+000~k30+900	2.25	8.93
k15+200~k15+700	4.90	14.68		9.06	23.72
	9.69	25.83		15.07	36.76
k26+600~k26+800	5.30	15.55	k39+700~k40+400	2.63	9.76

Evaluation of Alignment Consistency on Researched Sections

When researching the alignment consistency of the section from Xingshan to Fuxing on Heda Superhighway, this thesis mainly calculates and analyzes the operating speed coordination of large van and states the sections with the 85MSR value larger than 20 km/h. According to Table 3-2, the 85MSR of the sections of K1+400~k1+600, k7+700~k8+100, k15+400~k15+700, k22+700~k23+100, k30+300~k30+700 and adjacent section of k30+500~k30+900 are larger than 20km/h, and the alignment consistency of adjacent sections is poor.

Summary

The safe highway alignment design does not lie in horizontal or longitudinal qualifications of the whole line (or part of it), but in the consistency and balance of the entire alignment. Analyzing the alignment consistency with the combination of alignment parameters and operating speed can effectively overcome the disadvantage of design speed and guarantee the continuity and consistency when vehicles running on successive sections. Traditional ΔV_{85} does not sufficiently consider the operating speed of individual vehicle, so this thesis adopts the method of 85MSR and studies the alignment consistency of the section from Xingshan to Fuxing on Heda Superhighway, and then finds out the sections with poor alignment consistency and provides basic data for the analysis of traffic safety factors and road improvement.

References

[1] JTG D20-2006, Design Specifications for Highway Route[S].

[2] JTG/T B05－2004.Instruction for Safety Instruction of Highway Project [S].Beijing: China Communications Press.2004.10.

[3] Wang Heng, Fang Shou'en. Operating Speed Calculation with Consideration of Accelerated Speed [J].Shandong Transport Science. 2004.3:10～12.

[4] Liu Yuntong. Instruction for Road Traffic Safety [M].Beijing: China Communications Press.2004.7.

[5] McFadden J, Elefteriadou L. Evaluating horizontal alignment design consistency of two-lane rural highways: Development of new procedure [J]. Transportation Research Record 1737, Washington D. C., 9 -17, 2000.

[6] Young-Jin Park, Frank F. Saccomanno. Evaluating speed consistency between successive elements of a two-lane rural highway [J]. Transportation Research Part A 40 (2006) 375–385.

[7] Liu Zhiqiang, Wang Yunxia, Huang Cheng. Method Study of Highway Alignment Continuity Based on 85MSR [J]. Highway Transport Science. 2008.6:36～38.

doi:10.4028/www.scientific.net/AEF.5.333

High strength concrete small hollow blocks made with rock chips as aggregates

Zhang Yongquan [a], Yuan Jie [b], Ge Yong [c]

School of Transportation Science and Engineering, Harbin Institute of Technology, Harbin 150090, China

[a] zyqzygzs@126.com, [b] hityuanj@163.com, [c] hitbm@163.com

Keywords: rock chips; high strength concrete small hollow blocks; fractal dimension; curing methods; shrinkage

Abstract: It is more and more general of using industrial solid waste as the aggregates in construction materials for non-structural applications. But because of the developments and applications of reinforced blocks masonry structure in the modern masonry structure, especially in the mid-high and high storey buildings, there will be a growing interest of using industrial solid waste to produce high strength concrete small hollow blocks for structural applications. This experiment by mixing the different proportions of rock chips within the range of 30-70% as the replacement for sand prepared high strength concrete small hollow blocks which the compressive grade is MU 15.0, the influence of aggregates grading on the compressive strength of high strength concrete small hollow blocks was investigated at the same water/cement (w/c) ratio (0.45). In addition, the influence of the different curing methods on the compressive strength and shrinkage of high strength concrete small hollow blocks were also investigated, test results showed that high strength concrete small hollow blocks under the curing method which is the one-time pouring the ample amount of water, covered and sealed with plastic sheeting, the compressive strength had a better development, and the total shrinkage was larger than others.

1. Introduction

There will be a big development of Chinese housing construction in the future for a long period of time, which requires the construction industry must be according with sustainable development strategy, break the routine, develop the new wall materials [1]. Since “Eleventh Five-Year Plan”, the new building materials based on the building energy efficiency had a rapid development, the using of which played a “four of a green” objectives in the building structure [2]. The foreign researchers [3, 4] studied that the replacement of coarse and fine natural aggregates by recycled aggregates at the suitable levels had little effect on the compressive strength of the blocks, based on the laboratory work, factory trials showed that there were no practical problems with the use of recycled demolition aggregate in the manufacture of building blocks. Some domestic scholars [5-7] using industrial waste such as iron-tailings, steel slag, and gangue prepared the MU10.0 load-bearing concrete hollow blocks, which resulted in a good economic and social benefits. However, the study of preparing high strength concrete small hollow blocks more than MU15.0 and 45 percent hole rate with industrial waste is more lesser.

Concrete small hollow blocks are non-sintering prepared with a certain percentage gelled materials and aggregates by mechanical forming and curing, which performances are influenced by the changes of ambient temperature and humidity. In the former block masonry structure applications, the practical strength less than the design strength resulted the problems of missing edge off angle and cracks in walls, which even seriously affected the quality of the engineering, so how to ensure the excellent performances of concrete small hollow blocks become one of the widespread concerned problems [8]. Sunil Kumar [9] studied the influence of type of curing on the increase in strength and hardening of the blocks with time, and the results showed that the hot water curing leads to a greater degree of hardening, and higher strength, earlier compared to ordinary water curing. F.O. Ogunye [10] tested two different soil block samples, stablished with cement, lime and lime-gypsum at varying proportions and cured at both room temperature (RT) and elevated

temperature (ET), showed that the mass loss of the blocks cured at elevated temperature was smaller than the blocks cured at room temperature in the simulated rainfall. Ismail Demir [11] reported that optimal strength-thermal conductivity combination was obtained by the usage of silica fume and expanded perlite together. Improved strength properties were obtained by using hydrothermal curing conditions and super-plasticizer addition. Therefore, the curing methods are more important for the performance of concrete small hollow blocks.

This paper presents a recent study at the Harbin Institute of Technology on the feasibility of using rock chips replaced natural sand as aggregates for high strength concrete small hollow blocks. The main objective of this study was to develop the appropriate technologies for the production of high strength concrete small hollow blocks which hold better qualities.

2. Experimental Section

2.1 Materials

2.1.1 Cement

In this study, a Chinese standard 42.5 ordinary Portland cement was used and the corresponding properties are shown in Table 1.

Table 1 Chemical analysis of cement

CaO	SiO_2	Al_2O_3	Fe_2O_3	Na_2O	K_2O	MgO	SO_3
57.4	20.3	5.2	3.3	0.16	0.42	1.9	4.24

2.1.2 Rock chips

The rock chips were obtained from a quarry named Heng chang in A'Cheng, Harbin. The waste in the progress of gravel production is rock chips, which have the same chemical composition with parent rock. The particle size of rock chips is generally bellow 4.75mm, usually there is a certain content powder which particle size is less than 0.15mm. The technical indicators of rock chips such as the physical properties varied greatly because of the different production technology, the range of fineness modulus is between 1.7 and 4.6, apparent density between 2.64kg/m^3 and 2.84 kg/m^3, packing density between 1.38 kg/m^3 and 1.59 kg/m^3, porosity between 42% and 48%. Therefore, the physical properties of rock chips are similar with natural sand, it is more suitable material which can replace natural sands in the practical engineering applications. The properties of the rock chips were tested according to ASTM C136 and the results are presented in Table 2 and Table 3.

Table 2 The properties of the rock chips and river sand

	Fineness Modulus	Silt Content (%)	Voidage (%)	Gradation interval	Apparent Density (kg/m^3)
River sand	2.91	1.00	32.0	II	2580
Rock chips	3.50	5.0	32.5	I	2650

Table 3 Chemical analysis of stone powder

SiO_2	Fe_2O_3	Al_2O_3	CaO	Na_2O	K_2O	MgO	SO_3
57.3	6.1	14.6	5.4	6.3	2.9	1.9	0.3

2.1.3 River sand

River sand with a maximum size of 4.75mm and a fineness modulus of 2.91 was used the fine natural aggregates in this study. The properties of the sand were tested according to ASTM C136 and the results are presented in Table 3.

2.1.4 Crushed stone

Crushed stone obtained from the same quarry as rock chips was used as the coarse aggregate.

2.2 Mix proportions of high strength concrete small hollow blocks

Table 4 Mix proportions of high strength concrete small hollow blocks

Notation	Cement	Water	Coarse aggregate	Fine aggregate	
				Rock chips	Sand
RC50-1	360	162	914	274	640
RC55-2	360	162	823	402	603
RC60-3	360	162	731	549	548
RC65-4	360	162	640	713	475
RC70-5	360	162	548	896	384
BMP	340	153	667	868	372

2.3 Preparation of the blocks specimens

The high strength concrete small hollow blocks were fabricated in steel moulds with internal dimensions of 390mm in length, 190mm in width, 190mm in depth. Initially, cement, coarse and fine aggregates, were mixed in a pan mixer for approximately 3 min. After mixing, water was incrementally added to the mixtures until the desired moisture content for these dry mixtures was obtained. For fabrication of block specimens, only a small amount of water was required to prepare a cohesive mix but with zero slump (non-workability, which simulated the actual industrial production process of concrete blocks). The molding process was high frequency vibration and squeezing compacting, molding time was controlled at about 4s. The fabricated block specimens were putted on the steel layer boards, left at room temperature of 20±5℃ and 75±5 relative humidity (RH) for 4 h. The block specimens were then putted into the steam curing kiln and cured at a specific way which is warming up to 70℃ within 3h, then thermostating 3h, at last cooling for 6h.

2.4 Curing methods

High strength concrete small hollow blocks were cured in the storage yard after carried out steam curing kiln. According to the climatic characteristics of Harbin in May, this study designed the following three kinds of curing method as shown in Table 5.In order to better evaluate the three kinds of curing method, laboratory standard curing method was taken as the reference. The mix proportion of high strength concrete small hollow blocks was shown in Table 4 which number was BMP.

Table 5 Curing methods in the storage yard

Number	Specific details of curing method
A	covered and sealed with plastic sheeting, one-time pouring the ample of water
B	not covered with plastic sheeting, one-time pouring some water every day
C	not covered with plastic sheeting, one-time pouring some water every seven days

2.5 Test methods

2.5.1 Grading fractal dimension

Xie Heping [12] took a statistical analysis about the distribution of the particle size of broken rock, which has the statistical significance of the fractal behavior and self-similarity. The equations were obtained as follows.

$$M(r)/M = (R/\sigma)^{\alpha} \tag{2-1}$$

$$D_J = 3 - \alpha \tag{2-2}$$

Where M is the total mass of aggregates, $M(r)$ is the cumulative sieve of which size, and D_J is the fractal dimension, which is the measure of the complexity of distribution of the particle size. According to the solving model of the two equations calculated the grading fractal dimension using Matlab software.

2.5.2 Compressive strength

The compressive strength was determined by using a universal testing machine with a maximum capacity of 2000kN. The loading rate of 320kN/min was applied to the nominal area of the block specimen. Prior to the loading test, the compressive surfaces of the block specimens were made level by cement mortar which compressive strength is 28.6MPa. Three samples were tested for each mix proportion and curing method.

2.5.3 Shrinkage

After the steam curing, the two length measuring heads were fixed on half-height of any a surface of the block specimens along the horizontal direction by Epoxy resin, the initial length between them is 250mm. The tool of measuring length in this paper named hand-held strain gauge, which accuracy of measurement is 0.001mm. Then the block specimens were taken into storage yard under three curing methods showed in table until further measurement at 1st, 3rd, 7th, 14th, 28th, 45th day. Each value represents the average of three measurements.

3. Results and Discussion

3.1 Grading fractal dimension

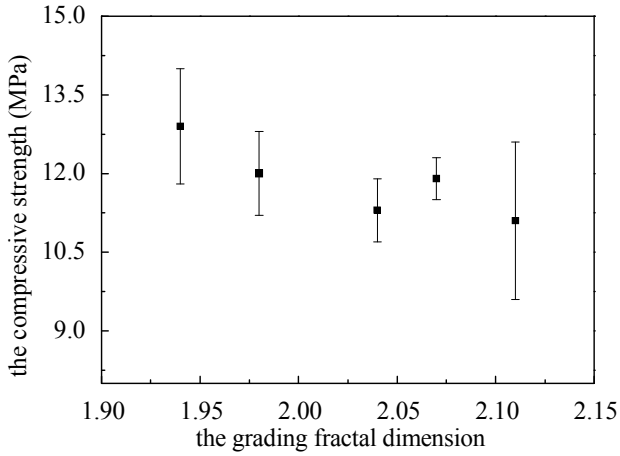

Fig 1 The influence of the grading dimension on the compressive strength of the blocks

It can be seen from the Fig 1 that when the grading dimension was between 1.94 and 2.11, the compressive strength of the blocks is between 11.1 and 12.9. With the increase of the grading fractal dimension the discreteness of values became larger, but in this experiment, the change of which was not too large, the compressive strength of high strength concrete small hollow blocks meet the design requirements. The grading fractal dimension expressed a range of grade, so any range of the grading fractal dimension is behalf of some a range of grade. In this paper, there is a certain practical significance that setting the grading fractal dimension to control the compressive strength of high strength concrete small hollow blocks.

3.2 Compressive strength

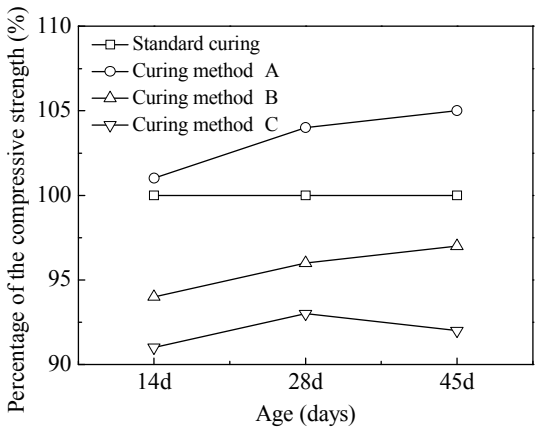

Fig 2 The influence of curing methods on the compressive strength of the blocks

It can be seen from the Fig 2 that the compressive strength of high strength concrete small hollow blocks at the age of 28 days and 45 days under the curing method A were bigger than two other curing methods, respectively was 108.3 percent and 107.1 percent of the blocks under the curing method B, was 110.6 percent and 112.9 percent of the blocks under the curing method C. With the increase of age the compressive strength of high strength concrete small hollow blocks were growing under the two curing methods A and B, the rate of growing were was more slowly, but the compressive of the blocks at the age of 45 days were smaller than the 28 days under the curing method C. After poured the ample amount of water, then covered and sealed with the plastic sheeting, the temperature and relative humidity of the closed system was respectively more than 50℃ and 95%, which is beneficial to the accelerating of hydration, so the compressive strength of the blocks under this curing method was growing faster. On the contrary, the compressive strength of the blocks was smaller in the open system, especially the curing method C. Poured one time every seven days, the relative humidity of outdoor climate is below 80%, so moisture lost too fast and there was no extra water supplied except the rain water, thereby the compressive strength of the blocks was growing slowly and even came up the negative growth because of the lower relative moisture content.

In another perspective, not covered the plastic sheeting, the compressive strength of high strength concrete small hollow blocks was seriously affected by the climate change, which will also take bad effects on the quality of high strength concrete small hollow blocks, so if high strength concrete small hollow blocks are not cured effectively, there will be asymmetrical in the compressive strength when the blocks are applied in walls at the age of 28 days.

3.3 Shrinkage

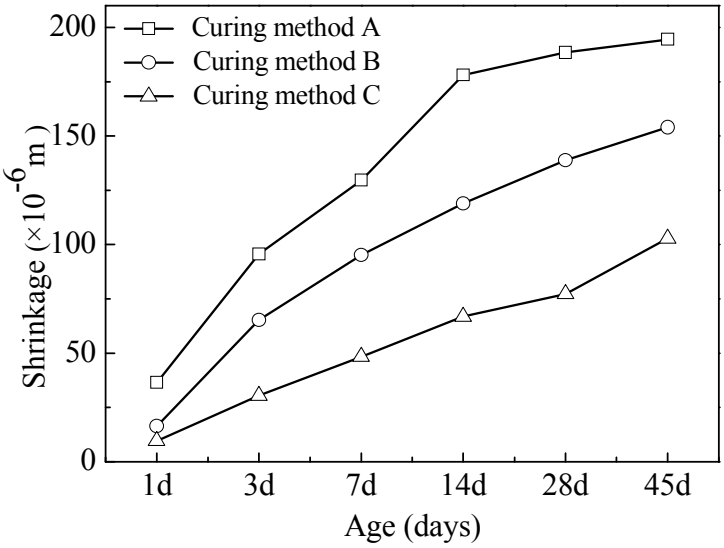

Fig 3 The influence of curing methods on the shrinkage of the blocks

It can be seen from Fig 3, the total shrinkage of high strength rock chips concrete small hollow blocks was the biggest under the curing method A among the three curing methods, reached 194μm/mm. The total shrinkage of high strength rock chips concrete small hollow blocks under the curing method C was the smallest, only reached 103μm/mm, and the total shrinkage of high strength rock chips concrete small hollow blocks under the curing method B was between them, reached 154μm/mm. The total shrinkage of the blocks under the curing method A at the age of 14 days was larger than the total shrinkage of the blocks under the curing methods B and C at the age of 45 days. Under the three curing methods, the main influencing factors of the total shrinkage were relative to hydration, the drying shrinkage of hardened cement pastes and moisture loss or migration. Continued hydration played a major role on the increasing shrinkage under the curing method A, because of the degree of hydration became more and more bigger, which directly resulted in the volume change of concrete. But to the curing method C, moisture loss or migration accounted for a major role, the loss or migration of moisture in pores of the cement gel could

generate capillary tension which caused the shrinkage of concrete. The three factors corporately played roles on the shrinkage of the blocks under the curing method B. As can be seen from the trend of the shrinkage, the slope of the curve A was changed at the age of 14 days, from which time to 45 days, the shrinkage of the blocks became slowly. The slopes of the curve B and C were almost unchanged in the 45 days, the shrinkage of them always increased, but the numerical value did not exceed the curve A. The strength of hardened cement pastes is rising with the hydration going on for the given concrete, so the absolute value of the shrinkage becomes smaller. When high strength concrete small hollow blocks under the curing methods B and C were applied in the construction buildings, there will be a bigger shrinkage because of temperature, humidity, stress and so on.

4. Conclusions

(1) Using the fractal dimension expressed the grading of aggregates is reasonable in some perspective. When the grading fractal dimensions were between 1.94 and 2.11, the compressive strength of high strength concrete small hollow blocks was larger, so by controlling the grading fractal dimension could control the quality of high strength concrete small hollow blocks.

(2) High strength concrete small hollow blocks under the curing method of one-time pouring ample amount of water, covered and sealed with plastic sheeting had larger shrinkage and bigger compressive strength. According to the theory, high strength concrete small hollow blocks at this curing method will not have any larger drying shrinkage applied in reinforced blocks masonry structure, and the quality of which can be better. So the problem of cracks in walls will be well solved from the new wall materials itself.

References

[1] Xu X, Xiao Y, Wu Q. Prospect and Measure of Construction Industry in China [J]. Journal of Shanghai Economic Management College, 2009, 4: 41-44.

[2] Wu H, Yang L, Li G. The development of new energy-saving building materials [J]. Shaanxi Architecture, 2008, 5: 1-4.

[3] C.S. Poon, S.C. Kou, L.Lam. Use of recycled aggregates in molded concrete bricks and blocks [J]. Construction and Building Materials, 2002(16): 281-289.

[4] Marios N. Soutsos, Kangkang Tang, Stephen G. Millard. Concrete building blocks made with recycled demolition aggregate [J]. Construction and Building Materials, 2011(25): 726-735.

[5] Deng Q, Li J. Concrete load-bearing small hollow blocks with iron tailings and slags [J]. China Construction Education, 2007.1: 47-49.

[6] Liu Y, Song S. Research on Steel Slag Concrete Small-Sized Hollow Block [J]. Journal of Beijing Institute of Civil Engineering and Architecture, 2007.3: 6-10.

[7] Xue C. Load-bearing blocks with gangue [J]. Fly Ash Comprehensive Utilization, 2002(2): 44-45.

[8] Lu C. Control of cracks in concrete hollow blocks wall [J]. Block-Brick-Tile, 2010, (2): 42-44.

[9] Sunil Kumar. A perspective study on fly ash–lime–gypsum bricks and hollow blocks for low cost housing development [J]. Construction and Building Materials, 2002, 16: 519-525.

[10] F. O. Ogunye, H. Boussabaine. Development of a rainfall test rig as an aid in soil block weathering assessment [J]. Construction and Building Materials, 2002(16):173-180.

[11] Ismail Demir, M. Serhat Baspinar. Effect of silica fume and expanded perlite addition on the technical properties of the fly ash–lime–gypsum mixture [J]. Construction and Building Materials, 2008, 22: 1299-1304.

[12] Xie H, Gao F. Fractal Fracture and Fragmentation in Rocks [J]. Journal of Seismology, 2003, 22(4): 1-9.

doi:10.4028/www.scientific.net/AEF.5.339

Asphalt Pavement Structural Health Monitoring Utilizing FBG Sensors

Zejiao Dong[1, a], Shenglong Li[2, b], Jiayu Wen[3, c], Hongchun Chen[4, d]

[1] School of Transportation Science & Engineering, Harbin Institute of Technology, Harbin 150090, China

[2] School of Transportation Science & Engineering, Harbin Institute of Technology, Harbin 150090, China

[3] School of Transportation Science & Engineering, Harbin Institute of Technology, Harbin 150090, China

[4] School of Transportation Science & Engineering, Harbin Institute of Technology, Harbin 150090, China

[a]hitdzj@hit.edu.cn, [b]lshlhit@hit.edu.cn, [c]wenjiayu521@sina.com, [d]291211@126.com

Keywords: Asphalt pavement; long-term monitoring; SHM; FBG sensors

Abstract. Assessment of pavement working state and service life is really meaningful for traffic security, design evaluation and road maintenance. However, this job seems to be a mission impossible, because it is unimaginable to learn exactly how a pavement works inside when the construction is finished. As a result, in this paper, current situation of pavement-design theory and testing methods was summarized, and at the same time the concept of Pavement Structural Health Monitoring (PSHM) was introduced, followed by the explanation of the FBG sensing component's basic theory. Then, an engineering application of utilizing FBG sensors in actual pavement was introduced, the monitoring effect was shown. Conclusions were that PSHM was of great importance and utilizing FBG sensors in PSHM was effective.

Introduction

Layered elastic system theory is the basic theroy in pavement design in China. Tensile stress of asphalt layer bottom, fatigue, and deflection are evalutaion indexes. Conventional survey and investigation methods adopted by researchers are core drilling, pavement cutting, Benkelman beam, FWD, automatic deflectometer, surface-curvature apparatus and etc. They are either destructive or with low-precision or low-frequency, and most important is that all of these methods are discontinuous and short-term. Long-term exposed in natural environment, pavement is deteriorating at the coupling effect of load, temperature, water and ultraviolet. It is difficult to veritably understand the mechanical response of pavement structure in actual environment by regular methods [1, 2].

Pavement condition has direct influence on traffic security, operating expenses, riding comfort and economic results in society. With the rapid development of the vehicle manufacturing technologies and cargo transporting demands, more and more heavy-duty asphalt pavements with superior performances have been constructed. Meanwhile, strain of the asphalt pavement will result in the destruction of pavement structure when it extends large enough. It is becoming a more and more outstanding problem, and adverse effects are following on.

Taking all the conditions having been illustrated above into consideration, necessity to monitor the service state of a pavement throughout its lifetime is apparently essential. Therefore, a new concept of asphalt pavement researching method has been put forward, that is PSHM. PSHM is a kind of advanced researching method which is a long-term and real-time process. The most common approach to PSHM is installing some sensors, including transverse strain sensors, vertical strain sensors, temperature sensors, and pressure cells, acquiring useful data and calculating them into

helpful parameters like strain, stress and temperature. In this way, pavement structural mechanical response can be veritably understood via embedded sensors within pavement structure. Hence, the performance and category of sensors being used in monitoring becomes the key point to the success.

FBG sensor

The past 20 years has witnessed the rapid growth of optical fiber sensing technology. FBG sensors, as one of optical fiber components, have been widely applied in sensing fields, such as strain sensors and temperature sensors [3]. Compared with conventional sensors, FBG sensors are the most promising candidates to effectively replace conventional strain gauges for long-term monitoring applications in harsh circumstances [4]. They exhibit several advantages such as, flexibility, embeddability, high frequency, EMI immunity and many other obvious advantages, showing in Table 1. In Table 1, M stands for medium, L for low, Y for yes, E for excellent, G stands for good, H for high, W for wide and N for narrow.

Table 1 Performance Index of Sensing Components

Index	*Materials and Sensing Components*					
	FBG	*Shape-Remembering Alloy*	*Piezoelectric Component*	*Resistance Strain Gauge*	*Carbon Fiber*	*Semi-Conductor*
Price	M	M	M	L	L	M
Distribution	Y	Y	Y	Y	Y	Y
Compatibility	E	E	E	M	E	G
Linearization	E	G	E	E	G	E
Sensitivity	H	H	H	M	M	H
Deformation Capacity	E	E	E	E	G	G
Stability	E	G	E	G	E	E
Endurance	E	M	G	M	M	E
Bandwidth of Response Frequency	W	N	W	N	W	W

The basic structure of fiber includes core, cladding, coating, reinforced fiber and protective material. Core and Cladding are the principal part of the fiber with the diameter 125 μm which play a key role in transmitting the light. While others, such as coating, reinforced fiber and protective material, isolate interferential light and protect fiber.

The basic principle of a FBG sensor is to monitor the wavelength shift of the returned Bragg signal as a function of the measurement (e.g. strain, temperature or force). The Bragg wavelength of grating can be expressed as:

$$\lambda_B = 2n_{eff}\Lambda . \tag{1}$$

Where:
n_{eff} = the effective refractive index and
Λ = grating period.

As shown in Eq. 1, the Bragg wavelength of fixating is related to the effective refractive index and grating period. Any physical process, which changes the effective refractive index and grating period, will induce the shift of Bragg wavelength of grating. The variation of Bragg wavelength of grating can be obtained as follows if a strain is applied on the fiber:

$$\Delta\lambda_B = \lambda_B \times (\frac{\partial\Lambda}{\Lambda} / \frac{\partial l}{l} + \frac{dn_{eff}}{n_{eff}} / \frac{\partial l}{l}) \times \frac{\Delta l}{l} . \quad (2)$$

Where:
l = grating length and
Δl = variation of fixating length.

As well as being sensitive to strain, the wavelength is also sensitive to temperature. The change of Bragg wavelength can be written as:

$$\Delta\lambda_B = \alpha_T \cdot \Delta T \cdot \lambda_B . \quad (3)$$

Where:
α_T = temperature sensitivity parameter of Bragg grating and
ΔT=temperature variation relative to calibration temperature.

As a result, the relative shift in the Bragg wavelength due to an applied strain and a change in temperature can be expressed by:

$$\Delta\lambda_B = \lambda_B \times (\frac{\partial\Lambda}{\Lambda} / \frac{\partial l}{l} + \frac{dn_{eff}}{n_{eff}} / \frac{\partial l}{l}) \times \frac{\Delta l}{l} + \alpha_T \cdot \Delta T \cdot \lambda_B . \quad (4)$$

Application of FBG sensor monitoring

Project design

The main idea for the project is to measure the vertical compressive strain at the top of subgrade, the transverse tensile strain at the bottom of aspalt layer and the vertical compressive strain at the middle of asphalt layer based on key mechanical information and position in flexible pavement[5], which can be seen in Table 2. Aiming at the approach of perpetual pavement constructing in Jilin, considering the different utilities of different sensors, other than strain gauges, a temperature sensor was also installed, given as Fig. 1. Then a final installation plan was settled, given in Table 4. We choosed Tider-FBG-LFRP as transverse strain gauge and Tider-FBG-SFRP as vertical strain gauge. Parameters of these two series of sensors are shown in Table 3.

Table 2 Key Mechanical Information and Position within Flexible Pavement Structure

Failure Types	*Mechanical Information*	*Key Position*
Fatigue Cracking	Transverse tensile strain/stress	Top/Bottom of asphalt layer
Permanent Deformation of Surface Layer	Vertical compressive strain/stress	Middle of asphalt layer
Permanent Deformation of Base Layer	Vertical compressive strain/stress	Base layer
Permanent Deformation of Subgrade	Vertical compressive strain/stress	Top of subgrade

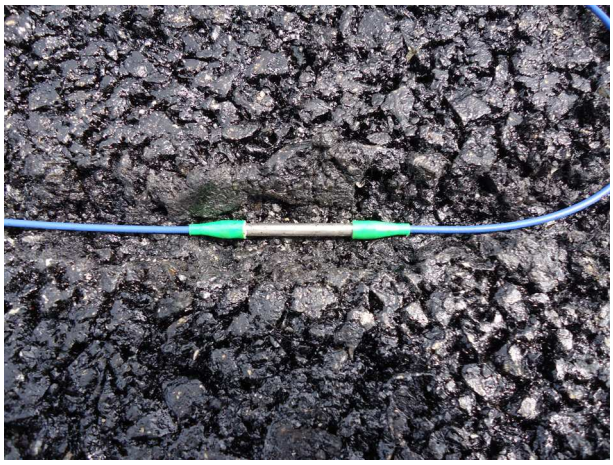

Fig. 1 Temperature sensor

Table 3 Parameters of FBG Sensors

Parameters	*Expanding Diameter [mm]*	*Packing Diameter [mm]*	*Length [mm]*	*Elastic Module [GPa]*	*Range [με]*	*Sensitivity Coefficient [pm/με]*
LFRP Series	20	4	70	50	±5000	1.2
SFRP Series	20	6	20	50	±5000	1.2

Table 4 Pavement Structural Information and Installation Position

Material	*Thickness*	*Installation Position*	*Type of Sensor*
SMA-16	5cm	Bottom	Temperature
AC-20	7cm	Bottom	Vertical strain sensor
AC-25	10cm	--	--
ATB-30	12cm	Bottom	Transverse strain sensor
Granular Base	20cm	--	--
Subgrade	--	Top	Vertical strain sensor

Sensor installation

In order to obtain accurate results, precise and cautious installation is necessary. Several steps as follows should be specially drawn attention to.

First, aclinic installation. To ensure the veracity of measurement, strain distraction must be eliminated. That means we have to level the surface where we set gauge, as Fig. 2(a) shows.

Second, cable binding. Given as Fig. 3. To avoid loss of signal for being pulled up, cables must be bound. According to NCAT's testing resulting, sensors' survive rate of which whose cables were bound was far higher than not[6]. When all of sensors in single layer had been installed, all cables should be bound together in the end, as Fig. 2(b) shows. We also can get a full view of sensor installation from Fig. 2(b).

Third, static compaction. When aspalt mixture was just being paved, there is not too much intensity in pavement to protect sensors from heavy duty. Therefore, the pavement should be compacted without vibration during first two times, as Fig. 4 shows.

(a) Vertical strain sensor

(b) Full view of installation

Fig. 2 Installation of FBG sensors

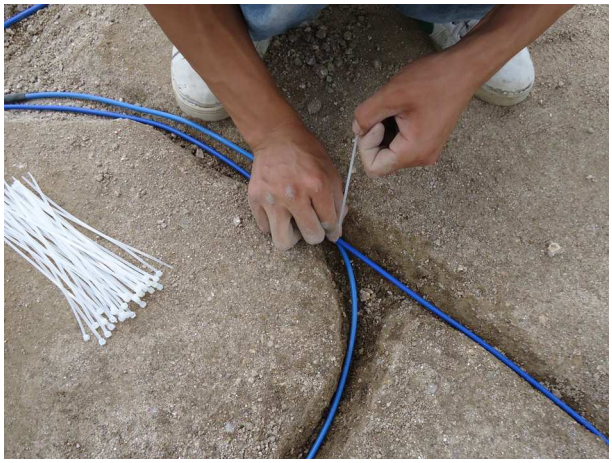

Fig. 3 Cable binding

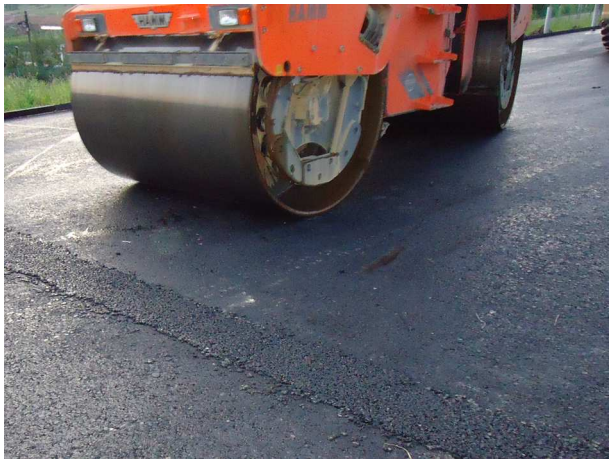

Fig. 4 Static compaction

Data acquisition

In this project, the FBG interrogator is TFBGD-9000 from Tider Co Ltd, China, with resolution of 1 pm, frequency of 300Hz, shown in Fig. 5. By comparatively long-term data acquiring and calculating, we got a temperature-time curve and some strain-time curves, given as Fig. 6, Fig. 7 and Fig. 8. From the temperature-time curve, we learn that how the pavement temperature changes in one day in May in Jilin. From strain-time curves, we exactly understand that how much the strain is at some certain points within the pavement. There is an issue should be explained, that is Fig. 7 and Fig. 8 are not the responses of the same vehicle.

Fig. 5 TFBGD-9000 interrogator

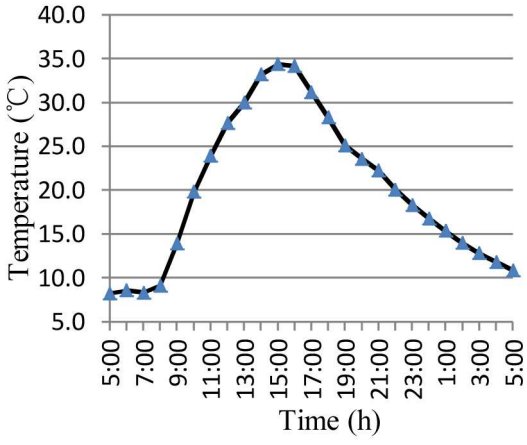

Fig. 6 Temperature of top layer

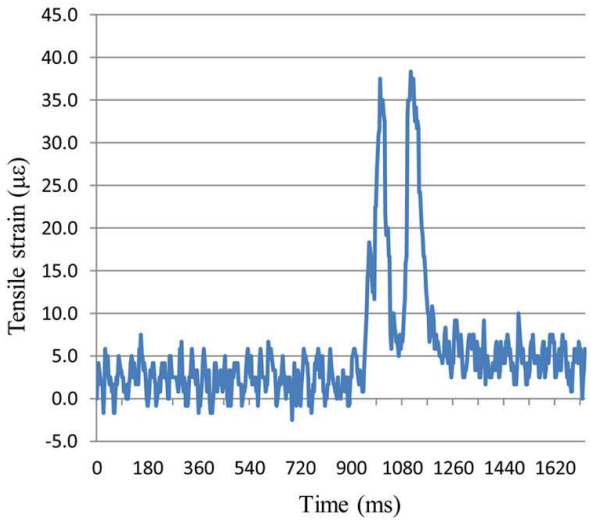

Fig. 7 Transverse sensor

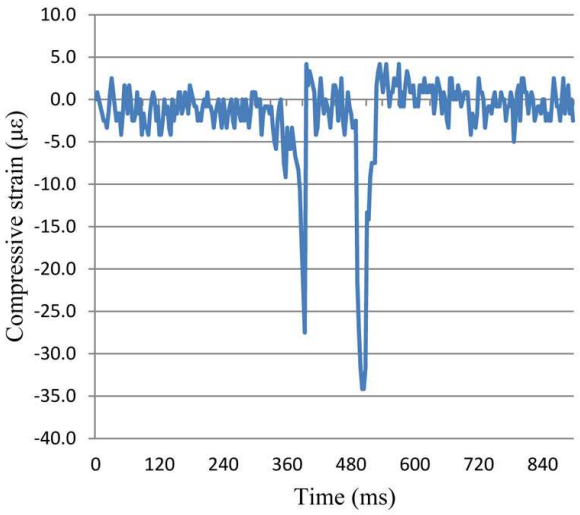

Fig. 8 Vertical sensor

Conclusions

The concept of Pavement Structural Health Monitoring was proposed in this paper. By analyzing conventional testing methods and results of application of FBG sensor monitoring, some key observations were:

1. By means of comparing with conventional pavement testing methods and effectiveness analysis, structural health monitoring is essentially necessary in pavement service lifetime, which brings a predominant researching method in highway field.
2. Using FBG sensors for strain and temperature monitoring in actual pavement, absolute temperature in a single day and dynamic response of a vehicle was obtained, good results were gained. This is a successful application of FBG sensor in pavement monitoring.

References

[1] Liu Shulong, Experimental Study on Monitoring Asphalt Pavement Performance Health Using Fiber Bragg Grating, Nanjing University of Aeronautics and Astronautics (2011).

[2] Li Chuanlin, Study on The Structure Test-Method of Asphalt Pavement Based on Internal Sensor Survey, Chang'an University, Xi'an, China (2008).

[3] Ren Liang, The Application of Fiber Bragg Grating Technology in Structure Health Monitoring, Dalian University of Technology (2008).

[4] X. F. Zhao, J. P. Ou, Long Sensing Gauge Fiber Bragg Grating Sensor with Pretension, J, ASCE (2003).

[5] Sun Zongjie, Initial Monitoring and Analysis on Dynamic Response of Pavement Structure, Harbin Institute of Technology (2011),pp:26-52.

[6] David H. Timm Angela L. Priest Thomas V. McEwen Design and Instrumentation of the Structural Pavement Experiment at the NCAT Test Track .NCAT Report 04-01 April 2004.

doi:10.4028/www.scientific.net/AEF.5.345

Analysis of Tire-Pavement Noise Spectrum of Noise Reduction Dense Asphalt-rubber Pavement

GUO Zhao-yang [1,2,a], FENG De-cheng[1,b], SHEN Guo-hui [2,c]

[1] School of Transportation Science and Engineering, Harbin Institute of Technology, Harbin 150090, China

[2]Research Institute of Highway Ministry of Transportation ,Beijing ,100088, China

[a]chaoyang226@163.com, [b]fdcgxy@vip.sina.com, [c]gh.shen@rioh.cn

Keywords: asphalt-rubber pavement; noise spectrum ; Close-Proximity (CPX) method ; tire-pavement noise ;

Abstract. The types of noise reduction asphalt pavement were summarized into the follows: single layer porous or two-layer porous asphalt pavement, elastic asphalt pavement, optimized surface texture pavement, and universally composable one based on these three types. Beijing of China was very drought and short of rainfall, there were large volume of traffic, heavy wheel load and many dirt things on the pavement surface taken by the tires too. So the dense asphalt-rubber pavement was the most common one for noise reduction, which was paved by gap-graded, macro-texture, dense asphalt concrete, belonging to the types of elastic and optimized surface texture noise reduction pavement. And it could reduce tire-pavement noise obviously and had excellent durability; all proved that it had gone through traffic and climate environment of Beijing well. It had measured tire-pavement noise of asphalt–rubber pavement and stone mustic asphalt pavement in Beijing from 2009 to 2012. This measurement was according to Measurement of close-proximity method which prepared by international organization for standardization in the year 2000. And the test vehicle was a trailer for measuring tire-pavement noise which met requirements of ISO/CD 11819-2:2000. The factors affecting tire-pavement noise spectrum were analyzed, such as temperature, speed, age of pavement and so on. It reveals that the tire-pavement noise sound level could get higher especially higher during the frequency 500Hz~2500Hz in the noise spectrum, while the testing speed increase, or the temperature decrease , or the age of pavement grow. While the frequency lay on the range of higher than 800 Hz, the asphalt–rubber pavement's noise sound level were lower than the stone mustic asphalt pavement's one in all situations, and when the temperature decreased from 30℃ to 0℃, the low limit frequency decreased from 800Hz to 63 Hz. It had tested dynamic modulus and phase angle of the two kinds of pavement materials under different temperature and load frequency with the help of Simple Performance Tester in order to show the reason, The result shows that, asphalt-rubber concrete has smaller Phase angle at wide temperature as well as frequency changes, it could be one of the main reasons to explain this phenomenon. It could provide reference for designing, constructing, maintaining and evaluating the noise reduction asphalt pavement.

Introduction

Asphalt-rubber pavement had been used in Beijing for more than 10 years primarily because it could reduce the premature failures of asphalt pavement. And it could recycle and utilize lots of waste tires by machining them into powder and adding them into asphalt mixture, and contributing to environmental protection of Beijing. Moreover, it could reduce tire-pavement noise, and had been extensively used in Beijing to obtain these benefits. The dense asphalt-rubber pavement was the most widely used in urban road in the last decade, whose nominal maximum aggregate sizes were mainly 13mm or 10mm. [1] However, its noise reducing properties is not well known compared with other asphalt pavement. There should be proof of adequate performance for dense asphalt-rubber pavement to be accepted as a noise mitigation tool.

Beijing Municipal Science & Technology Commission had spent RMB 2 million to study the technology of designing, constructing, maintaining and evaluating the noise reduction asphalt pavement in 2007. It would help to build greener and quieter Beijing, achieving the aim of improving the quality of life of citizens [2].

Research Institute of Highway Ministry of Transportation was asked to conduct the research. it had studied acoustic properties and mechanical properties of several types of asphalt mixture used in Beijing with the help of advanced test equipment, such as Simple Performance Tester, Universal Testing Machine, Asphalt Pavement Analyzer, Reverberation Room. And developed a new noise reduction asphalt pavement, which was paved by gap graded, macrotexture, dense asphalt-rubber mixture, It had invented a trailer with weight to measure tire-pavement noise in accordance with close-proximity method-proposed in ISO/CD 11819-2:2000. [2]

The preliminary findings presented here are analysis of tire-pavement noise spectrum of noise reduction dense asphalt-rubber pavement. After measuring tire-pavement noise five times in Chang'an Avenue from 2009 to 2012, it had gotten the difference between asphalt-rubber pavement's noise spectrum and stone mustic asphalt pavement's one. The factors affecting tire-pavement noise spectrum were analyzed, such as temperature, speed, age of pavement and so on. In order to show the reasons for the differences, this paper presents the correlations of noise spectrum with viscoelasticity of two kinds of pavement materials, by testing their dynamic modulus and phase angle under different temperature and load frequency.

Testing program

Close-Proximity Trailer (CPXT) method for tire-pavement noise [3]

Close-Proximity Trailer (CPXT) method is used for evaluating the noise characteristic of pavement in driving condition. CPXT method is recommended according to the close-proximity method—from Part 2 of Acoustics — Measurement of the influence of road surfaces on traffic noise in Technical Committee ISO/TC 43, Acoustics, Subcommittee SC 1, Noise. The average A-weighted sound pressure levels emitted by one specified reference tire are measured over a specified road distance, together with the vehicle testing speed, by at least two microphones, located close to the tires according to the method. The two mandatory microphones should be operated simultaneously and should have fixed positions relative to the test tire, such that the distance horizontally from the plane of the near test tires sidewall is 0.20 m (± 0.02 m). The two mandatory microphones should be mounted at a height above pavement level of 0.10 m (± 0.02 m). The front microphone should be mounted at an angle of 45° ± 5° to the rolling direction as and the rear microphone shall be mounted at an angle of 135° ± 5° to the rolling direction.

According to ISO 11819-2Acoustic, performance requirements of trailers used in measuring tire-pavement noise should be met mainly on two aspects: background noise and sound reflections against the enclosure. [4], [5]

The background noise of the entire test system must not influence the third octave-band levels more than 1 dB in the 500 Hz - 4000 Hz frequency range and more than 2 dB in the 315 Hz -400Hz range.

The influence of sound reflections against the enclosure should be smaller. Any influence greater than 1.0 dB in the third-octave-band spectra should be reported and all later measurements should be corrected accordingly to represent the case without enclosure (free-field).

Acoustics performance evaluation result of this trailer is shown in Table 1. The testing speed is 50km/h. Tire-pavement noise was evaluated by sound pressure level under the third octave-band frequency. The result is shown by average A-weight sound level.

Table 1: Performance test results of the trailer for tire-pavement noise measurements

Items	Results	Requirements
Pavement Temperature (℃)	22.0	23±3
Sound reflections against the enclosure dB（A）	0.6	＜1
Ambient noise dB（A）	50.0	＜Background noise sound pressure level
Background noise dB（A）	79.4	Field test
Tire -pavement sound pressure level dB（A）	91.2	Differential value exceeds 10dB, when compared with background noise

Test method for dynamic modulus and phase angle[6]

Simple Performance Tester was used, the test method for dynamic modulus and phase angle followed National Cooperative Highway Research Program (NCHRP) Project 9-19 simple performance tests.

Size of test specimen: cylindrical specimens of 15cm in diameter, 17cm in height by SGC; specimen of 10cm in diameter, 15cm in height made by coring and cutting;

Test parameters: four test temperatures (5℃, 20℃, 40℃ and 55℃); Nine loading frequency (25Hz, 20Hz, 10Hz, 5Hz, 2Hz, 1Hz, 0.5Hz, 0.2Hz and 0.1Hz). The load pattern could be half sinusoid. Each cyclic loading time is 0.1s while with 0.9s unloading time. While testing, the sequence of warming and lower frequency must be followed.

Data processing method: it fits dynamic modulus testing results into master curve with reference temperature of 20℃ on the basis of time-temperature equivalence principle of asphalt mixture. The master curve of dynamic modulus is fitted with Sigamodal function, and the master curve of phase angle is fitted with Gauss curve and adopted the same shift factor as dynamic modulus master curve.

Results and Discussion

Results of tire-pavement noise spectrum

Tire-pavement noise of asphalt-rubber pavement and stone mustic asphalt pavement had been measured for five times on Chang'an avenue, testing time included September 2009,October 2009, December 2009, January 2010, March 2012. At the time, the temperature was 30℃, 20℃, 0℃, 0℃ and 0℃in turn. The two sections of pavement were adjacent and had been built at the same time in August of 2009. The void of pavement was nearly the same, respectively 4.2% and 4.8%, as well as Texture depth on surface were 1.2 and 1.1. The testing speed was 50km/h, and the result is shown by average A-weight sound level under third octave-band frequency.

Table 2: Testing results of tire-pavement noise(CPXT method)

Item / Frequency (Hz)	30℃(2009)		20℃(2009)		0℃(2009)		0℃(2010)		0℃(2011)	
	ARAC-13	SMA-13	ARAC-13	SMA-13	ARAC-13	SMA-13	ARAC-13	SMA-13	ARAC-13	SMA-13
16	46.5	47.7	46.1	48.6	46.5	47.2	49.3	45.2	48.8	46.3
31.5	52.8	52.2	53.5	52.8	53.0	53.6	55.8	50.3	54.3	50.7
63	60.2	54.9	59.1	56.5	60.0	55.7	60.0	55.8	58.1	55.6
125	64.1	58.3	62.7	62.1	60.7	62.1	63.0	60.4	63.0	59.3
250	68.7	68.0	67.8	70.7	69.3	72.0	71.1	70.5	71.3	70.2
500	76.3	78.0	76.1	79.9	78.9	81.3	79.6	78.9	80.9	80.3
800	81.4	80.9	80.5	84.2	82.9	86.1	83.7	82.0	85.0	83.9
1000	84.1	87.4	85.2	88.4	86.7	91.2	87.6	88.1	89.7	88.5
2000	81.0	84.2	83.0	85.4	85.7	86.8	83.9	85.4	86.6	84.7
4000	71.2	72.0	71.5	73.5	74.3	73.7	73.6	76.1	74.1	73.0
5000	67.2	67.7	66.6	68.4	69.7	68.3	69.1	74.7	69.3	67.9
6300	60.0	59.5	59.3	63.8	62.8	63.7	64.8	72.9	64.4	63.0
8000	52.7	53.4	52.0	57.5	56.3	57.5	58.9	69.5	58.1	58.2
10000	48.8	50.9	48.3	53.5	52.2	52.8	55.8	68.1	54.0	54.6
Average sound level(dB)	91.2	94.1	92.4	95.4	94.2	97.3	94.9	98.6	96.5	99.1
Difference(dB)	2.9		3.0		3.1		3.7		2.6	

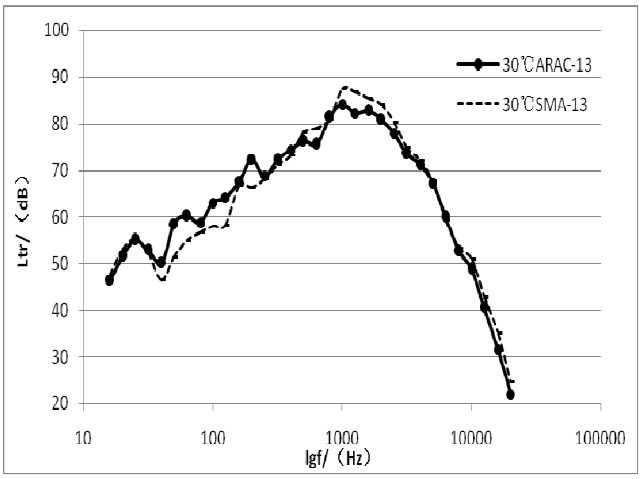

a:Temperature of pavement 30℃

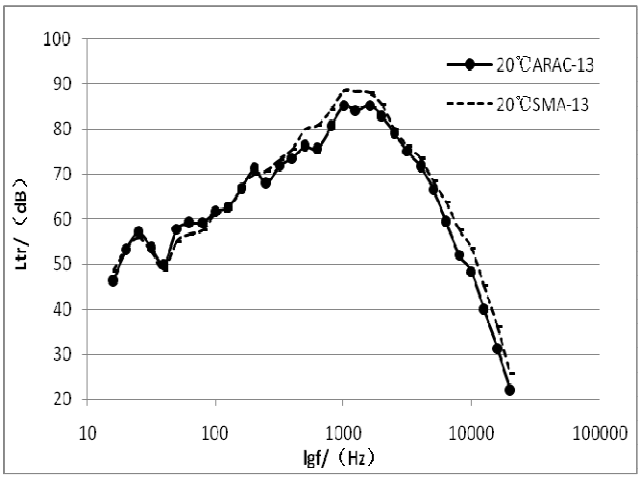

b:Temperature of pavement 20℃

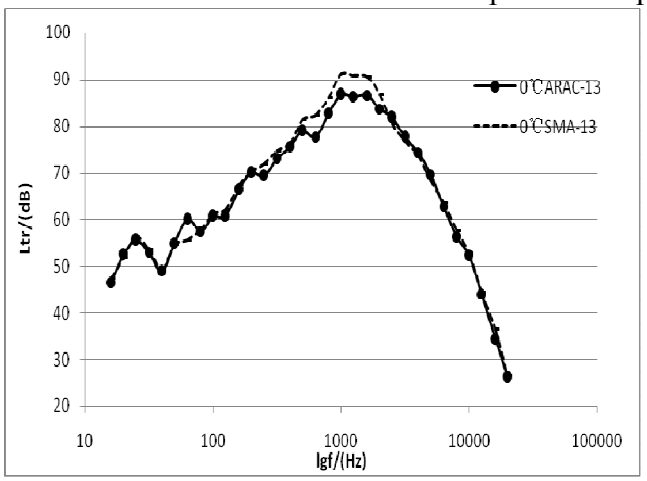

c:Temperature of pavement 0℃

Figure 1: Noise spectrum of two types of pavement under different temperature in 2009

Figure 1 shows the comparison of two types of pavement noise spectrum under different temperatures, namely, 30℃, 20℃ and 0℃. These noise spectrum of asphalt-rubber pavement was compared with that of stone mustic asphalt pavement, the shape was nearly the same, but the sound level is lower while the frequency lay on the range of higher than 800 Hz, and the low limit frequency decreased from 800Hz to 63 Hz when the temperature decreased from 30℃ to 0℃. It shows that asphalt-rubber pavement could reduce tire-pavement noise in a wide range of temperature and frequency, it could reduce about 3dB(A) compared with stone mustic asphalt pavement.

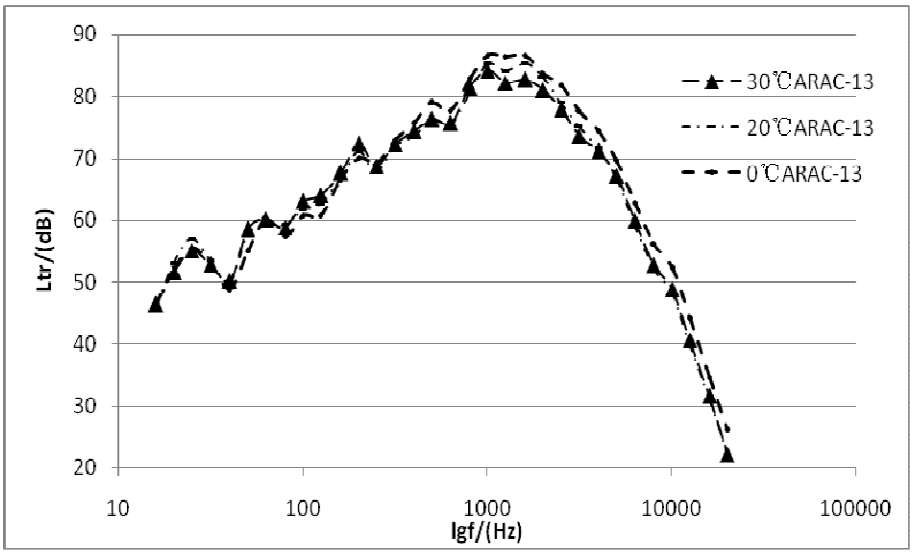

Figure 2: Noise spectrum of asphalt-rubber pavement under different temperature

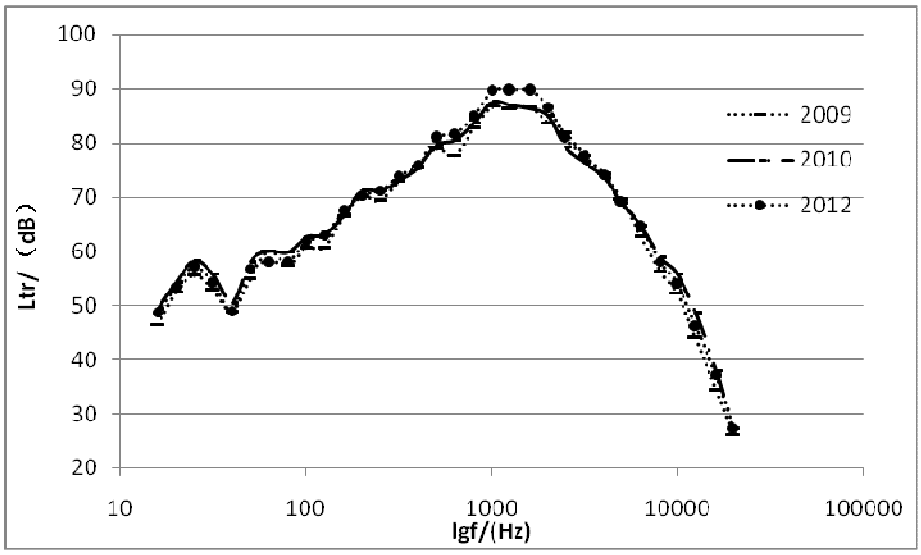

Figure 3: Noise spectrum of asphalt-rubber pavement in different age of pavement (0℃)

Figure 2 and Figure 3 shows regular pattern of noise spectrum of asphalt-rubber pavement changing with the temperature and age of pavement. The tire-pavement noise sound level could increase, especially sharply higher during the frequency 500Hz~2500Hz in the noise spectrum when the temperature is decreased and age of pavement grows.

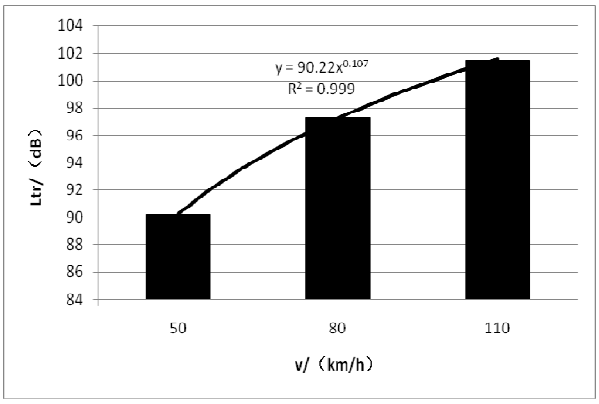

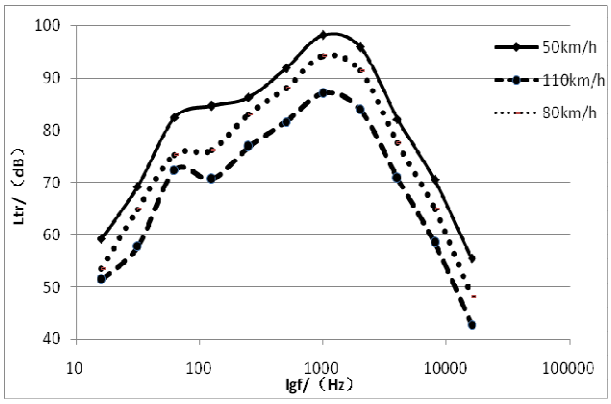

Figure 4: Average A-weight sound level of asphalt-rubber pavement at different testing speed
Figure 5: Noise spectrum of asphalt-rubber pavement at different testing speed

Figure 4 and Figure 5 show the effect of testing speed on tire-pavement noise of asphalt-rubber pavement. Another section of asphalt-rubber pavement in Beijing was chosen because of speed restriction in Chang'an avenue. The testing speeds were as follows:50km/h, 80km/h and 110km/h. Average A-weight sound level was increased in the form of approximate power law function with the increase of testing speed. The shape of noise spectrum shows no change, the sound level was increased during the entire range of testing frequency, and specially higher during the frequency 125Hz~2000Hz in the noise spectrum.

The difference of viscoelasticity between asphalt-rubber concrete and stone mustic asphalt concrete

The materials of asphalt-rubber concrete(ARAC-13) and stone mustic asphalt concrete(SMA-13) were just the same as the pavement of Chang'an avenue paved in 2009. And their air voids of specimens are all 4%. The results are shown as below:

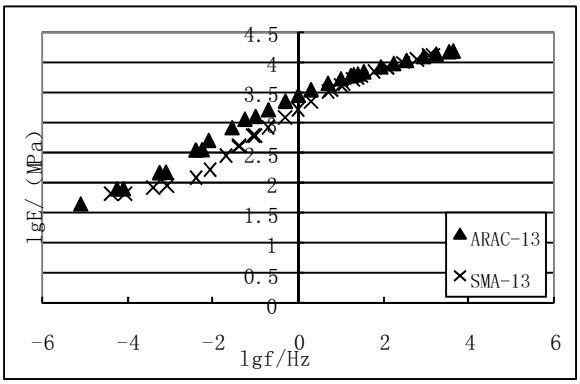

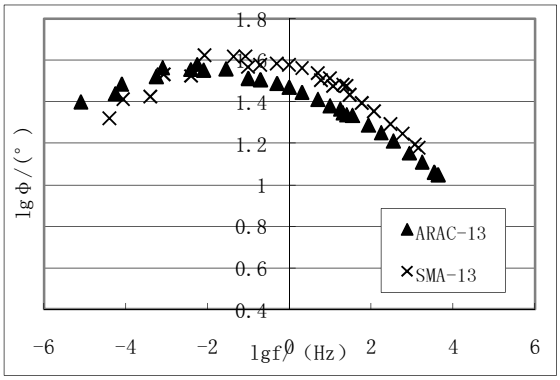

Figure 6: Dynamic modulus master curve of ARAC-13 and SMA-13 asphalt concrete
Figure 7: Phase angle master curve of ARAC-13 and SMA-13 asphalt mixture

As it can be seen from Figure 6 and Figure, ARAC-13 asphalt concrete's dynamic complex modulus was comparatively larger with more excellent elasticity in the most of frequency, and its phase angle is also comparatively smaller in the most of frequency compared with SMA-13 asphalt concrete. In other words, ARAC-13 asphalt concrete has more excellent elasticity than SMA-13 asphalt concrete in a wide range of frequency, which contributes to the reduction of tire-pavement noise greatly at wide vehicle speed as well as temperature change.

Conclusions

1. Asphalt-rubber pavement could reduce tire-pavement noise in a wide range of temperature and frequency and it could reduce about 3dB(A) in average A-weight sound level compared with stone mustic asphalt. Its sound level is lower while the frequency is based on the range higher than 800 Hz, and this low limit frequency decreased from 800Hz to 63 Hz when the temperature decreased from 30℃ to 0℃.

2.The tire-pavement noise sound level could get higher and higher during the frequency of 500Hz~2500Hz in the noise spectrum, while the testing speed increases, or the temperature decreases, or the age of pavement grows.

3.ARAC-13 asphalt concrete has better elasticity than SMA-13 asphalt concrete in a wide range of frequency, which contributes to the reduction of tire-pavement noise greatly at wide vehicle speed as well as temperature change.

4. The peak value concentrates on the range of frequency 500 Hz to 2500 Hz. So for noise spectrum of asphalt-rubber pavement, how to reduce noise sound level which lay on the range, and that is very important for the next step to research noise reduction asphalt-rubber pavement.

Acknowledgments

This material describes parts of research activities requested and sponsored by the Beijing Municipal Science & Technology Commission. Its sponsorship of the research and the contributions of Research Institute of Highway Ministry of Transportation are gratefully acknowledged. The contents of this publication reflect the views of the authors and do not necessarily reflect the official views or policies of Beijing Municipal Government or Research Institute of Highway Ministry of Transportation.

References

[1] WANG Xu-dong, LI Mei-jiang, LU Kai-ji. The Applied Technology of the Crumb Rubber in the Asphalt and Mixture [M]. Beijing: People's Communications Press, March 2008.

[2] Research Institute of Highway Ministry of Transport. Asphalt mixture Design Report of Maintenance Projects Chang'an Avenue in Beijing[R]. Beijing: Research Institute of Highway Ministry of Transport

[3] International Organization of Standardization. "ISO/CD 11819-2.Acoustics—Method for measuring the influence of road surfaces on traffic noise—Part 2: the close-proximity method" [S], ISO, Geneva, Switzerland, December 2000

[4] Paul R. Donavan, Dana M. Lodico. "Measuring Tire-Pavement Noise at the Source" [R]. Washington, D.C: Transportation Research Board, 2009

[5] Robert Otto Rasmussen."Tire/pavement and Environmental Traffic Noise Research Study" [R]. Denver: Colorado Department of Transportation DTD Applied and Innovation Branch, January 2011

[6] MA Xiang, NI Fu-jian, CHEN Rong-sheng. Dynamic Modulus Test of Asphalt Mixture and Prediction Model [J]. China Journal of Highway and Transport.2008.5.21(3) :P35

[7] Qing Lu, Erwin Kohler, John T. Harvey, Aybike Ongel. "Investigation of Noise and Durability Performance Trends for Asphaltic Pavement Surface Types: Three-Year Results" [R]. Davis: University of California Pavement Research Center UC Davis, UC Berkeley, January 2009

[8] Douglas I. Hanson, Robert S. James, Christopher NeSmith. "Tire/pavement Noise Study" [R]. Alabama: Auburn University, August 2004 [8] WANG Xu-dong, PENG Jing-wu, LI Mei-jiang, SHEN Guo-hui, ZHOU Xing-ye, ZHANG Lei. Trailer with Weight for Tre/road Noise Measurements, China: CN201327413 [P]:2010

[9] CHEN Ke-an, ZENG Xiang-yang, YANG You-liang. Acoustic Detecting [M].Beijing: China Machine Press, August 2010

doi:10.4028/www.scientific.net/AEF.5.352

Dynamic Water Effect on the High Temperature Stability of Asphalt Mixture

Hou Minghao[1,a], Tan Yiqiu[1,b], Hu Bin[2,c]

[1]Candidate of PhD, School of Traffic Science and Engineering, Harbin Institute of Technology, No.73 Huanghe Road Nangang District, Harbin, Hei Longjiang, China, 150090,
[1]Professor, School of Traffic Science and Engineering, Harbin Institute of Technology, No.73 Huanghe Road Nangang District, Harbin, Hei Longjiang, China, 150090,
[2]Candidate of PhD, Institute of Road Engineering, South China University of Technology, No.381 Wushan Road Tianhe District, Guangzhou, Guangdong, China, 510640,

[a]email:houminghao@hit.edu.cn [b]email: yiqiutan@163.com [c]email:hbhit@163.com

Keyword: dynamic water, asphalt mixture, high temperture, simulation device

Abstract: This paper introduces dynamic water effect into the test, develops a laboratory test device for simulating the dynamic water effect on asphalt pavement, and puts forward a test method of dynamic water effect working together with load, water and temperature. Based on this method, the high temperature stability of seven kinds of asphalt mixtures with the factors of asphalt grade, gradation and air voids are studied. The research shows that the effect of dynamic water can take adverse effect for the high temperature stability of asphalt mixture. The effect degree is different under different factors. It is the most disadvantaged when the air voids of the mixture is near 10%, the skeleton structure gradation of mixture is better than the suspended structure at the most disadvantage air voids, and the mixture made of high viscosity asphalt is more affected when the temperature is higher.

Introduction

Along with the increasing traffic volume, traveling speed and axle loads, serious premature failures occurred on many asphalt pavements soon after opening to the traffic, such as flooding oil, loose inside, frost boiling, settlement and bottom stripping [1]. The premature failures of asphalt pavements are one of the main problems of pavements' maintenance. Existing researches show that the premature failures are related to the water influence on asphalt pavement, the pressure of the dynamic water caused by high speed driving on the pavements is the main factor for premature failures [2]. In recent years, the research about water effect on asphalt pavement mainly concentrated on the cause and mechanism of water damage [3]. There are many test methods and standards for evaluation water damage of asphalt mixture, and also corresponding technical measures about control of water damage happened [4]. However, water-related damage of asphalt pavement continuously emerging in the practice engineering, that is because currently research for the dynamic water effect on the road performance of asphalt mixture is paid inadequate attention.

Most regions in our country, the high temperature season is also a rainy season, asphalt pavement under the effect of the water and high temperature. Because of the dynamic load of traffic and temperature expansion and contraction repeated affect, the water which enter the asphalt pavement voids continuously generate hydrodynamic pressure or the vacuum cycle, water gradually infiltrated into the interface of asphalt and aggregate, then the asphalt will be emulsified, the

strength of asphalt mixture will be declined [5]. Because of the dynamic water, asphalt membrane gradually stripped from the aggregate surface, the aggregate loss of bond strength between the asphalt mixtures arising out beads and loose, and then asphalt pavement appears pit and pushing deformation damage [6]. That is seriously reducing the use of pavement performance, endangering the traffic safety, shortening the life of asphalt pavement, and causing enormous economic losses. Therefore, the study of dynamic water effect of asphalt mixture high temperature stability is very necessary.

Mixture specimens preparation

This study uses three types gradation which are SMA-16, AC-16 and SAC-16. In order to research on the different asphalt grade, different gradation and different air voids of asphalt mixture, this paper select 90 #, 110 #, 130 # three type asphalt, three kinds of gradations which are AC-16, SAC-16 and SMA-16 and three kinds of air voids that are 6 %, 10%, 14% to prepare seven kinds of asphalt mixtures, their specific composition are shown in Table 1. Existing research shows that when the air voids of mixture is between 8% ~ 12%, the mixture will be more impacted by water. Engineering site investigation also found that the air voids of the roads which appear water damage are mostly in this context. Therefore, 10% air voids is selected as the main air voids of the asphalt mixture in this paper. The Mixture specimens sizes used in the study are 100mm × 63.5mm, the specimens are rotary compaction molding. The molding method can accurately control the shape of the specimen height, and thus better control the specimen's air voids.

Table 1. Basic composition of the asphalt mixtures

Mixture type	Asphalt grade	Gradation	Air voids (%)
A	90#	AC-16 median	10
B	110#	AC-16 median	10
C	130#	AC-16 median	10
D	110#	SAC-16 median	10
E	110#	SMC-16 median	10
F	110#	AC-16 median	6
G	110#	AC-16 median	14

Dynamic water effect test simulation

Dynamic water effect test device development The study designs a laboratory teat device simulating the dynamic water effect on asphalt mixture, the schematic diagram and actual picture of the device are shown in Fig. 1.

The main body of the device is scouring barrel, its wall thickness is 10mm. It is made of transparent plexiglass material, the mixture specimen can be put in it, there is support drums and clasp which will make the specimen at the fixed location. To ensure that device can withstand the test required pressure, the lateral wall of the barrel body is hooped with sheet iron, the cover and barrel are reinforced with steel plate and screw clamp. One said wall of the Barrel has two water districts separated by specimen which connected with a catheter; the other side has two valves, the lower valve is used for water injection and water drainage, the upper valve connect the external hydraulic pressure gage, which can measure the Real-time water pressure conveniently. In order to ensure the device is sealed, the contact area of the piston rod with the barrelhead and the barrelhead with barrel body are treated with the sealing tape and sealing ring. In addition the lateral edge of the mixture specimen in the scour barrel should be wrapped with thin rubber parcels, to strengthen its sealing relationship with the inner wall of device. Do the best to minimize the water stream from the gap over which causes the erosion effect weakening. During the test, the upper rod and lower base fixed at the upper and lower pressure head of MTS testing machine. Lubricating oil is put on the piston rod to ensure it well contacting with the barrelhead.

In the test, the MTS pressure head moves downward, water in the A district is pressed down into the air voids of specimen, some water through the specimen connectivity void into the B district, that process is simulating the water of the road surface is pressed into the road voids under the wheel load pressure. Similarly, when the MTS pressure head moves up rapidly, the water in the B district will make the opposite path enter into the A district, this situation is simulating the void water pumping effect when the wheels leave the road. MTS pressure head moves up and down repeatedly, so that the water in the device is repeatedly washing the specimen, which simulates the water at the wheel loads on the asphalt pavement washed repeatedly the air voids. The piston does not contact the specimen during the test.

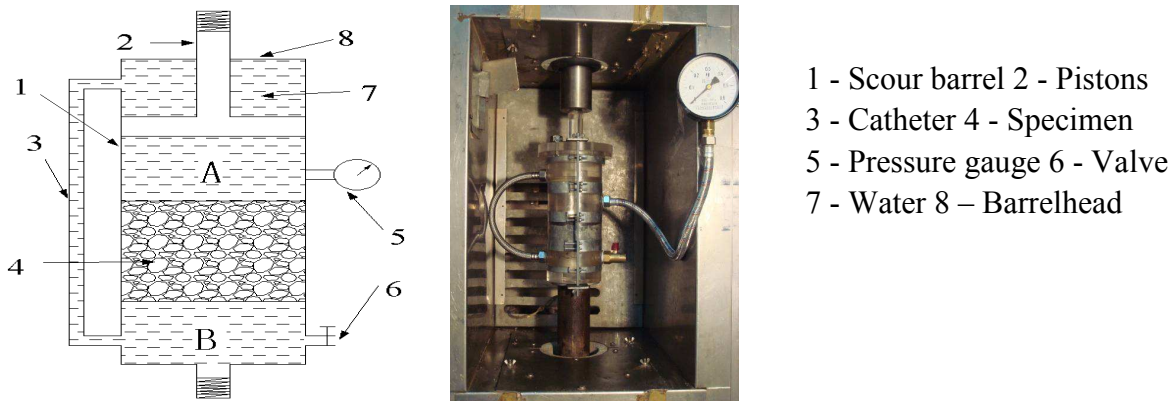

Fig. 1. The dynamic water test device

Dynamic water effect test conditions: For accurate simulation of dynamic water scouring effect on the mixture specimens, and quantitative analysis for it, the test conditions should be determined firstly. Selection of experimental conditions is considered with the simulation of the actual situation, and also with the difficult degree for the test implementation. According to the original selection of test condition scope for the scouring frequency, scouring pressure, scouring time and scouring temperature, the 15 ℃ splitting intensity ratio of the specimens are measured which are affected by the dynamic water test under different conditions, the test conditions are determined. The test temperature is 45℃, the scouring pressure is 0.4Mpa and the scouring time is 15 minutes. Based on that condition, the dynamic water test is conducted with the seven kinds of asphalt mixtures.

Influence of dynamic water on high temperature stability

Table 2. Creep rate change for mixtures before and after dynamic water effect

Mixture type	Creep rate (10^{-6}/s/Mpa)		Change rate (%)
	Before dynamic water effect	After dynamic water effect	
A	253.7	646.4	154.8
B	289.1	670.9	132.1
C	2062.0	3447.6	67.2
D	692.8	1178.3	70.1
E	561.3	878.8	56.6
F	289.1	670.9	132.1
G	2037.5	2160.2	6.0

Connected with reality, this study uses splitting creep test to evaluate the high temperature stability of asphalt mixture. Creep rate is selected as evaluation index in order to see the high-temperature resistance to deformation capacity of mixture more directly. The test temperature

is 45℃, load splitting tensile stress is 0.025Mpa. The test is separately carried on the specimens before and after the dynamic water effect of the seven kinds of asphalt mixtures. The test results are shown in Table 2.

Asphalt grade The physical properties of asphalt have impacted on the resistance to rutting performance of mixture. At a certain temperature and loading rate, the greater the viscosity of asphalt is, the greater the viscous resistance is, the stronger the anti-shear deformation ability is, and the resistance to rutting performance of asphalt mixture is better. Asphalt viscosity changes with temperature, the lower the temperature sensitivity is, then the formation of the corresponding asphalt mixtures have better high temperature stability, this relationship has been confirmed by the rapid loading test. Asphalt Binder provided the cohesive force is closely related to the nature performance of asphalt mixture, the asphalt content and the interaction between the asphalt and aggregate. The cohesive force of asphalt mixture is relevant to the cohesive force of asphalt at high temperature conditions.

To study the degree of the high temperature stability of mixtures with different asphalt grades under dynamic water effect, A, B and C are selected in this test, the experimental results are shown in Fig. 2-Fig.4. The real line in the diagram is representation for the creep curve of the specimens before dynamic water effect, and the broken line is representation for the creep curve of the specimens after dynamic water effect.

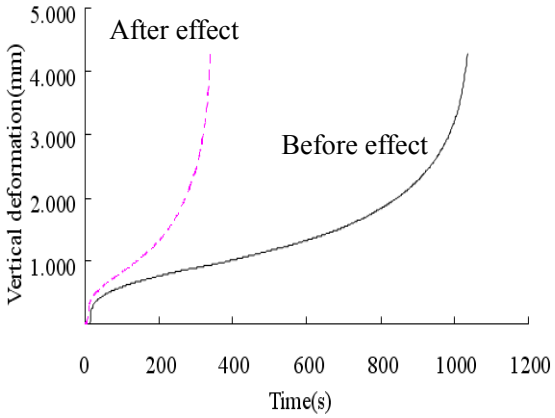

Fig. 2. Creep curve of A mixture

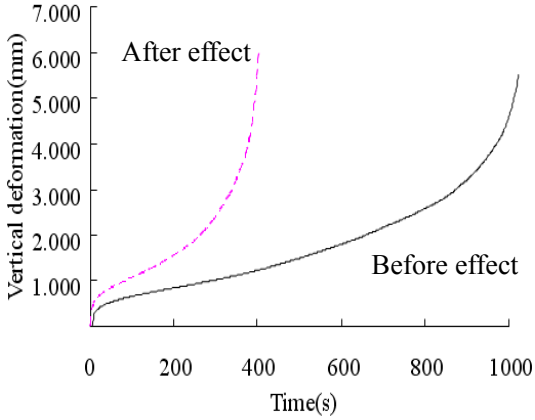

Fig.3. Creep curve of B mixture

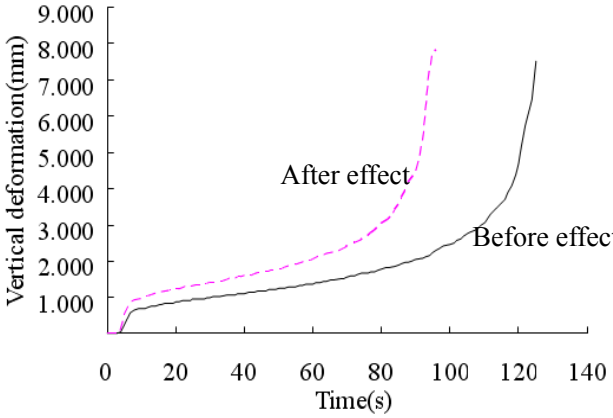

Fig. 4. Creep curve of C mixture

It can be seen that after the effect of dynamic water, the high temperature stability of asphalt mixtures with different grades have been reduced. The change rate of A is the most which the asphalt viscosity is high, and the change rate of B is the smallest which the asphalt viscosity is small. The order of arrangement according to the degree of reduction is A> B> C. This is because asphalt

of high viscosity contributes to the high temperature stability relatively more than the small viscosity, and when the asphalt adhesive is damage, its ability to resist deformation becomes weaker.

Gradation It is said on abroad research that 60% of the high temperature stability of asphalt depends on the skeleton effect of the aggregate gradation; asphalt binder can only have 40% contribution. In this part, B, D and E asphalt mixtures are selected to test which have different gradations, the same asphalt grade and same air voids. The experimental results are shown in Fig.5–Fig.7. The real line in the diagram is representation for the creep curve of the specimens before dynamic water effect, and the broken line is representation for the creep curve of the specimens after dynamic water effect.

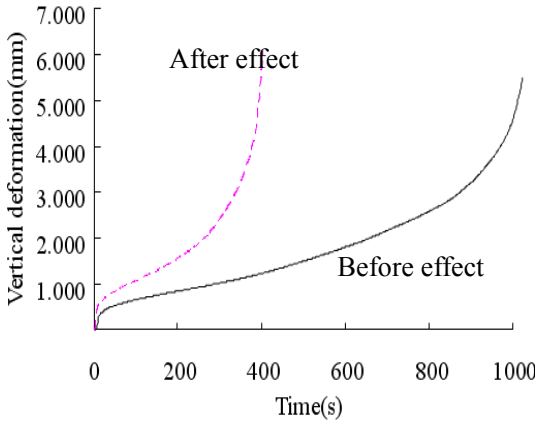

Fig. 5. Creep curve of B mixture

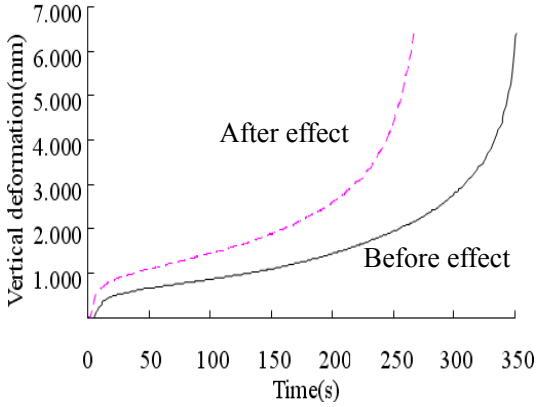

Fig. 6. Creep curve of D mixture

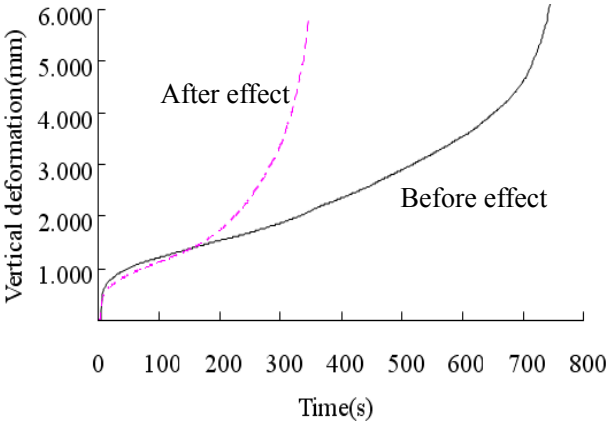

Fig. 7. Creep curve of E mixture

By the test results, the high temperature stability of asphalt mixture with different gradations which effected by dynamic water are all discount more or less. At the same 10% air voids, the high temperature stability of the dense structure of the AC-16 gradation mixture had reduced most; the skeleton structure of SMA mixture was affected by water relatively small. The order of arrangement of the three gradation according to dynamic water effect degree is AC-16> SAC-16> SMA-16. This is because after the adhesive effect attenuation between the asphalt and aggregate, the embedded squeeze support among aggregates plays a major role on high temperature deformation resistance of mixture, which is the SMA advantage.

Conclusion

This paper introduces the effect of dynamic water into the test, develops a laboratory test machine for simulating asphalt pavement effected by dynamic water, and puts forward a test method of dynamic water effect working together with load, water and temperature. Based on this method, the specimens should be pretreatment with the dynamic water effect, and then tests the changes for the high temperature stability of asphalt mixture. This paper focused on the effect of asphalt grade and gradation type on the high temperature stability of seven kinds of asphalt mixture. The results show that the effect of dynamic water can take adverse effect for the high temperature stability of asphalt mixture. The effect degree is different under different factors. Based on the reason for the mixture resisted the dynamic water effect, it is the most unfavorable that the void ratio of the mixture is near 10%, the asphalt mixture gradation of the skeleton structure is better than the suspended structure, the mixture made of the strong viscosity asphalt is more effected by water when the temperature is higher.

REFERENCES

[1] Sha Qing-lin. "*Premature Damage and Its Preservative Measures of Bituminous Pavement on Expressway*." China Communications Press,2011, 23-25.

[2] Plancher, Hetal. "Moisture-Induced Damage in Bituminous Pavement." International Symposium on Prograssi Nella Technologia Dei Bitumi, San Donato Milanese, Italy,1982.

[3] Theresa M Williams. "Use of environmental SEM to study asphalt-water interactions." *Journal of Materials in Civil Engineering*, 1998,10(2), 121-124.

[4] Saleh Al.Swailmi, Ronald L.Terrel. "Evaluation of Water Damage of Asphalt Concrete Mixtures Using the Environmental Conditioning System." *Association of Asphalt Paving Technologists,1998.*

[5] Zhao Jia-jun, Huang Zhi-fu. "Disease Dispose of Highway Asphalt Pavement." *East China Highway*, 2000,125, 34-36.

[6] Kennedy, T.W., Roberts, F.L., and Lee, K.W.. "Evaluation of Moisture Effects on Asphalt Concrete Mixtures." Presented at the meeting of the Transportation Research Board,1983.

doi:10.4028/www.scientific.net/AEF.5.358

Study of Road Performance between Rub-concrete and Normal Concrete Materials

Long Wang[1,a], Xiaoguang Xie[2,b], Lulu Fan[3,c]

[1] School of Transportation Science and Engineering, Harbin Institute of Technology, Harbin, China, 150090

[2] School of Transportation Science and Engineering, Harbin Institute of Technology, Harbin, China, 150090

[3] School of Transportation Science and Engineering, Harbin Institute of Technology, Harbin, China, 150090

[a]hitlongwang@sina.com, [b]xxg75@126.com, [c]fanlulu@163.com

Keyword: rubber cement concrete; flexural modulus; damping performance; fatigue performance ; surface properties ; performance prediction

Abstract. To improve the cement concrete deformation, small toughness traditional defects, with Adding the rubber grain in the concrete to form the rubber particles concrete; flexural modulus of Rubber particles of concrete and ordinary concrete was comparative studied, two kinds of concrete damping change was analyzed by using the finite element, through three point concrete trabecular bending test, the fatigue properties were comparative researched , the rutting test methods were used in proving the rubber particles of concrete of erosion performance; According to the test made the mechanical parameters of acquired in experiments , the applying the MEPDG 2002 design method, the road surface damage state were forecasted of the two kinds of concrete pavement in the design of the end; Experiment shows that rubber particles cement concrete flexural modulus is reduced by 12% than that of ordinary cement concrete, the damping ratio increased by 30%, the fatigue life have greatly improved, and surface erosion phenomenon did not happen; Theoretical analysis shows that, the rubber cement concrete panel breakage is lower 30% than ordinary concrete, Therefore, the rubber particles concrete pavement can overcome the traditional l defects of cement road and with has excellent road performance.

Introduction

At present, rubber particles cement concrete has achieved initial success in the application of industrial and civil architecture, such as the use of shock absorption and sound insulation function in seismic foundation, the railway sleepers and sound barriers has wide application, but it is still in the research stage in the cement concrete pavement, the researches show that the good deformation property of scrap tire rubber particle in the cement concrete has the following significance: from engineering application view, rubber particles mixed in cement concrete materials to help improve the brittleness shortcomings, promote its absorbing heat insulation, sound absorption damping performance, impact resistance and crack resistance[1].From the economic point, strongly built rubber particles of cement concrete pavement, to break the high cost of asphalt pavement monopoly situation, can promote the development of local economy[2].From the section of environmental protection, rubber particles of cement concrete to be able to deal with a large number of promotion waste tyre. Promote scrap tire the effective utilization of resources, stop to the occupation of the land by waste tires and has important significance good environmental protection prospects

[3].Rubber particle cement concrete road performance directly related to the development of it's prospects, so this paper for rubber particles concrete bending pull performance, driving damping performance, anti-fatigue properties and surface function system research, for rubber particles in the cement concrete pavement concrete application provides scientific guidance.

The Rubber Particles Cement Concrete Mixture Design

According to the results, with 10% rubber particles instead same volume sand on cement concrete mixture design[4], rubber particles concrete with cement: water: stone 1-3cm: stone 1-2cm: sand: rubber: water reducing agent = 360:120, 675, 675:376:15.5:5.5. Due to the rubber particles do not occur hydration reaction, the part replace some sand is equivalent to reduce fine aggregate, therefore, rubber particles cement concrete proportion design need reduced some water consumption compared to normal cement concrete, to meet the requirements of the mixing content workability[5].

Road Performance Comparison of Rubber Particles and Ordinary Cement Concrete Materials

The properties contrast with including the flexural strength, flexural modulus, shock absorption effect, fatigue properties and surface function five aspects.

The Flexural Strength. Highway cement concrete mixing materials requirements heavy traffic conditions 28 days folding strength not less than 5 MPa, two kind of mixture cement concrete curing to provisions of the cement flexural strength such as shown in table 1. Due to the 100 x 100 x 400 mm specimens, the flexural strength conversion coefficient is 0.85.

Table 1 Flexural strength contrast between rubber particles concrete with normal concrete

samples	number	failure load [kN]	flexural strength [MPa]	average flexural strength [MPa]
normal concrete	1	22.8	5.81	5.64
	2	22.4	5.71	
	3	21.2	5.41	
rub-concrete	1	22.6	5.76	5.49
	2	21.3	5.43	
	3	20.8	5.30	

By bending test results indicate that two kind of mixture bending strength are satisfy the standard requirement (more than 5 MPa). Rubber particles cement concrete flexural strength slightly lower than normal cement concrete, reduce the rate of 3% or so, compressive strength decline slightly big, about fell 6% or so[5]; Overall, both strength gap is not big.

Flexural Modulus. The concrete flexural elastic modulus in accordance with *Highway Engineering Cement and Concrete Test Regulations* (JTG T0559-2005), the use of a 100 mm x 100 mm x 400 mm specimens. 5 times cycle load test, take the fifth cycle of deflection value. The contrast flexural modulus of normal cement concrete and rubber particles cement concrete such as shown in table 2.

Table 2 The contrast flexural modulus of normal cement concrete and rub-concrete

samples	F_0[kN]	$F_{0.5}$[kN]	Δ [mm]	flexural modulus [GPa]	average flexural modulus [GPa]
normal concrete	3	11	0.0112	41.1	42.1
			0.0109	42.2	
			0.0107	43.0	
rub-concrete	3	10	0.0113	35.6	37.1
			0.0105	38.3	
			0.0108	37.3	

Rubber particles cement concrete flexural modulus is low 5 GPa than ordinary cement concrete reduced the rate is 12%, it shows the flexible performance increase[7], through calculation, it is known that the modulus reduce 5 GPa equivalent to total stress reducing 0.58 MPa unit deformation ,rubber particles to join, can improve the resistance of the cement concrete cracking.

Fatigue Performance. The three point bending trabecular fatigue test is adopted in the material fatigue test machine MTS. Load test using sine wave, the loading frequency is 10 Hz[11], equivalent to vehicles of the speed for 60 km/h. In order to speed up fatigue test, no gap between adjacent waveform.

At the beginning of test, 0.3kN stress is loaded on the specimen, in order to eliminate the error caused by bad contacts; under the premise of keeping stress in the same ratio (0.4, 0.6 and 0.8, three kinds of stress ratio) and the same stress level (5.28 MPa, 3.96 MPa and 2.64 MPa), fatigue performance of normal concrete and rubber cement concrete is contrasted, the test data such as shown in table 3 and Fig. 1.

Table 3 Normal and rubber cement concrete fatigue properties contrast

specimens name	stress ratio	stress level [MPa]	load recycle number[N]	logN
normal-concrete	0.8	5.28	88	1.94
	0.6	3.96	774	2.89
	0.4	2.64	2732	3.44
rub-concrete (same stress ratio)	0.8	5.04	7843	3.89
	0.6	3.78	8764	3.94
	0.4	2.52	11356	4.06
rub-concrete (same stress level)	0.83	5.28	304	2.48
	0.62	3.96	4060	3.61
	0.41	2.64	7893	3.90

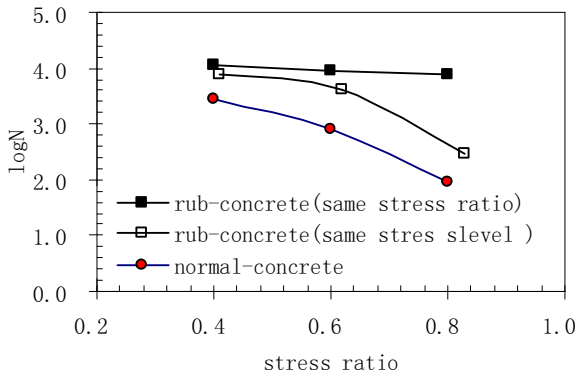

Fig. 1 Normal and rub-concrete fatigue properties contrast

Fig. 1 indicate that in the same stress than conditions, rub-concrete fatigue life is greater than normal cement concrete, with the improvement of the stress ratio, rub-concrete fatigue life is greater than that of normal concrete increased; In the same stress level, the two kinds of concrete are similar to the fatigue of the curve, the range of rub-concrete fatigue life increased basically the same under different stress level conditions. Whether using the same stress ratio and the same stress level to test, rub-concrete fatigue performance is better than normal cement concrete.

Rubber Concrete and Normal Concrete Pavement Performance Prediction and Contrast

Use the AASHTO MEPDG2002 road design guidelines; comparing using performance of two kinds of cement concrete pavement in the design age, analyzed the damage and flatness changes.

Pavement Structure. The maximum temperature gradient of experimental road 88℃/m, accumulative total axle load times is 500 x 10^4 times, belong to heavy traffic, cement concrete materials requirement flexural strength are greater than 5 MPa, pavement structure as shown in table 4. AASHTO climate model based on the database of the climate around the United States, due to the climate of Jilin province similar to the Minnesota, therefore, the climate model Minnesota adapted [12].

Table 4 The structure experimental road pavement

layer number	thickness[m]	layer name	modulus of resilience[MPa]	checking total stress[MPa]
1	0.30	normal concrete	42100	4.90
	0.28	rub-concrete	37100	4.87
2	0.18	cement stabilized macadam	1800	-
3	0.30	lime and cement stabilized soil	1200	-
4	0	soil base	40	-

Forecast Analysis Results. The change of flatness, damage of two kind of cement concrete pavement can be getting through calculation and analysis in service period; Two kinds of concrete pavement cracking rate are draw on the service years, as shown in Fig. 2.

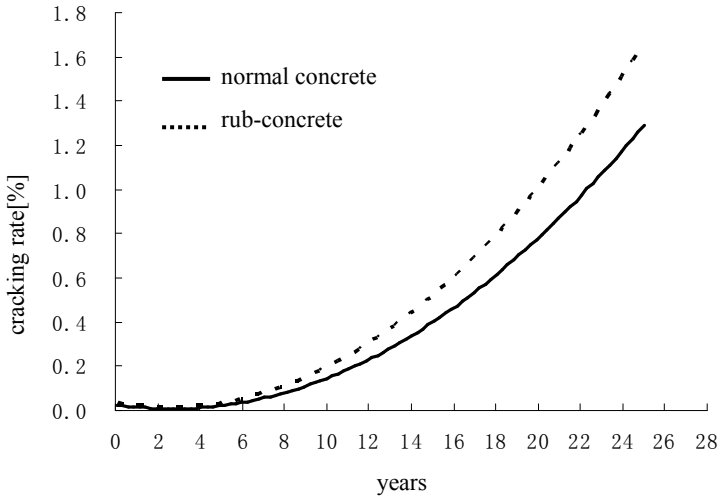

Fig. 2 Contrast of slab broken rate of two kinds of concrete pavement in different using years

From the results analysis, it is known that the IRI, cracking rate, faulting, cumulative damage of the rub-concrete pavement were less than normal concrete pavement in the end of service period. But the IRI and faulting does not significant difference. Through the Fig. 2 can see, rub-concrete pavement faulting in the process of using is far smaller than normal concrete pavement, and rub-concrete pavement Bottom-up and Top-down accumulative total crack damage also is smaller than normal concrete pavement, rub-cement concrete slab cracking rate is lower 30% than ordinary concrete slab. Therefore, in the using process, rub-concrete pavement has good flatness, and under the action of the load and climate, rub-concrete pavement disease such as cracking and slab broken are far lower than normal concrete pavement.

Conclusion

Trough the road performance comparison of normal cement concrete and rub-cement concrete, the following conclusions can be drawn:

(1) Compared to normal concrete cement concrete matrix, rub-concrete flexural strength fell by 3%, compressive strength fell by 6%, the flexural modulus lower by 12%, but the flexural strength to meet the requirements of the design specification heavy traffic.

(2) Fatigue resistance performance of rub-concrete is superior to that of normal concrete.

(3) Rub-concrete pavement broken rate, the cumulative damage are much lower than normal concrete pavement at the end of service year, and rub-concrete pavement IRI and faulting , are slightly better than normal concrete. Therefore, the rub-concrete pavement has good performance.

Reference

[1] M.G.Gregory. Analysis And Testing of Waste Tire Fiber Modified Concrete, Louisiana State University, may 2005:3~5.

[2] Han Cun Yu.Economics Comparison of Highway Cement Road Surface and Asphalt Pavement[J].Heilongjiang Transportation Science and Technology.2007,7:6-7.

[3] Li Rui, Wang Ling. The Research Progress of Portland Cement Concrete Containing Crumb Rubber [J].Concrete, 2006, 4:91-95.

[4] Hou Jie, Gao Pei Wei.Development Prospects of Highway Cement Concrete Pavement [J].Jiang Su Building Materials, 2006, 4:22-24.
[5] Liu Dong Liang,Wang Long, Fan Lu uninfluenced for Rub-concrete Road Performance of Waste Rubber Particles Processing Interface[J].HIGHWAY 2008,10:116-119.
[6] S.Pitil, C.Chalermphol. Concrete Pedestrian Block Containing Crumb Rubber from Recycled Tires.Thammasat Int.J.Sc.Tech., Vol.10, No.2, April-june 2005.
[7] Kang Jing Fu, Ren Hai Bo, hang Pin Zu.Cracing Resistance and Property of Rubberized Concrete [J].Journal of Composite Materials, 2006, 6:158-162.
[8] Sezan Qrak. Investigation of Vibration Damping on Polymer Concrete with Polyester Resin. Cement and concrete research, 2000, 30:171~174.
[9] Bai Wen Feng, Zhang Jian Hua,Wang Xin Li. Study on the Damping Ratio of Glass Fiber Reinforced Polymer Concrete [J]. Design and Research 2007, 10:71-74.
[10] Zhu Han. Adding Crumb Rubber into Exterior Wall Materials [J].Waste Management and Research.2003, 2:20-24.
[11] Ji Tian Jian,Wang Hui,Chen Rong Shen.Fatigue Characteristic of Recycling Cement Concrete[J].Journal of Traffic and Transportation Engineering.2002,2:16-18.
[12] AASHTO Guide for Design of New and Rehabilitated Pavement Structures [R].2002.

doi:10.4028/www.scientific.net/AEF.5.364

The Flexural Strength and Frost Resistance of Air Entrained Concrete

Xiuhua Zheng*[1,a], Qinfei Li[2,b], Jie Yuan[3,c], Yong Ge[4,d]

[1~4]School of Transportation Science and Engineering, Harbin Institute of Technology, P.R. China

[a]zhengxiuhua651@163.com, [b]hit_lee@163.com, [c]hityuanj@163.com, [d]hitbm@163.com

*Corresponding author. Tel/Fax: +86-451-86282191.
E-mail address: zhengxiuhua651@163.com (Xiuhua Zheng)

Key words: Flexural Strength, Frost Resistance, Freeze-thaw, Air Void Structure

Abstract. The flexural strength and frost resistance properties of air entrained concrete were tested in this study. Although the flexural strength of concrete does not change largely with increasing of air content, it still has a maximum value with air content of 4%. The test results show that the frost resistance increases with increasing of air content which makes the space parameter decreasing in the harden concrete. In air entrained concrete, the total air content is not the only factor that affect the final properties of the concrete, the air void structure parameters, including void size, shape, and distribution, are key factors as well. It was found that the air void structure and the frost resistance properties were influenced by the vibration time largely. The optimized vibration time is 30s.

Introduction

Since the air entrainment has been discovered in 1930s [1, 2], it has been regarded as an essential part for the freeze-thaw durability of concrete. Entrained air not just improves freeze-thaw durability, but also improves the workability of concrete, reduces segregation and bleeding in freshly mixed and placed concrete, and increases pump-ability of fresh concrete [3-5]. Therefore, it leads to the reduction of water to cement ratio, which results in more impermeable concrete and a better overall resistance to aggressive agents.

The common chemical used is vinsol resin based materials [6]. In recent years, some other air entraining admixtures, such as protein additives [7], used engine oil [8], were introduced as well.

Although the air entrained concrete has been widely accepted in hydraulic or port constructions, it was not applied on the roads and bridges in China until recent years. Especially in the cold area, the frost resistance property is quite important to the durability of the concrete. Since air entraining agents can improve the freeze-thaw properties largely [9], it was considered being used in roads and bridges in recent years.

Air entrainment has not come into practice widely even today due to concrete producers difficulties with air content in concrete, and the factors affecting air entrainment, such as, temperature, cement chemistry, and supplementary cementing materials, all quite important to the final properties of the concrete. A fundamental shortcoming of air entrainment today is that only total air content is typically specified. In fact, the air-void size and distribution are also quite important to the final properties of concrete, and they were affected by those factors mentioned above. In this study, the air void structure factors were discussed in detail.

Experimentals

The air entraining agents used in this study were DH-9 and SJ-2 (trademark), and their main chemical components were resin soap and triterpenoid saponin [4], respectively. Table 1 gives the mixture proportion of the concrete. Freeze-thaw test use the fast freeze-thaw test method.

Table1. Mixture proportion of concrete

No.	Fly Ash (%)	W/B	Water (kg/m^3)	Cement (kg/m^3)	Fly Ash (kg/m^3)	Sand (kg/m^3)	Aggregate (kg/m^3)	UNF-5 (%)	SJ-2 (0.01%)	Slump (mm)	Air content (%)
C40-I	15	0.44	188	363	83	627	1155	*	*	*	*
C40-II	15	0.44	171	331	76	644	1184	*	*	*	*
C45-I	15	0.42	150	303	70	634	1263	*	*	*	*
C60-I	15	0.31	157	432	99	614	1141	*	*	*	*

Note: The symbol, *, demonstrates that the content of SJ-2 or DH-9 is changing along with the requirements of design, and that the content of water-reducing agent is determined when the slump of fresh concrete reaches at 90mm~110mm. In addition, air content respectively arrives at 1%~8% with using the SJ-2, and I and II represent respectively Grade I and Grade II Fly Ash.

Results and Discussion

Flexural Strength. The flexural strength of C40 concrete as a function of air content, with 15% of grade I and grade II fly ash, is shown in Fig.1, as can be seen in this figure, the flexural strength does not change largely with increasing of air content when it is lower than about 7%. Although the change is not very obvious, it still can be found that the flexural strength reaches the highest value when the air content is about 3% - 4%.

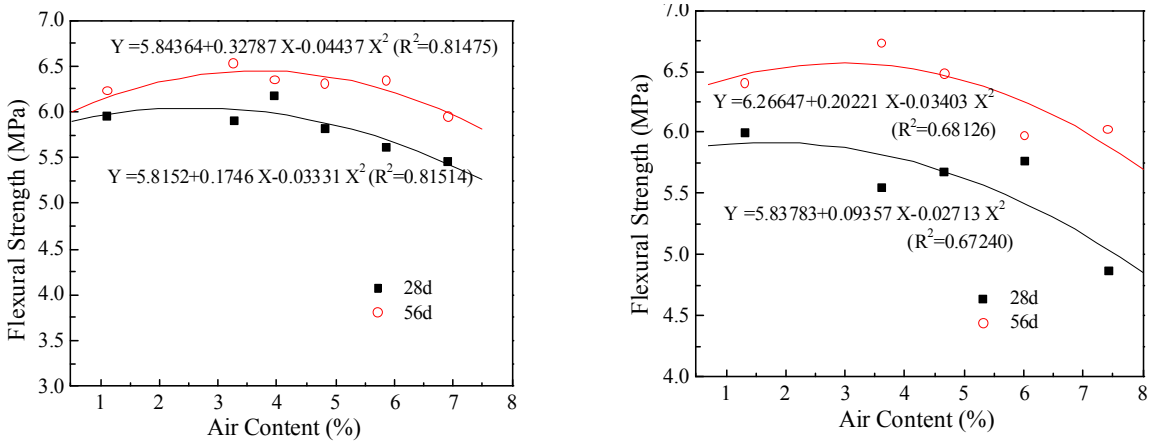

a) 15% of grade I fly ash b) 15% of grade II fly ash

Fig.1 Flexural strength of C40 concrete as a function of air content

This phenomenon is resulted from the air voids distribution in the fresh concrete. In general, the mechanical properties of the porous materials can be predicted by the following equation [10]:

$$\sigma = \sigma_0 \exp(-\alpha\theta) \quad (1)$$

As expressed in this equation, the mechanical properties of the porous materials should be decreased with increasing of air content. However, this is not observed in air entrained concrete when the air content is lower than about 7%. In the air entrained concrete, a small quantity of air bubbles will lead to more homogeneous distribution of aggregates and decrease bleeding and segregation in concrete, and some air bubbles occupied water position in the interfaces, which results in the increasing of the flexural strength. On the other hand, under the condition of the flexural load, cracking in interior concrete is gradual growth process. When growth of cracking is coming across an air void, its energy will be weakened slightly. Therefore, air entraining process makes the specific surface increasing greatly, which increases the susceptibility to resist cracking. However, the compressive strength plays an important role in flexural strength; the more air content, the more compressive strength is declining, so that the flexural strength takes on a downward tendency.

Frost Resistance. The freezing and thawing cycles as a function of relative dynamic elastic modulus with different air content of C45 and C60 concrete are shown in Fig. 2. As demonstrated in this figure, the C45 concrete specimen without air entrainment fractured at the 100 freeze-thaw cycles, relative dynamic elastic modulus was 90%. But in the test, the C45 concrete specimen fracture at 100 freeze-thaw cycles, and the C60 concrete specimen did not fracture until 300 freeze-thaw cycles. After the air was entrained into the concrete, the freeze-thaw property improved largely. The C45 concrete with air entrainment did not fracture after 300 freeze-thaw cycles. The C60 concrete with air content of 4.1% did not fracture until cycled 1,000 times. For the specimen with air content of 6.5%, the relative dynamic elastic modulus was 96% after 1,086 freeze-thaw cycles.

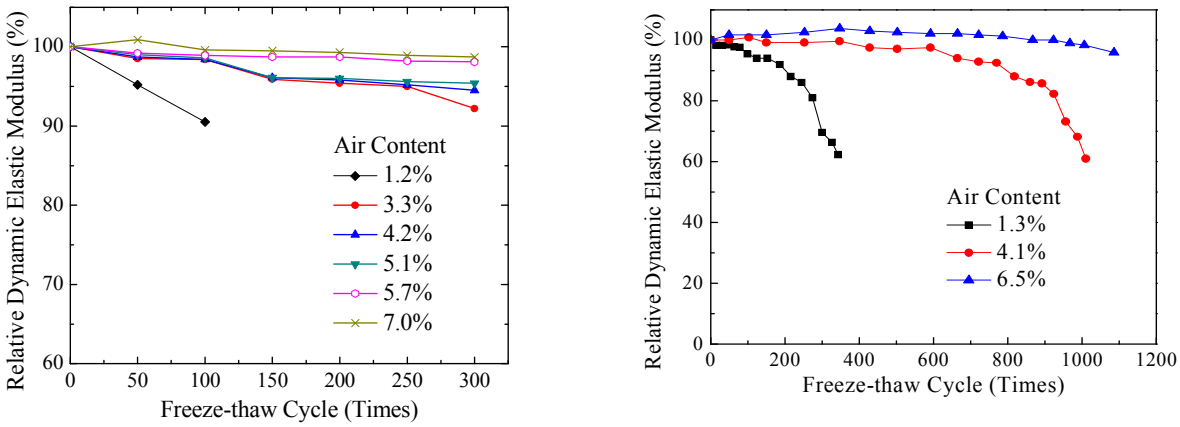

a) C45 concrete b) C60 concrete

Fig.2. Relative dynamic elastic modulus as a function of freeze - thaw cycle times

Table 2 lists the durability parameters of C45 concrete. As shown in this table, although the compressive strength decreases with increasing of air content, the frost resistance property improved largely. Generally, the durability parameters increase with increasing of air content, and decreasing of bubble space parameter. The bubble space parameter (spacing factor) decreased from 0.279mm to 0.197mm with the air content increase from 3.58% to 6.74%, and the durability factor increased from 92.2% to 98.7%. The durability factor can obtain values over 90% since the air content is higher than 3.3%. While the air content is considerable, the concrete has the ability to sustain somewhat the expansion bringing by freezing water in the concrete.

Table2. Durability parameters of C45 concrete

air content(%)	1.2	3.3	4.2	5.1	5.7	7.0
air content after cured(%)	1.74	3.58	4.12	4.74	5.4	6.74
air bubble space parameter (mm)	0.567	0.279	0.253	0.234	0.199	0.197
durability parameter(%)	30.2	92.2	95.2	96.6	98.1	99.8
28d compressive strength (MPa)	48.8	44.1	42.7	40.4	38.1	36.5

Vibration Time. In the air entrained concrete, the air void structure is another important factor that affects the final properties of the concrete. The pore structure parameters are pore size, shape, and distribution. The final properties of the air entrained concrete were different even with same air content but different air void structures. In porous materials, the pore structure can be affected by the temperature, humidity, chemical compositions or some other factors. In this study, different vibration time was used to change the pore structure factors.

Figure 3 shows the relative dynamic elastic modulus and mass loss as a function of freeze-thaw cycle times with different vibration time (vibration frequency 2850Hz/min). This section selects the C45-I as the primary object shown in Table1, and uses the SJ-2 air-entraining agent to control the 6% of air content in the fresh concrete.

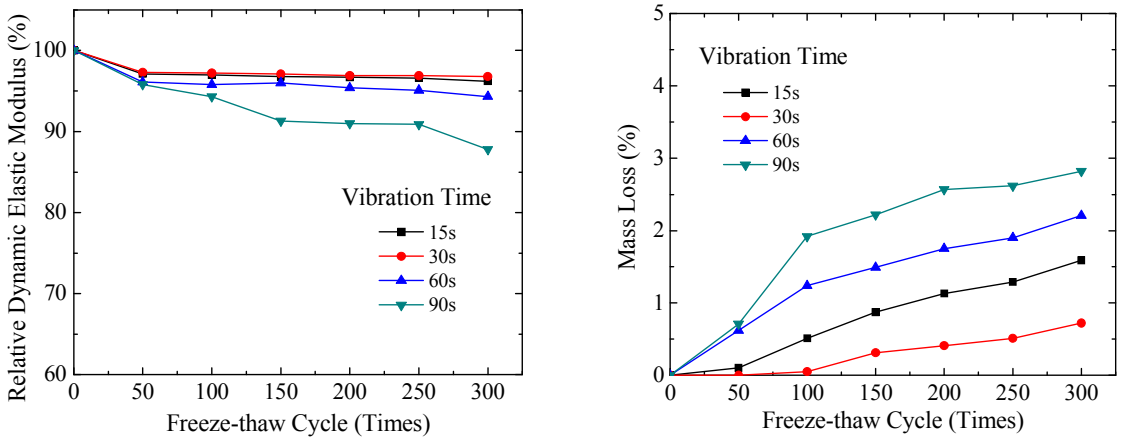

Fig .3 Relative dynamic elastic modulus and mass loss as a function of freeze-thaw cycle times with different vibration time

As can be seen in this figure, with same air content, the relative dynamic elastic modulus and mass loss increase with increasing of vibration time. This resulted from the different air void structures in concrete. The relative dynamic elastic modulus increases and mass loss decreases when the vibration time increases from 15s to 30s. But the relative dynamic elastic modulus decreases and mass loss increases sharply if the vibration time exceeds 60s.

During the vibration process, air voids keep changing in the concrete. In the beginning of the vibration process, the air bubbles start to distribute homogeneously, and this leads to the increasing properties of concrete after cure, however, with increasing of vibration time, some small air voids will merge and form bigger voids, and some bigger voids will break and form new smaller voids, which leads to segregation and breaks the homogeneous state of the concrete.

Table3 gives the air voids characterization parameters after curing 28 days. As shown in this table, the air voids structure was largely different at the top and the bottom of the specimen with different vibration time. As for the pore structure of upper section in the concrete, the optimal vibration time

in the upper concrete is 30 seconds, less than 60 seconds. However, as shown in the specific surface, the average radium, spacing factor and pore size distribution, the optimal vibration time in the bottom concrete is 60 seconds beyond the upper section. In sum, the optimal vibration time in the concrete is 30 seconds, less than 60 seconds.

Table3. Air voids characterization parameters after curing 28 days

vibration time (s)	test position	specific area (mm^2/mm^3)	average diameter (mm)	bubble space (mm)	air bubble diameter distribution (μm, %)			
					100~200	200~500	500~1000	>1000
15	top	29.0	0.104	0.121	86.1	11.3	1.7	0.9
	bottom	32.3	0.0930	0.143	88.5	8.5	2.3	0.7
30	top	32.0	0.0936	0.103	84.4	13.3	2.2	0
	bottom	39.6	0.0758	0.126	93.2	5.5	0.5	0.8
60	top	35.1	0.0855	0.127	92.0	6.1	0.9	0.9
	bottom	46.0	0.0653	0.103	93.3	5.2	0.5	0.7
90	top	31.7	0.0945	0.142	93.6	4.8	0	1.6
	bottom	39.6	0.0758	0.125	94.0	4.1	1.6	0.6

The parameter differences between the top and the bottom increase with increasing of vibration time. During the vibration process, the bigger bubbles tend to move upwards, displacing small bubbles, thus, the specific area difference changed obviously, and spacing factor increases from top to bottom. Since the bigger air bubbles move upward to the surface of the concrete, they will finally diminish with increasing vibration time, thus, the observed decrease in average air bubble diameter is reasonable. Vibrating is equivalently doing work on concrete, in other words, energy is added to it. In this case, some new air voids formed by this energy is coming out in fresh concrete, simultaneously, many old air void is occurring in the process of mergence and growth, and then they are collapsing or escaping from the concrete.

Conclusions

1. The flexural strength does not show obvious variation with increasing of air content, however, it still can be seen that the maximum value was obtained with air content of about 4%.
2. The entrained air improved largely the freeze-thaw property .C45 concrete specimen without air entrainment fractured at the 150 freeze-thaw cycles, but the C45 concrete with air of 3.3% did not fracture after 300 freeze-thaw cycles.
3. The C60 concrete with air content of 4.1% did not fracture until cycled 1,000 times. For the specimen with air content of 6.5%, the relative dynamic elastic modulus was 96% after 1,086 freeze-thaw cycles.
4. In air entrained concrete, the total air content is not the only factor that affects the final properties of concrete. The air void size, shape, and distribution are key factors as well. Different air void structures were realized at different durations of vibration. It was found the optimized vibration time was 30s.

References

[1] Chatterji S. (2003). "Freezing of air-entrained cement-based materials and specific actions of air-entrained agents" Cement Concrete Composites, Vol. 25, 759-765
[2] L. Du and Kevin J. Folliard, (2005). "Mechanisms of air entrainment in concrete" Cement and Concrete Research, Vol. 35, 1463-1471
[3] X. Ouyang, Y. Guo, and X. Qiu. (2008). "The feasibility of synthetic surfactant as an air entaining agent for the cement matrix" Construction and Building Materials, Vol. 22, 1774-1779
[4] John M. Stencel, Haiping Song, Federico Cangialosi. (2009). "Automated foam index test: Quantifiying air entraining agent addition and interactions with fly ash-cement admixtures" Cement and Concrete Research, Vol. 39, 362-370
[5] Q. Yang, *et.al.* (2000). "Properties of concrete with a new type of saponin air-entraining agent" Cement and Concrete Research, Vol. 30, 1313-1317
[6] Lamontagne A, Pigeon M., Pleau R, *et. al.*(1996). "Use of air-entraining admixtures in dry-mix shotcrete" ACI Mater. J., Vol. 93(1), 69-74
[7] Jasiczak J, Zielinski K. (2006). "Effect of protein additive on properties of mortar" Cement Concrete Composites, Vol. 28, 451-457
[8] Hamad BS, Rteil AA., El-Fadel M. (2003). "Effect of used engine oil on properties of fresh and hardened concrete" Construction and Building Materials, Vol. 17, 311-318
[9] S. Chatterji, (2003). "Freezing of air-entrained cement-based materials and specific actions of air-entraining agents" Cement and Concrete Composites Vol.25, 759–765
[10] W.Z.Shao, V.V.Ivanov, L.Zhen, *et.al.* (2004). "Effect of porosity and copper content on compressive strength of Cu/Cu2O cermet" Journal of Materials Science, Vol. 39, 731-732

doi:10.4028/www.scientific.net/AEF.5.370

A Dynamic Loading Test for Evaluating Permanent Deformation Resistance of Asphalt Mixtures

Xiaoguang Xie[1,a], Long Wang[2,b],Xiaorui Zhang[3,c]

[1]School of Transportation Science and Engineering Harbin Institute of Technology Harbin 150090, China

[2]School of Transportation Science and Engineering Harbin Institute of Technology Harbin 150090, China

[3]School of Transportation Science and Engineering Harbin Institute of Technology Harbin 150090, China

[a]xxg75@126.com , [b]hitlongwang@sina.com , [c]hagongdadaolu@163.com

Keywords: asphalt mixtures; deformation resistance; dynamic loading; permanent deformation

Abstract. Recent research shows that there is a serious need for accurate methods to evaluate the deformation resistance of asphalt mixtures at high temperatures, especially for stone-skeleton mixtures. To reflect the interlocking angle between coarse aggregates, confining pressure should be considered during testing. The dynamic loading test has been developed for applying different repetitive loads to a limited area of the specimen. This test can measure permanent deformation indices under different loads to evaluate the deformation resistance of asphalt mixtures at high temperature. The dynamic loading test is conducted on samples with different compaction rates and gradations. Further, the rutting resistance of two types of gradation is compared with a wheel tracking test and a dynamic loading test. The test results indicate that the dynamic loading test can apparently distinguish the influence of gradations on rutting resistance. It is also derived from this test that dense-graded mixtures have higher permanent deformation susceptibility than coarse-graded mixtures, which is consistent with experience in the field and validated by experiments. This test can reflect the entire permanent deformation and separate the compactive deformation and shear flow deformation. Furthermore, this test can simulate heavy and repeated loads to fully exhibit the deformation resistance of asphalt mixtures, especially for coarse-graded mixtures. However, this test is limited by the effects of rigid confinement, which can be improved by changing the confining pressure.

Introduction

At present, the ‘‘working environment’’ of roads are becoming more complex and severe. High traffic volumes and tire pressures combined with high ambient temperature accelerates the deterioration of asphalt pavement. Now one of the most common forms of failure of asphalt pavement is rutting [1]. For semi-rigid base asphalt pavement, rutting is primarily derived from the permanent deformation of the asphalt concrete layer at high temperatures. The gradation of hot-mix asphalts (HMA) should be accurately designed to improve rutting resistance. Literature research shows that 60% rutting resistance of asphalt mixtures is attributed to the interlocking forces provided by coarse particles, the other 40% coming from the cohesion of asphalt binder. In China, more and more asphalt-treated base (ATB) and asphalt-treated permeable base (ATPB) are applied to reduce the reflective cracking and moisture damage arising from the used semi-rigid base [2]. Therefore, it is essential to accurately evaluate the deformation resistance of stone-skeleton asphalt mixtures.

There are many methods to judge rutting resistance of asphalt mixtures including wheel tracking (WT), static creep, dynamic creep, indirect tensile strength (ITS) tests and an accelerated loading facility (ALF) test. ITS test is developed for elastic base and does not accurately estimate the rutting resistance of a mixture. Wheel-tracking tests are not quantified to be well correlated with rutting in the field under variable traffic loading and environmental conditions. However, it can be

used to rank mixtures according to rut potential. Wheel-tracking tests generate two rutting parameters (rutting depth and dynamic stability). Dynamic stability has limitation and sometimes conflicts with rutting depth, for it considers only the rutting depth at 45min and 60min, not the whole depth [3]. Experiences have shown that stone-skeleton mixtures, such as SMA and ATB, cannot be properly evaluated by means of conventional tests, such as the unconfined uniaxial static or dynamic creep tests [4]. Other studies for rutting evaluation use a creep loading or repeated loading in uniaxial or triaxial modes, however, these test procedures are relatively complex and are not widely used in field laboratories [5,6].

The existing experimental tests have limitations and lack rationalities to evaluate the deformation resistance of HMA, especially for stone-skeleton mixtures. It is essential to select an accurate test to evaluate the deformation properties of asphalt mixtures. The shear strength of stone-skeleton mixture is mainly derived from interlocking angle, φ used in the shear strength equation （$\tau = c + \sigma tg\varphi$）. To reflect the interlocking angle, φ confining pressure, σ should be considered. In general, rutting occurs mainly on wheel paths in the roads, the rest of the pavement section remaining almost intact. The spot under the wheel suffers stress and the immediate surrounding body acts as a restraining barrier for shear movement when the material underneath the tire begins to deform. According to this hypothesis, instead of applying load to the whole cross-sectional area of a specimen, a test method is developed to apply a dynamic load to a limited area with confining pressure. This test can reflect the deformation resistance of asphalt mixtures, especially for stone-skeleton mixtures at high temperatures, called as dynamic loading test.

Development of Dynamic Loading Test

Repetitive load tests apply an axial dynamic stress on a specimen with a sinusoidal loading pattern, close to the actual field loading conditions. Repetitive load tests are also thought to be more accurate than static testing to evaluate the characteristics of asphalt mixtures. The illustration above is the main reason to develop dynamic loading test in this research. Fig. 1 illustrates a periodic load applied to a specimen in a limited area (referring to CBR test). The applied load is haversine in shape and frequency is 0.1 hertz. Each level load increases by 10kN and 100 repetitions. The deformation curves under different load level are plotted through a sensor and displacement collecting system, as shown in Fig. 2. The elastic and plastic deformation can be directly derived from the deformation curve. The other deformation indices can be calculated, such as accumulative deformation, resilient and plastic modulus (equation 1).

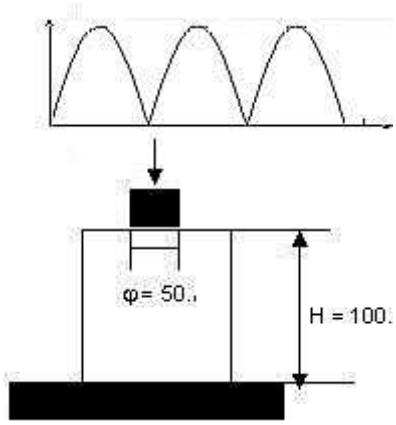

Fig. 1 Dynamic loading test (mm)

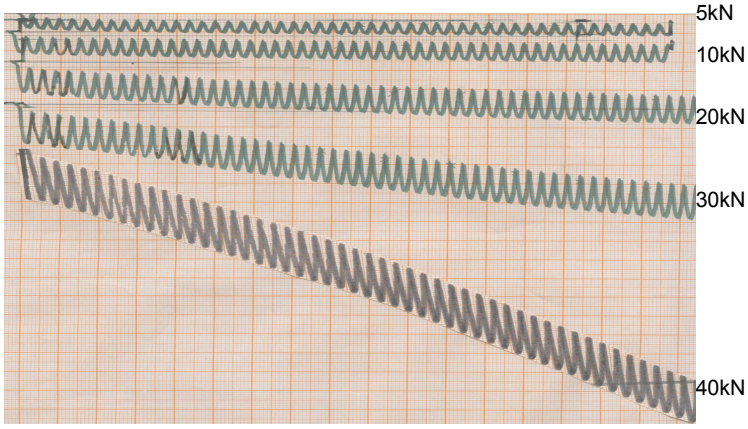

Fig. 2 Dynamic deformation curve of asphalt mixture at various loading

$$E = \frac{\pi D}{4} \times \frac{p}{l}(1 - \mu_0^{\,2}) \tag{1}$$

Where:

E —resilient or plastic modulus（MPa）;

μ_0 —poisson ratio (0.35);

D —the diameter of loading head（50mm）;

p —loading stress（MPa）;

l —elastic or plastic deformation（mm）;

Characteristics of the Test

The purpose of developing the new test method is to create a dynamic load-induced spot deformation similar to the one created by moving wheel. The dynamic loading test has a head (ϕ = 50 mm) on the specimen (ϕ = 150 mm) to simulate a variable wheel which has a circular tire imprint. Considering confining pressure, the dynamic loading test can evaluate interlock function between coarse aggregates under different loading levels, which is consistent with the actual stress state of asphalt pavement.

Permanent deformation in pavements has long been recognized to include two different modes according to Huang and Gokhale. The first mode is known as compactive deformation (consolidation of layers) and the second mode is plastic deformation (asphalt shear flow). The test system applies a dynamic load step-by-step from 5kN to 40kN, aiming to simulate the accumulative process of permanent deformation to attain different deformation stages. When the applying load is minor, deformation is known as compactive stage (the first mode). When the applying load increases, permanent deformation will increase consequently, the variable amplitude is not large, and deformation is known as accumulative stage. When the applying load increases further, the slope of deformation becomes larger sharply, which means the specimen failed, this deformation is known as shear flow. Fig. 2 shows the trend of deformation of an asphalt mixture.

The elastic and plastic deformation under different loading are separated from the test data. Further, the resilient modulus and permanent deformation can be calculated. The stress state is explicit in the uniaxial or triaxial creep tests and the objective is the cell, which represents the stress state of one point in the pavement. While the stress state of homogenate is nonuniform along the longitudinal and transverse distribution, the dynamic loading test reflects the entire homogeneous structure.

Loading Mode. The dynamic test with haversine loading cycles is repeated continually without any interval period. The repeated loadings are applied by a MTS machine. The maximum amplitudes are 5 kN, 10 kN, 20 kN, 30 kN, and 40 kN (2.55 MPa, 5.09 MPa, 10.19 MPa, 15.29 MPa and 20.38 MPa, respectively). The frequency is 0.1 hertz and cycle number is 100 each time.

Specimen Dimension. The stress distribution of the specimens is qualitatively analyzed using the finite element program in different heights and diameters. When specimen height is less than 100 mm, the position of the maximum normal stress is nearly half of the height. When specimen height is 150 mm, the position of the maximum normal stress value is 2/3 at 100 mm height. Therefore, the specimen dimension values selected are φ = 150 mm and H = 100 mm.

Experiment Temperature. The test temperature of evaluating deformation resistance of HMA at high temperature is, in general, between 40°C and 60°C. Through the summary of the literature, 45°C is selected for the asphalt mixture to evaluate permanent deformation resistance under high temperature.

Experimental Research

Materials. To prove the test susceptibility, five aggregate gradations are chosen, in which framework-void structure of asphalt mixtures are dominant, the other are dense-graded asphalt mixtures. Limestone aggregate is sampled from the Jilin rock quarry in China, and the 80-100 penetration asphalt cement comes from Panjin northern asphalt refinery. All materials and gradations demand Technical Specifications for Construction of Highway Asphalt Pavements in

China. Table 1 shows five used gradations. The gradation name respectively represents coarse aggregate, skeleton number-Taibo, an exponent *n* value of fine aggregate-filling coefficient. Every specimen should be brought to bear on different load level (2.55 MPa, 5.09 MPa, 10.19 MPa, 15.29 MPa and 20.38 MPa).

Table 1 Five Gradations in the Experiment Tests

Gradation Name	Air Void (%)	Seize Size(mm) Percentage Passing (%)										
		19.0	16.0	13.2	9.5	4.75	2.36	1.18	0.6	0.3	0.15	0.075
4-0.65-0.5	24.0	100	88.3	70.4	33.7	22.0	14.0	8.9	5.7	3.7	2.3	1.5
4-0.65-0.7	18.5	100	89.2	72.6	38.8	28.0	17.8	11.3	7.3	4.6	3.0	1.9
4-0.65-0.9	14.5	100	90.1	74.9	43.9	34.0	21.6	13.8	8.9	5.6	3.6	2.3
4-N-0.9	2.2	100	90.0	74.9	43.9	34.0	32.0	28.0	23.0	17.0	12.0	8.0
1-N-0.9	1.5	100	69.0	53.8	43.9	34.0	32.0	28.0	23.0	17.0	12.0	8.0

Aggregate Gradation Influence. Five gradations including 3 coarse-graded mixtures and 2 dense-graded mixtures (see Table 1) are fully compacted by the optimum compaction rate. Accordingly, deformation and modulus values are shown in Fig. 3 to Fig. 6.

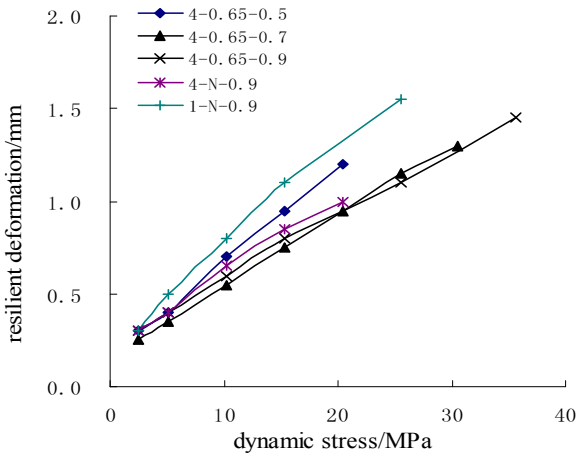

Fig. 3 Dynamic stress and resilient deformation of different gradations.

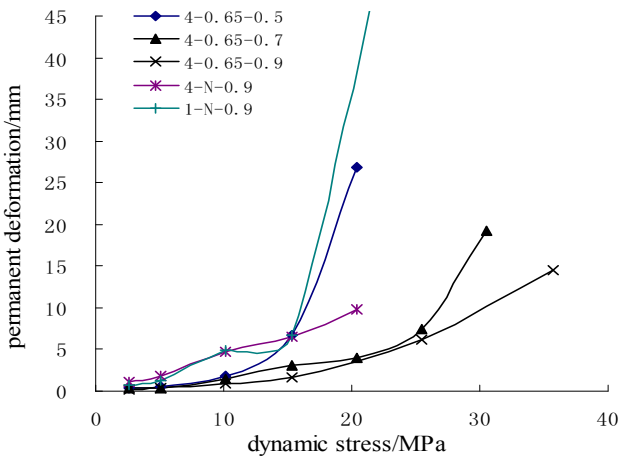

Fig. 4 Dynamic stress and permanent deformation of different gradations.

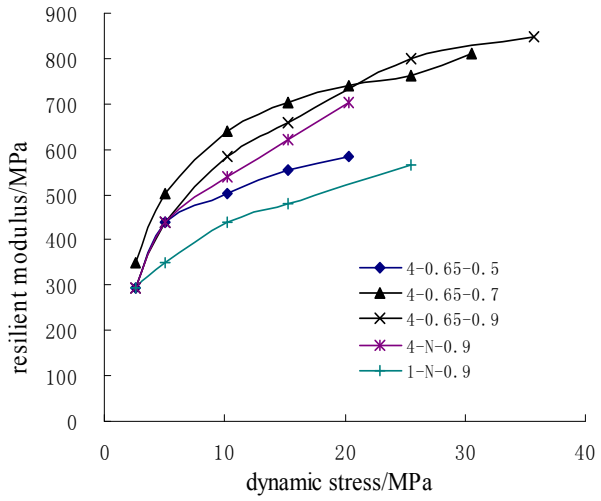

Fig. 5 Dynamic stress and resilient modulus of different gradations.

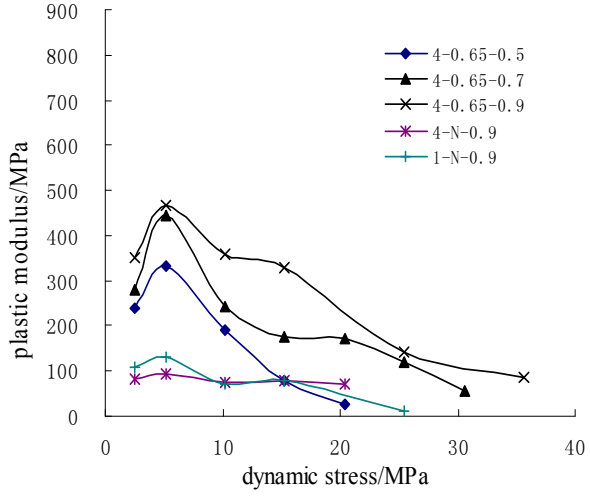

Fig. 6 Dynamic stress and plastic modulus of different gradations.

It can be clearly observed for both trends that as dynamic stress increases, resilient deformation and resilient modulus of different gradations are similar. There is a discrepancy in resilient deformation of 0 to 0.5 mm at the same dynamic stress (Fig. 3), while resilient modulus (Fig. 5) is 0 to 200 MPa. However, permanent deformation is quite different for different gradations. A discrepancy in permanent deformation is about 0 to 20 mm at the same dynamic stress (Fig. 4), while plastic modulus (Fig. 6) is 150 to 400 MPa. In Fig. 4, all five gradation mixtures are compacted efficiently, so permanent deformations under minor dynamic stress (less than 10 MPa) are nearly equal, which shows that asphalt mixtures compacted fully have little compactive deformation, regardless of any kind of aggregate gradation. While as dynamic stress increases (more than 25 MPa), the permanent deformations of different gradations are mainly attributed to asphalt shear flow, the value revealing significant distinctions of different gradations. Thus, it can be concluded that the discrepancy of deformation resistance of different gradation at high temperature can be measured through the dynamic loading test.

Fig. 6 shows that the plastic modulus reaches a maximum value at 5.09 MPa. As the dynamic stress increases, plastic modulus decreases. This indicates that when dynamic stress is no more than 5.09 MPa, deformation increases slowly and exhibits increasing modulus. As dynamic stress becomes more than 5.09 MPa, permanent deformation increases quickly and exhibits decreasing plastic modulus. It can be concluded that 5.09 MPa is a threshold for permanent deformation of asphalt mixtures, that is, compactive deformation in no more than 5.09 MPa and shear flow deformation in more than 5.09 MPa. It can be seen that this test reflects the entire deformation of asphalt mixture at high temperature.

Through analysis of coarse skeleton and filling coefficient of five asphalt mixtures and their influence on performance, it can be concluded that the coarse skeleton 4 bears heavier loading than coarse skeleton 1, which is in agreement with the research results of graded crush stone[7,8]. Fig. 4 and Fig. 5 show that an asphalt mixture with a filling coefficient of 0.9 is the optimum at the same coarse skeleton 4. Fig. 7 also displays the comparison results of the permanent deformation of dense-graded (4-N-0.9 and 1-N-0.9) and coarse-graded asphalt mixtures (such as 4-0.65-0.9) at 45°C temperature under different stress levels. Permanent deformation resistance of coarse-graded samples is more than dense-graded samples especially at heavy loads. This conclusion is validated by experience and field work, which also proves that dynamic loading test can reflect the deformation resistance of different types of gradations.

Contrast Analysis. Two aggregate gradations (4-0.65-0.9, 4-N-0.9) are used for preparing the specimen for the WT test and dynamic loading test. The curve in Fig. 7 shows accumulative permanent deformation increases along the time under different tire pressures. In general, with the tire pressure (from 0.7 MPa to 1.0 MPa) increases, vertical permanent deformation and the slope of asphalt mixtures increase too. When tire pressure increases to 1.15 MPa, the deformation slope is sharp before 20 min., then it slows. This phenomenon reveals two things, one is that dynamic stability derived from the deformation slope between 45 min. and 60 min. reflects the rutting resistance of asphalt mixtures, although not the whole permanent deformation; and secondly, such a phenomenon is possible that the dynamic stability of different asphalt mixtures are the same, while permanent deformations may be quite different. For instance, the deformation slopes of two gradations are similar, but the permanent deformation becomes different at 60 min. WT can exhibit the dynamic stability value under minor load (0.7 MPa), but it produces an error and leads to unreliable statistics in lieu of dimension effect when applying loads are heavy. Fig. 7 shows that the deformation slope of two gradations between 45 min. and 60 min. are the same under 1.15 MPa, but quite different in accumulative permanent deformation. Fig. 8 clearly presents that as dynamic stress increases, accumulative permanent deformation increases with different slopes for two gradations. The permanent deformation under different loads is able to be directly measured through the dynamic loading test, which significantly proves that the dynamic loading test effectively reflects the permanent deformation under different loads.

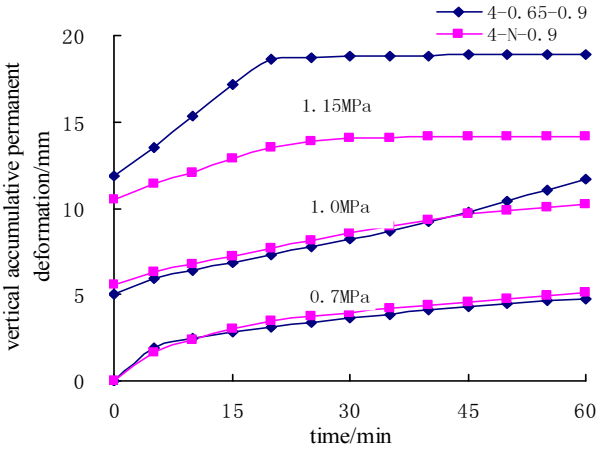

Fig. 7 Time and accumulative permanent deformation under different tire pressures.

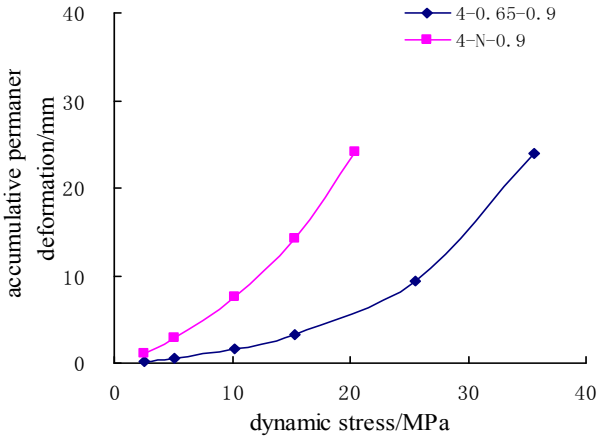

Fig. 8 Dynamic stress and accumulative permanent deformation.

Conclusions

For coarse skeleton asphalt mixtures, the shear strength is mainly derived from the interlocking forces provided by coarse aggregates. It is accurate to evaluate the deformation resistance of HMA considering the existence of confining pressure. The dynamic loading test is developed for applying different repetitive loads to a limited area of the specimen and utilizing mold confinement to evaluate the deformation resistance of asphalt mixtures at high temperatures.

This test can reflect the entire permanent deformation of asphalt mixtures at high temperature and separate the compactive deformation and shear flow deformation. Furthermore, the test can simulate different loads, especially heavy and repeated loads, which could fully exhibit the deformation resistance of asphalt mixtures, especially for coarse-graded mixtures.

The test is limited by the rigid confinement, which could be improved by changing the confinement.

References

[1] Tayfur, S., H. Ozen, and A. Aksoy. Investigation of Rutting Performance of Asphalt Mixtures Containing Polymer Modifiers. *Construction and Building Materials*, Vol. 21, 2006, pp. 328–337.

[2] Technical Specifications for Construction of Highway Asphalt Pavements in China. *JTG*, F40, 2004.

[3] Huihong, H. Assessment on Property of Wheel Tracks in Asphalt Mixtures. *Master's Thesis*. Harbin Institute of Technology, Harbin, P.R. China, 2000.

[4] Visser, A. T., F. Long, A. Verhaeghe, and A. Taute. Provisional Validation of the New South African Hot-mix Asphalt Design Method (Mix Design-1:7–6). Ninth International Conference on Asphalt Pavements. Copenhagen, Denmark, August 2002, p. 36–47.

[5] Krutz, N. C., R. Siddharthan, and M. Stroup-Gardiner. Investigation of Rutting Potential Using Static Creep Testing on Polymer-Modified Asphalt Concrete Mixture. In *Transportation Research Record (TRR): Journal of the Transportation Research Board*, No. 1317, Transportation Research Board (TRB) of the National Academies, Washington, D.C., 1991, pp. 100–118.

[6] Little, D. N. Performance Assessment of Binder of Binder-Rich Polyethylene-Modified Asphalt Concrete Mixtures (Novophalt). In *TRR: Journal of the TRB*, No. 1317, TRB of the National Academies, Washington, D.C., 1991, pp. 1–9.

[7] El Hussein, H. M., and Z. Yue. Criteria for Evaluation of Rut Potential Based on Repetitive Uniaxial Compression Test. In *TRR: Journal of the TRB*, No. 1454, TRB of the National Academies, Washington, D.C., 1994, pp. 74–81.

[8] Brown, S. F., and J. M. Gibb. Validation of Experiments for Permanent Deformation Testing of Bituminous Mixtures. *Journal of Asphalt Paving Technology*, Vol. 65, 1996, pp. 255–299.

doi:10.4028/www.scientific.net/AEF.5.376

Effect of Filler on Glass Transition of Asphalt Mastics

Meng Guo [1, a], Yi-qiu Tan [2,b] and Lei Zhang [3,c]

[1] School of Transportation Science and Engineering, Harbin Institute of Technology, Harbin 150090, Heilongjiang, PR China

[2] School of Transportation Science and Engineering, Harbin Institute of Technology, Harbin 150090, Heilongjiang, PR China

[3] School of Transportation Science and Engineering, Harbin Institute of Technology, Harbin 150090, Heilongjiang, PR China

[a]guomeng87@163.com, [b]yiqiutan@163.com, [c]hit.andy@foxmail.com

Keywords: Filler, Asphalt Mastics, Glass Transition, Dynamic Mechanic Analysis; Differential Scanning Calorimetry

Abstract. A study has been carried out on the glass transition of fifteen asphalt-filler mastics in three different filler types. The dynamic mechanical analysis (DMA) and differential scanning calorimetry (DSC) method were used. The results show that DMA method can measure the glass transition temperature (Tg) of asphalt-filler mastics more accurately than DSC; The glass transition temperature measured by DMA is generally higher by 20~40^{o}C than that measured by DSC; The glass transition temperature of the asphalt-filler mastics increase with the increase of the filler volume fraction, and andesite is the most sensitive; When the volume fraction of filler is greater than 0.5, the enhance capability of glass transition temperature of asphalt-filler mastics is in the order of andesite > granite > limestone, when the volume fraction of filler is smaller than 0.2, the enhance capability is in the order of granite > limestone > andesite.

1. Introduction

Asphalt-filler mastics is an important part of asphalt mixture, and its properties influences the performance of asphalt pavement directly. Fillers are used to lower the cost of materials, increase rigidity and give special properties to a material (such as colour or fire retardancy). The filler volume fraction and properties have considerable effects on the processing characteristics of materials such as mixing, pumping and compacting. The effects of fillers are therefore of vital importance. The performance of asphalt-filler mastics is different from base asphalt and asphalt mixtures.

Physical and rheological tests are known to correlate well with road performance. A certain similarity exists between the viscoelastic behavior of simple amorphous polymers and asphalt [1]. As the glass transition temperature (Tg) is a very important parameter of amorphous polymers [2], it should also be useful in interpreting the properties of asphalts. It is a reversible change in an amorphous domain from a viscous or rubbery state to a hard and relatively brittle glassy state, and vice versa.

Thermal analysis and dynamic mechanical analysis provide the possibility of determining Tg and morphology. Y. Edwards [3] used dynamic mechanical analysis (DMA) and differential scanning calorimetry (DSC) to demonstrate that bitumen composition was of decisive importance, and adding polyethylene wax or polyph-osphoric acid especially to a non-waxy bitumen, showed considerable positive effects on the rheological behaviour at medium and higher temperatures. P. Starck [4] measured the elastic modulus (stiffness), the glass transition temperature (Tg) of the bitumen phase, and the softening temperature by using DMA, and demonstrated that the viscosities of the blends increased significantly after the immersion in de-icing agents. Kim YR [5] used DMA to evaluate the fatigue and healing potential of asphalt binders in sand asphalt mixtures, and he considered several candidate fatigue failure parameters to assess fatigue life and the effect of rest periods on the extension of fatigue life through healing. Pavel Kriz [6] applied DSC to asphalt binders and

successfully identified binders that are sensitive to time hardening at low temperatures. In such binders, several thermodynamic and morphology parameters are strongly time-dependent, suggesting that the viscoelastic properties change with time. Wu SP [7] studied the thermal behavior and characterization of the ultraviolet aged asphalt binder. Their results indicated that the UV light ageing would lead to the improvement of thermal behavior and the growth of the glass transition temperature of asphalt binder. M. Garcĺa-Morales [8] conclude that the viscous properties of bitumen, at high temperature, are improved by adding recycled EVA copolymer in amounts that depend on bitumen penetration grade. Moreover, significant microstructural changes, related to the development of a polymer-rich phase, tend to occur in the bitumen as polymer concentration increased.

2. Materials and test methods

2.1. Experimental materials. Experimental materials used in this paper include 90# base asphalt and three kinds of mineral fillers, and their technical data are shown in Table 1 and Table 2. Fifteen asphalt mastics are prepared by mixing asphalt and fillers for 15 minutes at speed of 1000 rpm. Asphalt mastics are divided into three categories (limestone asphalt mastic, andesites asphalt mastic and granite asphalt mastic), and each categories include five filler volume fraction (Φ=0.1, 0.2, 0.3, 0.4 and 0.5).

Table 1. Technical data of 90# base asphalt

Test item	Measured value
25^{o}C Penetration (0.1mm)	83.0
Softening point (^{o}C)	46.3
15^{o}C Ductility (cm)	>140

Table 2. Physical properties of mineral powder

Filler type	Density (g/cm^3)	Sieve percentage (%)		
		0.6mm	0.15mm	0.075mm
Limestone	2.827	100	96.5	76.7
Andesites	2.864	100	98.7	76.7
Granite	2.614	100	85.7	74.2

2.2. Laboratory testing. Differential scanning calorimeter used in this paper is DSC200F3 produced by NETZSCH GmbH. The temperature range of tests is from -100°C to +100°C. Glass transition temperature is determined by analyzing the curve showing the relationship between heat flow and temperature (Figure 1). Pavel Kriz [6] pointed out that the repeatability and accuracy of Tg inflection point is good, but multi-component material include many Tg inflection point like asphalt, so using only one Tg inflection point can't show the whole property of the material; Tg midpoint can reflect the average of the glass transition region, but the value of Tg midpoint are sensitive to the selection of the start point and the end point, so this paper analyzed both of them. At first, we studied the influence of heating rate on measurement results (Figure 3).

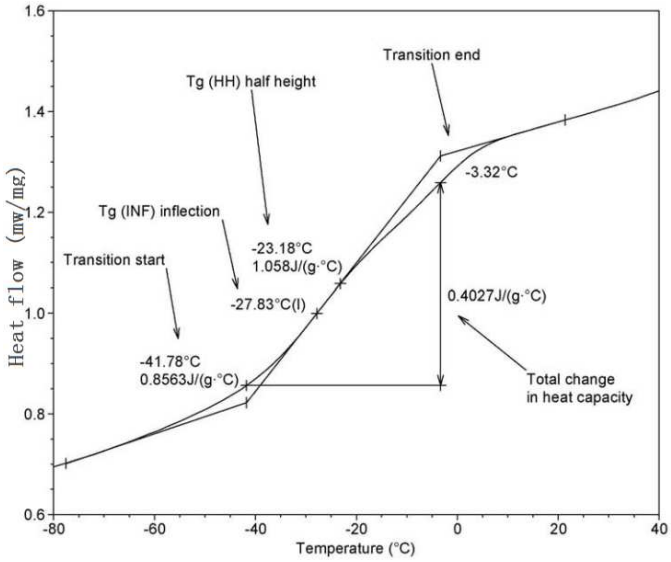

Fig.1. Determination of glass transition temperature by DSC.

Dynamic mechanical analysis method is an effective means of study the changing of polymer structural, molecular motion and performance. In this paper, the dynamic mechanical thermal analyzer DMA Q800 produced by TA was used to do a dynamic tension and compression testing on the asphalt-filler mastics, and the test parameters were selected as follows:

Temperature range: -60°C ~+50°C;

Heating rate: 5 °C /min;

Initial isothermal conditioning: 3 minutes;

Load mode： strain control, amplitude =0.05%, frenquecy=1Hz;

Specimen size: 17.33mm×4.50mm×2.40mm.

We can get the relationship of storage modulus, loss modulus, phase angle and temperature by doing the above test (Figure 2). By analyzing Figure 2, we can see that the peak value of loss modulus can reflect the glass transition temperature of asphalt-filler mastics accurately, but the cross point of tangents of storage modulus is imprecise in determining Tg of asphalt-filler mastics, because it's sensitive to the selection of the start point and the end point.

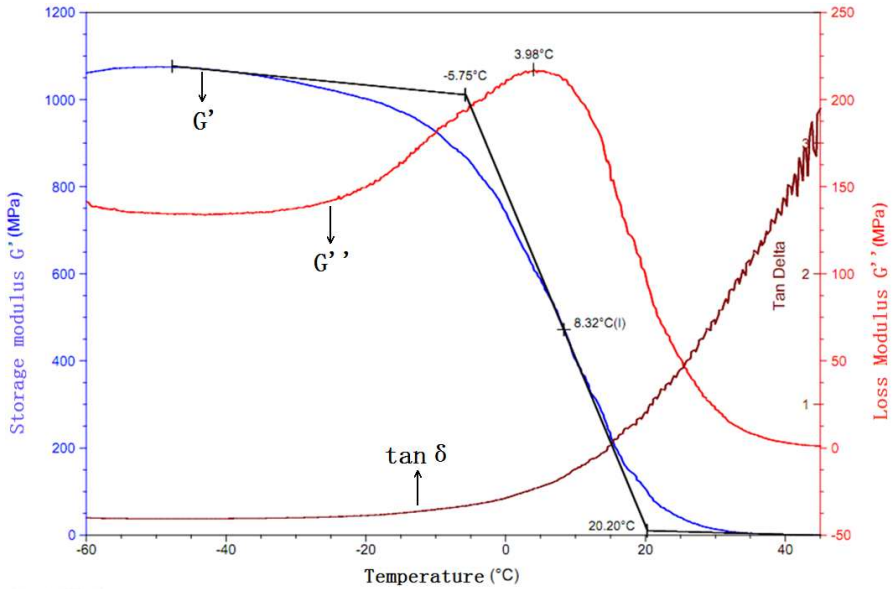

Fig.2. Determination of glass transition temperature by DMA.

3. Results and discussion

3.1. Results of DSC tests.

(1) The influence of heating rate on glass transition

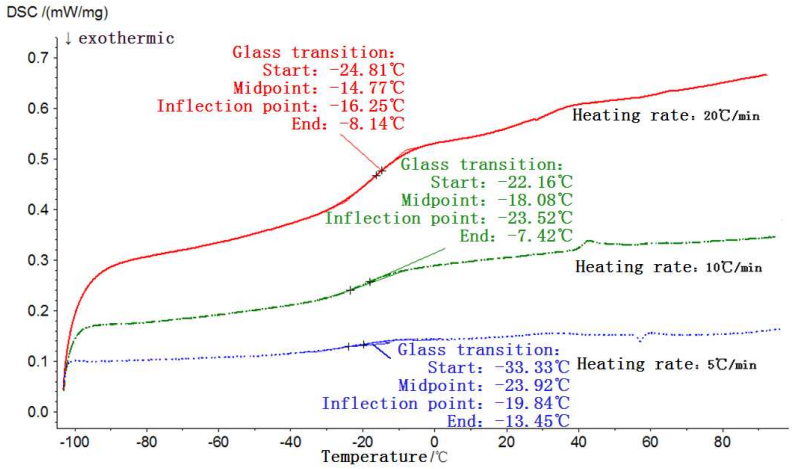

Fig.3. The influence of heating rate on glass transition.

It can be seen from Figure 3, with increasing heating rate, the glass transition is more obvious and more hysteretic, which is consistent with the time dependence of the chain segmental motion. If the time chain segment resisted stress is longer, they will have more time to make a response to the stress, the temperature of the glass transition will be much lower, which means that the glass transition is a dynamic process; The Tg midpoint increases with heating rate increases, but the Tg inflection point temperature presents ruleless.

(2) Effect of filler on Tg of asphalt mastic by DSC

The heating rate is set as 10°C/min, and the Tg measuring results of the various asphalt-filler mastics are shown in Figure 4 and Figure 5.

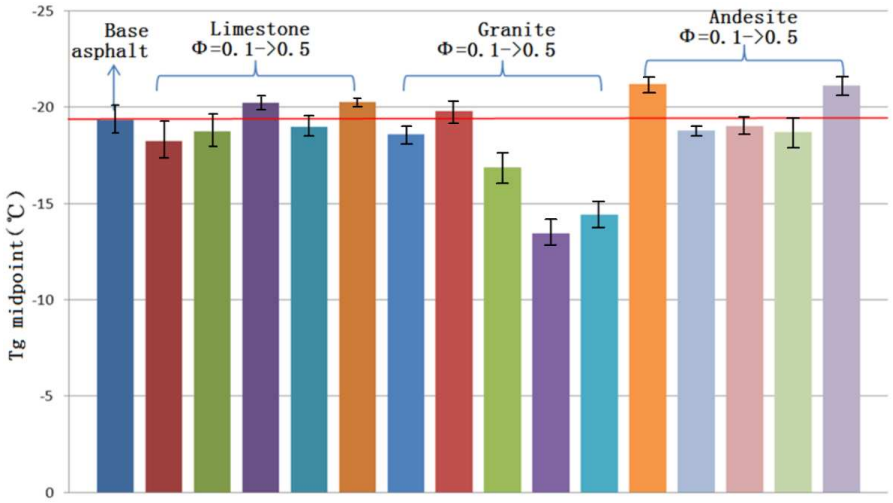

Fig.4. The Tg midpoint of various asphalt-filler mastics by DSC.

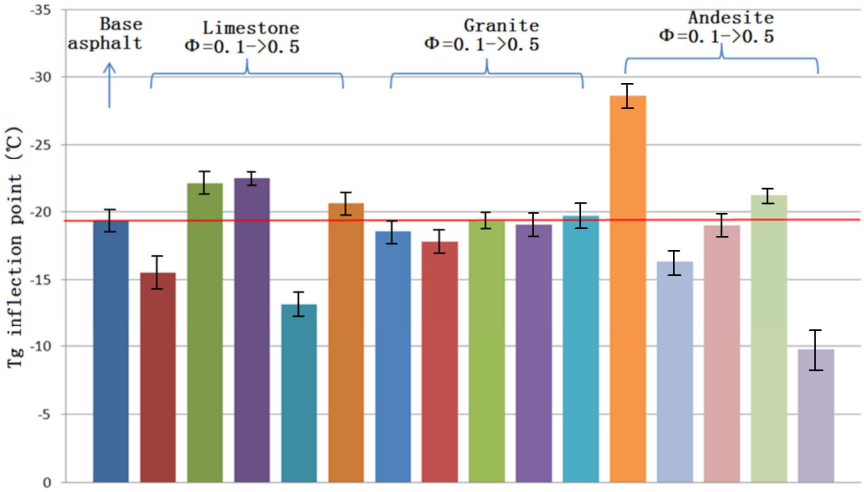

Fig.5. The Tg inflection of various asphalt-filler mastics by DSC.

It can be seen from Figure 4 and Figure 5 that Tg midpoint and Tg inflection point can't distinguish the glass transition of different asphalt-filler mastics clearly. The Tg midpoint of asphalt-filler mastics with granite filler has a weak regularity, which is the Tg midpoint increases with the increase of volume fraction.

3.2. Results of DMA tests

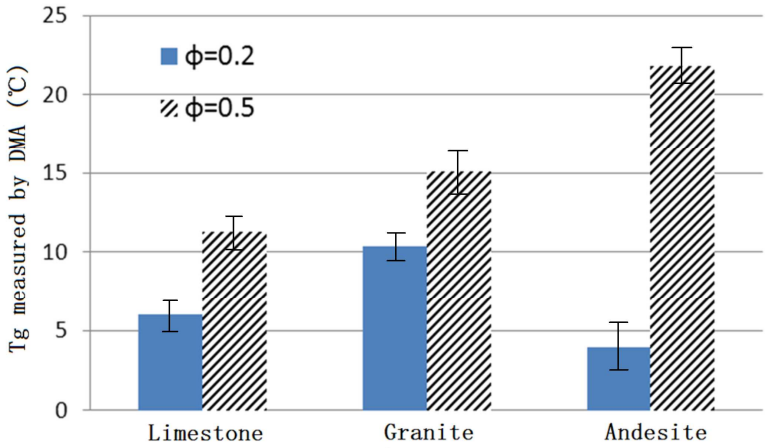

Fig.6. The Tg of various asphalt-filler mastics by DMA.

It can be seen from Figure 6 that dynamic mechanical analysis method has a better regularity in determining the glass transition temperature. The glass transition temperature of all asphalt-filler mastics have a same regularity, which is Tg increases with the increase of the filler volume fraction, and andesite is the most sensitive, which indicating that the more filler makes more interfacial layers, making the motion of asphalt molecular chain adsorbed on the surface of the filler particles become more difficult. The greater the filler content is, the stronger the effect is. When the volume fraction of filler is greater than 0.5, the enhance capability of glass transition temperature of asphalt-filler mastics is in the order of andesite > granite > limestone, which means that the more andesite filler will make the worst low-temperature performance; while the volume fraction of filler is smaller than 0.2, the enhance capability is in the order of granite > limestone > andesite, which indicates that less granite will the most decrease of glass transition temperature of asphalt-filler mastics.

By contrasting the Tg results obtained by the DSC method and DMA method, we can see that the DSC can't effectively reflect the influence of filling on the glass transition of the asphalt-filler mastics, while DMA have a considerable differentiation. The glass transition temperature measured by DMA is generally higher by 20~40°C than that measured by DSC, and the greater the filler volume fraction is, the greater the difference between the results of two methods is.

4. Summary and conclusions

Based on the testing and analysis presented herein, the conclusions of the study are summarized as follows:

1) The DMA method can measure asphalt Tg of asphalt-filler mastics accurately, and it can evaluate the impact of the type and volume fraction of filler on Tg. The glass transition temperature measured by DMA is generally higher by 20~40^{o}C than that measured by DSC, and the more filler will make a bigger difference. The Tg midpoint measured by DSC has a weak regularity, and Tg inflection point has no regularity.
2) The DMA tests demonstrated that the glass transition temperature of the asphalt-filler mastics increase with the increase of the filler volume fraction, and andesite is the most sensitive.
3) When the volume fraction of filler is greater than 0.5, the enhance capability of glass transition temperature of asphalt-filler mastics is in the order of andesite > granite > limestone; while the volume fraction of filler is smaller than 0.2, the enhance capability is in the order of granite > limestone > andesite.

References

[1] Giavarini C, Pochetti F. Characterization of Petroleum Products by DSC Analysis. Journal of Thermal Analysis and Calorimetry, 5 (1973): 83-94.

[2] Ngai KL. The Glass Transition and the Glassy State, Physical Properties of Polymers, Cambridge University Press, Cambridge, UK, 2004: 72-152.

[3] Y. Edwards, Y. Tasdemir, U. Isacsson. Rheological effects of commercial waxes and polyphosphoric acid in bitumen 160/220 – high and medium temperature performance. Construction and Building Materials. 21 (2007): 1899-1908.

[4] P. Starck, B. LÖfgren. Influence of de-icing agents on the viscoelastic properties of asphalt mastics. J Mater Sci. 42(2007): 676–685.

[5] Kim YR, Little DN, Lytton RL. Use of dynamic mechanical analysis (DMA) to evaluate the fatigue and healing potential of asphalt binders in sand asphalt mixtures. Journal of the Association of Asphalt Paving Technologists. 71 (2002): 176–206.

[6] Pavel Kriz，Jiri Stastna，Ludo Zanzotto. Glass Transition and Phase Stability in Asphalt Binders. Road Materials and Pavements Design. 1 (2007): 1-30.

[7] Wu SP, Zhu GJ, Liu G, Pang L. Laboratory research on thermal behavior and characterization of the ultraviolet aged asphalt binder. Journal of Thermal Analysis and Calorimetry. 95 (2009): 595-599.

[8] M. GarcÍa-Morales, P. Partal, F.J. Navarroa, F. MartÍnez-Boza, C. Gallegos, N. González, O. González, M.E. Muñoz. Viscous properties and microstructure of recycled eva modified bitumen. Fuel. 83 (2004): 31-38.

doi:10.4028/www.scientific.net/AEF.5.382

Effects of construction conditions on built-in temperature gradient of concrete pavement: a numerical study

Lei Quan[1,a], Bo Tian[1,2,b], Decheng Feng[1,c] Xinkai Li[1,d]

[1]School of Transportation Science and Engineering, Harbin Institute of Technology, Harbin 150090, China

[2]Research Institute of Highway Ministry of Transport, Beijing, 100080, China

[a]charly08@163.com,[b]b.tian@rioh.cn,[c]fdcgxy@vip.sina.com,[d]lxkhit@126.com

Key words: cement concrete pavement; built-in temperature gradient; construction conditions; numerical simulation

Abstract: The built-in temperature gradient of concrete pavement formed during hardening period caused by various construction conditions will permanently exist in the pavement, which will have significant influence on the service behavior of concrete pavement. However, it's still not involved in the current ***Specifications of Cement Concrete Pavement Design for Highway*** in China**.** In this paper, a user subroutine based on the ABAQUS code was developed to simulate the effects of weather condition, paving time, curing method, raw material temperature on built-in temperature gradient. The analyses indicate that these factors always produce obvious positive gradient in the slab and the influences of the first three aspects are obvious and the paving temperature of mixture has limited effect on the increasing of the final set temperature gradient. Furthermore, built-in temperature gradient is proposed as an index to evaluate the influences of various construction factors and optimize construction measures.

1 Introduction

Considering the whole life of cement concrete pavement from paving, early-age concrete experiences the hydration and hardening process including the flow state, plastic state and solid state respectively. During this period, the factors such as hydration heat of cement, the change of surrounding temperature and solar radiate will lead to the sustainable fluctuation of the temperature field of concrete pavement. Before final set, the plastic deformation insures the zero-stress in the slab, but after final set, temperature gradient will cause internal stress and deformation. Therefore, at the time of final set, the slab is still keep flat and zero-stress, but with temperature gradient through the depth. Under this initial status, the slab begins to bear loading and deformation. When the temperature gradient in the slab is zero, the slab curls upward rather than remaining flat. Thus, an effective negative temperature gradient is "built into" the slab, and is referred to as the built-in construction temperature gradient. The magnitude of the built-in temperature gradient is affected by air temperature and weather conditions during set and curing conditions [1]. The deformation caused by this effect is extremely unfavorable for the smoothness of concrete pavement [2,3] and this built-in temperature gradient will also produce significant influence on the service behavior of concrete slab [1,4-8]. However, it's still not involved in the current ***Specifications of Cement Concrete Pavement Design for Highway*** in China [9].

Based on the studies above, the objectives of this paper are as follows:

(1)Develop a program which can be used to calculate the temperature field of early-age concrete pavement;

(2)According to the heat transfer theory and construction conditions of concrete pavement, sort the influence factors and select the represented situations for numerical simulation;

(3)Analyze the effect regulations of each construction condition on built-in temperature gradient.

2 Numerical methodology

2.1 Governing equation of heat transfer

According to the heat transfer theory, heat will conduct from the high temperature part to the low temperature part. Thus the temperature of the body is a function of its position and time. Here we take a random part Ω1, and establish the heat transfer governing equation based on reserve energy principle [10].

$$\frac{d}{dt}\int_{\Omega 1} C_v(x)\rho(x)T(x,t)dV = \int_{\Omega 1} s(x,t)dV - \int_{\Omega 1} \nabla \bullet q(x,t)dV \tag{1}$$

where, C_v is the specific of concrete; ρ is the density of concrete; T is the temperature of concrete; s is hydration heat; q is the heat flow through surface of Ω1.

2.2 Concrete pavement model description

Finite element method is chosen to solve this problem. For 2 dimension concrete pavement system, the definite conditions for the solution of heat transfer equation are as follows [11]:

(1)Initial temperature field

(2) Convection

Convection heat transfer is expressed as:

$$q_{conv} = h(T_s - T_a) \tag{2}$$

where h is convective heat transfer coefficient; T_s is the temperature of concrete; T_a is the temperature of air, using the follow equation to fit, w=2π/24, t_0=9.

$$T_a = \frac{T_a^{\max} + T_a^{\min}}{2} + \frac{T_a^{\max} - T_a^{\min}}{2}\left[0.96\sin w(t-t_0) + 0.14\sin 2w(t-t_0)\right] \tag{3}$$

(3) Irradiation

$$q_{ir} = \varepsilon\sigma(T_s^4 - T_a^4) \tag{4}$$

where, ε is heat emissivity; σ is Stefan-Boltzmann constant.

(4) Solar radiation

$$q_r = \alpha_s q \tag{5}$$

where, α_s is surface heat absorptivity of concrete; q instantaneous solar radiation, using the follow equation to fit:

$$q(t) = \frac{a_0}{2} + \sum_{k=1}^{\infty} a_k \cos\frac{k\pi(t-12)}{12} \tag{6}$$

where, $a_0 = \frac{2q_0}{m\pi}$, q_0 is the max solar radiation at noon, $q_0 = 0.131mQ$; m=12/c ;Q is the total solar radiation; c is the effective solar radiation time.

$$a_k = \begin{cases} \frac{q_0}{\pi}\left[\frac{1}{m+k}\sin(m+k)\frac{\pi}{2m} + \frac{\pi}{2m}\right] & k = m \\ \frac{q_0}{\pi}\left[\frac{1}{m+k}\sin(m+k)\frac{\pi}{2m} + \frac{1}{m-k}\sin(m-k)\frac{\pi}{2m}\right] & k \neq m \end{cases}$$

(5) Conduction

$$q_{cond} = -k\frac{dT}{dx} \tag{7}$$

where, k is thermal conductivities of concrete

(6) Hydration heat

The heat of hydration is expressed as[12,13]:

$$Q_h(t_e) = H_u \cdot C_c \cdot (\frac{\tau}{t_e})^{\beta} \cdot \frac{\beta}{t_e} \cdot \alpha(t_e) \cdot \exp(\frac{E}{R}[\frac{1}{273+T_r} - \frac{1}{273+T_c}]) \quad (8)$$

where, $Q_h(t_e)$ is the heat release speed of hydration of concrete at equivalent age t_e; H_u is the total heat of hydration; C_c is cement content; τ, β, E, R are parameters, T_r is reference temperature; T_c is the temperature of concrete.

2.3 User subroutine development based on ABAQUS code

According to initial and boundary conditions above, develop the user subroutine based ABAQUS code. One issue needs to be noticed is that the equivalent age t_e should be set as global variable.

2.4 Validation of numerical model

(1) Adiabatic temperature rise

Adiabatic temperature rise calculated by the program is quite near to the experimental data in paper [14].

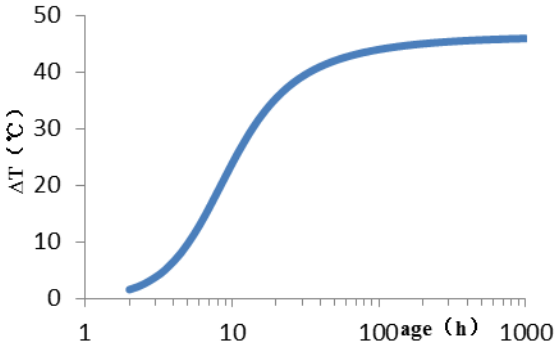

Fig. 1 Adiabatic temperature rise calculated by the program

(2)Temperature field of early-age concrete pavement

As shown in fig.2, compared with the data collected from field experiment [15], the calculated data of different layer of the slab can satisfy the requirements of engineering prediction.

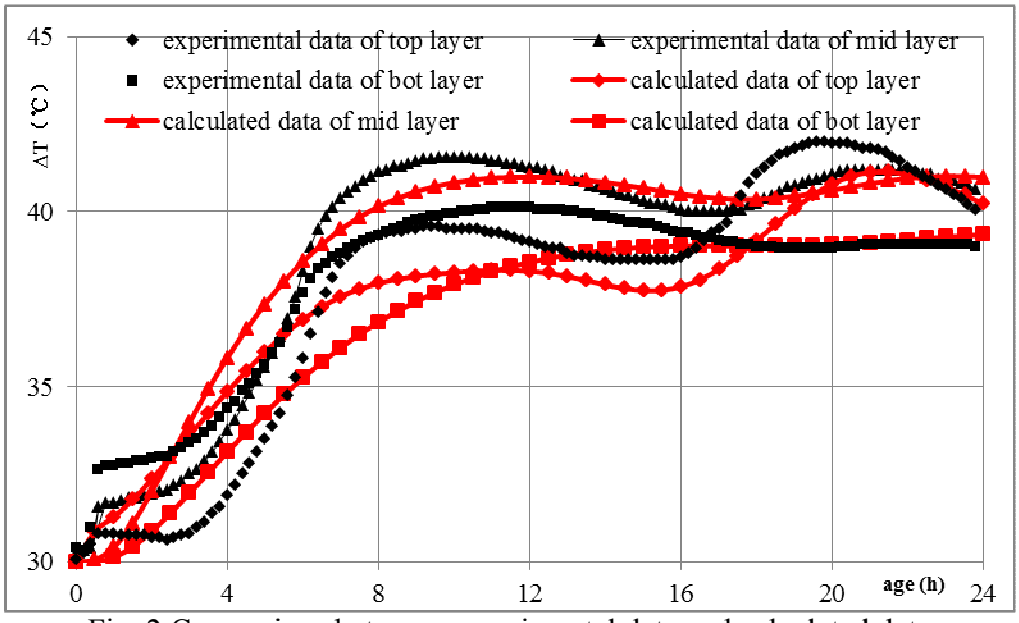

Fig. 2 Comparison between experimental data and calculated data

3 Numerical simulation Schemes

According to the study of Feng[16], the solar radiation absorption ratio and convection coefficient have the most obvious effects on the temperature field of pavement. Actually, during the construction period of concrete pavement, the following factors can exert influences on the definite conditions for the solution of heat transfer equation.

(1) Weather condition

According to the construction requirements select the represented weather condition: listed in table 1.

Reference situation: sunny day; Various situations: cloudy day

Table 1 Parameters of represented weather condition

parameters	spring	summer		autumn	winter
date	2009-4-28	2008-07-22 (sunny)	2008-07-15 (cloudy)	2008-10-19	2008-12-11
total solar radiation（MJ/m^2）	17	21	-	10	5
the effective solar radiation time（h）	14	15	-	12	10
maximum of air temperature（°C）	24.5	34.9	24.1	26.1	1.3
minimum of air temperature（°C）	12.0	22.3	18.5	7.9	-6.9

(2) Pavement structure and material

Choose the represented pavement structure and material of highway in China for the numerical model in this paper. The parameters are listed in table 2.

Although the pavement structure and thermal physical properties have influences on the temperature field, the values of these parameters are fixed in this paper because the structure and material are always chosen before construction.

Table 2 Parameters of represented pavement structure and material

parameters	cement concrete layer	cement stabilized gravel base	foundation
depth（cm）	26	40	300
thermal conductivity（J/m/h/°C）	7896	6000	4600
density（kg/m3）	2368	2270	1800
specific（J/kg/°C）	850	801	983

(3) Curing methods

Different curing materials have obvious difference in solar radiation absorption ratio and convection coefficient according to their color and material characteristics.

Reference situation: exposure curing without any curing materials, the value came from the thesis.

Various situations: the values are determined considering the limited situation (table 3).

Table 3 Parameters of different curing method

parameters	C1	C2	C3	C4	C5
surface heat absorptivity	0.1	0.1	0.9	0.9	0.24
heat emissivity	0.6	0.6	0.6	0.6	0.6
convective heat transfer coefficient（$J/m^2/h/°C$）	0	30*3600	0	30*3600	29552

(4) Paving time

The solar radiate and air temperature are fluctuating every year and every day, paving in different time will lead to the different concrete hardening process and final set temperature gradient. The selected represented situations are listed in table 6 according to the investigated distribution regulation of Beijing from June 2008 to June 2009.

Reference situation: paved at 8:00 am in summer;

Various situations: 0:00; 4:00; 12:00; 16:00; 20:00.

(5) Temperature of raw materials

The temperatures of raw materials will various with the saving status, which result in the temperature change of mixture and will have strong influence on the hydration process of cement. This factor is considered by the different placing temperature of concrete mixture.

Reference situation: 20℃; Various situations:0℃,10℃,30℃,40℃.

4 Results and discussion

(1) Influences of weather condition and paving time

Table 4 shows the weather conditions have a significant influence on the temperature gradient of concrete slab at final set time. The temperature gradients in sunny days are all higher than that in cloudy days. It indicates that the solar radiation is a non-negligible factor leading the temperature rise of concrete. In this table, we can also find that paving the concrete in different time of a day will cause obviously difference in built-in temperature gradient. The values of gradient built in the slab constructed in the daytime are higher as 51.4℃ and 11.8℃ for sunny and cloudy days, respectively, which have reached 4~9 times of the values in nighttime.

Table 4 Influences of weather condition and different paving time of a day

parameters		different paving time					
		SK1	SK2	SK3	SK4	SK5	SK6
		0:00	4:00	8:00	12:00	16:00	20:00
Sunny	final set time (h)	5.7	5.4	4.8	4.7	5.0	5.4
	T_{top}-T_{bottom} (°C)	3.2	9.0	13.4	12.3	6.5	3.5
	Temperature Gradient (°C/m)	12.4	34.7	51.4	47.4	25.1	13.7
cloudy	final set time (h)	6.0	5.9	5.7	5.6	5.7	5.9
	T_{top}-T_{bottom} (°C)	0.3	1.7	3.1	2.8	1.8	0.6
	Temperature Gradient (°C/m)	1.3	6.7	11.8	10.9	6.7	2.5

The meteorological conditions are always fluctuating in different months of a year, and the effects of paving season on built-in temperature gradient are given in table 5. The result in winter represents that the construction condition can also produce negative gradient in slab. This will lead to the totally opposite service behavior of concrete slab in the future days.

Table 5 Influences of different paving time of a year

group	paving season			
	spring	summer	autumn	winter
final set time（h）	5.9	4.8	5.8	10.7
T_{top}-T_{bottom}（℃）	10.3	13.4	8.2	-3.2
temperature gradient（℃/m）	39.4	51.4	31.5	-12.3

(2) Influences of curing method

Table 6 displayed the influences of various curing conditions. When solar radiation absorption is weak and convection is sufficient, the temperature difference between top and bottom surface of the slab is little, on the contrary, if solar radiation ratio is higher and convection is prevented by the curing material, the built-in gradient will come out quite high, which even exceeding the normal temperature gradient in concrete pavement. This issue needs a high level of concern.

Table 6 Influences of different curing methods

group	curing methods				
	YS1	YS2	YS3	YS4	YS5
final set time（h）	5.4	4.7	3.7	4.2	4.8
T_{top}-T_{bottom}（℃）	8.8	5.0	36.6	21.4	13.4
temperature gradient（℃/m）	33.9	19.3	140.9	82.4	51.4

(3) Influences of raw material temperature

The temperatures of raw materials will various with the surroundings, which result in the temperature change of mixture. As shown in table 7, the effects bring by this phenomenon is not so serious that this factor can be neglect compared with others.

Table 7 Influences of raw material temperature

group	temperature of raw material（℃）				
	0	10	20	30	40
final set time（h）	7.7	6.2	4.8	3.6	2.6
T_{top}-T_{bottom}（℃）	15.4	14.8	13.4	11.9	11.3
temperature gradient（℃/m）	59.3	56.9	51.4	45.7	43.6

5 Conclusions

(1) A user subroutine based on the ABAQUS code was developed which can be used to predict the temperature field of early-age concrete pavement. The validity of this program was verified through experimental result from literature and temperature field data collected from a full-scale concrete slab paved in the field.

(2) The effects of weather condition, paving time, curing method, raw material temperature on built-in temperature gradient were analyzed respectively based on the numerical simulation results. They indicate that these factors always produce positive gradient in the slab and the influences of the first three aspects are obvious and the paving temperature of mixture has limited effect on the increasing of the final set temperature gradient.

(3)The study in this paper shows that taking built-in temperature gradient as an index to evaluate the influences of various construction factors and optimize construction measures is effective. These works lay a foundation for the determination for the rational value of built-in temperature gradient based on service performance of concrete pavement.

References

[1]Rao, S. and Roesler, J.. Characterizing Effective Built-In Curling from Concrete Pavement Field Measurements[J]. Journal of Transportation Engineering. 2005,131(4):320~327

[2]Hveem, F. N.. Slab warping affects pavement joint performance[C]. American Concrete Institute.1951,47: 797~808

[3]Hveem, F. N., and Tremper, B.. Some factors influencing shrinkage of concrete pavements[C]. American Concrete Institute, 1957,53: 781~789.

[4]Zollinger, D. G., and Barenberg, E. J. ~1989!. “Proposed mechanistic based design procedure for jointed concrete pavements.” Illinois Cooperative Highway Research Program Project IHR-518, Univ. of Illionis, Urbana, Ill.

[5]Darter, M., Khazanovich, L., Snyder, M., Rao, S., and Hallin, J. (2001). “Development and calibration of a mechanistic design procedure for jointed plain concrete pavements.” Proc., 7th Int. Conf. on Concrete Pavements, Orlando, Fla.

[6]Beckemeyer, C. A., Khazanovich, L., and Yu, H. T. (2002). “Determining amount of built-in curling in jointed plain concrete pavement: Case study of Pennsylvania I-80.” Transp. Res. Rec., 1809, Transportation Research Board, Washington, D.C., 85–92.

[7]Hiller, J. E., and Roesler, J. R. (2002). “Transverse joint analysis for use in mechanistic–empirical design of rigid pavements.” Transp. Res. Rec., 1809, Transportation Research Board, Washington, D.C., 42–51.

[8]Steven A. Wellsa, Brian M. Phillipsa & Julie M. Vandenbosscheb. Quantifying built-in construction gradients and early-age slab deformation caused by environmental loads in a jointed plain concrete pavement[J]. International Journal of Pavement Engineering. 2006(7): 275-289

[9]Specmcations of Cement Concrete Pavement Design for Highway (JTG D40—2011)[S]. Beijing: People's Communication Press. 2002: Appendix B

[10]Zhu Bofang. Temperature stress and control method to mass concrete [M]. Beijing: China Electric Power Press. 1999.

[11]Jin-Hoon Jeong and Dan G. Zollinger. Finite-Element Modeling and Calibration of Temperature Prediction of Hydrating Portland CementConcrete Pavements[J]. JOURNAL OF MATERIALS IN CIVIL ENGINEERING.2006:317~324

[12]RW.J. Wilde. Computer-based guidelines for concrete pavements volume III—technical appendices[R], Federal Highway Administration Report FHWA-HRT- 04-127, McLean, VA, 2005

[13]ASTM C403/C403M-08. Standard Test Method for Time of Setting of Concrete Mixtures by Penetration Resistance. American Society of Testing and Materials, Pennsylvania. 1999

[14]Schindler, A.K. and Folliard, K.J. Influence of Supplementary Cementing on the Heat of hydration of Concrete[C]. Advances in Cement and Concrete IX Conference, August 2003

[15]Quan Lei. STUDY ON TEMPERATURE FIELD AND STRENGTH DEVELOPMENT OF EARLY-AGE CONCRETE SLAB UNDER DIFFERENT CURING METHODS [D],2011.

[16]FENG Decheng et al.Impact of Asphalt Pavement Thermophysical Property on Temperature Field and Sensitivity Analysis[J]. Journal of Highway and Transportation Research and Development.2011,11(28):12~19

Keywords Index

U

V

W

Z

Authors Index